SENSORY-MOTOR ASPECTS OF NERVOUS SYSTEMS DISORDERS: INSIGHTS FROM BIOSENSORS AND SMART TECHNOLOGY IN THE DYNAMIC ASSESSMENT OF DISORDERS, THEIR PROGRESSION, AND TREATMENT OUTCOMES

EDITED BY: Elizabeth B. Torres, Jonathan T. Delafield-Butt and Caroline Whyatt

PUBLISHED IN: Frontiers in Integrative Neuroscience,
Frontiers in Human Neuroscience,
Frontiers in Behavioral Neuroscience and
Frontiers in Aging Neuroscience

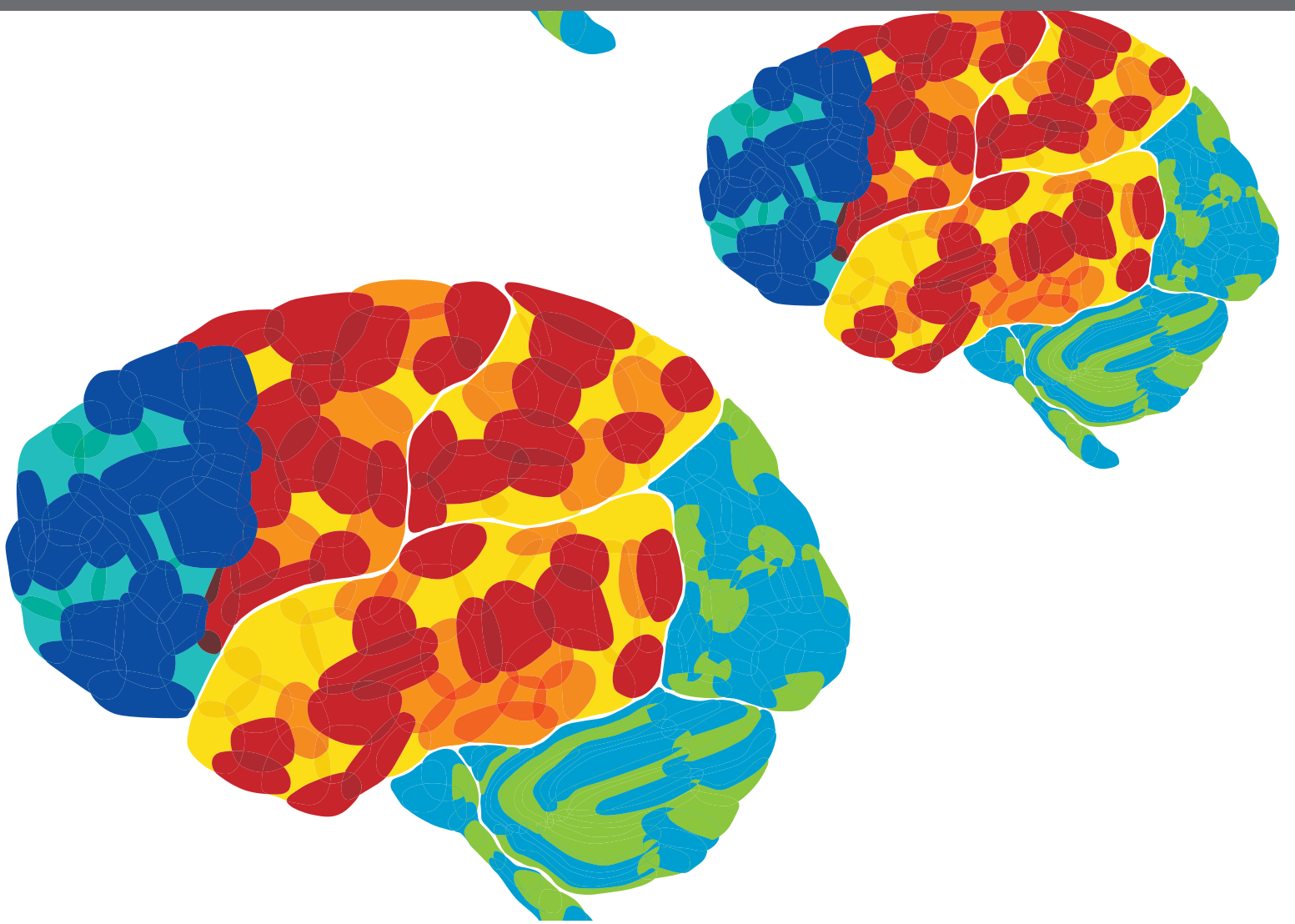

frontiers Research Topics

Frontiers eBook Copyright Statement

The copyright in the text of individual articles in this eBook is the property of their respective authors or their respective institutions or funders. The copyright in graphics and images within each article may be subject to copyright of other parties. In both cases this is subject to a license granted to Frontiers.

The compilation of articles constituting this eBook is the property of Frontiers.

Each article within this eBook, and the eBook itself, are published under the most recent version of the Creative Commons CC-BY licence. The version current at the date of publication of this eBook is CC-BY 4.0. If the CC-BY licence is updated, the licence granted by Frontiers is automatically updated to the new version.

When exercising any right under the CC-BY licence, Frontiers must be attributed as the original publisher of the article or eBook, as applicable.

Authors have the responsibility of ensuring that any graphics or other materials which are the property of others may be included in the CC-BY licence, but this should be checked before relying on the CC-BY licence to reproduce those materials. Any copyright notices relating to those materials must be complied with.

Copyright and source acknowledgement notices may not be removed and must be displayed in any copy, derivative work or partial copy which includes the elements in question.

All copyright, and all rights therein, are protected by national and international copyright laws. The above represents a summary only. For further information please read Frontiers' Conditions for Website Use and Copyright Statement, and the applicable CC-BY licence.

ISSN 1664-8714
ISBN 978-2-88963-895-6
DOI 10.3389/978-2-88963-895-6

About Frontiers

Frontiers is more than just an open-access publisher of scholarly articles: it is a pioneering approach to the world of academia, radically improving the way scholarly research is managed. The grand vision of Frontiers is a world where all people have an equal opportunity to seek, share and generate knowledge. Frontiers provides immediate and permanent online open access to all its publications, but this alone is not enough to realize our grand goals.

Frontiers Journal Series

The Frontiers Journal Series is a multi-tier and interdisciplinary set of open-access, online journals, promising a paradigm shift from the current review, selection and dissemination processes in academic publishing. All Frontiers journals are driven by researchers for researchers; therefore, they constitute a service to the scholarly community. At the same time, the Frontiers Journal Series operates on a revolutionary invention, the tiered publishing system, initially addressing specific communities of scholars, and gradually climbing up to broader public understanding, thus serving the interests of the lay society, too.

Dedication to Quality

Each Frontiers article is a landmark of the highest quality, thanks to genuinely collaborative interactions between authors and review editors, who include some of the world's best academicians. Research must be certified by peers before entering a stream of knowledge that may eventually reach the public - and shape society; therefore, Frontiers only applies the most rigorous and unbiased reviews.
Frontiers revolutionizes research publishing by freely delivering the most outstanding research, evaluated with no bias from both the academic and social point of view. By applying the most advanced information technologies, Frontiers is catapulting scholarly publishing into a new generation.

What are Frontiers Research Topics?

Frontiers Research Topics are very popular trademarks of the Frontiers Journals Series: they are collections of at least ten articles, all centered on a particular subject. With their unique mix of varied contributions from Original Research to Review Articles, Frontiers Research Topics unify the most influential researchers, the latest key findings and historical advances in a hot research area! Find out more on how to host your own Frontiers Research Topic or contribute to one as an author by contacting the Frontiers Editorial Office: researchtopics@frontiersin.org

SENSORY-MOTOR ASPECTS OF NERVOUS SYSTEMS DISORDERS: INSIGHTS FROM BIOSENSORS AND SMART TECHNOLOGY IN THE DYNAMIC ASSESSMENT OF DISORDERS, THEIR PROGRESSION, AND TREATMENT OUTCOMES

Topic Editors:
Elizabeth B. Torres, Rutgers, The State University of New Jersey, United States
Jonathan T. Delafield-Butt, University of Strathclyde, United Kingdom
Caroline Whyatt, University of Hertfordshire, United Kingdom

Citation: Torres, E. B., Delafield-Butt, J. T., Whyatt, C., eds. (2020). Sensory-Motor Aspects of Nervous Systems Disorders: Insights From Biosensors and Smart Technology in the Dynamic Assessment of Disorders, Their Progression, and Treatment Outcomes. Lausanne: Frontiers Media SA.
doi: 10.3389/978-2-88963-895-6

Table of Contents

05 ***Stochastic Signatures of Involuntary Head Micro-movements Can Be Used to Classify Females of ABIDE Into Different Subtypes of Neurodevelopmental Disorders***
Elizabeth B. Torres, Sejal Mistry, Carla Caballero and Caroline P. Whyatt

22 ***Sensory Disturbances, but Not Motor Disturbances, Induced by Sensorimotor Conflicts are Increased in the Presence of Acute Pain***
Clémentine Brun, Martin Gagné, Candida S. McCabe and Catherine Mercier

35 ***Effect of Electro-Acupuncture and Moxibustion on Brain Connectivity in Patients With Crohn's Disease: A Resting-State fMRI Study***
Chunhui Bao, Di Wang, Peng Liu, Yin Shi, Xiaoming Jin, Luyi Wu, Xiaoqing Zeng, Jianye Zhang, Huirong Liu and Huangan Wu

45 ***Automated Assessment of Endpoint and Kinematic Features of Skilled Reaching in Rats***
Ioana Nica, Marjolijn Deprez, Bart Nuttin and Jean-Marie Aerts

60 ***Large-Scale Brain Networks Supporting Divided Attention Across Spatial Locations and Sensory Modalities***
Valerio Santangelo

71 ***Characterization of Sensory-Motor Behavior Under Cognitive Load Using a New Statistical Platform for Studies of Embodied Cognition***
Jihye Ryu and Elizabeth B. Torres

90 ***The Effects of Tai Chi Intervention on Healthy Elderly by Means of Neuroimaging and EEG: A Systematic Review***
Zhujun Pan, Xiwen Su, Qun Fang, Lijuan Hou, Younghan Lee, Chih C. Chen, John Lamberth and Mi-Lyang Kim

102 ***A Review of the Pedunculopontine Nucleus in Parkinson's Disease***
Isobel T. French and Kalai A. Muthusamy

118 ***Olfactory Performance as an Indicator for Protective Treatment Effects in an Animal Model of Neurodegeneration***
Anja Meyer, Anne Gläser, Anja U. Bräuer, Andreas Wree, Jörg Strotmann, Arndt Rolfs and Martin Witt

136 ***Optogenetic Stimulation of GABAergic Neurons in the Globus Pallidus Produces Hyperkinesia***
Jun Tian, Yaping Yan, Wang Xi, Rui Zhou, Huifang Lou, Shumin Duan, Jiang Fan Chen and Baorong Zhang

147 ***Motor Sequence Learning is Associated With Hippocampal Subfield Volume in Humans With Medial Temporal Lobe Epilepsy***
Jinyi Long, Yanyun Feng, HongPeng Liao, Quan Zhou and M. A. Urbin

156 ***Impaired Performance of the Q175 Mouse Model of Huntington's Disease in the Touch Screen Paired Associates Learning Task***
Tuukka O. Piiponniemi, Teija Parkkari, Taneli Heikkinen, Jukka Puoliväli, Larry C. Park, Roger Cachope and Maksym V. Kopanitsa

173 ***The Role of Premotor Areas in Dual Tasking in Healthy Controls and Persons With Multiple Sclerosis: An fNIRS Imaging Study***
Soha Saleh, Brian M. Sandroff, Tyler Vitiello, Oyindamola Owoeye, Armand Hoxha, Patrick Hake, Yael Goverover, Glenn Wylie, Guang Yue and John DeLuca

184 ***Balance Training With a Vibrotactile Biofeedback System Affects the Dynamical Structure of the Center of Pressure Trajectories in Chronic Stroke Patients***
Kentaro Kodama, Kazuhiro Yasuda, Nikita A. Kuznetsov, Yuki Hayashi and Hiroyasu Iwata

191 ***Putting the "Sensory" Into Sensorimotor Control: The Role of Sensorimotor Integration in Goal-Directed Hand Movements After Stroke***
Lauren L. Edwards, Erin M. King, Cathrin M. Buetefisch and Michael R. Borich

206 ***Ecological Momentary Assessment of Head Motion: Toward Normative Data of Head Stabilization***
Peter Hausamann, Martin Daumer, Paul R. MacNeilage and Stefan Glasauer

219 ***Sensory Modulation Disorder (SMD) and Pain: A New Perspective***
Tami Bar-Shalita, Yelena Granovsky, Shula Parush and Irit Weissman-Fogel

229 ***Sensory Over-Responsivity as an Added Dimension in ADHD***
Shelly J. Lane and Stacey Reynolds

241 ***Effectiveness of Noise-Attenuating Headphones on Physiological Responses for Children With Autism Spectrum Disorders***
Beth Pfeiffer, Leah Stein Duker, AnnMarie Murphy and Chengshi Shui

frontiers in Integrative Neuroscience

ORIGINAL RESEARCH
published: 07 June 2017
doi: 10.3389/fnint.2017.00010

Stochastic Signatures of Involuntary Head Micro-movements Can Be Used to Classify Females of ABIDE into Different Subtypes of Neurodevelopmental Disorders

Elizabeth B. Torres[1,2]*, *Sejal Mistry*[3], *Carla Caballero*[1,2] and *Caroline P. Whyatt*[1,2]

[1] Department of Psychology, Rutgers University, Piscataway, NJ, United States, [2] Computer Science Department and Rutgers Center for Cognitive Science, Center for Biomedical Imaging and Modeling, New Brunswick, NJ, United States, [3] Department of Biomathematics, Rutgers University, Piscataway, NJ, United States

Background: The approximate 5:1 male to female ratio in clinical detection of Autism Spectrum Disorder (ASD) prevents research from characterizing the female phenotype. Current open access repositories [such as those in the Autism Brain Imaging Data Exchange (ABIDE I-II)] contain large numbers of females to help begin providing a new characterization of females on the autistic spectrum. Here we introduce new methods to integrate data in a scale-free manner from continuous biophysical rhythms of the nervous systems and discrete (ordinal) observational scores.

Methods: New data-types derived from image-based involuntary head motions and personalized statistical platform were combined with a data-driven approach to unveil sub-groups within the female cohort. Further, to help refine the clinical DSM-based ASD vs. Asperger's Syndrome (AS) criteria, distributional analyses of ordinal score data from Autism Diagnostic Observation Schedule (ADOS)-based criteria were used on both the female and male phenotypes.

Results: Separate clusters were automatically uncovered in the female cohort corresponding to differential levels of severity. Specifically, the AS-subgroup emerged as the most severely affected with an excess level of noise and randomness in the involuntary head micro-movements. Extending the methods to characterize males of ABIDE revealed ASD-males to be more affected than AS-males. A thorough study of ADOS-2 and ADOS-G scores provided confounding results regarding the ASD vs. AS male comparison, whereby the ADOS-2 rendered the AS-phenotype worse off than the ASD-phenotype, while ADOS-G flipped the results. Females with AS scored higher on severity than ASD-females in all ADOS test versions and their scores provided evidence for significantly higher severity than males. However, the statistical landscapes underlying female and male scores appeared disparate. As such, further interpretation of the ADOS data seems problematic, rather suggesting the critical need to develop an entirely new metric to measure social behavior in females.

Conclusions: According to the outcome of objective, data-driven analyses and subjective clinical observation, these results support the proposition that the female

OPEN ACCESS

Edited by:
Sidney A. Simon,
Duke University, United States

Reviewed by:
Marta Bieńkiewicz,
UMR7313 Institut des Sciences Moléculaires de Marseille (ISM2), France
Jorge V. Jose,
Indiana University Bloomington, United States

***Correspondence:**
Elizabeth B. Torres
ebtorres@rci.rutgers.edu

Received: *21 February 2017*
Accepted: *15 May 2017*
Published: *07 June 2017*

Citation:
Torres EB, Mistry S, Caballero C and Whyatt CP (2017) Stochastic Signatures of Involuntary Head Micro-movements Can Be Used to Classify Females of ABIDE into Different Subtypes of Neurodevelopmental Disorders. Front. Integr. Neurosci. 11:10. doi: 10.3389/fnint.2017.00010

phenotype is different. Consequently the "*social behavioral male ruler*" will continue to mask the female autistic phenotype. It is our proposition that new observational behavioral tests ought to contain normative scales, be statistically sound and combined with objective data-driven approaches to better characterize the females across the human lifespan.

Keywords: females, head micro-movements, autism, AS, stochastic signatures, resting state fMRI

INTRODUCTION

Autism Spectrum Disorder (ASD) presents a diagnosis ratio estimated between 4:1 and 5:1 males to females (Volkmar et al., 1993; Mandy et al., 2012), a figure that is further exacerbated by evidence indicating that females are diagnosed significantly later than males (Lai et al., 2015). Indeed, studies show that observational clinical tools, such as the Diagnostic Statistical Manual (DSM) [ASD; APA 4] and Autism Diagnostic Observation Schedule (ADOS) (Lord et al., 2000, 2012) may need modifications to detect symptomatology earlier in females. Such adaptations could help further our understanding of differential sex contribution to the ASD phenotype. Namely, the DSM-V shows a marked division from the DSM IV by encompassing ASD, Asperger's Syndrome (AS), and other similar developmental disorders under an umbrella diagnostic label of Autism Spectrum Disorders, yet the diagnostic implications with respect to sex-level differences has yet to be elucidated. Unfortunately, the current diagnostic rates present tangible difficulties in exploring ASD within the wider female population—most notably challenges in recruiting a sufficient number of female participants. The current methods are therefore grounded on the observation of social behaviors within the male phenotype. However, we know that expectations of social behavior vary from culture to culture. As such, they carry a heavy subjective weight. Thus, the question posed is, how can we use objective means and take advantage of contemporary data-driven techniques, to assess the question of sex differences in ASD?

In recent years, access to open scientific repositories of data has enabled researchers to rethink the issue of sex differences in ASD—providing access to a range of data to achieve higher levels of statistical power and female representation. For instance, a number of publications have pointed at presumed, fundamental, differences in brain signal variability (Takahashi et al., 2016) and patterns of connectivity between the typically developing (TD) brain and the ASD brain (Cheng et al., 2015; Falahpour et al., 2016) by drawing on brain imaging data banks. Importantly, such research highlights specific sex-based differences (Alaerts et al., 2016), including differentiations in structural organization of the motor systems, which are discussed in light of repetitive behaviors (Supekar and Menon, 2015), cortical volume and gyrification (Schaer et al., 2015), among other morphological parameters. Such evidence for fundamental, physiological differences in ASD expression between the sexes may allude to new, refined methods to isolate and quickly identify ASD symptomatology in females; a population that has been thus far difficult to diagnose.

But how accurate and reliable are these claims? A series of recent papers have begun to question the "black-box" treatment of functional magnetic resonance imaging (fMRI) data analyses (Power et al., 2012), particularly when related to ASD (Tyszka et al., 2014). More specifically, there is an analytic pipeline following a "one size fits all model" under assumptions of normality, linearity and stationarity in the imaging data that does not necessarily conform to the characteristics inherent in the variability of such data. Part of the problem stems from the pervasive effects of involuntary head motion on all measures of morphometry and functions derived from structural MRI or resting state fMRI data (rs-fMRI). As such, fMRI experiments require maximal dampening of head movements that may occur during the scanning session (i.e., while lying inside the scanner) to prevent artifacts due to involuntary movements (Deen and Pelphrey, 2012; Power et al., 2012; Tyszka et al., 2014). Yet, even upon padding the head during the scan to minimize movement, these minute fluctuations in head motion are detectable and known to confound the data if no motion correction procedures are in place (Friston et al., 1996; Hutton et al., 2002; Jenkinson et al., 2002). This problem often leads to the removal of large portions of datasets so as to enable statistical inferential analyses. Furthermore, recent work underscores the importance of not making *a priori* statistical assumptions about the underlying stochastic features of biophysical rhythms harnessed from the nervous systems (Torres, 2011, 2013a; Torres et al., 2013a, 2016a). In particular, such work demonstrates that when empirically estimated, the probability distributions that characterize such signals are generally not normal; rather, they are subject to non-linear and stochastic variations inherently present in signals derived from complex systems. These biophysical signals include those derived from fMRI involuntary head-motion related data (Eklund et al., 2016; Torres and Denisova, 2016).

Considering the inherent nature of the empirical data rather than *a priori* imposing theoretical assumptions for statistical inference seems particularly relevant when analyzing cross-sectional data from the population at large. Neurodevelopment is, indeed, non-uniform and highly non-linear in its early stages (Torres et al., 2016b), with the statistical properties of biorhythms from the developing nervous systems changing dramatically with age (**Figure 1**) (Torres et al., 2013a, 2016a). In particular, the degree to which spontaneous involuntary fluctuations in the nascent nervous systems can be dampened on command is in itself a sign of maturity (Torres et al., 2013a), as the nervous systems transition into more stable states. In the case of ASD and other neurodevelopmental disorders, the coping nature of

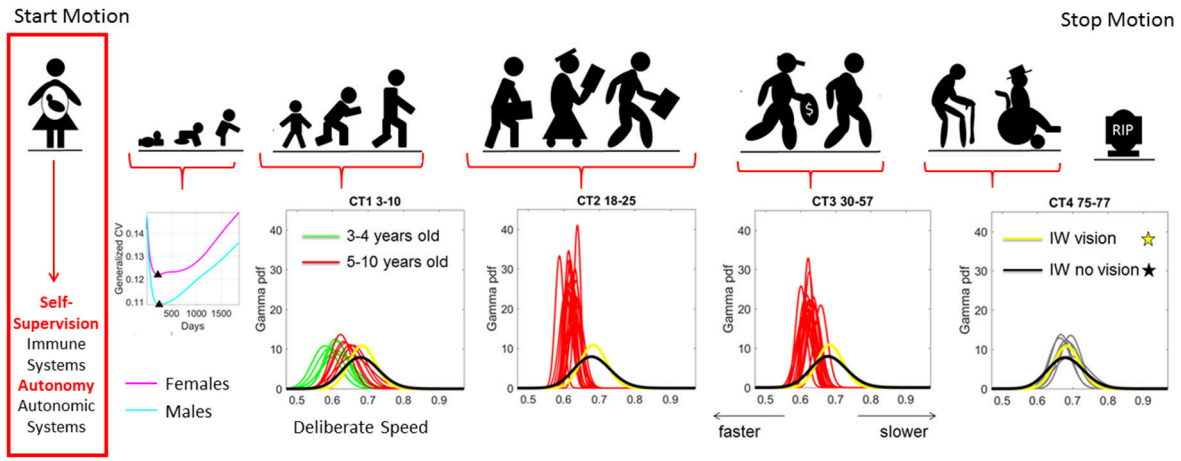

FIGURE 1 | Age dependent shifts in the non-Gaussian stochastic signatures of motion variability. Physical motion starts from conception and ends with death. We propose that during early stages of life the nascent immune and autonomic systems scaffold self-supervision and autonomy, respectively thus endowing the nervous systems with features to be poised to grow and mature intelligence by partly supervising and using its own feedback to learn and adapt. As such, the variability inherently present in the biorhythmic motions of the person—e.g., in deliberate voluntary motions, spontaneous involuntary motions and the inevitable autonomic motions serve as a form of kinesthetic feedback from various systems. It is our finding that these motions are not characterized by symmetric distributions with non-stationary properties. Rather, the probability density functions empirically derived from actual physical data are skewed; shift skewness with aging and the rates of change of the shifts in skewness change within different age groups. For example, early in neonatal stages the female and male phenotypes separate according to the generalized coefficient of variation (CV) of their rates of growth, which is reflected as well in their rate of change of motion stochastic signatures (Torres et al., 2016b) [Data obtained from 26,985 babies per summary point (13,623 girls, 13,362 boys) publicly available from the methods to build the WHO-CDC Growth Charts]. Babies were longitudinally tracked for 24 months upon which cross-sectional data was used to build the charts up to 5 years of age (Kuczmarski et al., 2002; de Onis and Onyango, 2003). Inset highlights the non-Gaussian nature of the variability of this parameter of physical growth and the inflecion point attained earlier (at 224 days) in females than males (at 252 days). Later on in life such sex differences are less obvious (Torres et al., 2013b), but using the fluctuations in motion parameters (e.g., those changing in cross-sectional data spanning 3–77 years of age) can be informative of subtle differences in speed micro-movements denoting different degrees of skewness and dispersion along with different age-dependent rates of change in this stochastic signatures (data extracted from controls (CT) in 176 participants reported in Torres et al., 2016a) Yellow and black PDFs are from a deafferented participant for reference of a system without (or very poor) kinesthetic reafference manifested in the typically aging elderly.

the nervous systems adds a layer of instability that can be tracked through the assessment of involuntary motions (Torres, 2013a), particularly those that are still present in excess in the system despite instructions to remain still (Torres and Denisova, 2016). Indeed, recent results on the role of head motion micro-movements during rs-fMRI revealed elevated levels of noise-to-signal ratio (NSR) in the ASD population at large (Torres and Denisova, 2016). These elevated NSR in involuntary head micro-movements were detected with or without medication intake, suggesting that the presence of involuntary motions with excess NSR levels could serve as an important biological feature of nervous systems with developmental problems. In addition, this previous work illustrated differences between individuals as a function of medication intake (Torres and Denisova, 2016); a comparison dominated by a cohort consisting of majority males participants.

The prior work, however, did not have a sufficiently large number of female participants to examine if male participants primarily drove the elevated NSR, or if the females with a diagnosis of ASD/or AS also have inherently elevated levels of NSR. If so, this signature of stochastic motor variability may provide a route of non-invasive diagnosis, one that may tap into underlying symptomatology associated with a diagnosis of ASD in females. Within the context of resting state imaging studies involving ASD participants, questions have therefore been raised over claims on connectivity and morphometry variation as individuals with a disorder of the nervous system—including those considered a "mental illness" by the DSM (American Psychiatric Association, 2013)—often move more, which impacts statistical inferences and interpretations made (Pardoe et al., 2016).

Given the pervasive noisy and random somatic motor micro-movements signal in ASD across sex and ages (Torres et al., 2013b), severity (Torres and Denisova, 2016) and levels of motor control (voluntary, Torres et al., 2013a; automatic, Torres et al., 2016c), autonomic (Torres and Lande, 2015; Kalampratsidou and Torres, 2016; Torres et al., 2016b), the present work aimed to investigate if involuntary micro-movements of head motion recorded within the scanner had a statistically different rate of noise accumulation in ASD *females* in relation to TD control females. Further, this was examined in light of male-specific ASD-TD differential patterns to consider the impact of gender. For the purposes of our inquiry, it was not as important to consider if the person affected with ASD moved more (since we suspected they did and others corroborated that guess already in affected adults, Tyszka et al., 2014). The question is whether the continuous random process that we used to characterize those fluctuations in head motion amplitude (as spike trains) revealed higher cumulative effects

of noise and randomness in females with ASD, (including as well those with a DSM-IV AS-related diagnosis) than in female controls. We report evidence that the ABIDE data sets contain information of use to help define the ASD female phenotype.

METHODS

Demographics of ABIDE I and ABIDE II

All datasets included in this study are from the Autism Brain Imaging Data Exchange (ABIDE) databases: ABIDE I (http://fcon_1000.projects.nitrc.org/indi/abide/abide_I.html) and ABIDE II (http://fcon_1000.projects.nitrc.org/indi/abide/abide_II.html). The work is in compliance with Frontiers guideline on the use of human subject's data. To that end, quoting from ABIDE "In accordance with HIPAA guidelines and 1,000 Functional Connectomes Project/INDI protocols, all datasets have been anonymized, with no protected health information included."

Collectively, these open access databases contain datasets with a much larger number of females (and males) than one could find in any given single study in the literature. The breakdown of demographics used in the present study is summarized in **Figure 2**. The study includes four main comparisons:

1. *ASD, AS, TD*: Comparison of stochastic signatures of head micro-movements extracted from individuals who have a formal DSM diagnosis of ASD, a DSM-IV-TR (American Psychiatric Association, 1994) diagnosis of AS and TD controls, but are not on medication.
2. *Medication vs. no Medication*: Comparison of individuals with a diagnosis who reported medication use *vs*. those who did not report medication use.
3. *ADOS-2 vs. ADOS-G*: Comparison of ADOS-2 and ADOS-G scores (Lord et al., 1989, 2000) whenever available for set in (1) above.
4. *Females vs. Males*: Comparison of females *vs*. males according to the above mentioned metrics and selected across ABIDE based on the inclusion/exclusion criterion next defined.

Inclusion/Exclusion Criterion

We included those sites in ABIDE I and II that contained information regarding participant medication intake (Table 1 of the Supplementary Material lists sites with summary information). From those sites, we first isolated female individuals who did not take medication ($n = 76$). From these individuals, we isolated those with a diagnosis of ASD and those with a diagnosis of either AS ($n = 27$), or a mixed diagnosis of AS or a pervasive developmental disorder not otherwise specified PDDNOS/PDD ($n = 32$). ABIDE I was published before the DSM-5 (American Psychiatric Association, 2013) was released and only reports information as per DSM-IV-TR (American Psychiatric Association, 1994) while ABIDE II reports both DSM-IV-TR and DSM-5 diagnostic information. Due to the augmentation of terminology in DSM-5 (American Psychiatric Association, 2013) leading to putative overlap between ASD and AS, the ASD individuals were from the non-DSM-IV column of the demographics data set. The AS individuals (and diagnosis) were isolated using the next column representing DSM-IV-TR classification only. Thus, the main question was whether the two groups (non-DSM-IV ASD and the DSM-IV AS) were in any way distinguishable. Then we examined 63 age-matched (TD) females, a group of comparable size, from ABIDE I as the control group.

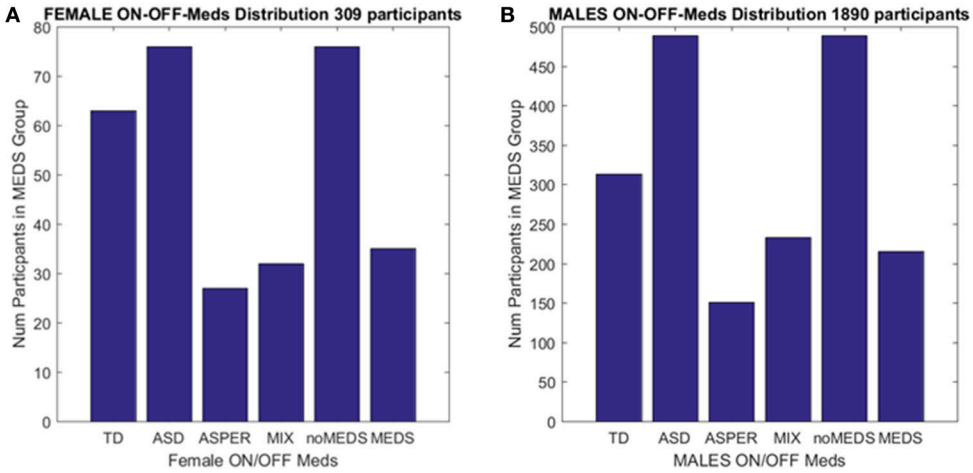

FIGURE 2 | Inclusion/Exclusion criteria for the ABIDE I and II data sets used in this study. **(A)** Females: TD females are from ABIDE I and include all individuals with no medication intake only from ABIDE I sites that reported medication intake in the demographics were included as the group size covered the proper age range and comparable number of participants to those with ASD. ASD females are from column 1 DSM of demographics records across ABIDE I and II with a diagnosis of ASD; DSM-IV-TR AS diagnosis of column 2 of demographics records; MIX includes all AS, PDDNOS, PDD from column 2 DSM-IV (no ASD from DSM IV). NoMEDS refers to all with a diagnosis of ASD (column 1 and 2 of the demographics records), all with a diagnosis of AS or PDDNOS or PDD who were not on medication (i.e., from all sites that reported medications). MEDS were as before, all participants with a diagnosis but not on medication. **(B)** The same as **(A)** for males.

A second level comparison was to select all participants with a given diagnosis (i.e., ASD from the first DSM column, ASD from the second column with the DSM-IV diagnosis and those with AS, PDDNOS, PDD) who were on medication ($n = 76$) and those who were not on medication ($n = 35$). Here, the goal was to compare their involuntary head micro-movements signatures and ask if medication intake in the *females* had an effect on the stochastic signatures of the head motions. **Figure 2** summarizes these demographics.

Lastly, we compared ADOS-2 and ADOS-G scores, whenever available, for the groups above and included the males selected under the same criteria for this comparison (Table 2 of the Supplementary Material lists sites with summary information). The idea was to uncover differential patterns (if any) between female-female statistically significant differences and male-male statistically significant differences. Summary of these results and the levels of statistical significance are shown in Tables 1, 2 of the Supplementary Material.

Motion Extraction

Motion extraction was performed using the Analysis of Functional NeuroImages (AFNI) software packages (Cox, 1996). Single subject processing scripts were generated using the afni_proc.py interface[1]. Skull stripping was performed on anatomical data and functional EPI data were co-registered to anatomical images. The median was used as the EPI base in alignment. Motion parameters, 3 translational (x, y, and z) and 3 rotational (pitch-about the x axis, roll-about the y axis, and yaw-about the z axis), from EPI time-series registration was saved.

Statistical Analyses

In the present work we assess the scan-by-scan velocity-dependent variations in the linear displacement and in the angular rotations of the head during rs-fMRI sessions. The analyses specifically refer to the stochastic signatures of the micro-movements (as generally defined below), their accumulation and empirically estimated statistical features under a statistical platform for individualized behavioral analysis (SPIBA). In the specific case of rs-fMRI data, the data types are not the original head motions *per se*, but rather derivative information pulled out from the original time series that the head-motion extraction methods create (Friston et al., 1995; Worsley and Friston, 1995). The commonly used methods to estimate volume-to-volume head movements from fMRI data were therefore used to obtain the original time series of (raw) head motion data (see section Methods for head motion extraction above).

Micro-Movements as a New Waveform Data Type for Analyses of Motions Embedded in the Biorhythms Harnessed from the Nervous Systems

Given the disparate sampling resolutions (SR) across sites reporting data to ABIDE, we here use a data type that is insensitive to the differences in stochastic processes that such different SR give rise to Caballero et al. (2017). The micro-movements (see below) are a new waveform introduced earlier to analyze motion data from various sensors used in motion caption sampling with different degrees of accuracy, frequency and temporal resolutions (Torres et al., 2013a). Instead of examining a time series of time dependent values, we rather focus on a waveform of the fluctuations in signal amplitude in the order in which the changes in the peaks of the signal occur. In the present work we use the raw linear and angular speeds extracted from the imaging data to build the micro-movements. To that end, we examine the changes in amplitude in a dynamic-independent fashion.

To derive the micro-movements, we obtained the series of local peaks (speed maxima) and divided them pointwise by the sum of the speed maximum value and the local average speed between the two minima,

$$NormSpeedMax = \frac{SpeedMax}{SpeedMax + AvrgSpeed} \quad (1)$$

The spike trains of amplitude fluctuations derived from this normalized version of the raw data are the waveform used as input to the SPIBA. We combine this waveform with a Gamma process to empirically estimate the Gamma parameters and track their values on the Gamma parameter plane, compute the probability distribution functions (PDFs), obtain the Gamma moments and the summary statistics (see **Figure 3**).

Presented in prior work (Torres, 2011, 2013a; Torres et al., 2013a, 2016a,c; Torres and Denisova, 2016) and patent pending technology (Torres and Jose, 2012), the micro-movement approach examines the orderly series of peaks and valleys across biophysical data continuously registered from physiological sensors, from which such spikes can be extracted. Specifically, the fluctuations in amplitude (and timing when the instrument's sampling resolution is uniform across the data set) of such spikes are assumed to characterize a continuous random process where events in the past may (or may not) accumulate evidence toward prediction of future events (see **Figure 4**). **Figure 4** provides a summary of the data types used in the stochastic analyses with sample raw data in **Figures 4A–D**, and micro-movements plots in **Figure 4E**.

This method has been applied to other biorhythms harnessed non-invasively from various processes of the nervous systems ranging from deliberate-voluntary to spontaneous-automatic, spontaneous-involuntary, to inevitable-autonomic (e.g., output from EEG, output from ECG, skin temperature probes, output from inertial measurement units, output from electromagnetic sensors, output from camera based systems, among others, Torres (2013b), Torres et al. (2013a), Kalampratsidou and Torres (2017), Ryu and Torres (2017), and Whyatt and Torres (2017).

Within this framework, the rate of change of raw linear displacement of the head position was obtained in vector form (a three-dimensional velocity field over time). For each velocity vector the Euclidean norm was used to obtain the magnitude of each element in this scalar field over time, i.e., the linear speed temporal profile corresponding to the given session (denoted LS). The time-series of the LS values were then plotted for

[1]https://afni.nimh.nih.gov/pub/dist/doc/program_help/afni_proc.py.html

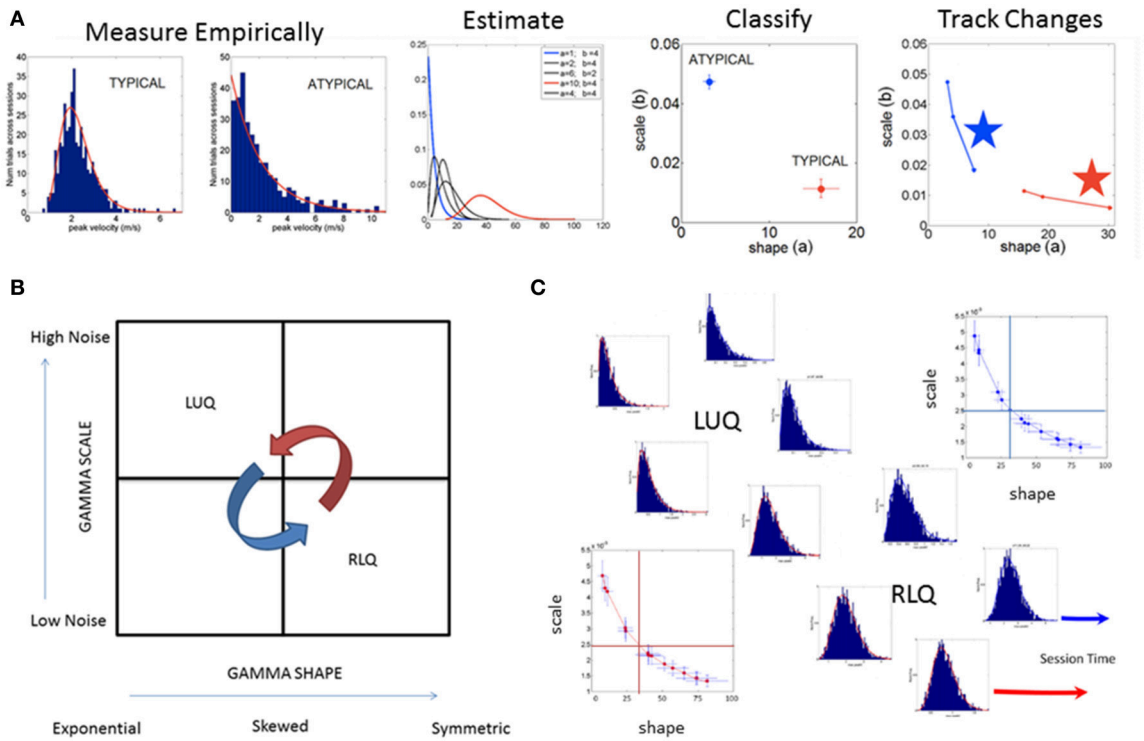

FIGURE 3 | SPIBA using the Gamma process for statistical inference and interpretation of biophysical data. **(A)** Obtain frequency histograms of biophysical parameter and derive micro-movements from the waveform. Empirically estimate the PDF's using maximum likelihood estimation with high confidence and plot the estimated parameters on the Gamma plane. **(B)** The Gamma plane statistical inference for interpretation of biophysical data, (e.g., the biophysical rhythms harnessed from the Central and Peripheral Nervous Systems) is shown here in schematic form. The empirical estimation of the shape and scale Gamma parameters has provided a range of empirical data from movements encompassing a range of voluntary control levels (e.g., autonomic, spontaneous, automatic, involuntary and voluntary). Along this gradient we have profiled the autistic phenotype and found empirical evidence for the prevalence of the Exponential distribution SHAPE value of 1 to the left of the shape-axis. In contrast, the typically developed young participants tend to manifest symmetric shapes to the right of the SHAPE-axis, with skewed distributions between these two extremes prevalent across the adult population at large. Along the SCALE-axis (denoting the noise to signal ratio (NSR) of the biophysical rhythms from movements comprising multiple levels of control) the autistic population remains high in ranges of NSR in relation to the typical controls with lower levels in the steady state regimes of a task (i.e., when the person is proficient at it). This empirical evaluation of human biorhythms harnessed during natural behaviors defines two quadrants of interest to track in any experimental setting involving individualized behavioral analyses: the left upper quadrant of the Gamma plane (LUQ) and the right lower quadrant (RLQ) of the Gamma plane. Each quadrant provides (theoretical) statistical inference information amenable to interpret the actual biophysical data. The subdivision has also been used to characterize and map out the statistical ranges of human behavior with pathologies of the nervous systems in relation to normative data from typical fellows. **(C)** Different scenarios of the Gamma plane and its statistical-inference quadrants are shown in schematic form to invite its use for the tracking of stochastic trajectories of a given individual derived during a given session of a given study. The longitudinal evolutions of the probability distribution functions from the LUQ to the RLQ are important to consider in individualized neurodevelopmental data but also possible to track in scenarios comprising cross-sectional data (such as the present one).

each participant as a linear speed profile where each unit time depends on the scan specs (frames per second in Hz) across the lengths of the scanning sessions (plotted in **Figures 4A,B** for the age-matched TD vs. ASD representative samples and in **Figures 4C,D** for age-matched TD vs. AS and PDDNOS participants).

The fluctuations in amplitude (of LS maxima) were then normalized as in Torres (2011) and Torres et al. (2013a), using equation 1 above, scaled between 0 and 1 to account for allometric (head or body size) effects in cross-sectional data from the population at large (Lleonart et al., 2000). This standardized way of examining physiological signals (the micro-movements data type) further permits grouping of the movement data using clinical and demographic features of participants with heterogeneous demographics and phenotypic information (Torres and Jose, 2012).

The normalized peaks in the order in which they appeared are plotted in **Figures 4E** and for each type of participant. This waveform then served as input to a Gamma process and stochastic characterizations of their fluctuations in amplitude were used to provide a signature of the ASD, AS, and TD groups. Thus, we examined the continuous spike train data of orderly speed amplitude shifts as a Gamma process under the general rubric of a Poisson Random Process (PRP), assuming independent and identically distributed (IID) random variables. This assumption will be relaxed in future work; but for the purposes of our examination concerning the traditional *a priori* assumption of normality in such biophysical data, it should

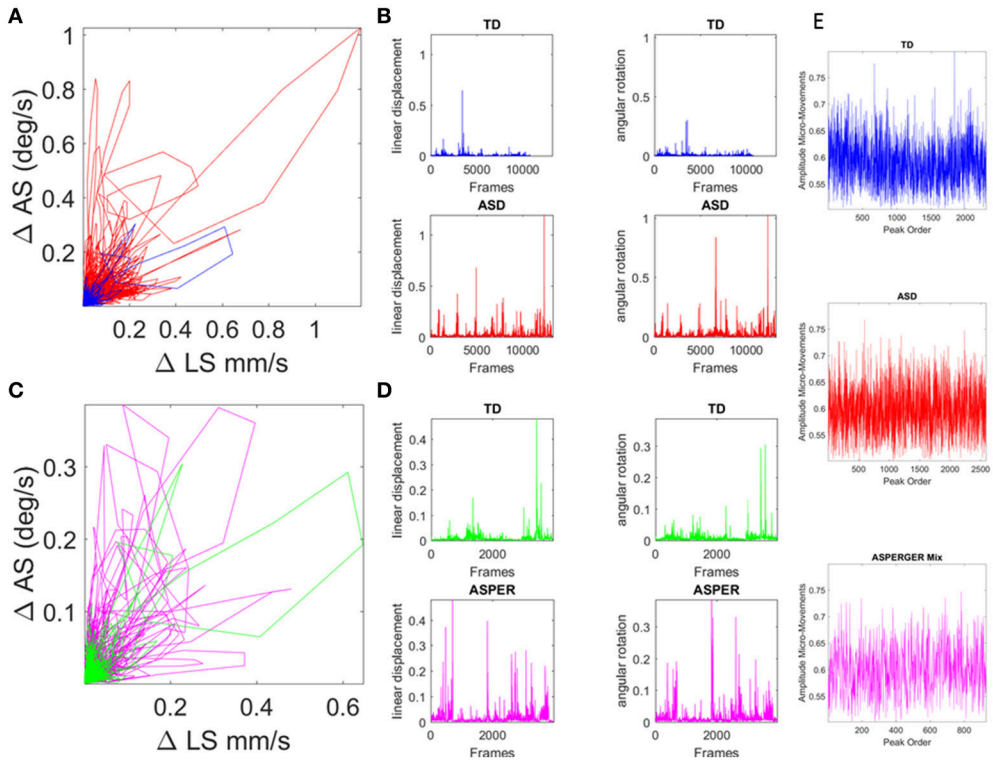

FIGURE 4 | Involuntary head excursions were detected during the resting state fMRI sessions. **(A)** Linear displacements vs. angular rotations of the head contrasting ASD females vs. age-matched TD controls. **(B)** Raw data consisting of linear speed and angular speed extracted from the position and orientation tri-axial trajectories contrasting TD vs. ASD participants. **(C,D)** Same as in **(A,B)** for the females of ABIDE I and II with a DSM-IV diagnosis of AS and PDDNOS vs. the age-matched TD controls in **(A)**. **(E)** Micro-movements extracted from rs-fMRI head linear displacements in TD, ASD, and AS combined with PDDNOS participants.

suffice to consider the simpler case of a point process where the distributions have various degrees of dispersion, skewness, i.e., are not normal and different kurtosis.

Briefly, the Gamma probability distribution function is given by: $y = f(x|a,b) = \frac{1}{\Gamma(a)b^a}x^{a-1}e^{\frac{-x}{b}}$, in which a is the shape parameter, b is the scale parameter, and Γ is the Gamma function (Ross, 1996). We used in-house developed software and MATLAB version 8.3 (R2014a) (The MathWorks, Inc., Natick, MA) functions to estimate the Gamma parameters and corresponding PDF (and CDF) using maximum likelihood estimation (MLE) with 95% Confidence Intervals (CIs). To that end, we compared different families of probability distributions (e.g., the Gaussian, Normal, Lognormal, Exponential and Gamma) and chose the best fit in an MLE sense. Owing to our prior work using the ABIDE sets (Torres and Denisova, 2016) we were able to determine that the Gamma had the best fit in an MLE sense. Of particular importance, the (NSR), a.k.a. the Fano Factor (FF, Fano, 1947) is obtained from the empirically estimated Gamma variance divided by the empirically estimated Gamma mean. The Gamma mean is given by $\mu = a \cdot b$ and the Gamma variance is given by $\sigma^2 = a \cdot b^2$. The NSR in this case is also the Gamma scale parameter since $\frac{\sigma^2}{\mu} = \frac{\cancel{a} \cdot b^{\cancel{2}}}{\cancel{a} \cdot \cancel{b}} = b$ (Ross, 1996). This is important as we will be assessing the levels of noise in relation to the empirical estimation of the Gamma parameters from the data as a function of group type. Higher levels of noise in the left upper quadrant of the Gamma plane (Gamma-LUQ) will correspond to increases of the *b scale* parameter along the vertical axes of the Gamma plane; whereas lower levels of noise in the right lower quadrant (Gamma-RLQ) will correspond to lower values along the *scale* axis of the Gamma plane. This is shown in **Figure 3B** in schematic form with schematic examples of stochastic trajectory evolution across the quadrants of interest in **Figure 3C**. The quadrant's limiting values (represented by the quadrant-dividing lines) are derived from the stochastic signatures of the evolution set as the median values of the scale or shape empirically estimated parameters.

It is also important to emphasize that when the *shape* parameter a of the Gamma family $a = 1$ at the Gamma-LUQ, the data follows the memory-less Exponential probability distribution. This is the most random distribution whereby events in the past do not accumulate information predictive of events in the future (Ross, 1996). Larger values of the shape parameter toward the Gamma-RLQ tend toward the symmetric distributions, with a variety of skewed distributions between the two extremes.

The scatter of points on the log-log Gamma plane gives rise to a power-law relation between the shape and the dispersion of the distributions [the scale parameter or Noise-to-Signal Ratio (NSR)]. The extent to which the scatter points deviate from

this pattern can be quantified. To that end, it is possible to measure the residuals from the linear polynomial fit (denoted here as delta) and obtain a parameter plane involving the delta values vs. the corresponding NSR for each point (representing a participant) in the scatter. This information can thus give rise to statistically driven clusters (Nguyen et al., 2016) to classify various subtypes of patients.

Here we adopt such a metric (that we introduced in Nguyen et al., 2016 and adapted to rs-fMRI data from ABIDE in Torres and Denisova, 2016) to ask if the females of the ABIDE sites that reported medication intake follow any type of automatic sub-group classification. Note here that we do not include females for whom medication status was unknown. To that end, we integrated information from the NSR and the delta residuals from the linear polynomial fit (power-law relation) associated to the scatter of the log-shape and log-scale values on the Gamma plane and will examine the ranges of parameter values within each group. In the text we will refer to the level of randomness in the empirically estimated shape parameter (when close to $a = 1$), the limiting Exponential case; or we will point out increasing values of the shape parameter toward more symmetric distributions tending to the Gaussian limiting case. Likewise we will refer to higher or lower NSR levels according to the empirically estimated b Gamma scale parameter value relative to the age-matched TD control values (as normative data) **Figure 3**A.

RESULTS

Significant Differences in Physical Head Excursions Distinguish ASD and AS Females from TD Females

We examined the relative head excursions during rs-fMRI sessions for each individual female in the cohort. To that end, the cumulative sum of speed values over all frames was obtained (i.e., the physical path length the head traveled) and divided by the number of frames for each participant. The rate of change raw data (before normalization) can be seen for TD vs. ASD in **Figure 4A** with their speed profiles in **Figure 4B**. **Figure 4C** shows the comparison for the TD age-matched vs. the AS. **Figure 4D** shows the corresponding speed profiles for each group.

The distributions of the relative head excursion ratios were well fit by the continuous family of Gamma PDFs. **Figure 5A** shows the empirical cumulative probability distribution (eCDFs) and the estimated CDFs for all three groups of age-matched females. The inset shows the estimated first and second Gamma PDFs. **Figure 5B** shows the signatures localized on the Gamma parameter plane. The estimated Gamma moments were also obtained and the results are summarized in Table 3 of the Supplementary Material.

We next focus on the linear displacements. We compare the *relative* head excursions pairwise across each female group. To that end we used the non-parametric Mann-Whitney-Wilcoxon U rank-sum test. We found statistically significant differences between the pooled data of ASD females and age-matched TD female controls (rank sum test $p < 2.22e\text{-}06$), with notably more head movement (as recorded by physical head excursion) for the ASD female group (see **Figures 4C,D** vs. **Figures 4A,B**). This was further identified in a significant comparison between the AS females, and age-matched TD female controls (rank sum test $p < 1.95e\text{-}05$), but no significant differences were found in the length of head excursions between ASD and AS females ($p < 0.39$). Furthermore, we used the Kolmogorov-Smirnov goodness-of-fit hypothesis test from MATLAB to compare two empirically estimated eCDFs. The pairwise comparison for the relative head excursion parameter yielded significant differences for TD vs. ASD ($p < 3.42e\text{-}05$) and for TD vs. AS ($p < 1.72e\text{-}04$) but was not

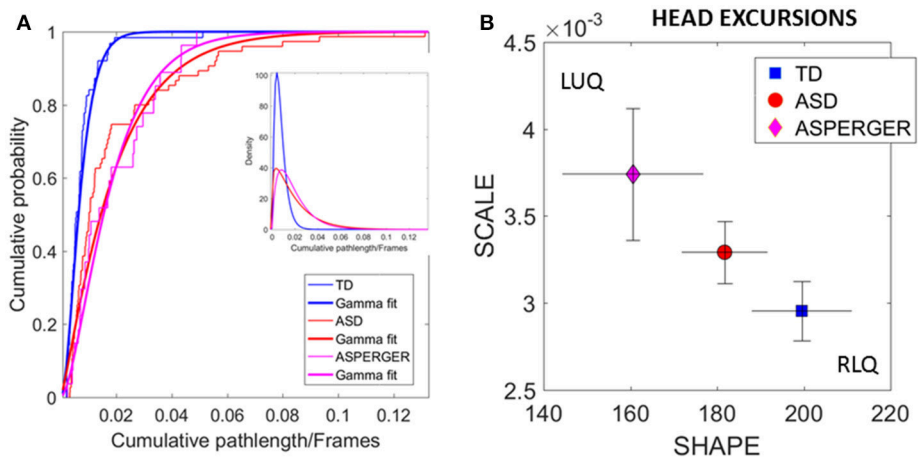

FIGURE 5 | Differences in relative physical head excursions manifest in female participants during rs-fMRI session upon instruction to remain still. **(A)** The empirical cumulative distribution functions (eCDFs) estimated using Gamma fits to the empirical data pooled across all subjects per pre-labeled group separate age-matched TD participants from ASD and AS. Note that eCDFs from ASD and AS participants also separate, but the separation has non-statistical significance (see text). The inset shows the estimated Gamma PDFs. **(B)** Using the SPIBA Gamma process the involuntary head micro-movements of each labeled cohort localize AS and ASD on the LUQ of the Gamma plane with more elevated NSR relative to TD controls localized on the RLQ of the Gamma plane.

significant for ASD vs. AS ($p < 0.54$). The ASD vs. AS proximity in the distributions can be appreciated in **Figure 5A** and the overlapping confidence intervals in **Figure 5B**, along with their separation form TD controls.

Similar analyses were performed to compare all females with a diagnosis on medication vs. those who reported not being on medications. No significant differences were found between the ASD and AS groups of females ($p < 0.31$).

Data-Driven Separation of ABIDE Females

We used SPIBA to examine the micro-movements of the head linear displacements extracted from the rs-fMRI. As explained in the methods section, these spike trains were used as inputs to a Gamma process and the Gamma shape and scale (the NSR) parameters are plotted on the Gamma plane (**Figure 6A**). The log-log plot of this scatter yielded a power relation, whereby a polynomial of degree 1 was fit using polyfit via the MATLAB curve fitting toolbox [Linear Model Poly1 $f(x) = p_1 \cdot x + p_2$ with $p_1 = -1.03(-1.09,\ 1.02)$ and $p2 = -0.369(-0.4185,\ -0.3194)$]. The goodness of fit was SSE 0.06, Adjusted R-square 0.9962 and RMSE 0.01.

The residuals (delta) from the linear fit against the actual scatter of points were examined and plotted on the bottom panel of **Figure 6A**. The deltas vs. the log of the Gamma scale (NSR) were plotted on a parameter plane in the random order in which they were examined. Three groups emerged with clear separation—see **Figure 6B**. The scatter was subsequently colored coded according to the diagnosis label (**Figure 6C**). As is evidenced in **Figure 6C**, the ASD females separated from the AS females, while both groups separated from the TD controls. We underscore here that the bottom panel of **Figure 6A** contains the deltas in random order. There is no a priori-selection that leads to **Figure 6B** systematic separation. It is rather a systematic separation that *self emerges* without the use of the labels (*unsupervised mode*). Then **Figure 6C** is colored with the labels (*supervised mode*). Further, the cumulative path/frame (head excursion ratio) was plotted along the *z-axis* (**Figure 6D**) and the groups further separated (surprisingly) showing the AS group as the farthest apart from the age-matched TD controls.

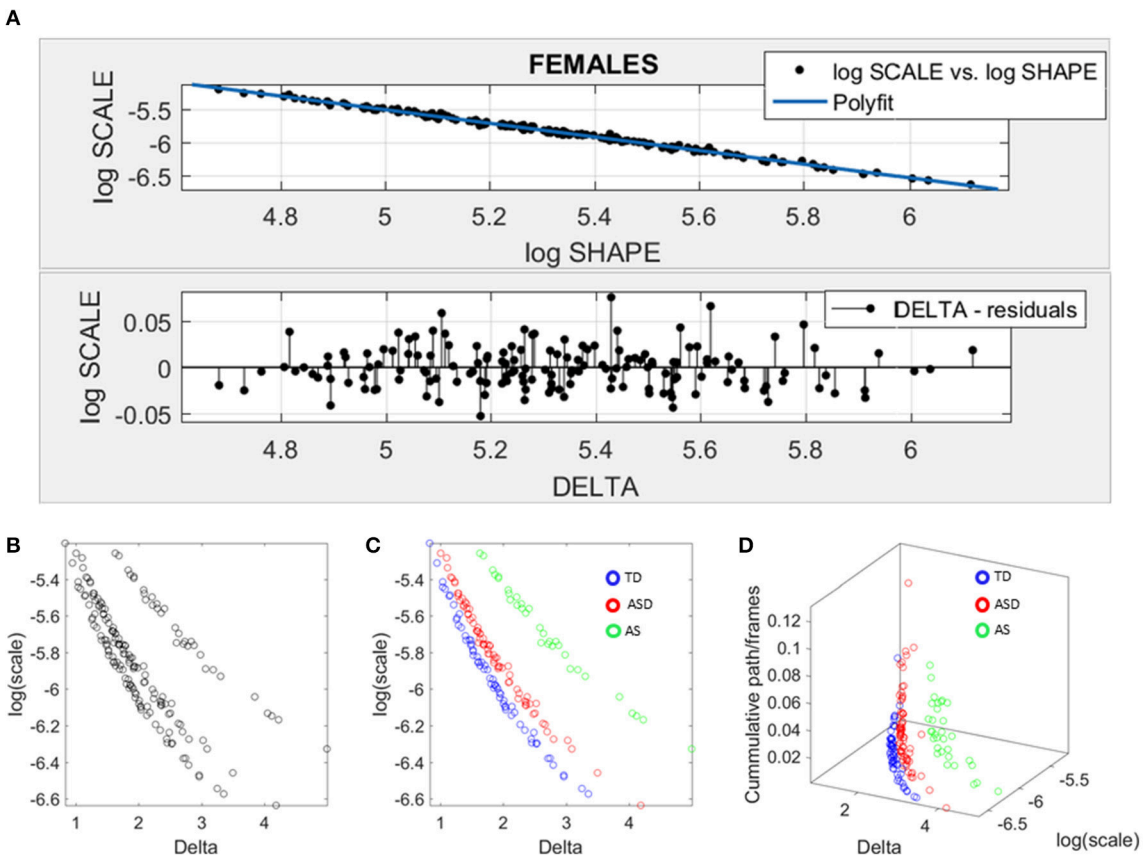

FIGURE 6 | Data-driven approach for cluster detection based on stochastic properties of the head micro-movements data of the females in ABIDE. **(A)** Individually estimated Gamma probability distributions of the females and power relation fit using polynomial of degree 1 on the log-shape vs. log-scale parameter plane (top panel). Bottom panel shows the residuals (delta) obtained from the error between the polynomial fit and the actual scatter points. **(B)** Parameter plane distinguishes three clusters along the Delta vs. log (scale) or noise to signal ratio (NSR). **(C)** Scatter colored by DSM labels reveal clusters congruent with the diagnosis. **(D)** Further separation of the groups emerges when using the relative head excursion (cumulative path length per frames), with the AS group singled out as the farthest apart from the age-matched TD controls.

Data-Driven Separation of ABIDE Males

Given the results in the female cohort, the SPIBA approach paired with the Gamma process was used to examine the males across ABIDE using the same inclusion-exclusion selection criteria as with the ABIDE females. **Figure 7** shows the resulting plots from these analyses. As in **Figure 6A** involving the females, we found that the log-log plot of this scatter yielded a power relation whereby a polynomial of degree 1 was fit using polyfit via the MATLAB curve fitting toolbox [Linear Model Poly1 $f(x) = p_1 \cdot x + p_2$ with $p_1 = -1.02(-1.024, 1.015)$ and $p2 = -0.423(-0.4364, -0.3879)$]. The goodness of fit was SSE 0.488, Adjusted R-square 0.9947 and RMSE 0.02, **Figure 7A**.

The delta residuals in random order are plotted in **Figure 7A**-bottom panel. They give rise to two main groups in the *unsupervised* case plotted in **Figure 7B**. The supervised case in **Figure 7C** reveals that in the males of ABIDE, the AS group overlaps with the TD controls. It is instead the male-ASD group that falls farther apart from the controls and AS groups. This comparison revealed a marked contrast with the ABIDE females in **Figure 6**, suggesting that the male ASD and the female ASD are two distinct *somatic-motor* phenotypic groups.

Impact of Clinical Severity

Given this result, severity metrics were examined to consider the symptomatology composition of the ASD and AS cohorts. As such, ADOS-2 (Autism Diagnostic Observation Schedule, Edition 2; Lord et al., 2012) and ADOS-G (Autism Diagnostic Observation Schedule Generic; Lord et al., 2000), scores were extracted where possible, to characterize associated severity. Table 2 of the Supplementary Material lists the ABIDE sites providing such information. Operationalizing clinical diagnostic criteria stipulated via the DSM (American Psychiatric Association, 1994, 2013), these "gold standard" (Lord et al., 1989, 2000, 2012; Gotham et al., 2008), clinical tools provide standardized scoring metrics to quantify and characterize axes of ASD, whereby "higher" scores are reflective of more pronounced symptoms, thus severity. The aims were therefore (1) to examine if female ASD and AS participants with DSM-based labels could be further refined by ADOS-based severity criteria; (2)

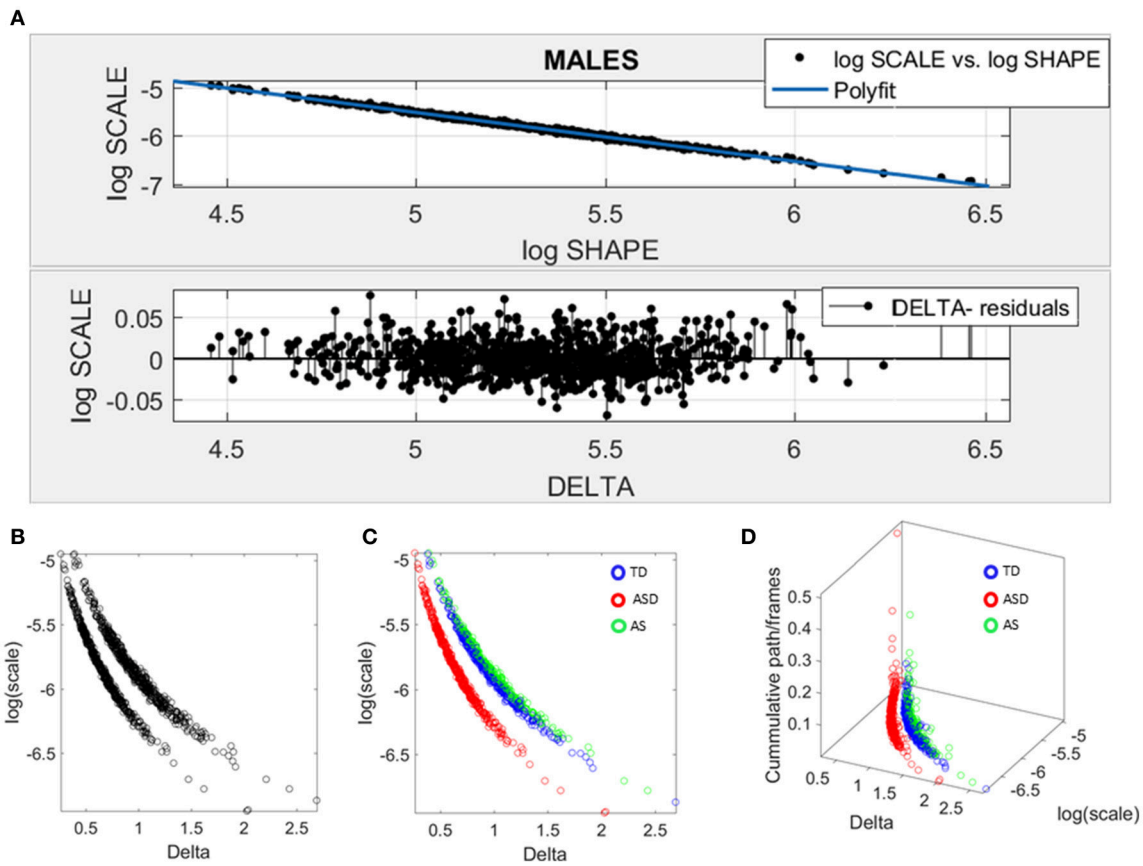

FIGURE 7 | Data-driven approach for cluster detection based on stochastic properties of the head micro-movements data of the males in ABIDE. **(A)** Individually estimated Gamma probability distributions of the females and power relation fit using polynomial of degree 1 on the log-shape vs. log-scale parameter plane (top panel). Bottom panel shows the residuals (delta) obtained from the error between the polynomial fit and the actual scatter points. **(B)** Parameter plane distinguishes three clusters along the Delta vs. log (scale) or noise to signal ratio (NSR). **(C)** Scatter colored by DSM labels reveal clusters congruent with the diagnosis. **(D)** Further separation of the groups emerges when using the relative head excursion (cumulative path length per frames), with the ASD group singled out as the farthest apart from the age-matched TD controls and AS subgroup overlapping with the TD controls.

to examine if male participants with ASD and AS DSM-based labels could be further refined by ADOS-based severity criteria and (3) if ADOS-based severity in males vs. females provided further information to further integrate both clinical and research criteria with the objectively determined subtypes (see **Figure 8** and Supplementary Materials for information on other ADOS-sub-scores).

To that end, the ADOS-G and ADOS-2 scores were first normalized relative to the maximum values allowed for each sub-score scale. Further, as age-related coping mechanisms in ASD appear to impact the stochastic signatures of micro-movements (Torres, 2013a; Torres et al., 2013a), the age of the participant at the time of the scan was used to correct for possible age differences due to the developing mechanisms. As such, we normalized the scores by age and set them on a 0–1 scale. These normalized scores reflect a measure obtained relative to the individual. However, due to the clinical characteristics of the ADOS-2 and ADOS-G scales (Lord et al., 2000), with no normalized population data for comparisons, it is difficult to anchor the ADOS-based scores to normative data to help interpret performance in relation to the neuro-typical population (unlike the analyses in **Figures 6**, **7** providing a relative metric, in relation to TD controls).

Comparisons were then made between the ADOS-2—total, severity and sub-scales (RRB–restricted repetitive behaviors and SA–social affect). As illustrated in Tables 1, 2 of the Supplementary Material, the overarching severity score and total scores were significantly different across the cohort. This pattern was further reflected in a significant difference between overarching ADOS-G total scores for each group. Yet, upon closer inspection of the metrics derived, these results illuminate a number of interesting, and somewhat puzzling findings.

First, the summative statistics, empirically derived through distribution fitting (rather than theoretically assuming normality), yielded higher average measures for each of the female and male AS sub-groups in relation to the corresponding ASD group. As measured by the ADOS-2, denoting the feature quantified by each element (sub-score and total metrics), the average was worse in AS females than in ASD females of comparable neuro-developmental age (as measured by the age

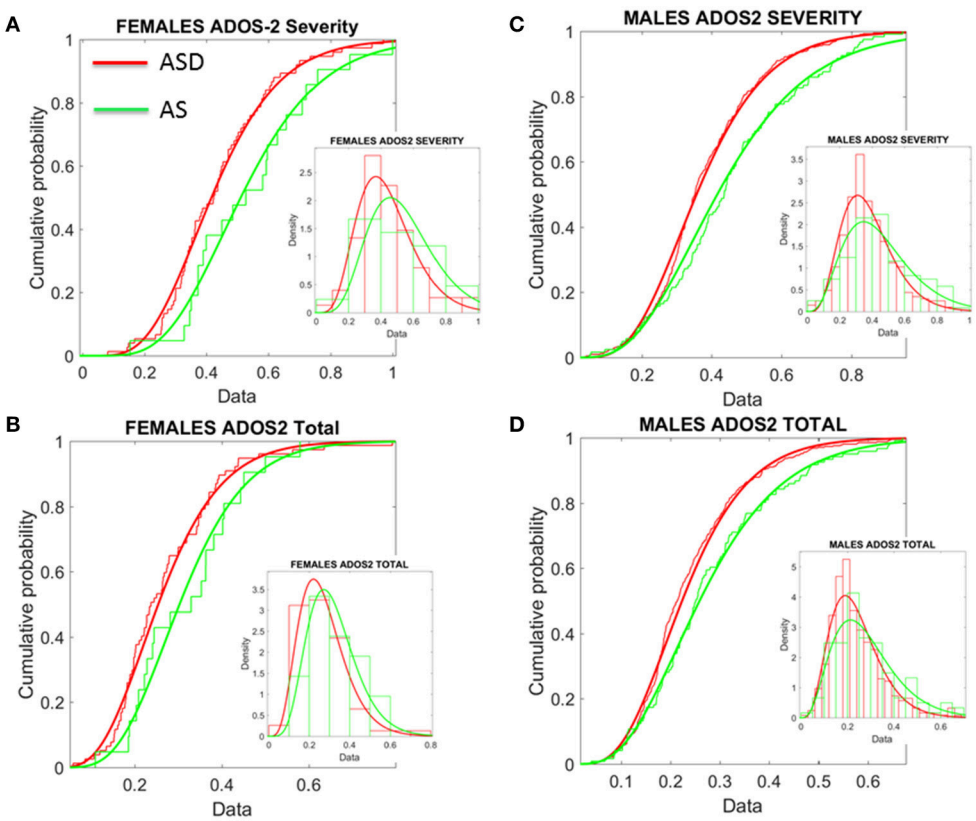

FIGURE 8 | Age corrected (incremental) ADOS-2 scores mark statistically significant differences between ASD and AS observational phenotypes in the cross-sectional data form ABIDE I and II of sites that reported medication status. **(A)** Females with an AS diagnosis have higher age-corrected ADOS-2 severity scores than ASD females (Table 1 in Supplementary Material) reports the Gamma fit first (mean) and second (sigma) moments from highly skewed distribution of incremental scores considering physical age of the person at the time of the test (i.e., this is different corrective criterion than adjusting for mental age, already factored into the module selection process). **(B)** Same trend as in **(A)** for the age-corrected ADOS2-total reveals worse scores for AS females. **(C,D)** The analyses of **(A,B)** for females were performed on the males. Similar statistical features were detected for the incremental age-corrected ADOS-2 scores: skewed distributions with higher mean values for AS in relation to ASD.

corrected scale). We underscore however, that this somewhat counterintuitive finding is underpinned by empirically derived estimates of the mean and variance, rather than *a priori* assumptions of normality across the data. In particular, the parameters of interest were extracted, normalized and the probability distribution function that best characterized the distribution of the data harnessed to extract both the mean and variance (see **Figure 8**). These results map onto the patterning derived through empirical, objective (*unsupervised*) examination of the underlying head micro-movement during rs-fMRI (see **Figure 6**), whereby female AS participants are found to be notably separated from the female TD group. Indeed, the female ASD group appears to display more commonality to the TD group at this objective level.

Second, this pattern is further mirrored in "higher" ADOS-G results for the female cohort, again implying pronounced symptomatology for the female AS group in comparison to the female ASD group. Yet, despite this pervasive finding across the female cohort, mapping well onto the pattern of grouping according to stochastic signature of physiological variability, the male cohort fail to display this feature consistently across the ADOS-G parameters. In particular, at this level, the male group inverts, whereby male participants diagnosed with ASD display "higher" ADOS-G scores in relation to the corresponding AS male group—a finding that is consistent across this clinical tool i.e., sub-scales and total metrics. More in keeping with traditional expectations (i.e., more pronounced symptomatology associated with ASD), this finding may also point to the similarities we unveiled in **Figure 7** between TD and AS male participants in relation to objective (*unsupervised*) profiling of the stochastic signature of micro-movements.

When examining the profile of significant differences between individuals with ASD and AS across the ADOS-2 and ADOS-G for both the female and male cohorts, further differences are highlighted. Specifically, fewer axes of both the ADOS-2 and ADOS-G significantly differentiate between female ASD and AS, whereas more consistently significant differences are found between the male ASD and AS groups (see Tables 1, 2 of the Supplementary Material). This pattern may be indicative of the sensitivity (or lack thereof) of the clinical assessment tools to quantify and classify symptomatology of ASD in females.

Further comparison between AS males and females, and ASD males and females were performed in relation to ADOS-G and ADOS-2 scores. These are provided on Tables 4, 5 of the Supplementary Material. All ADOS-G scores yielded significant differences with higher average scores for females (suggesting higher severity). Several ADOS-2 scores also yielded statistically significant differences and higher scores on average for the females. Yet, despite empirically derived, these summary statistics are based upon different probability distribution functions (in some instances) for each sex, as shown by Supplementary Tables and Figures. Indeed, overall, the distribution of ADOS-2 and ADOS-G sub-scores in the cases of ASD and AS females have very different tails than that of the males (**Figure 9**). This hints at a different statistical landscape altogether for the female case. Combined, such results caution that it may be inappropriate to continue the use of a *social-behavior male ruler* as imposed by clinical tools to measure the female ASD phenotype—a feature already unveiled by the somatic-motor metrics of involuntary motion in **Figures 6**, **7** underlying any behavior (social or otherwise.) See additional figures in Supplementary Material which provide sub-score distributions and Tables 4 and 5 lists the outcome from the male-female comparison with the caveat (as with Tables 1, 2 above) that we do not have any reference to normative population data (i.e., preventing us from using relative population scores) to anchor these results to (i.e., while using absolute population scores).

DISCUSSION

Arguably, the most striking result in the present work stems from the data-driven approach that revealed automatic clustering of subgroups with fundamentally different patterns between females and males. Specifically, the head motion patterns obtained from imaging data during resting state fMRI experiments—which are commonly used to remove motion artifacts from the images—can be harnessed to serve other purposes, namely to facilitate diagnosis and classification of separable subtypes. Indeed, groups appeared on a parameter plane according to the NSR within the head-motion signal, and the extent to which the participant's stochastic signature departs from a power relation between the shape and dispersion of the empirically estimated distributions derived from their involuntary head motions. Further, groups separated according to the relative head excursions that the individual experienced while resting in the fMRI session under the instruction to remain still. In the female cohort this result pointed at the AS group as the one having the most dissimilar involuntary micro-movements' signatures from the age-matched TD controls. In contrast, the male AS group overlapped with the TD male participants, potentially more in-line with expectations. Indeed, in this instance it was the ASD subgroup that emerged as the most dissimilar with respect to the TD controls.

Such results suggest that the stochastic signature of physiological variability may provide a physical, non-invasive method to objectively characterize the ASD phenotype. In particular, this method may provide a novel insight into the functioning and expression of ASD across the female population—a cohort known to be difficult to diagnose and examine. Indeed, current discussion points toward an under-diagnosis of ASD in the female population, with a number of females potentially missing diagnosis or being misdiagnosed in the clinical field (Gould and Ashton-Smith, 2011; Wing et al., 2011), developing coping strategies or mechanisms that result in the failure to diagnose and thus provide services to these females when exclusively basing their diagnosis on a male model of social behavior.

The extent to which these somatic-motor disturbances may be captured by observational tools may be reflected in the age-corrected ADOS-2 severity and total scores that reached statistical significance for comparisons between ASD vs. AS females. Specifically, the pattern of separation between the ASD and AS groups of females (at this observational level) is reflected in a distinct *unsupervised* separation of groups in relation to

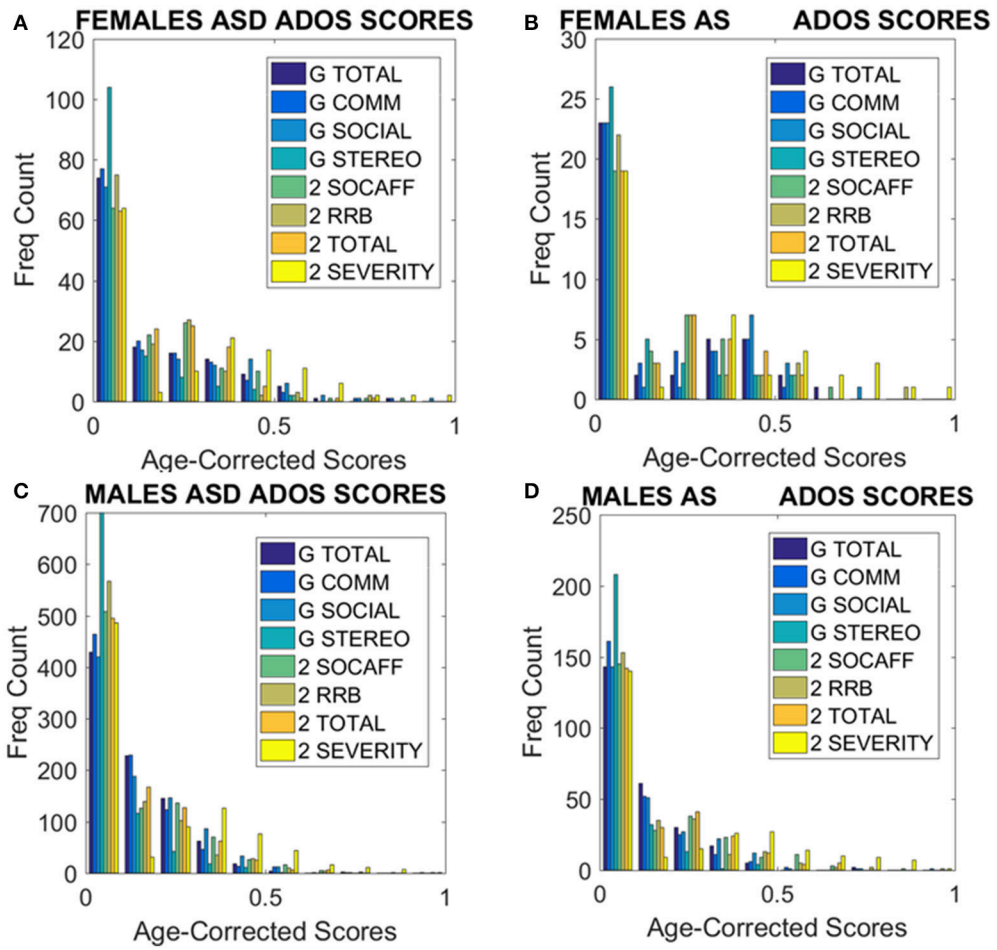

FIGURE 9 | ADOS-2 and ADOS-G scores at a glance taken from all subjects we included in the analyses. **(A)** Females with a non-DSM-IV diagnosis of ASD. **(B)** Females with a DSM-IV diagnosis of AS. **(C)** ASD Males as in **(A)**. **(D)** AS Males as in **(B)**. Note the skewness of these distributions and the differences in their tails separating the two sexes. As detected by the non-parametric Rank-Sum test, the ADOS-2 severity and the ADOS-2 total do not tapper off as the individual ages, physically grows and develops neutrally at irregular rates.

underlying stochastic signature of the physiological signature. Combined, these results suggest that an increase in somatic-motor noise in AS females distinguishes this group from the ASD group (and TD group)—a distinction reflected in the clinical tool assessment. Yet, interestingly, this separation is in a—perhaps counterintuitive—direction, with more pronounced difficulties or symptomatology recorded in female AS participants. When these analyses were extended to the males under similar criteria, the separation between ASD and AS males remained strong and the age-corrected ADOS-2 severity score also separated them with statistical significance. Yet, unlike in females, the head micro-movement analyses in males did not reveal fundamental statistical differences between the TD male controls and the males with an AS DSM-IV diagnosis.

The age-corrected ADOS-G scores provided a somewhat different landscape from those of the ADOS-2. Specifically, the pattern illustrated across the female cohort was inverted for the males. As demonstrated, AS females displayed systematically *higher age-corrected ADOS-G* scores than ASD females, a trend that persisted across both the ADOS-2 *and* ADOS-G. According to clinical interpretation, such results infer worse social-related symptoms in AS females than ASD females (communication, social and stereotypic behaviors)—a pattern also reflected at the physiological level. Yet, in comparison, the male AS cohort demonstrate systematically *lower age-corrected ADOS-G* sub-scores across all categories listed in the ADOS-G (see Table 2 of the Supplementary Material); a result that is an inversion to the pattern across the female group, and indeed, an inversion to the result displayed by the male AS group examined using the ADOS-2 (See summary **Figure 9** to see the results at a glance). This (implicitly) may imply that their social behavior as measured by these tests and the scores they provide (as properly corrected here by physical age) point at AS males being closer to TD controls than the ASD males. We underscore here the word "may implicitly imply" because the paper describing the ADOS-G explicitly states the need to test this inventory with typical control

participants. As such, we deduce that the scores of the ADOS-G as those of the ADOS-2 are absolute, rather than derived relative to normative data.

Yet, why the different pattern of results between sexes, and what can this tell us in light of the physiological metrics? First, the pattern of pronounced difficulty across the female AS cohort in relation to the ASD group may infer more pronounced symptoms in the female AS participant pool. Indeed, social-behaviors, such as those examined and quantified by the ADOS-2 and ADOS-G, intrinsically depend upon a level of motor control. As such, the result that individuals with higher levels of sensory-motor noise display "higher" scores capturing more pronounced ASD symptomatology may not be surprising. Further, it must be noted that the pattern of significant differences, across the clinical assessment are constrained to the total and severity metrics for the female cohort—perhaps reflective of the complexities associated with profiling the subtleties of ASD behaviors in the female population. Indeed, in line with physiological assessment, the one sub-scale (across both the ADOS-2 and ADOS-G) in which significant difference between the female sub-groups emerge is that of stereotyped behaviors in ADOS-G. It may be the case that this form of movement variability—both at an observational and micro-level—is a characteristic feature associated with AS in the female cohort. Secondly, the inversion of the male cohort at the level of ADOS-2 and ADOS-G is puzzling. With the ADOS-G outcomes sitting in line with the physiological metrics (i.e., with male AS participants being more in line with TD participants than those with ASD–see **Figure 8**), the objective physiologically driven results may place more weight on the outcomes of the ADOS-G. However, the ADOS-G criteria is (according to their authors) incomplete to completely render a diagnosis of ASD as it lacks the repetitive behavior sub-scores (Lord et al., 2000)–which we see here as the one sub-score with somewhat explicit motor component form *overt* observable behaviors that we could more directly relate to the data-driven results. On the other hand, the ADOS-2, which contains the sub-score from repetitive behaviors the ADOS-G lacks, does not align with the data-driven results based on involuntary motor issues. In fact, the males, which dominate ASD research due to the 5:1 male to female ratio, are according to the ADOS-2, better off in the non-DSM-IV ASD classification than in the DSM-IV AS classification (**Figure 10**, Tables 1–5 of the Supplementary Material). Yet, according to the ADOS-G, it is the opposite: the ASD males are worse off than the males with AS in all social and communication aspects. *Which one is it?*

A further element of potential concern with such observational clinical assessment tools, such as the ADOS-2 or ADOS-G aimed to operationalize the working DSM model, is the underlying assumption of a theoretical normal distribution across the population. This assumption underpins the ability for such tests to derive and report a (assumed) mean and standard deviation from their empirical computations. Yet, here the distribution of observational outcomes (i.e., those with the ADOS-2 and ADOS-G) were collated, the probability distribution that best characterized that metric *empirically estimated* (see Supplementary Material) were not symmetric. Such empirical work illustrates the inherent variability, even

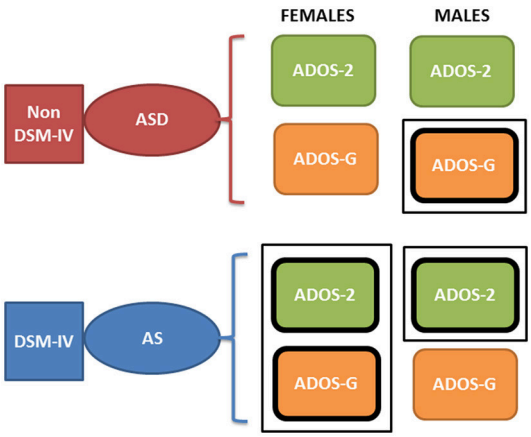

FIGURE 10 | Contradictory results between the ADOS-2 and ADOS-G reported demographics in ABIDE I and II in relation to the non-DSM-IV ASD and the DSM-IV AS phenotypes. According to the theoretical population assumptions underlying the ADOS-based scoring systems, if we were to have a random draw of one male individual with a diagnosis of ASD and one male individual with an AS diagnosis from the ABIDE population that reports medication, we would find that the ASD individual is likely to be worse off than the AS under ASD-G criteria (enclosed rectangle) but better off than the AS under the ADOS-2 criteria (enclosed rectangle). In contrast, if we were to do this with females, both ADOS-based criteria would yield a better outcome score for the ASD than the AS DSM-driven phenotype (enclosed rectangle comprising both ASD-2 and ASD-G). Note here that these are the outcomes of statistical tests. We are not interpreting here the data beyond that outcome from the ABIDE data (see *p*-values and empirically estimated summary statistics in Tables 1, 2 of the Supplementary Material).

at this level, of ASD characteristics, with the underlying distribution across the population of scores extracted from the ABIDE databases best characterized by PDFs including the Gamma family, the generalized extreme value, and exponential distributions. This raises a fundamental question on the ability of such population data to be accurately reflected in clinical tools; tools that largely dominate the research domain and advocate a "*one size fits all*" model (Torres et al., 2016a). Such a model is inadequate as it remains incongruent with empirical data from motions at all levels of nervous systems functioning that our proposed taxonomy defines (Torres, 2011): deliberate-voluntary (**Figure 1** and see Torres et al., 2016a); spontaneous-involuntary (explored in this work, Torres and Denisova, 2016; and inevitable-autonomic, Ryu and Torres, 2017).

The Question of Medication Intake

The present work also demonstrates atypically elevated levels of NSR and randomness in the amplitude fluctuations of the involuntary head micro-movements of female participants with ASD and ASD-related diagnoses (AS and PDDNOS, PDD) in relation to age-matched TD controls, *whether or not they took medication*. That is, even the medication naïve ASD and AS females demonstrated noisy and random involuntary motor signatures. It is our proposition (Brincker and Torres, 2013) that this excess noise from the periphery may compromise kinesthetic

feedback, echoing a form of persistently corrupted re-afferent feedback loop. This result is interesting in light of the prior work involving ABIDE I participants (Torres and Denisova, 2016), which had predominantly ASD male participants, but produced results that demonstrated differences according to the quantity of medication intake and medication classes. As such, there seems to be a difference between males and females on the spectrum regarding medication and involuntary head micro-movements. Larger sets involving females only with more detailed medication information (e.g., dosage, class, time on treatment, etc.) will be required to further investigate this hypothesis, nonetheless, the question of medication and mental illness is complex.

These new results are, however, a step forward toward the integration of ordinal *discrete data* from observational inventories with physically driven objective criteria from *continuous data*. In particular, the present criteria are derived directly from biorhythms of the nervous systems—which may mark nervous systems' disorders. Indeed, the 5:1 male to female ratio from observational methods currently employed to diagnose ASD strongly suggests that these observational criteria appear to "miss" the females early in life. In this sense, physical parameters providing objective assessments of somatic-motor measures and other related physiological signatures may boost the early detection rate and help distinguish sub-types of females in the spectrum relative to neuro-typical controls. Building on prior work quantifying differences in patterns of voluntary control that differentiate between males and females with ASD (Torres et al., 2013b) during a decision-making task, the present results demonstrate the ability to detect sex differences by analyzing involuntary head motion extracted from resting state activity during fMRI experiments. Perhaps combining these levels of enquiry we can further refine our understanding between different female subgroups. Specifically, we propose that neurodevelopmental fields dealing with criteria for mental illness, as defined by the DSM and ADOS, may utilize objective metrics grounded on somatic-motor physiology—in a move toward the Precision Psychiatry agenda (Torres et al., 2016a) and the Research Domain Criteria (RDoC) of the NIMH (Insel et al., 2010; Insel, 2014).

Unfortunately, both psychological (ADOS-2/ ADOS-G) and psychiatric (DSM) criteria for the diagnosis of ASD exclude somatic-motor criteria. For instance, the ADOS-2 manual states (author emphasis added):

> "*Note that the ADOS-2 was developed for and standardized using populations of children and adults* ***without significant sensory and motor impairments****. Standardized use of any ADOS-2 module presumes that the individual can walk independently and is free of visual or hearing impairments that could potentially interfere with use of the materials or participation in specific tasks*" (Lord et al., 2012).

While, the DSM-criteria also avoid somatic-motor issues on the grounds that many individuals on the autism spectrum, including infants and young children, are on psychotropic medication which may impact the nervous systems functioning. Indeed, under the DSM-5 (American Psychiatric Association, 2013) section entitled ***"Medication-Induced Movement Disorders and Other Adverse Effects of Medication"***, several disorders are listed as byproducts of adverse effects from psychotropic medication intake. Within this setting, the DSM-5 explicitly states, "**Although these movement disorders are labeled 'medication induced', it is often difficult to establish the causal relationship between medication exposure and the development of the movement disorder",** (DSM-5; medication section, American Psychiatric Association, 2013). While none of this section makes direct reference to developmental disorders like ASD or ADHD that under DSM-5 (but not under DSM-IV) are allowed to be comorbid (American Psychiatric Association, 1994, 2013), such developmental disorders are heavily medicated worldwide (Zito et al., 2003; Chai et al., 2012; Zhang et al., 2013) with uncertain consequences. Future consideration of the impact of medication intake on somatic-motor criteria may help separate involuntary motor issues from those present across the spectrum regardless of medication.

Finally, such results indicate that the ASD and ASD-related female phenotype (i.e., AS, PDDNOS and PDD) can be distinguished according to stochastic signatures of involuntary head micro-movements. Likewise, the ASD male phenotype can be distinguished from the AS and TD controls. However, the age groups in ABIDE start at 6 years of age. These distinctions need to be made within the first couple of years of life before an observational diagnosis or a diagnosis based on parental reports is already in place. By then, the problems are obvious to the naked eye, suggesting they have reached a more steady-state status with a tendency to become harder to readapt once the rates of adaptive change in the nervous systems slow down or plateau.

It is our proposition that perhaps to detect risk for a neurodevelopmental disorder earlier in life, we could begin to combine the types of neuro-motor control related biometrics explained here with patterns of physical growth that are already tracked by pediatricians in the newborn -as we did in a small cohort of 36 babies, some at risk of stunting in neurodevelopment (Torres et al., 2016b). Indeed, female newborn babies are already separable from the male newborn babies according to their patterns of physical growth. This should be particularly important in the nascent nervous systems of the newborn baby, or the rapidly developing nervous system of a young infant. During the pre-cognitive state of the neonate, accelerated rates of change in physical growth are accompanied by rapid neurodevelopment of motor control when typical development is in place (Torres et al., 2016b). Indeed failing to follow this coupled rate of change trajectory reveals stunting in neurodevelopment rather early. As such, objectively tracking physical parameters may help us identify the females with neurodevelopmental issues much earlier than current observational inventories or parental reports allow. The latter are of outmost importance. But if we were to complement them with physical criteria and properly derive and standardize their statistical ranges using normative approaches, more progress on the early detection of risk for neurodevelopmental issues would be ascertained.

CONCLUSIONS

The present methods were adapted to the personalized assessment of nervous systems biorhythms to objectively quantify: (1) the excess involuntary motions present as the person laid down in resting state and was instructed to remain still; (2) the cumulative effects of continuous head motions on the NSR and randomness of this physiological waveform; and to (3) distinguish females across the human spectrum of typical and atypical development resulting in an ASD or AS/PDDNOS diagnosis. Notwithstanding the limitations of the study owing to the need for more females of diverse age groups, more information on medication intake (dosage, classes, time of treatment, etc.), and the issues with the ADOS-based criteria, we demonstrate that it is possible to initiate the path of better defining the ASD female phenotype by employing objective quantitative means and publicly available large data sets. As our bodies are in constant motion (even when seemingly at rest) these methods may be extended to use with wearable sensing technology and cloud updating under the mobile-Health concept, contributing to progress toward a mathematically-driven model of Precision Psychiatry.

ETHICS STATEMENT

The datasets generated and/or analyzed during the current study are available in the ABIDE I repository, http://fcon_1000.projects.nitrc.org/indi/abide/abide_I.html.

AUTHOR CONTRIBUTIONS

ET designed and performed stochastic analyses and wrote paper; SM extracted all head motion data from ABIDE I and ABIDE II; ET, SM, CC, and CW analyzed demographics; ET, SM, and CW analyzed neonates data; SM, CC, and CW edited paper and all authors agreed to the last version of the MS. All authors read and approved the final manuscript. CC and CW independently reproduced all the ADOS-related statistical results and graphs reported in the paper and produced the Supplementary Materials.

FUNDING

The study was supported by the Nancy Lurie Marks Family Foundation Development Career Award to ET; the New Jersey Governor's Council for Research and Treatment of Autism to ET, CC, and CW. Funding sources for ABIDE are available at http://fcon_1000.projects.nitrc.org/indi/abide.

ACKNOWLEDGMENTS

We thank the participants in these studies and the researchers who contributed the data in ABIDE.

SUPPLEMENTARY MATERIAL

The Supplementary Material for this article can be found online at: http://journal.frontiersin.org/article/10.3389/fnint.2017.00010/full#supplementary-material

REFERENCES

Alaerts, K., Swinnen, S. P., and Wenderoth, N. (2016). Sex differences in autism: a resting-state fMRI investigation of functional brain connectivity in males and females. *Soc. Cogn. Affect. Neurosci.* 11, 1002–1016. doi: 10.1093/scan/nsw027

American Psychiatric Association (1994). *Task Force on DSM-IV, Diagnostic and Statistical Manual of Mental Disorders: DSM-IV, 4th Edn*. Washington, DC: American Psychiatric Association. xxvii, 886.

American Psychiatric Association (2013). *DSM-5 Task Force, Diagnostic and Statistical Manual of Mental Disorders: DSM-5, 5th Edn*. Washington, DC: American Psychiatric Association. xliv, 947.

Brincker, M., and Torres, E. B. (2013). Noise from the periphery in autism. *Front. Integr. Neurosci.* 7:34. doi: 10.3389/fnint.2013.00034

Caballero, C., Mistry, S., Vero, J., and Torres, E.B. (2017). "Reassessing the autistic phenotype using Big-Data from the autism brain imaging data exchange repository," in *Annual Meeting of the Society fot Neuroscience* (Washington, DC).

Chai, G., Governale, L., McMahon, A. W., Trinidad, J. P., Staffa, J., and Murphy, D. (2012). Trends of outpatient prescription drug utilization in US children, 2002–2010. *Pediatrics* 130, 23–31. doi: 10.1542/peds.2011-2879

Cheng, W., Rolls, E. T., Gu, H., Zhang, J., and Feng, J. (2015). Autism: reduced connectivity between cortical areas involved in face expression, theory of mind, and the sense of self. *Brain* 138(Pt 5), 1382–1393. doi: 10.1093/brain/awv051

Cox, R. W. (1996). AFNI: software for analysis and visualization of functional magnetic resonance neuroimages. *Comput. Biomed. Res.* 29, 162–173.

Deen, B., and Pelphrey, K. (2012). Perspective: brain scans need a rethink. *Nature* 491:S20. doi: 10.1038/491S20a

de Onis, M., and Onyango, A. W. (2003). The centers for disease control and prevention 2000 growth charts and the growth of breastfed infants. *Acta Paediatr.* 92, 413–419. doi: 10.1111/j.1651-2227.2003.tb00570.x

Eklund, A., Nichols, T. E., and Knutsson, H. (2016). Cluster failure: Why fMRI inferences for spatial extent have inflated false-positive rates. *Proc. Natl. Acad. Sci. U.S.A.* 113, 7900–7905. doi: 10.1073/pnas.1602413113

Falahpour, M., Wesley, T. K., Angela, A. E., Afrooz, J., Mark, M. E., Datko, M., et al. (2016). Underconnected, but not broken? Dynamic functional connectivity mri shows underconnectivity in autism is linked to increased intra-individual variability across time. *Brain Connect.* 6, 403–414. doi: 10.1089/brain.2015.0389

Fano, U. (1947). Ionization Yield of Radiations. II. The fluctuations of the number of ions. *Phys. Rev.* 72:26.

Friston, K. J., Holmes, A. P., Poline, J. B., Grasby, P. J., Williams, S. C., Frackowiak, R. S., et al. (1995). Analysis of fMRI time-series revisited. *Neuroimage* 2, 45–53.

Friston, K. J., Williams, S., Howard, R., Frackowiak, R. S., and Turner, R. (1996). Movement-related effects in fMRI time-series. *Magn. Reson. Med.* 35, 346–355.

Gotham, K., Risi, S., Dawson, G., Tager-Flusberg, H., Joseph, R., Carter, A., et al. (2008). A replication of the Autism Diagnostic Observation Schedule (ADOS) revised algorithms. *J. Am. Acad. Child Adolesc. Psychiatry* 47, 642–651. doi: 10.1097/CHI.0b013e31816bffb7

Gould, J., and Ashton-Smith, J. (2011). Missed diagnosis or misdiagnosis? Girls and women on the autism spectrum. *Good Autism Pract.* 12, 34–41.

Hutton, C., Bork, A., Josephs, O., Deichmann, R., Ashburner, J., and Turner, R. (2002). Image distortion correction in fMRI: a quantitative evaluation. *Neuroimage* 16, 217–240. doi: 10.1006/nimg.2001.1054

Insel, T., Cuthbert, B., Garvey, M., Heinssen, R., Pine, D. S., Quinn, K., et al. (2010). Research domain criteria (RDoC): toward a new classification framework for research on mental disorders. *Am. J. Psychiatry* 167, 748–751. doi: 10.1176/appi.ajp.2010.09091379

Insel, T. R. (2014). The NIMH Research Domain Criteria (RDoC) Project: precision medicine for psychiatry. *Am. J. Psychiatry* 171, 395–397. doi: 10.1176/appi.ajp.2014.14020138

Jenkinson, M., Bannister, P., Brady, M., and Smith, S. (2002). Improved optimization for the robust and accurate linear registration and motion correction of brain images. *Neuroimage* 17, 825–841. doi: 10.1006/nimg.2002.1132

Kalampratsidou, V., and Torres, E. B. (2016). "Outcome measures of deliberate and spontaneous motions," in *Third International Symposium on Movement and Computing MOCO'16* (Thessaloniki: ACM).

Kalampratsidou, V., and Torres, E. B. (2017). "Body-brain-avatar interface: a tool to study sensory-motor integration and neuroplasticity," in *Fourth International Symposium on Movement and Computing, MOCO'17* (London).

Kuczmarski, R. J., Ogden, C. L., Guo, S. S., Grummer-Strawn, L. M., Flegal, K. M., Mei, Z., et al. (2002). 2000 CDC growth charts for the united states: methods and development. *Vital. Health Stat.* 11, 1–190.

Lai, M. C., Baron-Cohen, S., and Buxbaum, J. D. (2015). Understanding autism in the light of sex/gender. *Mol. Autism* 6:24. doi: 10.1186/s13229-015-0021-4

Lleonart, J., Salat, J., and Torres, G. J. (2000). Removing allometric effects of body size in morphological analysis. *J. Theor. Biol.* 205, 85–93. doi: 10.1006/jtbi.2000.2043

Lord, C., DiLavore, P. C., and Gotham, K. (2012). *Autism Diagnostic Observation Schedule*. Torrance, CA: Western Psychological Services Torrance.

Lord, C., Risi, S., Lambrecht, L., Cook, E. H., Leventhal, B. L., DiLavore, P. C., et al. (2000). The autism diagnostic observation schedule—generic: a standard measure of social and communication deficits associated with the spectrum of autism. *J. Autism Dev. Disord.* 30, 205–223. doi: 10.1023/A:10055924 01947

Lord, C., Rutter, M., Goode, S., Heemsbergen, J., Jordan, H., Mawhood, L., et al. (1989). Autism diagnostic observation schedule: a standardized observation of communicative and social behavior. *J. Autism Dev. Disord.* 19, 185–212.

Mandy, W., Chilvers, R., Chowdhury, U., Salter, G., Seigal, A., and Skuse, D. (2012). Sex differences in autism spectrum disorder: evidence from a large sample of children and adolescents. *J. Autism Dev. Disord.* 42, 1304–1313. doi: 10.1007/s10803-011-1356-0.

Nguyen, J., Majmudar, U., Papathomas, T. V., Silverstein, S. M., and Torres, E. B. (2016). Schizophrenia: the micro-movements perspective. *Neuropsychologia* 85, 310–326. doi: 10.1016/j.neuropsychologia.2016.03.003

Pardoe, H. R., Kucharsky Hiess, R., and Kuzniecky, R. (2016). Motion and morphometry in clinical and nonclinical populations. *Neuroimage* 135, 177–185. doi: 10.1016/j.neuroimage.2016.05.005

Power, J. D., Barnes, K. A., Snyder, A. Z., Schlaggar, B. L., and Petersen, S. E. (2012). Spurious but systematic correlations in functional connectivity MRI networks arise from subject motion. *Neuroimage* 59, 2142–2154. doi: 10.1016/j.neuroimage.2011.10.018

Ross, S. M. (1996). *Stochastic Processes. 2nd Edn. Wiley Series in Probability and Statistics Probability and Statistics*. New York, NY: Wiley. xv, 510.

Ryu, J., and Torres, E. B. (2017). "Methods for Dynamically Coupled Brain Body Tracking," in *Fourth International Symposium on Movement and Computing, MOCO'17* (London).

Schaer, M., Kochalka, J., Padmanabhan, A., Supekar, K., and Menon, V. (2015). Sex differences in cortical volume and gyrification in autism. *Mol. Autism* 6:42. doi: 10.1186/s13229-015-0035-y

Supekar, K., and Menon, V. (2015). Sex differences in structural organization of motor systems and their dissociable links with repetitive/restricted behaviors in children with autism. *Mol. Autism* 6:50. doi: 10.1186/s13229-015-0042-z

Takahashi, T., Yoshimura, Y., Hiraishi, H., Hasegawa, C., Munesue, T., Higashida, H., et al. (2016). Enhanced brain signal variability in children with autism spectrum disorder during early childhood. *Hum. Brain Mapp.* 37, 1038–1050. doi: 10.1002/hbm.23089

Torres, E. B. (2011). Two classes of movements in motor control. *Exp. Brain Res.* 215, 269–283. doi: 10.1007/s00221-011-2892-8

Torres, E. B. (2013a). Atypical signatures of motor variability found in an individual with ASD. *Neurocase* 19, 150–165. doi: 10.1080/13554794.2011.654224

Torres, E. B. (2013b). The rates of change of the stochastic trajectories of acceleration variability are a good predictor of normal aging and of the stage of Parkinson's disease. *Front. Integr. Neurosci.* 7:50. doi: 10.3389/fnint.2013.00050

Torres, E. B., Brincker, M., Isenhower, R. W., Yanovich, P., Stigler, K. A., Nurnberger, J. I., et al. (2013a). Autism: the micro-movement perspective. *Front. Integr. Neurosci.* 7:32. doi: 10.3389/fnint.2013.00032

Torres, E. B., and Denisova, K. (2016). Motor noise is rich signal in autism research and pharmacological treatments. *Sci. Rep.* 6:37422. doi: 10.1038/srep37422

Torres, E. B., Isenhower, R. W., Nguyen, J., Whyatt, C., Nurnberger, J. I., Jose, J. V., et al. (2016a). Toward precision psychiatry: statistical platform for the personalized characterization of natural behaviors. *Front. Neurol.* 7:8. doi: 10.3389/fneur.2016.00008

Torres, E. B., Isenhower, R. W., Yanovich, P., Rehrig, G., Stigler, K., Nurnberger, J., et al. (2013b). Strategies to develop putative biomarkers to characterize the female phenotype with autism spectrum disorders. *J. Neurophysiol.* 110, 1646–1662. doi: 10.1152/jn.00059.2013

Torres, E. B., and Jose, J. V. (2012). *Novel Diagnostic Tool to Quantify Signatures of Movement in Subjects with Neurological Disorders, Autism and Autism Spectrum Disorders.* Rutgers University PCT Application (PCT/US2012/064805, dockets 2012–051, 2012–085.

Torres, E. B., and Lande, B. (2015). Objective and personalized longitudinal assessment of a pregnant patient with post severe brain trauma. *Front. Hum. Neurosci.* 9:128. doi: 10.3389/fnhum.2015.00128

Torres, E. B., Nguyen, J., Mistry, S., Whyatt, C., Kalampratsidou, V., and Kolevzon, A. (2016c). Characterization of the statistical signatures of micro-movements underlying natural gait patterns in children with phelan mcdermid syndrome: towards precision-phenotyping of behavior in ASD. *Front. Integr. Neurosci.* 10:22. doi: 10.3389/fnint.2016.00022

Torres, E. B., Smith, B., Mistry, S., Brincker, M., and Whyatt, C. (2016b). Neonatal diagnostics: toward dynamic growth charts of neuromotor control. *Front. Pediatr.* 4, 1–15. doi: 10.3389/fped.2016.00121

Tyszka, J. M., Kennedy, D. P., Paul, L. K., and Adolphs, R. (2014). Largely typical patterns of resting-state functional connectivity in high-functioning adults with autism. *Cereb. Cortex* 24, 1894–1905. doi: 10.1093/cercor/bht040

Volkmar, F. R., Szatmari, P., and Sparrow, S. S. (1993). Sex differences in pervasive developmental disorders. *J. Autism Dev. Disord.* 23, 579–591.

Whyatt, C., and Torres, E. B. (2017). "The social-dance: decomposing naturalistic dyadic interaction dynamics to the 'micro-level," in *Fourth International Symposium on Movement and Computing, MOCO'17* (London: ACM.)

Wing, L., Gould, J., and Gillberg, C. (2011). Autism spectrum disorders in the DSM-V: better or worse than the DSM-IV? *Res. Dev. Disabil.* 32, 768–773. doi: 10.1016/j.ridd.2010.11.003

Worsley, K. J., and Friston, K. J. (1995). Analysis of fMRI time-series revisited–again. *Neuroimage* 2, 173–181.

Zhang, T., Smith, M. A., Camp, P. G., Shajari, S., MacLeod, S. M., and Carleton, B. C. (2013). Prescription drug dispensing profiles for one million children: a population-based analysis. *Eur. J. Clin. Pharmacol.* 69, 581–588. doi: 10.1007/s00228-012-1343-1

Zito, J. M., Safer, D. J., DosReis, S., Gardner, J. F., Magder, L., Soeken, K., et al. (2003). Psychotropic practice patterns for youth: a 10-year perspective. *Arch. Pediatr. Adolesc. Med.* 157, 17–25. doi: 10.1001/archpedi.157.1.17

Conflict of Interest Statement: ET and Rutgers University hold patent pending agreements for the technology used in this manuscript to analyze the data.

The other authors declare that the research was conducted in the absence of any commercial or financial relationships that could be construed as a potential conflict of interest.

Copyright © 2017 Torres, Mistry, Caballero and Whyatt. This is an open-access article distributed under the terms of the Creative Commons Attribution License (CC BY). The use, distribution or reproduction in other forums is permitted, provided the original author(s) or licensor are credited and that the original publication in this journal is cited, in accordance with accepted academic practice. No use, distribution or reproduction is permitted which does not comply with these terms.

frontiers in Integrative Neuroscience

ORIGINAL RESEARCH
published: 21 July 2017
doi: 10.3389/fnint.2017.00014

Sensory Disturbances, but Not Motor Disturbances, Induced by Sensorimotor Conflicts Are Increased in the Presence of Acute Pain

*Clémentine Brun[1,2], Martin Gagné[1], Candida S. McCabe[3,4] and Catherine Mercier[1,2]**

[1] Center for Interdisciplinary Research in Rehabilitation and Social Integration, Québec, QC, Canada, [2] Department of Rehabilitation, Laval University, Québec, QC, Canada, [3] Royal National Hospital for Rheumatic Diseases, Bath, United Kingdom, [4] Department of Nursing and Midwifery, University of the West of England, Bristol, United Kingdom

Incongruence between our motor intention and the sensory feedback of the action (sensorimotor conflict) induces abnormalities in sensory perception in various chronic pain populations, and to a lesser extent in pain-free individuals. The aim of this study was to simultaneously investigate sensory and motor disturbances evoked by sensorimotor conflicts, as well as to assess how they are influenced by the presence of acute pain. It was hypothesized that both sensory and motor disturbances would be increased in presence of pain, which would suggest that pain makes body representations less robust. Thirty healthy participants realized cyclic asymmetric movements of flexion-extension with both upper limbs in a robotized system combined to a 2D virtual environment. The virtual environment provided a visual feedback (VF) about movements that was either congruent or incongruent, while the robotized system precisely measured motor performance (characterized by bilateral amplitude asymmetry and medio-lateral drift). Changes in sensory perception were assessed with a questionnaire after each trial. The effect of pain (induced with capsaicin) was compared to three control conditions (no somatosensory stimulation, tactile distraction and proprioceptive masking). Results showed that while both sensory and motor disturbances were induced by sensorimotor conflicts, only sensory disturbances were enhanced during pain condition comparatively to the three control conditions. This increase did not statistically differ across VF conditions (congruent or incongruent). Interestingly however, the types of sensations evoked by the conflict in the presence of pain (changes in intensity of pain or discomfort, changes in temperature or impression of a missing limb) were different than those evoked by the conflict alone (loss of control, peculiarity and the perception of having an extra limb). Finally, results showed no relationship between the amount of motor and sensory disturbances evoked in a given individual. Contrary to what was hypothesized, acute pain does not appear to make people more sensitive to the conflict itself, but rather impacts on the type and amount of sensory disturbances that they experienced in response to that conflict. Moreover, the results suggest that some sensorimotor integration processes remain intact in presence of acute pain, allowing us to maintain adaptive motor behavior.

Keywords: body image, body schema, acute pain, virtual reality, sensorimotor integration

OPEN ACCESS

Edited by:
Christophe Lopez, Centre National de La Recherche Scientifique (CNRS), France

Reviewed by:
Alessandra Sciutti, Fondazione Istituto Italiano di Technologia, Italy
Guilherme Lucas, University of São Paulo, Brazil

***Correspondence:**
Catherine Mercier
catherine.mercier@rea.ulaval.ca

Received: *28 February 2017*
Accepted: *05 July 2017*
Published: *21 July 2017*

Citation:
Brun C, Gagné M, McCabe CS and Mercier C (2017) Sensory Disturbances, but Not Motor Disturbances, Induced by Sensorimotor Conflicts Are Increased in the Presence of Acute Pain. Front. Integr. Neurosci. 11:14. doi: 10.3389/fnint.2017.00014

INTRODUCTION

To maintain accurate movements that are adapted to the outside world, the sensory feedback arising from our actions is systematically compared to our motor intentions (Blakemore et al., 2000; Frith et al., 2000). While this function is critical to detect unexpected perturbations, correct for inadequate planning and support motor learning, Harris (1999) has proposed that a discordance between motor intention and sensory feedback (creating a sensorimotor conflict) may result in the sensation of pain acting as an "error signal". The most obvious example that has been proposed by Harris to illustrate this theory is the case of phantom limb pain, in which the intention to move the phantom limb cannot result in appropriate sensory feedback from the missing body part. However, sensorimotor conflicts can also arise when the limb is still present. For instance, in complex regional pain syndrome a conflict can arise between the intended movement (e.g., completely open the hand) and the limited movement that can actually be performed (McCabe and Blake, 2008). Interestingly, canceling out the discordance between motor intention and visual feedback (VF) by spatially superposing a mirror image of the non-painful limb on the painful limb can alleviate pain in various chronic pain populations (Ramachandran and Rogers-Ramachandran, 1996; McCabe et al., 2003; Mercier and Sirigu, 2009; McCabe, 2011). In contrast, creating an experimental sensorimotor conflict with a mirror can transiently exacerbate painful sensations and other sensory disturbances (as feelings of peculiarity, loss of control, perceived extra limb or loss of limb, changes in weight or temperature) (McCabe et al., 2007; Daenen et al., 2010, 2012). Changes in motor performance have also been observed during exposure to the mirror feedback, but reports have focused more on the sensory consequences of those changes in performance rather than recording a specific trajectory change (McCabe et al., 2005, 2007). For example, participants with and without chronic pain describe a loss of awareness and control of limbs, and the researchers observe altered limb trajectory and poor bilateral alignment of the limbs (McCabe et al., 2005, 2007).

In healthy volunteers, sensorimotor conflicts produced experimentally generate the same type of sensory disturbances (Daenen et al., 2010; Foell et al., 2013; Roussel et al., 2015), but to a lesser extent to what is observed in chronic pain populations (McCabe et al., 2007; Daenen et al., 2010). These conflicts have even been reported to sometimes induce painful sensations (McCabe et al., 2005), although this remains controversial (Foell et al., 2013; Don et al., 2017). Less robust body representations in the presence of pain could contribute to explain this difference in the intensity of the response to sensorimotor conflicts between individuals with chronic pain and healthy individuals, as well as altered sensory perception and motor performance that are often observed in chronic pain populations (Lotze and Moseley, 2007; Nijs et al., 2012).

Indeed various chronic pain states are associated with alterations in sensory perception and body representations, such as an overestimation of the size of the painful limb (Lewis et al., 2007; Peltz et al., 2011; Nishigami et al., 2015), an altered sense of position (Gelecek et al., 2006; Moseley, 2008; Lewis et al., 2010) and movement (Roosink et al., 2015). These alterations in body representations have sometimes been reported to be associated with the severity of motor disturbances observed in chronic pain populations (Bank et al., 2013; Hamacher et al., 2016). In healthy volunteers, the induction of experimental acute pain can also transiently alter body representations, as shown by shifts in the subjective body midline toward the painful side (Bouffard et al., 2013), overestimation of the size of the painful limb (Gandevia and Phegan, 1999) and altered sense of position (Eva-Maj et al., 2013) Finally, patients with chronic pain have altered somatosensory (Flor et al., 1997; Di Pietro et al., 2013) and motor (Lotze et al., 2001; Maihöfner et al., 2007) cortical representations. A recent study has shown that the presence of acute pain enhances the corticospinal excitability changes induced by subsequent transient deafferentation of the hand (Mavromatis et al., 2016). Together, these results support the view that pain might make the body representations more plastic, both at the cortical and perceptual level.

The general objective of this study was to assess sensory and motor disturbances induced by sensorimotor conflicts, and to test whether these disturbances are influenced by the presence of experimental pain. We hypothesized that both sensory and motor disturbances would be increased in presence of pain, which would support the idea that pain makes body representations less robust. To test this hypothesis, participants realized cyclic asymmetric movements of flexion-extension with both upper limbs in a robotized system combined with a 2D virtual environment. The virtual environment allowed the provision of VF about movements that were either congruent or incongruent, while the robotized system allowed precise measurement of motor performance (in addition to subjective perception of the participant), before and during exposure to different types of VF. The effect of experimental pain was compared to three control conditions (no somatosensory stimulation, tactile distraction and proprioceptive masking) to ensure that the effect of pain was not due to a simple distraction or to an impact of pain on the integration of proprioceptive information. Indeed, integration of proprioceptive information has been reported to be altered in the presence of pain. (Lee et al., 2010; Sheeran et al., 2012; Eva-Maj et al., 2013).

A secondary objective was to determine whether the amount of sensory disturbances induced by sensorimotor conflicts was associated with the extent of motor disturbances.

MATERIALS AND METHODS

Participants and Ethics Statement

Thirty healthy caucasian participants (26 right-handed as determined in the Edinburgh Inventory Test (Oldfield, 1971)—15 females—mean ± SD age: 27.7 ± 5.9 years) were recruited from Laval University. None of them had a history of visual, nervous system or musculoskeletal disease that could affect task performance. All participants provided their written informed consent prior to admission to the study. The experiment was performed in accordance with the tenets of the Declaration of Helsinki and the study protocol was approved by the local ethical

review board (Institut de réadaptation en déficience physique de Québec, Canada, n°2015-461).

Study Design

The experiment was conducted on two experimental sessions separated by 6.9 ± 2.7 days (**Figure 1A**). In total, each participant was exposed to 16 experimental conditions (described in details in Section Experimental Conditions) presented in a factorial within-subject design: [*Somatosensory conditions* ("No Stimulation" or "Tactile Distraction" or "Proprioceptive Masking" or "Experimental Pain")] × [*Visual conditions* ("Congruent VF " or "No VF" or "Flipped VF" or "Mirror VF")].

In each of the two sessions, participants realized two blocks of trials, each block corresponding to one of the four somatosensory conditions (No Stimulation, Tactile Distraction, Proprioceptive Masking or Experimental Pain, **Figure 1B**). Each block included 8 trials, i.e., two trials of each of the 4 visual conditions (Congruent VF, No VF, Flipped VF or Mirror VF, see **Figure 2**) presented in a pseudo-random order. Note that given that the effect of experimental pain (induced with capsaicin) does not vanish immediately after the removal of the capsaicin cream, the Experimental Pain condition was systematically the last block in the session. However, the order to the four somatosensory conditions was counterbalanced in such a way that the average rank of all somatosensory conditions was similar. Each participant performed a total of 32 experimental trials (4 Visual conditions X 4 Somatosensory conditions X 2 trials) over the two sessions (i.e., 16 trials by session).

Instrumentation and Experimental Task

The experiment was conducted using the KINARM (BKIN Technologies, Kingston ON, Canada; see **Figure 3A**), a robotized bilateral exoskeleton that allows combined movements of the shoulder (horizontal abduction-adduction) and elbow (flexion-extension) joints in order to move upper limbs (ULs) in the horizontal plane. A 2D virtual environment (47″) created the illusion of two virtual ULs replacing participant's ULs (with appropriate vision of depth), that were always obstructed from view (Dexterit-E software version 3.4.2; **Figure 3B**). These virtual ULs that were driven by participant' ULs in real-time provided the possibility to manipulate the VF given to the participant in a much more flexible manner than the mirror box set-up that is typically used in this type of experiments: we had the possibility to program virtual ULs to move synchronously or asynchronously with the real movement of the participant, or to disappear, giving us an ideal scenario to create varied sensorimotor conflicts while recording the impact of these conflicts on the movement of each UL. Joint angular positions for both the shoulder and elbow were obtained from KINARM motor encoders and sampled at 1 kHz,

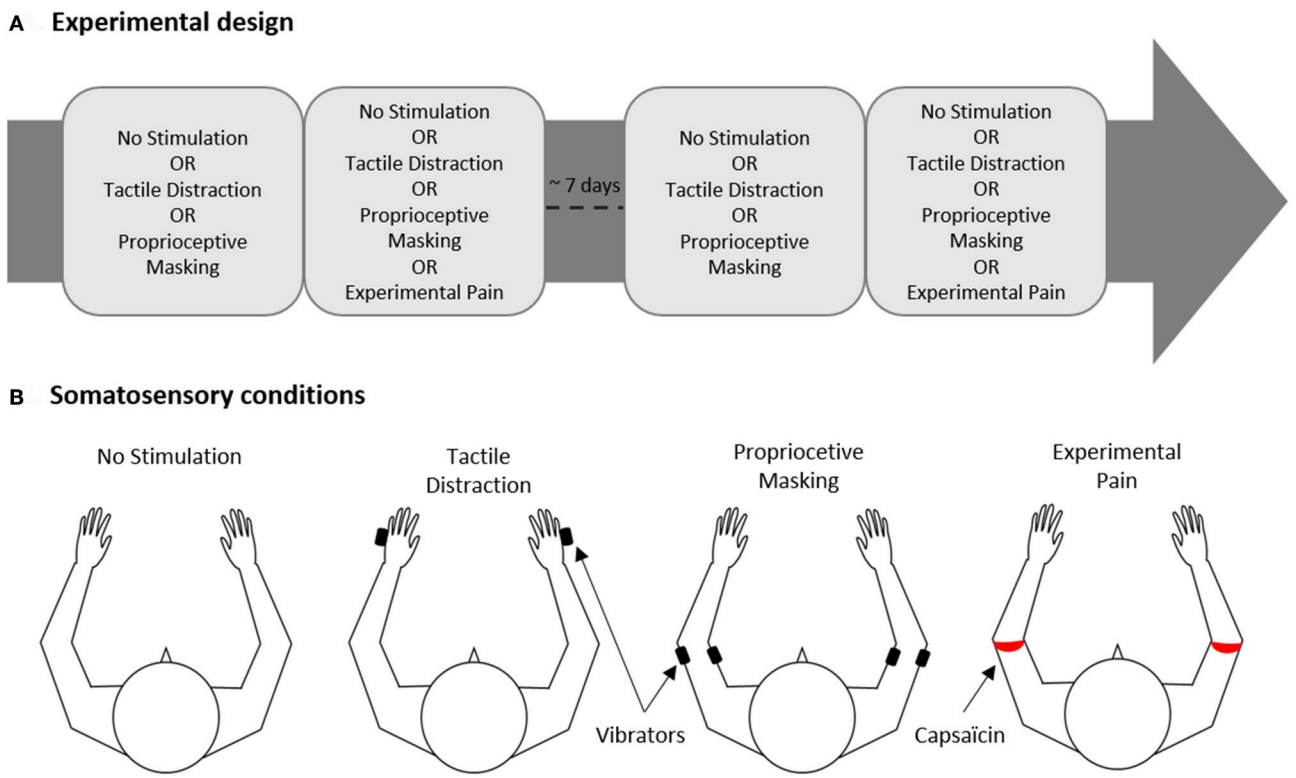

FIGURE 1 | Experimental design. **(A)** The experiment was carried out on two experimental sessions separated by ∼7 days for each participant. Each session comprised two blocks of trials, one block corresponded to one of the four somatosensory conditions. **(B)** Somatosensory conditions. Black and red rectangles indicate the site of application of vibrators or capsaicin cream, respectively.

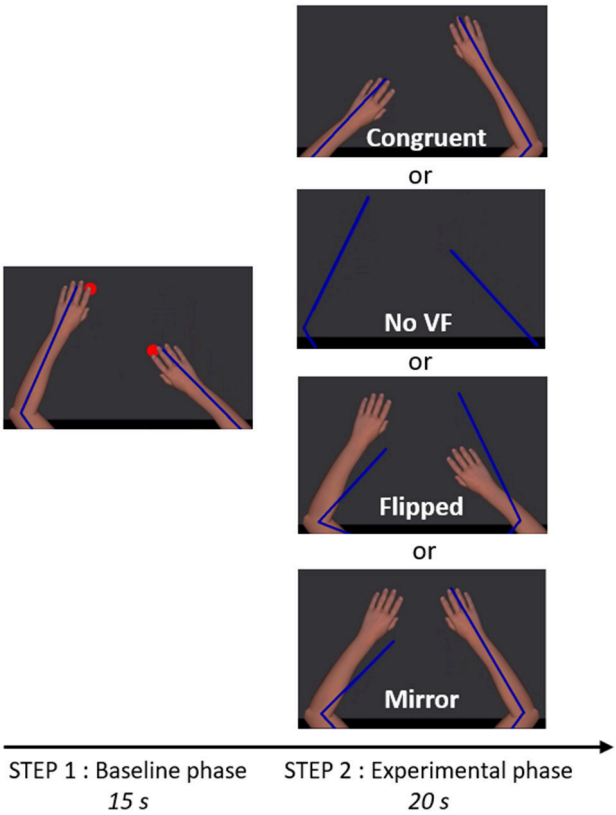

FIGURE 2 | Trial timeline and visual conditions. The participant saw exclusively the virtual upper limbs (Step 1 and 2) as well as the red targets (Step 1). Blue lines depict the real position of the upper limbs. The size and the center of rotation of virtual upper limbs were adjusted to correspond to the real upper limbs of the participant. In Step 1, two red targets were alternating in anti-phase at 1.25 Hz and participants were instructed to reach successively toward the targets, in order to create a bilateral anti-phase movement. In Step 2, the red targets were disappearing and one of the four visual conditions depicted was presented, providing either congruent or incongruent visual feedback (VF) about the limb movement.

and the position of the index was computed in real-time. Data processing was made with Matlab (MathWorks, R2011b).

Each session began with two trials of familiarization with the motor task (35 s each), in which the virtual ULs reproduced faithfully the movement of the participants' ULs (corresponding to Step 1 described below). **Figure 2** illustrates the task that was then used throughout the experiment and comprised two steps. Before each trial, participants had to position their ULs on two green targets (2 cm of diameter) corresponding to an angular position of 85° for the elbows and 40° for the shoulders.

In Step 1 (baseline phase, 15 s), the virtual ULs were always congruent with the position of the real ULs. Two red targets (2 cm diameter) were appearing and alternating in anti-phase at 1.25 Hz. Location of the red targets was 10 cm anterior or posterior to the position of the green targets. Participants were instructed to reach successively toward red targets, in order to create a bilateral anti-phase movement (i.e., when one UL was in its peak of flexion, the other was in its peak of extension, with an endpoint movement amplitude of 20 cm in the antero-posterior axis for each UL). Participants were instructed to execute a fluid movement, without stopping on the red targets. To help participants to follow the rhythm, a metronome beat the time every 800 ms. Red targets were only present during this step, in order to help the participant to achieve the expected movement amplitude, but the metronome beat was maintained until the end of Step 2 to help keeping the rhythm. After the baseline phase (Step 1) and just before the experimental phase (Step 2), the red targets and the virtual ULs were disappearing for 0.8 s, while the metronome was still beating.

In Step 2 (experimental phase, 20 s), one of the four visual conditions (Congruent VF, No VF, Flipped VF, or Mirror VF) was presented. Except in the No VF condition, in which the screen remained completely black, participants were seeing their virtual ULs (although the position/movement was not necessarily congruent with their movements). Participants were instructed to continue to do the same movement and to always look at both virtual ULs, even if the visual condition was troubling (see Supplementary Material for a video of an experimental trial).

At the end of each trial, participants had to respond to questions about their sensations and perceptions in their ULs during the experimental phase.

Experimental Conditions

Visual Conditions (Present Only in Step 2)

Four visual conditions were studied (**Figure 2**), one control condition (Congruent VF) and three sensorimotor conflict conditions (No VF, Flipped VF and Mirror VF):

(1) *Congruent VF*: the virtual UL reproduced faithfully the movements of the participant;
(2) *No VF*: participants were watching a black screen (with eyes open);
(3) *Flipped VF*: the left virtual UL reproduced the movement of the right UL and the right virtual arm reproduced the movement of the left UL;
(4) *Mirror VF*: both virtual ULs reproduced the movement of the non-dominant UL.

Somatosensory Conditions (Present through Both Step 1 and Step 2)

Four somatosensory conditions were studied (**Figure 1B**):

(1) *No stimulation*: no somatosensory stimulation applied to the ULs;
(2) *Tactile Distraction*: a 40-Hz vibration was applied on each hand (5th metacarpal; irrelevant to the task performed) to control for attentional effects related to the application of somatosensory stimuli to ULs;
(3) *Proprioceptive Masking* was achieved by co-vibrating the biceps and triceps of both ULs at 40 Hz. Vibration preferentially activates muscle spindle endings (Roll and Vedel, 1982). When the vibration is applied to a single muscle, illusory movements or a reflexive contraction can be elicited (Calvin-Figuière et al., 1999). However, when the vibration is applied equally to agonist-antagonist muscles these effects are canceled out and the co-vibration

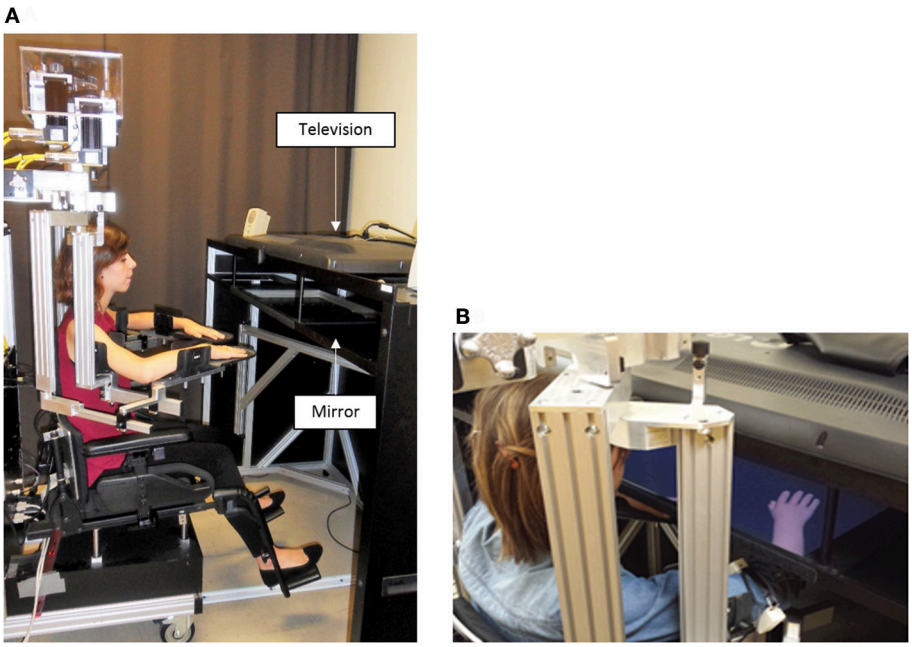

FIGURE 3 | Experimental set up. Exoskeleton robot **(A)** and 2D virtual environment **(B)** are the 2 elements of the KINARM. The exoskeleton is fitted to the anthropometric characteristics of the participant. The virtual environment consists in the projection of virtual upper limbs on a semi-transparent mirror (47″) thanks to a television. Upper limbs rest on the exoskeleton under the semi-transparent mirror and are obstructed from the participant' view.

method degrades proprioceptive responsiveness (Bock et al., 2007). Although the preferential frequency used is 80 Hz (Bock et al., 2007), 40 Hz is sufficient to degrade proprioception (Cordo et al., 1995; Chancel et al., 2016) without inducing discomfort (to maintain a clear distinction with the Experimental Pain condition). When vibrators were installed, biceps and triceps were first stimulated separately to evoke an illusory movement of extension and flexion, and then we ensured that co-vibration canceled out these illusory movements. All participants except one reported illusory movements when the biceps or triceps were stimulated separately, and this illusion was always canceled out during co-vibration;

(4) *Experimental Pain* was induced with a single topical application of 1% capsaicin cream. A thin layer (∼1 mm) of cream forming a 1 cm ring was applied around the upper arm, just proximal to the elbow, on both ULs. This location was selected because elbow joints were the most directly involved in the motor task performed by the subject, and that location was visible on the virtual ULs. Moreover, the fact that capsaicin was applied all around the arm creates a penetrating and irradiating burning sensation, which aimed to reproduce neuropathic pain. When the capsaicin cream was applied, participants were required to verbally rate their pain intensity using a numeric pain rating scale (NPRS) ranging from 0 (no pain) to 10 (the worst pain imaginable). Experimental block began when the pain reached an intensity of 5/10 for both ULs, or when the pain reached a plateau (average of 18 ± 4 min). The average of pain intensity reported at the beginning of the experimental block was 5.4 ± 1.6 for the left arm, 5.3 ± 1.6 for the right arm, and did not differ between both ULs ($p = 0.96$).

Measures and Data Analysis

Each outcome was expressed as a change from the baseline phase in order to cancel out any direct effect that the somatosensory condition could have had on the movement or the perception of the limb.

Sensory Disturbances

After each trial, participants had to verbally answer to nine yes-no questions: *"In the last trial, when the red targets were not present, did you feel any change or the appearance of...?"* (i.e., dichotomic choice without intensity rating, but with the possibility to add comments). Questions were targeting perceptions of pain, discomfort, losing a limb, temperature change, weight change, having an extra limb, losing control, peculiarity or any other sensations. Participants had to report any changes from the baseline phase, meaning for example that in the Experimental Pain condition, participants were instructed to answer no to the question about pain if the pain level was similar between the baseline period and the experimental condition. This questionnaire is based on previous studies assessing the impact of sensorimotor conflict on sensory disturbances in healthy volunteers (McCabe et al., 2005; Foell et al., 2013) and in chronic pain populations (McCabe et al., 2007) using open questions. The descriptors obtained through open questions in these studies

were used to produce yes-no question for the present study, allowing quantification of the changes induced in the sensations across conditions. However, the last question (to report any other changes) allowed participants to report changes that were not covered by the questionnaire. A total score for the nine items was computed, corresponding to the mean percentage of sensory disturbances. For one experimental condition, a score of 0% indicated that the participant experienced no sensory disturbances for the nine items on the two trials. A score of 100% indicated that the participant experienced sensory disturbances on every item in both trials.

Motor Performance

Two main outcomes were used to assess motor performance, both based on the position of the endpoint (index finger):

(1) *Amplitude asymmetry* between both upper limbs: y-coordinates for both indexes were encoded for each peak of flexion and extension. For each movement half-cycle, the amplitude on the y-axis was extracted for each UL, and then the absolute difference between both ULs was calculated (see **Figure 6** for an example).
(2) *Medio-lateral drift*: for each movement half-cycle, the x-coordinate of the maximal deviant point was extracted. The difference between the highest (i.e., most lateral point) and the lowest (i.e., most medial point) values was then calculated to obtain the range of the medio-lateral drift. Values of both ULs were pooled because they did not differ ($p = 0.19$) (see **Figure 6** for an example).

The motor performance for both outcomes in the Baseline phase are presented in Supplementary Figure 1. Both motor outcomes were expressed as a change from the baseline phase in order to cancel out effects of the somatosensory condition, as we were not interested in the effect of vibration or pain on motor control *per se*, but rather on alteration in motor performance induced by the conflict. Such normalization was needed as there was a small, but significant, effect of somatosensory condition on the amplitude asymmetry ($p < 0.01$), less asymmetry being observed in Tactile Distraction condition compared to the three others ($p < 0.05$). No effect of somatosensory condition was observed for medio-lateral drift ($p = 0.20$). Change from baseline was calculated by subtracting the performance during the last 10 s of the baseline phase from the performance during experimental phase. A positive value indicates a degradation of motor performance (i.e., more interlimb amplitude asymmetry or more medio-lateral drift) and a negative value an improvement.

Statistics

Sensory disturbances and the two motor outcomes were analyzed using 4 × 4 repeated-measures analyses of variance (rmANOVA). *Post-hoc* tests were performed using Tuckey's correction for multiple comparisons. Statistical significance was set at $p < 0.05$. *P*-values were Huynh–Feldt corrected for sphericity when necessary. Mean ± standard deviation are reported in the results. Statistical analysis was performed with R software (version 3.1.2).

To answer the secondary objective of the study—to determine whether the sensory disturbances induced by sensorimotor conflicts were associated with motor disturbances—participants were arbitrarily split into two equal groups ($n = 15$/group), that were named the Minimal and the High disturbances group (see **Figure 7A**). The three sensorimotor conflict conditions were pooled together to classify participants according to their sensitivity to conflicts during No Stimulation and Experimental Pain conditions. Then, the effect of Group on motor outcomes was tested with *t*-test.

RESULTS

Sensory Disturbances

The rmANOVA revealed a strong main effect of vision ($p < 0.0001$, $\eta_p = 0.42$). As it can be seen on **Figure 4**, participants reported more sensory disturbances in conditions of sensorimotor conflicts (Flipped $VF = 15 \pm 14\%$, Mirror $VF = 15 \pm 16\%$, No $VF = 9 \pm 13\%$) than in Congruent VF ($3 \pm 5\%$, $p < 0.05$). Flipped and Mirror VF did not differ from each other ($p = 0.99$), but both induced more sensory disturbances than No VF condition ($p < 0.05$). Furthermore, a main effect of somatosensory condition was observed ($p < 0.001$, $\eta_p = 0.24$). Experimental Pain ($15 \pm 16\%$) induced more sensory disturbances than Proprioceptive Masking ($8 \pm 11\%$, $p < 0.001$), Tactile Distraction ($10 \pm 11\%$, $p < 0.001$) and No Stimulation ($9 \pm 11\%$, $p < 0.001$) conditions. Proprioceptive Masking, Tactile Distraction and No Stimulation conditions did not differ from each other ($p > 0.75$). Finally, no significant interaction was observed between somatosensory and visual conditions ($p = 0.60$).

As Proprioceptive Masking and Tactile distraction conditions did not differ from the No Stimulation condition, further comparisons focused solely on the differences between Experimental Pain and No Stimulation conditions. **Figure 5** displays the number of individuals who reported each specific type of disturbance in each visual condition. Note that no statistical analyses were undertaken due to the large variability

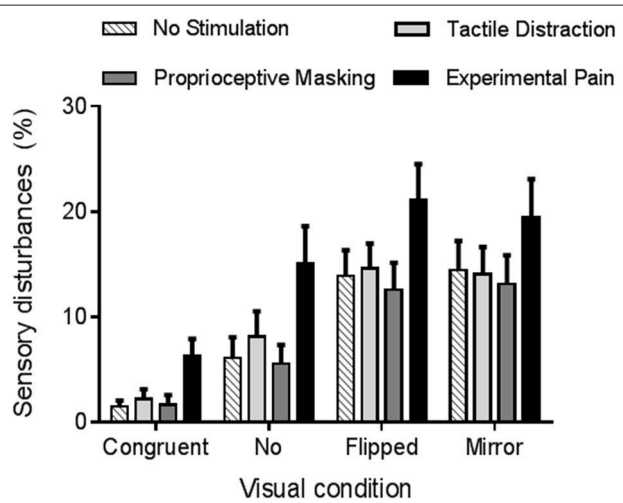

FIGURE 4 | Average amount of sensory disturbances reported in each experimental condition. Error bars represent the standard error of the mean.

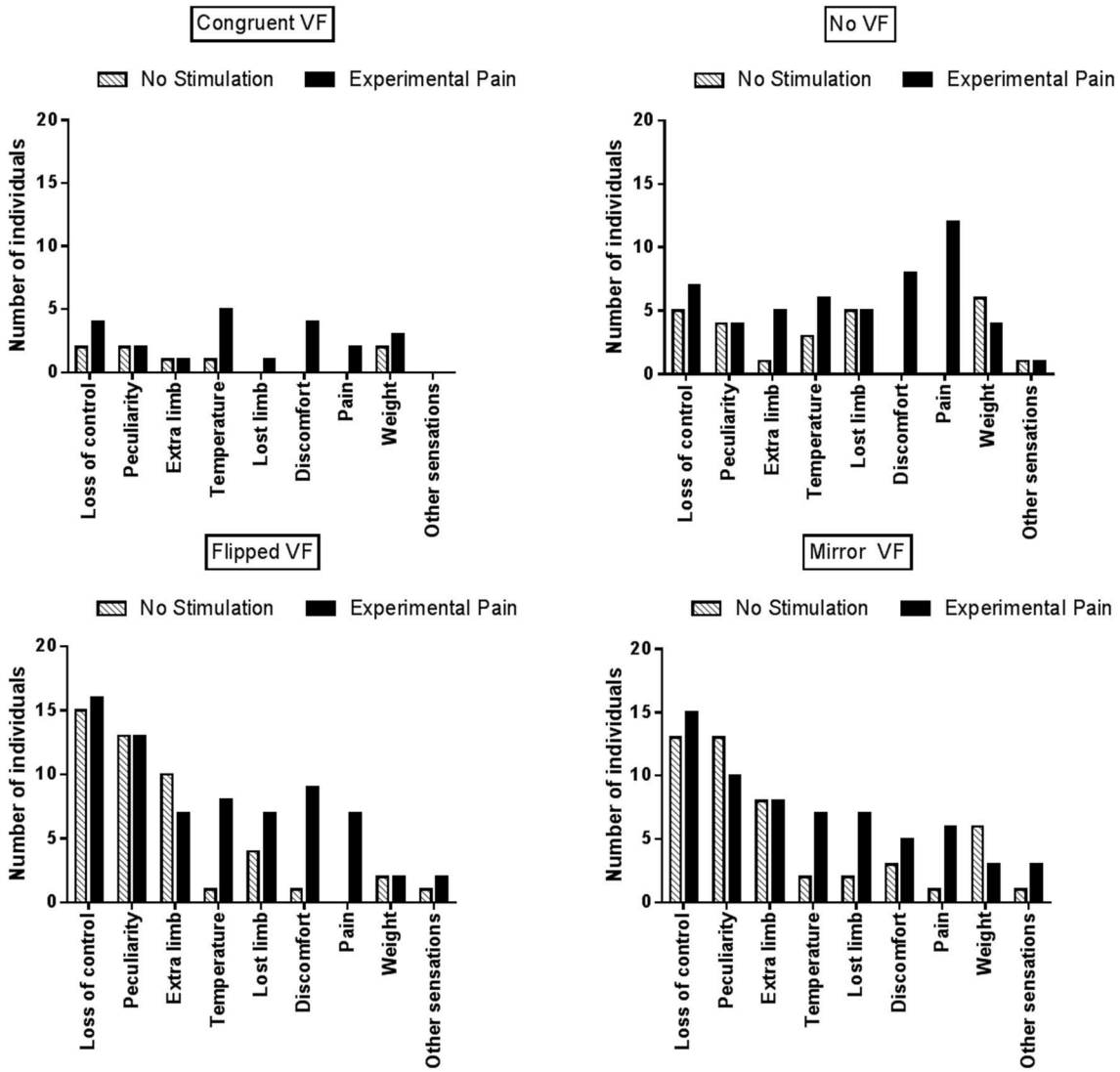

FIGURE 5 | Number of individuals who reported at least one disturbance for a given item, reported as a function of the experimental condition.

across items and the fact that the proportion of participants reporting a given item was often low: these results should therefore be considered as exploratory. During sensorimotor conflicts (No VF, Flipped VF, and Mirror VF), participants reported mainly a sensation of loss of control, peculiarity and the perception of having an extra limb. However, the occurrence of these three items was not influenced by the presence of Experimental Pain. It was rather the disturbances related to changes in intensity of pain or discomfort, changes in temperature (hotter or colder, depending on the participant) or the impression of a missing limb that appeared to differ between Experimental Pain and No Stimulation condition. Such effects were observed in the three conditions of sensorimotor conflict. Importantly very few participants reported disturbances related to changes in intensity of pain in the Congruent VF condition performed in the presence of Experimental Pain, which shows that the participants understood well that they were expected to report only pain increases, and not pain sensations *per se* (which were obviously present in all Experimental Pain trials). The other disturbances experienced by participants during sensorimotor conflicts were nausea, dizziness and numbness in the hand. Finally, when Experimental Pain was applied five participants reported the perception of an extra limb like "having a phantom hand" in the No VF condition.

Motor Performance

Figure 6A provides an example of motor disturbances induced by sensorimotor conflicts in the absence of somatosensory stimulation for two representative participants. Visual inspection of the data shows that motor disturbances are observed both in the antero-posterior and in the medio-lateral axis, and illustrates

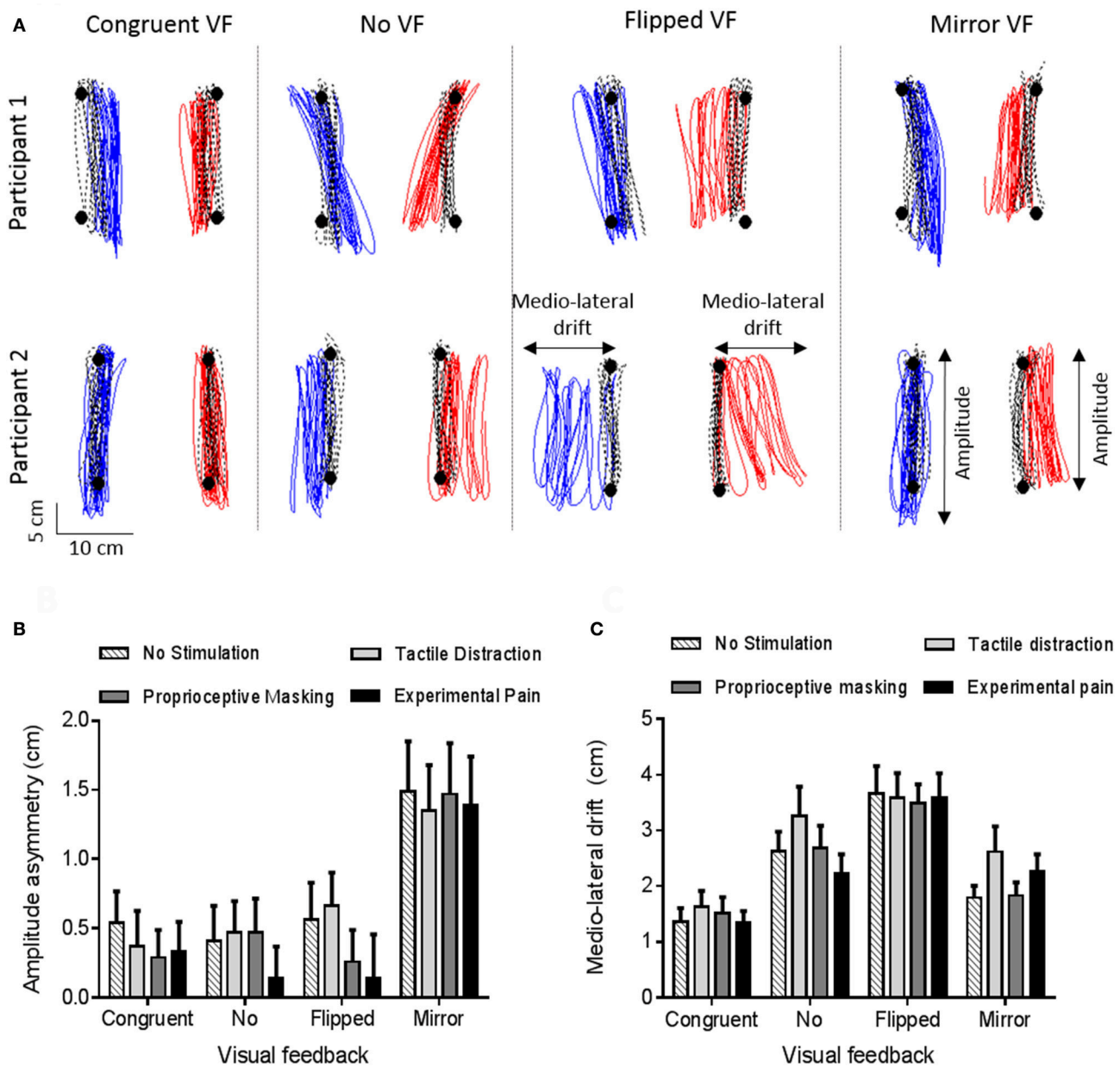

FIGURE 6 | Motor disturbances. **(A)** Individual data for two representative participants, in absence of somatosensory stimulation. Black circles and black dashed lines represent, respectively, targets and trajectory of ULs during the baseline phase (Step 1). Blue and red lines represent, respectively, the trajectory of the left and right ULs during the experimental phase (Congruent VF, No VF, Flipped VF or Mirror VF—Step 2). **(B,C)** Amplitude asymmetry between left and right ULs **(B)** and medio-lateral drift **(C)**. A positive value indicates a degradation of motor performance relative to baseline. Error bars represent the standard error of the mean.

how the two motor outcome variables (Amplitude asymmetry and Medio-lateral drift) capture these disturbances. Moreover, we can see that motor disturbances differ according to the visual condition, and that some variability is present across participants. Finally, motor disturbances in the Congruent VF comparatively to the Baseline phase are observed and are explained by the fact that the red targets were disappearing during the Experimental phase (in order to avoid visual cues about errors in the conflict conditions).

Amplitude Asymmetry

A significant main effect of vision ($p < 0.0001$, $\eta_p = 0.29$) was observed. As shown on **Figure 6B**, the asymmetry was larger in the Mirror VF condition (1.4 ± 1.9) than in the Congruent VF (0.4 ± 1.2, $p < 0.0001$), No VF (0.4 ± 1.3, $p < 0.0001$) and Flipped VF (0.4 ± 1.5, $p < 0.0001$) conditions. In Mirror VF, the dominant UL (for which incongruent VF was provided) did smaller movements than the non-dominant UL (for which congruent VF was provided). Congruent VF, No VF and Flipped

VF conditions were not statistically different ($p > 0.99$). The somatosensory condition had no significant effect on Amplitude asymmetry ($p = 0.54$) and no significant interaction was observed between the somatosensory and the visual conditions ($p = 0.93$).

Medio-Lateral Drift

The ANOVA revealed a main effect of vision ($p < 0.0001$, $\eta_p = 0.36$). As shown on **Figure 6C**, participants drifted more in Flipped VF (3.6 ± 2.4 cm) than in the three other conditions ($p < 0.05$). Moreover, Mirror VF (2.1 ± 1.7 cm) and No VF (2.7 ± 2.2 cm) did not differ statistically from each other ($p = 0.26$), but only No VF differed statistically from Congruent VF (1.5 ± 1.4 cm, $p < 0.05$). However, there were no significant main effect of somatosensory conditions ($p = 0.20$) and no significant interaction between visual and somatosensory conditions ($p = 0.31$).

Perception and Motor Performance

Figure 7A shows the variability in the amount of sensory disturbances experienced across participants in condition of sensorimotor conflicts during No Stimulation somatosensory condition, ranging from 0% (no disturbances at all in the three sensorimotor conflict conditions) to 42.6%. Based on this average score of sensory disturbances, participants were arbitrarily split in to two equal groups to explore factors related to the sensitivity to sensorimotor conflicts as assessed by sensory disturbances. No difference was observed between the Minimal and the High disturbances group in terms of gender and age ($p = 0.96$). To explore whether groups also differed on the amount of motor disturbances, they were compared on the motor outcome that was the most sensitive to each type of conflict, i.e., the medio-lateral drift for No VF (**Figure 7B**) and Flipped VF (**Figure 7C**) conditions and amplitude asymmetry for the Mirror VF (**Figure 7D**). No significant difference was observed on motor performance between the Minimal and the High disturbances groups for any of the sensorimotor conflict in the No stimulation condition (**Figure 7**). The same result was observed for the Experimental Pain condition, (all $p > 0.32$; Supplementary Figure 2). Importantly, the intensity of pain reported by both groups following the application of capsaicin was similar ($p = 0.84$).

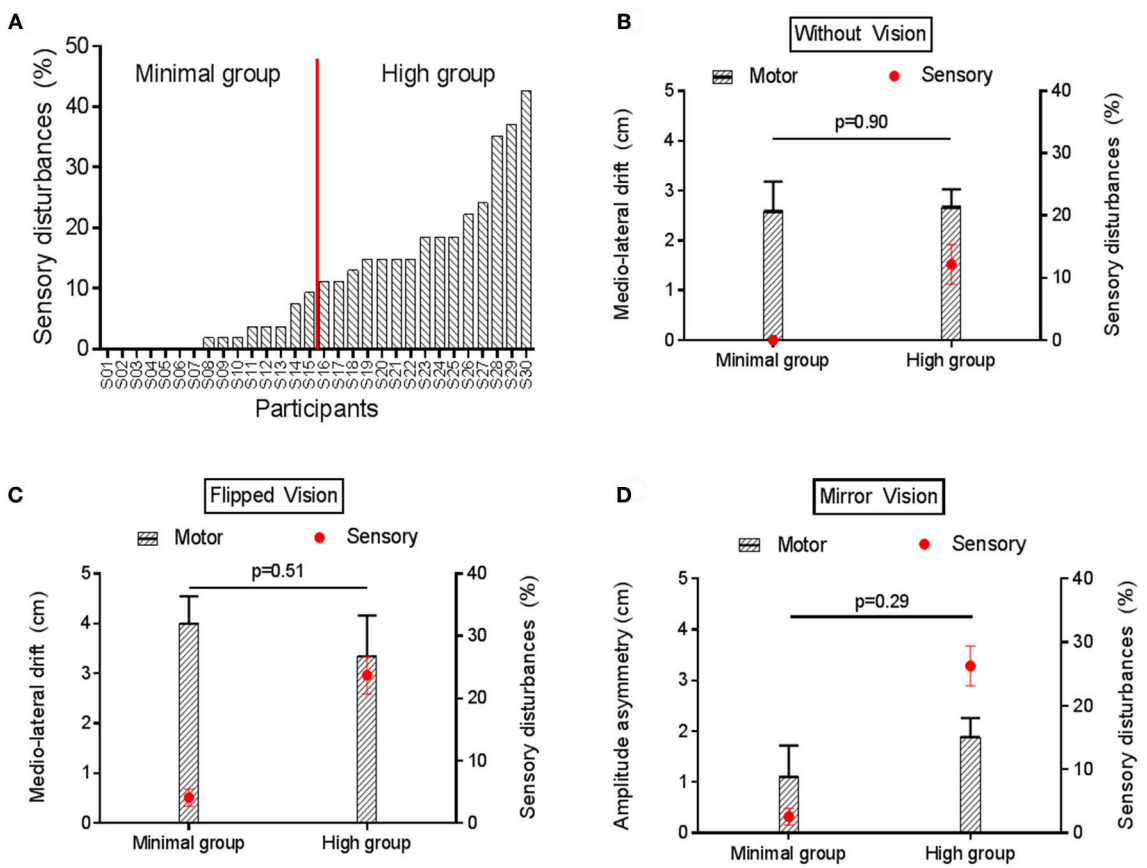

FIGURE 7 | Motor and sensory disturbances induced by sensorimotor conflict in the No Stimulation condition. **(A)** represents the amount of sensory disturbances across participants for the three sensorimotor conflict conditions during No Stimulation condition. **(B,C)** compares the average medio-lateral drift (black bars) and amount of sensory disturbances (red circles) between groups with Minimal vs. High sensory disturbances, in the No VF and Flipped VF conditions, respectively. **(D)** compares the average amplitude asymmetry (black bars) and amount of sensory disturbances (red circles) between groups with Minimal vs. High sensory disturbances in the Mirror VF condition. Error bars represent the standard error of the mean. *P*-values are reported only for motor disturbances (as groups were formed based on amount of sensory disturbances).

DISCUSSION

While previous studies on sensorimotor conflicts have focused only on evoked sensory disturbances in pain-free individuals and chronic pain patients, the two main original contributions of the present study were to investigate simultaneously sensory and motor disturbances evoked by such conflict, as well as to assess how they are influenced by the presence of acute pain. Results of the present study show that looking at virtual ULs which provide VF about movement that is incongruent with our actual movement induces sensory and motor disturbances in healthy participants. Contrary to what we hypothesized—that both motor and sensory disturbances would increase in the presence of pain—only sensory disturbances were enhanced during the experimental pain condition comparatively to the three control conditions (no stimulation, tactile distraction or proprioceptive masking). Moreover, this increase did not depend on the VF condition (congruent or incongruent). Finally, results show that motor and sensory disturbances induced by sensorimotor conflicts are not related with each other.

Sensory disturbances reported by the participants, involving mainly perceptions of loss of control, of peculiarity or of having an extra limb, are consistent with previous studies in which sensorimotor conflicts were induced with a mirror (McCabe et al., 2005; Daenen et al., 2010; Foell et al., 2013; Roussel et al., 2015). Sensory disturbances were also reported during the Congruent VF, but significantly less than in condition of sensorimotor conflicts. This could be explained by the fact that although virtual ULs were realistic in shape and adjusted to the arm's length of each participant, the match with the real arms was never perfect, thus creating a minor sensorimotor conflict. Moreover, our results showed that even in the absence of VF (i.e., when virtual ULs, present during Step 1, were suddenly disappearing during Step 2) participants reported more sensory disturbances than in the Congruent VF condition, but to a lesser extent than Flipped and Mirror VF. In line with this result, individuals with fibromyalgia report increased sensory disturbances when they close their eyes, including the perception of an extra limb. The induction of sensory disturbances by sensorimotor conflicts is a large and robust effect: 42% of the variance in sensory disturbances was explained by the visual condition in our study, and similar effects have been reproduced several times both in healthy participants (McCabe et al., 2005; Daenen et al., 2010; Foell et al., 2013; Roussel et al., 2015) and in chronic pain populations (McCabe et al., 2007; Daenen et al., 2010, 2012). It supports the idea that sensory disturbances might be acting as a warning signal when a discordance occurs between our motor intentions and the sensory feedback of the action. It has been suggested that a sensorimotor conflict can be sufficient to trigger painful sensations in healthy subjects (Harris, 1999; McCabe et al., 2005, 2009), but this remains controversial (Don et al., 2017). In our study, only one participant out of thirty reported painful sensations in the No Stimulation condition, supporting the idea that painful sensations can sometimes be elicited with sensorimotor conflicts in healthy individuals (McCabe et al., 2005), but that this is the exception rather than the rule.

The presence of acute pain, but not of other sensory manipulations, was found to enhance sensory disturbances in all visual conditions, including conditions of sensorimotor conflicts, consistent with the fact that chronic pain populations report more sensory disturbances than pain-free individuals (McCabe et al., 2007; Daenen et al., 2012). However, no statistically significant interaction between visual and somatosensory conditions was observed, which question whether this effect was specific to the situation of sensorimotor incongruence. An aspect that makes quantitative comparisons between conditions difficult in this type of study is the fact that although a large proportion of individuals report abnormal sensations in response to conflict, different types of disturbances are experienced and simply counting the number of sensations reported is certainly an imperfect approach. It is possible that some types of sensations (e.g., discomfort, pain, lost limb) reflect a higher degree of disturbance than others (e.g., change in weight or temperature). Interestingly, items that were the most sensitive to sensorimotor conflicts in the absence of pain (loss of control, feelings of peculiarity, perception to having an extra-limb) were not increased in the presence of experimental pain. New types of sensations (changes in intensity of pain or discomfort, changes in temperature or the impression of a missing limb) were rather appearing, mainly in the three conditions of conflict. This suggests that, contrary to our initial hypothesis, pain does not make individuals generally more sensitive to sensorimotor conflicts. Based on this hypothesis, we would have expected to see an increase in the frequency of reports of the type of sensations that were typically evoked by the conflicts in the absence of experimental pain. Our results rather suggest that while pain does not make people more sensitive to the conflict itself, it impacts on the type and amount of sensory disturbances that they experienced in response to that conflict. This idea is supported by a recent study comparing EEG cortical sources in healthy subjects under conditions of sensorimotor congruence or incongruence, while taking into account the amount of discomfort generated during sensorimotor incongruence (Nishigami et al., 2014). Interestingly, they reported that sensorimotor incongruence was associated with increased activation in the right posterior parietal cortex, irrespective of whether discomfort was experienced or not. However, individuals who were highly sensitive to discomfort exhibited more activation in two pain-related areas: anterior cingulate cortex and posterior cingulate cortex. In light of these results, we could hypothesize that in the presence of acute pain, the effect of the sensorimotor conflict on posterior parietal cortex activity would not be modified (i.e., no change in the sensitivity to conflict *per se*) but that the activity in pain-related areas would be increased, resulting in a different (and larger) set of sensory symptoms.

In contrast with our observations in acute pain, comparison between individuals with fibromyalgia and healthy controls suggests that chronic pain results in an increase in the frequency of reports of the disturbances that are typically evoked by sensorimotor conflict, in addition to sensory disturbances that appear to be more pain-specific (McCabe et al., 2007). This might indicate that chronic pain, but not acute pain, make individuals

more sensitive to sensorimotor conflicts. This difference between acute and chronic pain could be explained by the fact that parietal dysfunctions has been reported in individual with chronic pain (Cohen et al., 2013; Kim et al., 2015), and that sensorimotor incongruence is associated with increased parietal activations (Nishigami et al., 2014).

Results on motor disturbances evoked by the sensorimotor conflicts also contradict the hypothesis that acute pain makes individuals generally more sensitive to sensorimotor conflicts. If it was the case, we would expect to see an impact of pain on both sensory and motor disturbances, while no effect of pain on motor disturbances was observed. This, and the observation that the amount of sensory disturbances perceived is not indicative of the amount of motor disturbances exhibited suggest that sensory and motor disturbances depend on different mechanisms. These results indirectly support the multiple body representations model, which dissociates the body schema governing the motor action, and the body image underlying the perceptual judgment. This theory was built according the Perception-Action model (Haffenden and Goodale, 1998) which suggests a dissociation between the "where"—*ventral pathway*—and the "what"—*dorsal pathway*. Although this theory of multiple body representations originally explained pathological cases like deafferentation or neglect syndrome (Paillard, 1999; De Vignemont, 2010), it had been shown that such dissociation also exists in healthy volunteers (Kammers et al., 2009). In light of that theory, our results would be interpreted as indicating that acute pain alters body image (perceptual judgment), but without impacting on body schema. This suggests that some sensorimotor integration processes remain intact in the presence of pain which allows us to maintain adaptive motor behavior, a view supported by two recent studies showing that acute pain does not interfere with sensorimotor integration as measured by short afferent inhibition paradigm (Burns et al., 2016; Mercier et al., 2016). However, it is possible that pain of a longer duration is needed to impact on body schema, given that movement disorders become more prevalent in complex regional pain syndrome as the disease progresses (Van Hilten, 2010).

Some limitations of the present study need to be highlighted. First, it is surprising that no effect of co-vibration was observed on motor performance, questioning whether proprioceptive masking was effectively achieved. Although the preferential frequency used for co-vibration is 80 Hz (Bock et al., 2007), we used a 40 Hz frequency to avoid inducing discomfort (to maintain that condition independent of the Experimental Pain condition). However, the lack of effect of bilateral co-vibration on motor performance does not necessarily indicate that proprioception was not degraded, as previous studies showing a degradation of bimanual coordination used co-vibration on only one UL, therefore creating an asymmetry on the proprioceptive feedback from both sides (Swinnen et al., 2003; Metral et al., 2014; Brun and Guerraz, 2015). Second, for the sensory perception questionnaire performing statistical analyses for each item was considered inappropriate in view of the large inter-subject variability, therefore these results should be interpreted cautiously. For future studies, using a scale that allows the assessment of the intensity of the disturbances (e.g., a Likert scale) rather than a binary answer (yes-no question) might provide more sensitivity. Another interesting approach would be to measure objectively the sensory disturbances induced by sensorimotor conflict, e.g., change in skin temperature (Moseley et al., 2013). Third, although all participants exhibited motor disturbances in presence of sensorimotor conflicts, the exact manner in which the movement disorganized was quite variable from one subject to another. Although we have been able to successfully identify motor outcomes that were sensitive to the visual condition, it is possible that these variables were not the most sensitive to the effect of pain. The use of a simpler motor task, for example a unilateral task (which is not possible to do with a mirror but could be achieved with virtual reality) or of a single-joint bilateral task, might allow to decrease inter-subject variability and therefore increase the sensitivity of the measure for future studies. Finally, tonic pain was used in order to mimic a neuropathic pain condition, as sensory disturbances are predominantly reported in populations with neuropathic pain. Using a phasic pain model, in which the occurrence of pain would be related to a specific movement of the participant, could have more impact on the motor disturbances.

In conclusion, acute pain does not appear to make people more sensitive to sensorimotor conflict itself, but rather impacts on the type and amount of sensory disturbances that they experience in response to that conflict. However, it needs to be kept in mind that the impact of acute pain on body representation might differ from that of chronic pain. Moreover, results showed no relationship between the amount of motor and sensory disturbances evoked in a given individual. This suggests that some sensorimotor integration processes remain intact in the presence of acute pain, allowing us to maintain adaptive motor behavior even though limb perception is altered.

AUTHOR CONTRIBUTIONS

CM, CSM, and CB designed the study; CB and MG performed data collection; CB, MG, CSM, and CM analyzed and interpreted the data; CB and CM drafted the paper, CSM and MG commented on the paper and approved the final version.

ACKNOWLEDGMENTS

We thank Nicolas Robitaille, eng. Ph.D., and Steve Forest for their help in the development of the task and technical support. This study was supported by a Discovery grant from Natural Sciences and Engineering Research Council of Canada (NSERC, grant number: RGPIN 355896-2012). CB was supported by fellowships from Centre interdisciplinaire de recherche en réadaptation et en intégration sociale (CIRRIS), from Centre thématique de recherche en neurosciences (CTRN) and from the Faculté de médecine de l'Université Laval. CM is supported by a salary award from Fonds de recherche Québec-Santé (FRQS, grant number: 29251).

SUPPLEMENTARY MATERIAL

The Supplementary Material for this article can be found online at: http://journal.frontiersin.org/article/10.3389/fnint.2017.00014/full#supplementary-material

REFERENCES

Bank, P. J., Peper, C. L. E., Marinus, J., Beek, P. J., and van Hilten, J. J. (2013). Motor dysfunction of complex regional pain syndrome is related to impaired central processing of proprioceptive information. *J. Pain* 14, 1460–1474. doi: 10.1016/j.jpain.2013.07.009

Blakemore, S. J., Wolpert, D., and Frith, C. (2000). Why can't you tickle yourself?. *Neuroreport* 11, R11–R16. doi: 10.1097/00001756-200008030-00002

Bock, O., Pipereit, K., and Mierau, A. (2007). A method to reversibly degrade proprioceptive feedback in research on human motor control. *J. Neurosci. Methods* 160, 246–250. doi: 10.1016/j.jneumeth.2006.09.010

Bouffard, J., Gagné, M., and Mercier, C. (2013). Effect of painful and non-painful sensorimotor manipulations on subjective body midline. *Front. Hum. Neurosci.* 7:77. doi: 10.3389/fnhum.2013.00077

Brun, C., and Guerraz, M. (2015). Anchoring the "floating arm": use of proprioceptive and mirror visual feedback from one arm to control involuntary displacement of the other arm. *Neuroscience* 310, 268–278. doi: 10.1016/j.neuroscience.2015.09.052

Burns, E., Chipchase, L. S., and Schabrun, S. M. (2016). Primary sensory and motor cortex function in response to acute muscle pain: a systematic review and meta-analysis. *Eur. J. Pain* 20, 1203–1213. doi: 10.1002/ejp.859

Calvin-Figuière, S., Romaiguère, P., Gilhodes, J. C., and Roll, J. P. (1999). Antagonist motor responses correlate with kinesthetic illusions induced by tendon vibration. *Exp. Brain Res.* 124, 342–350. doi: 10.1007/s0022100 50631

Chancel, M., Brun, C., Kavounoudias, A., and Guerraz, M. (2016). The kinaesthetic mirror illusion: how much does the mirror matter? *Exp. Brain Res.* 234, 1459–1468. doi: 10.1007/s00221-015-4549-5

Cohen, H., McCabe, C., Harris, N., Hall, J., Lewis, J., and Blake, D. R. (2013). Clinical evidence of parietal cortex dysfunction and correlation with extent of allodynia in CRPS type 1. *Eur. J. Pain* 17, 527–538. doi: 10.1002/j.1532-2149.2012.00213.x

Cordo, P., Gurfinkel, V. S., Bevan, L., and Kerr, G. K. (1995). Proprioceptive consequences of tendon vibration during movement. *J. Neurophysiol.* 74, 1675–1688.

Daenen, L., Nijs, J., Roussel, N., Wouters, K., Van Loo, M., and Cras, P. (2012). Sensorimotor incongruence exacerbates symptoms in patients with chronic whiplash associated disorders: an experimental study. *Rheumatology* 51, 1492–1499. doi: 10.1093/rheumatology/kes050

Daenen, L., Roussel, N., Cras, P., and Nijs, J. (2010). Sensorimotor incongruence triggers sensory disturbances in professional violinists: an experimental study. *Rheumatology* 49, 1281–1289. doi: 10.1093/rheumatology/keq067

De Vignemont, F. (2010). Body schema and body image—Pros and cons. *Neuropsychologia* 48, 669–680. doi: 10.1016/j.neuropsychologia.2009.09.022

Di Pietro, F., McAuley, J. H., Parkitny, L., Lotze, M., Wand, B. M., Moseley, G. L., et al. (2013). Primary somatosensory cortex function in complex regional pain syndrome: a systematic review and meta-analysis. *J. Pain* 14, 1001–1018. doi: 10.1016/j.jpain.2013.04.001

Don, S., Voogt, L., Meeus, M., De Kooning, M., and Nijs, J. (2017). Sensorimotor incongruence in people with musculoskeletal pain: a systematic review. *Pain Practice* 17, 115–128. doi: 10.1111/papr.12456

Eva-Maj, M., Hans, W., Per-Anders, F., Mikael, K., and Måns, M. (2013). Experimentally induced deep cervical muscle pain distorts head on trunk orientation. *Eur. J. Appl. Physiol.* 113, 2487–2499. doi: 10.1007/s00421-013-2683-y

Flor, H., Braun, C., Elbert, T., and Birbaumer, N. (1997). Extensive reorganization of primary somatosensory cortex in chronic back pain patients. *Neurosci. Lett.* 224, 5–8. doi: 10.1016/S0304-3940(97)13441-3

Foell, J., Bekrater-Bodmann, R., McCabe, C. S., and Flor, H. (2013). Sensorimotor incongruence and body perception: an experimental investigation. *Front. Hum. Neurosci.* 7:310. doi: 10.3389/fnhum.2013.00310

Frith, C. D., Blakemore, S. J., and Wolpert, D. M. (2000). Abnormalities in the awareness and control of action. *Philos. Trans. R. Soc. Lond. B Biol. Sci.* 355, 1771–1788. doi: 10.1098/rstb.2000.0734

Gandevia, S. C., and Phegan, C. M. L. (1999). Perceptual distortions of the human body image produced by local anaesthesia, pain and cutaneous stimulation. *J. Physiol.* 514, 609–616. doi: 10.1111/j.1469-7793.1999.609ae.x

Gelecek, N., Başkurt, Z., and Başkurt, F. (2006). Effects of chronic osteoarthritis pain on the pressure-pain thresholds and proprioceptive sense. *J. Musculoskelet. Pain* 14, 45–50. doi: 10.1300/J094v14n02_06

Haffenden, A. M., and Goodale, M. A. (1998). The effect of pictorial illusion on prehension and perception. *J. Cogn. Neurosci.* 10, 122–136. doi: 10.1162/089892998563824

Hamacher, D., Hamacher, D., Krowicki, M., and Schega, L. (2016). Gait variability in chronic back pain sufferers with experimentally diminished visual feedback: a pilot study. *J. Mot. Behav.* 48, 205–208. doi: 10.1080/00222895.2015.1073136

Harris, A. J. (1999). Cortical origin of pathological pain. *Lancet* 354, 1464–1466. doi: 10.1016/S0140-6736(99)05003-5

Kammers, M. P. M., de Vignemont, F., Verhagen, L., and Dijkerman, H. C. (2009). The rubber hand illusion in action. *Neuropsychologia* 47, 204–211. doi: 10.1016/j.neuropsychologia.2008.07.028

Kim, H., Kim, J., Loggia, M. L., Cahalan, C., Garcia, R. G., Vangel, M. G., et al. (2015). Fibromyalgia is characterized by altered frontal and cerebellar structural covariance brain networks. *Neuroimage Clin.* 7, 667–677. doi: 10.1016/j.nicl.2015.02.022

Lee, A. S., Cholewicki, J., Reeves, N. P., Zazulak, B. T., and Mysliwiec, L. W. (2010). Comparison of trunk proprioception between patients with low back pain and healthy controls. *Arch. Phys. Med. Rehabil.* 91, 1327–1331. doi: 10.1016/j.apmr.2010.06.004

Lewis, J. S., Kersten, P., McCabe, C. S., McPherson, K. M., and Blake, D. R. (2007). Body perception disturbance: a contribution to pain in complex regional pain syndrome (CRPS). *Pain* 133, 111–119. doi: 10.1016/j.pain.2007.03.013

Lewis, J. S., Kersten, P., McPherson, K. M., Taylor, G. J., Harris, N., McCabe, C. S., et al. (2010). Wherever is my arm? Impaired upper limb position accuracy in complex regional pain syndrome. *Pain* 149, 463–469. doi: 10.1016/j.pain.2010.02.007

Lotze, M., Flor, H., Grodd, W., Larbig, W., and Birbaumer, N. (2001). Phantom movements and pain An fMRI study in upper limb amputees. *Brain* 124, 2268–2277. doi: 10.1093/brain/124.11.2268

Lotze, M., and Moseley, G. L. (2007). Role of distorted body image in pain. *Curr. Rheumatol. Rep.* 9, 488–496. doi: 10.1007/s11926-007-0079-x

Maihöfner, C., Baron, R., DeCol, R., Binder, A., Birklein, F., Deuschl, G., et al. (2007). The motor system shows adaptive changes in complex regional pain syndrome. *Brain* 130, 2671–2687. doi: 10.1093/brain/awm131

Mavromatis, N., Gagné, M., Voisin, J. I. A. V., Reilly, K. T., and Mercier, C. (2016). Experimental tonic hand pain modulates the corticospinal plasticity induced by a subsequent hand deafferentation. *Neuroscience* 330, 403–409. doi: 10.1016/j.neuroscience.2016.06.008

McCabe, C. (2011). Mirror visual feedback therapy. A practical approach. *J. Hand Ther.* 24, 170–179. doi: 10.1016/j.jht.2010.08.003

McCabe, C. S., and Blake, D. R. (2008). An embarrassment of pain perceptions? Towards an understanding of and explanation for the clinical presentation of CRPS type 1. *Rheumatology* 47, 1612–1616. doi: 10.1093/rheumatology/ken254

McCabe, C. S., Cohen, H., and Blake, D. R. (2007). Somaesthetic disturbances in fibromyalgia are exaggerated by sensory–motor conflict: implications for chronicity of the disease? *Rheumatology* 46, 1587–1592. doi: 10.1093/rheumatology/kem204

McCabe, C. S., Cohen, H., Hall, J., Lewis, J., Rodham, K., and Harris, N. (2009). Somatosensory conflicts in complex regional pain syndrome type 1 and fibromyalgia syndrome. *Curr. Rheumatol. Rep.* 11, 461–465. doi: 10.1007/s11926-009-0067-4

McCabe, C. S., Haigh, R. C., Halligan, P. W., and Blake, D. R. (2005). Simulating sensory–motor incongruence in healthy volunteers: implications for a cortical model of pain. *Rheumatology* 44, 509–516. doi: 10.1093/rheumatology/keh529

McCabe, C. S., Haigh, R. C., Ring, E. F. J., Halligan, P. W., Wall, P. D., and Blake, D. R. (2003). A controlled pilot study of the utility of mirror visual feedback in the treatment of complex regional pain syndrome (type 1). *Rheumatology* 42, 97–101. doi: 10.1093/rheumatology/keg041

Mercier, C., Gagné, M., Reilly, K. T., and Bouyer, L. J. (2016). Effect of experimental cutaneous hand pain on corticospinal excitability and short afferent inhibition. *Brain Sci.* 6:45. doi: 10.3390/brainsci6040045

Mercier, C., and Sirigu, A. (2009). Training with virtual visual feedback to alleviate phantom limb pain. *Neurorehabil. Neural Repair* 23, 587–594. doi: 10.1177/1545968308328717

Metral, M., Guinot, M., Bresciani, J. P., Luyat, M., Roulin, J. L., and Guerraz, M. (2014). Bimanual coordination with three hands: is the mirror hand of any help? *Neuropsychologia* 52, 11–18. doi: 10.1016/j.neuropsychologia.2013.10.027

Moseley, G. L. (2008). I can't find it! Distorted body image and tactile dysfunction in patients with chronic back pain. *Pain* 140, 239–243. doi: 10.1016/j.pain.2008.08.001

Moseley, G. L., Gallace, A., Di Pietro, F., Spence, C., and Iannetti, G. D. (2013). Limb-specific autonomic dysfunction in complex regional pain syndrome modulated by wearing prism glasses. *Pain* 154, 2463–2468. doi: 10.1016/j.pain.2013.07.026

Nijs, J., Daenen, L., Cras, P., Struyf, F., Roussel, N., and Oostendorp, R. A. (2012). Nociception affects motor output: a review on sensory-motor interaction with focus on clinical implications. *Clin. J. Pain* 28, 175–181. doi: 10.1097/AJP.0b013e318225daf3

Nishigami, T., Mibu, A., Osumi, M., Son, K., Yamamoto, S., Kajiwara, S., et al. (2015). Are tactile acuity and clinical symptoms related to differences in perceived body image in patients with chronic non-specific lower back pain?. *Man. Ther.* 20, 63–67. doi: 10.1016/j.math.2014.06.010

Nishigami, T., Nakano, H., Osumi, M., Tsujishita, M., Mibu, A., and Ushida, T. (2014). Central neural mechanisms of interindividual difference in discomfort during sensorimotor incongruence in healthy volunteers: an experimental study. *Rheumatology* 53, 194–1199. doi: 10.1093/rheumatology/ket494

Oldfield, R. C. (1971). The assessment and analysis of handedness: the Edinburgh inventory. *Neuropsychologia* 9, 97–113. doi: 10.1016/0028-3932(71)90067-4

Paillard, J. (1999). "Body schema and body image—A double dissociation," in *Motor Control: Today and Tomorrow*, eds G. N. Gantchev, S. Mori, and J. Massion (Sofia: Academic Publishing House "Prof. M. Drinov"), 197–214.

Peltz, E., Seifert, F., Lanz, S., Müller, R., and Maihöfner, C. (2011). Impaired hand size estimation in CRPS. *J. Pain* 12, 1095–1101. doi: 10.1016/j.jpain.2011.05.001

Ramachandran, V. S., and Rogers-Ramachandran, D. (1996). Synaesthesia in phantom limbs induced with mirrors. *Proc. R. Soc. Lond. B Biol. Sci.* 263, 377–386. doi: 10.1098/rspb.1996.0058

Roll, J. P., and Vedel, J. P. (1982). Kinaesthetic role of muscle afferents in man, studied by tendon vibration and microneurography. *Exp. Brain Res.* 47, 177–190. doi: 10.1007/BF00239377

Roosink, M., McFadyen, B. J., Hébert, L. J., Jackson, P. L., Bouyer, L. J., and Mercier, C. (2015). Assessing the perception of trunk movements in military personnel with chronic non-specific low back pain using a virtual mirror. *PLoS ONE* 10:e0120251. doi: 10.1371/journal.pone.0120251

Roussel, N. A., De Kooning, M., Nijs, J., Cras, P., Wouters, K., and Daenen, L. (2015). The role of sensorimotor incongruence in pain in professional dancers. *Motor Control* 19, 271–288. doi: 10.1123/ijsnem.2013-0074

Sheeran, L., Sparkes, V., Caterson, B., Busse-Morris, M., and van Deursen, R. (2012). Spinal position sense and trunk muscle activity during sitting and standing in non-specific chronic low back pain: classification analysis. *Spine* 37, E486–E495. doi: 10.1097/brs.0b013e31823b00ce

Swinnen, S. P., Puttemans, V., Vangheluwe, S., Wenderoth, N., Levin, O., and Dounskaia, N. (2003). Directional interference during bimanual coordination: is interlimb coupling mediated by afferent or efferent processes. *Behav. Brain Res.* 139, 177–195. doi: 10.1016/S0166-4328(02)00266-8

Van Hilten, J. J. (2010). Movement disorders in complex regional pain syndrome. *Pain Med.* 11, 1274–1277. doi: 10.1111/j.1526-4637.2010.00916.x

Conflict of Interest Statement: The authors declare that the research was conducted in the absence of any commercial or financial relationships that could be construed as a potential conflict of interest.

Copyright © 2017 Brun, Gagné, McCabe and Mercier. This is an open-access article distributed under the terms of the Creative Commons Attribution License (CC BY). The use, distribution or reproduction in other forums is permitted, provided the original author(s) or licensor are credited and that the original publication in this journal is cited, in accordance with accepted academic practice. No use, distribution or reproduction is permitted which does not comply with these terms.

frontiers in Human Neuroscience

ORIGINAL RESEARCH
published: 17 November 2017
doi: 10.3389/fnhum.2017.00559

Effect of Electro-Acupuncture and Moxibustion on Brain Connectivity in Patients with Crohn's Disease: A Resting-State fMRI Study

Chunhui Bao[1†], Di Wang[1†], Peng Liu[2], Yin Shi[3], Xiaoming Jin[4], Luyi Wu[1], Xiaoqing Zeng[5], Jianye Zhang[6], Huirong Liu[3] and Huangan Wu[1]**

[1]Key Laboratory of Acupuncture and Immunological Effects, Shanghai University of Traditional Chinese Medicine, Shanghai, China, [2]Life Sciences Research Center, School of Life Sciences and Technology, Xidian University, Xi'an, China, [3]Outpatient Department, Shanghai Research Institute of Acupuncture and Meridian, Shanghai University of Traditional Chinese Medicine, Shanghai, China, [4]Stark Neurosciences Research Institute, Indiana University School of Medicine, Indianapolis, IN, United States, [5]Department of Gastroenterology, Zhongshan Hospital, Fudan University, Shanghai, China, [6]Department of Radiology, Shanghai Mental Health Center, Shanghai Jiaotong University School of Medicine, Shanghai, China

OPEN ACCESS

Edited by:
Elizabeth B. Torres,
Rutgers University, The State University of New Jersey,
United States

Reviewed by:
Junhua Li,
National University of Singapore,
Singapore
Yan Wang,
University of North Carolina at Chapel Hill, United States

***Correspondence:**
Huirong Liu
lhr_tcm@139.com
Huangan Wu
wuhuangan@126.com

[†]These authors have contributed equally to this work.

Received: 02 August 2017
Accepted: 06 November 2017
Published: 17 November 2017

Citation:
Bao C, Wang D, Liu P, Shi Y, Jin X, Wu L, Zeng X, Zhang J, Liu H and Wu H (2017) Effect of Electro-Acupuncture and Moxibustion on Brain Connectivity in Patients with Crohn's Disease: A Resting-State fMRI Study. Front. Hum. Neurosci. 11:559. doi: 10.3389/fnhum.2017.00559

Acupuncture and moxibustion have been shown to be effective in treating Crohn's disease (CD), but their therapeutic mechanisms remain unclear. Here we compared brain responses to either electro-acupuncture or moxibustion treatment in CD patients experiencing remission. A total of 65 patients were randomly divided into an electro-acupuncture group (n = 32) or a moxibustion group (n = 33), and treated for 12 weeks. Eighteen patients in the electro-acupuncture group and 20 patients in the moxibustion group underwent resting-state functional magnetic resonance imaging at baseline and after treatment. Seed-based analysis was used to compare the resting-state functional connectivity (rsFC) between bilateral hippocampus and other brain regions before and after the treatments, as well as between the two groups. The CD activity index (CDAI) and inflammatory bowel disease questionnaire (IBDQ) were used to evaluate disease severity and patient quality of life. Electro-acupuncture and moxibustion both significantly reduced CDAI values and increased IBDQ scores. In the electro-acupuncture group, the rsFC values between bilateral hippocampus and anterior middle cingulate cortex (MCC) and insula were significantly increased, and the changes were negatively correlated with the CDAI scores. In the moxibustion group, the rsFC values between bilateral hippocampus and precuneus as well as inferior parietal lobe (IPC) were significantly elevated, and the changes were negatively correlated with the CDAI scores. We conclude that the therapeutic effects of electro-acupuncture and moxibustion on CD may involve the differently modulating brain homeostatic afferent processing network and default mode network (DMN), respectively.

Keywords: acupuncture, moxibustion, Crohn's disease, fMRI, functional connectivity

Abbreviations: CD, Crohn's disease; CDAI, Crohn's disease activity index; DMN, default mode network; HADS, hospital anxiety and depression scale; HIPP, hippocampus; HCs, healthy control subjects; IBDQ, inflammatory bowel disease questionnaire; IPC, inferior parietal cortex; MCC, middle cingulate cortex; rsFC, resting-state functional connectivity.

INTRODUCTION

Crohn's disease (CD) is a chronic inflammatory disease that most commonly affects the terminal ileum and neighboring colon, but can affect the entire digestive tract. The main clinical manifestations include abdominal pain, diarrhea and weight loss. Current therapeutic strategies are aimed at inducing and maintaining disease remission, preventing the incidence of complications, and preventing disease progression (Torres et al., 2016). Although medications such as mesalazine, glucocorticoids, and immunosuppressants are efficient in controlling the acute activity of disease, the side effects caused by long-term administration of these medications hinder their continuous usage (Clark et al., 2007; Saibeni et al., 2014). Emerging biological agents, for example tumor necrosis factor alpha (TNF-α) inhibitors, bring hope to some patients. However, the use of these agents places a heavy financial burden on them (Clark et al., 2007).

Recently, the importance of brain-gut axis dysfunction in the development and progression of inflammatory bowel disease (IBD) has drawn more attention (Bonaz and Bernstein, 2013; Al Omran and Aziz, 2014). Numerous recent studies have shown that structural and functional abnormalities of the brain may play crucial roles in the development of CD (Bao et al., 2015; Bao C. et al., 2016; Bao C. H. et al., 2016; Rubio et al., 2016; Thomann et al., 2016). As a principal structure of the limbic system, hippocampus affects the intestinal tract through multiple pathways, including the hypothalamic-pituitary-adrenal (HPA) axis, the vagus nerve and the immune system (Lathe, 2001). Studies using animal models of chemically-induced CD have revealed changes in the excitability and behavior of the central nervous system, such as activation of hippocampal microglia, changes in glutamate transmission and neuronal plasticity, increased levels of TNF-α, inducible nitric oxide synthase (iNOS), and nitrites in the hippocampus (Riazi et al., 2008; Heydarpour et al., 2016), and declined neuronal regeneration (Riazi et al., 2015; Zonis et al., 2015). These findings provide evidence for potential interaction between the hippocampus and intestinal inflammation as well as immunity. Previous neuroimaging studies have demonstrated alterations in gray matter volume and functional activity of the hippocampus in CD patients when compared to healthy volunteers (Bao et al., 2015; Bao C. et al., 2016; Bao C. H. et al., 2016). Hence, the hippocampus may play a pivotal role in the development, progression and remission of CD.

As an important complementary therapy and alternative to standard medicine, acupuncture and moxibustion have been used for thousands of years in the prevention and treatment of different diseases, and have been widely used for gastrointestinal diseases globally (Schneider et al., 2007; Cheifetz et al., 2017). Randomized controlled trials have indicated that acupuncture and moxibustion can help control intestinal inflammation and improve CD patient quality of life (Joos et al., 2004; Bao et al., 2014), but the underlying mechanisms have not yet been fully elucidated. Previous evidence has suggested that the clinical outcome of acupuncture treatment relies on its modulation of central nervous system activity (Han et al., 1982; Takahashi, 2011; Huang et al., 2014). Electro-acupuncture is a form of acupuncture with improved therapeutic efficacy, in which small electrical currents at certain frequencies are passed through acupuncture needles. Moxibustion is a therapy that consists of burning dried mugwort on acupoints to generate warm stimulation on the local regions. Herb-partitioned moxibustion is a form of moxibustion in which herbs are ground into powder, prepared as a certain size of herbal disc using a mold, and the moxa cone is burned to warm the herb-partition, which stimulates acupoints. Electro-acupuncture and moxibustion are two stimulation approaches, generally producing similar clinical outcomes. However, in our previous study, we found that electro-acupuncture and moxibustion induced different brain responses in CD patients (Bao C. et al., 2016). The use of electro-acupuncture or moxibustion treatment can correct abnormal brain function in CD patients, and these changes are closely associated with clinical outcomes (Bao C. et al., 2016). Considering the principle role of the hippocampus in the brain-gut axis, it is important to investigate if electro-acupuncture and moxibustion treatment can affect the resting-state functional connectivity (rsFC) of the hippocampus in CD patients, and the potential differences between the two approaches.

Seed-based rsFC analysis can clarify the correlation of time series signals of low frequency oscillation between brain areas of interest (seeds) and other brain areas within the same neuroanatomical system. It has been used to evaluate the synchronization of neuronal activity in varied brain regions to study brain function, and identify functional networks associated with a seed region (Biswal et al., 1995; Fox and Raichle, 2007; Bullmore and Sporns, 2009). This method has also been used to investigate the mechanisms underlying several diseases and acupuncture and moxibustion treatment (Chen et al., 2015; Deng et al., 2016; Wang et al., 2016; Ning et al., 2017). This study aimed to investigate the effects of electro-acupuncture or moxibustion treatment on rsFC using bilateral hippocampus as seeds, to compare the differences in brain response between the two approaches, and to further explore the correlation between these changes and clinical outcomes in CD patients experiencing remission.

MATERIALS AND METHODS

Subjects

This study was approved by the Ethical Committee of Yueyang Hospital of Integrated Translational Chinese and Western Medicine, Shanghai University of Traditional Chinese Medicine. It was registered in the clinical trials database (NCT01696838)[1]. All participants were informed and signed a consent form and the study was carried out in accordance with the Declaration of Helsinki (Edinburgh version, 2000).

A total of 65 CD patients from the Specialist Outpatient Department of IBD, Shanghai Research Institute of Acupuncture and Meridian, and the Endoscopy Center of Zhongshan Hospital,

[1]https://clinicaltrials.gov/

Fudan University, were recruited in this study. All patients received systemic and gastrointestinal screening, including colonoscopy and biopsy, by an experienced gastroenterologist from the Department of Gastroenterology, Zhongshan Hospital, Fudan University. Disease severity was scored according to the CD Index of Severity (CDEIS; Mary and Modigliani, 1989). In addition, data were collected for patient serum C-reactive protein level, erythrocyte sedimentation rate, and platelet count. Patient mental health was evaluated by a psychiatrist from Shanghai Mental Health Center according to DSM-IV criteria, and participants with psychological and psychiatric disorders were excluded.

Patients who met the following criteria were included for this study: 18–70 years of age; education history $\geq$6 years; right-hand dominant; disease remission >1 year; Crohn's disease activity index (CDAI) score $\leq$150; CDEIS score <3; and no history of acupuncture or moxibustion treatment. Patients were excluded if they met any of the following criteria: serum C-reactive protein >10 mg/L; erythrocyte sedimentation rate >20 mm/h; platelet level $>300 \times 10^9$/L; presence of abdominal fistula or sinus tract; history of medical therapy with glucocorticoids, immunosuppressants, anti-TNF-α agents or other biologics, mental health medications, or opioids in the past 3 months; in a pregnant state; currently experiencing or had a history of mental/neurological disease, brain trauma, or loss of consciousness; with chronic damage or disease of the heart, liver, or kidneys; or had experienced tuberculosis, acute suppurative disease, or an infectious disease.

Patients under the following conditions were excluded from MRI examination: history of abdominal surgery related to CD; claustrophobia; presence of metal inside the body; or over 50 years of age (brain structure and function in these subjects have greater variation; Liu et al., 2016; Wu et al., 2016).

Participants taking mesalazine continued the drug administration with unchanged dosing during the study.

Randomization

In this study, simple randomization was used. A random number table was generated using SPSS 16.0 statistical software by a non-related individual, and a random distribution table was passed to the experimental researchers. Participants that met the inclusion criteria were assigned to a random number sequentially according to their admission number. Subjects with odd random numbers were assigned to the electro-acupuncture group (n = 32) and those with even random numbers were assigned to the moxibustion group (n = 33). During treatment, patients in the two groups were admitted to separate treatment units in the study center to avoid interpersonal communication.

Electro-Acupuncture and Moxibustion Treatments

According to our previous studies (Bao et al., 2014; Bao C. et al., 2016), four acupoints were selected for both groups, including bilateral ST25 (*stomach, Tianshu, bilateral*), CV6 (*conception vessel, Qihai*) and CV12 (*Zhongwan*; **Figure 1**).

Electro-Acupuncture Procedures

Following local disinfection, an acupuncture needle (0.30 × 40 mm; Hwato, Suzhou Medical Appliance Factory) was rapidly inserted through the skin, then slowly inserted an additional 20–25 mm into the subcutaneous region. After achieving a Qi sensation of acupuncture, the needles were connected to a Han's Acupoint Nerve Stimulator (HANS-100). Two electrodes of the stimulators (not divided into positive and negative charge) were connected to the left ST25 and CV6, as well as the right ST25 and CV12. The two clips did not touch each other. Dense disperse waves (frequency 2/100 Hz, current intensity 1–2 mA) were used, and the needles were left in place for 30 min. Patients were given electro-acupuncture treatment once every other day (3 days per week) for a total of 12 weeks (36 total sessions).

Moxibustion Procedures

An herbal disc used in herb-partitioned moxibustion was composed of Monkshood, *Coptis chinensis, Radix aucklandiae*, *Carthamus tinctorius*, Salvia and *Angelica sinensis*. Each herbal disc contained 2.8 g raw power. The powder was mixed with maltose (3 g) and made into a paste with warm water. The herbal disc was prepared to a uniform size using a mold (23 mm in diameter, 5 mm in thickness). Refined pure mugwort (size, 18 mm × 200 mm; Hanyi; Nanyang Hanyi Moxibustion Technology Development Co., Ltd.) was cut to a 16 mm height (final weight 1.8 g) for herb-partitioned moxibustion treatment. For each acupoint, two moxa-cones were burnt. The therapeutic course was the same as electro-acupuncture treatment (36 sessions over 12 weeks).

Outcome Measurement

CDAI (Best et al., 1979) is a globally accepted index for accurate evaluation of the disease severity and therapeutic outcome for CD patients. CDAI $\leq$150 was identified as remission, and CDAI >150 was identified as active disease. The inflammatory bowel disease questionnaire (IBDQ; Irvine et al., 1994) is a questionnaire used to efficiently evaluate the health-related quality of life in adults with IBD. It contains 32 questions, with each question having a seven-point Likert scale. The total score ranges from 32 to 224 points. A higher score represents a better quality of life. Patients were assessed at baseline and after the 12-week treatment.

MRI Protocol and Image Acquisition

The MRI experiments were conducted using a 3.0 Tesla clinical scanner (MagnetomVerio, Siemens, Erlangen, Germany) in the Department of Radiology, Shanghai Mental Health Center, Shanghai Jiaotong University (Shanghai, China). The MRI scans were performed 3 days before the treatment and 3 days after the end of treatment. During the MRI scan, all participants were instructed to relax and keep their eyes closed but not to fall asleep and not to think of anything in particular. Resting-state fMRI was performed with an echo-planar imaging sequence (TR/TE: 2000 ms/30 ms, flip

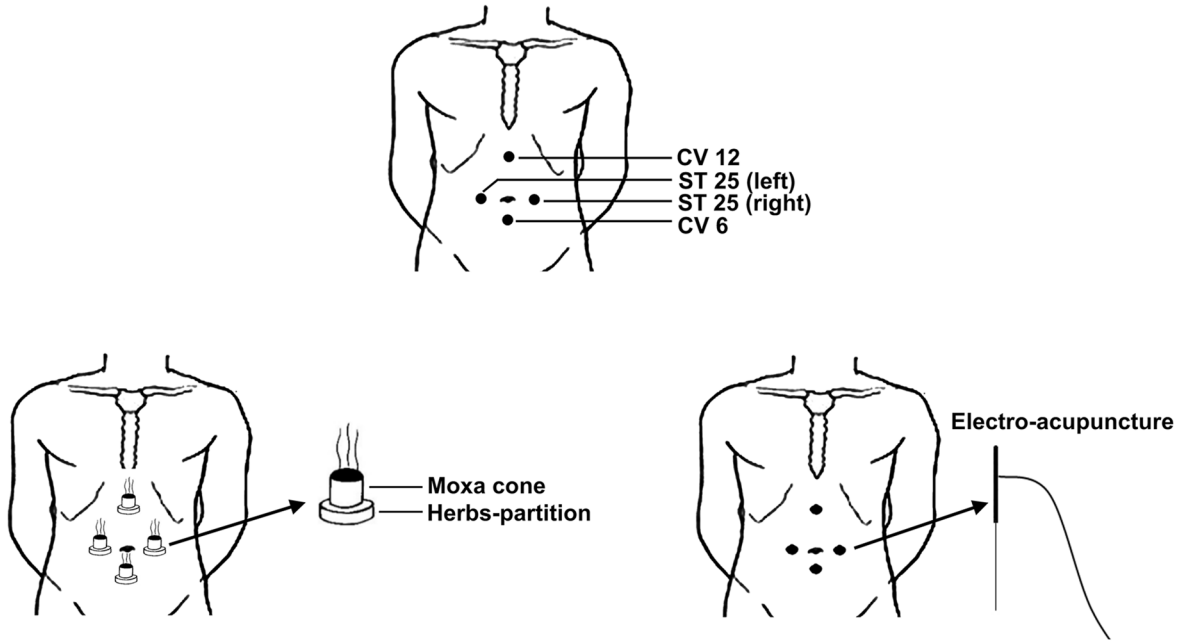

FIGURE 1 | Locations of selected acupoints and schematic diagram of electro-acupuncture and moxibustion treatment. The acupoints were ST25 (*stomach, Tianshu, bilateral*), CV6 (*conception vessel, Qihai*) and CV12 (*Zhongwan*).

angle = 90°, field of view (FOV) = 240 mm × 240 mm, matrix size = 240 × 240, in-plane resolution = 1 mm × 1 mm, slice thickness = 5 mm with no gaps and 32 slices). High resolution three-dimensional T_1-weighted imaging was performed with a multi-echo magnetization-prepared rapid gradient-echo (MPRAGE) sequence with the following parameters: TR/TE = 2300/2.98 ms, FOV = 256 mm × 256 mm, matrix size = 256 × 256, flip angle = 9°, slice thickness = 1.0 mm and 176 slices.

Image Data Processing

The resting-state fMRI datasets were processed using statistical parametric mapping software (SPM8)[2]. The first 10 images of each dataset were removed due to instability of the initial MRI signal and adaptation of participants to the environment. The remaining images were analyzed. Briefly, images from each subject were slice-time corrected and head-motion corrected. After realignment, all images were normalized to the standard Montreal Neurological Institute (MNI) template, and then resampled into 3 × 3 × 3 mm^3 resolution. Next, the images were smoothed with a Gaussian kernel of 6 mm full-width at half maximum (FWHM). Six head motion parameters, signals of the cerebrospinal fluid (CSF), and signals from white matter were used as nuisance covariates to reduce the effects of head motion and non-neuronal blood oxygenation level-dependent (BOLD) fluctuations (Graybiel, 2008; Montembeault et al., 2012). To reduce low-frequency drift and high-frequency respiratory and heart rhythms, the linear trend in the fMRI data was removed, and the images were temporally bandpass filtered (0.01–0.1 Hz).

FC Analysis

Seed-based, whole-brain rsFC analyses were performed using the Conn Toolbox (Whitfield-Gabrieli and Nieto-Castanon, 2012). In this study, the WFU Pickatlas Tool[3] was used to define the bilateral hippocampus, as demonstrated in previous studies (Rasetti et al., 2014; Duan et al., 2017; **Figure 2A**). Correlation maps were created by computing the correlation coefficients between the mean BOLD time course from the seed region and those from all other brain voxels. Correlation coefficients were then converted to *z* values using Fisher's r-to-z transformation to improve the normality.

Statistical Analysis

Twenty patients in each group were scheduled for MRI scans at baseline and at the end of treatment. In the electro-acupuncture group, one patient had head motion during the MRI scan, and one patient was not scanned due to a conflict of schedule. Therefore, a total of 18 MRI datasets from the electro-acupuncture group and 20 from the moxibustion group were included for final analysis. Among the 25 patients who were not scheduled for MRI scans, 12 patients were in the electro-acupuncture group (five were older than 50 years of age, three had metal implants in their body, and four had refused to receive the MRI scan) and 13 patients were in the moxibustion group (five were older than 50 years of age, six had metal

[2]http://www.fil.ion.ucl.ac.uk/spm

[3]http://www.nitrc.org/projects/wfu_pickatlas/

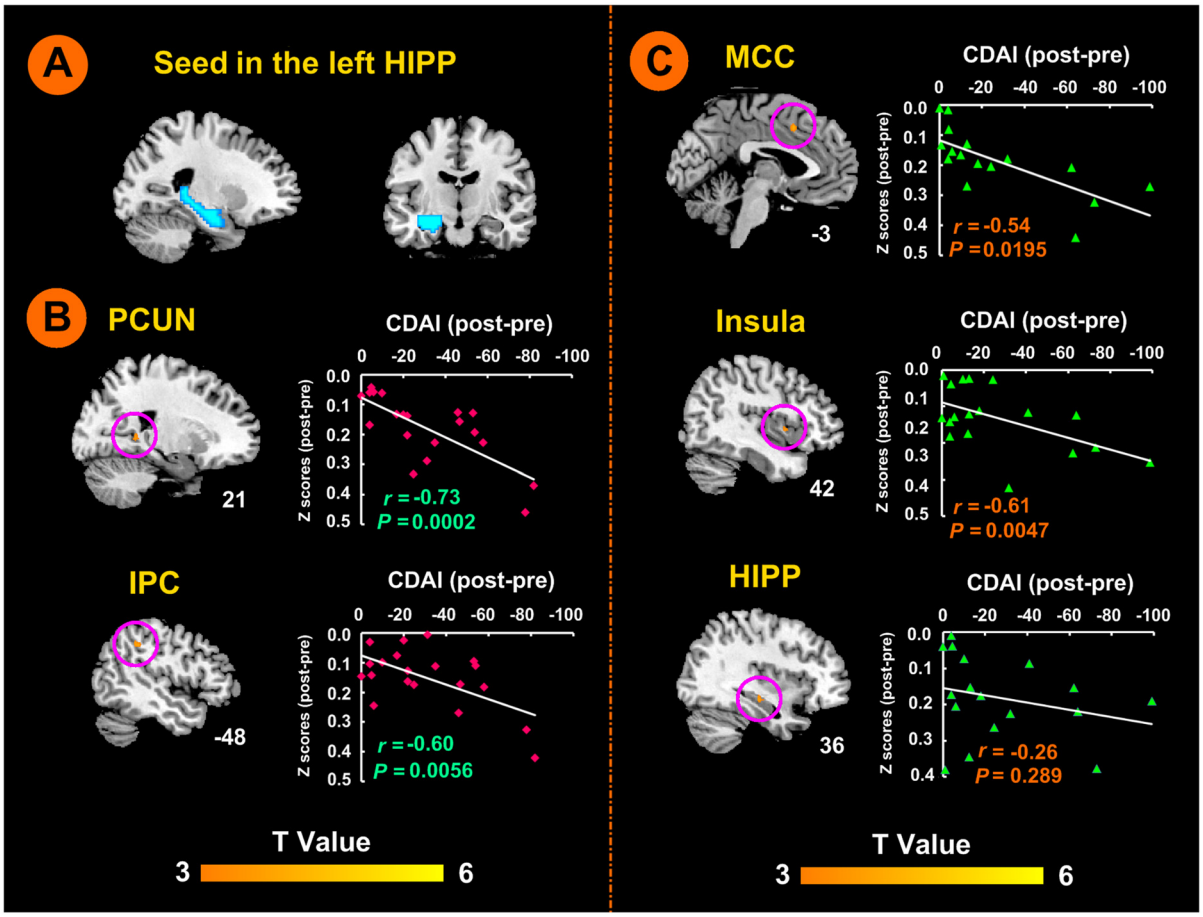

FIGURE 2 | Left hippocampal seed locations and brain responses to electro-acupuncture and moxibustion treatment. **(A)** Seed region in the left hippocampus. **(B)** Brain regions showing an increase of rsFC with the left hippocampus following moxibustion compared to electro-acupuncture treatment, and the correlation between rsFC and CDAI scores. **(C)** Brain regions showing less of an increase of rsFC with the left hippocampus after electro-acupuncture compared to moxibustion treatment, and the correlation between rsFC and CDAI score changes. CDAI, Crohn's disease activity index; HIPP, hippocampus; IPC, inferior parietal cortex; MCC, middle cingulate cortex; PCUN, precuneus; rsFC, resting-state functional connectivity.

implants in their body, and two had refused to receive the MRI scan).

A paired *t*-test was used to evaluate rsFC alterations induced by different treatments within the two groups (electro-acupuncture and moxibustion; $P < 0.05$, false discovery rate (FDR) corrected and the cluster size ≥48). The differences of rsFC between the two groups were evaluated using a two sample *t*-test (post-treatment minus pre-treatment; $P < 0.05$, FDR corrected and the cluster size ≥48). To analyze the relationships between changes in rsFC and disease severity (CDAI scores), Pearson's correlation was then calculated in patient groups with $P < 0.05$ using the Bonferroni correction.

SPSS 16.0 software (SPSS Inc., Chicago, IL, USA) was used for statistical analysis of the clinical variables. All clinical data were subjected to an intention-to-treat (ITT) analysis using the last observation carried forward approach. Measurement data that were normally distributed were compared by independent sample *t*-test between groups. Measurement data without normal distribution were subjected to non-parametric tests. Enumeration data were compared between groups using a Chi-squared test or Fisher's exact test. Two-tailed tests were applied for all analyses and $P < 0.05$ was considered statistically significant.

RESULTS

Clinical Outcome

Table 1 shows a comparison of clinical and demographic variables of CD patients between the two groups who completed MRI scanning. There was no significant difference in the gender, age, height, weight, disease duration, concomitant medication (mesalazine), or the CDAI and IBDQ scores between the two groups of patients (all $P > 0.05$). **Table 2**

TABLE 1 | Demographic and clinical characteristics of CD patients at baseline in each group.

	Electro-acupuncture group (*n* =18)	Moxibustion group (*n* =20)	Statistical value	*P* value
Age (years), mean ± SD	30.89 ± 6.09	29.35 ± 7.73	$t = -0.676$	0.503
Gender (male/female), *n*	13/5	13/7	$X^2 = 5.158$	0.023
Concomitant medication (mesalazine, yes/no), *n*	15/3	20/0	$X^2 = 26.947$	0.000
Height (cm), mean ± SD	170.44 ± 6.53	170.00 ± 7.77	$t = -0.190$	0.851
Weight (kg), mean ± SD	58.56 ± 9.14	56.85 ± 8.53	$t = -0.595$	0.556
Disease duration (years)	5.42 ± 4.22	5.93 ± 3.80	$t = 0.391$	0.698
CDAI	78.28 ± 40.95	71.85 ± 40.84	$t = -0.484$	0.631
IBDQ	171.72 ± 20.17	176.10 ± 32.23	$t = 0.495$	0.623
HADS-A	6.33 ± 6.33	5.35 ± 3.62	$t = -0.894$	0.377
HADS-D	5.61 ± 3.16	3.65 ± 3.82	$t = -1.713$	0.095

CD, Crohn's disease; CDAI, Crohn's disease activity index; HADS-A, Hospital Anxiety and Depression Scale-Anxiety; HADS-D, Hospital Anxiety and Depression Scale-Depression; IBDQ, inflammatory bowel disease questionnaire; SD, standard deviation.

TABLE 2 | Clinical outcome measurements.

Items	Electro-acupuncture group (*n* = 18)		Moxibustion group (*n* = 20)
CDAI			
Baseline, mean ± SD	78.28 ± 40.95		71.85 ± 40.84
Post-treatment, mean ± SD	51.53 ± 31.80		40.90 ± 27.78
T value	6.876		6.584
P value	0.000		0.000
Changes from baseline to post-treatment	−26.74 ± 29.23		−30.95 ± 24.83
T value		−0.479	
P value		0.634	
IBDQ			
Baseline, mean ± SD	171.72 ± 20.17		176.10 ± 32.23
Post-treatment, mean ± SD	187.18 ± 18.69		192.05 ± 21.45
T value	42.486		40.048
P value	0.000		0.000
Changes from baseline to post-treatment	15.44 ± 18.02		15.95 ± 17.28
T value		0.088	
P value		0.930	

CDAI, Crohn's disease activity index; IBDQ, inflammatory bowel disease questionnaire; SD, standard deviation, compared with baseline.

shows that the CDAI scores were significantly reduced ($P < 0.01$), while the IBDQ scores were significantly increased ($P < 0.01$) following treatment in both groups. There was no significant difference in the CDAI ($P = 0.634$) or IBDQ scores ($P = 0.93$) between the two groups after treatment.

Additionally, the clinical outcomes of either male or female population was similar to those when the both populations were combined (Supplementary Tables S1–S4).

Modulation of rsFC between Left Hippocampus and Other Brain Regions by Electro-Acupuncture and Moxibustion Treatment

There was no significant difference in the rsFC baseline characteristics between the two groups ($P > 0.05$). After the 12-week treatment, the electro-acupuncture group showed significant increases in rsFC values between the left hippocampus seed region (shown in **Figure 2A**) and the left anterior middle cingulate cortex (MCC), the right insula, and the right hippocampus. In the moxibustion group, the rsFC values were significantly elevated between the left hippocampus seed region and the right precuneus (PCUN), and the left inferior parietal lobe (IPC; $P < 0.05$, FDR corrected). We did not detect any brain region that showed reduced rsFC with the left hippocampus ($P < 0.05$, FDR corrected).

As shown in **Figure 2B**, the moxibustion group showed a greater increase in the rsFC between the left hippocampus seed and the right PCUN and left IPC compared to the electro-acupuncture group ($P < 0.05$, FDR corrected). As shown in **Figure 2C**, the electro-acupuncture showed a greater increase in the rsFC between the left hippocampus seed and left MCC, right insula and right hippocampus compared to the moxibustion group ($P < 0.05$, FDR corrected).

In the moxibustion group, the increase of rsFC between the left hippocampus seed and the right PCUN and left IPC was negatively correlated with a reduction in the CDAI score ($r = -0.73$, $P < 0.001$; $r = -0.60$, $P < 0.01$; **Figure 2B**). In the electro-acupuncture group, the increase of rsFC between the left hippocampus seed and the left anterior MCC and right insula was negatively correlated to the reduction in the CDAI score ($r = -0.54$, $P < 0.05$; $r = -0.61$, $P < 0.005$; **Figure 2C**); the increase of rsFC between the left hippocampus

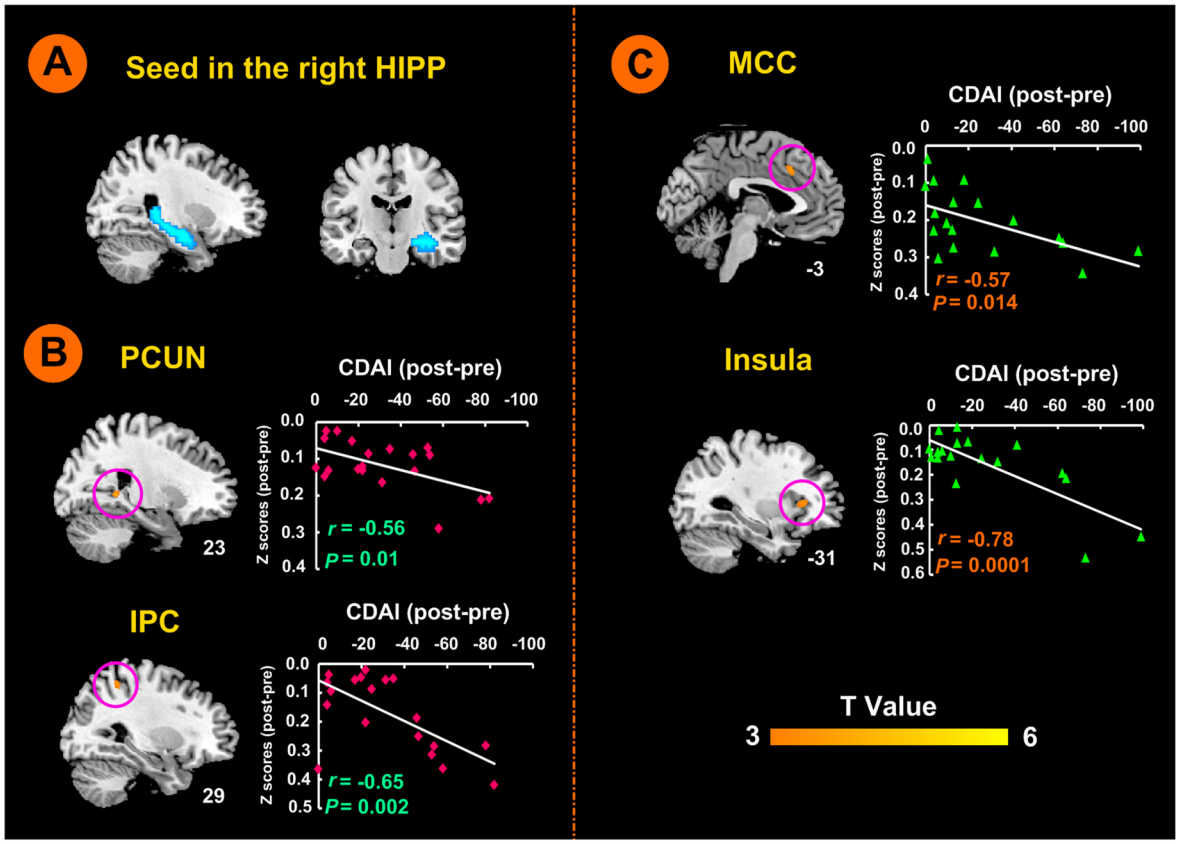

FIGURE 3 | Right hippocampal seed locations and brain responses to electro-acupuncture and moxibustion treatment. **(A)** Seed region in the right hippocampus. **(B)** Brain regions showing an increase of rsFC with the right hippocampus following moxibustion compared to electro-acupuncture treatment, and the correlation between rsFC and CDAI scores. **(C)** Brain regions showing less of an increase of rsFC with the right hippocampus after electro-acupuncture compared to moxibustion treatment, and the correlation between rsFC and CDAI score changes. CDAI, Crohn's disease activity index; HIPP, hippocampus; IPC, inferior parietal cortex; MCC, middle cingulate cortex; PCUN, precuneus; rsFC, resting-state functional connectivity.

seed and the right hippocampus was not significantly correlated to the reduction in the CDAI score ($r = -0.26$, $P > 0.05$; **Figure 2C**).

Modulation of rsFC between Right Hippocampus and Other Brain Regions by Electro-Acupuncture and Moxibustion Treatment

There was no significant difference in the rsFC baseline characteristics between the two groups ($P > 0.05$). After the 12-week treatment, the rsFC value in the electro-acupuncture group was significantly increased between the right hippocampus seed region (shown in **Figure 3A**) and the left anterior MCC and the left insula. In the moxibustion group, the rsFC value was significantly elevated between the right hippocampus seed region and the right precuneus (PCUN), and the right IPC ($P < 0.05$, FDR corrected). We did not detect any brain region that showed reduced rsFC with the right hippocampus ($P < 0.05$, FDR corrected).

As shown in **Figure 3B**, the moxibustion group showed a greater increase in the rsFC between the right hippocampus seed and the right PCUN and right IPC compared to the electro-acupuncture group ($P < 0.05$, FDR corrected). As shown in **Figure 3C**, the electro-acupuncture showed a greater increase in the rsFC between the right hippocampus seed and left MCC and left insula compared to the moxibustion group ($P < 0.05$, FDR corrected).

In the moxibustion group, the increase of rsFC between the right hippocampus seed and the right PCUN and right IPC was negatively correlated with a reduction in the CDAI score ($r = -0.56$, $P = 0.01$; $r = -0.65$, $P < 0.01$; **Figure 3B**). In the electro-acupuncture group, the increase of rsFC between the right hippocampus seed and the left anterior MCC and left insula was negatively correlated to the reduction in the CDAI score ($r = -0.57$, $P < 0.05$; $r = -0.78$, $P < 0.001$; **Figure 3C**).

DISCUSSION

Our results demonstrate that electro-acupuncture and moxibustion treatments resulted in similar improvements in clinical outcomes but different changes in brain connectivity

in CD patients in remission. Electro-acupuncture primarily modulates the homeostatic afferent processing network, whereas moxibustion treatment mainly regulates the default mode network (DMN). Our findings suggest that electro-acupuncture and moxibustion may help improve clinical outcomes through different central integration patterns, and provide new insight for understanding the therapeutic mechanisms of these two approaches.

Previous studies have showed abnormality in the homeostatic afferent processing network and DMN in CD patients in remission (Bao et al., 2015; Bao C. et al., 2016). The homeostatic afferent processing network participates in the regulation of visceral sensation, pain, emotion and homeostasis. Non-painful and painful stimulation from the viscera and body, as well as emotional stimulation, can activate this network (Mayer et al., 2006; Van Oudenhove et al., 2007). The DMN is mainly involved in monitoring external environment, which is a spontaneous cognitive process (Buckner et al., 2008; Mantini and Vanduffel, 2013).

Following electro-acupuncture treatment, the functional connectivity between the bilateral hippocampus and the homeostatic afferent processing network (insula and anterior MCC) was enhanced. In addition, the clinical outcomes of electro-acupuncture treatment were significantly correlated with increases in rsFC between the bilateral hippocampus and these two areas. The insula is considered the "interoceptive cortex" that processes different modalities of sensory information regarding the internal state of the body (Van Oudenhove et al., 2007). The MCC is a component of the medial pain system that processes pain-related emotional and cognitive information. The anterior MCC and subcortical structures, such as hypothalamus and PAG, constitute the descending pain modulation system, which functions in processing endogenous pain. The system mediates nociceptive information at the level of the spinal dorsal horn and controls the perception of pain (Wiech et al., 2008; Blankstein et al., 2010). Electro-acupuncture may help restore the homeostatic afferent processing network function, improve the cerebral integration of the gastrointestinal afferents, and balance homeostasis in CD patients by modulating the functional connectivity between brain regions related to visceral sensation, pain, and internal perception. This result is consistent with our previous findings (Bao C. et al., 2016) as well as results of a neuroimaging study that used electro-acupuncture for the treatment of functional dyspepsia (Zeng et al., 2012).

Following moxibustion treatment, the functional connectivities between the bilateral hippocampus and the DMN (PCUN and IPC) were enhanced, which were positively correlated with the clinical outcomes. The PCUN and IPC are two important components of the DMN. The PCUN plays a pivotal role in the processing of emotions associated with self-introspection and episodic memory (Maddock, 1999; Schneider et al., 2008), whereas the IPC is linked to concentration (Binder et al., 2009). During moxibustion treatment, the abdomen of the patient was always warm. The patient was pleased and felt positive regarding the warm stimulation generated by moxibustion treatment, which increased the attention of the patient on the abdomen. The warm stimulation is a key factor for the outcome of moxibustion treatment (Pach et al., 2009; Yi, 2009), and may mediate moxibustion-induced influences on DMN-associated brain regions. In summary, moxibustion treatment may enhance body attention, enhance functional connectivity between the bilateral hippocampus and the PCUN and IPC, and trigger the re-integration of the DMN, all of which may positively regulate gastrointestinal function in patients. These results are consistent with our previous findings (Bao C. et al., 2016).

The different effects of acupuncture and moxibustion on brain connectivity are likely due to a difference in their stimulation properties. Electro-acupuncture combines mechanical and electrical stimulation, while moxibustion is a kind of warm stimulation. Afferent input from electro-acupuncture stimulation ascends to thalamus and projects to multiple targets including the limbic system and cerebro-cerebellar (Hui et al., 2005), and were represented by the response of the homeostatic afferent processing network in CD patients. While the warm stimulation of moxibustion makes a subject to feel comfortable in the abdomen, resulting in a pleasure emotional experience, which may activate the DMN responsible for internal and external environmental monitoring and concentration. The input signals of both treatments may be carried primarily by mechanosensory, and pain and temperature sensation pathways. However, because acupuncture is shown to mainly activate Aβ and Aδ afferent fibers while the warm stimulus of moxibustion mainly activates C afferent fibers (Han, 2009, 2016), these two stimulus signals likely activate specific peripheral and central pathways and ultimately lead to the activation of different brain regions that underlie the observed differences in brain connectivity in CD patients.

The main limitation of this study is the lack of a positive control group (e.g., medication administration) or a negative control (e.g., placebo). Because of the progressive and recurring nature of CD, the Ethical Committee rejected our initial protocol to include a placebo control group, even if the subjects were all in remission. Therefore, we cannot rule out the non-specific effects of electro-acupuncture and moxibustion treatment. The ethical issue may be addressed in future through shortening treatment period and a positive control may also be considered in the future.

CONCLUSION

Our study demonstrated that electro-acupuncture and moxibustion treatments were both effective in improving symptoms in CD patients in remission but they may have different brain mechanism by enhancing different brain connectivity. Electro-acupuncture treatment may modulate brain function mainly through the homeostatic afferent processing network (insula and anterior MCC), whereas moxibustion treatment may modulate the activity of the DMN (PCUN and IPC). These findings provide a new insight on the brain mechanism and clinical application of acupuncture and moxibustion.

AUTHOR CONTRIBUTIONS

CB, PL, HL and HW: study protocol and design; CB, YS, LW, JZ and XZ: data acquisition; PL, CB and DW: data analysis and interpretation; CB and DW: drafting of the manuscript; XJ and YS: manuscript revision.

ACKNOWLEDGMENTS

Many thanks to Dr. Lili Ma at Zhongshan Hospital of Fudan University for endoscopy examination and scoring. This work was supported by the National Key Basic Research Program of China (973 program), No. 2009CB522900, 2015CB554501; the Program for Outstanding Medical Academic Leader, No. 80; the Program of Shanghai Academic Research Leader, No. 17XD1403400 and the National Natural Science Foundation of China, No. 81471738.

SUPPLEMENTARY MATERIAL

The Supplementary Material for this article can be found online at: https://www.frontiersin.org/articles/10.3389/fnhum.2017.00559/full#supplementary-material

REFERENCES

Al Omran, Y., and Aziz, Q. (2014). The brain-gut axis in health and disease. *Adv. Exp. Med. Biol.* 817, 135–153. doi: 10.1007/978-1-4939-0897-4_6

Bao, C., Liu, P., Liu, H., Jin, X., Calhoun, V. D., Wu, L., et al. (2016). Different brain responses to electro-acupuncture and moxibustion treatment in patients with Crohn's disease. *Sci. Rep.* 6:36636. doi: 10.1038/srep36636

Bao, C. H., Liu, P., Liu, H. R., Wu, L. Y., Jin, X. M., Wang, S. Y., et al. (2016). Differences in regional homogeneity between patients with Crohn's disease with and without abdominal pain revealed by resting-state functional magnetic resonance imaging. *Pain* 157, 1037–1044. doi: 10.1097/j.pain.0000000000000479

Bao, C. H., Liu, P., Liu, H. R., Wu, L. Y., Shi, Y., Chen, W. F., et al. (2015). Alterations in brain grey matter structures in patients with Crohn's disease and their correlation with psychological distress*. *J. Crohns Colitis* 2015, 532–540. doi: 10.1093/ecco-jcc/jjv057

Bao, C. H., Zhao, J. M., Liu, H. R., Lu, Y., Zhu, Y. F., Shi, Y., et al. (2014). Randomized controlled trial: moxibustion and acupuncture for the treatment of Crohn's disease. *World J. Gastroenterol.* 20, 11000–11011. doi: 10.3748/wjg.v20.i31.11000

Best, W. R., Becktel, J. M., and Singleton, J. W. (1979). Rederived values of the eight coefficients of the Crohn's disease activity index (CDAI). *Gastroenterology* 77, 843–846.

Binder, J. R., Desai, R. H., Graves, W. W., and Conant, L. L. (2009). Where is the semantic system? A critical review and meta-analysis of 120 functional neuroimaging studies. *Cereb. Cortex* 19, 2767–2796. doi: 10.1093/cercor/bhp055

Biswal, B., Yetkin, F. Z., Haughton, V. M., and Hyde, J. S. (1995). Functional connectivity in the motor cortex of resting human brain using echo-planar MRI. *Magn. Reson. Med.* 34, 537–541. doi: 10.1002/mrm.1910340409

Blankstein, U., Chen, J., Diamant, N. E., and Davis, K. D. (2010). Altered brain structure in irritable bowel syndrome: potential contributions of pre-existing and disease-driven factors. *Gastroenterology* 138, 1783–1789. doi: 10.1053/j.gastro.2009.12.043

Bonaz, B. L., and Bernstein, C. N. (2013). Brain-gut interactions in inflammatory bowel disease. *Gastroenterology* 144, 36–49. doi: 10.1053/j.gastro.2012.10.003

Buckner, R. L., Andrews-Hanna, J. R., and Schacter, D. L. (2008). The brain's default network: anatomy, function, and relevance to disease. *Ann. N Y Acad. Sci.* 1124, 1–38. doi: 10.1196/annals.1440.011

Bullmore, E., and Sporns, O. (2009). Complex brain networks: graph theoretical analysis of structural and functional systems. *Nat. Rev. Neurosci.* 10, 186–198. doi: 10.1038/nrn2575

Cheifetz, A. S., Gianotti, R., Luber, R., and Gibson, P. R. (2017). Complementary and alternative medicines used by patients with inflammatory bowel diseases. *Gastroenterology* 152, 415.e15–429.e15. doi: 10.1053/j.gastro.2016.10.004

Chen, X., Spaeth, R. B., Freeman, S. G., Scarborough, D. M., Hashmi, J. A., Wey, H. Y., et al. (2015). The modulation effect of longitudinal acupuncture on resting state functional connectivity in knee osteoarthritis patients. *Mol. Pain* 11:67. doi: 10.1186/s12990-015-0071-9

Clark, M., Colombel, J. F., Feagan, J. F., Fedorak, B. C., Hanauer, K. N., Kamm, S. B., et al. (2007). American gastroenterological association consensus development conference on the use of biologics in the treatment of inflammatory bowel disease, June 21–23, 2006. *Gastroenterology* 133, 312–339. doi: 10.1053/j.gastro.2007.05.006

Deng, D., Liao, H., Duan, G., Liu, Y., He, Q., Liu, H., et al. (2016). Modulation of the default mode network in first-episode, drug-Naïve major depressive disorder via acupuncture at baihui (GV20) acupoint. *Front. Hum. Neurosci.* 10:230. doi: 10.3389/fnhum.2016.00230

Duan, G., Liu, H., Pang, Y., Liu, P., Liu, Y., Wang, G., et al. (2017). Hippocampal fractional amplitude of low-frequency fluctuation and functional connectivity changes in premenstrual syndrome. *J. Magn. Reson. Imaging* doi: 10.1002/jmri.25775 [Epub ahead of print].

Fox, M. D., and Raichle, M. E. (2007). Spontaneous fluctuations in brain activity observed with functional magnetic resonance imaging. *Nat. Rev. Neurosci.* 8, 700–711. doi: 10.1038/nrn2201

Graybiel, A. M. (2008). Habits, rituals, and the evaluative brain. *Annu. Rev. Neurosci.* 31, 359–387. doi: 10.1146/annurev.neuro.29.051605.112851

Han, J. S. (2009). *Neuroscience.* China: Peking University Medical Press.

Han, J. S. (2016). Research on acupuncture anesthesia-analgesia. *Zhen Ci Yan Jiu* 41, 377–387. doi: 10.13702/j.1000-0607.2016.05.001

Han, J. S., Xie, G. X., Zhou, Z. F., Folkesson, R., and Terenius, L. (1982). Enkephalin and β-endorphin as mediators of electro-acupuncture analgesia in rabbits: an antiserum microinjection study. *Adv. Biochem. Psychopharmacol.* 33, 369–377.

Heydarpour, P., Rahimian, R., Fakhfouri, G., Khoshkish, S., Fakhraei, N., Salehi-Sadaghiani, M., et al. (2016). Behavioral despair associated with a mouse model of Crohn's disease: role of nitric oxide pathway. *Prog. Neuropsychopharmacol. Biol. Psychiatry* 64, 131–141. doi: 10.1016/j.pnpbp.2015.08.004

Huang, R., Zhao, J., Wu, L., Dou, C., Liu, H., Weng, Z., et al. (2014). Mechanisms underlying the analgesic effect of moxibustion on visceral pain in irritable bowel syndrome: a review. *Evid. Based Complement. Alternat. Med.* 2014:895914. doi: 10.1155/2014/895914

Hui, K. K., Liu, J. O., Napadow, V., Haselgrove, C., Kwong, K. K., Kennedy, D. N., et al. (2005). The integrated response of the human cerebro-cerebellar and limbic systems to acupuncture stimulation at ST 36 as evidenced by fMRI. *Neuroimage* 27, 479–496. doi: 10.1016/j.neuroimage.2005.04.037

Irvine, E. J., Feagan, B., Rochon, J., Archambault, A., Fedorak, R. N., Groll, A., et al. (1994). Quality of life: a valid and reliable measure of therapeutic efficacy in the treatment of inflammatory bowel disease. Canadian Crohn's Relapse Prevention Trial Study Group. *Gastroenterology* 106, 287–296. doi: 10.1016/0016-5085(94)90585-1

Joos, S., Brinkhaus, B., Maluche, C., Maupai, N., Kohnen, R., Kraehmer, N., et al. (2004). Acupuncture and moxibustion in the treatment of active

Crohn's disease: a randomized controlled study. *Digestion* 69, 131–139. doi: 10.1159/000078151

Lathe, R. (2001). Hormones and the hippocampus. *J. Endocrinol.* 169, 205–231. doi: 10.1677/joe.0.1690205

Liu, H., Wang, L., Geng, Z., Zhu, Q., Song, Z., Chang, R., et al. (2016). A voxel-based morphometric study of age- and sex-related changes in white matter volume in the normal aging brain. *Neuropsychiatr. Dis. Treat.* 12, 453–465. doi: 10.2147/ndt.s90674

Maddock, R. J. (1999). The retrosplenial cortex and emotion: new insights from functional neuroimaging of the human brain. *Trends Neurosci.* 22, 310–316. doi: 10.1016/s0166-2236(98)01374-5

Mantini, D., and Vanduffel, W. (2013). Emerging roles of the brain's default network. *Neuroscientist* 19, 76–87. doi: 10.1177/1073858412446202

Mary, J. Y., and Modigliani, R. (1989). Development and validation of an endoscopic index of the severity for Crohn's disease: a prospective multicentre study. Groupe d'Etudes Thérapeutiques des Affections Inflammatoires du Tube Digestif (GETAID). *Gut* 30, 983–989. doi: 10.1136/gut.30.7.983

Mayer, E. A., Naliboff, B. D., and Craig, A. D. (2006). Neuroimaging of the brain-gut axis: from basic understanding to treatment of functional GI disorders. *Gastroenterology* 131, 1925–1942. doi: 10.1053/j.gastro.2006.10.026

Montembeault, M., Joubert, S., Doyon, J., Carrier, J., Gagnon, J. F., Monchi, O., et al. (2012). The impact of aging on gray matter structural covariance networks. *Neuroimage* 63, 754–759. doi: 10.1016/j.neuroimage.2012.06.052

Ning, Y., Li, K., Fu, C., Ren, Y., Zhang, Y., Liu, H., et al. (2017). Enhanced functional connectivity between the bilateral primary motor cortices after acupuncture at yanglingquan (GB34) in right-hemispheric subcortical stroke patients: a resting-state fmri study. *Front. Hum. Neurosci.* 11:178. doi: 10.3389/fnhum.2017.00178

Pach, D., Brinkhaus, B., and Willich, S. N. (2009). Moxa sticks: thermal properties and possible implications for clinical trials. *Complement. Ther. Med.* 17, 243–246. doi: 10.1016/j.ctim.2009.01.002

Rasetti, R., Mattay, V. S., White, M. G., Sambataro, F., Podell, J. E., Zoltick, B., et al. (2014). Altered hippocampal-parahippocampal function during stimulus encoding: a potential indicator of genetic liability for schizophrenia. *JAMA Psychiatry* 71, 236–247. doi: 10.1001/jamapsychiatry.2013.3911

Riazi, K., Galic, M. A., Kentner, A. C., Reid, A. Y., Sharkey, K. A., and Pittman, Q. J. (2015). Microglia-dependent alteration of glutamatergic synaptic transmission and plasticity in the hippocampus during peripheral inflammation. *J. Neurosci.* 35, 4942–4952. doi: 10.1523/JNEUROSCI.4485-14.2015

Riazi, K., Galic, M. A., Kuzmiski, J. B., Ho, W., Sharkey, K. A., and Pittman, Q. J. (2008). Microglial activation and TNFα production mediate altered CNS excitability following peripheral inflammation. *Proc. Natl. Acad. Sci. U S A* 105, 17151–17156. doi: 10.1073/pnas.0806682105

Rubio, A., Pellissier, S., Van Oudenhove, L., Ly, H. G., Dupont, P., Tack, J., et al. (2016). Brain responses to uncertainty about upcoming rectal discomfort in quiescent Crohn's disease—a fMRI study. *Neurogastroenterol. Motil.* 28, 1419–1432. doi: 10.1111/nmo.12844

Saibeni, S., Meucci, G., Papi, C., Manes, G., and Fascì-Spurio, F. (2014). Low bioavailability steroids in inflammatory bowel disease: an old chestnut or a whole new ballgame? *Expert Rev. Gastroenterol. Hepatol.* 8, 949–962. doi: 10.1586/17474124.2014.924396

Schneider, F., Bermpohl, F., Heinzel, A., Rotte, M., Walter, M., Tempelmann, C., et al. (2008). The resting brain and our self: self-relatedness modulates resting state neural activity in cortical midline structures. *Neuroscience* 157, 120–131. doi: 10.1016/j.neuroscience.2008.08.014

Schneider, A., Streitberger, K., and Joos, S. (2007). Acupuncture treatment in gastrointestinal diseases: a systematic review. *World J. Gastroenterol.* 13, 3417–3424. doi: 10.3748/wjg.v13.i25.3417

Takahashi, T. (2011). Mechanism of acupuncture on neuromodulation in the gut—a review. *Neuromodulation* 14, 8–12. doi: 10.1111/j.1525-1403.2010.00295.x

Thomann, A. K., Thomann, P. A., Wolf, R. C., Hirjak, D., Schmahl, C., Ebert, M. P., et al. (2016). Altered markers of brain development in Crohn's disease with extraintestinal manifestations—a pilot study. *PLoS One* 11:e0163202. doi: 10.1371/journal.pone.0163202

Torres, J., Mehandru, S., Colombel, J. -F., and Peyrin-Biroulet, L. (2016). Crohn's disease. *Lancet* 389, 1741–1755. doi: 10.1016/S0140-6736(16)31711-1

Van Oudenhove, L., Coen, S. J., and Aziz, Q. (2007). Functional brain imaging of gastrointestinal sensation in health and disease. *World J. Gastroenterol.* 13, 3438–3445. doi: 10.3748/wjg.v13.i25.3438

Wang, X., Wang, Z., Liu, J., Chen, J., Liu, X., Nie, G., et al. (2016). Repeated acupuncture treatments modulate amygdala resting state functional connectivity of depressive patients. *Neuroimage Clin.* 12, 746–752. doi: 10.1016/j.nicl.2016.07.011

Whitfield-Gabrieli, S., and Nieto-Castanon, A. (2012). Conn: a functional connectivity toolbox for correlated and anticorrelated brain networks. *Brain Connect.* 2, 125–141. doi: 10.1089/brain.2012.0073

Wiech, K., Ploner, M., and Tracey, I. (2008). Neurocognitive aspects of pain perception. *Trends Cogn. Sci.* 12, 306–313. doi: 10.1016/j.tics.2008.05.005

Wu, M., Kumar, A., and Yang, S. (2016). Development and aging of superficial white matter myelin from young adulthood to old age: mapping by vertex-based surface statistics (VBSS). *Hum. Brain Mapp.* 37, 1759–1769. doi: 10.1002/hbm.23134

Yi, S. H. (2009). Thermal properties of direct and indirect moxibustion. *J. Acupunct. Meridian Stud.* 2, 273–279. doi: 10.1016/S2005-2901(09)60068-6

Zeng, F., Qin, W., Ma, T., Sun, J., Tang, Y., Yuan, K., et al. (2012). Influence of acupuncture treatment on cerebral activity in functional dyspepsia patients and its relationship with efficacy. *Am. J. Gastroenterol.* 107, 1236–1247. doi: 10.1038/ajg.2012.53

Zonis, S., Pechnick, R. N., Ljubimov, V. A., Mahgerefteh, M., Wawrowsky, K., Michelsen, K. S., et al. (2015). Chronic intestinal inflammation alters hippocampal neurogenesis. *J. Neuroinflammation* 12:65. doi: 10.1186/s12974-015-0281-0

Conflict of Interest Statement: The authors declare that the research was conducted in the absence of any commercial or financial relationships that could be construed as a potential conflict of interest.

Copyright © 2017 Bao, Wang, Liu, Shi, Jin, Wu, Zeng, Zhang, Liu and Wu. This is an open-access article distributed under the terms of the Creative Commons Attribution License (CC BY). The use, distribution or reproduction in other forums is permitted, provided the original author(s) or licensor are credited and that the original publication in this journal is cited, in accordance with accepted academic practice. No use, distribution or reproduction is permitted which does not comply with these terms.

frontiers in Behavioral Neuroscience

ORIGINAL RESEARCH
published: 04 January 2018
doi: 10.3389/fnbeh.2017.00255

Automated Assessment of Endpoint and Kinematic Features of Skilled Reaching in Rats

Ioana Nica[1], Marjolijn Deprez[2], Bart Nuttin[2,3] and Jean-Marie Aerts[1]**

[1]Measure, Model & Manage Bioresponse (M3-BIORES), Department of Biosystems, KU Leuven, Leuven, Belgium, [2]Research Group Experimental Neurosurgery and Neuroanatomy, KU Leuven, Leuven, Belgium, [3]Department of Neurosurgery, University Hospitals Leuven, Leuven, Belgium

Background: Neural injury to the motor cortex may result in long-term impairments. As a model for human impairments, rodents are often used to study deficits related to reaching and grasping, using the single-pellet reach-to-grasp task. Current assessments of this test capture mostly endpoint outcome. While qualitative features have been proposed, they usually involve manual scoring.

Objective: To detect three phases of movement during the single-pellet reach-to-grasp test and assess completion of each phase. To automatically monitor rat forelimb trajectory so as to extract kinematics and classify phase outcome.

Methods: A top-view camera is used to monitor three rats during training, healthy and impaired testing, over 33 days. By monitoring the coordinates of the forelimb tip along with the position of the pellet, the algorithm divides a trial into reaching, grasping and retraction. Unfulfilling any of the phases results in one of three possible errors: miss, slip or drop. If all phases are complete, the outcome label is success. Along with endpoints, movement kinematics are assessed: variability, convex hull, mean and maximum reaching speed, length of trajectory and peak forelimb extension.

Results: The set of behavior endpoints was extended to include miss, slip, drop and success rate. The labeling algorithm was tested on pre- and post-lesion datasets, with overall accuracy rates of 86% and 92%, respectively. These endpoint features capture a drop in skill after motor cortical lesion as the success rate of 59.6 ± 11.8% pre-lesion decreases to 13.9 ± 8.2% post-lesion, along with a significant increase in miss rate from 7.2 ± 6.7% pre-lesion to 50.2 ± 18.7% post-lesion. Kinematics reveals individual-specific strategies of improvement during training, with a common trend of trajectory variability decreasing with success. Correlations between kinematics and endpoints reveal a more complex pattern of relationships during rehabilitation (18 significant pairs of features) than during training (nine correlated pairs).

Conclusion: Extended endpoint outcomes and kinematics of reaching and grasping are captured automatically with a robust computer program. Both endpoints and kinematics capture intra-animal drop in skill after a motor cortical lesion. Correlations between kinematics and endpoints change from training to rehabilitation, suggesting different mechanisms that underlie motor improvement.

Keywords: motor cortical lesions, rehabilitation, reach-to-grasp test, image processing, kinematics

OPEN ACCESS

Edited by:
Elizabeth B. Torres, Rutgers University, The State University of New Jersey, United States

Reviewed by:
Karunesh Ganguly, University of California, San Francisco, United States
Kazutaka Takahashi, University of Chicago, United States

****Correspondence:***
Ioana Nica
ioanagabriela.nica@kuleuven.be
Jean-Marie Aerts
jean-marie.aerts@kuleuven.be

Received: *06 October 2017*
Accepted: *14 December 2017*
Published: *04 January 2018*

Citation:
Nica I, Deprez M, Nuttin B and Aerts J-M (2018) Automated Assessment of Endpoint and Kinematic Features of Skilled Reaching in Rats. Front. Behav. Neurosci. 11:255. doi: 10.3389/fnbeh.2017.00255

INTRODUCTION

Neural damage due to trauma, stroke, or tumor resection, for example, may induce long-term impairments that are widely studied with the use of animal models. Rodents are excellent subjects to explore the understanding of fine motor impairments that neurological damage induces in humans (Krakauer et al., 2012). In this context, the single pellet reaching task is an established method of evaluating skilled reaching in rodents, either to assess effects of motor cortex lesions (Whishaw, 2000), of models of stroke (Schaar et al., 2010; Lai et al., 2015) or to study neural mechanisms of movement in healthy subjects (Azim et al., 2014; Li et al., 2017). The test involves training rats to reach and grasp for individual food pellets. Once the animals become proficient, the test can be further used to study disruption of skilled reaching and grasping, after a cortical lesion has been induced, for example. After an initial drop of performance, with focused training of the impaired limb, animals often reach similar preoperative performance levels (Whishaw, 2000; Schaar et al., 2010). However, a prevalent question arising in clinical rehabilitation in recent years that most current studies do not address is how to study the underlying mechanism of motor improvement and whether it reflects true neural recovery or merely learning and training of new compensatory behaviors, to overcome the underlying persisting impairment (Jones and Adkins, 2015; Kwakkel et al., 2015; Hylin et al., 2017; Jones, 2017). The intact motor cortex is widely thought to be involved both in the acquisition and execution of new motor skills. However, it remains unclear how neural mechanisms related to training a new motor skill compare to recovery after neurological damage, which may involve neural repair and/or learning new compensatory behaviors to preserve that motor skill. One common way of assessing behavioral recovery is whether an endpoint has been achieved that is similar to the preoperative performance of the animal or to the performance of an intact control (Hylin et al., 2017). Such standard performance outcomes are: reaching success, first-try success, or number of attempts (Schaar et al., 2010). On the other hand, very detailed qualitative assessments have also been described in literature, where a reaching and grasping task is divided in up to ten phases, each scored independently (Whishaw, 2000; Gharbawie et al., 2005). Such detailed studies have so far revealed evidence of compensatory limb behaviors that are qualitatively different compared to true behavioral recovery. However, such approaches are yet to be used prevalently. This is due to the relative ease of evaluating the more standard endpoint features, whereas qualitative phase-based features require evaluation on a frame-by-frame basis, making the task very cumbersome. More recent kinematic studies are using multiple cameras to reconstruct 3-D trajectory of reaching (Azim et al., 2014; Guo et al., 2015), and to extend the set of biomarkers of impairment and recovery by using semi-autonomous tracking algorithms (Lai et al., 2015). However, the step to detailed automatic segmentation of movement is yet to be made. To our knowledge, no study so far aimed to compellingly study the relationship between computer-assessed kinematics and endpoint outcomes during learning and during rehabilitation.

In this study, we developed and assessed a computer program that uses image processing to monitor the kinematics of forelimb during the pellet test and infers based on it a label for the task outcome. The program can discriminate between three movement phases: reaching, grasping and retrieval and can give a label for each of them, thus discriminating between success and three types of mistakes: miss, slip, drop. We developed the algorithm on data from three rats monitored during 8 days of learning the task. We then validated it on data acquired during tests on the highly-skilled rats while they are healthy and after a motor cortical lesion in the region controlling their most dexterous forelimb has been induced. The kinematics revealed an individual strategy to optimally accomplish the task during the training phase. Moreover, the cortical lesion altered the fine spatio-temporal structure of reaching, grasping and retraction phases, triggering compensatory behavior, which cannot be captured just by monitoring the percentage of successful attempts, but also the type and distribution of errors. Thus, the analysis revealed the need for longitudinal, intra-animal studies that focus on individualized kinematics of movement, where improvements in endpoint measures are accompanied by a significant reduction in subjects' trajectory variability. Correlation analysis between endpoint features and kinematics revealed different patterns of linear relationships between the training and the post-lesion rehabilitation stages, underlying strategies of performing the reach and grasp task.

Thus, this study emphasizes the need for individualized methods of monitoring performance that fuse traditional endpoint features with kinematics of movement and raises questions on how such variables help explain improvement and change our definition of recovery, be it due to true neural repair or learned compensatory behavior.

MATERIALS AND METHODS

Subjects

Three male Sprague-Dawley rats weighing ∼300 g were housed individually in standard plastic cages (light on a 14:10 h cycle beginning at 7:00 AM; room temperature 22°C). The animals were 8 weeks old at the beginning of the experiment. Five days prior to the start of training, the animals were gradually food deprived to reach 90% of their body weight by the start of the experiment. The animals were fed standard laboratory chow (1 g per 50 g of body weight) after the testing period each day. By the time testing began at 10:00 AM, all three rats had no remaining food in their cage, thus being sufficiently restricted and motivated to perform the task. The experiments were approved by the Animal Ethics Committee KU Leuven, and all procedures were in accordance with the Belgian and European laws and guidelines for animal experimentation, housing and care (Belgian Royal Decree of 29 May 2013 and European Directive 2010/63/EU on the protection of animals used for scientific purposes of 20 October 2010, project number: P218/2014).

Reaching Task

The pellet test setup and training paradigm were based on established methods (Whishaw, 2000). The animals were trained

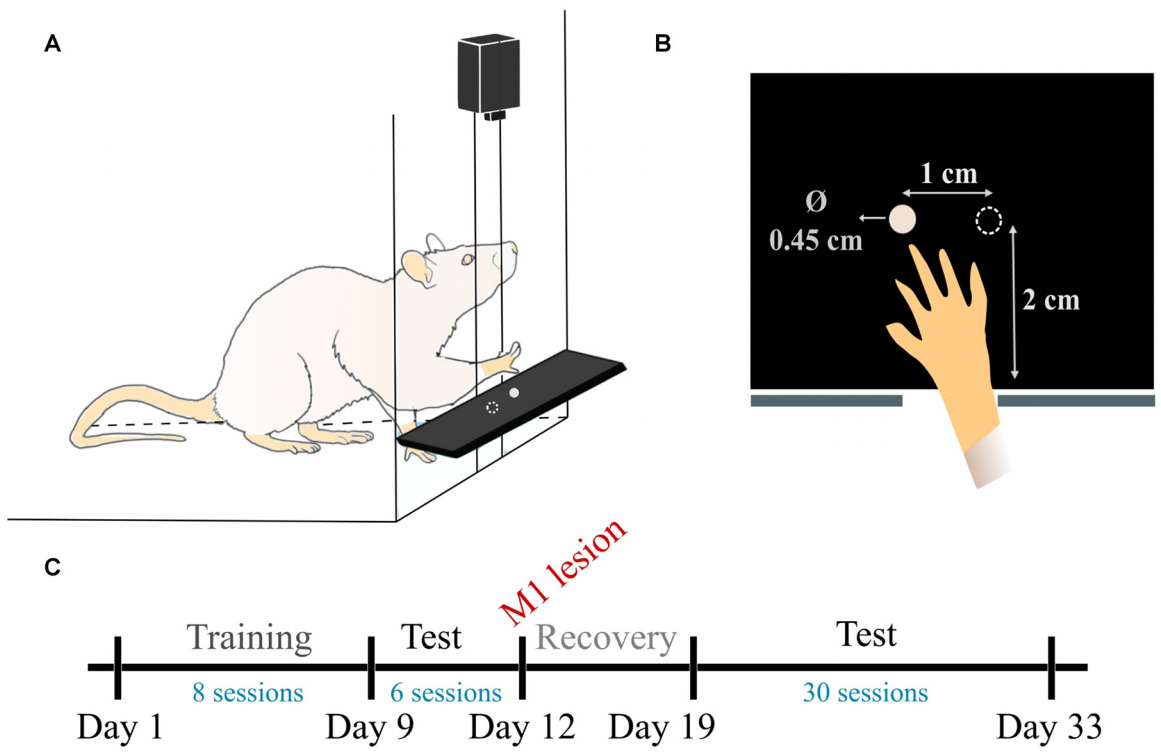

FIGURE 1 | Pellet test setup and experimental timeline. **(A)** Schematic view of the reaching box. **(B)** Top-view illustration of the pellet placement with respect to the slit. **(C)** Timeline of the data experiment and data acquisition. During training (days 1–8) one test/day was recorded. During pre-lesion (days 9–11) and post-lesion (days 19–33) testing periods, two tests/day were recorded.

to reach and grasp in a clear Plexiglas reaching box (19.5 cm long, 8 cm wide, and 20 cm high), with a 1 cm-wide slit in the anterior side. A plastic shelf (8 cm long, 6 cm wide, 2 cm tall) was mounted in front of the box. Two indentations were created in the shelf, 2 cm away from the slit, and symmetrical to its edges, spaced 1 cm away from each other (**Figure 1A**).

Two days before start of training, the rats were habituated to the cage. Pellets were initially available on the cage floor and within tongue distance on the shelf. Pellets were gradually placed farther away on the shelf until the rats were forced to reach to retrieve the food. The pellets were placed in both indentations initially, allowing the animals to display forelimb preference.

Since day 1, once we started recording the training phase, we solely used the indentation contralateral to the preferred forepaw, which allows the rat to obtain the pellet with the most dexterous forelimb and not with the tongue or the other forelimb (**Figure 1B**). The training consisted of reaching for 20 food pellets (Dustless precision pellets, 45 mg, Bio-Serv, Flemington, NJ, USA) until they were all consumed. The experimenter re-placed the pellet in the indentation as many times as needed before the rat managed to successfully retrieve it. The training session was performed once a day, for 8 days.

Once the rats achieved a mean success rate higher than 40% over three consecutive days, we proceeded to test them. A test session differed from a training session in that each of the 20 pellets was offered only once. The rat was allowed to reach for the pellet until it either displaced it, in which case the experimenter took it away, or until it could retrieve it through the opening, into the box. If the rats missed the target or touched the pellet without knocking it away from the indentation, they were allowed to continue. We collected six tests for each animal, during 4 days (days 9–12). The average success rate was 59.7% (±5.7%), comparable to other similar behavior studies (Gharbawie et al., 2005; Alaverdashvili and Whishaw, 2008; Alaverdashvili et al., 2008). Thus the animals were considered trained for the task and we proceeded to inducing cortical lesions.

Surgery

A lesion in the area of the primary motor cortex was induced on day 12. Rats were anesthetized with a mixture of ketamine (Nimatek®) and medetomidine hydrochloride (Narcostart®). A craniotomy over the forelimb area of the primary motor cortex contralateral to the preferred forelimb (right hemisphere in one, left hemisphere in two animals) was made, using coordinates: 1.5 mm posterior to 5 mm anterior to Bregma, and 0.5 mm to 4.5 mm lateral to Bregma, after which the exposed brain tissue was aspirated to a depth of 1.5 mm. Lesions were made to include the rostral and caudal forelimb areas. We defined these coordinates in a preliminary mapping experiment performed in

TABLE 1 | Histology results.

	Lesion location (mm)						Lesion extent (mm)		
Rat	**A**	**P**	**M**	**L**	**D**	**V**	**A-P**	**M-L**	**D-V**
R1	2.52	1.92	1	2.4	0.2	3	4.44	1.4	2.8
R2	5.64	0	1	2.6	0.4	3	5.64	1.6	2.6
R3	4.68	1.44	1.6	2.8	0.6	2.6	6.12	1.2	2
Mean	4.28	1.12	1.2	2.6	0.4	2.87	5.4	1.4	2.47
SD	1.60	0.99	0.35	0.20	0.2	0.23	0.87	0.2	0.42

Lesion location and lesion extent are determined based on the most anterior point (A), most posterior point (P), medial (M) and lateral (L) borders at the widest point and dorsal (D) and ventral (V) borders at the deepest point. Lesion extent is shown in terms of length (antero-posterior spread, A-P), width (medial-lateral spread, M-D) and depth (dorsal-ventral spread, D-V). All values represent distances (mm) to Bregma.

animals of the same sex, age and weight that had been trained for a similar skilled task (data not published).The animals were returned to their home cages, and the pellet test was resumed on day 19, following 1 week of rest.

Histology

Rats received a pentobarbital overdose (Nembutal, CEVA Santé Animale, Belgium; 3 ml i.p.) after which they were perfused intracardially with a solution of 10% sucrose (D(+)-Saccharose, VWR International BVBA, Belgium), followed by a 4% formaldehyde solution (37% dissolved in water, stabilized with 5%–15% methanol, Acros organics, Belgium; 10× diluted in DI water). The brain was removed, embedded in paraffin and was then sliced with a microtome (Leica Biosystems GmbH, Germany) to obtain 10 μm slices. Slices were stained with cresyl violet (0.5% cresyl violet acetate in dH_2O, Merck KGaA, Germany), and were then microscopically inspected and visually compared to a Paxinos stereotactic atlas (Paxinos and Watson, 2005) to determine the lesion extent and location (with the observer blinded for group allocation). Lesion depth and width were estimated based on the deepest and widest point of the lesion, respectively, and results are summarized in **Table 1**. On average, the lesions extended between 1.12 ± 0.99 mm posterior to 4.28 ± 1.6 mm anterior and 1.2 ± 0.35 mm medial to 2.6 ± 0.2 mm lateral. The lesions were rather large, but representative of those described previously (Whishaw, 2000).

Video Recording and Timeline of Data Acquisition

We performed top-view recordings of the task with a Sony DSRPD100 camera (30 Hz sample rate, 120° wide angle, resolution 1920 × 1080) placed ∼10 cm above the reaching table. As shown in **Figure 1C**, data was collected in three phases: training, pre-lesion testing and post-lesion testing. In total, we collected eight training phase sessions, as the rats learned to execute the task (days 1–8), 6 tests pre-lesion, when the animals were healthy and well skilled for the task (days 9–12) and 30 sessions in post-lesion rehabilitation, as the rats gradually improved their skill over 15 days (days 19–33).

Pre-processing

To remove the effect of lens distortion, we determined camera distortion parameters with a checkerboard calibration pattern, by using Matlab Single Camera Calibration App (Computer Vision System Toolbox, Mathworks, Natwick, MA, USA). These parameters were further used in the video monitoring routines, to undistort each frame before analysis. To account for millimeter variations in the way the camera was positioned for each test and to reconstruct 2-D world coordinates of the forelimb, we determined the pixel/centimeter ratio of each video, by taking as reference the reaching table, a black object of exactly 5 cm width.

Behavioral Monitoring

We hypothesized that both training and the motor lesion would not only impact the success rate, which is quantifiable manually, but it would also alter the fine spatio-temporal structure of the reaching, grasping and retraction phases. The objective of the behavioral monitoring was thus two-fold: to assess movement kinematics but also to use kinematics to infer the outcome of the test, be it success or error. Furthermore, we hypothesized the type of error would provide insight into the mechanisms of learning or rehabilitation, so we extended the possible classes of errors to three categories: miss, slip, drop. All video analyses were performed in Matlab, using the Computer vision toolbox (in pre-processing and step (i)) and Image processing toolbox (in step (i)), along with custom designed functions.

Behavioral monitoring was performed off-line, in three steps. In step (i), the algorithm analyzed all frames in a recording session to identify and digitize location of the pellet and the forelimb tip along with features of the forelimb's shape. Rats identify food by olfaction (Alaverdashvili and Whishaw, 2008). However, we observed instances when rats reach towards an empty indentation, either before the pellet was placed in the indentation by the experimenter, or after they had displaced it. Consequently, we programed the algorithm to first identify the pellet with respect to the indentation, so as to ensure that such attempts were excluded and only reaches aimed at a correctly positioned pellet were quantified. The position of the indentation was defined manually for each video, since the contrast was not high enough to determine it by means of image processing. This was the only manually required input. A rectangle of size 0.5 × 0.5 cm centered on the indentation is generated as the preliminary region of interest (ROI). In this preliminary ROI, the pellet can be identified by means of pixel intensity discrepancy, since the pellet is almost white in color, against the dark background of the reaching table (**Figure 2A**). However, the metallic forceps used to place the pellet in the indentation was

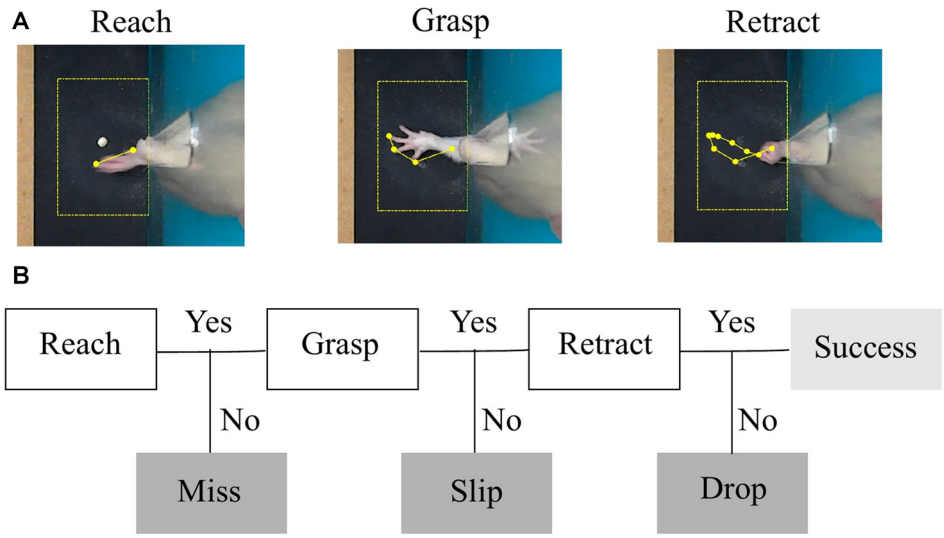

FIGURE 2 | Task phases and error categories. **(A)** The three phases of a successful trial captured by a top-view camera. The region of interest centered around the detected pellet and the trajectory of the forelimb tip are plotted in yellow. **(B)** Decision tree that treats each phase as a condition for success and labels the type of outcome.

also occasionally transiting this region, so to ensure such noise is excluded, an extra condition was imposed. Once an object was detected, its perimeter, P and area A are used to test if the object is round, using circularity C defined as

$$C = P^2/(4\pi A)$$

C has a value of 1 for circles and more than 1 for all other objects. Roundness and not area was the only condition for detecting the pellet, since bigger objects would not fit in the preliminary ROI.

Once the pellet was confirmed to be in the indentation, the search for the forelimb was triggered, in an ROI of 4 × 6 cm centered on the detected pellet. The size of the ROI was devised to monitor reaching once the forelimb passed through the slit. The activity of the forelimb in the cage was obscured by the animal's head and it could not be reliably quantified. The cropped image was converted to a binary image. Because the limb of the rat is light in color, it can easily be identified against the black reaching table without the need to use skin markers (**Figure 2A**). Using the Matlab function "regionprops" (Image Processing Toolbox), forelimb shape features like centroid, area, orientation, minor and major axes, x- and y-coordinates of the tip were assessed. Timestamps for the position of the pellet and forelimb tip, the coordinates of the indentation and the ROIs, and forelimb shape features were saved.

In step (ii), pellet and forelimb coordinates are analyzed as time series, to determine the interval of a reaching attempt. **Figures 3A,B** shows examples of reaching trajectories reconstructed based on forelimb tip coordinates between the timestamps for start of reach and grasping. These timestamps were extracted in step (ii). The most robust feature to detect an attempt was the maxima in the time series of forepaw shape area, marking the moments of maximum forelimb extension. The start of an attempt was defined as the first frame before the forepaw area started increasing monotonically. This condition was imposed rather than just detecting the timestamp when the forelimb enters through the box slit and is detectable in the ROI, so as to exclude intervals when the rat was resting its forelimb on the reaching table or was hesitating before moment of attack. The moment of grasping was detected in the frames following the maximum forelimb extension, based on velocity profile (**Figure 3C**). A decrease in speed succeeded the change in x-axis direction, as the rat retrieved the forepaw from maximum extension position and hovered above the pellet location before touching it. While reaching towards the pellet is quite a uniform and repeatable phase of the attempt, the behavior following grasping was variable. Thus, in this stage only the timestamps for start of reach and grasping (hovering) were detected. Kinematic features based on the reaching phase were extracted in this step, such as maximum speed of reaching, mean speed of reaching, total reaching length, mean peak extension, variability of reaching trajectories and convex hull (see "Behavioral Endpoints" section).

In step (iii), a decision tree was implemented to assess the outcomes of each attempt. As explained in step (ii), we aimed to segment movement in three phases: reaching, grasping and retraction. Forelimb position and direction of movement with respect to the pellet was used by the algorithm to label the outcome of each attempt into four possible categories: miss, no grasp, drop and success (see **Figure 2B**). We used the timestamps for start to reach and hovering/grasping detected in step (ii), to create a decision tree algorithm that labels attempt outcome after the rat reached for the pellet (**Figure 4B**). Starting from the first frame where hovering is detected, the algorithm checks how many objects are detected in the ROI for the next 25 frames (∼0.8 s) or until no objects is detected,

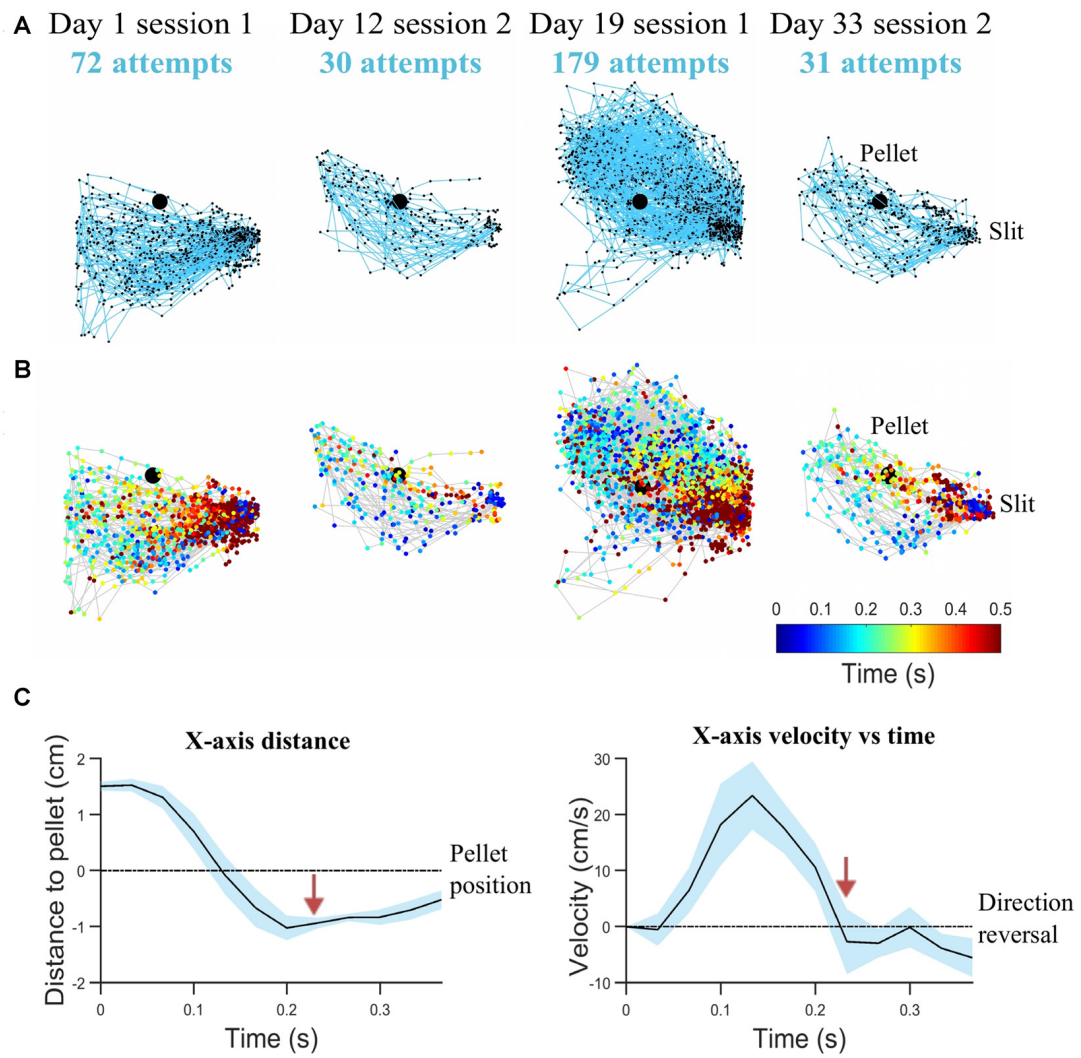

FIGURE 3 | Reaching kinematics. **(A)** Tracked forelimb trajectories capture skill variability. Trajectories of all reaching, grasping and retraction attempts are plotted for a representative rat on start of training (day 1), last test before lesion induction (day 12), first rehabilitation test (day 19), last rehabilitation test (day 33). All trajectory coordinates are normalized with respect to the pellet (represented as the black filled circle). The slit, from which movement is initiated and completed, is indicated on the right-hand side. **(B)** Corresponding spatio-temporal representation for trajectories represented in **(A)**. Each trajectory coordinate is plotted as a colored circle, where the color represents the time from the start of the attempt (see Legend). **(C)** Mean kinematics from a representative rat captured between the start of a reaching attempt and grasping (average over 20 attempts). Shaded regions represent 95% confidence intervals. Transition from reach to hovering phase delineated by red arrows, as velocity decreases. Velocity crossing of zero indicates direction reversal. For clarity, variations of velocity and distance with time are shown with respect to x-axis direction.

meaning the forelimb was completely retracted. Assuming the rat missed the target, the position of the pellet will be unchanged as the forelimb retracts. We excluded a miss when Δ_{Pellet}, the distance between indentation and current pellet position, didn't exceed a value of 0.04 cm. If the rat touches the pellet without grasping it, or grasps it correctly, but drops it while retracting, the pellet will again become visible in the ROI, in a changed position. The algorithm detects a drop if the position of the pellet is within 1 cm away from the slit ($\Delta_{\text{Slit-Pellet}} < 1$). The other cases are taken as a slip. An example of how the algorithm detects a slip is pictured in **Figure 4A**. The algorithm gives a label of success if the pellet is at no time detected in the ROI until the forepaw is completely retracted out of the ROI.

Behavioral Endpoints

All endpoint and kinematic parameters were calculated individually for each animal and for each session.

Task Outcome

As shown in **Figure 2A**, the reaching phase consisted of an extension of the limb within the cage slit and beyond

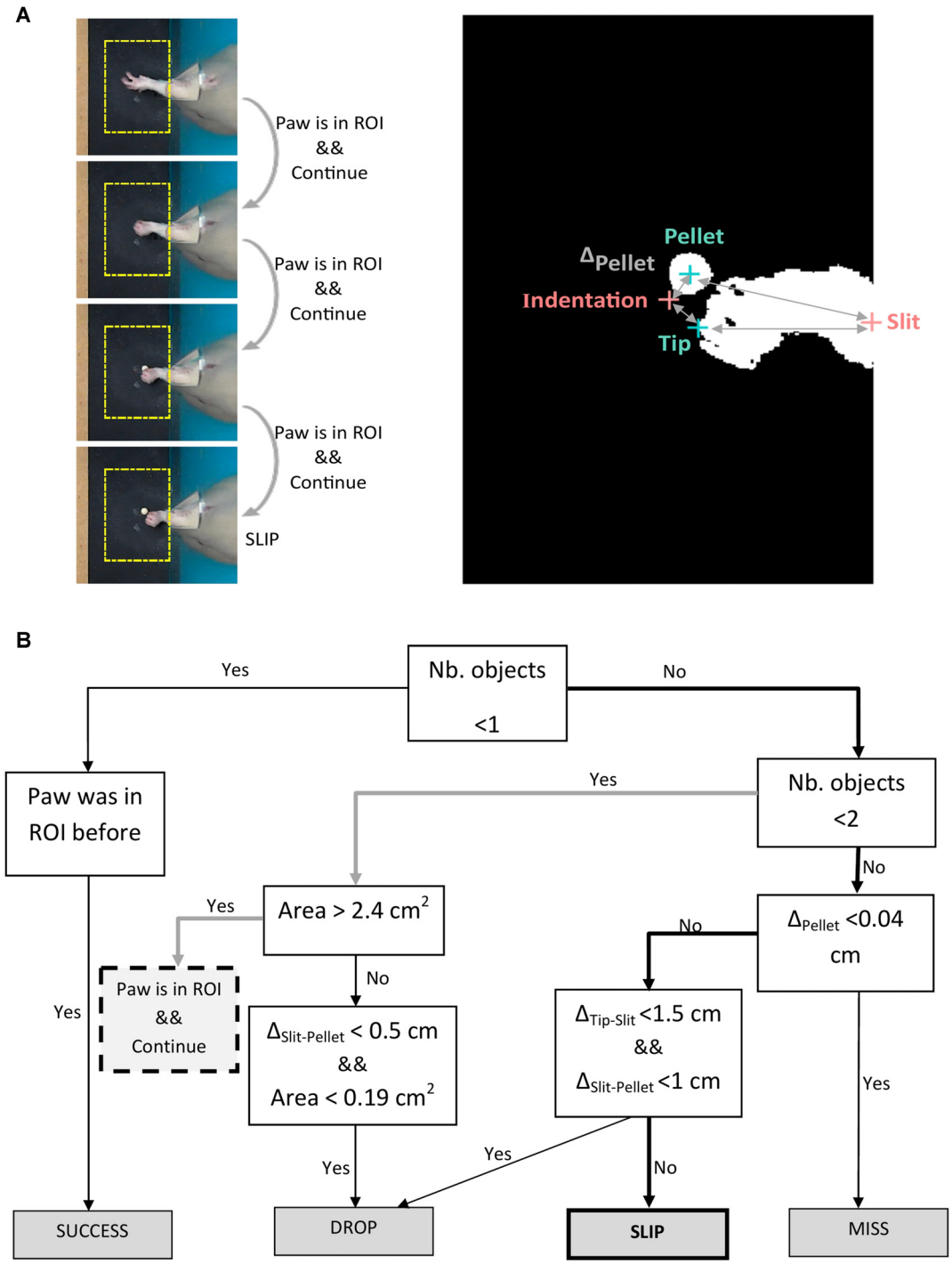

FIGURE 4 | Algorithm for outcome labeling. **(A)** Left panel: example of algorithm decision on four frames succeeding maximum forepaw extension. Right panel: binary image of the frame in which the slip occurs, showing detected objects (forepaw tip, pellet) and fixed landmarks (indentation, slit). **(B)** Decision tree algorithm iterated on the frames succeeding maximum forepaw extension. Description of abbreviations: Δ_{Pellet} = distance between indentation and current pellet position; $\Delta_{Tip\text{-}Slit}$ = distance between forepaw tip and slit; $\Delta_{Slit\text{-}Pellet}$ = distance between pellet and slit.

the position of the pellet. The limb then returned and hovered above the pellet with a decreased speed. Then, the grasping phase occurred. In the retraction phase, the animal returned the forelimb holding the pellet back in the cage. These were the movements captured with our setup. We did not capture behavior inside the cage, e.g., the start of

reaching or the eating of the pellet. However, the phases described were still informative as to the skill of reaching and grasping.

As described in "Behavioral Monitoring" section, the instantaneous position of the forelimb, its velocity profile (speed and direction of the tip of the forelimb) along with the position of the pellet with respect to the indentation allowed us to develop a decision tree algorithm that identified phases of movement and labeled the outcome of the attempt (**Figure 2B**). Based on total number of attempts executed in the session, we calculated miss, slip, drop and success percentages as endpoint measures of one session.

Variability

Dynamic time warping is a distance measure that allows for time shifting and can thus match similar shapes even when they have a time phase difference. Since reaching trajectories were of varying time lengths, we calculated intra-animal variability by using pairwise dynamic time warping distance between all trajectories recorded in one session.

Convex Hull

The convex hull of one training session is the area containing all x-y coordinates tracked during that session. This surface was drawn between the most extreme points of the forelimb coordinates. While variability is a function of time-aligned space coordinates, the convex hull provides solely space information, as it quantifies the spread of the reaching trajectories performed during one session.

Mean and Maximum Speed

Mean speed was averaged during each individual reach, then averaged between all reaches in one session. Maximum speed was taken as the absolute maximum speed achieved between all reaches in one session.

Reaching Length

The length of each reaching trajectory, calculated between the start of the reach and the positioning of the paw above the pellet was taken as the reaching length. All reaching length values were averaged over one session.

Peak Limb Extension

As shown in **Figures 3A,B**, the animals extended their limb beyond the position of the pellet, before returning to grasp it. Peak limb extension is the length of the forelimb at the moment of maximum limb extension. All values were averaged over attempts within one session. While the pasta matrix test directly assesses physical limits of reaching, with the reach-to-grasp test, the pellet is well within the limits of reaching for each rat. Thus, shorter peak limb extensions should not be interpreted as a proof of impairment, since the animal might have a more directed reaching strategy even as an intact subject. However, changes in peak limb extension might signal changes in strategy of reaching, which in turn may reflect compensatory behavior.

Statistical Analysis

Statistical analyses were performed using MATLAB with a significance level $\alpha = 0.05$. To assess the effect of the lesion on performance and the effect of the rehabilitation, we created two groups with the post-lesion data, comprising, respectively, the first six tests after lesion induction (days 19–21) and the last six tests of the rehabilitation (days 31–33). The third set included the six tests recorded pre-lesion (days 9–12) when the rats were well skilled. We compared outcome percentage and kinematic parameters in these three sets using the non-parametric Kruskal-Wallis test with Dunn-Sidak *post hoc* pairwise comparisons. To test linear relationships between kinematic parameters and task outcome, we calculate Pearson coefficient. *P*-values were adjusted with a Bonferroni correction.

RESULTS

Task Outcome

Labeling Accuracy

We assessed accuracy of the labeling algorithm by manually scoring a subset of the videos for each experimental stage: the three acclimation sessions from day 0, before training began, were used together with 38% of videos from training phase (days 1–8) to develop and validate the training set. We included the three acclimation sessions in order to capture more extreme behavior and make the algorithm more robust. To test the algorithm, 33% of videos from pre-lesion tests and 20% of videos of post-lesion testing were used. The percentages are equal for all animals. This allowed us to estimate the rates of predicted labels with respect to actual labels, and the results are presented in confusion matrices (see **Tables 2–4**). The reason for assessing each dataset separately is that the distribution of labels differs from one stage to the next. **Figure 3A** captures the kinematics of impairment after lesion. As seen in **Figure 5**, the animals are very successful in the pre-lesion stage, while exhibiting high percentages of misses or slips in the post-lesion testing. Moreover, since the rats exhibit task-unrelated behavior especially in the beginning of the training period and at the start of the rehabilitation period respectively, we defined an additional

TABLE 2 | Confusion matrix with correctly and incorrectly classified attempts from the training phase (days 1–8).

True class	Miss	**86**	3	0	1	0	96%
	Slip	2	**182**	0	8	0	95%
	Drop	0	2	**18**	5	0	72%
	Success	2	2	4	**163**	2	94%
	Other	1	3	0	4	**20**	71%
							= TPR
		99%	97%	99%	94%	99%	= Specificity
		Miss	Slip	Drop	Success	Other	
		Predicted class					

The algorithm outcome was validated on 38% of videos selected randomly from the training phase. Five labels (N = 509) are correctly classified in 92% of cases. TPR = true positive rate = sensitivity. In bold are the correctly classified instances (true positives).

TABLE 3 | Confusion matrix with correctly and incorrectly classified attempts from the test phase (days 9–11).

True class	Miss	Slip	Drop	Success	Other	
Miss	**11**	2	0	0	0	85%
Slip	1	**49**	0	6	0	88%
Drop	0	0	**10**	1	0	91%
Success	0	1	0	**71**	2	96%
Other	0	4	0	7	**2**	15%
						= TPR
	99%	93%	100%	85%	98%	= Specificity
	Miss	Slip	Drop	Success	Other	
	Predicted class					

The algorithm outcome was validated on 33% of videos selected randomly from the test dataset. Five labels (N = 167) are correctly classified in 86% of cases. TPR = true positive rate = sensitivity. In bold are the correctly classified instances (true positives).

TABLE 4 | Confusion matrix with correctly and incorrectly classified attempts from the rehabilitation phase (days 19–33).

True class	Miss	Slip	Drop	Success	Other	
Miss	**194**	4	1	1	1	97%
Slip	9	**295**	1	8	1	93%
Drop	0	0	**31**	0	0	100%
Success	0	6	4	**117**	6	88%
Other	0	4	0	9	**50**	79%
						= TPR
	98%	97%	99%	97%	99%	= Specificity
	Miss	Slip	Drop	Success	Other	
	Predicted class					

The algorithm outcome was validated on 20% of videos selected randomly from the rehabilitation phase. Five labels (N = 747) are correctly classified in 92% of cases. TPR = true positive rate = sensitivity. In bold are the correctly classified instances (true positives).

label, "Other" for all non-attempt movements captured by the forelimb monitoring algorithm that could be discarded by the labeling routine. These include movements of the forelimb in the region of interest that are not related to or not according to the instructions for the skilled reaching task, like keeping the forelimb stationary on the table, or grasping the pellet straight from the forceps before the experimenter could position it on the indentation. The overall accuracy for development and validation sets was 92% (**Table 2**). Similar accuracy was obtained for the pre-lesion test (86%, **Table 3**) and the post-lesion test (92%, **Table 4**).

Training Phase

Early training sessions exhibited a high number of attempts and high percentages of misses (**Figure 5**). The rats became more successful in locating the pellet and the rate of misses decreased at under 10% in only 3 days of training. The precision of grasping stayed variable between days as slips remain the main type of error the animals made throughout the training period. The percentage of drops was constantly under 5%. Success rate steadily increased with each day of training, and it became the main test outcome in the last 3 days of training at rates of 45%–50%.

Pre- vs. Post-lesion Tests

As seen in the timeline of outcomes from **Figure 5**, a drop in performance after lesion induction occurred, but rats progressively became more successful during the 15 days of post-lesion testing. We compared the rate of misses, slips, drops and success between three phases: days 9–11 when the healthy animals were well skilled for the task, day 19–21, the first on resuming training when the effect of the lesion was most severe, and days 31–33, to test the effect of rehabilitation. The results of the comparisons along with individual data points are summarized in **Figure 6**.

The relative rate of missed attempts increased significantly from $7.2 \pm 6.7\%$ pre-lesion to $50.2 \pm 18.7\%$ post lesion ($p \ll 0.01$) and remained significantly high at $21.6 \pm 9.3\%$ with respect to pre-lesion testing after 15 days of rehabilitation ($p < 0.01$), although it also decreased significantly with respect to the beginning of rehabilitation ($p < 0.01$). The relative rate of slips did not change significantly after lesion induction: $28.1 \pm 13.1\%$ pre-lesion and $31.9 \pm 8.9\%$ post-lesion ($p > 0.05$). However, the rate of slips increased by the end of rehabilitation to $43.63 \pm 8.1\%$, significantly higher with respect to pre-lesion tests ($p \ll 0.01$), and to the start of rehabilitation ($p = 0.02$). There was no significant change in drop percentage, which remained under $5 \pm 3.2\%$ during all three testing phases. The rate of success decreased significantly from a mean of $59.6 \pm 11.8\%$ pre-lesion to $13.9 \pm 8.2\%$ post-lesion ($p \ll 0.01$). Success rate increased to $30 \pm 9.2\%$ at the end of rehabilitation, significantly higher with respect to beginning of rehabilitation ($p = 0.011$) but still significantly below the levels before lesion induction ($p \ll 0.01$). For all outcome labels, no between-animal differences were significant.

Kinematics

As with outcome labels, kinematic features were compared among three phases of the experiment using Kruskal-Wallis test with Dunn-Sidak *post hoc* for pairwise comparisons. Based on observed reaching trajectories, it seems that rats developed individual strategies for reaching, so additionally, we tested in the same way if kinematics can help discriminate between the animals.

Variability

We tested intra-rat variability, finding a significant increase in the beginning of rehabilitation at 11.5% (±3%) from pre-lesion tests, where the mean was 9.2% (±1.6%). By the end of rehabilitation, the mean was 9.2% (±1.1%), similar to that of the pre-lesion tests. Rat 1 exhibited values significantly lower than rats 2 and 3 ($p \ll 0.01$).

Convex Hull

The convex hull increased significantly ($p \ll 0.01$) from 4.2 (±0.6) cm^2 pre-lesion to 6.4 (±1.8) cm^2 post-lesion, but the difference disappeared by the end of rehabilitation, when the mean convex hull was 4.3 (±0.3) cm^2. There were also differences between rats, with rat 1 trajectories (4.1, ±0.8 cm^2) having significantly ($p = 0.03$) lower convex hulls than rats 2

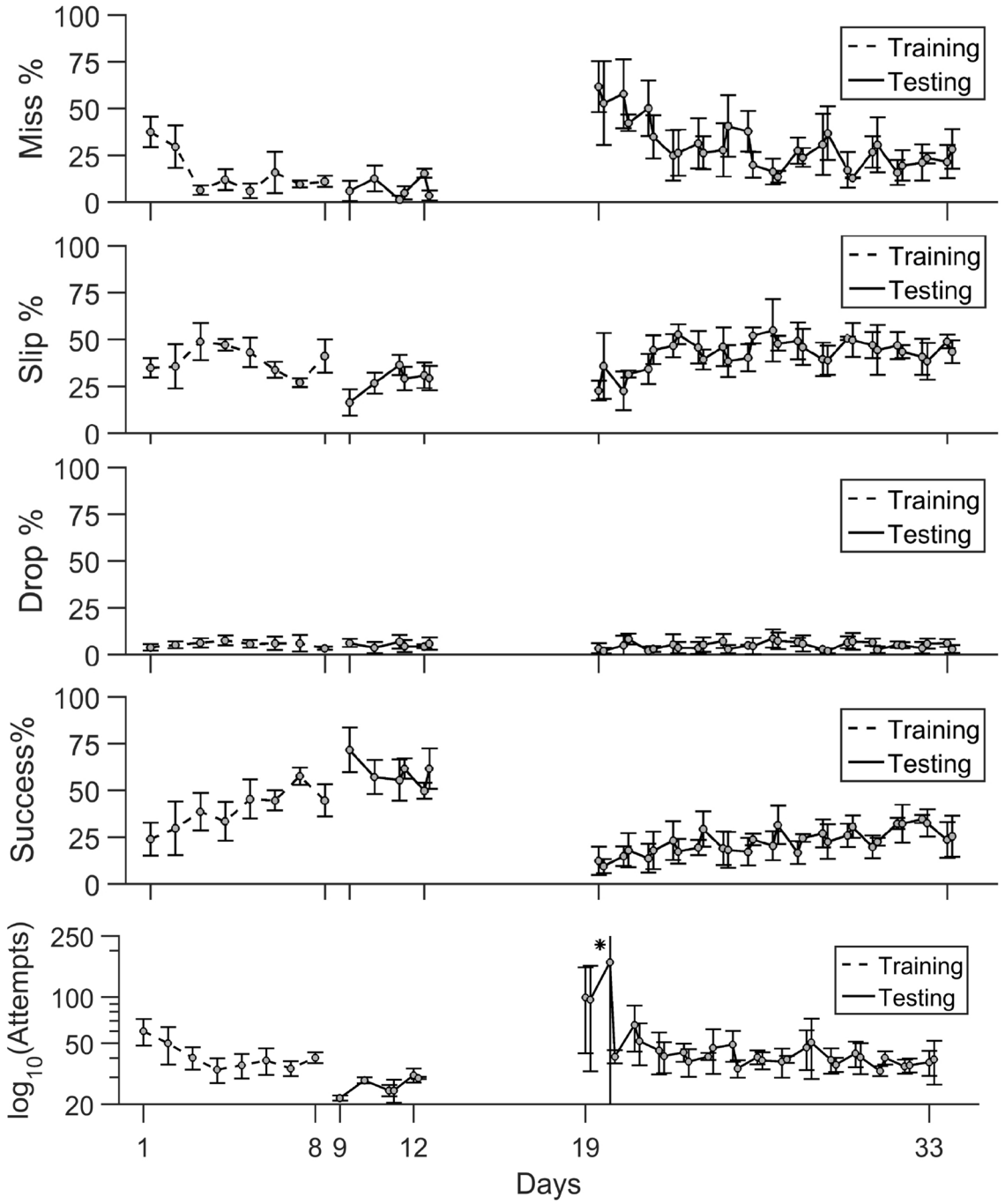

FIGURE 5 | Timeline of task phase outcome. The percentage of misses, slips and drops together with success rate and number of attempts are shown during training (days 1–8), testing (days 9–11) and rehabilitation (days 19–33). Mean values ± standard deviation are shown. (*) In panel (v), the number of attempts is represented on a log scale. The mean value ± standard deviation on day 20 were [8.5 329.5].

(5.1 ± 1.1 cm^2) and 3 (5.6 ± 2 cm^2). There were no differences between rats 2 and 3.

Mean Speed and Maximum Speed of Reaching

Mean speed of reaching decreased at the end of rehabilitation with respect to the start of rehabilitation, but the difference was not significant. There were no significant differences with respect to pre-lesion tests. There were also no significant differences between rats.

Maximum speed decreased significantly ($p = 0.05$) from 45.8 ($\pm$3.5) cm/s pre-lesion to 43.4 ($\pm$4.2) cm/s in the beginning of rehabilitation, but the difference was not significant by the end

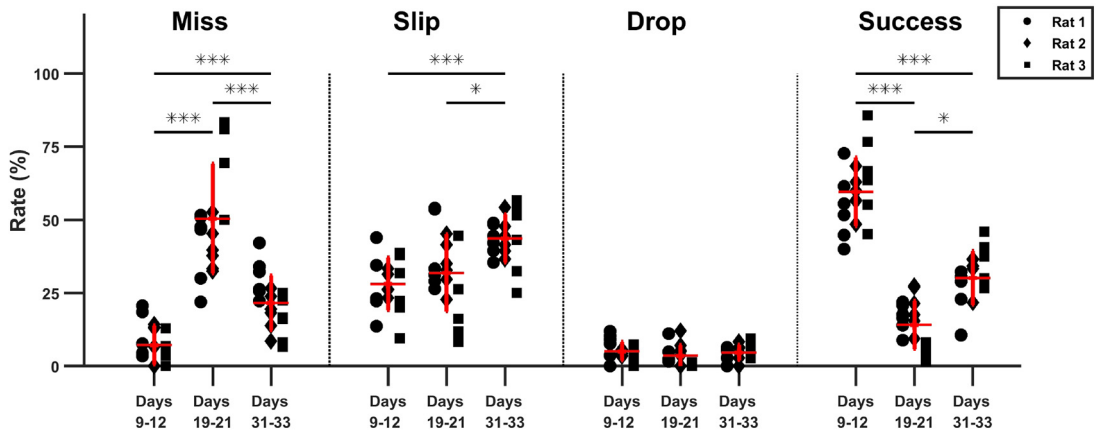

FIGURE 6 | Comparison of task phase outcome. The percentage outcome is compared between pre-lesion testing, the start and the end of rehabilitation (*$p < 0.05$, ***$p < 0.01$).

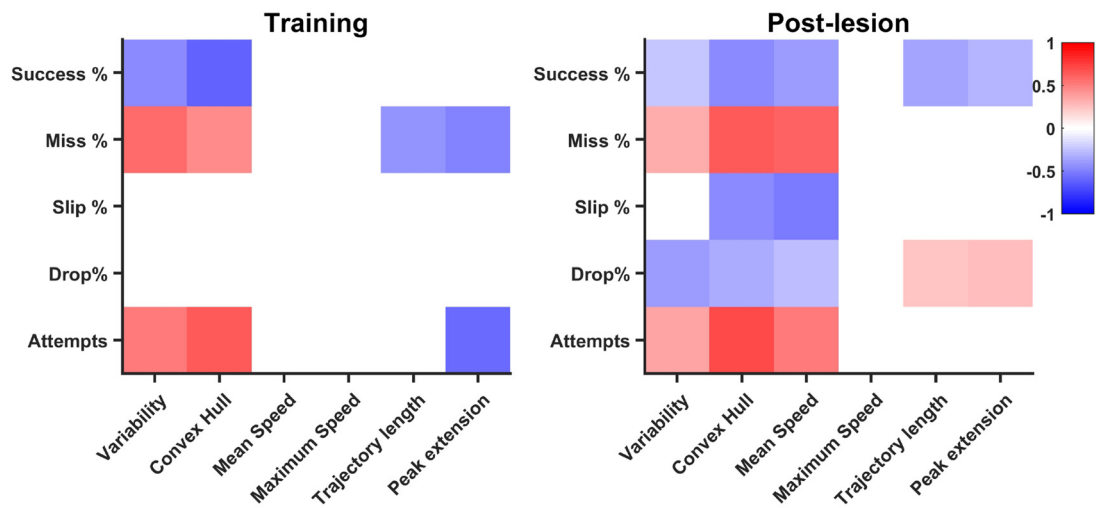

FIGURE 7 | Correlation of endpoint outcome with kinematics. Significant ($p < 0.05$) correlation pairs are represented. The pattern of correlations increases in the post-lesion dataset (days 19–33) with respect to the training phase (days 1–8).

of rehabilitation. Rat 2 had a significantly faster maximum speed ($p < 0.01$) at 46.7 (±3.9) cm/s than rat 3 (42.3 ± 2.2 cm/s), but not rat 1 (43.2 ± 3.5).

Length of Trajectory

Although there were no significant differences in trajectory length (4.17 ± 0.02 cm) between the phases of the experiment, there were significant differences between rats ($p < 0.01$), as rat 2 shows significantly shorter trajectories (3.9 ± 0.3 cm), than rat 1 (4.4 ± 0.3 cm, $p < 0.01$) and rat 3 (4.2 ± 0.3 cm, $p = 0.03$).

Peak Limb Extension

Peak limb extension decreased significantly ($p < 0.01$) in the beginning of rehabilitation (2.8 ± 0.2 cm) with respect to pre-lesion (3.07 ± 0.23 cm) and remained significantly lower ($p = 0.01$) at the end of rehabilitation (2.8 ± 0.18 cm). There were no differences in peak limb extension between animals.

Task Outcome and Kinematics during Training and Rehabilitation

Performance improved in both the training phase and the post-lesion phase, with similar trends, as shown in **Figure 5**: success rate increased as miss percentage lowers, slip is consistently the most prevalent type of mistake, while drop rates are insignificant. To examine if kinematics help explain improvement in task outcome and if the mechanisms for improvement are similar in training and in rehabilitation, we calculated correlations between kinematic features and

behavioral endpoints independently for each phase. We took the Pearson coefficient as a measure of correlation and we set a significance level of $p = 0.05$. All correlation strengths for non-significant pairs of features were subsequently set to zero.

The training phase revealed a number of nine significantly correlated pairs of features, with an increase in the rehabilitation stage to 18 pairs, suggesting overall a different contribution of kinematic features to task success (see **Figure 7**). Number of attempts was positively correlated with variability ($R = 0.51$) and convex hull ($R = 0.65$) in the training phase, a relationship that is maintained during rehabilitation ($R = 0.37$ and $R = 0.72$, respectively). The negative correlation with peak limb extension ($R = -0.58$) during the training phase became insignificant during rehabilitation, while additionally, a positive correlation with mean speed ($R = 0.53$) occurred during rehabilitation. There was a similar trend with miss percentage, where positive correlations with variability ($R = 0.57$) and convex hull ($R = 0.46$) in the training phase were maintained during post-lesion phase ($R = 0.33$ and $R = 0.64$, respectively) during post-lesion phase. Additionally, miss rate was positively correlated with mean speed during rehabilitation ($R = 0.62$). Interestingly, as trajectory length and peak limb extension increase during training, miss percentage decreases ($R = -0.41$ and $R = -0.49$, respectively). These negative correlations were not maintained during post-lesion tests, suggesting that precision of reaching was achieved in different ways in the two phases. While slip rate was not correlated with any kinematic features during training, it was negatively correlated with convex hull ($R = -0.45$) and mean speed ($R = -0.51$) during post-lesion tests. Drop rates were not significantly correlated with any kinematic features during the training phase, but were negatively correlated with variability ($R = -0.38$) and convex hull ($R = -0.32$) in the rehabilitation stage and weakly correlated with trajectory length and peak limb extension ($R < 0.3$). Success rate was negatively correlated with variability ($R = -0.44$) and convex hull ($R = -0.61$) in the training phase, which weakened during rehabilitation ($R = -0.23$ and $R = -0.46$, respectively) and additionally, small negative correlations with mean speed ($R = -0.38$), trajectory length ($R = -0.37$) and peak limb extension ($R = -0.3$) arose during this phase.

DISCUSSION

The present study demonstrates the feasibility of automatically tracking reaching and grasping without additional need of skin markers. Monitoring the forelimb from top-view recordings generated a kinematic profile of movement. Based on it, we developed necessary conditions for the algorithm to segment the task into reaching, grasping and retraction. Top-view monitoring proved sufficient to reliably detect the outcome of the three movement phases and thus distinguish between the following types of errors: miss, slip and drop along with overall task success. The Matlab algorithms were developed on a dataset consisting of training sessions and the overall accuracy achieved on new datasets was of 86% (pre-lesion test set) and 92% (post-lesion test set).

Combinations of front-view and lateral-view cameras (usually infra-red or near-infra-red sensitive), have been used in recent studies to reconstruct 3-D kinematics of reaching and grasping in rodents. While kinematic assessment could be achieved autonomously (using infra-red reflective markers to track the forelimb, in Azim et al., 2014) or semi-autonomously (tracking with machine learning techniques, while segmentation of movement is achieved manually by Guo et al., 2015), these studies didn't extend their automatic tracking to more descriptive measures of movement and no measure of algorithm performance is reported. Lai et al. (2015) used a side-view camera together with a tilted mirror to reconstruct reaching trajectories in a sagittal and coronal plane and extended types of kinematic parameters to characterize reaching, grasping and retrieval, but did not use kinematics to further extend or explain endpoint measures. Esposito et al. (2014) proposed a segmentation of movement and types of errors similar to the one we used, but the forelimb tracking and classification are achieved manually. Two recent studies (Wong et al., 2015; Ellens et al., 2016) developed a fully automated apparatus to perform the pellet test and assess success or failure online.

On the other hand, very detailed, but manually scored qualitative measures have been proposed, either to segment reaching and grasping movement into 10 phases (Whishaw, 2000, 2002; Whishaw et al., 2004), to study individual digit movement (Alaverdashvili and Whishaw, 2008) or types of gestures that arise with impairment (Alaverdashvili et al., 2008). These qualitative approaches are very informative and capture adaptation strategies to induced impairments, but given the burden of manual scoring, they have not been widely adopted. The main findings of these studies point towards decreased wrist rotation, additional adaptive body rotation, decreased individual movement of digits and increase in gestures with impairment, highlighting the role of compensation after neural damage.

In comparison, in our study we developed an algorithm that uses image processing to semi-autonomously reconstruct the kinematics of reaching, which are then further used to gain insight into the quality of movement, by segmenting attempts into three phases of movement. We used one camera placed on top to capture x-y-coordinates of movement (transverse plane). A front view analysis is very difficult to implement with a computer routine, given the lack of contrast between the paw of the rat and its body, both light in color. A side view recording, while offering a better glimpse at the activity of the limb inside the cage, and in the sagittal plane, would miss movement in the transversal plane, which proved very informative in our study. In comparison with most studies cited, we used a rather low sampling rate of 30 Hz. This caused occasional blurring, especially during the reaching phase, when the speed of the forepaw was maximum. However, since we quantified trajectories based on the tip of the paw instead of the centroid, the blurring did not affect the result during the reaching phase. We did not observe blurring during retraction

in the frames we manually quantified for scoring and validating the result of the classification, possibly because the speed of the paw decreases during retraction (**Figure 3C**). Higher sampling rates would also provide more accurate estimates of kinematic features, especially when estimating maximum speed. When the animals move fast, we might be underestimating the distance between two consecutive forelimb coordinates, due to the low frame rate. Since top-view recordings with a rather low sampling rate were sufficient in our study to reach an overall accuracy percentage of 86%–92% in scoring outcome, it would be informative to assess what further information can be extracted from an additional dimension at a higher time resolution, possibly features like rotation of the wrist, which can lead to further movement segmentation and outcome classification.

While using the classical single pellet reaching test setup (Whishaw, 2000), we did not force the rat to execute true grasping rather than dragging the pellet and we also did not distinguish between dragging and grasping with our algorithm. We attempted to quantify grasping by assessing the minor-axis length of the forepaw shape (the width), but this feature didn't prove robust enough (data not shown). However, this strategy may be used robustly if bigger variations in shape width can be captured, for example while testing non-human primates or humans performing similar reaching and grasping tests. Also, while animals exhibited dragging rather than grasping since the training phase, we did not associate dragging with impairment. While not eliminating dragging, detecting it would be possible by increasing the frame rate, which may provide more robust results. In other studies that automatically quantify kinematics of the reach and grasp test, dragging was detected from sagittal plane recordings (Lai et al., 2015). One possibility to eliminate dragging would be a change of experimental setup and such a solution has been proposed by Hays et al. (2013), who developed a novel setup, called the isometric pull task, to quantify both reach-to-grasp dexterity and forelimb strength (Sloan et al., 2015).

Analysis of phase outcome captured disruption in motor skill and prevalence of abnormal behavior, as rates of misses increased seven times between pre- and post-lesion tests. By the end of rehabilitation, the percentage of misses had decreased, but it was still three times higher than in pre-lesion tests. Significant increases of slip percentage during rehabilitation were also observed. A study focused on gesture analysis (Alaverdashvili et al., 2008) reported an increased number of gestures with rehabilitation, related, among other phases, also to reaching towards the pellet and grasping it. It is possible that we captured the same kind of increased abnormal behavior, since such gestures would translate in our study to failures of reaching, miss or failures of grasping, slip. Further analysis is needed to compare the quality of mistakes pre- and post-lesion. Success rates decreased severely after lesion, as reported widely in literature, and increased over the 2 weeks of rehabilitation, but not to the pre-lesion percentages. Our study focused on intra-rat comparisons, but we also tested for differences between animals. Interestingly, no differences were found between rats based on endpoint features. Thus, endpoint performance features are a useful tool to assess error rates and types of errors on a group level. More importantly, the phase analysis revealed which interval of the reaching and grasping movement was more prone to error. Moreover, this study reveals that different phases of movement are problematic in the timeline of recovery. Miss rates, possibly reflecting the inability to control the forelimb so as to aim at a target, are higher in early stages, whereas slips, caused by inexact grasping, dominate error rates in later stages of recovery. Such insight is essential in developing a rehabilitation strategy that targets specific aspects of movement. With further refinements in movement segmentation, this assessment of behavior outcome could be used to gain insight into neural mechanisms of movement acquisition and execution in healthy subjects, or in mechanisms of recovery, in studies focused on motor impairments.

On the other hand, inspection of trajectories clearly shows independence in strategy between animals, findings supported by other studies that focused on kinematic quantification (Esposito et al., 2014; Guo et al., 2015; Lai et al., 2015). Variability, convex hull and maximum speed increase significantly at the start of rehabilitation with respect to pre-lesion. These differences were not significant with respect to pre-lesion values by the end of rehabilitation. In all features except mean speed, significant differences between rats were detected. Thus, kinematics proved much more sensitive to individual differences than endpoint task outcome, even when they could not capture changes in state between pre- and post-lesion behavior. This result further emphasizes the need for individualized rehabilitation strategies, where kinematics and endpoint behavior measures are used jointly to infer what aspects of movement allow improvement in motor performance. Additional features such as curvature of reaching trajectories might provide further insight into individual strategies of completing the task and into how behavior changes with impairment.

While correlation does not necessarily imply causation, it is still informative to compare the general pattern in kinematics and outcome percentages. We found that variability and convex hull decreased as success rates increased, a relationship significant both in learning and rehabilitation, confirming the idea that kinematics stabilize as endpoint performance increases (Kawai et al., 2015). A high number of attempts, mostly ending in a miss, characterize both the beginning of training and that of rehabilitation and this non-structured pattern of searching for the position of the pellet translates kinematically in high trajectory variability and high convex hull. Thus, it is not surprising that the correlation between convex hull, variability and miss rate, number of attempts, stays significant both in training and rehabilitation. Additionally, more significant relationships of lower magnitude develop during rehabilitation. Interestingly, mean speed was correlated with all endpoint features. Based on observation, animals tended to make fast, imprecise movements in the beginning of rehabilitation, which translated to an indirect correlation of mean speed with success and direct correlation with miss rate and number of attempts. However, the indirect correlations with slip and drop rates may

be a by-product of using relative outcome rates. With less misses, the rats proceed further in the task, increasing the probability of making mistakes during further phases, like slips of drops. Thus, we believe further investigations are needed to confirm a true relationship with slip and drop rates. Trajectory length and peak extension decreased with miss and number of attempts in training, an interesting result, suggesting the rats learn to optimize their pellet search with training. This relationship no longer holds in rehabilitation, however, as inverse correlations of trajectory length and peak extension arise with success rate, suggesting optimized pellet search most likely results in overall success. A weak direct correlation of peak limb extension was also found with drop rate, suggesting that longer searches for the pellet, even after a successful grasp, are more likely to result in a drop before the retraction can be successfully completed. Overall, more linear relationships between kinematic parameters and phase outcome arise during rehabilitation, suggesting a change in strategy with respect to training. This is an unsurprising result, since compensation has often been reported as the more prevalent mechanism for achieving improvement after neural damage (Whishaw, 2000; Whishaw et al., 2004; Alaverdashvili and Whishaw, 2008; Alaverdashvili et al., 2008).

Recent review articles assess the important role of compensation in and the lack of features to discriminate it from normal recovery (Kwakkel et al., 2015; Hylin et al., 2017; Jones, 2017). Developing algorithms that can achieve refined detailed behavior description, both robustly and efficiently has become a necessity. Algorithms that assess automatically types of mistakes, not just overall task outcome, together with kinematics of movement may help elucidate the question of what recovery really means and what rehabilitation should focus on: achieving true neural repair and pre-injury behavior quality, or improving ability to adapt to impairments.

CONCLUSION

The present study focused on implementing a detailed evaluation of the classical pellet test in a computer program: (i) we developed an algorithm that automatically tracks the movement of the rat's forelimb using image processing methods; (ii) we expand on existing endpoint behavior features and we assess them along with kinematics of movement, achieving accuracy rates of 86%–92%; (iii) with this extended analysis we captured perturbation of skill after a motor cortical lesion was induced; (iv) analysis of kinematics of movement revealed that rats developed individual strategies to achieve the task; and (v) that learning is distinct from rehabilitation.

AUTHOR CONTRIBUTIONS

IN, MD, BN and J-MA designed the research and wrote or revised the manuscript. IN and MD performed experiments and analyzed the data. IN developed the algorithms.

ACKNOWLEDGMENTS

This study was supported by the Interdisciplinary Research Programs of KU Leuven (IDO/12/024).

REFERENCES

Alaverdashvili, M., Foroud, A., Lim, D., and Whishaw, I. Q. (2008). "Learned baduse" limits recovery of skilled reaching for food after forelimb motor cortex stroke in rats: a new analysis of the effect of gestures on success. *Behav. Brain Res.* 188, 281–290. doi: 10.1016/j.bbr.2007.11.007

Alaverdashvili, M., and Whishaw, I. Q. (2008). Motor cortex stroke impairs individual digit movement in skilled reaching by the rat. *Eur. J. Neurosci.* 28, 311–322. doi: 10.1111/j.1460-9568.2008.06315.x

Azim, E., Jiang, J., Alstermark, B., and Jessell, T. M. (2014). Skilled reaching relies on a V2a propriospinal internal copy circuit. *Nature* 508, 357–363. doi: 10.1038/nature13021

Ellens, D. J., Gaidica, M., Toader, A., Peng, S., Shue, S., John, T., et al. (2016). An automated rat single pellet reaching system with high-speed video capture. *J. Neurosci. Methods* 271, 119–127. doi: 10.1016/j.jneumeth.2016.07.009

Esposito, M. S., Capelli, P., and Arber, S. (2014). Brainstem nucleus MdV mediates skilled forelimb motor tasks. *Nature* 508, 351–356. doi: 10.1038/nature13023

Gharbawie, O. A., Gonzalez, C. L., and Whishaw, I. Q. (2005). Skilled reaching impairments from the lateral frontal cortex component of middle cerebral artery stroke: a qualitative and quantitative comparison to focal motor cortex lesions in rats. *Behav. Brain Res.* 156, 125–137. doi: 10.1016/j.bbr.2004.05.015

Guo, J.-Z., Graves, A. R., Guo, W. W., Zheng, J., Lee, A., Rodríguez-González, A., et al. (2015). Cortex commands the performance of skilled movement. *Elife* 4:e10774. doi: 10.7554/eLife.10774

Hays, S. A., Khodaparast, N., Sloan, A. M., Hulsey, D. R., Pantoja, M., Ruiz, A. D., et al. (2013). The isometric pull task: a novel automated method for quantifying forelimb force generation in rats. *J. Neurosci. Methods* 212, 329–337. doi: 10.1016/j.jneumeth.2012.11.007

Hylin, M. J., Kerr, A. L., and Holden, R. (2017). Understanding the mechanisms of recovery and/or compensation following injury. *Neural Plast.* 2017:7125057. doi: 10.1155/2017/7125057

Jones, T. A. (2017). Motor compensation and its effects on neural reorganization after stroke. *Nat. Rev. Neurosci.* 18, 267–280. doi: 10.1038/nrn.2017.26

Jones, T. A., and Adkins, D. L. (2015). Motor system reorganization after stroke: stimulating and training toward perfection. *Physiology* 30, 358–370. doi: 10.1152/physiol.00014.2015

Kawai, R., Markman, T., Poddar, R., Ko, R., Fantana, A. L., Dhawale, A. K., et al. (2015). Motor cortex is required for learning but not for executing a motor skill. *Neuron* 86, 800–812. doi: 10.1016/j.neuron.2015.03.024

Krakauer, J. W., Carmichael, S. T., Corbett, D., and Wittenberg, G. F. (2012). Getting neurorehabilitation right—what can we learn from animal models? *Neurorehabil. Neural Repair* 26, 923–931. doi: 10.1177/1545968312440745

Kwakkel, G., Veerbeek, J. M., van Wegen, E. E. H., and Wolf, S. L. (2015). Constraint-induced movement therapy after stroke. *Lancet Neurol.* 14, 224–234. doi: 10.1016/S1474-4422(14)70160-7

Lai, S., Panarese, A., Spalletti, C., Alia, C., Ghionzoli, A., Caleo, M., et al. (2015). Quantitative kinematic characterization of reaching impairments in mice after a stroke. *Neurorehabil. Neural Repair* 29, 382–392. doi: 10.1177/1545968314545174

Li, Q., Ko, H., Qian, Z.-M., Yan, L. Y. C., Chan, D. C. W., Arbuthnott, G., et al. (2017). Refinement of learned skilled movement representation in motor cortex deep output layer. *Nat. Commun.* 8:15834. doi: 10.1038/ncomms15834

Paxinos, G., and Watson, C. (2005). *The Rat Brain in Stereotaxic Coordinates.* 5th Edn. San Diego, CA: Elsevier Academic Press.

Schaar, K. L., Brenneman, M. M., and Savitz, S. I. (2010). Functional assessments in the rodent stroke model. *Exp. Transl. Stroke Med.* 2:13. doi: 10.1186/2040-7378-2-13

Sloan, A. M., Fink, M. K., Rodriguez, A. J., Lovitz, A. M., Khodaparast, N., Rennaker, R. L., et al. (2015). A within-animal comparison of skilled

forelimb assessments in rats. *PLoS One* 10:e0141254. doi: 10.1371/journal.pone.0141254

Whishaw, I. Q. (2000). Loss of the innate cortical engram for action patterns used in skilled reaching and the development of behavioral compensation following motor cortex lesions in the rat. *Neuropharmacology* 39, 788–805. doi: 10.1016/s0028-3908(99)00259-2

Whishaw, I. Q. (2002). An endpoint, descriptive, and kinematic comparison of skilled reaching in mice *(Mus musculus)* with rats *(Rattus norvegicus)*. *Behav. Brain Res.* 78, 101–111. doi: 10.1016/0166-4328(95)00236-7

Whishaw, I. Q., Piecharka, D. M., Zeeb, F., and Stein, D. G. (2004). Unilateral frontal lobe contusion and forelimb function: chronic quantitative and qualitative impairments in reflexive and skilled forelimb movements in rats. *J. Neurotrauma* 21, 1584–1600. doi: 10.1089/neu.2004.21.1584

Wong, C. C., Ramanathan, D. S., Gulati, T., Won, S. J., and Ganguly, K. (2015). An automated behavioral box to assess forelimb function in rats. *J. Neurosci. Methods* 246, 30–37. doi: 10.1016/j.jneumeth.2015.03.008

Conflict of Interest Statement: The authors declare that the research was conducted in the absence of any commercial or financial relationships that could be construed as a potential conflict of interest.

Copyright © 2018 Nica, Deprez, Nuttin and Aerts. This is an open-access article distributed under the terms of the Creative Commons Attribution License (CC BY). The use, distribution or reproduction in other forums is permitted, provided the original author(s) or licensor are credited and that the original publication in this journal is cited, in accordance with accepted academic practice. No use, distribution or reproduction is permitted which does not comply with these terms.

frontiers in Integrative Neuroscience

ORIGINAL RESEARCH
published: 27 February 2018
doi: 10.3389/fnint.2018.00008

Large-Scale Brain Networks Supporting Divided Attention across Spatial Locations and Sensory Modalities

Valerio Santangelo [1,2]*

[1]Department of Philosophy, Social Sciences & Education, University of Perugia, Perugia, Italy, [2]Neuroimaging Laboratory, Santa Lucia Foundation, Rome, Italy

Higher-order cognitive processes were shown to rely on the interplay between large-scale neural networks. However, brain networks involved with the capability to split attentional resource over multiple spatial locations and multiple stimuli or sensory modalities have been largely unexplored to date. Here I re-analyzed data from Santangelo et al. (2010) to explore the causal interactions between large-scale brain networks during divided attention. During fMRI scanning, participants monitored streams of visual and/or auditory stimuli in one or two spatial locations for detection of occasional targets. This design allowed comparing a condition in which participants monitored one stimulus/modality (either visual or auditory) in two spatial locations vs. a condition in which participants monitored two stimuli/modalities (both visual and auditory) in one spatial location. The analysis of the independent components (ICs) revealed that dividing attentional resources across two spatial locations necessitated a brain network involving the left ventro- and dorso-lateral prefrontal cortex plus the posterior parietal cortex, including the intraparietal sulcus (IPS) and the angular gyrus, bilaterally. The analysis of Granger causality highlighted that the activity of lateral prefrontal regions were predictive of the activity of all of the posteriors parietal nodes. By contrast, dividing attention across two sensory modalities necessitated a brain network including nodes belonging to the dorsal frontoparietal network, i.e., the bilateral frontal eye-fields (FEF) and IPS, plus nodes belonging to the salience network, i.e., the anterior cingulated cortex and the left and right anterior insular cortex (aIC). The analysis of Granger causality highlights a tight interdependence between the dorsal frontoparietal and salience nodes in trials requiring divided attention between different sensory modalities. The current findings therefore highlighted a dissociation among brain networks implicated during divided attention across spatial locations and sensory modalities, pointing out the importance of investigating effective connectivity of large-scale brain networks supporting complex behavior.

Keywords: divided attention, frontoparietal, central executive, salience, network, independent component analysis (ICA), Granger, causality

OPEN ACCESS

Edited by:
Elizabeth B. Torres, Rutgers University, The State University of New Jersey, United States

Reviewed by:
Britt Anderson, University of Waterloo, Canada
Yifeng Wang, University of Electronic Science and Technology of China, China

Correspondence:
Valerio Santangelo
valerio.santangelo@unipg.it

Received: *21 December 2017*
Accepted: *12 February 2018*
Published: *27 February 2018*

Citation:
Santangelo V (2018) Large-Scale Brain Networks Supporting Divided Attention across Spatial Locations and Sensory Modalities. Front. Integr. Neurosci. 12:8. doi: 10.3389/fnint.2018.00008

INTRODUCTION

It is by now well established that higher-order cognitive processes rely on the interplay between large-scale neural networks (Bressler and Menon, 2010; Raichle, 2015; Wig, 2017). However, how such multiple networks interact to support a complex cognitive process such as divided attention is largely unknown. Divided attention consists in the capability to monitor and select multiple information at the same time (Jans et al., 2010). Previous research has demonstrated that monitoring of multiple streams of information typically results in a decrement of processing efficacy (Shaw and Shaw, 1977; Eriksen and St. James, 1986; Castiello and Umiltà, 1990, 1992; Müller M. M. et al., 2003; Müller N. G. et al., 2003). At a neurophysiological level, divided attention was shown to recruit high-level brain regions, such as the dorsal frontoparietal attention network (Fagioli and Macaluso, 2009, 2016; Santangelo et al., 2010), showing modulatory effects on sensory cortices deputed to process the incoming, multiple information (McMains and Somers, 2004, 2005; Sreenivasan et al., 2014).

However, one limitation of the previous studies devoted to the understanding of the neural correlates of divided attention relies on the use of subtraction paradigms that, by definition, are not sensitive to the co-activation of distinct networks (Friston et al., 1996). As such, less is known to date about whether the neurophysiological underpinnings of divided attention involve a dynamical interplay between multiple networks. Based on the re-analysis of previous data (Santangelo et al., 2010, reporting standard fMRI analyses), the current study aims at highlighting large-scale brain networks involved with divided attention, and more specifically, with divided attention across different spatial locations vs. different stimuli and sensory modalities. Attentional resources can be employed to monitor for a given stimulus that might appear from different locations (divided attention across multiple locations) or to monitor for different stimuli originating from the same spatial locations (divided attention across multiple stimuli). In this latter case, the stimuli to be monitored might come from the same or different sensory modalities, e.g., visual or auditory.

Previous research (Fagioli and Macaluso, 2009) reported that the dorsal frontoparietal attention network (encompassing the frontal eye-fields (FEF) and the intraparietal sulci (IPS), bilaterally) activated both when subjects divided attention across different spatial locations and across simultaneously presented visual stimuli (e.g., geometrical shapes of different colors). Fagioli and Macaluso (2009) interpreted these findings as suggesting a key role played by the dorsal frontoparietal network both for spatial and non-spatial divided attention. This might also indicate the existence of an interplay between divided attention and working memory, with increased working memory load when trying to monitor multiple visual stimuli at different locations, supported by frontoparietal regions (e.g., see for review Smith and Jonides, 1999; D'Esposito, 2001; see also Johnson and Zatorre, 2005, 2006; Johnson et al., 2007). However, following research (Santangelo et al., 2010) showed that dividing attention between two sensory modalities depended on the spatial distribution of attention, unlike monitoring two stimulus categories in the visual unisensory context. In fact, the behavioral cost of monitoring two vs. one sensory modality was shown to decrease when paying attention to two vs. one hemifield. These findings suggest that there is higher interference (greater behavioral costs) in monitoring two independent sensory modalities when attention is focused on a given spatial location as compared to multiple spatial locations. Overall, this suggests greater availability of processing resources when attending for different sensory modalities at different spatial locations. The more efficient performance in monitoring two modalities at separated locations compared to the same location was found to be supported by the posterior nodes of the dorsal frontoparietal network, namely the posterior parietal cortex, which might provide additional processing resources under this condition (Santangelo et al., 2010). This specific interplay between spatial- and sensory-related factors might indicate that—at least in multisensory contexts—divided attention across different spatial locations or sensory modalities might be subserved by different brain networks.

In the current study participants were asked to monitor streams of visual and/or auditory stimuli in one or two spatial locations for detection of occasional targets. This experimental design allowed contrasting conditions in which participants monitored one stimulus/modality (either visual or auditory) in two locations, i.e., the left and right hemifields ("att2loc") vs. conditions in which participants monitored two stimuli/modalities (both visual and auditory) in one location ("att2mod"). The analysis of the independent components (ICA) was used to highlight any large-scale brain network operating during divided attention across spatial locations vs. sensory modalities. Based on the existent literature (Fagioli and Macaluso, 2009, 2016; Santangelo et al., 2010; Santangelo and Macaluso, 2013a), there might be expected a main involvement of the frontoparietal network during divided attention tasks, but also brain differences related to the specific interplay between spatial- and sensory-related factors in multisensory contexts (see, Santangelo et al., 2010) during divided attention over different spatial locations or sensory modalities. To investigate the specific contribution of regions within the ICs supporting either divided attention across spatial locations or sensory modalities Granger Causality Analysis (GCA) was employed. This allowed to assess any causal relationships (i.e., the effective connectivity) among the main nodes of the emerging ICs.

MATERIALS AND METHODS

Participants

Thirteen right-handed healthy volunteers took part in the study. All participants had normal hearing and normal or corrected-to-normal visual acuity (with contact lenses). Because of poor accuracy on the task (<75%), one participant was excluded from statistical analysis, leaving 12 participants (6 males, age range: 20–33 years, mean age: 25.2 years). The independent Ethics Committee of the Santa Lucia Foundation (Scientific Institute

for Research Hospitalization and Health Care) approved the study. Participants gave written informed consent before their participation.

Stimuli and Task

Stimuli and task were fully described in Santangelo et al. (2010), where we performed standard univariate analyses of this data set. Briefly, the participants' task was to detect visual and/or auditory targets (i.e., one or two target modalities) in either or both hemifields (i.e., one or two target locations). During fMRI scanning, participants viewed a central display via a mirror system (see **Figure 1A**). Through the display, participants were presented with visual instructions regarding the upcoming attention task and with a central fixation cross (1.2° × 1.2°), which was displayed throughout the task. During the task participants were present with four simultaneous streams of stimuli, that is, a visual and an auditory stream on each hemifield. Two rubber pipes conducting sounds (i.e., bursts of white noise, sound pressure level, SPL = 115 dB) from two loudspeakers placed outside the MR room were used to present the auditory stimuli. The pipes were horizontally aligned with the fixation cross and connected to the left and right side of the coil. Participants were presented with either single (duration = 160 ms) or double bursts (160 ms on, 160 ms off, 160 ms on), with the latter serving as to-be-detected targets, when presented in the to-be-attended auditory stream. Optical fibers (diameter = 1 mm) connected with yellow light emitting diode (LED; luminance = 30 cd/m^2) were instead used to present visual stimuli. Each optical fiber was located into a rubber pipe: this procedure allowed delivering visual and auditory stimuli from approximately the same locations, that is, around 30° to the left and right of central fixation point. As for the auditory stimuli, single (duration = 160 ms) and double flashes (160 ms on, 160 ms off, 160 ms on) were presented, with the latter serving as targets when delivered in the to-be-attended visual stream. Notably, the amount of stimulation was identical on both hemifields, with visual and auditory stimuli presented concurrently, regardless of the selective attention task that participants had to carry out.

The four simultaneous streams were presented in blocks of 25 s, corresponding to 10 consecutive trials. At the beginning of each block an instruction display indicating the location(s) and modality(ies) to be monitored was presented to the participants. The instruction display (duration = 3 s) included the text string "Instruction", plus one or two letters on the left and/or right side ("V" for "monitor vision" and "A" for "monitor audition"). The arrangement of letter(s) and position(s) provided the relevant side and modality to be monitored in that block of trials (see **Figure 1A**). According to the instruction, the participants performed one of four possible attention tasks: (1) attend to one single modality in one hemifield, that is, detect either visual or auditory target in either the left or the right hemifield; (2) attend to one single modality in both hemifields, that is, detect either visual or auditory targets in both the right and left hemifield; (3) attend to both modalities in the same hemifield, that is, detect both visual and auditory targets in either the left or right hemifield and (4) attend to one modality in one hemifield, and the other modality in the opposite hemifield, that is, detect visual targets in the left hemifield and auditory targets in the right hemifield or vice versa. According to the main aim of the current study, here we directly compared task 2 vs. task 3, involving, respectively, "divided attention across two spatial locations" (att2loc) and "divided attention across two sensory modalities" (att2mod).

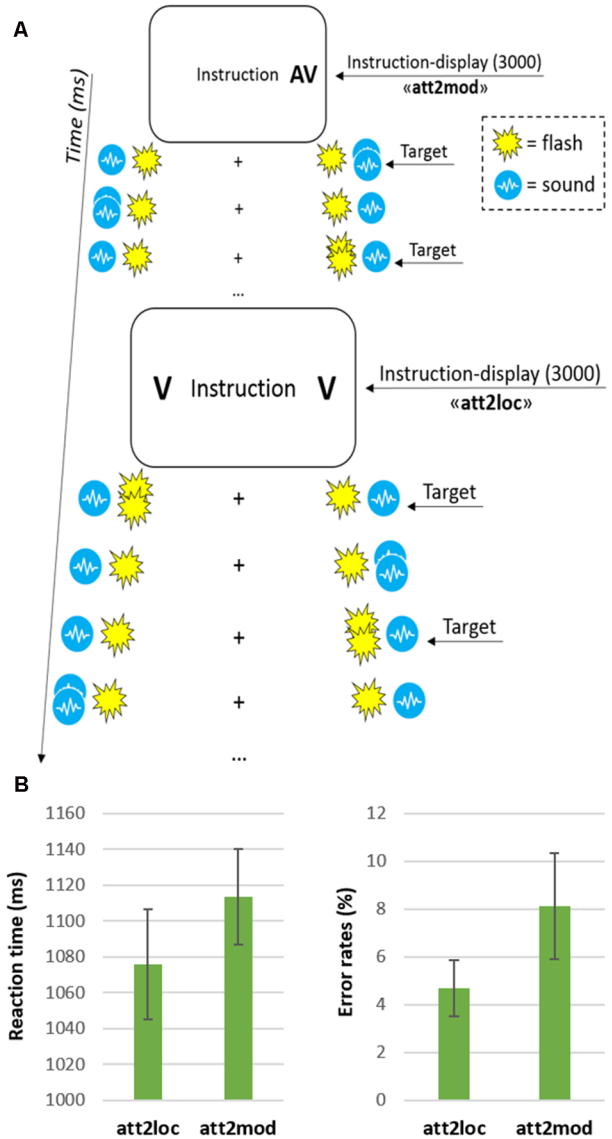

FIGURE 1 | (A) Schematic diagram showing from top to bottom an example of a few trials in the "attending two modalities" (att2mod) and "attending two locations" (att2loc) conditions. Each block consisted of 10 trials and began with an instruction display signaling the current task. On each trial, the stimulation was always bilateral with two independent audiovisual streams on each side. Depending on the current condition, participants monitored one or two of the four sensory streams in one or two hemifields, responding to double pulses (i.e., the targets) in the relevant stream/streams while ignoring all other stimuli; **(B)** Reaction times (left graph) and error rates (right graph) for the two main conditions (att2loc and att2mod). The error bars represent the standard error of the means.

Participants task consisted in the detection of visual (double flashes) and/or auditory (double bursts) targets in one of the currently attended streams, while ignoring all the stimuli in the currently irrelevant streams. Participants signaled target detection by pressing a response button with their right index-finger. Each block included 10 trials, which started 2000 ms after the offset of the instruction display. Every 2500 ms a new trial started. The sequence of trials entailed two constraints: First, two target stimuli were never presented in the same trial when participants had to monitor for multiple streams. Second, there were always five targets in each currently relevant stream. Participants underwent four fMRI runs, each lasting about 6 min. Each run included 12 blocks, i.e., four tasks repeated three times. Overall, each participant was therefore presented with an amount of 480 trials, that is, 120 repetitions for each of the four attention tasks.

fMRI Methods

Image Acquisition

A Siemens Allegra (Siemens Medical Systems, Erlangen, Germany) operating at 3T and equipped for echo-planar imaging (EPI) was used to acquire the functional magnetic resonance images. A quadrature volume head coil was used for radio frequency transmission and reception. Head movement was minimized by mild restraint and cushioning. Thirty-two slices of functional MR images were acquired using blood oxygenation level-dependent imaging (3×3 mm, 2.5 mm thick, 50% distance factor, repetition time = 2.08 s, time echo = 30 ms), covering the entirety of the cortex.

Image Processing

I used SPM12 (Wellcome Department of Cognitive Neurology) implemented in MATLAB R2012b (The MathWorks Inc., Natick, MA, USA) for data preprocessing and GLM. Each participant underwent four fMRI-runs, each comprising 477 volumes. After having discarded the first four volumes of each run, all images were corrected for head movements. Slice-acquisition delays were corrected using the middle slice as reference. All images were normalized to the standard SPM12 EPI template, resampled to 2 mm isotropic voxel size, and spatially smoothed using an isotropic Gaussian kernel of 8 mm FWHM. Time series at each voxel for each participant were high-pass filtered at 220 s and pre-whitened by means of autoregressive model AR(1).

Independent Component Analysis

The main aim of the current study was to highlight any large-scale brain network involved with divided attention across multiple spatial locations and sensory modalities. These brain networks were identified by the ICA. ICA is a blind-source computational method for separating a multivariate signal into additive subcomponents. The main assumption is that each subcomponent is statistically independent from each other. ICA was here implemented by means of the "Group ICA of fMRI Toolbox" (GIFT; Calhoun et al., 2001, 2009). This method involves performing ICA on functional data concatenated over every participant, creating a series of spatial maps and associated time courses for the group. The number of components was estimated to be 24 using the minimum description length criteria. The infomax algorithm was repeated 20 times with randomly initialized decomposition matrices and the same convergence threshold using ICASSO approach in GIFT (Himberg et al., 2004). As a finite set of data never result in exactly the same ICA model, ICASSO was introduced to estimate the overall reliability of the generated components. Back reconstruction was then used to create individual time courses and spatial maps from each participant's functional data. Based on the spatio-temporal characteristics of each identified independent component (IC), 12 components reflecting noise were discarded after careful visual inspection (see **Supplementary Figure S1** and Beckmann, 2012), leaving 12 components for further analyses.

Identification of Independent Components Related to Divided Attention

ICs with time courses related to the experimental design were identified using multiple regressions and the temporal sorting feature of the GIFT toolbox. Individual performance at the two main attention tasks was modeled with SPM12. Single subject models comprised two regressors, one including the onsets of "att2loc" blocks and the other including the onsets of "att2mod" blocks, plus a covariate of no interest including the onsets of the remaining blocks of trials (i.e., task 1: Attend to one single modality in one hemifield, and task 4: Attend to one modality in one hemifield, and the other modality in the opposite hemifield). All blocks were modeled with a duration of 25 s, i.e., 10 trials by 2500 ms each, time locked at the onset of the first trial of the block. The onsets of instruction displays were also included in the multiple regression model as covariates of no interest, with a duration of 5 s. All predictors were convolved with the SPM12 hemodynamic response function.

We tested the significance of the component time courses by doing statistics on the beta weights obtained after the temporal sorting, using the "Stats on Beta Weights" GIFT utility. Specifically, this utility allowed to assess the temporal fitting of the time course of a given IC with the events modeled with SPM. In accordance with the main aim of the current study, we assessed which component was involved with divided attention across spatial locations, by testing "att2loc > att2mod", and with divided attention across sensory modalities, by testing "att2mod > att2loc", by means of two-tailed paired *t*-tests. Holm-Bonferroni's correction was applied to account for the risk of increased false positives as a function of an increased number of ICs tested (Gaetano, 2013). This procedure enabled to highlight two different brain networks, one operating during divided attention across space (IC 8), and the other operating during divided attention across sensory modalities (IC 15; see **Table 1**).

Granger Causality Analysis

The effective connectivity among the main nodes of ICs supporting divided attention across spatial locations and sensory modalities was then assessed. While "functional"

TABLE 1 | Two-tailed paired *t*-tests assessing the involvement of independent components (ICs) with "att2loc > att2mod", denoted by positive *t*-values, and with "att2mod > att2loc", denoted by negative *t*-values, showing the involvement of IC 8 and IC 15, respectively.

IC	*t*-value	*p*-value
2	2.11	0.295
3	−1.64	0.427
5	−2.77	0.163
7	3.12	0.098
8	4.59	0.008
9	−1.76	0.427
11	2.45	0.225
13	−0.95	0.693
14	2.33	0.240
15	−5.79	0.001
18	0.98	0.693
23	−2.67	0.175

P-values are corrected by Holm-Bonferroni's procedure for multiple comparisons.

connectivity allows assessing the co-variation between two or more neurophysiological measures (i.e., time-series) without providing any information about directionality or causality, "effective" connectivity allows investigating which time-series is causing which other, thus drastically reducing the possibility of alternative interpretations (Stephan and Roebroeck, 2012). To investigate the effective connectivity among IC nodes GCA was used. CGA has the advantage with respect to other effective connectivity measures (e.g., dynamic causal modeling, DCM) of not requiring any *a priori* knowledge about within-network connectivity (Friston et al., 2013).

CGA is based on the notion that, if a time-series "X" causes a time-series "Y", then knowledge of X should improve the prediction of Y more than information already in the past of Y. GCA allows computing causality by comparing the variance of the residuals after an autoregressive (AR) application to the reference signal Y, with the same variance obtained when autoregression is evaluated by combining both the past values of the signal Y and the past values of the potentially causing signal X. Previous literature has already demonstrated that CGA is a viable technique for analyzing fMRI time-series (Barnett and Seth, 2011; Seth et al., 2013; Wen et al., 2013) and that provides results that are consistent with other effective connectivity measures (i.e., DCM; Bajaj et al., 2016). We therefore modelled directional causality among multiple time series using GCA, as implemented in the "Multivariate Granger Causality Toolbox" (MVGC; Barnett and Seth, 2014; see also Seth, 2010).

As showed in **Figure 2**, the IC 8 that was selectively involved during divided attention across spatial locations (att2loc > att2mod) included bilateral regions of the posterior parietal cortex and left regions of prefrontal cortex (see "Results" section below). On the other hand, IC 15 that was selectively involved with divided attention across sensory modalities (att2mod > att2loc), included both regions belonging

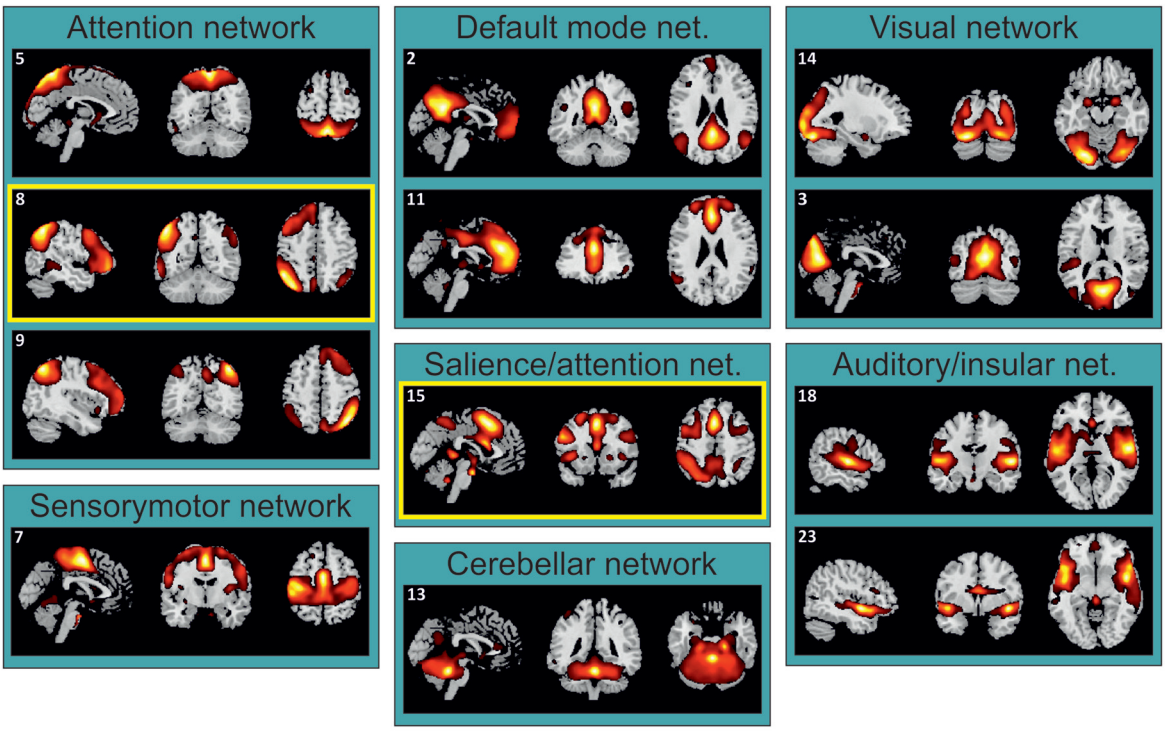

FIGURE 2 | Task-related independent components (ICs) grouped according to their functional similarity. IC 8 and IC 15, supporting divided attention across space and sensory modalities, respectively (see **Table 1**), were highlighted by yellow boxes.

TABLE 2 | MNI coordinates of areas selected as regions of interest (ROI) in the IC 8 and IC 15, supporting divided attention across space and sensory modalities, respectively.

Divided attention across space (IC 8)			
Area	***x***	***y***	***z***
L DLPFc	−50	10	30
L VLPFc	−56	18	8
L IPL	−48	50	54
R IPL	46	−48	52
L Ang	−42	−66	48
R Ang	54	−60	38
Divided attention across modalities (IC 15)			
Area	***x***	***y***	***z***
ACC	−2	14	42
L aINS	−30	24	−4
R aINS	36	22	−2
L FEF	−28	2	58
R FEF	30	2	58
L IPS	−34	−48	46
R IPS	34	−46	48

The time courses of the bold signal originated from these ROIs were used for the Granger causality analysis. Note: DLPFc, dorsolateral prefrontal cortex; VLPFc, ventrolateral prefrontal cortex; IPL, inferior parietal lobule; Ang, angular gyrus; ACC, anterior cingulate cortex; aIC, anterior insular cortex; FEF, frontal eye-fields; IPS, intraparietal sulcus.

to the dorsal frontoparietal network and regions belonging to the salience network. Accordingly, these areas (see **Table 2**) were selected as regions of interest (ROI) for the GCA. Each ROI consisted of a sphere (diameter = 8 mm, matching the FWHM of the smoothing filter) centered on the peak of activity of the regions belonging to IC 8 and IC 15 (**Table 2**). MarsBar SPM toolbox (v. 0.44) was used to extract and average time series from single subject designs within each ROI. Holm-Bonferroni correction was applied to account for the risk of increased false positives as a function of an increased number of comparisons across the nodes of the ICs tested.

RESULTS

Behavioral Data

The analysis of the behavioral performance—illustrated in **Figure 1B**—revealed that participants made more errors (including both false alarms and missed responses) when monitoring two sensory modalities (mean = 8.1%) compared with two spatial locations (4.7%; two-tailed paired *t*-test: $t_{(11)} = 2.9$, $p = 0.015$). Despite only marginally significant, the RT data were consistent with the latter finding, with slower target detection when participants monitored two sensory modalities (1114 ms) compared with two spatial locations (1076 ms; $t_{(11)} = 2.1$, $p = 0.059$; see, for extended behavioral results, Santangelo et al., 2010).

fMRI Data

The ICA identified 24 ICs. Twelve of these ICs were unnoisy and related to the main attention tasks (**Figure 2**). Each of these ICs was attributed to a particular network on the basis of the previous literature (e.g., Damoiseaux et al., 2006; Shirer et al., 2012). These components were further analyzed in order to highlight which of them underlies divided attention across spatial locations and divided attention across sensory modalities.

Divided Attention across Spatial Locations: ICA and GCA

Trials requiring dividing attention across the two hemifields involved the selective contribution of IC 8, as revealed by the analysis of beta weights that contrasted "att2mod > att2mod" (see **Table 1**). IC 8 included several regions of the posterior parietal cortex, extending from the inferior parietal lobule (IPL) to the angular gyrus (Ang), bilaterally. This component also included regions of the prefrontal cortex, but only on the left hemisphere, namely the left dorsolateral prefrontal cortex (DLPFc) and the left ventrolateral prefrontal cortex (VLPFc; see **Figure 3A** and **Table 2**).

The effective connectivity among these regions was investigated with GCA (**Figure 3B** and **Table 3**). Significant causal relationships were observed at both intra-regional (i.e., within the prefrontal and within the posterior parietal cortex) and inter-regional level (i.e., prefrontal/posterior parietal effective connectivity). This causal relationships are schematically illustrated in **Figure 3C**. Mutual causality was observed between the dorsolateral and ventrolateral regions of the prefrontal cortex. Similarly, an high level of mutual causality was observed within the posterior parietal cortex, although this was mainly driven by the left and right IPL, which were found to predict the activity of the left and right Ang. At the inter-regional level, the prefrontal regions were found to significantly predict the activity of the posteriors parietal nodes. In fact, both the DLPFc and the VLPFc showed causal relations with each single node of the posterior parietal cortex (see cyan lines in **Figure 3C**). By contrast, the posterior parietal cortex showed overall a reduced causal influence of the prefrontal nodes. This was evidenced by the fact that only the right IPL and the left Ang showed causal relations with the left DLPFc and the VLPFc, respectively, and that these two latter connections were bi-directional, i.e., not indicating any specific causal influence of the posterior parietal over the prefrontal nodes during trials requiring divided attention across different spatial locations.

Divided Attention across Sensory Modalities: ICA and GCA

The analysis of beta weights revealed that IC 15 was selective involved with events requiring to divide attention across stimuli originated from different sensory modalities ("att2mod > att2loc"; see **Table 1**). IC 15 included regions belonging to the dorsal frontoparietal network (Corbetta and Shulman, 2002; Corbetta et al., 2008; Duncan, 2013), such as the FEF and the IPS, bilaterally. IC 15 also included regions belonging to the salience network (Menon and Uddin, 2010; Uddin, 2015), such as the anterior cingulate cortex (ACC) and the anterior insular cortex (aIC), bilaterally (see **Figure 4A** and **Table 2**).

As before, the effective connectivity among these regions was analyzed with GCA (**Figure 4B** and **Table 4**). Extensive intra- and

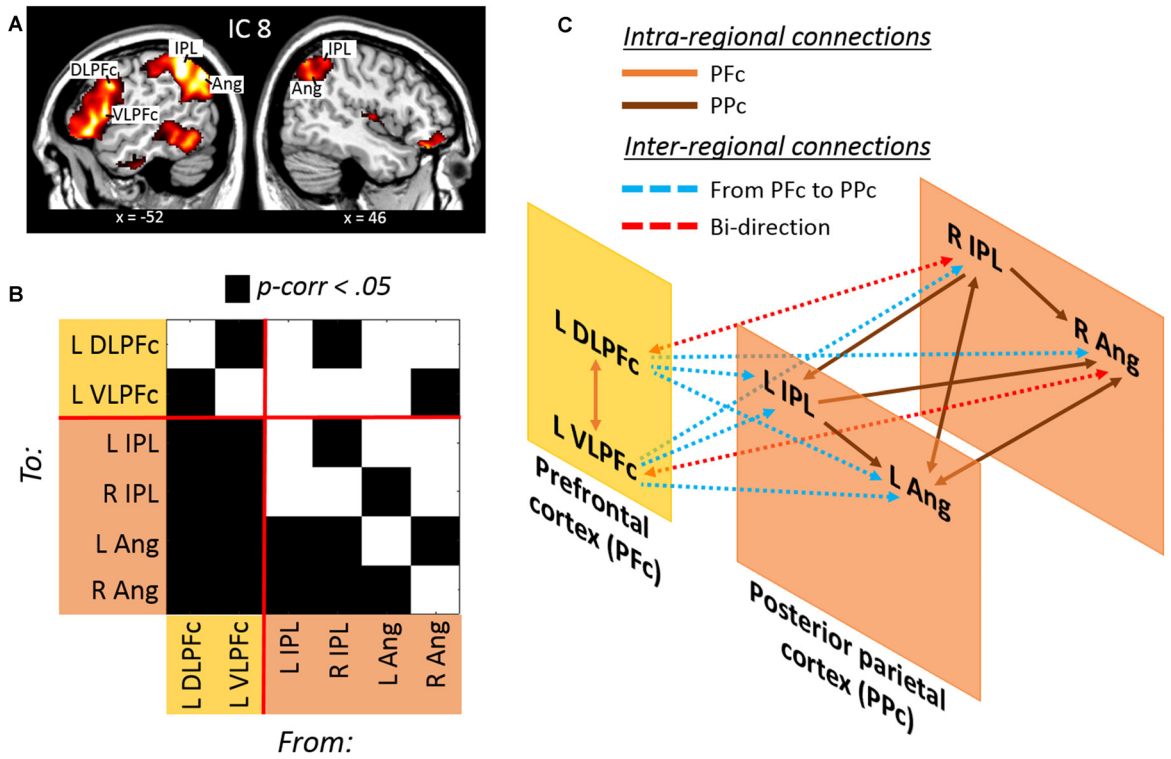

FIGURE 3 | (A) Lateral prefrontal and posterior parietal regions derived from the IC no. 8 involved with divided attention across space. **(B)** Results of the Granger Causality Analysis (GCA) highlighting **(C)** a model of effective connectivity between prefrontal and posterior parietal regions. The model illustrates a prefrontal over posterior parietal control during divided attention across space (see the main text for further details).

inter-network causal relationships were observed, and these are schematically illustrated in **Figure 4C**. In the salience network, each of the three nodes showed mutual causal relationships with each of the other nodes. Similarly, mutual causality relations were observed among the nodes of the dorsal frontoparietal network, with the exception of the left IPS that did not predicted activity in the left and right FEF. At inter-network level, the GCA showed a number of mutual causal relationships between the dorsal frontoparietal and the salience network, highlighting a tight interdependence between these two networks. This was exemplified by the seven red lines in **Figure 4C**. By contrast, the GCA showed only a few uni-directional causal relationships from the dorsal frontoparietal to the salience network (two yellow lines) and from the salience to the dorsal frontoparietal network (three purple lines).

DISCUSSION

The current study aimed at characterizing large-scale brain networks supporting divided attention by re-analyzing previously reported fMRI data (Santangelo et al., 2010). Consistent with standard fMRI analyses reported by the previous literature (Fagioli and Macaluso, 2009, 2016; Santangelo et al., 2010; Santangelo and Macaluso, 2013a), the current study found that divided attention was sustained by regions belonging to the frontal and parietal cortices. However, the current data-driven approach based on ICA and CGA also revealed novel findings compared to the previous literature. Specifically, important differences were observed depending on whether attentional resources were divided across different spatial locations or different sensory modalities, which is in agreement with the

TABLE 3 | Holm-Bonferroni's corrected *p*-values derived from the Granger causality analysis carried out among the nodes of the ICs no. 8 (see also **Figure 3B**).

To:	L DLPFc	—	0.000	0.090	0.000	0.350	0.195
	L VLPFc	0.000	—	0.456	0.209	0.456	0.008
	L IPL	0.000	0.000	—	0.000	0.063	0.448
	R IPL	0.000	0.000	0.116	—	0.000	0.090
	L Ang	0.001	0.000	0.000	0.021	—	0.000
	R Ang	0.004	0.000	0.000	0.000	0.000	—
		L DLPFc	L VLPFc	L IPL	R IPL	L Ang	R Ang
				From:			

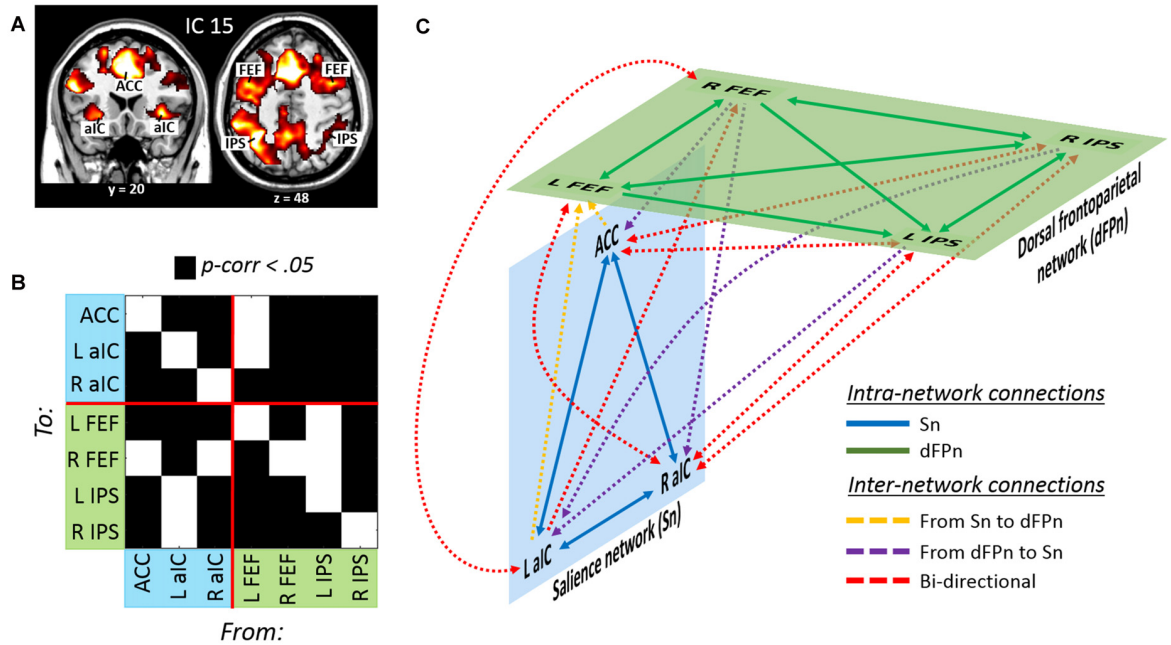

FIGURE 4 | (A) Dorsal frontoparietal, anterior cingulate and insular regions derived from the IC no. 15 involved with divided attention across sensory modalities. **(B)** Results of the GCA highlighting **(C)** a model of effective connectivity between the nodes of the dorsal frontoparietal and the salience network. Overall, the model illustrates a tight interdependence between the two networks during divided attention across sensory modalities (see the main text for further details).

current behavioral data showing decreased performance when participants had to monitor both visual and auditory streams compared to when they had two monitor both the left and right hemifield.

As revealed by the ICA, dividing attentional resources across two spatial locations necessitated the recruitment of a brain network involving the left ventro- and dorso-lateral prefrontal cortex, plus the posterior parietal cortex, including the IPS and the angular gyrus, bilaterally (IC 8, **Figure 3A**). There is by now a large consensus about the key role played by the posterior parietal cortex in spatial-related tasks. In fact, the posterior parietal cortex has been associated with spatial attention (Corbetta et al., 2000; Yantis et al., 2002; Vandenberghe et al., 2005; Molenberghs et al., 2007; Kelley et al., 2008; Nardo et al., 2011, 2014), as well as with the storage of spatial information in working memory (Munk et al., 2002; Leung et al., 2004; Xu and Chun, 2006; Santangelo and Macaluso, 2013b; Santangelo et al., 2015; see also, for reviews, Zimmer, 2008; Santangelo, 2015). The lateral prefrontal cortex is instead thought to be deeply implicated in executive control (see, for reviews, Yuan and Raz, 2014; Koechlin, 2016) and to play a central role in strategic monitoring during working memory processes (see, for a review, Sreenivasan et al., 2014). While the posterior parietal cortex has been shown to be centrally involved with the maintenance of spatial representation, the activation of the lateral prefrontal cortex has been more related to the control of the information that is actually maintained in the posterior parietal cortex (Champod and Petrides, 2007). Consistently, several recent studies demonstrated that neural populations in the lateral prefrontal cortex can encode multiple task variables (Barak et al., 2010; Stokes et al., 2013), which allows high-dimensional representation of behavioral priorities. For instance, Machens et al. (2010) showed that single lateral prefrontal neurons contributed to the maintenance of multiple information, such as stimulus identity and elapsed time, but that each type of information can be independently extracted from the population code.

TABLE 4 | Holm-Bonferroni's corrected *p*-values derived from the Granger causality analysis carried out among the nodes of the ICs no. 15 (see also **Figure 4B**).

To:	ACC	—	0,000	0,000	0,454	0,000	0,000	0,013
	L aIC	0.000	—	0.000	0.454	0.000	0.000	0.000
	R aIC	0.000	0.000	—	0.006	0.000	0.000	0.000
	L FEF	0.000	0.000	0.000	—	0.000	0.369	0.000
	R FEF	0.052	0.000	0.086	0.000	—	0.158	0.000
	L IPS	0.021	0.136	0.000	0.001	0.000	—	0.000
	R IPS	0.000	0.136	0.000	0.014	0.000	0.000	—
		ACC	L aIC	R aIC	L FEF	R FEF	L IPS	R IPS
				From:				

All this literature is consistent with the current findings showing the involvement of lateral prefrontal and posterior parietal regions during divided attention across spatial locations. The current data demonstrates for the first time in the context of divided attention that the posterior parietal regions are under controls of the ventro- and dorso-lateral prefrontal cortex. As revealed by the GCA, the prefrontal regions (i.e., the left DLPFc and the VLPFc) of IC 8 were found to predict the activity of all of the posteriors parietal nodes (see cyan lines in **Figure 3C**). Conversely, the causal influences of the posterior parietal nodes towards the prefrontal regions is rather limited, showing no uni-directional causal relationships with the prefrontal cortex. In agreement with the existent literature, the involvement of the lateral prefrontal cortex might be related to the effort of maintaining the current target representation, implemented by the posterior parietal cortex, on multiple spatial locations. The lateral prefrontal/posterior parietal mechanism might then pre-activate sensory cortices (McMains and Somers, 2004, 2005; Sreenivasan et al., 2014), thus enabling correct target detection among the continuous flow of audiovisual information across both hemifields.

The current findings demonstrated instead quite different neural resources implicated for monitoring multiple stimulus types/sensory modalities. As revealed by the ICA, dividing attention across different stimuli/sensory modalities necessitated the recruitment of IC 15. This brain network involved nodes belonging to the dorsal frontoparietal cortex (Corbetta and Shulman, 2002; Corbetta et al., 2008; Duncan, 2013), such as the FEF and the IPS, bilaterally, and the salience network (Menon and Uddin, 2010; Uddin, 2015), including the anterior cingulated cortex and the left and right aIC. The analysis of Granger causality highlights a tight interdependence between the dorsal frontoparietal and the salience network in trials requiring divided attention between different sensory modalities. In fact, most of the link between the two networks were bi-directional, indicating mutual causal relationships, which is in agreement with recent literature showing positive correlation between the frontoparietal and the salience network in a variety of tasks (see, for a review, Uddin, 2015). The current findings further extends the notion of frontoparietal/salience network co-variation in the domain of divided attention, showing that mutual interrelations between the dorsal frontoparietal and salience network might be fundamental to monitor concurrent stimuli coming from different sensory modalities. The salience network has key nodes in the aIC and ACC and is thought to be critical for detecting stimuli that are potentially relevant from a behavioral point of view (Menon and Uddin, 2010). Recently, the aIC has been shown to play an important role during multisensory attention. Chen et al. (2015) reported an fMRI study in which participants were asked to perform three different "oddball" tasks based on visual, auditory and auditory-visual stimuli. Chen et al. (2015) observed that the activity of the right anterior insula influenced the activity of all of the other emerging multisensory-related areas (i.e., frontal, cingulate and parietal cortex). The authors found that the role of the right anterior insula was more compatible with an "integrated signaling model" based on the simultaneous deployment of attention to both auditory and visual stimuli in the oddball task, rather than a "segregated signaling model" based on uncorrelated signals coming from each single sensory modality. What is more, this integrated model was particularly effective in accounting for the signals originating from the anterior cingulate and posterior parietal cortices, two important nodes of the salience and the frontoparietal network, respectively. These results were interpreted as an evidence that the anterior insula might serve as a control hub for the deployment of attentional resources on multisensory stimuli.

Consistent with Chen et al. (2015), monitoring simultaneous multisensory streams entailed here the recruitment of the salience network. However, the current data showed an interdependency between the salience and the dorsal frontoparietal network, more than a "control" role played by the salience over the dorsal frontoparietal network. This might be related to a key difference in task demands: while Chen et al. (2015) employed a task based on audio-visual integration (i.e., with audiovisual targets), in the current task participants were asked to monitor concurrent but separated audiovisual streams for detecting visual and auditory targets. The current requirement to monitor independent auditory and visual streams might have necessitated an increased interplay between the salience and the dorsal frontoparietal network.

To conclude, this study highlighted the key role played by the lateral prefrontal cortex in splitting attentional resources over multiple spatial locations, and by the salience network to divide attention towards multiple (visual and auditory) stimuli originating from the same location. Both the lateral prefrontal cortex and the salience network were shown to necessitate the contribution of different regions of the frontoparietal network during divided attention: dorsal frontoparietal regions (FEF and IPS) were linked to the salience network during divided attention towards audiovisual stimuli, while ventral regions of the posterior parietal cortex (IPL and Ang) were linked to the lateral prefrontal cortex during divided attention towards the left and right hemifield. The current findings therefore brought to light a dissociation between the brain networks implicated during divided attention across spatial location and sensory modalities, overall highlighting the importance of instigating the effective connectivity among large-scale brain networks supporting complex behavior.

AUTHOR CONTRIBUTIONS

VS conceived the study, collected and analyzed the data and wrote the manuscript.

SUPPLEMENTARY MATERIAL

The Supplementary Material for this article can be found online at: https://www.frontiersin.org/articles/10.3389/fnint.2018.00008/full#supplementary-material

FIGURE S1 | Discarded independent components.

REFERENCES

Bajaj, S., Adhikari, B. M., Friston, K. J., and Dhamala, M. (2016). Bridging the gap: dynamic causal modeling and granger causality analysis of resting state functional magnetic resonance imaging. *Brain Connect.* 6, 652–661. doi: 10.1089/brain.2016.0422

Barak, O., Tsodyks, M., and Romo, R. (2010). Neuronal population coding of parametric working memory. *J. Neurosci.* 30, 9424–9430. doi: 10.1523/JNEUROSCI.1875-10.2010

Barnett, L., and Seth, A. K. (2011). Behaviour of Granger causality under filtering: theoretical invariance and practical application. *J. Neurosci. Methods* 201, 404–419. doi: 10.1016/j.jneumeth.2011.08.010

Barnett, L., and Seth, A. K. (2014). The MVGC multivariate Granger causality toolbox: a new approach to Granger-causal inference. *J. Neurosci. Methods* 223, 50–68. doi: 10.1016/j.jneumeth.2013.10.018

Beckmann, C. F. (2012). Modelling with independent components. *Neuroimage* 62, 891–901. doi: 10.1016/j.neuroimage.2012.02.020

Bressler, S. L., and Menon, V. (2010). Large-scale brain networks in cognition: emerging methods and principles. *Trends Cogn. Sci.* 14, 277–290. doi: 10.1016/j.tics.2010.04.004

Calhoun, V. D., Adali, T., Pearlson, G. D., and Pekar, J. J. (2001). A method for making group inferences from functional MRI data using independent component analysis. *Hum. Brain Mapp.* 14, 140–151. doi: 10.1002/hbm.1048

Calhoun, V. D., Liu, J., and Adali, T. (2009). A review of group ICA for fMRI data and ICA for joint inference of imaging, genetic, and ERP data. *Neuroimage* 45, S163–S172. doi: 10.1016/j.neuroimage.2008.10.057

Castiello, U., and Umiltà, C. (1990). Size of the attentional focus and efficiency of processing. *Acta Psychol.* 73, 195–209. doi: 10.1016/0001-6918(90)90022-8

Castiello, U., and Umiltà, C. (1992). Splitting focal attention. *J. Exp. Psychol. Hum. Percept. Perform.* 18, 837–848. doi: 10.1037//0096-1523.18.3.837

Champod, A. S., and Petrides, M. (2007). Dissociable roles of the posterior parietal and the prefrontal cortex in manipulation and monitoring processes. *Proc. Natl. Acad. Sci. U S A* 104, 14837–14842. doi: 10.1073/pnas.0607101104

Chen, T., Michels, L., Supekar, K., Kochalka, J., Ryali, S., and Menon, V. (2015). Role of the anterior insular cortex in integrative causal signaling during multisensory auditory-visual attention. *Eur. J. Neurosci.* 41, 264–274. doi: 10.1111/ejn.12764

Corbetta, M., Kincade, J. M., Ollinger, J. M., McAvoy, M. P., and Shulman, G. L. (2000). Voluntary orienting is dissociated from target detection in human posterior parietal cortex. *Nat. Neurosci.* 3, 292–297. doi: 10.1038/73009

Corbetta, M., Patel, G., and Shulman, G. L. (2008). The reorienting system of the human brain: from environment to theory of mind. *Neuron* 58, 306–324. doi: 10.1016/j.neuron.2008.04.017

Corbetta, M., and Shulman, G. L. (2002). Control of goal directed and stimulus-driven attention in the brain. *Nat. Rev. Neurosci.* 3, 201–215. doi: 10.1038/nrn755

D'Esposito, M. (2001). "Functional neuroimaging of working memory," in *Handbook of Functional Neuroimaging of Cognition*, eds R. Cabeza and A. Kingstone (Cambridge, MA: The MIT Press), 293–327.

Damoiseaux, J. S., Rombouts, S. A., Barkhof, F., Scheltens, P., Stam, C. J., Smith, S. M., et al. (2006). Consistent resting-state networks across healthy subjects. *Proc. Natl. Acad. Sci. U S A* 103, 13848–13853. doi: 10.1073/pnas.0601417103

Duncan, J. (2013). The structure of cognition: attentional episodes in mind and brain. *Neuron* 80, 35–50. doi: 10.1016/j.neuron.2013.09.015

Eriksen, C. W., and St. James, J. D. (1986). Visual attention within and around the field of focal attention: a zoom lens model. *Percept. Psychophys.* 40, 225–240. doi: 10.3758/bf03211502

Fagioli, S., and Macaluso, E. (2009). Attending to multiple visual streams: interactions between location-based and category-based attentional selection. *J. Cogn. Neurosci.* 21, 1628–1641. doi: 10.1162/jocn.2009.21116

Fagioli, S., and Macaluso, E. (2016). Neural correlates of divided attention in natural scenes. *J. Cogn. Neurosci.* 28, 1392–1405. doi: 10.1162/jocn_a_00980

Friston, K., Moran, R., and Seth, A. K. (2013). Analysing connectivity with Granger causality and dynamic causal modelling. *Curr. Opin. Neurobiol.* 23, 172–178. doi: 10.1016/j.conb.2012.11.010

Friston, K. J., Price, C. J., Fletcher, P., Moore, C., Frackowiak, R. S., and Dolan, R. J. (1996). The trouble with cognitive subtraction. *Neuroimage* 4, 97–104. doi: 10.1006/nimg.1996.0033

Gaetano, J. (2013). Holm-Bonferroni sequential correction: an EXCEL calculator (1.2). Microsoft Excel workbook. Available online at: https://www.researchgate.net/publication/242331583_Holm-Bonferroni_Sequential_Correction_An_EXCEL_Calculator_-_Ver._1.2

Himberg, J., Hyavrinen, A., and Esposito, F. (2004). Validating the independent components of neuroimaging time series via clustering and visualization. *Neuroimage* 22, 1214–1222. doi: 10.1016/j.neuroimage.2004.03.027

Jans, B., Peters, J. C., and De Weerd, P. (2010). Visual spatial attention to multiple locations at once: the jury is still out. *Psychol. Rev.* 117, 637–684. doi: 10.1037/a0019082

Johnson, J. A., Strafella, A. P., and Zatorre, R. J. (2007). The role of the dorsolateral prefrontal cortex in bimodal divided attention: two transcranial magnetic stimulation studies. *J. Cogn. Neurosci.* 19, 907–920. doi: 10.1162/jocn.2007.19.6.907

Johnson, J. A., and Zatorre, R. J. (2005). Attention to simultaneous unrelated auditory and visual events: behavioral and neural correlates. *Cereb. Cortex* 15, 1609–1620. doi: 10.1093/cercor/bhi039

Johnson, J. A., and Zatorre, R. J. (2006). Neural substrates for dividing and focusing attention between simultaneous auditory and visual events. *Neuroimage* 31, 1673–1681. doi: 10.1016/j.neuroimage.2006.02.026

Kelley, T. A., Serences, J. T., Giesbrecht, B., and Yantis, S. (2008). Cortical mechanisms for shifting and holding visuospatial attention. *Cereb. Cortex* 18, 114–125. doi: 10.1093/cercor/bhm036

Koechlin, E. (2016). Prefrontal executive function and adaptive behavior in complex environments. *Curr. Opin. Neurobiol.* 37, 1–6. doi: 10.1016/j.conb.2015.11.004

Leung, H. C., Seelig, D., and Gore, J. C. (2004). The effect of memory load on cortical activity in the spatial working memory circuit. *Cogn. Affect. Behav. Neurosci.* 4, 553–563. doi: 10.3758/cabn.4.4.553

Machens, C. K., Romo, R., and Brody, C. D. (2010). Functional, but not anatomical, separation of "what" and "when" in prefrontal cortex. *J. Neurosci.* 30, 350–360. doi: 10.1523/JNEUROSCI.3276-09.2010

McMains, S. A., and Somers, D. C. (2004). Multiple spotlights of attentional selection in human visual cortex. *Neuron* 42, 677–686. doi: 10.1016/s0896-6273(04)00263-6

McMains, S. A., and Somers, D. C. (2005). Processing efficiency of divided spatial attention mechanisms in human visual cortex. *J. Neurosci.* 25, 9444–9448. doi: 10.1523/JNEUROSCI.2647-05.2005

Menon, V., and Uddin, L. Q. (2010). Saliency, switching, attention and control: a network model of insula function. *Brain Struct. Funct.* 214, 655–667. doi: 10.1007/s00429-010-0262-0

Molenberghs, P., Mesulam, M. M., Peeters, R., and Vandenberghe, R. R. C. (2007). Remapping attentional priorities: differential contribution of superior parietal lobule and intraparietal sulcus. *Cereb. Cortex* 17, 2703–2712. doi: 10.1093/cercor/bhl179

Müller, N. G., Bartelt, O. A., Donner, T. H., Villringer, A., and Brandt, S. A. (2003). A physiological correlate of the "Zoom Lens" of visual attention. *J. Neurosci.* 23, 3561–3565.

Müller, M. M., Malinowski, P., Gruber, T., and Hillyard, S. A. (2003). Sustained division of the attentional spotlight. *Nature* 424, 309–312. doi: 10.1038/nature01812

Munk, M. H., Linden, D. E., Muckli, L., Lanfermann, H., Zanella, F. E., Singer, W., et al. (2002). Distributed cortical systems in visual short-term memory revealed by event-related functional magnetic resonance imaging. *Cereb. Cortex* 12, 866–876. doi: 10.1093/cercor/12.8.866

Nardo, D., Santangelo, V., and Macaluso, E. (2011). Stimulus-driven orienting of visuo-spatial attention in complex dynamic environments. *Neuron* 69, 1015–1028. doi: 10.1016/j.neuron.2011.02.020

Nardo, D., Santangelo, V., and Macaluso, E. (2014). Spatial orienting in complex audiovisual environments. *Hum. Brain Mapp.* 35, 1597–1614. doi: 10.1002/hbm.22276

Raichle, M. E. (2015). The restless brain: how intrinsic activity organizes brain function. *Philos. Trans. R. Soc. Lond. B. Biol. Sci.* 370:20140172. doi: 10.1098/rstb.2014.0172

Santangelo, V. (2015). Forced to remember: when memory is biased by salient information. *Behav. Brain Res.* 283, 1–10. doi: 10.1016/j.bbr.2015.01.013

Santangelo, V., Di Francesco, S. A., Mastroberardino, S., and Macaluso, E. (2015). Parietal cortex integrates contextual and saliency signals during the encoding of natural scenes in working memory. *Hum. Brain Mapp.* 36, 5003–5017. doi: 10.1002/hbm.22984

Santangelo, V., Fagioli, S., and Macaluso, E. (2010). The costs of monitoring simultaneously two sensory modalities decrease when dividing attention in space. *Neuroimage* 49, 2717–2727. doi: 10.1016/j.neuroimage.2009.10.061

Santangelo, V., and Macaluso, E. (2013a). The contribution of working memory to divided attention. *Hum. Brain Mapp.* 34, 158–175. doi: 10.1002/hbm.21430

Santangelo, V., and Macaluso, E. (2013b). Visual salience improves spatial working memory via enhanced parieto-temporal functional connectivity. *J. Neurosci.* 33, 4110–4117. doi: 10.1523/JNEUROSCI.4138-12.2013

Seth, A. K. (2010). A MATLAB toolbox for Granger causal connectivity analysis. *J. Neurosci. Methods* 186, 262–273. doi: 10.1016/j.jneumeth.2009.11.020

Seth, A. K., Chorley, P., and Barnett, L. C. (2013). Granger causality analysis of fMRI BOLD signals is invariant to hemodynamic convolution but not downsampling. *Neuroimage* 65, 540–555. doi: 10.1016/j.neuroimage.2012.09.049

Shaw, M. L., and Shaw, P. (1977). Optimal allocation of cognitive resources to spatial locations. *J. Exp. Psychol. Hum. Percept. Perform.* 3, 201–211. doi: 10.1037/0096-1523.3.2.201

Shirer, W. R., Ryali, S., Rykhlevskaia, E., Menon, V., and Greicius, M. D. (2012). Decoding subject-driven cognitive states with whole-brain connectivity patterns. *Cereb. Cortex* 22, 158–165. doi: 10.1093/cercor/bhr099

Smith, E. E., and Jonides, J. (1999). Storage and executive processes in the frontal lobes. *Science* 283, 1657–1661. doi: 10.1126/science.283.5408.1657

Sreenivasan, K. K., Curtis, C. E., and D'Esposito, M. (2014). Revisiting the role of persistent neural activity during working memory. *Trends Cogn. Sci.* 18, 82–89. doi: 10.1016/j.tics.2013.12.001

Stephan, K. E., and Roebroeck, A. (2012). A short history of causal modeling of fMRI data. *Neuroimage* 62, 856–863. doi: 10.1016/j.neuroimage.2012.01.034

Stokes, M. G., Kusunoki, M., Sigala, N., Nili, H., Gaffan, D., and Duncan, J. (2013). Dynamic coding for cognitive control in prefrontal cortex. *Neuron* 78, 364–375. doi: 10.1016/j.neuron.2013.01.039

Uddin, L. Q. (2015). Salience processing and insular cortical function and dysfunction. *Nat. Rev. Neurosci.* 16, 55–61. doi: 10.1038/nrn3857

Vandenberghe, R., Geeraerts, S., Molenberghs, P., Lafosse, C., Vandenbulcke, M., Peeters, K., et al. (2005). Attentional responses to unattended stimuli in human parietal cortex. *Brain* 128, 2843–2857. doi: 10.1093/brain/awh522

Wen, X., Rangarajan, G., and Ding, M. (2013). Is Granger causality a viable technique for analyzing fMRI data? *PLoS One* 8:e67428. doi: 10.1371/journal.pone.0067428

Wig, G. S. (2017). Segregated systems of human brain networks. *Trends Cogn. Sci.* 21, 981–996. doi: 10.1016/j.tics.2017.09.006

Xu, Y., and Chun, M. M. (2006). Dissociable neural mechanisms supporting visual short-term memory for objects. *Nature* 440, 91–95. doi: 10.1038/nature04262

Yantis, S., Schwarzbach, J., Serences, J. T., Carlson, R. L., Steinmetz, M. A., Pekar, J. J., et al. (2002). Transient neural activity in human parietal cortex during spatial attention shifts. *Nat. Neurosci.* 5, 995–1002. doi: 10.1038/nn921

Yuan, P., and Raz, N. (2014). Prefrontal cortex and executive functions in healthy adults: a meta-analysis of structural neuroimaging studies. *Neurosci. Biobehav. Rev.* 42, 180–292. doi: 10.1016/j.neubiorev.2014.02.005

Zimmer, H. D. (2008). Visual and spatial working memory: from boxes to networks. *Neurosci. Biobehav. Rev.* 32, 1373–1395. doi: 10.1016/j.neubiorev.2008.05.016

Conflict of Interest Statement: The author declares that the research was conducted in the absence of any commercial or financial relationships that could be construed as a potential conflict of interest.

Copyright © 2018 Santangelo. This is an open-access article distributed under the terms of the Creative Commons Attribution License (CC BY). The use, distribution or reproduction in other forums is permitted, provided the original author(s) and the copyright owner are credited and that the original publication in this journal is cited, in accordance with accepted academic practice. No use, distribution or reproduction is permitted which does not comply with these terms.

frontiers in Human Neuroscience

ORIGINAL RESEARCH
published: 06 April 2018
doi: 10.3389/fnhum.2018.00116

Characterization of Sensory-Motor Behavior Under Cognitive Load Using a New Statistical Platform for Studies of Embodied Cognition

Jihye Ryu[1] *and Elizabeth B. Torres*[2]*

[1]*Sensory Motor Integration Laboratory, Department of Psychology, Rutgers University, Piscataway, NJ, United States,* [2]*Computational Biomedical Imaging and Modeling Center, Department of Psychology and Computer Science, Rutgers University Center for Cognitive Science, Rutgers University, Piscataway, NJ, United States*

The field of enacted/embodied cognition has emerged as a contemporary attempt to connect the mind and body in the study of cognition. However, there has been a paucity of methods that enable a multi-layered approach tapping into different levels of functionality within the nervous systems (e.g., continuously capturing in tandem multi-modal biophysical signals in naturalistic settings). The present study introduces a new theoretical and statistical framework to characterize the influences of cognitive demands on biophysical rhythmic signals harnessed from deliberate, spontaneous and autonomic activities. In this study, nine participants performed a basic pointing task to communicate a decision while they were exposed to different levels of cognitive load. Within these decision-making contexts, we examined the moment-by-moment fluctuations in the peak amplitude and timing of the biophysical time series data (e.g., continuous waveforms extracted from hand kinematics and heart signals). These spike-trains data offered high statistical power for *personalized* empirical statistical estimation and were well-characterized by a Gamma process. Our approach enabled the identification of different empirically estimated families of probability distributions to facilitate inference regarding the continuous physiological phenomena underlying cognitively driven decision-making. We found that the same pointing task revealed shifts in the probability distribution functions (PDFs) of the hand kinematic signals under study and were accompanied by shifts in the signatures of the heart inter-beat-interval timings. Within the time scale of an experimental session, marked changes in skewness and dispersion of the distributions were tracked on the Gamma parameter plane with 95% confidence. The results suggest that traditional theoretical assumptions of stationarity and normality in biophysical data from the nervous systems are incongruent with the true statistical nature of empirical data. This work offers a unifying platform for personalized statistical inference that goes far beyond those used in conventional studies, often assuming a "*one size fits all model*" on data drawn from discrete events such as mouse clicks, and observations that leave out continuously co-occurring spontaneous activity taking place largely beneath awareness.

Keywords: embodied cognition, cognitive load, heart rate variability, sensory-motor integration, pointing movements, stochastic processes

OPEN ACCESS

Edited by:
Stephane Perrey,
Université de Montpellier, France

Reviewed by:
Pablo Varona,
Universidad Autonoma de Madrid, Spain
Claudia Repetto,
Università Cattolica del Sacro Cuore, Italy
Annalisa Bosco,
Università degli Studi di Bologna, Italy

***Correspondence:**
Elizabeth B. Torres
torreselizabeth248@gmail.com

Received: *06 September 2017*
Accepted: *12 March 2018*
Published: *06 April 2018*

Citation:
Ryu J and Torres EB (2018) Characterization of Sensory-Motor Behavior Under Cognitive Load Using a New Statistical Platform for Studies of Embodied Cognition. Front. Hum. Neurosci. 12:116. doi: 10.3389/fnhum.2018.00116

INTRODUCTION

Cognitive Science as a field has focused primarily on the study of the mind, with few studies addressing the mind-body interactions. In recent years, the field of embodied cognition has emerged to fill this gap and try to connect mental representations with physically enacted actions (Wilson, 2002; Mahon and Caramazza, 2008). However, progress in this nascent field has stalled, partly because there are no proper ways to statistically quantify cognition and action under a common framework. Given that motor action is a result of the central and peripheral nervous systems working together, it is necessary to study continuous output signals from all layers of the nervous systems in tandem. These include the brain, the heart and the body in motion. Conventional studies are often based on *discrete* epochs of biophysical signals obtained during constrained (unnatural) actions whereby decisions are marked by mouse clicks, self-reports and/or observation. Such classes of actions contrast with signals obtained during naturalistic and self-generated *continuous* behaviors.

In the naturalistic case, spontaneous movement segments coexist with deliberate ones and are performed largely beneath the person's awareness (Torres, 2011). Indeed, naturalistic actions involve varying levels of functional control, which range from those that are intentional and goal-directed, to those that are autonomic in nature (**Figure 1A**). Activities of daily living require the coordination and control of motions along all these levels of functionality. Accordingly, it is important to understand the evolving dynamics of biophysical signals across the multiple layers of the nervous systems, under different levels of functional control within these systems. To that end, the current study introduces a new theoretical and methodological framework that assesses the influences of cognitive loads on bodily motions. We use the hand's and the heart's rhythmic motions during continuously repeated pointing gestures to indicate cognitive-loaded decisions.

In order to understand the interactive dynamics across the different nervous systems, we introduce a new theoretical framework (Torres et al., 2013a) grounded on the principle of reafference (Von Holst and Mittelstaedt, 1950), from the works of Von Holst and Mittelstaedt, stating that "*Voluntary movements show themselves to be dependent on the returning stream of afference which they themselves cause*." Our work expands the use of this principle to other non-voluntary movements' functionalities and to movements that may be independent of the returning afferent stream but coexisting within voluntary actions. These include supportive motions that occur spontaneously and do not pursue a goal, involuntary motions inherent in the person's system, automated and autonomic motions. These motions have different dynamics and funnel differently the influences of dynamics on the geometry of the paths their trajectories describe—as compared to those intended to a goal, i.e., deliberately performed with intent or purpose (Torres, 2001, 2010, 2011; Torres and Zipser, 2004; Torres and Andersen, 2006; Torres et al., 2013c). They also have the common feature that the person is less aware of them than those performed under voluntary control.

Within this framework, studying physiological signals with varying levels of functional control, it is then essential to understand co-existing levels of functionality permeating the closed feedback loops between the CNS, the PNS, and within the PNS, the ANS. These multi-modal flows of information exert influences over one another. For instance, it has been shown that spontaneous actions (e.g., retracting motion of the pointing hand) co-exist with, and are instrumental to the goal-directed segments of complex motions, as they provide fluidity to behavior at large (Torres, 2011). Along those lines, prior work concerning neuromotor features of complex actions with coexisting multi-functional movement segments examined the interplay between deliberate and spontaneous movements to characterize their stochastic signatures among athletes vs. novices (Torres, 2011, 2013b). Within the realm of basic perceptual science, the new framework has been used to examine top down influences of visual illusions on multi-functional motor control (Nguyen et al., 2013, 2014a,b). In the health space, these new methods under the aforementioned theoretical construct have been used to examine individuals with autism spectrum disorders (Torres, 2013c; Torres et al., 2013a), schizophrenia (Nguyen et al., 2016), Parkinson's disease (Torres et al., 2011), stroke (Torres et al., 2010) and deafferentation (Torres et al., 2014). More generally, these methods have been deployed as a new platform for personalized medicine drawing on principles of the Precision Medicine approach (Torres et al., 2016a,b) for Big Data analyses (Torres and Denisova, 2016; Torres et al., 2017) and mobile health concepts (Torres, 2013a; Torres and Lande, 2015; Torres et al., 2016c). The use of the fluctuations in amplitude and timing extracted from parameters in biophysical signals provides a proper level of detail to detect preferences in sensory guidance and help evoke and steer the system's autonomy, its volitional control and ultimately its agency (**Figures 1B,C**).

We posit that interactions among signals from the full range of functionalities and from different nervous systems are necessary for the development and maintenance of *deliberate autonomy* (i.e., the ability to deliberately maintain a robust course of action on demand, impervious to external/environmental influences).

Under the lens of this framework, to examine how increase in cognitive demands are manifested across different nervous systems, we assessed the variability inherent in the biophysical rhythms that we harnessed noninvasively from the various layers of the nervous systems. We characterize the influences of increases in cognitive demands on the hand movement kinematics and the heart signals, using new statistical methods under the renovated kinesthetic reafference framework, as applied to the multi-layered and multi-functional nervous systems. Here, we vary the level of cognitive demands during a pointing task to communicate a decision. Under those conditions, we examine: (1) the goal-directed segment of the pointing motion; (2) the supplemental segments of the retracting motions; and (3) the heart rate variability, as these provide a window into the individual's mental states during cognitive decisions, in an interactive closed-loop between the central and the peripheral nervous systems.

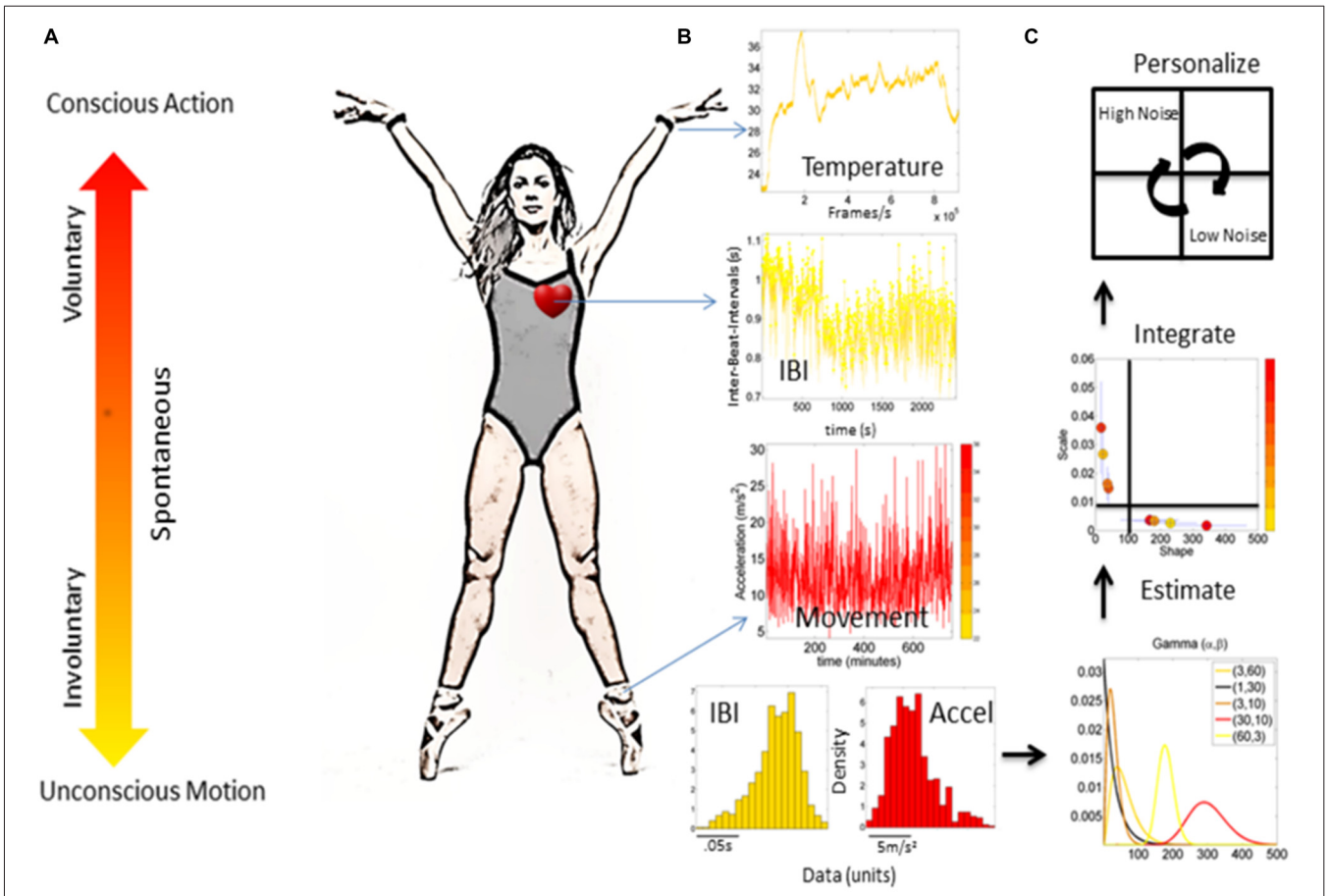

FIGURE 1 | Micro-movements from different nervous systems' biorhythms. **(A)** Continuum of different levels of control ranging from those that are conscious and goal-directed to those that are autonomic and unconscious (taken from Torres, 2011). **(B)** Different waveforms from different instrumentations (e.g., heart activity, temperature and movement) registered from physiological sensors. Raw biophysical signals give rise to a time series of peaks and valleys, which vary in amplitude and timing. The fluctuations in the amplitude and timing of the peaks are the "micro-movements" of biophysical signals. **(C)** The micro-movements datatype can be used in an empirical estimation of families of probability distributions (e.g., using a Gamma process) to estimate parameters of the probability distribution functions (PDFs), track the integrated signatures from different layers of the nervous systems on the Gamma parameter plane, and separate regimes of low vs. high noise-to-signal ratio (NSR), and low vs. high symmetry of the distribution based on the shape values.

MATERIALS AND METHODS

Participants

Nine undergraduate students (two males and seven females) between the ages 18 and 22 were recruited from the Rutgers human subject pool system and received credit for their participation. This study took place at the Sensory Motor Integration Laboratory of Rutgers University. All participants signed the consent form approved by the Rutgers University Institutional Review Board (IRB). The entire study protocol was approved by the Rutgers University IRB. The study conforms to the guidelines of the Helsinki Act for the use of human subjects in research. Two participants were left-handed, and all had normal or corrected-to-normal vision.

During the experiment, the motor and heart signals were recorded from each participant. However, one participant's heart signals did not record successfully due to instrumentation malfunctioning, resulting in an analysis on motor data for nine individuals and heart data for eight individuals.

Sensor Devices

In this study, two sensor devices—motion capture system and a wireless heart rate monitor—were used to record the signals coming from the bodily movements and the heart. The data obtained from these two devices were analyzed separately.

Motion Capture

Fifteen electromagnetic sensors at a sampling frequency of 240 Hz (Polhemus Liberty, Colchester, VT, USA) were used to continuously capture the participant's movements across the upper body. Nine sensors were placed on the following body segments using sports bands to optimize unrestricted movement of the body: center of the forehead, thoracic vertebrate T7, right and left scapula, right and left upper arm, right and left forearm, the dominant hand's index finger. An additional sensor was used

to digitize the body in constructing a biomechanical model using the Motion Monitor (Innovative Sports Training Inc., Chicago, IL, USA) software. One sensor was placed at the backside center of the iPad (Apple, Cupertino, CA, USA) display screen. This sensor served to measure the physical position of the fixed target, to help obtain a distance-based criterion to automatically classify motions into forward (from the resting position of the hand to the target) and backward (from the target to the resting position). There were also four positional sensors placed at the four corners of the table on which the iPad was standing. This physical information enables us to build computational models of these movements to study Bernstein's degree of freedom problem (Torres and Zipser, 2002; but that work is beyond the scope of this article). During the experiment, the participant's motion was captured in real-time, recording the location and speed of the upper body movements.

Heart Rate Monitor

Heart signals were obtained via electrocardiogram (ECG) from a wireless Nexus-10 device (Mind Media BV, Netherlands) and Nexus 10 software Biotrace (Version 2015B) at a sampling rate of 256 Hz. Three electrodes were placed on the chest according to the standardized lead II method and were attached with adhesive tape. A typical ECG data includes a set of QRS complexes and detecting R-peaks (within the QRS complex) is essential, as the heart rate metrics needed for this study focuses on the oscillation of intervals between consecutive heartbeats. To remove any baseline wandering and to accurately detect the R-peaks, ECG data were preprocessed using the Butterworth IIR band pass filter for 5–30 Hz at 2nd order. The range of the band pass filter was selected based on the finding that a QRS complex is present in the frequency range of 5–30 Hz (Kathirvel et al., 2011). To retrieve the time between R-peaks (i.e., inter-beat intervals, IBI) from the preprocessed ECG data, simple peak detection method was used, and was plotted using Matlab graphics to ensure that there were no missed R-peaks.

Stimulus Apparatus and Experimental Procedure

Once all sensors were donned and calibrated, participants were seated at a table facing an iPad used as a touchscreen display. An in-house developed MATLAB (Release 2015b, The MathWorks, Inc., Natick, MA, USA) program controlled the presentation displayed on the touchscreen display and recorded the timing and location of the touches made by the participant. The MATLAB program was presented on the touchscreen display using the TeamViewer (Germany) application.

As shown in the schematics of **Figure 2**, for each trial, the participant was presented with a circle on the center of the display screen. This presentation prompted the participant to touch the circle on the screen within 5 s. After the touch, the participant heard a tone at 1000 Hz for 100 ms. The duration between the touch and the tone was randomly set to be 100 ms, 400 ms, or 700 ms. Then, on the display screen, the participant was presented with a sliding scale ranging from 0 to 1. On the sliding scale, the participant indicated how long they perceived the time to have elapsed between the touch and the tone, by touching the corresponding number on the scale within 5 s. Note, the 5 s time-windows allowed ample time for the participant to touch the screen at their own pace, as the time to reach the screen and then to retract the hand took approximately 1.5 s. Supplementary Table S1 of the Supplementary Material summarizes the median time to move the hand under each condition.

The experiment consisted of three conditions—control, low cognitive load and high cognitive load condition. Under the control condition, the participant simply performed this task for 60 trials. Under the low cognitive load condition, the participant performed these tasks for 60 trials, while repeatedly counting out loud one through five. Under the high cognitive load condition, the participant performed these tasks for 60 trials, while counting backwards from 400 subtracting by 3.

Participants performed the conditions in the order of control-baseline, low cognitive load condition, and high cognitive load condition. Note, the order was not counterbalanced, because performing high cognitive load tasks prior to low load tasks would have caused cognitive load and fatigue to be carried over to the low cognitive load condition. This might have influenced the effect of cognitive load to be mixed with fatigue, but this was necessary to keep the low cognitive load tasks to be minimally taxing as possible. For both low and high cognitive load conditions, the participant was instructed to count at a comfortable pace. Participants took breaks in between conditions, and the entire experiment took about 40 min.

Justification and Assessment of Levels of Cognitive Load

To illustrate the effects of subtle increases in cognitive demands on the hand kinematics, we use **Figure 3A** where the hand speed profiles for the low and high cognitive load conditions show marked differences in variability as the movements unfold in each trial, and as they are performed from trial to trial. Besides the speed profiles, these differences can be appreciated in plots of heat maps where the peaks are highlighted for 60 trials. Indeed, the results extend to the heart beat, as illustrated in **Figure 3B** using similar format as in **Figure 3A** (i.e., the waveform of the raw signal and the heat map of the peaks).

To justify the use of this paradigm to test influences of cognitive demands on movement kinematics, we evaluated the number of peaks in the angular acceleration waveform for both the deliberate portion of the reach (forward to the target) and the spontaneous retraction (backward to rest).

The effects of the increase in cognitive demands manifested in statistically significant changes in the accuracy of the task and the time of performance. The group incurred a significant increase in the time to point ($t_{(8)} = 0.15$, $p < 0.01$) explained by the statistically significant increase in the number of angular acceleration peaks as the cognitive demands increased. The accumulation of peaks in the rates of hand angular speed with higher cognitive load resulted in higher physical effort, as the participants had longer angular excursions with higher cognitive demands. The insets in **Figure 3C** show the increase in number of peaks for both types of motions under consideration (forward and backwards). Lastly, we confirmed that the increase in cognitive demands affected their accuracy in estimating time.

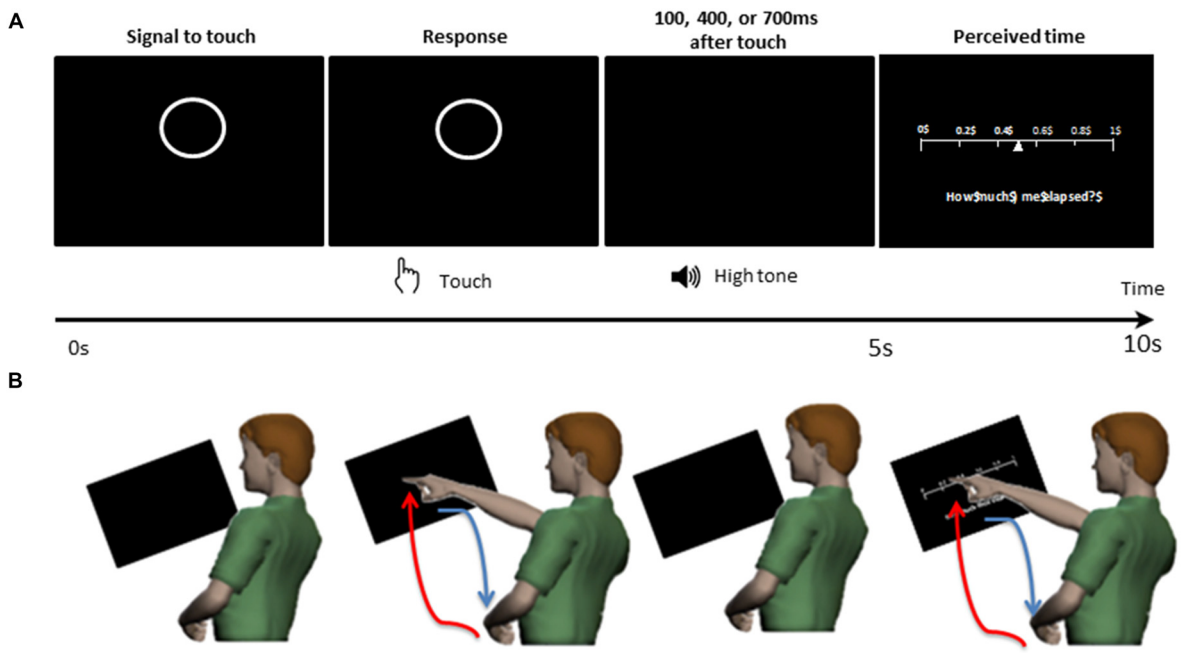

FIGURE 2 | Experimental design. The participant was presented with a display screen as shown on **(A)**. During the first 5 s, the screen presented a circle prompting the participant to touch the circle on the screen. After the touch, the participant heard a tone. The duration between the touch and the tone was randomly set to be 100 ms, 400 ms, or 700 ms. In the next 5 s, the participant was presented with a sliding scale, where the participant would indicate how long they perceived the time to have elapsed between the touch and the tone, by touching the corresponding number on the scale. **(B)** For each trial, the participant made a pointing gesture to touch the circle and to indicate their time estimation on the sliding scale. The pointing movement is composed of a voluntary/goal-directed forward segment (red) and a spontaneous backward segment (blue).

This is shown in **Figure 3D**, where the increase in the cognitive loads resulted in statistically significant higher errors of the time estimation ($t_{(8)} = 4.21$, $p < 0.01$). All these preliminary tests confirmed that the motor task we designed was adequate to assess variations in cognitive load and their potential effects on physiological parameters of interest. We then proceeded to examine these physiological waveforms' peaks in terms of spike trains under the general rubric of continuous stochastic processes.

Data Analysis

The Statistical Platform for Individualized Behavioral Analyses (SPIBA)

The current study employs a new platform, Statistical Platform for Individualized Behavioral Analyses (SPIBA; Torres and Jose, 2012), which was created for personalized assessments required in the Precision Medicine and mobile Health concepts (Hawgood et al., 2015). For the present study, the SPIBA was used to first characterize each participant individually, which could potentially be used to automatically (without heuristics of e.g., machine learning algorithms to classify labeled data) identify self-emerging clusters of participants based on their similar statistical patterns in subsequent studies. This platform stands in stark contrast to current approaches in health sciences (e.g., significant hypothesis testing method), which tend to compare hand-picked grouped data under some inclusion/exclusion criteria and assumed to follow a normal distribution with homogenous variance. The pitfalls of such methods have been discussed by others (Gallistel, 2009; Gallistel and King, 2009) and the Bayesian framework has been offered (e.g., in fields of Cognitive Science and Neuroscience) as an alternative to address some of the known weaknesses of traditional approaches to statistical inference. However, the Bayesian approach has not been adapted to analyze multiple types of biophysical data in tandem, obtained from different layers of the nervous systems, including those that are internally generated with disparate levels of functionality.

The SPIBA framework, with the use of a new datatype coined "*the micro-movements*" of biophysical signals (explained in the following section), was precisely designed to longitudinally tackle the emergence, dynamic development, maintenance and degeneration of the signals produced by the multi-layered nervous systems, including those with different pathologies over the human lifespan (Torres et al., 2016a).

New Data Type: Definition of Micro-Movements

The raw biophysical data continuously registered from physiological sensors (i.e., physiological signals obtained by ECG, respiration patterns, kinematics from bodily, head and eye movements, tremor data, etc.) give rise to time series of peaks and valleys, which vary in amplitude and timing (**Figure 3**). The fluctuations in amplitude and timing of the peaks are treated as spikes and assumed to follow a continuous

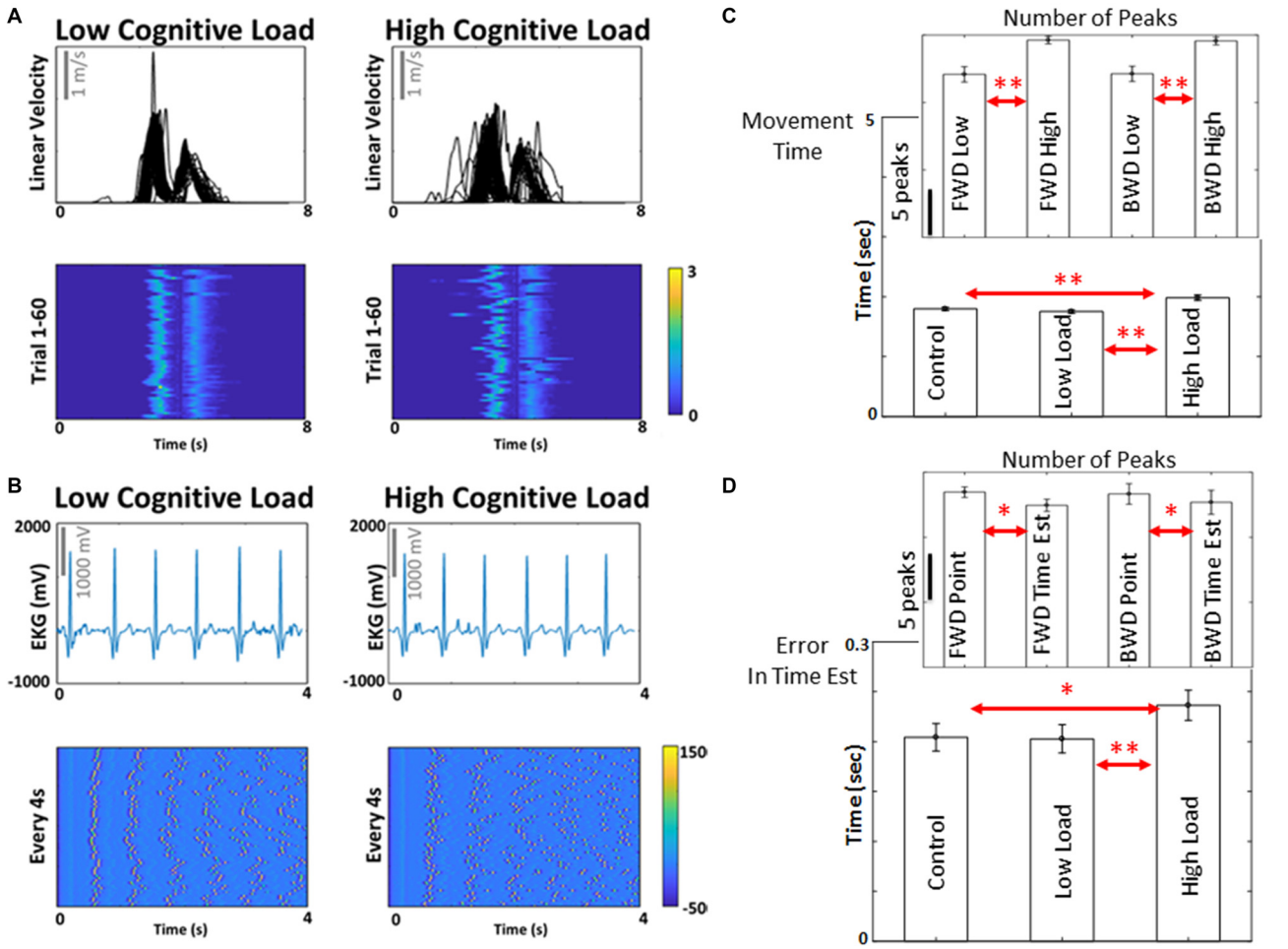

FIGURE 3 | Biorhythms from different nervous systems and motor/behavioral results from cognitive load. **(A)** Biorhythm of motor signals, from hand pointing movements, in the form of temporal speed profiles across 60 trials, exhibit moment by moment variations with different levels of cognitive load. Motions are aligned to the touch of the screen and heat maps are used to show the speed peaks (cm/s) for the forward and backwards motions. Peaks of the electro-cardiogram signals (ECG) are aligned (4 s) and represented in **(B)** as spikes. Later in the analyses, these peaks become standardized as unit-less micro-movements ranging on the real-valued scale from 0 to 1 for further stochastic analyses (see "Materials and Methods" section). **(C,D)** To validate the effect of cognitive load, movement time (i.e., time was registered from the time when the participant was prompted to reach the target, to time of completion of the reach by touching the screen), error in time estimation, and average number of angular acceleration peaks per trial were compared between the high and low cognitive load conditions, and between pointing and time estimation tasks. Movement time showed significant difference between control and high cognitive load condition ($t_{(8)} = 3.53$, $p < 0.01$) and between low and high cognitive load condition ($t_{(8)} = 0.15$, $p < 0.01$). Error in time estimation also showed significant difference between control and high cognitive load condition ($t_{(8)} = 2.89$, $p = 0.04$) and low and high cognitive load condition ($t_{(8)} = 4.21$, $p < 0.01$). Number of angular acceleration peaks were significantly different between low and high cognitive load conditions for forward motions ($t_{(8)} = 5.4$, $p < 0.01$) and backward motions ($t_{(8)} = 7.6$, $p < 0.01$); and between pointing and time estimation tasks for forward motions ($t_{(8)} = 2.2$, $p = 0.05$) and borderline significant for backward motions ($t_{(8)} = 2.1$, $p = 0.07$). $^{**}p < 0.01$; $^{*}p < 0.05$. The experimental paradigm described in **Figure 2** proved efficient to probe cognitive demands and characterize cognitive loads by time series of peaks in trajectories described by the hand's angular acceleration. See Supplementary Tables S2–S4 for all pairwise comparisons of these metrics.

random process where events in the past may (or may not) accumulate evidence towards the prediction of future events. Under this framework, we distinguish the processes, whereby the consequences of the signals *dependent on the returning stream of afference which the (voluntary) motions themselves cause*, from the independent processes. The latter are those for which the present events are independent of the past events. All fluctuations treated as standardized spikes in the 0–1 unit-less real number range are the "*the micro-movements*" of biophysical signals. To model them, we build on our original work (Torres et al., 2013a) whereby random variables follow a Gamma process (rationale behind this is explained in next).

For the current study, the goal is to show an example of using SPIBA and micro-movement data involving signals harnessed in tandem from the PNS and ANS while performing CNS driven decisions. To that end, we will examine biophysical data from body movements and the heart activities in a personalized fashion, as each participant is exposed to a decision-making task with different levels of cognitive load.

Different Classes of Movement Segments—Forward vs. Backward

The continuous positional trajectory of the participant's dominant hand index finger was decomposed into forward and backward movements (schematics of **Figure 2** (bottom panel) and sample hand movement trajectory in **Figure 4A**). The forward movement corresponds to the movement when the hand resting on the table would reach out to touch the display screen. As this movement involves an explicit goal in mind (i.e., to touch the display screen), this movement involves a high level of intention. On the other hand, the backward movement corresponds to the movement when the hand touching the display screen would spontaneously (without any instruction) retract back to the table. Because this uninstructed movement does not involve an explicit goal and is more automatic, it involves a relatively lower level of intention. Note, this forward-

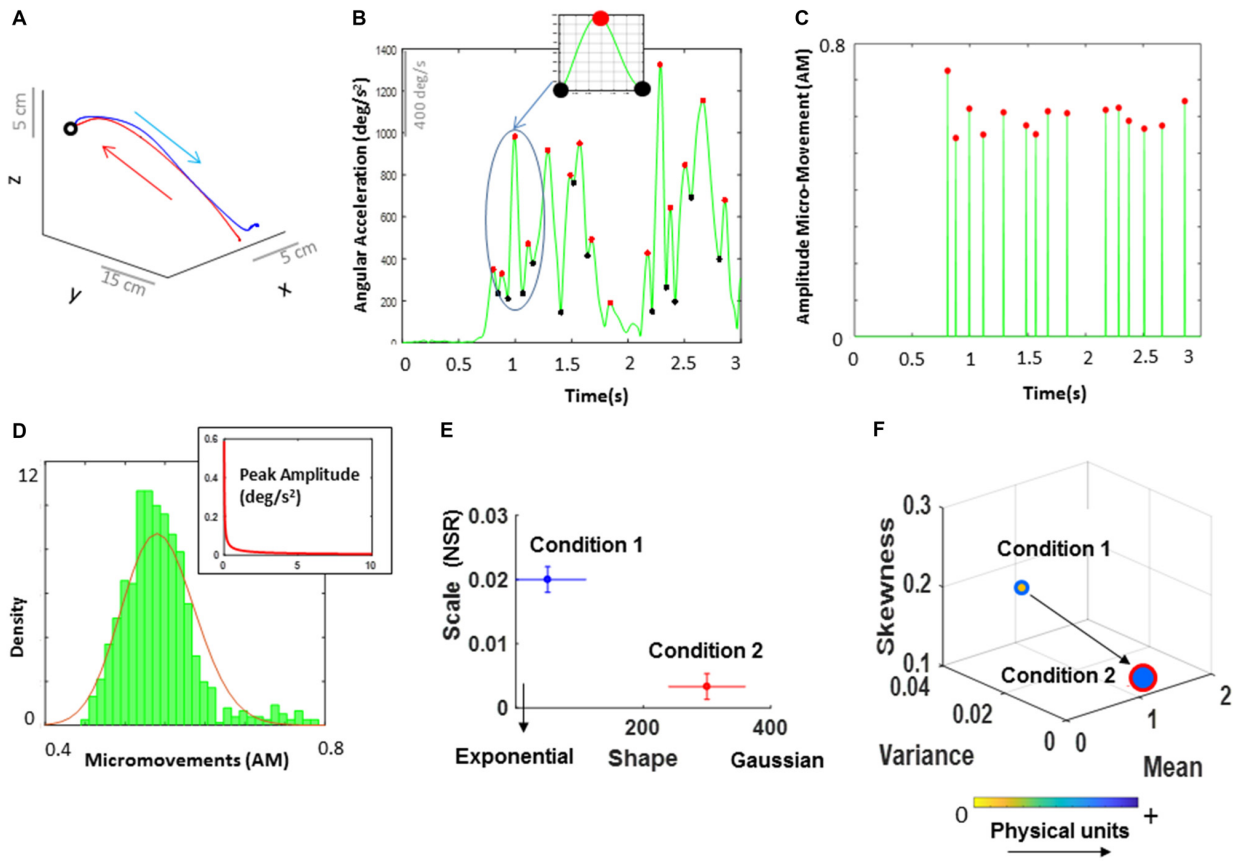

FIGURE 4 | Analytical and visualization methods. **(A)** Continuous positional trajectory of the dominant hand performing a single pointing movement loop forward to the target (instructed) and backwards to rest (spontaneous). Forward motion corresponds to the movement from the time when the index finger is resting on the table and lifts to move until the time the finger touches the target displayed on the screen and stops. The backward movement corresponds to the movement from the time the index finger leaves the target and retracts back to the table. **(B)** Time series of angular acceleration of the dominant hand's index finger rotations during a typical pointing task. Peaks (maxima) and valleys (minima) are shown in red and black dots, respectively. The inset shows a zoomed-in picture of a single angular acceleration segment (i.e., two local minima and a single local peak in between). This is a schematic of computing the amplitude micro-movements (AM; i.e., normalized peak amplitude) from a continuous time series of signal data, where the AM is computed by dividing the peak value by the sum of the peak value and the average of the signal values between the two local minima (see equation 1). **(C)** Spike train for a typical pointing task. All peak values from **(B)** are normalized between 0 and 1, while all non-peak values are set to 0. **(D)** All AM values were identified and gathered across all trials. For these data, a frequency histogram was then plotted, and fitted with a Gamma PDF using maximum likelihood estimation (MLE). In addition to the AM values (used here to explain these methods), we can also plot an inset PDF of the raw data (i.e., angular acceleration or time to peak TM) to show the differences in PDF between the raw data and the data scaled by equation (1). **(E)** The estimated Gamma parameters from the fitted probability distribution corresponding to the parameters registered in two sample conditions (e.g., high load and low load) were then plotted on a Gamma parameter plane, with lines representing the 95% confidence interval (CI). **(F)** Empirically estimated Gamma moments: mean, variance, and skewness plotted on the x, y, and z axes respectively. The size of the marker reflects the level of kurtosis, where larger size indicates high kurtosis level of the fitted PDF. The arrows connecting the markers indicate the order of the task conditions. The marker's face color represents the median values of the underlying physical units (e.g., the range values of deg/s^2). For example, the marker with blue edge representing Condition 1, is yellow, signaling a color of lower values in the color bar than the blue color of the marker with red edge representing Condition 2. This representation to visualize the data means that from Condition 1 to Condition 2, the skewness dropped towards the 0-value reference for symmetric distributions (also marked by a right-shift in **(E)** along the shape axis); a decrease in kurtosis (peakier distribution in Condition 2 than in Condition 1) with a drop in the NSR in **(E)** along the scale axis from Condition 1 to Condition 2. Further, the shift from Condition 1 to Condition 2 shows an increase in the mean with a reduction in the variance (explaining the drop in NSR, i.e., mean/var).

retraction motion paradigm has been developed (Nguyen et al., 2014a) and translated in clinical (Torres et al., 2010, 2011, 2013a,b, 2016a; Yanovich et al., 2013; Hong et al., 2014; Amano et al., 2015; Nguyen et al., 2016) and sports research (Torres, 2011).

For each trial, as the participant moved the dominant hand from the table to the display screen and back to the table, the movement trajectory consisted of a single forward and backward movement segment. Within the trajectory, the two movement segments were extracted, by identifying the time when the distance between the index finger and the display screen was at the minimum. Naturally, the linear velocity of the index finger reaches near instantaneous zero at that point. Hence, the forward movement would correspond to the movement from the time when the index finger is resting on the table until the time the finger stops at the display screen. The backward movement, on the other hand, would correspond to the movement from the time when the index finger stops at the display screen until it reaches back to the table and rests (i.e., the speed value is near zero again).

As explained above, the rationale behind the separation between forward and backward movement is that one is instructed and goal-directed, while the other is not, thus differing in their levels of intent. The latter is spontaneously self-initiated by the person without instruction. The statistical characteristics have been shown to differ between forward and backward movements (i.e., motion segment with high vs. low level of intent) during reaching, pointing, and grasping actions among different patient populations and across the general human population (Torres et al., 2010, 2011, 2013a, 2014; Nguyen et al., 2016). For that reason, we expect that separating the movements in such a manner would allow us to examine the impact of cognitive load on movements involving different levels of intent.

Analyses of the sensors from other body parts are beyond the scope of this article and will be disseminated in future work.

Motivation and Rationale: Micro-Movements Analytics for Motor Signals

For each forward and backward movement, we examined the linear and angular positional data and their higher order derivatives: the linear velocity, the angular velocity, the linear acceleration and the angular acceleration. For each time-series data the peak amplitudes and inter-peak intervals were identified, converted to micro-movements (see below) and gathered across all trials. Among the four types of parameters, for both forward and backward movements, angular acceleration was analyzed, as it has the largest number of peaks and provides the signal with the highest statistical power (hundreds of peaks per person) to carry on our stochastic estimation with high (95%) confidence.

We underscore that the current paradigm relies on the statistical power of an estimation procedure (which will be detailed in the next paragraph) so the higher the number of samples used to make an empirical estimation for a given person, the less taxing the experiment is to the participant, as it takes less time to attain a robust estimate. For instance, during a typical point-to-point reaching action, which consists of a single forward and backward movement, the linear velocity would typically provide at least two salient samples (peaks; see **Figure 3A**), one for forward and one for backward movement. To gain enough peak data from the linear velocity speed profile during a single experimental session and attain proper statistical power, the participant would need to perform at least 100 reaches. These would give us statistical power for the estimation of the probability distribution function (PDF) describing each segment but would likely lead to fatigue-related effects. However, using underlying kinematic parameters with higher number of samples (i.e., higher order of peak data) instead can result in shorter experiments. In turn, this would allow us to include additional conditions to manipulate various contextual parameters. For that reason, the current study focused on examining the peak data obtained from *angular acceleration*, as this provides the most power in the statistical estimation within the shortest time. The tradeoff here is that higher order derivatives of the position/orientation data (such as angular acceleration) can introduce large fluctuations from instrumentation noise. However, we have developed in house filtering/smoothing methods (Nguyen et al., 2014a) and combined them with traditional filtering (Paarmann, 2001) to eliminate such potential issues when using higher order derivatives of the position and orientation data. In the present work, we further rely on a variety of filtering algorithms embedded in the data collection interface we used (Sports Inn, The Motion Monitor, Chicago, IL, USA).

To build a unit-less normalized scale, and to address possible allometric effects (Mosimann, 1970) due to individual anatomical differences, the peak amplitudes of the angular acceleration were normalized as:

$$Norm\ Peak\ Amplitude\ (AM) = \frac{Peak\ Amplitude}{Peak\ Amplitude + Avrg_{\text{Min to Min}}} \quad (1)$$

Normalized peak amplitude (coined *amplitude micro-movements* (AM), Torres et al., 2013a) provides a scaled summary of the continuous data, and is computed using equation (1), by dividing each local peak amplitude by the sum of the peak amplitude and the average of the signals sampled within the neighboring points of two local minima surrounding the peak (**Figure 4B** inset). While we convert the analog continuous signal into a point process and treat it as a continuous random process for statistical estimation, the averaging in the denominator preserves the information contained in the points surrounding the maxima. Higher values of the AM imply lower values of the signal amplitude on average. Likewise, shifts towards lower values of AM imply increases on the magnitude of the amplitude values on average. We emphasize that representation of spike trains is not reduced to a binary scale (unlike the binary representation of cortical neuronal spikes). We work with a continuous (normalized) scale with real values ranging from 0 to 1. Further the averaged peaks in the denominator are Gamma distributed and so are the peaks in the numerator. As such the resulting scaled value is also Gamma distributed.

Besides the amplitude information, peak data can provide estimates related to the motion's temporal dynamics. To that

end, normalized inter-peak interval timings were computed by extracting the time elapsed between consecutive peaks (*timing* TM) and normalizing the array of these TM values using Equation 1 (coined *timing micro-movements* NTM). The two types of normalized, unitless spike-dependent data (i.e., AM, NTM) can be visualized in a spike train format as shown in **Figure 4C**. Further, the physical ranges (deg/s^2 and seconds) of the original peaks can be used to color code the graphs and show the range of parameters of each participant as shown in **Figure 4F**. This is a personalized approach that enables us to distinguish the physiological features of each person, while automatically unveiling self-emerging trends in a group.

The micro-movements are then used as input to a Gamma process. These spike-train data are accumulated within a time window that depends on the sampling resolution of the sensors and on the physical phenomena under investigation. In this case, the sampling resolution is 240 Hz and the physical phenomena (i.e., a self-generated pointing movement consisting of a forward and backward motion, produced by the nervous system) are on the order of approximately 1500 ms each (see Supplementary Table S1). As such, we have many sample peaks within a single minute. Usually, we set the size of the sampling window to 1 min (e.g., when we collect data continuously for 12 h in a hospital setting; Torres and Lande, 2015), but in the present article we use all trials in a given condition accrued across the experimental session. The time window for the estimated statistical parameters is the duration of the session (see experimental epochs for one trial in **Figure 2**). For each condition we gather all peaks of the angular acceleration and plot a frequency histogram using optimal binning (Freedman and Diaconis, 1981; Shimazaki and Shinomoto, 2007; **Figure 4D**). The histogram is then fitted using maximum likelihood estimation (MLE; see Supplementary Figure S3) to estimate the best continuous family of probability distributions that fits the data with high confidence. We have set the confidence intervals (CIs) for the empirically estimated Gamma parameters to 95%.

Prior work from our lab was the first to explore in human data the differences between multiplicative (e.g., lognormal family) and additive (e.g., exponential families) random processes of the micro-movement spike trains during voluntary, automatic and involuntary motions (Torres, 2011). Among these are micro-movements data from boxing routines involving voluntary and spontaneously performed movements (Torres, 2011, 2013c), forward-retracting motor loops during target-directed reaches (Torres et al., 2010, 2011, 2013a, 2014; Nguyen et al., 2016), natural walking involving automatic gait patterns (Torres et al., 2016b), and involuntary head motions during resting state within fMRI experiments (Torres and Denisova, 2016; Torres et al., 2017). In all cases, the continuous Gamma family of probability distributions has been the best fit (based on MLE and Kolmogorov-Smirnov tests (KSTs) for empirically derived cumulative distributions), showing that the human data has a wide range of PDFs, ranging from the exponential to the normal distribution. This contrasts with the assumption of a one size fits all model guided by the theoretical Gaussian distribution. Given that we found good fitting for the Gamma family under MLE, here we opted for the Gamma process to represent our spike trains of micro-movements. The Gamma PDF is given by:

$$y = f(x|a,b) = \frac{1}{\Gamma(a)b^a} x^{a-1} e^{\frac{-x}{b}} \tag{2}$$

in which a is the shape parameter, b is the scale parameter, and Γ is the Gamma function (Ross, 1996). The two parameters in equation (2)—shape (a) and scale (b)—were estimated for each histogram of the micro-movement data, as mentioned, using MLE with 95% CIs. The estimated parameters with their CI were plotted on a Gamma parameter plane, where the x-axis represents the shape parameter value and the y-axis represents the scale parameter value (**Figure 4E**).

The Gamma scale value conveys the noise to signal ratio (NSR) since the Gamma mean $\mu_\Gamma = a \cdot b$ and the Gamma variance is $\sigma_\Gamma = a \cdot b^2$, the scale:

$$b = NSR = \frac{\sigma_\Gamma}{\mu_\Gamma} = \frac{\cancel{a} \cdot \cancel{b}^2}{\cancel{a} \cdot \cancel{b}} \tag{3}$$

In this sense, according to equation (3), the scale axis of the Gamma parameter plane allows us to infer behaviors leading to higher noise levels vs. lower noise levels. Along the shape axis, the Exponential distributions at $a = 1$ are found in autism cases (Torres, 2011, 2013c). Using this approach, we can track processes whereby events in the past do not contribute to the prediction of future events and are well characterized by the Exponential (the most random) distribution. We can also track processes where the events in the past predict future events with high certainty and observe skewed to symmetric distributions along the shape axis with the Gaussian distribution at the opposite extreme of the Exponential case. We have indeed done so and provided the first empirical characterization of human motions on the Gamma parameter plane (Torres et al., 2016a).

Additionally, the estimated Gamma moments were obtained and plotted in a four-dimensional graph (**Figure 4F**). Here, the empirically estimated mean, variance and skewness of the fitted Gamma PDFs are plotted on the x, y and z axes respectively. The size of the marker reflects the level of kurtosis, where larger size indicates higher kurtosis level (distributions with sharper peaks) of the fitted PDF. Negative skewness means that the data are spread out more to the left of the mean than to the right. Positive skewness means that the data are spread out more to the right. Zero skewness indicates a perfectly symmetric distribution. This four-dimensional graph allows us to visualize the statistical features of the micro-movements and understand how the stochastic signatures shift across different conditions and/or individuals. The arrows are included to indicate the orderly flow of changes across different conditions. Note, that we standardized the waveform to a unit-less real-number ranging from 0 to 1 and lost the original range of the physical units. To capture the physical range of the raw data for each person, we include color as a fifth dimension to visualize the gradient of physical ranges of the data underlying the AM (expressed in deg/s^2) and NTM (expressed in second), giving us the change in physical units along this color gradient for each participant. The marker's face represents the median of the physical values within a condition, and the marker's edge is used as another

feature to represent the condition (i.e., cognitive load type). This visualization tool allows us to see the physical ranges of each individual person in transition from one condition to another, while expressing all parameters along a common unit-less standard scale. Note that reporting on the physical parameter ranges of each instrument while maintaining the standardized unit-less scale for statistical estimation and inference is amenable for data exchange and reproducibility of results in our fields of study.

Graphs such as **Figures 4E,F** produce a useful visualization tool to uncover patterns (see Torres et al., 2016a, 2017) for examples of large population groups that self-cluster according to nervous systems pathologies using these methods). Here, we can visualize participants as a group and uncover self-emerging clusters of the general population, without *a priori* hand-picking homogeneous groups for significant hypothesis testing comparison (as it is traditionally done across the fields of brain and health sciences). This is very important because the patterns that we uncover are entirely *data-driven*, as the patterns self-emerge from the inherent variability of the nervous systems signals.

In the present work, we only have nine participants. However, we underscore the personalized and empirically driven nature of this statistical platform, as the statistical power lies in the number of samples per person. The population family of Gamma distributions for the human spectrum has been *empirically* characterized in prior work (Torres et al., 2016a) for this basic pointing task. This platform enables us to make well-informed statistical inferences and interpret the empirically-driven statistical phenomena under consideration.

Note also that we can examine the deliberate and spontaneous processes by analyzing the micro-movement of forward and backward motor signals, since the empirical data showed that these processes map well onto voluntary goal-directed motions and automatic uninstructed/goal-less motions, respectively (Torres, 2011, 2013c).

Analytics for Heart Signals (Inter-Beat Interval)

Like the analysis performed on the micro-movement peak data of motor signals (i.e., AM, NTM), we applied the distributional analyses on the IBI data for each condition. As with the hand kinematics, we fitted the PDF using MLE (see Supplementary Figure S4). Histograms for the IBI data were fitted among the Gamma, exponential, lognormal, and normal for each condition, and we determined that the continuous Gamma family of distributions would be appropriate for fitting the IBI data. For that reason, the parameters of the Gamma PDF were estimated for each histogram of the IBI data, and the shape and scale values were plotted on the Gamma parameter plane with 95% CIs, and the Gamma moments of the estimated PDFs were plotted on a 4D graph. Through this analysis, we could examine the inevitable processes emerging from the ANS.

RESULTS

Given the preliminary analyses of **Figure 3C**, demonstrating statistically significant effects given by increases in cognitive demands on the participants' performance (accuracy and time), and their influences on the number of peaks of the biophysical signals, we felt confident to explore the stochastic nature of signals and more precisely characterize such effects at different levels of functionality and control.

ANS Assessment of (Inevitable) Autonomic Control of IBI

The estimated Gamma parameters characterizing the PDFs of the IBI showed a distinct trend in the separation between the two conditions at 95% CI. **Figure 5A** shows the individualized profiling of each participant's stochastic transitions from low to high cognitive load condition, with the arrow marking the order of those conditions. As the cognitive load increases, there is a trend across participants to increase the PDF skewness (note, the PDF shape is symmetric when the skewness value is 0), and an overall tendency to increase the variance.

The increase in the IBI's timing variance as the cognitive load increases is reflected in the increase of the NSR (i.e., the value of the Gamma scale parameter in **Figure 5B** bottom panel showing the Gamma parameter shape-scale plane) across all participants. Each participant's PDF for low (blue) and high (red) cognitive load is plotted in the inset of **Figure 5A**. Each point on the Gamma parameter plane represents a single participant, and the CIs are set to 95% level. **Figure 5C** illustrates the results of using the KST to compare two empirically estimated PDFs estimated under each condition. In particular, rows 1–3 are Low vs. High; Low vs. Control baseline pointing; and High vs. Control respectively; while the fourth and fifth rows of the color matrix in **Figure 5C** show the departure of the estimated PDF from the normal distribution for the low and high load condition respectively. In all cases, a significant shift of the PDF can be appreciated for different conditions performed during the same pointing task.

In contrast to the task requiring different cognitive demands, the time estimation task elicited modest changes when compared to the baseline pointing task in the estimated Gamma PDF parameters of the IBI, as is shown in **Figures 5D–F**. Yet, the comparison of the empirically estimated PDFs to those of the normal distribution did yield significance (**Figure 5F** rows 2 and 3 of the matrix). This underscores the skewed nature of these distributions and the variety of the family across the general population (see inset in **Figure 5D**). Although the changes in dispersion and shape were more modest in time estimation-pointing task than in the high-low cognitive load task, the overall shifts in PDF recorded within one experimental session and the variations in skewness and dispersion across subjects were quantifiable and significant.

Further distinction between the two tasks can be appreciated in the fitting line to the log-log of the scatter and the behavior of the scatter on the line. These are shown in insets to **Figures 5B,E**. There, the high-load case shows a broader variety of PDFs with a broader and more separable distributions per condition; while the time estimation case shows a narrower range of PDFs and a more mixed scatter of points between the baseline pointing and the pointing during time estimation. Both slopes and intercepts of the fitting line were similar (Low/High

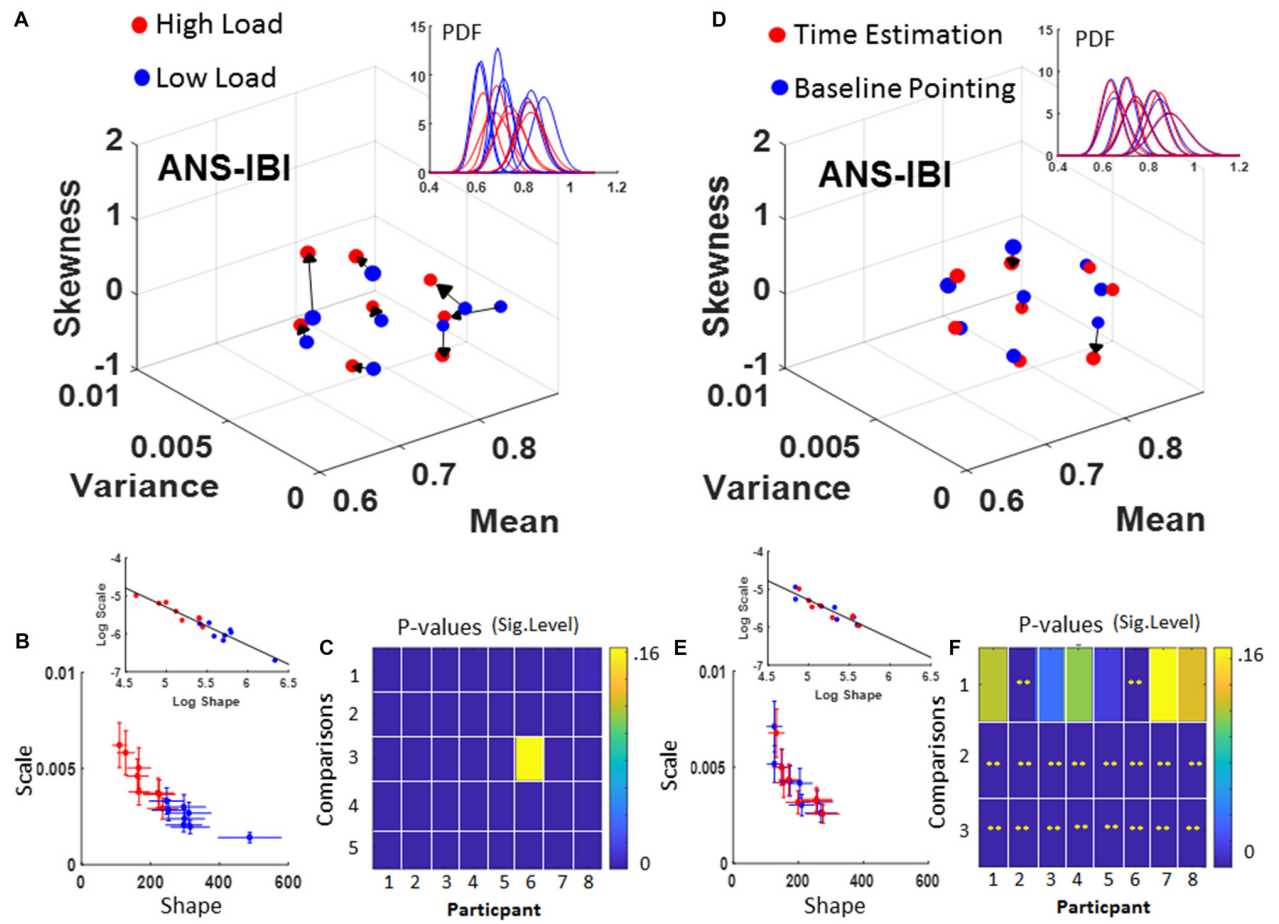

FIGURE 5 | ANS autonomic control assessment under high and low cognitive load conditions. Inter-beat intervals (IBI) signal. When comparing between high and low cognitive load conditions **(A–C)** and basic pointing with pointing during time estimation **(D–F)**. **(A)** Shifts in the empirically estimated Gamma moments of the IBI distinguish Condition 1 (low load) from Condition 2 (high load) along moment axes, and PDFs spanning a family (inset). **(B)** Gamma parameters separate conditions whereby high load have higher NSR and lower shape (higher skewness) than low load condition. Insets show the linear fitting of the log-log scatter (see **Table 1** for slope and intercept values). **(C)** Pairwise Kolmogorov-Smirnoff test (KST) for empirically estimated distributions (1–3 are Low vs. High; Low vs. Control; and High vs. Control respectively). Comparisons 4, 5 refer to the KST for each empirically estimated distribution vs. the theoretical normal for low and high cognitive load respectively. **(D)** Similar plots as in **(A–C)** in reference to the basic pointing and pointing during time estimation. **(E)** Note the different location of the scatter on the Gamma parameter plane and the difference in slope and intercept of the inset. **(F)** Pairwise comparison of empirically estimated distributions using KST for each participant: (1) baseline point vs. time estimation; (2) baseline pointing vs. normal distribution; (3) Time estimation vs. normal distribution.

load slope −1.01 intercept −0.27; Point/Time estimation slope −1.01 intercept −0.23; also see **Table 1**) while the scatters shifted along the line.

CNS Assessment of Deliberate and Spontaneous Processes in Hand Kinematics

Low Cognitive Load vs. High Cognitive Load

The estimated Gamma parameters characterizing the PDFs of the hand kinematics were extracted from the pointing task and separated into a deliberate forward movement segment and a spontaneous backward movement segment. Then, for each of these segments, the stochastic transitions of kinematic micro-movements were examined between the low and high cognitive load conditions.

Fluctuations in normalized inter-peak-time intervals (NTM)

The changes in the estimated Gamma moments referring to the fluctuations in timing information are shown in **Figure 6**. Both the deliberate (forward) and the spontaneous (retraction) motions showed a large departure from 0-shift across all participants. This means that the PDF of each participant shifted to a different PDF altogether; thus, strongly advising against the assumption of a theoretical uniform statistical approach to assess the entire group. This is the *one size fits all* model currently in use by traditional approaches and discussed in Supplementary Figure S1.

The PDFs that we empirically estimated for each participant were skewed, as is shown in the insets of **Figures 6B,D**; thus, strongly advising against the theoretical assumption of symmetric distributions such as the Gaussian distribution

TABLE 1 | Power law fit of estimated gamma parameters.

Parameter	Scatter points from	Slope	Intercept
IBI	Low load vs. High load	−1.0053	−0.2703
	Point vs. Time estimation	−1.0109	−0.2278
NTM forward	Low load vs. High load	−1.0304	−0.3678
	Point vs. Time estimation	−1.0352	−0.3372
NTM backward	Low load vs. High load	−1.0178	−0.4466
	Point vs. Time estimation	−1.0409	−0.3131
AM forward	Low load vs. High load	−1.0260	−0.3856
	Point vs. Time estimation	−1.0226	−0.4055
AM backward	Low load vs. High load	−1.0003	−0.5324
	Point vs. Time estimation	−1.0133	−0.4600

for statistical inference. Besides visual inspection, this result was further verified using the Kolmogorov Smirnov test to compare the empirically estimated distribution against the normal distribution, yielding significant departure from normality ($p \ll 0.01$) across all participants (see Supplementary Figure S5D).

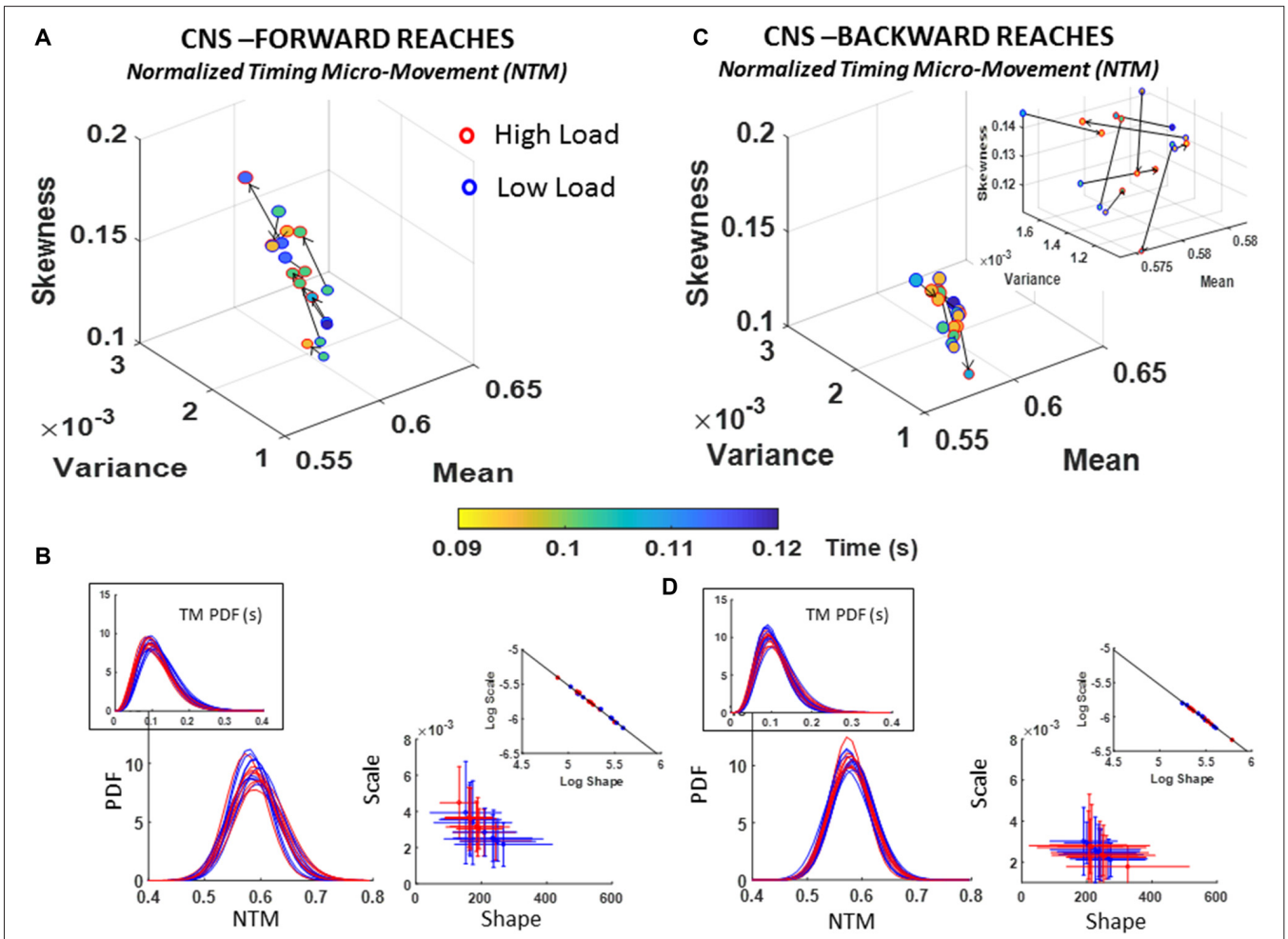

FIGURE 6 | CNS voluntary control assessment of goal-directed forward normalized inter-peak-time intervals (NTM) **(A,B)** and CNS automatic backward NTM **(C,D)** during low and high cognitive load conditions. **(A)** Estimated Gamma moments showing shifts in NTM distribution parameters from low to high cognitive load condition for forward motions, and color gradient denoting the range of physical parameter (time, seconds), where marker color for each participant noticeably shifts range between conditions. **(B)** PDFs family across participants for the unitless NTM along with those for the raw TM in inset (left) and Gamma parameter plane (right). Log-log scale aligns scatter along linear fit (see **Table 1** for slope and intercept information). **(C)** Same as in **(A)** for spontaneous retractions with inset plotted at local scale to appreciate the shifts in PDFs moments. **(D)** Estimated NTM PDF family along with raw TM PDFs in inset (left) and Gamma parameters (right). Inset shows the shift of the scatter along the line fitted to the log-log plot (see **Table 1** for slope and intercept values and Supplementary Figure S5 for detailed comparisons of pairwise KST distribution comparisons for each participant).

Furthermore, comparisons of the parameters of the estimated Gamma PDFs and moments yielded differences in skewness and dispersion with the task. In the forward case of **Figure 6A**, a trend denoting an increase in skewness and dispersion of the fluctuations in timing with the increase in cognitive demands was quantified. The large shifts in PDFs for forward motions contrasted with the backwards reach (retracting the hand to rest without instructions), where the changes were more modest (see **Figure 6C**). Specifically, each participant had a unique type of shift in PDF as the cognitive load increased during backward reaches (i.e., spontaneous process). Inset in **Figure 6C** zooms in the scatter to show the shifts in the moments of the PDF estimated and shown in **Figure 6D** for the backwards case.

The results of assessing these stochastic transitions with the Kolmogorov Smirnov test are detailed for each participant in Supplementary Figure S5A. Importantly, besides the shifts in PDFs, we also quantified shifts in the physical range of the parameters underlying the NMT (i.e., the range concerning the number of seconds the original inter-peak time intervals manifested). These are appreciated in **Figures 6A,C**, where the changes of marker-face colors should be examined following the arrow representing the order of presentation (from low to high cognitive load). The shifts in physical range correspond to the color gradient in the color bar.

To further quantify the shifts in PDFs between forward and backward cases, we used the line fitting the scatter represented in log-log transform of the Gamma parameter plane. These are depicted in the insets of **Figure 6B**-right panel and **Figure 6D**-right panel along the shape and scale axes. Forward slope −1.03 intercept −0.37; Backward slope −1.02 intercept −0.45; also see **Table 1** reflect similarity in the fitting lines with different locations and spread of the scatters. In the forward motions the stochastic signatures of the NTM have a broader and more uniform spread along the line while in the backward motions the spread tended to lower NSR ranges and more symmetric shapes (down and to the right of the line). This suggests a stochastic process in the spontaneous retractions that is more predictable (towards the Gaussian ranges) and less random (away from Exponential ranges) than those quantified in the deliberate case.

Fluctuations in angular acceleration amplitude micro-movements (AM)

The analyses of the fluctuations in the amplitude of the angular acceleration, as normalized by the micro-movements data type (AM) using equation (1) show departure from 0-change in PDF for all participants. As with the TM and NTM cases, these results also advise against the use of a *grand average* treatment to these biophysical data. Each participant manifested a different stochastic shift. Further, there were no visible patterns across all participants. Here, both the forward and backwards cases showed unique shifting patterns for each person's stochastic signatures. The trend was rather in the physical ranges of angular acceleration, which tended to decrease with the increase in cognitive load for the forward reaches. This trend in reduction of angular acceleration amplitude (**Figure 7A**) was generally opposite in the backwards retractions (**Figure 7C**), with some variations unique to each participant. The color bar (deg/s^2) of **Figures 7A,C** provide information on the median physical range.

Of note is the skewed (Exponential-fit) distributions of the original peaks of the angular acceleration shown in **Figures 7B,D** insets. The scaling of equation (1) transformed the micro-movements data from Exponential to Gamma distributed angular acceleration micro-movements, as shown on the Gamma parameter plane and corresponding PDFs of **Figures 7B,D**. This family of PDFs estimated within the time span of a section further confirms that the motor signatures under cognitive load are non-stationary. They shift stochastic signatures in quantifiable ways even within the experimental session, in the first 10–20 min.

As with the NTM parameter, here, besides uncovering individual shifts between high and low cognitive loads for each movement type, it is also possible to ascertain the overall shifts of the group scatter between the deliberate and spontaneous movements. In the log-log Gamma parameter planes of **Figure 7B** vs. **Figure 7D** we can see these shifts in the slope and intercepts of the line fitting the log-log transform of the scatter (Forward slope −1.03 intercept −0.39; backward slope −1.00 intercept −0.53; see also **Table 1**). For the forward case there is broader spread (as in the case of NTM) than the backwards case. The latter shows a trend to PDFs with lower NSR (lower dispersion) and more symmetric shape. See also the PDF plots corresponding to **Figure 7B** (flatter) and **Figure 7D** (peakier). These features are reflected as well in lower skewness and higher kurtosis when comparing the Gamma moments across forward and backward reaches (**Figure 7A** vs. **Figure 7C**).

Pointing vs. Time Estimation (Decision-Making) Task

Deliberate forward and spontaneous backward reaches revealed systematic shifts in PDFs for all participants and parameters under examination, when comparing the basic pointing task to the pointing task under time estimation. Several features for each parameter are reported below.

Fluctuations in normalized inter-peak-time intervals (NTM)

A trend across all participants in the deliberate forward reaches was a marked decrease in parameter range (time in seconds) underlying the NTM data. Namely, basic pointing on average took longer time between peaks (blue range of the color gradient in **Figure 8A**) than pointing under time estimation, exhibited by shifts in color gradient towards green/yellow range. These shorter time intervals between peaks denote faster transitions in the acceleration of the hand's rotations. Another trend with the time estimation task was a decrease in the dispersion (shown along the scale axis of the Gamma parameter plane) with most participants shifting to lower NSR and towards distributions of higher shape value (more symmetric), as shown in **Figure 8B**. For backward motions (**Figures 8C,D**), the patterns of the underlying physical time reverted, whereby marker colors in **Figure 8C** shifted from light to dark blue ranges for some, indicating an increase in the number of time between peaks (i.e., slower rates of rotation).

The stochastic transitions in PDF signatures were tested against the normal distribution for each estimated PDFs across conditions for both forward and backward motions and showed to significantly depart from the normality (details can be found in

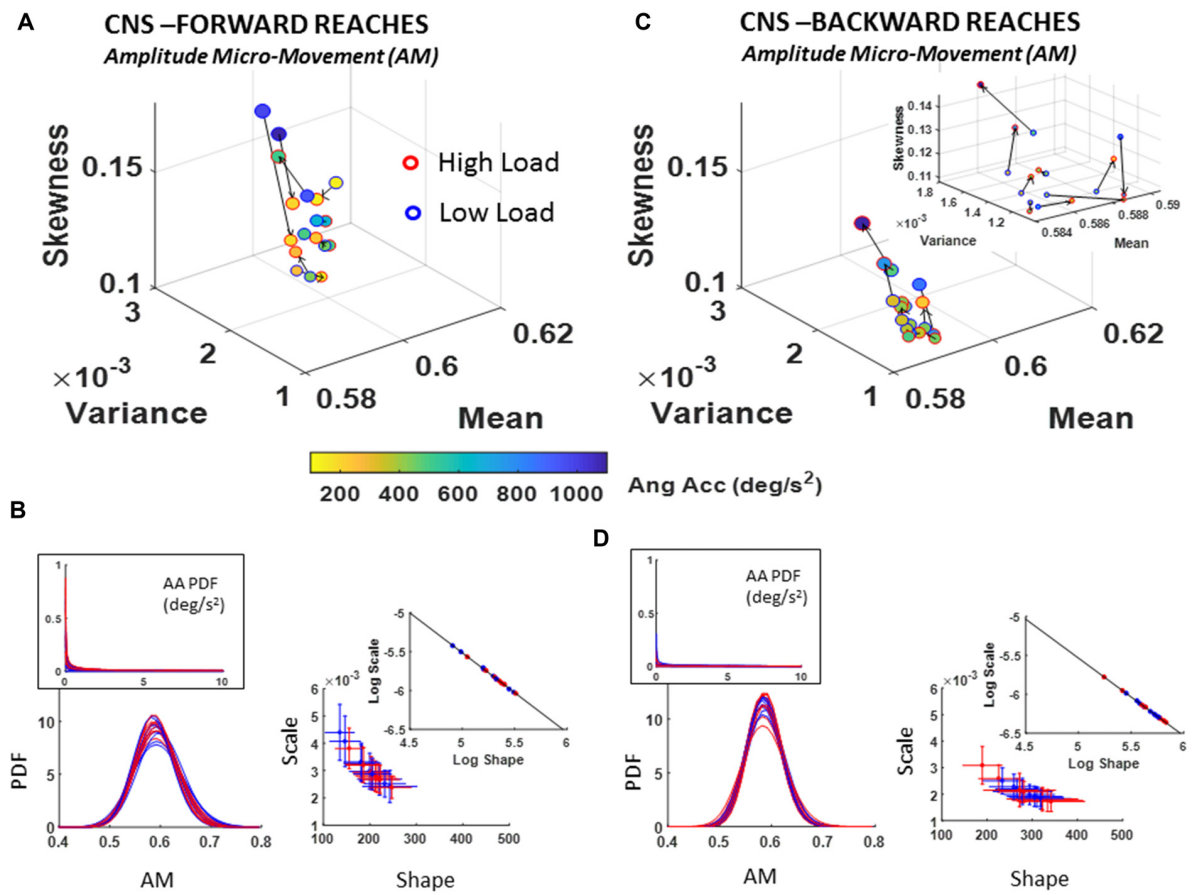

FIGURE 7 | CNS voluntary control assessment of goal-directed forward AM **(A,B)** and CNS automatic backward AM **(C,D)** during low and high cognitive load conditions. **(A)** Estimated Gamma moments showing shifts in AM PDF from low to high cognitive load condition for forward motions, and **(B)** its AM estimated family of PDFs along with raw angular acceleration peaks PDF in the inset (left) and Gamma parameters (right). **(C)** Same as in **(A)** for the spontaneous retractions. **(D)** Same as **(B)**, showing the shifts in PDFs towards lower dispersion and more symmetric shapes on the Gamma parameter plane and the log-log inset showing the linear fit (see **Table 1** for slope and intercept reports and Supplementary Figure S5 for detailed comparisons of pairwise KST distribution comparisons for each participant).

Supplementary Figure S5E). We obtained the slope and intercept of the line fitting the log-log transform of the scatters (Forward slope −1.04 intercept −0.34; backward slope −1.04 intercept −0.31; also see **Table 1**) and found a more modest shift down and to the right of the line than in the conditions involving low vs. high loads. Nonetheless, the changes can be best appreciated in the insets showing the PDFs whereby the more skewed distributions in **Figure 8B** as compared to **Figure 8D** inset are evident. Further the reduction in dispersion from inset PDFs in **Figure 8B** as compared to inset PDFs in **Figure 8D** is also evident. These visible effects were quantified and their significance shown in Supplementary Figure S5.

Fluctuations in angular acceleration amplitude (AM)

A change in the estimated PDF from basic pointing to pointing during time estimation was registered for the fluctuations in the amplitude of the angular acceleration peaks, AM, as scaled by equation (1). The individual shifts in the empirically estimated Gamma moments were registered for both the forward and backward reaches. The overall trend in the scatter of forward reaches of **Figure 9A** is an increase in skewness of AM distributions corresponding with higher ranges of physical angular accelerations (see color gradient depicting median range values of deg/s^2).

Comparing between the movement classes, forward reaches tended to have distributions with higher skewness as quantified in the moments graphs of **Figure 9A** vs. **Figure 9C**. Further, **Figure 9B** vs. **Figure 9D** show the differences between these deliberate and spontaneous processes reflected in the NSR (Gamma scale) and the Gamma shape estimated values for each movement class.

In the forward goal-directed motion, the stochastic signatures had higher NSR and lower shape parameters than the spontaneous backward motions. The lower shape corresponds to the higher positive skewness of Gamma moments plot in **Figure 9A**. These features are visualized and apparent in the corresponding panels of PDFs in **Figure 9B** vs. **Figure 9D**. They are also quantifiable as shifts of the overall scatter along the line fitting the log-log transform of the Gamma parameter plane. The slope and intercepts of the log-log transform of the scatters for

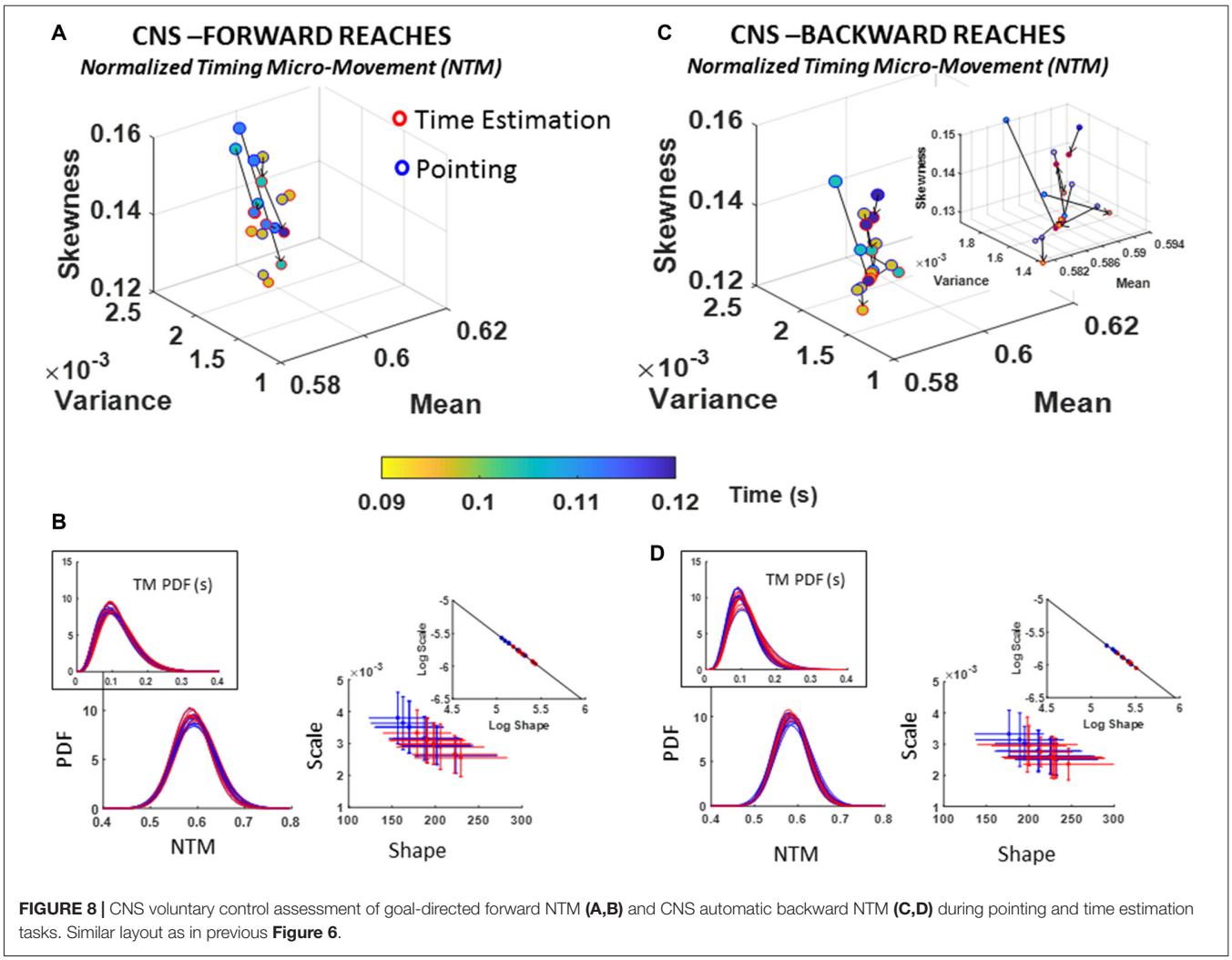

FIGURE 8 | CNS voluntary control assessment of goal-directed forward NTM **(A,B)** and CNS automatic backward NTM **(C,D)** during pointing and time estimation tasks. Similar layout as in previous **Figure 6**.

the forward and backward reaches are similar (Forward slope −1.02 intercept −0.41; backward slope −1.01 intercept −0.46; also see **Table 1**); yet the scatter in the backwards motions shifted down and to the right towards more distributions with lower dispersion (downward-shift) and higher shape (right-shift). Furthermore, Supplementary Figure S5B points the reader to differences in the PDF between the two tasks as quantified by the KST. These differences were significant as shown in various parameters.

DISCUSSION

This work provides a new theoretical research framework, datatypes, and analytics combined with an experimental paradigm to study the interactions between mental states and physical actions. We systematically probed the variability inherently present in the biophysical rhythms across the multiple layers of the nervous systems, as participants pointed to communicate their decisions, and as they were exposed to different levels of cognitive loads. Under such conditions, and through a simple pointing task, we examined the influences of cognitive demands across multiple layers of the nervous systems and through fundamentally different processes—*deliberate, spontaneous and inevitable*. These proposed processes have specific characteristics and can be studied (non-invasively) through the variability of various somatic-sensory-motor and heart signals harnessed in tandem (Ryu and Torres, 2017).

We detected the effects of cognitive load in multi-modal signals across different levels of functionality, and identified specific parameters characterizing cognitive load through the stochastic shifts of biophysical signals. Specifically, using a personalized method of statistical analyses, we found families of skewed probability distributions better describing the empirical variability of the data, as opposed to assuming the normal distribution for statistical inference.

Within the time span of minutes, the stochastic signatures of parameters from the pointing motions shifted for each participant in ways that were well-characterized by a Gamma process. Using the new datatype that converts continuous analog kinematic signals to real-valued spike trains normalized between 0–1 and treating the various types of cognitive demands as a continuous stochastic process, we were able to capture marked

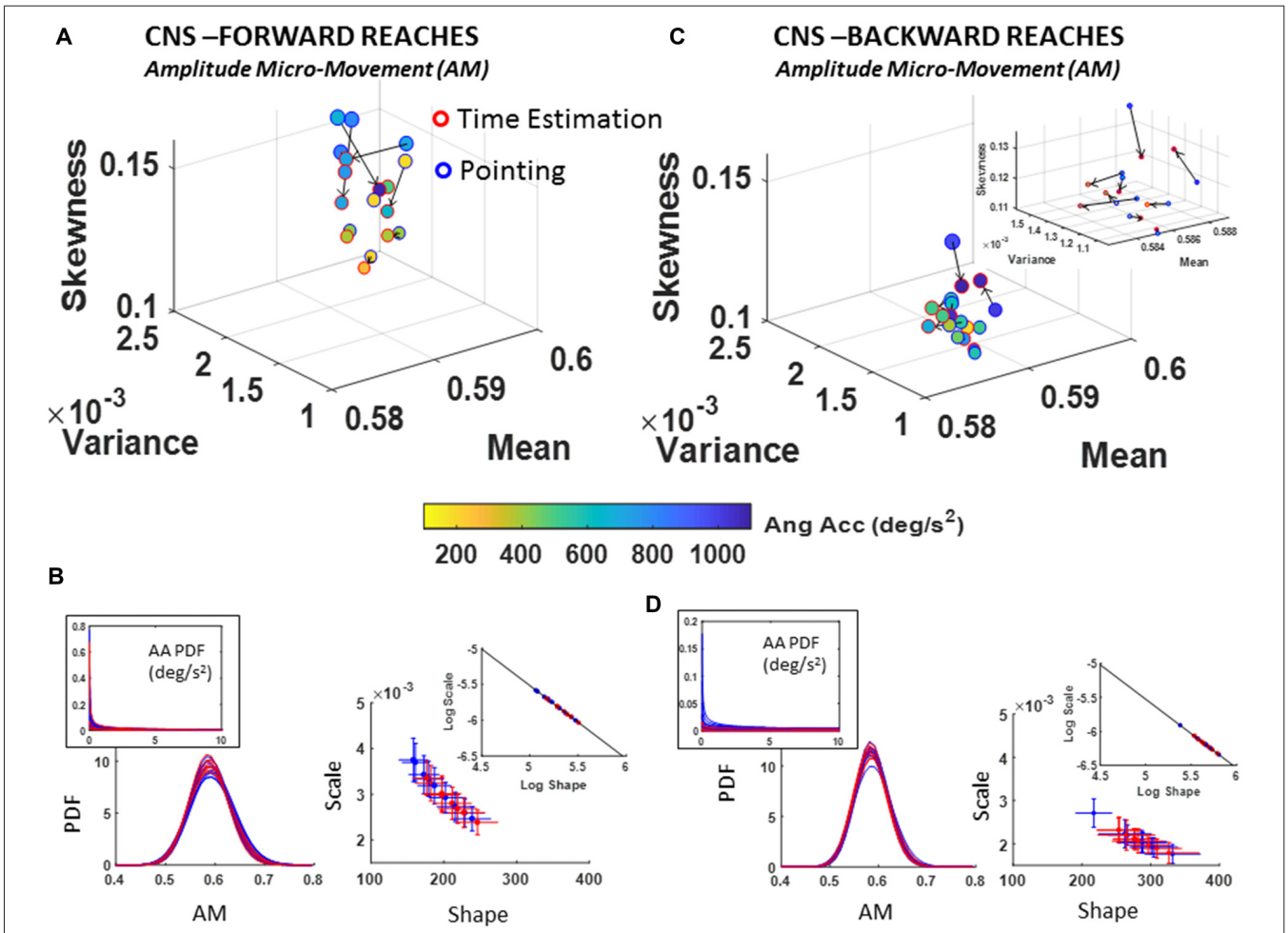

FIGURE 9 | CNS voluntary control assessment of goal-directed forward AM **(A,B)** and CNS spontaneous backward AM **(C,D)** during baseline pointing and pointing during time estimation tasks. Format as in **Figure 7**. Note the shift of the scatter in the insets of **(B,D)** whereby the PDFs denote distributions with lower dispersion and more symmetric shapes in the backwards reaches.

effects of cognitive load on the somatic-motor parameters. A simple pointing task performed with the same biomechanical structure, but while making decisions on time estimations, or while counting backwards, was sufficient to help us read out in the motor and heart variability code, the various mental influences across deliberate, spontaneous and (inevitable) autonomic processes.

Of relevance here, we highlight the marked differences we found in IBI with changes in the cognitive demands of the task, transitioning from low to high cognitive loads. Changes in PDF of the IBI were not as marked with the time estimation task, perhaps inviting thoughts about differences between a task with higher cognitive demands (counting backward) and one with lower demands (estimating time). Indeed, the mere quantification of the number of angular acceleration peaks during the higher cognitive loads denoted higher demands in bodily motions: i.e., the hand moved significantly more at the micro-level with higher cognitive demands. As such, when viewed cumulatively over the timespan of the task, the system overall required more energy. This may be reflected as well in the shifts in IBI with higher cognitive loads. In this sense, we found a statistically quantifiable link between cognitive loads and physical motions whereby differences are detectable and have characteristic values that we summarized in various ways. Among these, the slope and intercept of the log-transform of the scatter points on the Gamma plane was similar for each experiment (i.e., low-high cognitive load vs. pointing and pointing while estimating time), denoting a power-law relation between the shape and scale estimated parameters for each participant. Yet the location of the scatter along the fitting line of these points representing the personalized family of PDFs changed across conditions and between the deliberate and spontaneous classes of motions. They also changed for the IBI timings of the autonomic motions. The main shift from deliberate to spontaneous mode was down and to the right on the Gamma parameter plane, consistently denoting distributions with lower NSR and more symmetric shapes. During these tasks, across all parameters, the spontaneous

retractions were unexpectedly more controlled (lower noise and higher predictability) than the forward ones. Yet it was the forward motions that broadcasted more clearly the shifts across conditions in the signatures of variability of the kinematic parameters. These shifts were also noted in the IBI activity.

One limitation of the present methods is that they depend on the sampling resolution of the sensors and accordingly, on the time length of the task. In this study, due to time constraint of the experiment (to avoid fatigue) we were only able to examine angular acceleration as a kinematic parameter. As explained in the methods and Supplementary Figure S2, within the time constraints of this task, the angular acceleration provided enough peaks in its waveform for statistical power in our distribution-parameter estimation (we needed above 100 peaks for tight CIs). If we were to conduct this experiment for a longer period, we could examine other position-related parameters, such as linear speed and hand trajectory curvatures. However, this would have caused participants to experience fatigue during a prolonged experiment with conditions involving multiple levels of cognitive loads. The linear speed has fewer peaks-though we have recently studied the micro-movements in the context of basic pointing in autism (Wu et al., 2018). To make these methods amenable to use with commercially available biosensors like the inertial measurement units (IMUs embedded in smart phones) we could use linear acceleration. Linear accelerations would provide us with sufficient number of peaks in its waveforms, so we could possibly use these wearable devices in future studies. The trade-off is that we would then lose the positional data that we have access to with the present research-grade sensors.

The main take home message from the study is that even subtle fluctuations in timing and amplitude of the biophysical signals that we recorded could be detected under the proposed framework. Thus, the exact same task funneled out very different stochastic scenarios under slightly different conditions. The mere act of having to decide or having to do so under different cognitive loads changed these heart and kinematics parameters in ways we could capture here. These stochastic shifts would have been missed if we had averaged across the group or relied only on observation. In this sense, the present methods allowed us to detect *change* at the individual level on more than one statistical dimension. It also allowed us to examine the cohort as a group and within each condition, look at the effects of the cognitive demands on the deliberate, spontaneous and autonomous functional somatic-motor classes.

We underscore here that these stochastic shifts in the biophysical parameters were empirically characterized. We did not assume *a priori* any PDF, nor did we assume stationarity of the random processes under examination (Supplementary Figure S1). The shifts in the *empirically estimated* parameters of the continuous Gamma family of probability distributions, that we quantified here, occurred on the time scale of minutes, i.e., the duration of the experimental session. They strongly suggest that prior assumptions involving kinematics data analyses may be insufficient to capture the richness of cognitive phenomena, pertaining to their effects on the somatic-motor signals. Here, we showed that cognitive phenomena do not merely elicit a change in the mean or variance of somatic-motor related variables under a single PDF. Rather, different PDFs are needed altogether to better characterize cognitive phenomena for each person under examination, as it is continuously funneled through physical activity that leads to shifts in the signatures. The process changes dynamically along the multiple layers of the nervous systems.

Another aspect of the results alludes to the motor control literature examining pointing behavior. There, the uninstructed retraction segments, during which the hand automatically returns to rest (i.e., backward movement), are hardly ever considered as part of the overall behavior. However, when we examined those retraction segments, we quantified the effect of cognitive load on biophysical signals from spontaneous processes in the moment-by-moment variations of the angular acceleration NTM. Indeed, their stochastic signatures showed statistically significant shifts in the empirically estimated parameters of the Gamma PDF family (i.e., statistically significant departure from zero-valued change across all participants for all Gamma moments).

Pointing is a very automatic task, and yet several motor signals from the peripheral end-effector were significantly affected by simply adding an additional task requiring decision-making (see Supplementary Figure S5 whereby for each participant at least one change in PDF is highly significant across pairwise compared conditions). This result implies that decision-making processes driven by central controllers at the CNS level can be quantified using the continuous flow of the motor signal, as the voluntarily generated bodily motions unfold to communicate the decision; and as the fast-automatic segments of the motion spontaneously unfold. In this sense, a parallel between slow-fast (deliberate-automatic; Kahneman, 2011) decision-making processes and deliberate-spontaneous somatic-motor signals can be established and well characterized using continuous physiological signals beyond discrete mouse clicks. Our conceptualization of multi-layered influences across the different functional levels of the nervous systems adds the *inevitable* (autonomic) afferent processes feeding back to the cognitive systems. As such, we provide a new experimental paradigm and a unifying statistical framework to study *embodied cognitive decision-making* under a renewed theoretical construct of multi-modal, multi-functional *recursive* kinesthetic afference.

EMBODIED APPROACH TO STUDY COGNITION

The current study employs a novel methodology to assess features of *embodied* cognition. The new method extracts continuous signals obtained from the PNS, including the ANS, and statistically characterizes those signals under a common unit-less (i.e., normalized) scale, using different levels of cognitive loads (driven by the CNS), thereby allowing us to gain a glimpse into the *brain-body coupled stochastic dynamics*. In this sense, we have characterized cognitive load

with sensory and somatic-motor signals, alluding to processes that occur in a closed (recursive) loop between the many layers of the brain and the body (the body that the brain aims to control at will); including also those spontaneous processes that fall largely beneath observational and/or sensing awareness. For instance, the input signals from the micro-movements of the movement-kinematics and the heart signals can be thought of as fluctuations providing an important source of guidance to the brain. They may be a form of re-afferent feedback, to help the brain compensate for synaptic transductions and transmission delays. By selectively shifting the signatures of statistical variability under different levels of cognitive load, different functional relations (in terms of probabilistic maps) between bodily responses and environmental demands (including cognitive loads) may be built, to be able to predict ahead the sensory consequences of bodily actions, even in the absence of, or the intermittent availability of relevant sensory information.

This multi-layered, multi-modal and multi-functional embodied approach to the study of cognitive processes has the potential to provide a more holistic perspective on our overall understanding of cognition and its development. Indeed, this simple paradigm was useful to examine the changes in bodily signals across multiple layers of the nervous systems and characterize the sensory-motor behavior that underlies cognitively driven performance. Furthermore, by adopting the renovated kinesthetic reafferent framework in this study, we could capture the variations of motor and multifaceted sensory inputs that must be integrated to drive cognitive processes (e.g., goal-selection, planning, decision making) under varying levels of control, ranging from voluntary to automatic to autonomic.

CONCLUSION

The current study provides important evidence to justify an embodied and personalized approach to studying cognition (Gallagher, 2014). This study offers a renovated theoretical construct grounded on the principle of kinesthetic reafference, a new unifying statistical method, datatypes and experimental paradigms to assess voluntary, automatic and autonomic signals through a common lens. As such, this work is an invitation to use such tools to help advance the field of embodied cognition.

AUTHOR CONTRIBUTIONS

JR designed experiment, collected and analyzed data and wrote the article. EBT designed experiment, designed analyses and wrote the article. Both authors agreed to the final version of the manuscript.

ACKNOWLEDGMENTS

This work was funded in part by the New Jersey Governor's Council for Medical Research and Treatment of Autism and the New Jersey Department of Health. It was also supported by the Nancy Lurie Marks Family Foundation Career Development Award to EBT.

SUPPLEMENTARY MATERIAL

The Supplementary Material for this article can be found online at: https://www.frontiersin.org/articles/10.3389/fnhum.2018.00116/full#supplementary-material

REFERENCES

Amano, S., Hong, S. L., Sage, J. I., and Torres, E. B. (2015). Behavioral inflexibility and motor dedifferentiation in persons with Parkinson's disease: bilateral coordination deficits during a unimanual reaching task. *Neurosci. Lett.* 585, 82–87. doi: 10.1016/j.neulet.2014.10.007

Freedman, D., and Diaconis, P. (1981). On the histogram as a density estimator: L theory. *Probab. Theory* 57, 453–476.

Gallagher, S. (2014). In your face: transcendence in embodied interaction. *Front. Hum. Neurosci.* 8:495. doi: 10.3389/fnhum.2014.00495

Gallistel, C. R. (2009). The importance of proving the null. *Psychol. Rev.* 116, 439–453. doi: 10.1037/a0015251

Gallistel, C. R., and King, A. P. (2009). *Memory and The Computational Brain: Why Cognitive Science will Transform Neuroscience.* Chichester, West Sussex, UK, Malden, MA: Wiley-Blackwell.

Hawgood, S., Hook-Barnard, I. G., O'Brien, T. C., and Yamamoto, K. R. (2015). Precision medicine: beyond the inflection point. *Sci. Transl. Med.* 7:300ps317. doi: 10.1126/scitranslmed.aaa9970

Hong, S. L., Isenhower, R. W., José, J. V., and Torres, E. B. (2014). Cognitive load results in motor overflow in essential tremor. *Neurocase* 20, 397–406. doi: 10.1080/13554794.2013.791859

Kahneman, D. (2011). *Thinking, Fast and Slow.* Basingstoke: MacMillan.

Kathirvel, P., Manikandan, M. S., Prasanna, S., and Soman, K. (2011). An efficient R-peak detection based on new nonlinear transformation and first-order Gaussian differentiator. *Cardiovasc. Eng. Technol.* 2, 408–425. doi: 10.1007/s13239-011-0065-3

Mahon, B. Z., and Caramazza, A. (2008). A critical look at the embodied cognition hypothesis and a new proposal for grounding conceptual content. *J. Physiol. Paris* 102, 59–70. doi: 10.1016/j.jphysparis.2008.03.004

Mosimann, J. E. (1970). Size allometry: size and shape variables with characterizations of the lognormal and generalized gamma distributions. *J. Am. Stat. Assoc.* 65, 930–945. doi: 10.2307/2284599

Nguyen, J., Isenhower, R., Yanovich, P., Ravaliya, J., Papathomas, T., and Torres, E. B. (2013). *Quantifying Changes in the Kinesthetic Percept Under a 3D Perspective Visual Illusion.* Naples, FL: Vision Science Society.

Nguyen, J., Majmudar, U., Papathomas, T. V., Silverstein, S. M., and Torres, E. B. (2016). Schizophrenia: the micro-movements perspective. *Neuropsychologia* 85, 310–326. doi: 10.1016/j.neuropsychologia.2016.03.003

Nguyen, J., Papathomas, T., Ravaliya, J., and Torres, E. B. (2014a). Methods to explore the influence of top-down visual processes on motor behavior. *J. Vis. Exp.* 86:e51422. doi: 10.3791/51422

Nguyen, J., Silverstein, S. M., Papathomas, T. V., and Torres, E. B. (2014b). *Characterization of Visuomotor Behavior in Patients with Schizophrenia Under a 3D-depth Inversion Illusion.* Washington, DC: Society for Neuroscience.

Paarmann, L. D. (2001). *Design and Analysis of Analog Filters: a Signal Processing Perspective.* Boston, MA: Kluwer Academic Publishers.

Ross, S. M. (1996). *Stochastic Processes.* New York, NY: Wiley.

Ryu, J., and Torres, E. B. (2017). "Methods for dynamically coupled brain body tracking," in *Fourth International Symposium on Movement and Computing, MOCO'17* (London), 1–8.

Shimazaki, H., and Shinomoto, S. (2007). A method for selecting the bin size of a time histogram. *Neural Comput.* 19, 1503–1527. doi: 10.1162/neco.2007.19.6.1503

Torres, E. B. (2001). *Theoretical Framework for the Study of Sensory-Motor Integration.* San Diego, CA: University of California.

Torres, E. B. (2010). New symmetry of intended curved reaches. *Behav. Brain Funct.* 6:21. doi: 10.1186/1744-9081-6-21

Torres, E. B. (2011). Two classes of movements in motor control. *Exp. Brain Res.* 215, 269–283. doi: 10.1007/s00221-011-2892-8

Torres, E. B. (2013a). The rates of change of the stochastic trajectories of acceleration variability are a good predictor of normal aging and of the stage of Parkinson's disease. *Front. Integr. Neurosci.* 7:50. doi: 10.3389/fnint.2013.00050

Torres, E. B. (2013b). Signatures of movement variability anticipate hand speed according to levels of intent. *Behav. Brain Funct.* 9:10. doi: 10.1186/1744-9081-9-10

Torres, E. B. (2013c). Atypical signatures of motor variability found in an individual with ASD. *Neurocase* 19, 150–165. doi: 10.1080/13554794.2011.654224

Torres, E., and Andersen, R. (2006). Space-time separation during obstacle-avoidance learning in monkeys. *J. Neurophysiol.* 96, 2613–2632. doi: 10.1152/jn.00188.2006

Torres, E. B., Brincker, M., Isenhower, R. W., Yanovich, P., Stigler, K. A., Nurnberger, J. I., et al. (2013a). Autism: the micro-movement perspective. *Front. Integr. Neurosci.* 7:32. doi: 10.3389/fnint.2013.00032

Torres, E. B., Isenhower, R. W., Yanovich, P., Rehrig, G., Stigler, K., Nurnberger, J., et al. (2013b). Strategies to develop putative biomarkers to characterize the female phenotype with autism spectrum disorders. *J. Neurophysiol.* 110, 1646–1662. doi: 10.1152/jn.00059.2013

Torres, E. B., Quian Quiroga, R., Cui, H., and Buneo, C. A. (2013c). Neural correlates of learning and trajectory planning in the posterior parietal cortex. *Front. Integr. Neurosci.* 7:39. doi: 10.3389/fnint.2013.00039

Torres, E. B., Yanovich, P., and Metaxas, D. N. (2013d). Give spontaneity and self-discovery a chance in ASD: spontaneous peripheral limb variability as a proxy to evoke centrally driven intentional acts. *Front. Integr. Neurosci.* 7:46. doi: 10.3389/fnint.2013.00046

Torres, E. B., Cole, J., and Poizner, H. (2014). Motor output variability, deafferentation, and putative deficits in kinesthetic reafference in Parkinson's disease. *Front. Hum. Neurosci.* 8:823. doi: 10.3389/fnhum.2014.00823

Torres, E. B., and Denisova, K. (2016). Motor noise is rich signal in autism research and pharmacological treatments. *Sci. Rep.* 6:37422. doi: 10.1038/srep37422

Torres, E. B., Heilman, K. M., and Poizner, H. (2011). Impaired endogenously evoked automated reaching in Parkinson's disease. *J. Neurosci.* 31, 17848–17863. doi: 10.1523/JNEUROSCI.1150-11.2011

Torres, E. B., Isenhower, R. W., Nguyen, J., Whyatt, C., Nurnberger, J. I., Jose, J. V., et al. (2016a). Toward precision psychiatry: statistical platform for the personalized characterization of natural behaviors. *Front. Neurol.* 7:8. doi: 10.3389/fneur.2016.00008

Torres, E. B., Nguyen, J., Mistry, S., Whyatt, C., Kalampratsidou, V., and Kolevzon, A. (2016b). Characterization of the statistical signatures of micro-movements underlying natural gait patterns in children with phelan McDermid syndrome: towards precision-phenotyping of behavior in ASD. *Front. Integr. Neurosci.* 10:22. doi: 10.3389/fnint.2016.00022

Torres, E. B., Smith, B., Mistry, S., Brincker, B., and Whyatt, C. (2016c). Neonatal diagnostics: toward dynamic growth charts of neuromotor control. *Front. Pediatr.* 4:121. doi: 10.3389/fped.2016.00121

Torres, E. B., and Jose, J. V. (2012). *Novel Diagnostic Tool to Quantify Signatures of Movement in Subjects with Neurological Disorders, Autism and Autism Spectrum Disorders.* New Brunswick, NJ: Office of Technology Commercialization, Rutgers, The State University of New Jersey.

Torres, E. B., and Lande, B. (2015). Objective and personalized longitudinal assessment of a pregnant patient with post severe brain trauma. *Front. Hum. Neurosci.* 9:128. doi: 10.3389/fnhum.2015.00128

Torres, E. B., Mistry, S., Caballero, C., and Whyatt, C. P. (2017). Stochastic signatures of involuntary head micro-movements can be used to classify females of ABIDE into different subtypes of neurodevelopmental disorders. *Front. Integr. Neurosci.* 11:10. doi: 10.3389/fnint.2017.00010

Torres, E. B., Raymer, A., Gonzalez Rothi, L. J., Heilman, K. M., and Poizner, H. (2010). Sensory-spatial transformations in the left posterior parietal cortex may contribute to reach timing. *J. Neurophysiol.* 104, 2375–2388. doi: 10.1152/jn.00089.2010

Torres, E. B., and Zipser, D. (2002). Reaching to grasp with a multi-jointed arm. I. Computational model. *J. Neurophysiol.* 88, 2355–2367. doi: 10.1152/jn.00030.2002

Torres, E. B., and Zipser, D. (2004). Simultaneous control of hand displacements and rotations in orientation-matching experiments. *J. Appl. Physiol.* 96, 1978–1987. doi: 10.1152/japplphysiol.00872.2003

Von Holst, E., and Mittelstaedt, H. (1950). "The principle of reafference: interactions between the central nervous system and the peripheral organs," in *Perceptual Processing: Stimulus Equivalence and Pattern Recognition*, ed. P. C. Dodwell (New York, NY: Appleton-Century-Crofts), 41–72.

Wilson, M. (2002). Six views of embodied cognition. *Psychon. Bull. Rev.* 9, 625–636. doi: 10.3758/bf03196322

Wu, D., José, J. V., Nurnberger, J. I., and Torres, E. B. (2018). A biomarker characterizing neurodevelopment with applications in autism. *Sci. Rep.* 8:614. doi: 10.1038/s41598-017-18902-w

Yanovich, P., Isenhower, R. W., Sage, J., and Torres, E. B. (2013). Spatial-orientation priming impedes rather than facilitates the spontaneous control of hand-retraction speeds in patients with Parkinson's disease. *PLoS One* 8:e66757. doi: 10.1371/journal.pone.0066757

Conflict of Interest Statement: The authors declare that the research was conducted in the absence of any commercial or financial relationships that could be construed as a potential conflict of interest.

Copyright © 2018 Ryu and Torres. This is an open-access article distributed under the terms of the Creative Commons Attribution License (CC BY). The use, distribution or reproduction in other forums is permitted, provided the original author(s) and the copyright owner are credited and that the original publication in this journal is cited, in accordance with accepted academic practice. No use, distribution or reproduction is permitted which does not comply with these terms.

frontiers in Aging Neuroscience

SYSTEMATIC REVIEW
published: 18 April 2018
doi: 10.3389/fnagi.2018.00110

The Effects of Tai Chi Intervention on Healthy Elderly by Means of Neuroimaging and EEG: A Systematic Review

Zhujun Pan[1], Xiwen Su[2], Qun Fang[1], Lijuan Hou[2], Younghan Lee[1], Chih C. Chen[1], John Lamberth[1] and Mi-Lyang Kim[3]*

[1] Department of Kinesiology, Mississippi State University, Starkville, MS, United States, [2] Exercise Physiology Laboratory, College of Physical Education and Sports, Beijing Normal University, Beijing, China, [3] Department of Sports, Leisure and Recreation, Soonchunhyang University, Asan, South Korea

Aging is a process associated with a decline in cognitive and motor functions, which can be attributed to neurological changes in the brain. Tai Chi, a multimodal mind-body exercise, can be practiced by people across all ages. Previous research identified effects of Tai Chi practice on delaying cognitive and motor degeneration. Benefits in behavioral performance included improved fine and gross motor skills, postural control, muscle strength, and so forth. Neural plasticity remained in the aging brain implies that Tai Chi-associated benefits may not be limited to the behavioral level. Instead, neurological changes in the human brain play a significant role in corresponding to the behavioral improvement. However, previous studies mainly focused on the effects of behavioral performance, leaving neurological changes largely unknown. This systematic review summarized extant studies that used brain imaging techniques and EEG to examine the effects of Tai Chi on older adults. Eleven articles were eligible for the final review. Three neuroimaging techniques including fMRI ($N = 6$), EEG ($N = 4$), and MRI ($N = 1$), were employed for different study interests. Significant changes were reported on subjects' cortical thickness, functional connectivity and homogeneity of the brain, and executive network neural function after Tai Chi intervention. The findings suggested that Tai Chi intervention give rise to beneficial neurological changes in the human brain. Future research should develop valid and convincing study design by applying neuroimaging techniques to detect effects of Tai Chi intervention on the central nervous system of older adults. By integrating neuroimaging techniques into randomized controlled trials involved with Tai Chi intervention, researchers can extend the current research focus from behavioral domain to neurological level.

Keywords: Tai Chi, aging, neuroimaging, EEG, neural plasticity

OPEN ACCESS

Edited by:
Sarah A. Schoen,
STAR Institute for Sensory Processing Disorder, United States

Reviewed by:
Xu Lei,
Southwest University, China
Deep R. Sharma,
SUNY Downstate Medical Center, United States

****Correspondence:***
Zhujun Pan
zp147@msstate.edu

Received: *09 January 2018*
Accepted: *03 April 2018*
Published: *18 April 2018*

Citation:
Pan Z, Su X, Fang Q, Hou L, Lee Y, Chen CC, Lamberth J and Kim M-L (2018) The Effects of Tai Chi Intervention on Healthy Elderly by Means of Neuroimaging and EEG: A Systematic Review. Front. Aging Neurosci. 10:110. doi: 10.3389/fnagi.2018.00110

INTRODUCTION

Older adults experience gradual regression of abilities. In addition to the physiological changes such as loss of muscular strength and declined vision, neurological ability declines with advanced aging. Tomasi and Volkow (2012) proposed that age-related decrease in motor and cognitive functions is associated with degeneration of the brain networks and changes in brain

anatomy. Other studies indicated that decrease in functional connectivity as well as atrophy in gray matter and basal ganglia result in lack of motor control in older adults (Seidler et al., 2010; Hoffstaedter et al., 2015). However, aging process is reversible due to the plasticity and adaptivity of the human brain to experience-specific tasks (Adkins et al., 2006; Petzinger et al., 2010). Brain plasticity implies that reorganization of brain structure and functional connectivity is possible in older adults (Erickson et al., 2007). The finding suggested that appropriate intervention protocols such as exercise and motor training can counteract declines associated with advanced aging (Erickson et al., 2007; Seidler et al., 2010). For example, older adults participating in a 6-month aerobic exercise demonstrated better cardiovascular fitness and enhanced brain plasticity than the sedentary counterparts. Specifically, increased brain volume in gray and white matter were considered evidence of intact central nervous system and contributed to cognitive improvement (Colcombe et al., 2004, 2006). Bearing with the perception as to the significant role of brain plasticity in mitigating or even reversing the course of aging, researchers attempt to understand the neural mechanisms underlying exercise-related improvement in cognitive and motor performance.

Regular exercise is a practical approach to enhancing brain plasticity (Erickson et al., 2013; Voss et al., 2013). Tai Chi, a multimodal mind-body exercise integrating gracefulness, mindfulness, and gentleness, is a recommended form of physical activity for older adults (Wong et al., 2001). Benefits of practicing Tai Chi were reported in cognitive performance (Lam et al., 2011; Wayne et al., 2014) and motor functions such as postural control (Ni et al., 2014), fall prevention (Tousignant et al., 2013; Jain et al., 2017), muscle strength (Reid et al., 2016), and agility (Wayne et al., 2014). Given that neural plasticity shapes performance modification (Paré and Munoz, 2000), it is reasonable to assume that evolution of behavior associated with Tai Chi practice should be detected in the corresponding brain regions. Noninvasive neuroimaging techniques allow researchers to identify neural correlates of exercise-induced changes in the aging brain. Electroencephalography (EEG) produces spontaneous neuroelectric feedback on brain activity (Hatta et al., 2005; Fong et al., 2014). Magnetic Resonance Imaging (MRI) provides *in vivo* measures of brain anatomy and physiology (Giedd et al., 2015). Researchers used the technique to investigate structural changes in brain volume (Colcombe et al., 2006) and cortical thickness (Wei et al., 2013). Functional Magnetic Resonance Imaging (fMRI) detects brain connectivity based on blood oxygenation level-dependent (BOLD) signal in distinct brain regions (Fox et al., 2007). This technique has been applied to probe exercise-induced changes in brain activation and functional connection (Erickson et al., 2007; Seidler et al., 2010).

The current review summarized extant studies that applied Tai Chi to promote health for the following reasons. First, Tai Chi is an increasingly popular physical activity, which has been recommended for older adults and people with chronic disease. Second, despite the encouraging outcomes observed at the behavioral level, neural mechanisms underlying the promoted functions remain largely unknown (Voss et al., 2013). Neuroimaging (fMRI and MRI) and neuroelectric techniques (EEG) are the instruments that expand current knowledge on the correlates between neural plasticity and modified function. In this context, we aim to investigate three main issues: (1) Tai Chi-incurred benefits in older adults; (2) improved functions and corresponding changes in the brain; and (3) the direction of future study. To our knowledge, it is the first review to systematically investigate the benefits of Tai Chi exercise from the perspective of neural plasticity. With an increasing application of neuroimaging techniques, researchers should elevate the current study of interest from mere performance to neurological level.

METHODS

Literature Search

Five electronic databases (Google scholar, PubMed, Cochrane Library, Scopus, and Web of science) were searched for relevant studies published since 1990. The following terms were entered in multiple combinations, including older adults, elderly, seniors, aging, Tai Chi Chuan, Tai chi, Taichi, and Tai Ji. Terms for neuroimaging techniques include brain imaging, electroencephalography (EEG), event-related potentials (ERP) diffuse optical tomography (DOT), diffuse optical imaging (DOI), event-related optical signal (EROS), magnetic resonance imaging (MRI), Functional magnetic resonance imaging (fMRI), diffusion tensor imaging (DTI) arterial spin labeling (ASL), magnetoencephalography (MEG), computed tomography (CT), positron emission tomography (PET), and single-photon emission computerized tomography (SPECT). Manual search was conducted for known articles in the area by titles instead of keywords search.

Eligibility criteria

Studies were eligible for inclusion if the following criteria were met: (1) subjects were healthy older adults or middle-aged adults (average age of Tai Chi group must be over 50); (2) Tai Chi was applied to exercise intervention; (3) brain imaging methods including MRI, fMRI, EEG, ERP etc. were used to assess variables of interest. The screening process consisted of two phases. First, two reviewers (XS & ZP) independently examined title, keywords, and abstracts of retrieved articles. In the second phase, a third author (QF) was responsible to deal with any disagreement between the reviewers.

Studies that failed to conform to one of the specified criteria were considered ineligible. To gain a comprehensive understanding of Tai Chi-related changes in the central nervous system of older adults, there were no restrictions on the types of studies. However, conference abstracts, review articles, monograph, and videos were excluded.

Quality Assessment

The methodological quality was assessed by Delphi list for quality assessment (Verhagen et al., 1998). To reduce the risk of bias in assessment, two reviewers (XS & ZP) independently scored the quality of the included articles. Inconsistencies between the two reviewers were solved after discussing with a third author.

Data Extraction

Study characteristics encompass basic information of the selected articles, including author(s) of study and year of publication, study design, place of study, sample size and attribution rate, intervention frequency and duration, age of subjects, and measures. Age of subjects refers to the average group age, which should be above 50. Measures applied to the studies must include neuroimaging (fMRI or MRI) or neuroelectric techniques (EEG). Rationale, findings, and practical implications were summarized according to the purpose, results, and conclusions of the retrieved studies.

RESULTS

Study Selection

A total of 40 articles were retrieved from the initial search. Examination of titles and abstracts excluded 13 irrelevant articles. Further analysis of the remaining 27 items screened off 16 articles for the following reasons: lack of Tai Chi intervention ($N = 10$), participants with health issues ($N = 2$), non-journal articles ($N = 2$), lack of brain imaging method ($N = 1$), and review paper ($N = 1$). Finally, 11 studies were eligible for full-text critical appraisal. **Figure 1** indicates the study selection process.

Study Characteristics

Effects of Tai Chi intervention on participants' neurological changes received an increasing attention in recent years as nine of the included studies ($N = 11$) were published in the past 5 years. China is the major country where relevant studies were conducted ($N = 8$) due to the prevalence of Tai Chi in the region. Subjects were mostly seniors. The average age of Tai Chi group in the studies ranged between 50.5 and 68.6 years. The study design included pre- and post-tests ($N = 1$), RCT ($N = 5$), and Quasi-experiment ($N = 5$). Seven studies compared the subjects' performance of Tai Chi group with that of control group before and after the intervention. The other four studies examined the difference between experienced Tai Chi practitioners and people with a relatively sedentary lifestyle.

Scales and instruments such as Attention Network Test (ANT) and Memory Scale (MS) were used to assess behavioral and cognitive performance. On the other hand, MRI, fMRI, and EEG provided evidence of neural plasticity. MRI presented the image of brain structures (Wei et al., 2013, 2014; Zheng et al., 2015). fMRI examined functional connectivity (Li et al., 2014; Tao et al., 2016, 2017) and brain neural activity (Yin et al., 2014). EEG detected the spontaneous electric activity when a subject is performing a specific task (Liu et al., 2003; Field et al., 2010; Fong et al., 2014; Hawkes et al., 2014). Combining performance assessment with neuroimaging evidence allows researchers to investigate Tai Chi-induced outcomes at both behavioral and neural levels. Study characteristics are listed in **Table 1**.

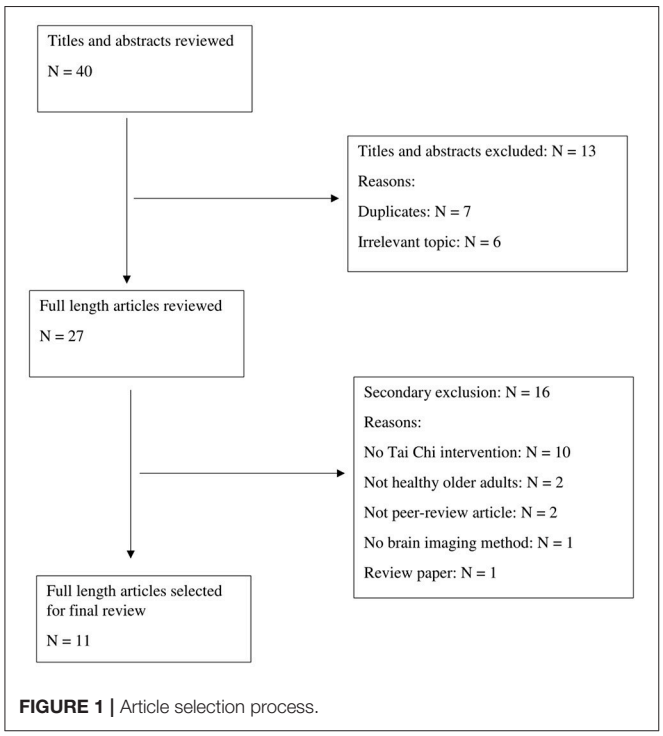

FIGURE 1 | Article selection process.

Quality Assessment of Eligible Studies

Most of the included studies exhibited moderate ($N = 5$) to high ($N = 5$) quality of study design, with only one being categorized as low quality. Five cross-sectional studies aimed to identify different features between experienced Tai Chi practitioners and sedentary counterparts. Participants were recruited and allocated based on Tai Chi-related experiences and thus failed to meet the requirement of random allocation. For the studies without adopting intervention protocols, criterions such as similar at baseline (SB) and therapist blinded (TB) were not applicable to the studies ($N = 5$). Details of quality assessment are listed in **Table 2**.

Summary of Evidence

Summary of the studies involved with four categories of interest regarding the impacts of Tai Chi on brain structures, functional connectivity, neural activity, and electric activity. Details of the summarized evidence are displayed in **Table 1**.

Brain Structures

One study examined the differences in the brain structures between experienced Tai Chi practitioners and people lacking routine exercise. MRI image identified thicker cortex in the left and right hemisphere of long-term Tai Chi practitioners in comparison to the cortical regions of people with a sedentary lifestyle. The study suggested that cortex thickness in the left medial occipitotemporal sulcus and lingual sulcus is subject to the intensity of Tai Chi practice (Wei et al., 2013).

Functional Connectivity

Tai Chi-induced benefits in cognitive function were observed after elderly participants receiving a 6-week multimodal intervention, which consisted of Tai Chi exercise, group counseling, and cognitive training. Changes in functional

TABLE 1 | Summary of reviewed articles.

References	Aim/Purpose	Design	Place of study	Sample size (attribution%)	Age group (year)	Intervention frequency & duration	Measurment instruments/ Measures	Results	Conclusion
Tao et al., 2017	To investigate the impact of Tai chi chuan and Baduanjin on the cognitive control network (CCN) especially on the DLPFC part. To explain the underlying mechanism of the fact that Taichi and Baduanjin can help improve mental control function.	RCT	Gulou District, Fuzhou City, China	TC: 21 BDJ:16 CG:25 $N = 62$	50–70 years TC: 62.38 ± 4.55 BDJ: 62.33 ± 3.88 CG: 59.76 ± 4.83	TC: 60 min/d, 5d/week, last for 12 weeks. BDJ: 60 min/d, 5d/ week, last for 12 weeks. CG: maintain original physical activity habits for 12 weeks.	WMS-CR fMRI	In TC, the rsFC decreases significantly between the DLPFC and the left SFG and ACC. In BDJ, the rsFC decreases significantly between the DLPFC and the left putamen and insula. Mental control improvement was negatively associated with rsFC DLPFC-putamen changes across all subjects.	The practice of Tai Chi and Baduanjin could significantly increases the participant's mental control function.
Tao et al., 2016	To investigate how longitudinal Tai Chi Chuan and Baduanjin can modulate memory function and HPC resting-state functional connectivity (rs-FC) in elderly adults and the relation between them.	RCT	Gulou District, Fuzhou City, China	TC: 21 BDJ:16 CG:25 $N = 62$	50–70 years TC: 62.38 ± 4.55 BDJ: 62.33 ± 3.88 CG: 59.76 ± 4.83	TC: 60min/d, 5d/week, last for 12 weeks. BDJ: 60min/d, 5d/week, last for 12 weeks. CG: maintain original physical activity habits for 12 weeks.	MQ (WMS-CR) fMRI	The MQ significantly increased in TC and BDJ compared to CG. The rs-FC between the bilateral HPC and mPFC significantly increased in the TC compared to the CG. The rs-FC increases between the bilateral HPC and mPFC were significantly associated with corresponding memory function improvement across all subjects.	Both Tai Chi Chuan and Baduanjin may be effective exercises to prevent memory decline during aging.
Field et al., 2010	To determine the immediate effects of a combined form of Tai chi/yoga.	pretest/ posttest	Coral Gables, Florida, United States.	$N = 38$ $M = 2.7$ on the HSI (57% Caucasian, 14% Hispanic, 14% Asian, 5% Black, and 10% other.)	21–59 years (averaged 41.0)	20 min long, including 10min of Taichi movements and 10 min of yoga postures.	STAI EKG EEG Math computations	A trend for increased EEG theta activity was detected but the result was not significant enough ($p = 0.10$).	The increased relaxation may have contributed to the increased speed and accuracy noted on math computations following the Tai chi/yoga class.

(Continued)

TABLE 1 | Continued

References	Aim/Purpose	Design	Place of study	Sample size (attribution%)	Age group (year)	Intervention frequency & duration	Measurment instruments/ Measures	Results	Conclusion
Wei et al., 2013	To investigate whether brain structural difference existed between highly experienced TCC practitioners and healthy control non-TCC practitioners.	Quasi-experiment	Beijing, China	ETC: 22(7 males) CG: 18 *N* = 40	ETC: 52 ± 6 years CG: 54 ± 6 years	No intervention.	ANT (RT & error scores) MRI	ETC showed significantly thicker cortex in the right PG, IS and MFS, also in the left MOTS and LS. Thicker cortex in left MOTS and LS was associated with greater intensity of TCC practice.	TCC practice could induce regional structural change in the brain. TCC might share similar patterns of neural correlates with meditation and aerobic exercise.
Wei et al., 2014	To examine TCC-associated changes in the human brain's intrinsic architecture and the relevant gains in behavioral performance.	Quasi-experiment	Beijing, China	ETC: 22(7 males) CG: 18(8 males) *N* = 40	ETC: 52.4 ± 6.8 years CG: 54.8 ± 6.8 years	No intervention.	ANT R-fMRI 2dReHo	The ETC had significantly greater fHo in the right PosCG and less fHo in the left ACC and the right DLPFC. Increased functional homogeneity in the PosCG was correlated with TCC experience. Decreases in fHo in the left ACC and increases in fHo in the right PosCG both predicted performance gains on ANT.	These findings provide evidence for the functional plasticity of the brain's intrinsic architecture toward optimizing locally functional organization.
Fong et al., 2014	To determine the relationship between physical activity and the task-switching aspect of executive function. (by investigating the modulating roles of age, modality of physical activity, and type of cognitive function using behavioral and event-related potential (ERP) assessments.	Quasi-experiment	Taipei, Taiwan	OEE: 16 OTC: 16 OSL: 16 YA: 16 *N* = 64	OA: 65–75 years OEE: 68.37 ± 3.68 OTC:67.31 ± 4.92 OSL: 68.93 ± 4.28 YA: 20–30 years (22.43 ± 2.58)	No intervention	Questionnaire MMSE IPAQ ERP	YA, OEE, and OTC had significantly larger P3 amplitude compared with OSL under homogeneous and heterogeneous conditions, while no differences were observed among the former three groups. YA exhibited shorter P3 latency than OSL. The ERP findings support the model of the STAC.	Regular participation in endurance exercise and Tai Chi Chuan may have equivalent beneficial effects on cognition at the behavioral and neuroelectric levels. Age and participation in physical activity influence the relationship between physical activity and task-switching, and a positive relationship was observed regardless of the modality of physical activity and type of cognitive function.

(Continued)

TABLE 1 | Continued

References	Aim/Purpose	Design	Place of study	Sample size (attribution%)	Age group (year)	Intervention frequency & duration	Measurment instruments/ Measures	Results	Conclusion
Li et al., 2014	To investigate the functional plasticity in resting-state connectivity of the prefrontal cortex and MTL in older adults.	RCT	Beijing, China	IG: 17(9 men) CG: 17(11 men) $N = 34$	IG: 68.6 ± 5.7 years CG: 71.7 ± 4.0 years	Cognitive intervention (MT& EFT): 1-h session, 3 sessions/week, last for 6 weeks Tai Chi: 1-h session, 3 sessions/week, last for 6 weeks, Yang-Style 24-form Tai Chi Group counseling: 90-min session, 1 time/week, last for 6 weeks CG: two 120 min health-related lectures	Participants criteria: MoCA CES-D ADL standardized assessments: PALT digit span TMT Stroop Test CFT Health status: MOS SF-36 SSRS SWLS IWB Image acquisition: fMRI	After the training activities, IG showed dramatic increment in functional correlation between mPFC and PHC.L, and significantly increased functional connectivity between the mPFC and left PHG. CG showed significantly decreased connectivity between mPFC and MFG. IG showed significant correlation between the changes in the FC of mPFC-PHG and the changes in cognitive performance (CFT). IG's level of mPFC-PHC.L connectivity at the post-training scan correlated significantly with individual performance on the TMT.	Multimodal intervention could postpone the effects of aging and improve the function of the regions that are most heavily influenced by aging, as well as play an important role in preserving the brain and cognition during old age.
Yin et al., 2014	To examine the effects of a multimodal intervention on spontaneous brain activity in healthy older adults, and the relationship between individual differences in baseline spontaneous activity and intervention-induced changes in behavioral performance.	RCT	Beijing, China	IG: 17(9 men) CG: 17(11 men) $N = 34$	61–79 years IG: 68.6 ± 5.7 years CG: 71.7 ± 4.0 years	Cognitive intervention (MT& EFT): 1-h session, 3 sessions/week, last for 6 weeks Tai Chi: 1-h session, 3 sessions/week, last for 6 weeks, Yang-Style 24-form Tai Chi Group counseling: 90-min session, 1 time/week, last for 6 weeks CG: two 120 min health-related lectures	Participants criteria: MoCA CES-D ADL standardized assessments: PALT digit span TMT Stroop Test CFT Health status: MOS SF-36 SSRS SWLS IWB Image acquisition: fMRI	IG showed significantly increased ALFF in the right MFG, left SFG and left ACL, while the mean ALFF in all three ROIs was significantly reduced in CG. In IG, increased ALFF in the right MFG was significantly correlated with changes in the TMT and SWLS, and in the left ACL the ALFF increase was significantly correlated with changes in social support. The baseline ALFF in the right MFG was significantly correlated with changes in the TMT and SWLS.	Multimodal intervention is effective in improving cognitive functions and well-being and can induce functional changes in the aging brain. The study suggested resting-state ALFF as a marker of intervention-induced plasticity in older adults.

(Continued)

TABLE 1 | Continued

References	Aim/Purpose	Design	Place of study	Sample size (attribution%)	Age group (year)	Intervention frequency & duration	Measurment instruments/ Measures	Results	Conclusion
Zheng et al., 2015	To explore the regionally functional plasticity by using the ReHo method to do an exploratory analysis in the whole brain.	RCT	Beijing, China	IG: 17(9 men) CG: 17(11 men) *N* = 34	IG: 68.59 ± 5.65 years CG: 71.65 ± 4.00 years	Cognitive intervention (MT& EFT): 1-h session, 3 sessions/week, last for 6 weeks Tai Chi: 1-h session, 3 sessions/week, last for 6 weeks, Yang-Style 24-form Tai Chi Group counseling: 90-min session, 1 time/week, last for 6 weeks CG: two 120 min health-related lectures	Participants criteria: MoCA CES-D ADL standardized assessments: PALT digit span TMT Stroop Test CFT Health status: MOS SF-36 SSRS SWLS IWB Image acquisition: fMRI	In IG, ReHo significantly increased in the left STG and left PCL, but decreased in the left MTG. In CG, ReHo significantly decreased in the left STG and PCL and increased in bilateral MTG. In IG, the intervention-related ReHo changes in the left STG were significantly positively correlated with changes in the CFT, and changes in the right MTG were negatively correlated with increase in the total PALT scores.	The present study confirms that the combined intervention induces regionally brain functional reorganization, and it could optimize the intrinsic functional brain architecture in the temporal cortex and cerebellum in the normal elderly.
Hawkes et al., 2014	To determine if people who were long-term Tai Chi practitioners would show enhancements to executive function and aerobic capacity.	Quasi-experiment	Eugene and Springfield, Oregon	TC: 10(3 female) MEG: 16(6 female) AEG: 16(8 female) SG: 12(10 female) *N* = 54	TC: 55.4 ± 12.99 MEG: 48.63 ± 15.00 AEG: 44.09 ± 16.2 SG: 46.92 ± 12.81	No intervention	Rockport 1-mile walk VSTS test with EEG Button press response	TC and MEG showed significantly larger P3b switch amplitudes than sedentary controls, while AEG and SG did not differ significantly on this key executive function measure. P3b switch latency showed no significant differences between groups.	Long-term practice of Tai Chi may benefit a neurophysiological index of executive function.

(Continued)

TABLE 1 | Continued

References	Aim/Purpose	Design	Place of study	Sample size (attribution%)	Age group (year)	Intervention frequency & duration	Measurment instruments/ Measures	Results	Conclusion
Liu et al., 2003	To examine the different physiological and psychological effects of 24TJQ in middle-aged women.	Quasi-experiment	Osaka, Japan	SkG: 10 NG: 10 $N = 20$	SkG: 50.56 ± 5.45 NG: 53.66 ± 4.9	6-min 24TJQ exercise, with 3-min rest (before) and recovery (after)	Concurrently measure with the exercise: HR RR exercise intensity physical fitness test EEG (used telemeter system to avoid noise) EMG ST	SkG showed significantly higher values of alpha%-power in eye-closed rest and recovery period compared to NG, but they have nearly the same values during exercise. SG showed a tendency of higher beta%-power during experiment than NG. SG showed a significant increase of alpha%-power in central region compared to occipital region after exercise while there was no significant change in NG.	24TJQ is beneficial to keep or improve agility, flexibility, and muscle strength or endurance ability in middle-aged women, and gives a special effect on the cardio-respiratory system.

RCT, randomized controlled trial; TC, Tai chi group; BDJ, Baduanjin group; CG: control group; WMS-CR, Wechsler Memory Scale–Chinese Revision; fMRI, functional magnetic resonance imaging; resting state functional connectivity, rsFC; DFPLC, bilateral dorsolateral prefrontal cortex; SFG, superior frontal gyrus; ACC, anterior cingulate cortex; MQ, memory quotient; HPC, hippocampus; mPFC, medial prefrontal cortex; HIS, Hollingshead Socioeconomic Index; STAI, the State Anxiety Inventory; HIS, Hollingshead Socioeconomic Index; STAI, State Anxiety Inventory; EKG, Electrocardiogram; EEG, Electroencephalogram; ETC, experienced Taichi practitioners; ANT, Attention Network Test; MRI, magnetic resonance imaging; PG, precentral gyrus; IS, insula sulcus; MFS, middle frontal sulcus; STG, superior temporal gyrus; MOTS, medial occipitotemporal sulcus; LS, lingual sulcus; R-fMRI, Resting-state functional magnetic resonance imaging; 2dReHo, 2d surface-based regional homogeneity; fHo, functional homogeneity; PosCG, post-central gyrus; ERP, event-related potential; OEE, older adults performing endurance exercise; OTC, older adults practicing Tai Chi Chuan; OSL, older adults with a sedentary lifestyle; YA, young adults; OA, older adults; MMSE, Mini-Mental State Examination; IPAQ, International Physical Activity Questionnaire; STAC, scaffolding theory of aging and cognition; MTL, medial temporal lobe; IG, Intervention group; MT, mnemonic training; EFT, executive function training; MoCA, Montreal Cognitive Assessment; CES-D, Center for Epidemiologic Depression Scale; ADL, activities of daily living; PALT, Paired Associative Learning Test; TMT, Trail Making Test; CFT, Category Fluency Test; MOS SF-36, Medical Outcomes Study Short Form-36; SSRS, Social Support Rating Scale; SWLS, Satisfaction with Life Scale; IWB, Index of Well-Being; mPFC, medial prefrontal cortex; HF, hippocampal formation; PHC, parahippocampal cortex; MFG, medial frontal gyrus; PHG, parahippocampal gyrus; FC, functional connectivity; SFG, superior frontal gyrus; ACL, anterior cerebellum lobe; ROI, region of interest; STG, superior temporal gyrus; PCL, posterior lobe of cerebellum; MTG, middle temporal gyrus; MEG, meditation plus exercise group; AEG, aerobic exercise group; SG, sedentary group; VSTS, Visuo-spatial task switch; 24TJQ, 24-style Taijiquan; SkG, skilled group; NG, novices' group; HR, heart rate; RR, respiratory rate; EMG, electromyography; ST, surface thermograph.

TABLE 2 | Quality assessment of reviewed studies.

Study	EC	RA	CA	SAB	SB	TB	AB	DR	ITA	BC	PM	OSQ
Tao et al., 2017	Yes	Yes	Yes	Yes	Yes	Yes	Yes	No	Yes	Yes	Yes	High
Tao et al., 2016	Yes	Yes	Yes	Yes	Yes	Yes	Yes	No	Yes	Yes	Yes	High
Field et al., 2010	No	CD	CD	CD	No	Yes	CD	Yes	Yes	NA	No	Low
Wei et al., 2013	Yes	No	No	NA	Yes	NA	Yes	Yes	NA	Yes	Yes	Moderate
Wei et al., 2014	Yes	No	No	NA	Yes	NA	Yes	Yes	NA	Yes	Yes	Moderate
Fong et al., 2014	Yes	No	No	NA	Yes	NA	Yes	Yes	NA	Yes	Yes	Moderate
Li et al., 2014	Yes	Yes	Yes	Yes	Yes	Yes	Yes	No	Yes	Yes	Yes	High
Yin et al., 2014	Yes	Yes	Yes	Yes	Yes	Yes	Yes	No	Yes	Yes	Yes	High
Zheng et al., 2015	Yes	Yes	Yes	Yes	Yes	Yes	Yes	No	Yes	Yes	Yes	High
Hawkes et al., 2014	Yes	No	No	NA	Yes	NA	Yes	Yes	NA	Yes	Yes	Moderate
Liu et al., 2003	Yes	No	No	NA	Yes	NA	Yes	Yes	NA	Yes	Yes	Moderate

EC, eligibility criteria; RA, random allocation; CA, concealed allocation; SAB, similar at baseline; SB, subject blinded; TB, therapist blinded; AB, assessor blinded; DR, drop-out rate; ITA, intention-to-treat analysis; BC, between-group comparison; PM, points measures; OSQ, overall study quality; CD, cannot determine; NA, not applicable.

connectivity included enhanced rsFC between the medial prefrontal cortex and the medial temporal lobe (Li et al., 2014). Given the fact that Tai Chi was the only form of physical activity in the intervention program, it is reasonable to assume that, to a certain extent, Tai Chi exercise contributed to the enhanced functional connectivity in correlation to improved cognitive performance.

Tao and colleagues examined correlates of mental control and functional connectivity (Tao et al., 2016, 2017). Participants who completed Tai Chi or a similar exercise (Baduanjin) over the 12-week intervention achieved a significant improvement in mental control and memory function. fMRI identified a significant decrease in the resting state functional connectivity (rsFC) between bilateral dorsolateral prefrontal cortex (DLPFC) and putamen, suggesting a negative relationship between mental control improvement and rsFC DLPFC-putamen connectivity (Tao et al., 2017). Superior memory function was found in alignment with increased rsFC between bilateral hippocampus and medial prefrontal cortex (Tao et al., 2016). Both studies substantiated the association between cognitive function and functional connectivity in prefrontal areas.

Brain Neural Activity

Regional homogeneity (ReHo) and amplitude of low-frequency fluctuations (ALFF) in BOLD signal of fMRI revealed spontaneous neuronal activity (Zang et al., 2004; Fox and Raichle, 2007). The previous study found that ALFF declines with aging (Zuo and Xing, 2014). A multimodal intervention including Tai Chi, cognitive training, and group counseling benefited the intervention group in which strengthened ALFF in the middle frontal gyrus, superior frontal gyrus, and anterior cerebellum lobe was observed (Yin et al., 2014). Another study following similar protocols identified reorganized ReHo in the superior and middle temporal gyri, and the posterior lobe of the cerebellum (Zheng et al., 2015). Enhanced intrinsic brain activity is the evidence of Tai Chi-induced benefits in promoting cognitive functions.

Brain Electric Activity

EEG detects brain electric activity, which is subject to physical activity. Participants showed better performance in math computation after Tai Chi and yoga practice (Field et al., 2010). Increased theta activity indicated immediate relaxation during exercise. The study suggested that Tai Chi and yoga exerted an immediate impact on brain activity. Brain plasticity was partially evident in that brain activity was adaptive to specific task.

Liu et al. (2003) investigated spontaneous brain activity of Tai Chi experts and novices during practice. Experts indicated a significantly higher alpha-wave amplitude than novices in eye-close resting and recovery period, suggesting that the experts could quickly and effectively reach a psychological relaxation. Also, the experts exhibited a higher beta-wave amplitude than novices, implying that experts tend to be more physiologically excited than novices throughout the practice. Experts indicated well-developed mind concentration capacity, which was evident in the alpha shift tendency from occipital lobe to central or frontal regions.

Cognitive function was assessed by event-related potential (ERP) while subjects conducting a task-switch test under homogeneous and heterogeneous conditions (Fong et al., 2014). P3 amplitude exhibited no difference between young adults and older adults with either regular endurance training or Tai Chi exercise. However, all three groups indicated significantly larger P3 amplitude than that indicated in the group of sedentary older adults. Similar P3 patterns between young and older adults participating in long-term exercise provided evidence regarding the benefits of endurance training and Tai Chi exercise on cognitive function. Another study examining P3b amplitude of subjects conducting task-switch test confirmed the benefits of long-term Tai Chi practice in the neural substrates of executive function (Hawkes et al., 2014).

DISCUSSION

The included studies reported positive outcomes of Tai Chi practice in older adults. Specifically, Tai Chi-induced benefits

involved with superior capacities in respect to mental control (Tao et al., 2017), memory (Tao et al., 2016), fitness (Liu et al., 2003; Wei et al., 2013), cognition (Fong et al., 2014; Li et al., 2014; Wei et al., 2014; Yin et al., 2014), and executive function (Field et al., 2010; Hawkes et al., 2014; Zheng et al., 2015). Findings as to physiological and psychological improvement substantiated the significant role of Tai Chi practice in counteracting age-related decline in motor and cognitive function. More importantly, neural imaging techniques applied to the included studies provided evidence on the connection between improved performance and changes in the neural system. Aging brain still retains some plasticity, which may contribute to delaying or reversing neurological deterioration in the aging process (Kramer et al., 2004; Gabbard, 2011). Wei et al. (2013) identified effects of Tai Chi intervention on reshaping brain structures. The finding is consistent with previous studies, which observed greater cortical thickness in older adults after memory training (Engvig et al., 2010), meditation practice (Lazar et al., 2005), and aerobic exercise (Colcombe et al., 2006). Functional change is associated with the development of new neurons and synapses in the brain (Honey et al., 2009; Cai et al., 2014). In alignment with other forms of exercise, Tai Chi exercise mitigates brain structural and functional deficits (Seidler et al., 2010). Older adults maintaining an active lifestyle by routinely practicing Tai Chi indicated enhanced neural plasticity (Liu et al., 2003; Field et al., 2010; Fong et al., 2014; Hawkes et al., 2014). The included studies provided evidence-based explanation on the neural mechanisms underlying the exercise-induced improvement in motor and cognitive performance.

The reviewed studies only adopted tasks related to cognition, working memory, and executive function. Motor tasks, however, have yet been incorporated into EEG, fMRI, or MRI scan. In comparison to the EEG detection, which allows moderate physical activity, fMRI and MRI require subjects to maintain a resting state. Even small head motions may produce noise in brain scans (Power et al., 2012; Satterthwaite et al., 2012; Van Dijk et al., 2012), which proposed a challenge of integrate neuroimaging techniques into motor tasks. Researchers have designed a few tasks, which require a small range of motion such as finger tapping (Stoodley et al., 2012; Gardini et al., 2016), reaching and grasping (Culham et al., 2003), and lower limb joint motions (Kapreli et al., 2006). To expand knowledge on neural correlates of motor performance, feasible motor tasks should be developed to fit the setting of research employing the neuroimaging techniques.

Older adults experience reduced hemispheric asymmetry due to age-related deficits in neural connectivity (Cabeza, 2002). Evidence from fMRI scan indicated symmetric brain activations when older adults were performing cognitive tasks (Grady, 2000). A recent study involved with older adults also identified reduced asymmetry in movement patterns between dominant and non-dominant hand, suggesting a potential connection to the reduced hemispheric asymmetry (Przybyla et al., 2011). However, the theory remains to be an assumption without direct evidence from a study, which applies fMRI to motor tasks. By investigating the change in motor performance, whether it is associated with age-related degeneration or Tai Chi-incurred improvement, researchers can better understand neural mechanisms underlying the aging process.

The lack of robust empirical research on Tai Chi-incurred changes for older adults is a limitation of the review. The inherent risk of bias in the study design, paired with the limited literature, suggests the necessity of an increasing number of RCTs in this field. Only two of the included studies reported effect size, which makes it difficult to compare the effectiveness between studies. Future research should report the effect size so that critical conclusion can be reached based on statistical evidence.

CONCLUSION

The literature review summarized 11 studies, which employed neuroimaging techniques and EEG to investigate effects of Tai Chi on hemispheric reorganization. The reviewed articles provide evidence that there may be cognitive improvement associated with modified brain activity, functional connectivity, and brain structures in older adults through Tai Chi exercise. Future studies should account for the potential connection between changed motor functions and corresponding neural mechanisms underlying the aging process. RCTs are needed to provide powerful evidence on the effect of Tai Chi intervention. In contrast to previous research focusing on performance, future studies should analyze the effects of intervention from the neurological standpoint. Applying neuroimaging techniques and EEG to Tai Chi intervention is worth investigating, which allows researchers to explore the neural mechanisms related to the effectiveness of Tai Chi exercise on counteracting the aging process.

AUTHOR CONTRIBUTIONS

ZP and XS contributed to the conception and design of the review. ZP, XS, and QF applied the search strategy. All authors applied the selection criteria. All authors completed assessment of risk of bias. All authors analyzed the data and interpreted data. XS, QF, and ZP wrote this manuscript. LH, YL, CC, JL, and M-LK critically edited the manuscript.

FUNDING

This research was supported by a combination of institutions as stated below: National Natural Science Foundation of China (NSFC31401018); The National Research Foundation of Korea Grant funded by the Korean Government (MOE) (NRF 2017S1A2A2039405); Mississippi State University College of Education Undergraduate Student Research Grant.

REFERENCES

Adkins, D. L., Boychuk, J., Remple, M. S., and Kleim, J. A. (2006). Motor training induces experience-specific patterns of plasticity across motor cortex and spinal cord. *J. Appl. Physiol.* 101, 1776–1782. doi: 10.1152/japplphysiol.00515.2006

Cabeza, R. (2002). Hemispheric asymmetry reduction in older adults: the HAROLD model. *Psychol. Aging* 17, 85–100. doi: 10.1037/0882-7974.17.1.85

Cai, L., Chan, J. S., Yan, J. H., and Peng, K. (2014). Brain plasticity and motor practice in cognitive aging. *Front. Aging Neurosci.* 6:31. doi: 10.3389/fnagi.2014.00031

Colcombe, S. J., Erickson, K. I., Scalf, P. E., Kim, J. S., Prakash, R., McAuley, E., et al. (2006). Aerobic exercise training increases brain volume in aging humans. *J. Gerontol. Ser. A Biol. Sci. Med. Sci.* 61, 1166–1170. doi: 10.1093/gerona/61.11.1166

Colcombe, S. J., Kramer, A. F., Erickson, K. I., Scalf, P., McAuley, E., Cohen, N. J., et al. (2004). Cardiovascular fitness, cortical plasticity, and aging. *Proc. Natl. Acad. Sci. U.S.A.* 101, 3316–3321. doi: 10.1073/pnas.0400266101

Culham, J. C., Danckert, S. L., De Souza, J. F., Gati, J. S., Menon, R. S., and Goodale, M. A. (2003). Visually guided grasping produces fMRI activation in dorsal but not ventral stream brain areas. *Exp. Brain Res.* 153, 180–189. doi: 10.1007/s00221-003-1591-5

Engvig, A., Fjell, A. M., Westlye, L. T., Moberget, T., Sundseth, Ø., Larsen, V. A., et al. (2010). Effects of memory training on cortical thickness in the elderly. *Neuroimage* 52, 1667–1676. doi: 10.1016/j.neuroimage.2010.05.041

Erickson, K. I., Colcombe, S. J., Wadhwa, R., Bherer, L., Peterson, M. S., Scalf, P. E., et al. (2007). Training-induced plasticity in older adults: effects of training on hemispheric asymmetry. *Neurobiol. Aging* 28, 272–283. doi: 10.1016/j.neurobiolaging.2005.12.012

Erickson, K. I., Gildengers, A. G., and Butters, M. A. (2013). Physical activity and brain plasticity in late adulthood. *Dialogues Clin. Neurosci.* 15, 99–108.

Field, T., Diego, M., and Hernandez-Reif, M. (2010). Tai chi/yoga effects on anxiety, heartrate, EEG and math computations. *Complement. Ther. Clin. Pract.* 16, 235–238. doi: 10.1016/j.ctcp.2010.05.014

Fong, D. Y., Chi, L. K., Li, F., and Chang, Y. K. (2014). The benefits of endurance exercise and Tai Chi Chuan for the task-switching aspect of executive function in older adults: an ERP study. *Front. Aging Neurosci.* 6:295. doi: 10.3389/fnagi.2014.00295

Fox, M. D., and Raichle, M. E. (2007). Spontaneous fluctuations in brain activity observed with functional magnetic resonance imaging. *Nat. Rev. Neurosci.* 8, 700–711. doi: 10.1038/nrn2201

Fox, M. D., Snyder, A. Z., Vincent, J. L., et al. (2007). Intrinsic fluctuations within cortical systems account for intertrial variability in human behavior. *Neuron* 56, 171–184. doi: 10.1016/j.neuron.2007.08.023

Gabbard, C. P. (2011). *Lifelong Motor Development.* San Francisco, CA: Pearson Higher Ed.

Gardini, S., Venneri, A., McGeown, W. J., Toraci, C., Nocetti, L., Porro, C. A., et al. (2016). Brain activation patterns characterizing different phases of motor action: execution, choice and ideation. *Brain Topogr.* 29, 679–692. doi: 10.1007/s10548-016-0491-5

Giedd, J. N., Raznahan, A., Alexander-Bloch, A., Schmitt, E., Gogtay, N., and Rapoport, J. L. (2015). Child psychiatry branch of the National Institute of Mental Health longitudinal structural magnetic resonance imaging study of human brain development. *Neuropsychopharmacology* 40, 43–49. doi: 10.1038/npp.2014.236

Grady, C. L. (2000). Functional brain imaging and age-related changes in cognition. *Biol. Psychol.* 54, 259–281. doi: 10.1016/S0301-0511(00)00059-4

Hatta, A., Nishihira, Y., Kim, S. R., Kaneda, T., Kida, T., Kamijo, K., et al. (2005). Effects of habitual moderate exercise on response processing and cognitive processing in older adults. *Jpn. J. Physiol.* 55, 29–36. doi: 10.2170/jjphysiol.R2068

Hawkes, T. D., Manselle, W., and Woollacott, M. H. (2014). Tai Chi and meditation-plus-exercise benefit neural substrates of executive function: a cross-sectional, controlled study. *J. Complement. Integr. Med.* 11, 279–288. doi: 10.1515/jcim-2013-0031

Hoffstaedter, F., Grefkes, C., Roski, C., Caspers, S., Zilles, K., and Eickhoff, S. B. (2015). Age-related decrease of functional connectivity additional to gray matter atrophy in a network for movement initiation. *Brain Struct. Funct.* 220, 999–1012. doi: 10.1007/s00429-013-0696-2

Honey, C. J., Sporns, O., Cammoun, L., Gigandet, X., Thiran, J. P., Meuli, R., et al. (2009). Predicting human resting-state functional connectivity from structural connectivity. *Proc. Natl. Acad. Sci. U.S.A.* 106, 2035–2040. doi: 10.1073/pnas.0811168106

Jain, A., Taylor, J., Sanzo, P., and Zerpa, C. (2017). The effect of Tai Chi on functional lower extremity mobility and strength, ankle proprioception, and postural adaptation in older adults. *American J. Med. Med. Sci.* 7, 229–237. doi: 10.5923/j.ajmms.20170706.01

Kapreli, E., Athanasopoulos, S., Papathanasiou, M., Van Hecke, P., Strimpakos, N., Gouliamos, A., et al. (2006). Lateralization of brain activity during lower limb joints movement. An fMRI study. *Neuroimage* 32, 1709–1721. doi: 10.1016/j.neuroimage.2006.05.043

Kramer, A. F., Bherer, L., Colcombe, S. J., Dong, W., and Greenough, W. T. (2004). Environmental influences on cognitive and brain plasticity during aging. *J. Gerontol. Ser. A Biol. Sci. Med. Sci.* 59, M940–M957. doi: 10.1093/gerona/59.9.M940

Lam, L. C., Chau, R. C., Wong, B. M., Fung, A. W., Lui, V. W., Tam, C. C., et al. (2011). Interim follow-up of a randomized controlled trial comparing Chinese style mind body (Tai Chi) and stretching exercises on cognitive function in subjects at risk of progressive cognitive decline. *Int. J. Geriatr. Psychiatry* 26, 733–740. doi: 10.1002/gps.2602

Lazar, S. W., Kerr, C. E., Wasserman, R. H., et al. (2005). Meditation experience is associated with increased cortical thickness. *Neuroreport* 16:1893. doi: 10.1097/01.wnr.0000186598.66243.19

Li, R., Zhu, X., Yin, S., Niu, Y., Zheng, Z., Huang, X., et al. (2014). Multimodal intervention in older adults improves resting-state functional connectivity between the medial prefrontal cortex and medial temporal lobe. *Front. Aging Neurosci.* 6:39. doi: 10.3389/fnagi.2014.00039

Liu, Y., Mimura, K., Wang, L., and Ikuda, K. (2003). Physiological benefits of 24-style Taijiquan exercise in middle-aged women. *J. Physiol. Anthropol. Appl. Human Sci.* 22, 219–225. doi: 10.2114/jpa.22.219

Ni, M., Mooney, K., Richards, L., Balachandran, A., Sun, M., Harriell, K., et al. (2014). Comparative impacts of tai chi, balance training, and a specially-designed yoga program on balance in older fallers. *Arch. Phys. Med. Rehabil.* 95, 1620.e30–1628.e30. doi: 10.1016/j.apmr.2014.04.022

Paré, M., and Munoz, D. P. (2000). Immediate neural plasticity shapes motor performance. *J. Neurosci.* 20:RC52. doi: 10.1523/JNEUROSCI.20-01-j0005.2000

Petzinger, G. M., Fisher, B. E., Van Leeuwen, J. E., Vukovic, M., Akopian, G., Meshul, C. K., et al. (2010). Enhancing neuroplasticity in the basal ganglia: the role of exercise in Parkinson's disease. *Mov. Disord.* 25(Suppl. 1), S141–S145. doi: 10.1002/mds.22782

Power, J. D., Barnes, K. A., Snyder, A. Z., Schlaggar, B. L., and Petersen, S. E. (2012). Spurious but systematic correlations in functional connectivity MRI networks arise from subject motion. *Neuroimage* 59, 2142–2154. doi: 10.1016/j.neuroimage.2011.10.018

Przybyla, A., Haaland, K. Y., Bagesteiro, L. B., et al. (2011). Motor asymmetry reduction in older adults. *Neurosci. Lett.* 489, 99–104. doi: 10.1016/j.neulet.2010.11.074

Reid, K., Price, L., Harvey, W., et al. (2016). Changes in leg muscle strength and power after Tai Chi exercise in patients with symptomatic knee osteoarthritis. *Osteoarthr. Cartil.* 24:S430. doi: 10.1016/j.joca.2016.01.776

Satterthwaite, T. D., Wolf, D. H., Loughead, J., Ruparel, K., Elliott, M. A., Hakonarson, H., et al. (2012). Impact of in-scanner head motion on multiple measures of functional connectivity: relevance for studies of neurodevelopment in youth. *Neuroimage* 60, 623–632. doi: 10.1016/j.neuroimage.2011.12.063

Seidler, R. D., Bernard, J. A., Burutolu, T. B., Fling, B. W., Gordon, M. T., Gwin, J. T., et al. (2010). Motor control and aging: links to age-related brain structural, functional, and biochemical effects. *Neurosci. Biobehav. Rev.* 34, 721–733. doi: 10.1016/j.neubiorev.2009.10.005

Stoodley, C. J., Valera, E. M., and Schmahmann, J. D. (2012). Functional topography of the cerebellum for motor and cognitive tasks: an fMRI study. *Neuroimage* 59, 1560–1570. doi: 10.1016/j.neuroimage.2011.08.065

Tao, J., Chen, X., Egorova, N., Liu, J., Xue, X., Wang, Q., et al. (2017). Tai Chi Chuan and Baduanjin practice modulates functional connectivity of the cognitive control network in older adults. *Sci. Rep.* 7:41581. doi: 10.1038/srep41581

Tao, J., Liu, J., Egorova, N., Chen, X., Sun, S., Xue, X., et al. (2016). Increased hippocampus–medial prefrontal cortex resting-state functional connectivity and memory function after tai chi chuan practice in elder adults. *Front. Aging Neurosci.* 8:25. doi: 10.3389/fnagi.2016.00025

Tomasi, D., and Volkow, N. D. (2012). Aging and functional brain networks. *Mol. Psychiatry* 17, 471, 549–558. doi: 10.1038/mp.2012.27

Tousignant, M., Corriveau, H., Roy, P. M., et al. (2013). Efficacy of supervised Tai Chi exercises versus conventional physical therapy exercises in fall prevention for frail older adults: a randomized controlled trial. *Disabil. Rehabil.* 35, 1429–1435. doi: 10.3109/09638288.2012.737084

Van Dijk, K. R., Sabuncu, M. R., and Buckner, R. L. (2012). The influence of head motion on intrinsic functional connectivity MRI. *Neuroimage* 59, 431–438. doi: 10.1016/j.neuroimage.2011.07.044

Verhagen, A. P., de Vet, H. C., de Bie, R. A., Kessels, A. G., Boers, M., Bouter, L. M., et al. (1998). The Delphi list: a criteria list for quality assessment of randomized clinical trials for conducting systematic reviews developed by Delphi consensus. *J. Clin. Epidemiol.* 51, 1235–1241. doi: 10.1016/S0895-4356(98)00131-0

Voss, M. W., Erickson, K. I., Prakash, R. S., Chaddock, L., Kim, J. S., Alves, H., et al. (2013). Neurobiological markers of exercise-related brain plasticity in older adults. *Brain Behav. Immun.* 28, 90–99. doi: 10.1016/j.bbi.2012.10.021

Wayne, P. M., Walsh, J. N., Taylor-Piliae, R. E., Wells, R. E., Papp, K. V., Donovan, N. J., et al. (2014). Effect of Tai Chi on cognitive performance in older adults: systematic review and meta-analysis. *J. Am. Geriatr. Soc.* 62, 25–39. doi: 10.1111/jgs.12611

Wei, G. X., Dong, H. M., Yang, Z., Luo, J., and Zuo, X. N. (2014). Tai Chi Chuan optimizes the functional organization of the intrinsic human brain architecture in older adults. *Front. Aging Neurosci.* 6:74. doi: 10.3389/fnagi.2014.00074

Wei, G.-X., Xu, T., Fan, F.-M., et al. (2013). Can Taichi reshape the brain? A brain morphometry study. *PLoS ONE* 8:e61038. doi: 10.1371/journal.pone.0061038

Wong, A. M., Lin, Y. C., Chou, S. W., Tang, F. T., and Wong, P. Y. (2001). Coordination exercise and postural stability in elderly people: effect of Tai Chi Chuan. *Arch. Phys. Med. Rehabil.* 82, 608–612. doi: 10.1053/apmr.2001.22615

Yin, S., Zhu, X., Li, R., Niu, Y., Wang, B., Zheng, Z., et al. (2014). Intervention-induced enhancement in intrinsic brain activity in healthy older adults. *Sci. Rep.* 4:7309. doi: 10.1038/srep07309

Zang, Y., Jiang, T., Lu, Y., He, Y., and Tian, L. (2004). Regional homogeneity approach to fMRI data analysis. *Neuroimage* 22, 394–400. doi: 10.1016/j.neuroimage.2003.12.030

Zheng, Z., Zhu, X., Yin, S., Wang, B., Niu, Y., Huang, X., et al. (2015). Combined cognitive-psychological-physical intervention induces reorganization of intrinsic functional brain architecture in older adults. *Neural Plast.* 2015:713104. doi: 10.1155/2015/713104

Zuo, X. N., and Xing, X. X. (2014). Test-retest reliabilities of resting-state FMRI measurements in human brain functional connectomics: a systems neuroscience perspective. *Neurosci. Biobehav. Rev.* 45, 100–118. doi: 10.1016/j.neubiorev.2014.05.009

Conflict of Interest Statement: The authors declare that the research was conducted in the absence of any commercial or financial relationships that could be construed as a potential conflict of interest.

Copyright © 2018 Pan, Su, Fang, Hou, Lee, Chen, Lamberth and Kim. This is an open-access article distributed under the terms of the Creative Commons Attribution License (CC BY). The use, distribution or reproduction in other forums is permitted, provided the original author(s) and the copyright owner are credited and that the original publication in this journal is cited, in accordance with accepted academic practice. No use, distribution or reproduction is permitted which does not comply with these terms.

frontiers in Aging Neuroscience

REVIEW
published: 26 April 2018
doi: 10.3389/fnagi.2018.00099

A Review of the Pedunculopontine Nucleus in Parkinson's Disease

Isobel T. French and Kalai A. Muthusamy*

Division of Neurosurgery, Department of Surgery, University Malaya, Kuala Lumpur, Malaysia

The pedunculopontine nucleus (PPN) is situated in the upper pons in the dorsolateral portion of the ponto-mesencephalic tegmentum. Its main mass is positioned at the trochlear nucleus level, and is part of the mesenphalic locomotor region (MLR) in the upper brainstem. The human PPN is divided into two subnuclei, the pars compacta (PPNc) and pars dissipatus (PPNd), and constitutes both cholinergic and non-cholinergic neurons with afferent and efferent projections to the cerebral cortex, thalamus, basal ganglia (BG), cerebellum, and spinal cord. The BG controls locomotion and posture via GABAergic output of the substantia nigra pars reticulate (SNr). In PD patients, GABAergic BG output levels are abnormally increased, and gait disturbances are produced via abnormal increases in SNr-induced inhibition of the MLR. Since the PPN is vastly connected with the BG and the brainstem, dysfunction within these systems lead to advanced symptomatic progression in Parkinson's disease (PD), including sleep and cognitive issues. To date, the best treatment is to perform deep brain stimulation (DBS) on PD patients as outcomes have shown positive effects in ameliorating the debilitating symptoms of this disease by treating pathological circuitries within the parkinsonian brain. It is therefore important to address the challenges and develop this procedure to improve the quality of life of PD patients.

Keywords: Pedunculopontine nucleus, mesenphalic locomotor region, basal ganglia, substantia nigra, brainstem, Parkinson's disease, deep brain stimulation

OPEN ACCESS

Edited by:
Elizabeth B. Torres, Rutgers University, The State University of New Jersey, United States

Reviewed by:
Jose Bargas, Universidad Nacional Autónoma de México, Mexico
Tipu Z. Aziz, John Radcliffe Hospital, United Kingdom

****Correspondence:***
Isobel T. French
belleitf88@gmail.com

Received: *31 May 2017*
Accepted: *22 March 2018*
Published: *26 April 2018*

Citation:
French IT and Muthusamy KA (2018) A Review of the Pedunculopontine Nucleus in Parkinson's Disease. Front. Aging Neurosci. 10:99. doi: 10.3389/fnagi.2018.00099

THE PEDUNCULOPONTINE NUCLEUS

The pedunculopontine nucleus (PPN) is situated in the upper pons in the dorsolateral part of the ponto-mesencephalic tegmentum. Its main mass is located at the level of trochlear nucleus, and is part of the mesenphalic locomotor region (MLR) in the upper brainstem (Olszewski and Baxter, 1954; Geula et al., 1993). Olszewski and Baxter (1954) divided the human PPN into two subnuclei, the pars compacta (PPNc) and pars dissipatus (PPNd). The PPNc is more prominent with a compact cluster of large neurons, whereas the PPNd is composed of small and medium-sized neurons scattered inside the superior cerebellar peduncle (SCP) and central tegmental tract (Olszewski and Baxter, 1954). The PPN comprises both cholinergic and non-cholinergic neurons, and possesses afferent and efferent projections to the cerebral cortex, thalamus, basal ganglia (BG), cerebellum, and spinal cord.

Eighty to ninety percentage of the PPNc contains cholinergic neurons amassed along the dorsolateral border of the SCP at trochlear nucleus levels with few dopaminergic neurons (Jones, 1991; Pahapill and Lozano, 2000; Winn, 2008). These thin unmyelinated axons diverge extensively over the brain supply nuclei in the BG, cerebellum, reticular formation in the lower brainstem, and

also the spinal cord (Stein, 2009). PPNd neurons dispersed along the SCP from mid-encephalic to mid-pontine levels constitute mainly glutamatergic neurons (Rye et al., 1987; Lavoie and Parent, 1994a) while the rest are cholinergic (Mesulam et al., 1989).

The PPNc and PPNd also possess GABAergic inhibitory neurons, whereas cholinergic neurons also contain neuropeptides and novel neuromodulators (Vincent et al., 1986; Vincent and Kimura, 1992; Lavoie and Parent, 1994a,b,c; Bevan and Bolam, 1995). The PPN possesses ascending and descending afferent and efferent (see **Figure 1**) projections, and PPN inputs approach from above and below its level. Descending networks from the cerebral cortex project via the BG and extrapyramidal system to the PPN, including the face, arm, trunk, and leg areas of the motor cortex (MCx), specifically Brodmann area 4 (von Monakow et al., 1979). The PPNc is also a primary constituent in a feedback loop to the thalamus from the spinal cord and limbic system (Pahapill and Lozano, 2000) and is a component of the ascending reticular activating system (ARAS), where cortical stimulation is modulated via ascending cholinergic connections to the thalamus (Steriade, 2004).

The PPN enhances the movement, motivational, and cognitive aspects of multifaceted behavioral responses (Garcia-Rill, 1986; Inglis and Winn, 1995; Reese et al., 1995; Takakusaki et al., 2004a). Stimulation of this area induces locomotion in animals, whereas damage leads to a number of neurological disorders included in Parkinson's disease (PD), Alzheimer's disease and schizophrenia due to its close ties with the BG and thalamus.

PPN Connectivity and Physiology

Motor Cortical Connections

The PPN possesses dense connections to the upper extremity regions of the MCx, followed by the lower extremity, trunk, and orofacial regions. Connections are more dense in the pre-MCx and frontal lobe compared to other regions (Muthusamy et al., 2007). Reciprocal connections also exist with the ipsilateral prefrontal MCx (Pahapill and Lozano, 2000). The PPN also obtains direct cortical afferent fibers from the primary and somatosensory motor area, pre-supplementary, dorsal, and ventral pre-MCx, as well as frontal eye fields (Kuypers and Lawrence, 1967; Moonedley and Graybiel, 1980; Matsumura et al., 2000). These connections implicate the PPN in cortical functions such as movement, cognition and sleep.

Abbreviations: Ach, Acetylcholine; ARAS, Ascending reticular activating system; BG, Basal ganglia; BG-BS, Basal ganglia-brainstem; CN, caudate nucleus; CuN, Cuneiform nucleus; DA, Dopamine; DBS, Deep brain stimulation; GABA, Gamma aminobutyric acid; GiN, Gigantocellular reticular nucleus; GP, Globus pallidus; GPe, Globus pallidus externa; GPi, globus pallidus interna; LN, Lewy neurites; LB, Lewy bodies; LDT, Laterodorsal tegmental nucleus; MCx, Motor cortex; MLR, mesenphalic locomotor region; NAcc, Nucleus accumbens; PPN, Pedunculopontine nucleus; PPNc; Pedunculopontine nucleus pars compacta; PPNd, Pedunculopontine nucleus pars dissipatus; PD, Parkinson's disease; REMS, Rapid eye movement sleep; VTA, Ventral tegmental area; VA, ventral anterior nucleus; VL, ventrolateral nucleus; SC, Superior colliculus; SN, Substantia nigra; SNc, Substantia nigra pars compacta; SNr, Substantia nigra pars reticulate; STN, Subthalamic nucleus.

Striatal Connections

PPN efferent projections contacting the striatum are poorly arborized, excluding the ventral and peri-pallidal zone of the putamen (Lavoie and Parent, 1994c). These connections indicate that the PPN is also involved in limbic function. This is seen in the ventral striatum, also known as the nucleus accumbens (NAcc). Ascending PPN connections provide control over striatal input and output via connections with the thalamus and cerebral cortex, even in the absence of direct projections (Winn, 1998). PPN stimulation increases bursting activity in the NAcc (Floresco et al., 2003), where changes in release accompanying different firing patterns reveal two forceful conditions in dopamine (DA) levels in the striatum and NAcc. This is namely a tonic state with truncated but stable DA levels, and a phasic state correlated to behavioral actions and reactions to environmental stimuli. PPN cholinergic inputs therefore provide a functional duality ensuring the basal level of DA neurons response, whether stimulus-specific or anatomically diffuse. This also determines the response required in precise circumstances (Mena-Segovia et al., 2008b).

Thalamic Connections

Ascending PPN outputs project via the ventral and dorsal tegmental bundle pathways carry major cholinergic projections (Garcia-Rill, 1991) to all thalamic nuclei (Lavoie and Parent, 1994b). Strong cholinergic innervations to the intralaminar and reticular nuclei were also revealed (Mesulam et al., 1992a). These studies suggest that the thalamus obtains major cholinergic PPN input, especially toward "nonspecific" nuclei associated with the ARAS. The ARAS (Moruzzi and Magoun, 1949) stimulates the cortex using cholinergic input to the thalamus largely via PPN cholinergic cells (Pare et al., 1988; Steriade et al., 1988). This projection then travels to non-specific thalamic nuclei and produces rapid cortical oscillatory activity associated with arousal and rapid eye movement sleep (REMS) (Steriade, 2004). This stimulates reticular formation neurons in a positive-feedback procedure, whereas termination is induced through inhibitory activity of REMS-off aminergic neurons via REMS-on stimulated neuronal regulation positioned in the laterodorsal tegmental nucleus (LDT), and PPN regions (French and Muthusamy, 2016).

Pallidal Connections

The globus pallidus interna (GPi) of the globus pallidum (GP) sends inhibitory efferent fibers to the ipsilateral PPN. Anterograde tracer studies reveal that the PPN sends substantial efferent fibers to the GPi (Lavoie and Parent, 1994b) rather than the globus pallidus externa (GPe). In humans, the GP receives cholinergic innervations from the brainstem (Mesulam et al., 1983). Pallidal efferent pathways descend along the pallidotegmental tract to the Forel's field before dividing into the medial & lateral descending pathway into the PPN and midbrain tegmentum. The medial pathway then joins the medial longitudinal fasciculus in the pre-rubral field & terminates in the PPN, whereas the lateral pathway descends in the ventrolateral tegmentum before intermingling with the medial lemniscus and terminating in the PPN (Carpenter, 1976; DeVito et al., 1980).

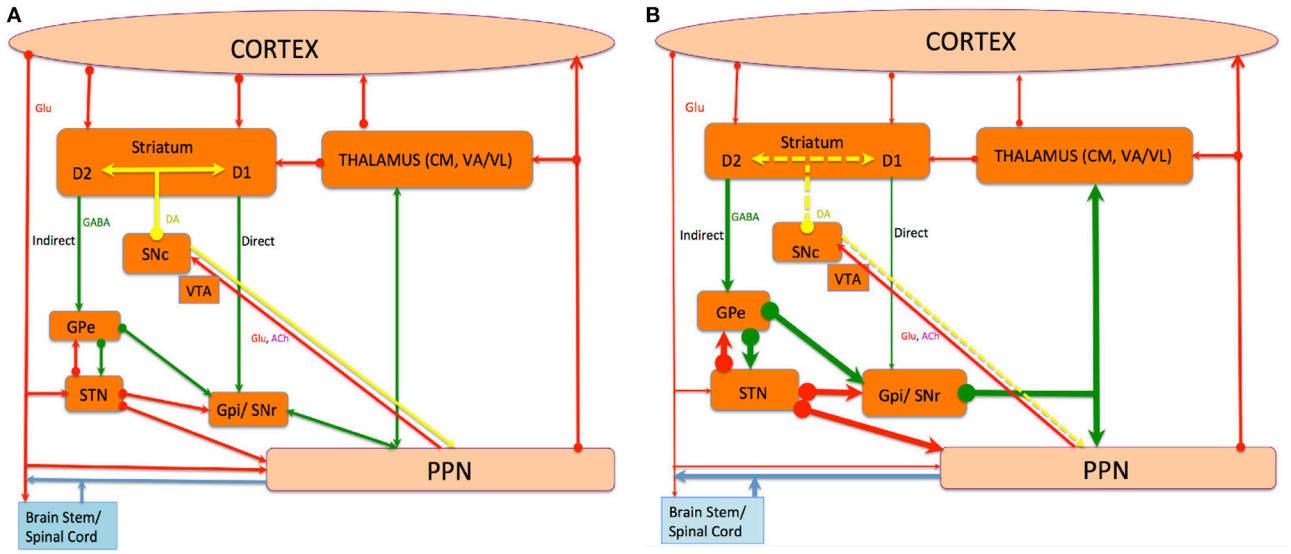

FIGURE 1 | The connections of The PPN, and the direct and indirect pathway of BG-thalamocortical circuits under normal **(A)** and PD **(B)** conditions. Red, green, and yellow lines denote glutamatergic, GABAergic and dopaminergic projections respectively, while blue lines indicate chemically amalgamated projections. Thickening lines show increased activity whereas thinning lines show decreased activity when alterations occur in the average activity rate of specific projection pathways in PD compared with the normal state. Dotted yellow lines indicate loss. The striatum and STN deliver input from incoming cortical information to the BG. The GPi and SNr deliver output information from the BG to the rest of the brain and apply robust inhibitory control on targets in the thalamus and the brainstem. This tonic inhibitory input must be disinhibited to permit normal movements to occur. The striatum applies opposite influences on the GPi and SNr via two distinct classes of efferent neurons, namely the D1-receptor-rich "direct pathway" positively modulated by DA and the D2-receptor-rich "indirect pathway" negatively modulated by DA. The loss of DA in PD's causes disequilibrium in the activity of these two striatofugal pathways and their corresponding cortical inputs.

Nigral Connections

Afferent gamma aminobutyric acid (GABA) endings from the substantia nigra (SN) profusely contact with synapses of PPN cell bodies and dendrites (Granata and Kitai, 1991). Reciprocally, the PPN sends efferent glutamatergic and cholinergic fibers to dopaminergic SN pars compacta (SNc) neurons (Charara et al., 1996) via multiple contacts with dendrites and cell bodies (Bolam et al., 1991; Mesulam et al., 1992b; Charara et al., 1996). These connections propose that strong excitatory influences on dopaminergic SNc neurons exerted from the PPN as pedunculonigral fibers branch more profusely in the SNc than SN pars reticulata (SNr).

The PPN also receives DA innervation over its anteroposterior extent (Rolland et al., 2009) from the SNc at posterior and mediodorsal levels, crossing through the medial lemniscus and reticular formation. These fibers tend to avoid cholinergic cell bodies but converge in neighboring non-cholinergic PPN parts through an anteroposterior and ventrodorsal gradient, particularly in the ventral cuneiform nucleus (CuN) located dorsally to the PPN. Furthermore, cell bodies analogous to the dopaminergic peri- and retrorubral cell clusters decrease rapidly posteriorly in the anterior PPN. Lavoie and Parent (1994b) also report that DA and cholinergic cells dominate adjoining but definite regions, with the dopaminergic population more anteriorly and laterodorsally located. Thus, the PPN along with the CuN receives dopaminergic innervation, endorsing that DA has a role in neural activity modulation of these structures. Intriguingly, DA fibers are heterogeneously dispersed, with central concentrations in the non-cholinergic PPN and ventral CuN border. This implies that functions such as postural muscle tone controlled by the PPN or locomotion via the CuN (Takakusaki et al., 2003) are directly influenced by DA. Furthermore, PPN and nigral dopaminergic neurons ascertain a direct loop moderating motor activity as both the cholinergic and especially non-cholinergic PPN project back to dopaminergic neurons of the SNc and ventral tegmental area (VTA) (Lavoie and Parent, 1994b; Mena-Segovia et al., 2008a).

PPN cholinergic projections have an expansive effect upon midbrain DA systems innervating both SNc and VTA neurons. Though less significant in controlling burst firing and population action of DA neurons, PPN neurons could be associated with sustaining the muscarinic-dependent tonic discharge of DA and specifying DA neuronal phasic signals to time sensory events. This suggests a responsibility for the PPN in associative learning. These phasic signals most likely work as a part of the ARAS in contribution of acetylcholine (ACh), to thalamocortical neuronal coherence in sensory stimuli integration.

PPN connections to the SNc and VTA alters DA release in different regions of the striatum, further affecting striatal inputs such as the cortex and thalamus. This modifies activity throughout the BG that eventually leads to behavioral changes. PPN afferents increase the number of neuronal burst firing in the VTA, though only in neurons that are already firing (Floresco et al., 2003). Extensive bilateral cholinergic innervation is also observed in the VTA, deriving primarily from the LDT and caudal PPN. An ipsilateral cholinergic projection originating

from less dense regions of the cholinergic group projects to the SN. Cholinergic and glutamatergic PPN cells projecting to the SN and VTA (Beninato and Spencer, 1987; Bolam et al., 1991; Futami et al., 1995). This activates midbrain DA cells with short latencies (Scarnati et al., 1984; Lokwan et al., 1999) and evokes DA release in dopaminergic innervation areas (Forster and Blaha, 2003). Such topography indicates that cholinergic outflow from the PPN to functionally different systems vary depending on where afferent input is received. Input to dense cores of the group appears to affect cholinergic outflow to the mesolimbic DA system rather than the nigrostriatal system. However, this does not negate its influence on the nigrostriatal system as SN-projecting cells are also found throughout areas containing cholinergic cells. This implies that input received by an SN-projecting cell is more likely to affect the ipsilateral nigrostriatal system rather than the contralateral side. The VTA, however, appears to receive input from both sides of the cholinergic group. The identification of a distinct difference in cholinergic innervation of the SN and VTA relays important information on how cholinergic systems regulate CNS-controlling behavioral states including arousal and motor functions (Steriade and Buzsaki, 1990). Relative to this, the PPN also works with a parallel cholinergic input arising from the LDT. The PPN is thus part of two interrelated systems arising from cholinergic brainstem neurons modulating DA systems in the midbrain, another of which is the LDT.

Subthalamic Nuclei Connections

Glutamatergic afferents from the subthalamic nucleus (STN) to the PPN function through a positive feed-forward circuit arising from PPN cholinergic neurons. These projections converge with inputs from the cortex and GPe, affecting the activity of direct and indirect pathways (Bevan and Bolam, 1995).

A subpopulation of PPN neurons with ascending projections to the STN are distinct from neurons with descending projections to the gigantocellular reticular nucleus (GiN) (Mena-Segovia et al., 2008a; Ros et al., 2010). PPN projections are predominantly discrete to these two motor components, although cholinergic and non-cholinergic projections also surface from neurons within similar areas (Mena-Segovia et al., 2008a; Ros et al., 2010). This suggests that projection neurons in both pathways interact with each other, advocating an integrative role within PPN microcircuits. Similarly, the distribution of cholinergic, GABAergic, and glutamatergic neurons (Mena-Segovia et al., 2009; Wang and Morales, 2009; Martinez-Gonzalez et al., 2012) suggests that the rostral PPN is chiefly inhibitory being GABAergic, while the caudal PPN is chiefly excitatory being glutamatergic. Hence, motor projections to the STN and GiN are primarily glutamatergic with distinctive subtypes as they contain a diverse balance of calcium-binding proteins. Nonetheless, GABAergic constituents also exist (Bevan and Bolam, 1995). The quantity of cholinergic neurons in the caudal PPN is larger connecting to both targets, suggesting that cholinergic-mediated excitation of motor structures arise from the caudal PPN. Descending non-cholinergic neurons showed distinct electrophysiological properties compared to ascending non-cholinergic neurons, supporting the existence of functional differentiations concerning these two routes (Ros et al., 2010). Thus, descending PPN projections mediated via reticulospinal neurons of the GiN excites inhibitory interneurons in the spinal cord and modulate excitatory MLR output (Takakusaki et al., 2004a; Takakusaki, 2008). This concurs that the PPN is implicated in locomotion initiation (see **Figure 1A**).

Cerebellar and Spinal Cord Connections

Efferent fibers from deep cerebellar nuclei send collaterals to the PPN before reaching the thalamus (Hazrati and Parent, 1992), suggesting that the PPN acts as a well-designed consolidation epicenter between the BG and the cerebellum. Matsumura et al. (1997) also suggests that the PPN acts as a dispatch between the cerebral cortex and spinal cord, performing as a brainstem regulator center for interlimb movement synchronization and bimanual motor performance (Matsumura et al., 1997).

PARKINSON'S DISEASE

PD is a collection of neurodegenerative conditions affecting the brain, particularly pigmented nuclei in the extrapyramidal system of the midbrain and brainstem, the olfactory tubercle, cerebral cortex, and components of the peripheral nervous system (Braak et al., 2003). Ultimate physical debilities ensuing from these pathologies are motor deficiencies termed "parkinsonism." These comprise dearth and movement slowness, known as akinesia and bradykinesia, muscle rigidity and resting tremor. Parkinsonism is produced primarily through BG functional impairments.

Principally, these problems result from dopaminergic neuronal degeneration in the midbrain leading to DA deficiency in areas receiving dopaminergic inputs, specifically from the post-commissural putamen and other BG areas (Braak et al., 2003). However, before dopaminergic degeneration occurs in the midbrain, Lewy neurites (LNs), and bodies (LBs), first form in the non-catecholaminergic dorsal glossopharyngeus-vagus complex and intermediate reticular zone projection neurons, and exclusive gain setting system nerve cell types, which are the coeruleus-subcoeruleus complex, caudal raphe nuclei, GiN, and olfactory bulb, tract, and/or anterior nucleus before nigral involvement (Del Tredici et al., 2002). This is possibly why PD patients develop anosmia during initial stages. This multisystem disorder first involves few susceptible nerve cell types in particular areas of the human nervous system, where the intracerebral development of abnormal proteinaceous LBs and LNs commences at definite locations and progress in a topographic order (Braak and Del Tredici, 2004). As the disease advances, constituents of the autonomic, limbic, and somatomotor systems become increasingly compromised. During pre-symptomatic stages 1–2, LB inclusion pathology is constricted to the medulla oblongata/pontine tegmentum and olfactory bulb/anterior nucleus. This means that SN involvement presumes an obvious prevailing pathology in the medulla oblongata. If it were possible to detect PD during this stage with an underlying therapy available, consequent neuronal loss in the SN could probably be prevented (Braak et al., 2003). In stages 3–4, the SN and other midbrain gray nuclei and forebrain undergo severe pathological changes as the process develops

in an ascending manner traversing the upper border of the pontine tegmentum and enters midbrain and forebrain basal portions. More explicitly, the very first solitary LNs are observed in the SNc leading to granular aggregations, pale bodies, and LBs in melanized projection neurons, all of which are thin and sparsely myelinated axons (Braak et al., 2004). Classically, nigral pathology initiates in the SNc postero-lateral subnucleus (Braak and Braak, 1985; Gibb and Lees, 1991) and continue on in the postero-superior and posteromedial subnuclei, circumventing the SN magnocellular and anterior subnuclei while causing trivial lesions (Braak et al., 2003). Nuclear gray pathology from earlier stages is now severely exacerbated. Concurrently, the process impinges on the central amygdala subnucleus before extending into basolateral nuclei. LN complexes progressively fill the central subnucleus and characterize it off from contiguous structures (Sims and Williams, 1990; Amaral et al., 1992; Braak et al., 1994; Bohus et al., 1996). Other brain regions involved include the cholinergic PPN (Garcia-Rill, 1991; Inglis and Winn, 1995; Rye, 1997; Pahapill and Lozano, 2000), oral raphe nuclei, cholinergic magnocellular nuclei of the basal forebrain (Candy et al., 1983; Whitehouse et al., 1983; Mesulam et al., 1992a), and hypothalamic tuberomamillary nucleus (Del Tredici and Braak, 2004).

Excluding the SN and PPN, other striatal loop axes begin early myelination and oppose undergoing pathological changes (Braak et al., 2004). At stage 4, the poorly myelinated temporal mesocortex involving the transentorhinal region between the allocortex and neocortex is engaged in disease development for the first time (Braak et al., 2003). Most patients transcend into the symptomatic stages at this juncture. In the last stages 5–6, the disease reveals itself in all of its clinical dimensions as the process crosses the mature neocortex (Braak et al., 2004). During this stage, a plexus of LNs develop in the second sector of Ammon's horn (Dickson et al., 1994). This feature is typical of stages 4–6 that even when sections through the SN are unavailable, PD can be diagnosed based on Ammon's horn lesions alone (Del Tredici and Braak, 2004). During these final stages, the neurodegenerative progression reaches its supreme topographic degree. The SN appears practically stripped of melanoneurons, appearing colorless upon macroscopic inspection (Braak et al., 2004).

THE BG AND PD

The BG comprises the neostriatum containing the caudate nucleus (CN) and putamen, the GP containing the GPe and GPi, the STN, and the SN consisting of the SNr and SNc. These structures contribute to anatomically and functionally isolated loops involving certain thalamic and cortical regions. These parallel circuits differ based on the cortical function involved and are separated into "motor," "associative," and "limbic" loops (Alexander et al., 1986; Alexander and Crutcher, 1990; Middleton and Strick, 2000; Kelly and Strick, 2004). Reciprocal projections concerning the striatum and GPi/SNr are divided into two distinct pathways, namely a "direct" monosynaptic connection, and an "indirect" projection via the interpolated GPe/STN. GPi/SNr output projects mainly to ventral anterior (VA) and ventrolateral (VL) thalamic nuclei, which project to the cerebral cortex. Minor BG projections extend to the intralaminar centromedian and parafascicular thalamic nuclei, and brainstem structures such as the superior colliculus (SC), PPN, and reticular formation. The striatum also obtains prominent dopaminergic SNc input (Galvan and Wichmann, 2008). The BG are a major brain system modulated by dopaminergic input from the SN (Albin et al., 1989) with profound effects on behavior.

The striatum and STN obtains glutamatergic afferents from exclusive cerebral or thalamic regions and transfer this information to BG output nuclei, namely the GPi and SNr. These BG output nuclei fire tonically and rapidly (DeLong and Georgopoulos, 2011), thus brain areas receiving inputs from the BG are continuously under strong tonic inhibitions (Hikosaka, 2007). Decreases in SNr/ GPi neuronal activity is caused by direct input from the neostriatum, which are also GABAergic and inhibitory (Yoshida and Precht, 1971; Hikosaka et al., 1993b). An appealing theory states that the BG's chief purpose is apt behavior selection (Hikosaka et al., 1993a; Mink, 1996; Nambu et al., 2002), where unwanted behaviors are subdued by SNr/GPi-induced inhibition preservation or increment whilst required behaviors are liberated by SNr/GPi-induced inhibition decrement or elimination. Patients with BG dysfunctions portray involuntary movement disorders such as tremor, dyskinesia, dystonia, chorea, athetosis, and ballism (Denny-Brown, 1968). These involuntary movements are instigated by a disruption of the SNr/GPi-induced inhibition, consistent with parkinsonian symptoms displaying involuntary tremulous movements, diminished muscular power whether in activation or not, impaired posture with an inclination to bend the trunk forwards, festination from walking to running or poverty and slowness of movement without paralysis (DeLong and Wichmann, 2007), where the senses and intellect are uninjured initially. However, these patients also display difficulty in initiating purposeful movements known as akinesia, or slow and small movements known as bradykinesia and hypokinesia (see **Figure 2**). This movement disorder is elicited by an incomplete disinhibition of the SNr/GPi-induced inhibition on thalamocortical systems (Burbaud et al., 1998; Stein, 2009), ensuing in gait disturbances with difficulties initiating or terminating walking (Azulay et al., 2002). Additionally, dyskinesias induced by the DA pre-cursor levodopa (L-DOPA) or DA agonist apomorphine, are concomitant with the inadequate suppression of BG GABAergic output (Nevet et al., 2004). This leads to abnormal oscillatory firing of motor neurons in the aforementioned areas, inducing tremor or other involuntary movements.

The BG is known for controlling locomotion and posture via SNr-GABAergic output (Takakusaki et al., 2004c). In PD patients, GABAergic BG output levels are abnormally increased (Miller and DeLong, 1987; DeLong, 1990; Filion, 1991). Takakusaki et al. (2004b) proposed that gait disturbances in PD are produced by abnormal increases in SNr-induced inhibition of the MLR. Furthermore, muscle rigidity might result from abnormally increased PPN inhibition that would otherwise produce muscle relaxation (see **Figure 1B**). Dystonia could be triggered by BG GABAergic output diminution to the PPN, depicted by focal

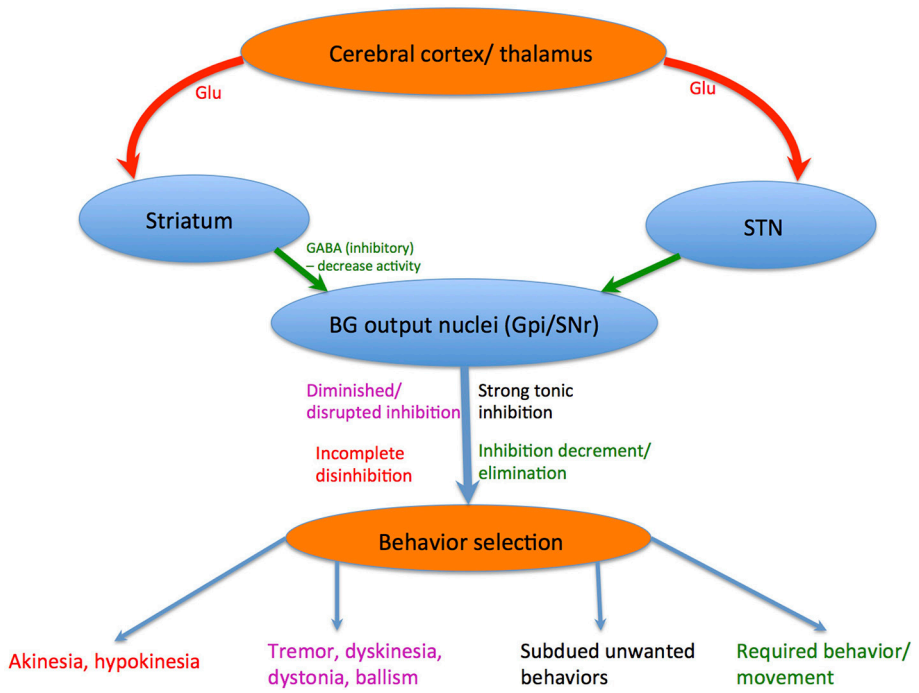

FIGURE 2 | Behavior selection: Red lines depict glutamatergic pathways, whereas green lines depict GABAergic pathways. Blue lines depict chemically composite pathways. The corresponding colored notations show how each different movement disorder is elicited.

and involuntary muscle tone, posture, or movement changes (Starr et al., 2005). Augmented GABAergic outputs would thus overwhelm target areas including the SC, MLR, PPN, thalamo-cortical circuits, and feasibly mouth movement and vocalization centers, ensuing in akinesia or hypokinesia (see **Figure 2**).

Another reason for a deranged BG-GABAergic output in the SNr/GPi would result from inputs coming from the GPe/neostriatum (Hikosaka, 2007). These motor features are often accompanied by non-motor issues such as depression, anxiety, autonomic dysfunction, sleep disorders, and cognitive impairment as a result of DA deficiency in non-motor portions of the striatum and more widespread progressive pathologic changes in the brainstem, thalamus, and eventually, the cerebral cortex (Braak et al., 2003).

THE PPN AND BG-BRAINSTEM SYSTEM

Ascending PPN projections provide substantial innervation to the SNc, STN, and GP (Mehler and Nauta, 1974; Graybiel, 1977; Nomura et al., 1980; Saper and Loewy, 1982; Edley and Graybiel, 1983; Jacobs and Azmitia, 1992; Spann and Grofova, 1992; Lavoie and Parent, 1994a,b,c). The inconsistency between the number of ascending and descending projections indicate that the PPN is not a major output component, but a modulating structure as it is part of the many auxiliary loops in BG circuitry and activity. This is because of its strategic position and network with the MCx, thalamus, SN, STN, and CuN. PPN neurons exert excitatory action upon various BG components facilitated mainly by Ach (Woolf and Butcher, 1986). However, the presence of glutamate and various neuropeptides within (Clements and Grant, 1990; Clements et al., 1991; Côté and Parent, 1992) suggest that the PPN also applies an expansive range of effects upon BG neurons through various chemo-specific neuronal systems (Parent and Hazrati, 1995). PPN neurons directly influence BG output nuclei, namely the SNr and GPi, and therefore directly affect information processed within the BG before approaching targets such as the thalamus. Since the PPN establishes highly reciprocal connections with the BG than any other brain region, both these structures exhibit complex physiological interdependence crucial for physiologic function (Mena-Segovia et al., 2004, 2008b). These structures are interconnected either directly or indirectly with every element, and the BG receives large converging input from the PPN (Garcia-Rill, 1991; Pahapill and Lozano, 2000; Mena-Segovia et al., 2004; Alderson and Winn, 2005).

The BG–brainstem (BG–BS) system functions throughout the mesopontine tegmentum in controlling diverse behavioral expressions. This includes automatic movement control comprising periodic limb movements and postural muscle tone adjustments throughout locomotion integrated with voluntary control. It is also involved in awake–sleep state regulation. The BG-BS system is thus accountable for the manifestation of volitionally-directed and emotionally-instigated motor behavior consolidation, and dysfunction of this system together with the cortico-BG loop triggers behavioral disorders (Takakusaki et al., 2004c). The BG performs planning and implementation of deliberate movements through parallel BG-thalamocortical loop sequences (Alexander and Crutcher, 1990; DeLong, 1990;

Turner and Anderson, 1997), directing outflow to motor networks in the brainstem (Inglis and Winn, 1995; Hikosaka et al., 2000; Takakusaki et al., 2003) where central neuronal complexes for muscle tone and locomotor movement control are located (Garcia-Rill, 1991). Thus, BG outputs project through thalamocortical loops to the brainstem, and are involved in postural muscle tone and locomotion integrative assimilation (Takakusaki et al., 2004b). Hikosaka et al. (2000) postulates that the BG utilizes two types of output to regulate movements; one via thalamocortical systems, and another via brainstem motor networks (see **Figure 3**).

BG output to the cerebral cortex regulates voluntary movement control processes, whereas specific movement patterns such as saccades (Hikosaka and Wurtz, 1983a,b,c; Hikosaka, 1991; Hikosaka et al., 2000; Sparks, 2002), vocalization (Düsterhöft et al., 2000), and locomotion (Rossignol, 1996) are generated by exclusive neuronal systems in the brainstem and spinal cord. MCx projections are directed to the PPN (Matsumura et al., 2000) and pontomedullary reticular formation (Matsuyama and Drew, 1997), where muscle tone regulation and the locomotor system are coordinated simultaneously by dual feedback via net BG inhibition and MCx excitation to the brainstem. In PD, GABAergic BG output is overactive (Wichmann and DeLong, 1996, 2003), ensuing in sluggishness and movement decreases by thalamocortical neurons, known as bradykinesia and hypokinesia respectively. Contrarily, increases in BG inhibition together with PPN cortical excitation reductions would increase the level of muscle tone, known as hypertonus. Likewise, excessive MLR inhibitions and cortical excitation decreases in the brainstem reticular formation would educe gait failure. Furthermore, primary MCx inactivity would disrupt the locomotor programming necessary for defined gait control (Hanakawa et al., 1999; Pahapill and Lozano, 2000). Resultantly, this would constrain the degree of freedom for locomotion (Takakusaki et al., 2004c). Gait disturbances where delays are seen in freezing of gait (FoG), stance phase increases in movement sequences and movement speed decreases are also seen in PD invalids (Morris et al., 1994; Pahapill and Lozano, 2000). BG–BS system impairment would be the principal foundation for PD-induced gait deficiencies (Takakusaki et al., 2004c) as these gait failures resemble SNr-stimulated movement (Takakusaki et al., 2003).

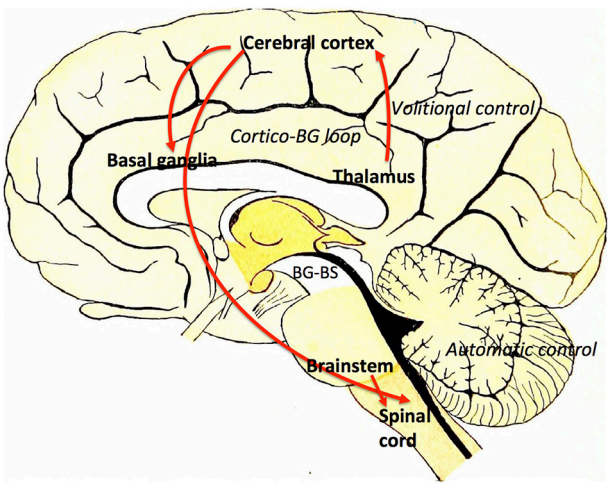

FIGURE 3 | Volitional and automatic control of locomotor movements by the BG-BS system: GABAergic BG output to thalamocortical and brainstem neurons assimilates volitional and automatic movement control processes. Adapted from Villiger and Piersol (1912).

In saccadic control, the direct and indirect pathways within the BG (Alexander and Crutcher, 1990; DeLong, 1990) cause GABAergic SNr tonic neuronal inhibition of SC output neurons, consequently preventing unnecessary saccades. The direct pathway from the CN to SNr results in SC neuronal disinhibition by eradicating this constant inhibition. Specifically, phasic GABAergic output neuronal activity in the CN permits saccade occurrence via tonic SNr-SC inhibition suspension (Hikosaka, 1989). The indirect pathway, involving the GPe and STN, further enhances the SNr-SC inhibition via excitatory cortical input (Nambu et al., 2002). Hence, direct CN-SNr and indirect CN-GPe-STN-SNr pathways induce contrasting SNr-SC system effects. Concurrent interactions within the two pathways generate additional discriminating information and heighten the target systems' neural signal spatial contrast. Inversely, behavior interchange from locomotor subdual when the indirect pathway dominates, to locomotor induction when the direct pathway dominates, is produced via consecutive communication of the pathways. This effect enhances temporal contrast. Thus, BG saccadic control can be summarized via two mechanisms. The first is by enhancement of tonic inhibition and disinhibition, while the second mechanism is through converging and sequencing. These two modules are elicited via direct and indirect pathway communication, and might influence brainstem networks besides thalamocortical networks (Hikosaka et al., 2000) (see **Figure 4**).

Similarly, disinhibition and inhibition regulations are key mechanisms for BG postural muscle tone and locomotion control. Locomotor and muscle tone control systems are normalized by the direct and indirect pathway balance via muscle tone inhibitory regions in the PPN, MLR, and SC receiving GABAergic input from the SNr. During locomotor movement preparation, tonic SNr neuronal tonic activity continuously inhibits both systems. When an activating signal occurs, the direct pathway releases activity in these systems, causing locomotion initiation followed by muscle tone level reduction. Parallel SNr organization to the MLR/PPN also regulates muscle tone level accompanying the initiation and termination of locomotion (Takakusaki et al., 2004c).

Cholinergic PPN neuronal loss in PD (Hirsch et al., 1987; Zweig et al., 1987, 1989; Jellinger, 1988) also attributes to attentive and cognitive damages and sleep defects (Scarnati and Florio, 1997). This validates that the BG-BS are also involved in non-motor function, specifically in REMS regulation, arousal and emotional motor behaviors (Takakusaki et al., 2004c).

Gait and Locomotion

As mentioned, the PPN is a central part of the MLR within the brainstem, where it generates and supports lower controlled

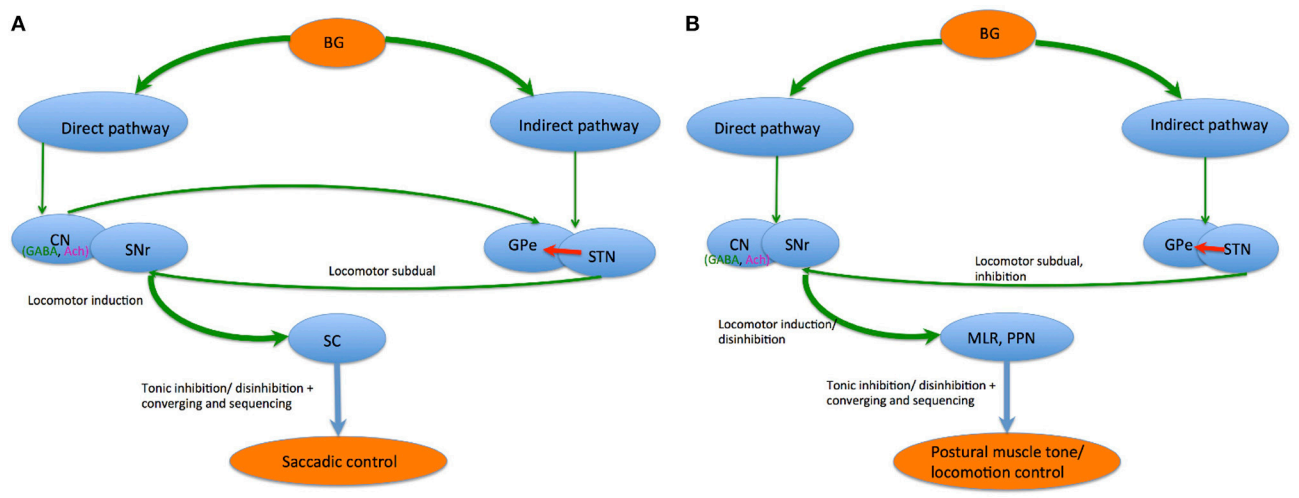

FIGURE 4 | Saccadic control **(A)** and postural muscle tone/ locomotion control **(B)** by the direct and indirect pathways.

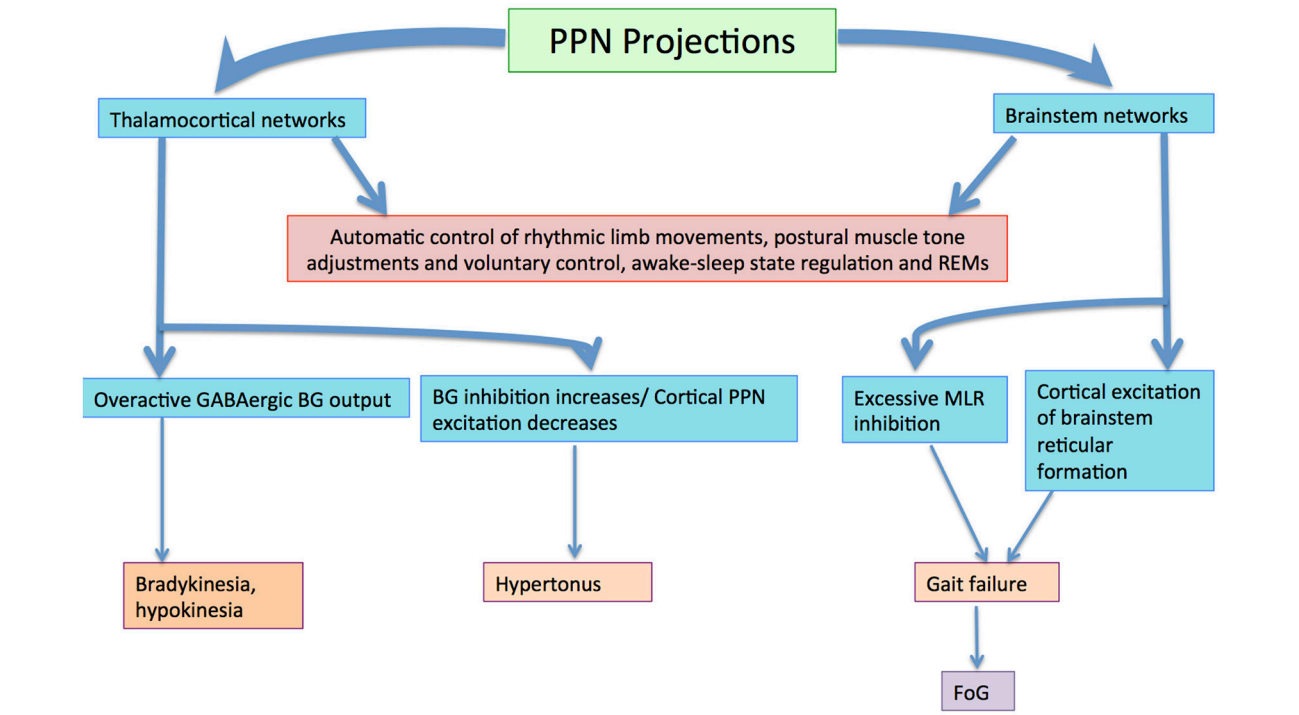

FIGURE 5 | The involvement of the PPN in the neuropathology of PD.

locomotion (Skinner and Garcia-Rill, 1984; Skinner et al., 1990) via descending projections innervating foci in the lower brainstem and medulla, comprising the oral pontine reticular nucleus, the GiN, the medioventral medulla, and spinal cord regions (Mitani et al., 1988; Rye et al., 1988; Nakamura et al., 1989; Semba et al., 1990; Grofova and Keane, 1991; Scarnati et al., 2011). These projections are associated with gait control and posture primarily via locomotion inhibition, where increasing levels of high stimulation drives the frequency of stepping from walking to running (see **Figure 5**) (Garcia-Rill et al., 1987; Garcia-Rill, 1991).

The cholinergic PPNc induces locomotion (Garcia-Rill et al., 1987) together with other brainstem regions via prominent sensory nuclei stimulating locomotion through direct outputs to spinal cord regions of recognized locomotor generators (Pahapill and Lozano, 2000). PPN neuronal response to somatosensory excitation (Grunwerg et al., 1992; Reese et al., 1995) combined with cholinergic PPN neuronal thalamic projections and inputs

from lamina 1 of the spinal cord, advocates that the PPN modulates sensory information to thalamic nuclei. Thus, the PPN plays a role as a dispatch amid the cerebral cortex and spinal cord, providing feedback information vital for posture and gait initiation modulation. This is enabled by ascending thalamic cholinergic projections and deep cerebellar nuclei networks (Pahapill and Lozano, 2000).

Non-cholinergic PPNd neurons receive input from the BG and limbic structures, propositioning that the PPN acts as an assimilator for BG motor choice output and incentive-motivated commands from the striatal-pallidal complex to deliver motivationally influenced activation of motor pattern generators in the pons, medulla and spinal cord (Inglis and Winn, 1995). Such factors affect motor function like kinesia paradoxica. Treatment via PPN activation would improve motor planning and permit increasing motivational ability in stimulating preserved motor programs for stereotyped movements (Pahapill and Lozano, 2000).

Reward, Motivation, and Compulsion

The PPN is accountable for the phasic activity bursts in SNc DA cells, which plays a key role in learning and preserving instrumental tasks (Scarnati et al., 1988; Futami et al., 1995). Primary PPN reward stimuli originate from the lateral hypothalamus, but excitatory reward-prediction stimuli spawns a condition stimulus-elicited DA surge traversing the ventral striatum–pallidum pathway, receiving predominantly limbic cortex input (Schultz et al., 1992). Striosomal cells regulate response to primary reward after conditioning via suppressing DA burst response through the striosomal-SNc pathway (Gerfen, 1992). Striosomal cells also modulate the adaptive scheduled reward expectation that annuls the predicted reward at the predicted interval (Schultz et al., 1997). DA cell activity is therefore an exclusive parallel act of PPN inactivation, compared to a secondary influence on motivation or abridged capability of task performance. The PPN thus serves as an integrative interface amidst innumerable stimuli necessary for executing intended behaviors (Kobayashi et al., 2004). This enables the fundamental activities for motor command initiation and external sensory dispensation via arousal regulation and attentive conditions through dopaminergic systems (Takakusaki et al., 2004c).

PPN lesions ensued in impaired attention (Inglis et al., 2001) and memory learning during a trained incitement and a prime reward (Inglis et al., 1994, 2000). This advocates that PPN inactivation has variable effects on non-dopaminergic cells in the VTA. Firstly, PPN neurons respond to the same task stimuli, whether visual- or auditory-activating DA cells. Secondly, PPN responses are governed by phasic inception patterns observed in DA cells. Thirdly, PPN cells respond before DA cells, permitting PPN-DA information transfer. Finally, PPN suppression subdues DA cell responses to stimuli without upsetting baseline firing frequency (Pan and Hyland, 2005). Therefore, auditory, visual, and somatosensory trained incitements stimulate DA cells (Romo and Schultz, 1990; Schultz and Romo, 1990), with bias toward auditory incitements at tremendously brief latencies, strictly programmed to the stimulus interval. The preference of PPN cells for tone and light increases the likelihood that homogenous afferent projections regulate DA cell action, with biasness for either constituent (Wallace and Fredens, 1988; Comoli et al., 2003). Thus, the PPN and SC supplement each other in dispatching sensory knowledge of different stimuli. PPN neuronal activity predisposed toward auditory responses has a functionally imperative role in reducing DA cell responses without substantial effects on baseline firing rate via a visual component inactivation. This establishes that the PPN selectively controls DA cell bursting rather than tonic resting activity (Floresco et al., 2003), and that PPN inputs are necessary for producing DA cell surge reactions to significant sensory stimuli (Schultz, 1998; Brown et al., 1999). The PPN is therefore imperative for arousal, attention, motivation, learning, and specifically stimulated–reward conditions (Steckler et al., 1994).

PPN lesions do not disrupt brain stimulation reward value however (Waraczynski and Perkins, 1998), suggesting that it performs as a primary sensory and motivational system interface toward delivering communication signals irrespective of reward value. DA cells typically react staggeringly when signals are reward-connected, while PPN cells react non-contingently, suggesting that separate, reward-information-bearing pathways gate PPN inputs. Hence PPN inputs have a dual role, to provide precise and brief latent information toward sensory stimuli intervals and advanced-level function information transmission concerning signals dispatched via sensory-attention regulating mechanisms (Pan and Hyland, 2005).

Research establishes that lateral hypothalamic brain stimulation not only rewards, but also drive-induces (Coons et al., 1965; Glickman and Schiff, 1967). Rewarding hypothalamic brain stimulation depends on trans-synaptic induced release of Ach in the VTA (Yeomans et al., 1993), where dominant portions of these fibers synapse in PPN cholinergic efferents relaying messages back to the VTA (Yeomans et al., 1993). These cholinergic PPN neurons provide non-specific facilitation for reward-connecting behaviors, and therefore act as a relay amid limbic-incentive organization and brainstem locomotor machinery (Steckler et al., 1994). Due to its position within the mesolimbic DA system encompassing the VTA and NAcc, it is entangled in brain mechanisms and neural circuitry formation involved in reward processing, which can lead to motivation and compulsion.

Rapid Eye Movement Sleep (REMS)

PPN and LDT cholinergic neurons are involved in arousal state maintenance and REMS generation (Rye, 1997). During sleep, PPN cholinergic activation of the cortex transpires via projections to the thalamocortical network to subdue slow delta waves and elicit cortical stimulation (Belaid et al., 2014). This leads to REMS, through REM-on and –off cellular activity together with the locus coeruleus and dorsal raphe nuclei (DRN) (McCarley and Chokroverty, 1994). Reduced inhibitory input from the SNr/GPi nuclei to the PPN results in higher intrinsic activity causing cortical activation and electroencephalography (EEG) desynchronization (Reiner et al., 1988) leading to REMS (Steriade, 1996). These neuronal mechanisms that induce REMS

and muscular atonia together with PPN cholinergic projections are under SNr GABAergic inhibition regulation.

PD patients are known to experience several sleep disorders, including reduction of REMS sleep period and REMS behavior disorder (RBD) (Bliwise et al., 2000; Eisensehr et al., 2001). This is because decreases in BG dopaminergic activities is also involved in REMS reduction and RBD (Rye et al., 1999; Albin et al., 2000), hence providing a lucid explanation for the pathogenesis of sleep disturbances in PD (Takakusaki et al., 2004c; French and Muthusamy, 2016). A summary of the different maladies associated with the PPN in PD are listed in **Table 1**.

TREATMENT/DEEP BRAIN STIMULATION

Electrode recordings in deep brain stimulation (DBS) postulate that uncontrolled abnormal pathological oscillations throughout motor networks in the STN, GP, and thalamus are concomitant with motor symptoms in PD (Hammond et al., 2007). Similarly BG networks oscillating at a pathological beta (β) range of 20 Hz, driven by cerebral neurons firing in either "burst" or "tonic" modes is associated with akinesia (Stein, 2009). Successful alleviation of akinesia with L-DOPA enables the system to break away from this pathological beta repression (Kühn et al., 2008). High frequency stimulation, applied via DBS also subdues pathological synchronization (Brown and Eusebio, 2008). PD symptoms are lessened by DBS via preventing pathological neuronal network oscillations that destabilize them, and are successful as they abolish nodes responsible for oscillation generation itself. DBS is thus permanently effective by driving neurons tonically so that pathological oscillations causing the burst/silence mode are reversible.

Neurophysiologically, cortical bursts normally govern PPN input and orchestrate field potentials and neuronal discharges to the cortical rhythm so that PPN local field potentials and neuronal discharges are synchronized with those of MCx activity (Aravamuthan et al., 2008). However, these synchronies reverse after cell lesions and PPN neurons fire mostly throughout positive swings in the cortex when they should be silent. This indicates that inhibitory GP and SNr output is predominant input to the PPN, rather than excitatory MCx output. Stimulation of the GP and SNr also requires adequate glutamate conduction. This substitutes dominant PPN firing via inhibitory input for normal excitatory input from the MCx and STN to the PPN. The β-band is responsible for associated akinesia, where β suppression increases with the complexity of the intended movement while its latency predicts movement onset. This means that the earlier the suppression, the shorter the movement latency. Therapeutic interventions reducing akinetic symptoms reduce enhanced synchronization in the β band and facilitates regular gamma oscillations (Brown et al., 2001).

TABLE 1 | Maladies associated with the PPN in PD, the source and affected brain components, as well as its consequence/ indications.

Malady type	Source	Brain components affected	Consequence/ Indications
LOCOMOTOR			
Akinesia/bradykinesia/hypokinesia	Overactive GABAergic BG output	MCx, thalamus, BG, PPN, SC, MLR	Decreases in velocity and amount of movement
Hypertonus	Increases in BG inhibition Increases in PPN inhibition Decreases in cortical PPN excitation Direct-indirect pathway imbalance via increased SNr inhibition	MCx, BG, PPN	Increased muscle tone
Dystonia	Diminution or instability of BG GABAergic outputs to the PPN	BG (SNr, Gpi), PPN	Central and spontaneous fluctuations in muscle tone, posture, or locomotion
Gait disturbances/ failure	Excessive MLR inhibition via SNr-GABAergic output Cortical excitation of brainstem reticular formation Decreases in cortical stimulation of the brainstem reticular formation Inactivity of the PMC Dysfunction of BG-BS system Direct-indirect pathway imbalance	MLR MCx, brainstem Primary MCx SNr, PPN, MLR, SC	Uncontrolled gait Limited movement Freezing of gait, increases in stance phases in locomotor cycles and decreases in locomotor velocity
COGNITIVE			
Impaired attention and memory learning	PPN lesions	PPN	Inability to concentrate, unable to retain memory
Motivation and compulsion	PPN lesions, impaired brain mechanisms and neural circuitry formation involved in reward processing	NAcc, VTA, PPN	Obsessive compulsive disorder
SLEEP			
REMS	Decreases in BG dopaminergic activity	SNr, GPi, DRN, LDT, PPN	REMS behavior disorder

The PPN area might be a good prospective DBS objective concerning freezing and other gait disorders' treatment associated with PD, where data shows that cholinergic denervation due to PPN neuronal degeneration causes DA non-responsive gait and balance impairment (Karachi et al., 2010; Grabli et al., 2013). Imaging studies in PD patients propose that unilateral PPN DBS intensifies cerebral blood flow bilaterally into the central thalamus and cerebellum (Ballanger et al., 2009). However, recognized assessments support bilateral DBS (Khan et al., 2012) ascertained to be superior particularly for controlling FoG. Thevathasan et al. (2012) further supports this, concluding that bilateral stimulation was more successful in a specific subgroup of PD patients by ∼200%. This study exhibited concrete unprejudiced, double-blinded proof that an explicit subcategory of Parkinsonian patients benefit from bilateral stimulation of a caudal PPN region just below the pontomesenphalic junction that discriminately improves FoG. This did not include inconsistencies in step length however, which could be furtive freezing interrupting the smooth execution of gait (Thevathasan et al., 2012). Long-term outcomes would unquestionably need further substantiation via supplementary studies or randomized trials with longer follow-up periods involving a higher number of patients and exclusive criteria.

Most PPN DBS studies denote alleviation in patients disturbed by freezing and falls although outcomes are variable. This possibly reflects patient choice, target option heterogeneity, surgical procedure differences and stimulation protocols (Hamani et al., 2016a). This leads to a number of challenges to be solved, including the prime target identification, surgical method choice that optimizes electrode placement, precision, and impact of surgical procedures, intraoperative target reliability, and procedural modifications in postoperative electrode position validation. Nonetheless, the procedure appears to provide benefit to selected patients and is comparatively safe. One important limitation in comparing studies from different centers and analyzing outcomes is great target variability and surgical techniques (Hamani et al., 2016b).

Chronic PPN stimulation is usually combined with stimulation of other targets, including the STN, GPi, and the caudal zona incerta due to its superiority compared to PPN DBS alone. However, combined stimulation poses challenges in the effectual assessment of DBS in each target, and also in enlightening the complex relationship between medication and stimulation. A particular problem is the use of low-frequency PPN stimulation and high-frequency stimulation in other targets, where this necessitates intricate programming or utilization of a supplementary pulse generator. Another issue is the concordance on the ideal target position within the PPN region, where it is ambiguous as to whether electrodes should be implanted in the rostral PPN at the level of the inferior colliculus or caudal PPN in a region about 4 mm below the inferior colliculus. A reasonable approach would be to insert contacts in both rostral and caudal PPN regions since available data is still vague, and also because the PPN is oriented along the long axis of the brainstem. Since the PPN is partially degenerated in PD, smaller-spaced electrodes might be preferable. It would also be vital to develop a specified set of resting and movement-related intraoperative local field potentials while conducting PPN DBS as frequency bands in the alpha, β, and theta ranges and movement-related potential were all recorded from the PPN region (Hamani et al., 2016b).

PPN DBS is still a relatively novel intervention in PD, and the numerous challenges mentioned before must be resolved. Despite these trials, the procedure provides benefit to selected patients and appears relatively safe. The future role of PPN DBS in the armamentarium of surgery for PD patients is still uncertain. Unquestionably, more studies are needed to provide more solid data on the advantages and limits of chronic stimulation (Hamani et al., 2016b).

CONCLUSION

Understanding the function of the PPN and its utility in the many neuronal circuitries of the brain is vital for neurophysiological knowledge. This would ensue in the understanding of how maladies such as Parkinson's disease occurs along amid its consequences, and subsequently help in producing the appropriate treatment needed to cure and control these disorders. A promising and long-term treatment would be DBS, which could vastly improve patients' quality of life. Further studies would definitely need to be conducted to elucidate further on such disorders especially in terms of genetics and biochemistry.

AUTHOR CONTRIBUTIONS

IF was the main author of this paper who wrote this manuscript as part of a research project in order to understand better and summarize the physiology and pathophysiology of the pedunculopontine nucleus in associated with Parkinson's disease. KM provided the main oversight and general guidance in the completion of this manuscript.

ACKNOWLEDGMENTS

This review was prepared in accordance with research conducted in conjunction with the High Impact Research Grant of University of Malaya (HIR -UM.C/625/1/HIR-MOHE/CHAN/12) and University Malaya Department of Surgery.

REFERENCES

Albin, R. L., Koeppe, R. A., Chervin, R. D., Consens, F. B., Wernette, K., Frey, K. A., et al. (2000). Decreased striatal dopaminergic innervation in REM sleep behavior disorder. *Neurology* 55, 1410–1412. doi: 10.1212/WNL.55.9.1410

Albin, R. L., Young, A. B., and Penney, J. B. (1989). The functional anatomy of basal ganglia disorders. *Trends Neurosci.* 12, 366–375. doi: 10.1016/0166-2236(89)90074-X

Alderson, H. L., and Winn, P. (2005). "The pedunculopontine and reinforcement," in *The Basal Ganglia VIII*, (Boston, MA: Springer), 523–532.

Alexander, G. E., and Crutcher, M. D. (1990). Functional architecture of basal ganglia circuits, neural substrates of parallel processing. *Trends Neurosci.* 13, 266–271. doi: 10.1016/0166-2236(90)90107-L

Alexander, G. E., DeLong, M. R., and Strick, P. L. (1986). Parallel organization of functionally segregated circuits linking basal ganglia and cortex. *Annu. Rev. Neurosci.* 9, 357–381. doi: 10.1146/annurev.ne.09.030186.002041

Amaral, D. G., Price, J. L., Pitkanen, A., and Carmichael, S. T. (1992). "Anatomical organization of the primate amygdaloid complex," in *The Amygdala: Neurobiological Aspects of Emotion, Memory, and Mental Dysfunction*, ed J. P. Aggleton (New York, NY: Wiley-Liss), 1–66.

Aravamuthan, B. R., Bergstrom, D. A., French, R. A., Taylor, J. J., Parr-Brownlie, L. C., and Walters, Jr. (2008). Altered neuronal activity relationships between the pedunculopontine nucleus and motor cortex in a rodent model of Parkinson's disease. *Exp. Neurol.* 213, 268–280. doi: 10.1016/j.expneurol.2008.05.023

Azulay, J. P., Mesure, S., Amblard, B., and Pouget, J. (2002). Increased visual dependence in Parkinson's disease. *Percep. Motor Skills* 95(3 Suppl), 1106–1114. doi: 10.2466/pms.2002.95.3f.1106

Ballanger, B., Lozano, A. M., Moro, E., van Eimeren, T., Hamani, C., Chen, R., et al. (2009). Cerebral blood flow changes induced by pedunculopontine nucleus stimulation in patients with advanced Parkinson's disease: A [15O] H2O PET study. *Hum. Brain Mapp.* 30, 3901–3909. doi: 10.1002/hbm.20815

Belaid, H., Adrien, J., Laffrat, E., Tandé, D., Karachi, C., Grabli, D., et al. (2014). Sleep disorders in Parkinsonian macaques: effects of L-dopa treatment and pedunculopontine nucleus lesion. *J. Neurosci.* 34, 9124–9133. doi: 10.1523/JNEUROSCI.0181-14.2014

Beninato, M., and Spencer, R. F. (1987). A cholinergic projection to the rat substantia nigra from the pedunculopontine tegmental nucleus. *Brain Res.* 412, 169–174. doi: 10.1016/0006-8993(87)91455-7

Bevan, M. D., and Bolam, J. P. (1995). Cholinergic, GABAergic, and glutamate-enriched inputs from the mesopontine tegmentum to the subthalamic nucleus in the rat. *J. Neurosci.* 15, 7105–7120.

Bliwise, D. L., Willians, M. L., Irbe, D., Ansari, F. P., and Rye, D. B. (2000). Inter-rater reliability for identification of REM sleep in Parkinson's disease. *Sleep* 23, 671–676.

Bohus, B., Koolhaas, J. M., Luiten, P. G., Korte, S. M., Roozendaal, B., and Wiersma, A. (1996). The neurobiology of the central nucleus of the amygdala in relation to neuroendocrine and autonomic outflow. *Prog. Brain Res.* 107, 447–460. doi: 10.1016/S0079-6123(08)61881-6

Bolam, J. P., Francis, C. M., and Henderson, Z. (1991). Cholinergic input to dopaminergic neurons in the substantia nigra: a double immunocytochemical study. *Neuroscience* 41, 483–494. doi: 10.1016/0306-4522(91)90343-M

Braak, H., and Braak, E. (1985). Nuclear configuration and neuronal types of the nucleus niger in the brain of the human adult. *Hum. Neurobiol.* 5 , 71–82.

Braak, H., and Del Tredici, K. (2004). Poor and protracted myelination as a contributory factor to neurodegenerative disorders. *Neurobiol. Aging* 25, 19–23. doi: 10.1016/j.neurobiolaging.2003.04.001

Braak, H., Braak, E., Deniz, Y., de Vos, R. A., Jansen, E. N. , Bohl, J., et al. (1994). Amygdala pathology in Parkinson's disease. *Acta Neuropathol.* 88, 493–500. doi: 10.1007/BF00296485

Braak, H., Del Tredici, K., Rüb, U., de Vos, R. A., Jansen, E. N., and Braak, E. (2003). Staging of brain pathology related to sporadic Parkinson's disease. *Neurobiol. Aging* 24, 197–211.

Braak, H., Ghebremedhin, E., Rüb, U., Bratzke, H., and Del Tredici, K. (2004). Stages in the development of Parkinson's disease-related pathology. *Cell Tissue Res.* 318, 121–134. doi: 10.1007/s00441-004-0956-9

Brown, J., Bullock, D., and Grossberg, S. (1999). How the basal ganglia use parallel excitatory and inhibitory learning pathways to selectively respond to unexpected rewarding cues. *J. Neurosci.* 19, 10502–10511.

Brown, P., and Eusebio, A. (2008). Paradoxes of functional neurosurgery: clues from basal ganglia recordings. *Mov. Disord.* 23, 12–20. doi: 10.1002/mds.21796

Brown, P., Oliviero, A., Mazzone, P., Insola, A., Tonali, P., and Di Lazzaro, V. (2001). Dopamine dependency of oscillations between subthalamic nucleus and pallidum in Parkinson's disease. *J. Neurosci.* 21, 1033–1038.

Burbaud, P., Bonnet, B., Guehl, D., Lagueny, A., and Bioulac, B. (1998). Movement disorders induced by gamma-aminobutyric agonist and antagonist injections into the internal globus pallidus and substantia nigra pars reticulata of the monkey. *Brain Res.* 780, 102–107. doi: 10.1016/S0006-8993(97)01158-X

Candy, J. M., Perry, R. H., Perry, E. K., Irving, D., Blessed, G., Fairbairn, A. F., and Tomlinson, B. E. (1983). Pathological changes in the nucleus of Meynert in Alzheimer's and Parkinson's diseases. *J. Neurol. Sci.* 59 , 277–289.

Carpenter, M. B. (1976). Anatomical organization of the corpus striatum and related nuclei. *Res. Publ. Assoc. Res. Nerv. Ment. Dis.* 55, 1.

Charara, A., Smith, Y., and Parent, A. (1996). Glutamatergic inputs from the pedunculopontine nucleus to midbrain dopaminergic neurons in primates: *Phaseolus vulgaris*-leucoagglutinin anterograde labeling combined with postembedding glutamate and GABA immunohistochemistry. *J. Comp. Neurol.* 364, 254–266. doi: 10.1002/(SICI)1096-9861(19960108)364:2<254::AID-CNE5>3.0.CO;2-4

Clements, J. R., Toth, D. D., Highfield, D. A., and Grant, S. (1991). "Glutamate-like immunoreactivity is present within cholinergic neurons of the laterodorsal tegmental and pedunculopontine nuclei," in *The Basal Forebrain*, (Boston, MA: Springer), 127–142.

Clements, J. R., and Grant, S. (1990). Glutamate-like immunoreactivity in neurons of the laterodorsal tegmental and pedunculopontine nuclei in the rat. *Neurosci. Lett.* 120 , 70–73.

Comoli, E., Coizet, V., Boyes, J., Bolam, J. P., Canteras, N. S., Quirk, R. H., et al. (2003). A direct projection from superior colliculus to substantia nigra for detecting salient visual events. *Nat. Neurosci.* 6, 974–980. doi: 10.1038/nn1113

Coons, E. E., Levak, M., and Miller, N. E. (1965). Lateral hypothalamus: learning of food-seeking response motivated by electrical stimulation. *Science* 150, 1320–1321.

Côté, P. V., and Parent, A. (1992). Calbindin D-28k and choline acetyltransferase are expressed by different neuronal populations in pedunculopontine nucleus but not in nucleus basalis in squirrel monkeys. *Brain Res.* 593, 245–252. doi: 10.1016/0006-8993(92)91314-5

Del Tredici, K., and Braak, H. (2004). "Idiopathic Parkinson's Disease: Staging an α-Synucleinopathy with a Predictable Pathoanatomy," in *Madame Curie Bioscience Database [Internet]* (Austin, TX: Landes Bioscience), 2000–2013.

Del Tredici, K., Rüb, U., De Vos, R. A., Bohl, J. R. E., and Braak, H. (2002). Where does Parkinson disease pathology begin in the brain? *J. Neuropathol. Exp. Neurol.* 61, 413–426. doi: 10.1093/jnen/61.5.413

DeLong, M. R. (1990). Primate models of movement disorders of basal ganglia origin. *Trends Neurosci.* 13, 281–285. doi: 10.1016/0166-2236(90)90110-V

DeLong, M. R., and Georgopoulos, A. P. (2011). Motor functions of the basal ganglia. *Compr. Physiol.* doi: 10.1002/cphy.cp010221

DeLong, M. R., and Wichmann, T. (2007). Circuits and circuit disorders of the basal ganglia. *Arch. Neurol.* 64, 20–24. doi: 10.1001/archneur.64.1.20

Denny-Brown, D. (1968). Clinical symptomatology of diseases of the basal ganglia. *Handb. Clin. Neurol.* 6, 133–172.

DeVito, J. L., Anderson, M. E., and Walsh, K. E. (1980). A horseradish peroxidase study of afferent connections of the globus pallidus in *Macaca mulatta*. *Exp. Brain Res.* 38, 65–73. doi: 10.1007/BF00237932

Dickson, D. W., Schmidt, M. L., Lee, V. M., Zhao, M. L., Yen, S. H., and Trojanowski, J. Q. (1994). Immunoreactivity profile of hippocampal CA2/3 neurites in diffuse Lewy body disease. *Acta Neuropathol.* 87, 269–276. doi: 10.1007/BF00296742

Düsterhöft, F., Häusler, U., and Jürgens, U. (2000). On the search for the vocal pattern generator. A single-unit recording study. *Neuroreport* 11, 2031–2034.

Edley, S. M., and Graybiel, A. M. (1983). The afferent and efferent connections of the feline nucleus tegmenti pedunculopontinus, pars compacta. *J. Comp. Neurol.* 217, 187–215. doi: 10.1002/cne.902170207

Eisensehr, I., Lindeiner, H. V., Jäger, M., and Noachtar, S. (2001). REM sleep behavior disorder in sleep-disordered patients with versus without Parkinson's disease, is there a need for polysomnography? *J. Neurol. Sci.* 186, 7–11. doi: 10.1016/S0022-510X(01)00480-4

Filion, M. (1991). Abnormal spontaneous activity of globus pallidus neurons in monkeys with MPTP-induced parkinsonism. *Brain Res.* 547, 140–144. doi: 10.1016/0006-8993(91)90585-J

Floresco, S. B., West, A. R., Ash, B., Moore, H., and Grace, A. A. (2003). Afferent modulation of dopamine neuron firing differentially regulates tonic and phasic dopamine transmission. *Nat. Neurosci.* 6, 968–973. doi: 10.1038/nn1103

Forster, G. L., and Blaha, C. D. (2003). Pedunculopontine tegmental stimulation evokes striatal dopamine efflux by activation of acetylcholine and glutamate receptors in the midbrain and pons of the rat. *Eur. J. Neurosci.* 17, 751–762. doi: 10.1046/j.1460-9568.2003.02511.x

French, I. T., and Muthusamy, K. A. (2016). A Review of sleep and its disorders in patients with Parkinson's Disease in relation to various brain structures. *Front. Aging Neurosci.* 8:114. doi: 10.3389/fnagi.2016.00114

Futami, T., Takakusaki, K., and Kitai, S. T. (1995). Glutamatergic and cholinergic inputs from the pedunculopontine tegmental nucleus to dopamine neurons in the substantia nigra pars compacta. *Neurosci. Res.* 21, 331–342. doi: 10.1016/0168-0102(94)00869-H

Galvan, A., and Wichmann, T. (2008). Pathophysiology of parkinsonism. *Clin. Neurophysiol.* 119, 1459–1474. doi: 10.1016/j.clinph.2008.03.017

Garcia-Rill, E. (1986). The basal ganglia and the locomotor regions. *Brain Res. Rev.* 11, 47–63. doi: 10.1016/0165-0173(86)90009-3

Garcia-Rill, E. (1991). The pedunculopontine nucleus. *Prog. Neurobiol.* 36, 363–389. doi: 10.1016/0301-0082(91)90016-T

Garcia-Rill, E., Houser, C. R., Skinner, R. D., Smith, W., and Woodward, D. J. (1987). Locomotion-inducing sites in the vicinity of the pedunculopontine nucleus. *Brain Res. Bull.* 18, 731–738. doi: 10.1016/0361-9230(87)90208-5

Gerfen, C. R. (1992). The neostriatal mosaic: multiple levels of compartmental organization in the basal ganglia. *Annu. Rev. Neurosci.* 15, 285–320. doi: 10.1146/annurev.ne.15.030192.001441

Geula, C., Schatz, C. R., and Mesulam, M. M. (1993). Differential localization of NADPH-diaphorase and calbindin-D 28k within the cholinergic neurons of the basal forebrain, striatum and brainstem in the rat, monkey, baboon and human. *Neuroscience* 54, 461–476.

Gibb, W. R., and Lees, A. J. (1991). Anatomy, pigmentation, ventral and dorsal subpopulations of the substantia nigra, and differential cell death in Parkinson's disease. *J. Neurol. Neurosurg. Psychiatry* 54, 388–396. doi: 10.1136/jnnp.54.5.388

Glickman, S. E., and Schiff, B. B. (1967). A biological theory of reinforcement. *Psychol. Rev.* 74, 81. doi: 10.1037/h0024290

Grabli, D., Karachi, C., Folgoas, E., Monfort, M., Tande, D., Clark, S., et al. (2013). Gait disorders in parkinsonian monkeys with pedunculopontine nucleus lesions: a tale of two systems. *J. Neurosci.* 33, 11986–11993. doi: 10.1523/JNEUROSCI.1568-13.2013

Granata, A. R., and Kitai, S. T. (1991). Inhibitory substantia nigra inputs to the pedunculopontine neurons. *Exp. Brain Res.* 86, 459–466. doi: 10.1007/BF00230520

Graybiel, A. M. (1977). Direct and indirect preoculomotor pathways of the brainstem: an autoradiographic study of the pontine reticular formation in the cat. *J. Comp. Neurol.* 175, 37–78. doi: 10.1002/cne.901750105

Grofova, I., and Keane, S. (1991). Descending brainstem projections of the pedunculopontine tegmental nucleus in the rat. *Anat. Embryol.* 184, 275–290. doi: 10.1007/BF01673262

Grunwerg, B. S., Krein, H., and Krauthamer, G. M. (1992). Somatosensory input and thalamic projection of pedunculopontine tegmental neurons. *Neuroreport* 3, 673–675. doi: 10.1097/00001756-199208000-00004

Hamani, C., Aziz, T., Bloem, B. R., Brown, P., Chabardes, S., Coyne, T., et al. (2016a). Pedunculopontine nucleus region deep brain stimulation in Parkinson disease: surgical anatomy and terminology. *Stereotact. Funct. Neurosurg.* 94, 298–306. doi: 10.1159/000449010

Hamani, C., Lozano, A. M., Mazzone, P. A., Moro, E., Hutchison, W., Silburn, P. A., et al. (2016b). Pedunculopontine nucleus region deep brain stimulation in Parkinson Disease: surgical techniques, side effects, and postoperative imaging. *Stereotact. Funct. Neurosurg.* 94 , 307–319. doi: 10.1159/000449011

Hammond, C., Bergman, H., and Brown, P. (2007). Pathological synchronization in Parkinson's disease: networks, models and treatments. *Trends Neurosci.* 30, 357–364. doi: 10.1016/j.tins.2007.05.004

Hanakawa, T., Katsumi, Y., Fukuyama, H., Honda, M., Hayashi, T., Kimura, J., et al. (1999). Mechanisms underlying gait disturbance in Parkinson's disease. *Brain* 122, 1271–1282. doi: 10.1093/brain/122.7.1271

Hazrati, L. N., and Parent, A. (1992). Projection from the deep cerebellar nuclei to the pedunculopontine nucleus in the squirrel monkey. *Brain Res.* 585, 267–271. doi: 10.1016/0006-8993(92)91216-2

Hikosaka, O. (1989). "Role of basal ganglia in initiation of voluntary movements," in *Dynamic Interactions in Neural Networks: Models and Data*, (New York, NY: Springer), 153–167. doi: 10.1007/978-1-4612-4536-0_9

Hikosaka, O. (1991). Role of the forebrain in oculomotor function. *Prog. Brain Res.* 87:101. doi: 10.1016/S0079-6123(08)63049-6

Hikosaka, O. (2007). GABAergic output of the basal ganglia. *Prog. Brain Res.* 160, 209–226. doi: 10.1016/S0079-6123(06)60012-5

Hikosaka, O., and Wurtz, R. H. (1983a). Visual and oculomotor functions of monkey substantia nigra pars reticulata. II. Visual responses related to fixation of gaze. *J. Neurophysiol.* 49, 1254–1267.

Hikosaka, O., and Wurtz, R. H. (1983b). Visual and oculomotor functions of monkey substantia nigra pars reticulata. III. Memory-contingent visual and saccade responses. *J. Neurophysiol.* 49, 1268–1284.

Hikosaka, O., and Wurtz, R. H. (1983c). Visual and oculomotor functions of monkey substantia nigra pars reticulata. IV. Relation of substantia nigra to superior colliculus. *J. Neurophysiol.* 49, 1285–1301.

Hikosaka, O., Matsumura, M., Kojima, J., and Gardiner, T. W. (1993a). "Role of basal ganglia in initiation and suppression of saccadic eye movements," in *Role of the Cerebellum and Basal Ganglia in Voluntary Movement*, eds N. Mano, I. Hamada, and M. R Delong (Okazaki: Elsevier Science Publishers), 213–219.

Hikosaka, O., Sakamoto, M., and Miyashita, N. (1993b). Effects of caudate nucleus stimulation on substantia nigra cell activity in monkey. *Exp. Brain Res.* 95, 457–472. doi: 10.1007/BF00227139

Hikosaka, O., Takikawa, Y., and Kawagoe, R. (2000). Role of the basal ganglia in the control of purposive saccadic eye movements. *Physiol. Rev.* 80, 953–978. doi: 10.1152/physrev.2000.80.3.953

Hirsch, E. C., Graybiel, A. M., Duyckaerts, C., and Javoy-Agid, F. (1987). Neuronal loss in the pedunculopontine tegmental nucleus in Parkinson disease and in progressive supranuclear palsy. *Proc. Natl. Acad. Sci. U.S.A.* 84, 5976–5980. doi: 10.1073/pnas.84.16.5976

Inglis, W. L., and Winn, P. (1995). The pedunculopontine tegmental nucleus, where the striatum meets the reticular formation. *Prog. Neurobiol.* 47, 1–29. doi: 10.1016/0301-0082(95)00013-L

Inglis, W. L., Dunbar, J. S., and Winn, P. (1994). Outflow from the nucleus accumbens to the pedunculopontine tegmental nucleus: a dissociation between locomotor activity and the acquisition of responding for conditioned reinforcement stimulated by d-amphetamine. *Neuroscience* 62, 51–64. doi: 10.1016/0306-4522(94)90314-X

Inglis, W. L., Dunbar, J. S., and Winn, P. (2000). Pedunculopontine tegmental nucleus lesions impair stimulus–reward learning in autoshaping and conditioned reinforcement paradigms. *Behav. Neurosci.* 114:285. doi: 10.1037/0735-7044.114.2.285

Inglis, W. L., Olmstead, M. C., and Robbins, T. W. (2001). Selective deficits in attentional performance on the 5-choice serial reaction time task following pedunculopontine tegmental nucleus lesions. *Behav. Brain Res.* 123, 117–131. doi: 10.1016/S0166-4328(01)00181-4

Jacobs, B. L., and Azmitia, E. C. (1992). Structure and function of the brain serotonin system. *Physiol. Rev.* 72, 165–229. doi: 10.1152/physrev.1992.72.1.165

Jellinger, K. (1988). The pedunculopontine nucleus in Parkinson's disease, progressive supranuclear palsy and Alzheimer's disease. *J. Neurol. Neurosurg. Psychiatry* 51, 540–543. doi: 10.1136/jnnp.51.4.540

Jones, B. E. (1991). Paradoxical sleep and its chemical/structural substrates in the brain. *Neuroscience* 40, 637–656. doi: 10.1016/0306-4522(91)90002-6

Karachi, C., Grabli, D., Bernard, F. A., Tandé, D., Wattiez, N., Belaid, H., et al. (2010). Cholinergic mesencephalic neurons are involved in gait and postural disorders in Parkinson disease. *J. Clin. Invest.* 120, 2745–2754. doi: 10.1172/JCI42642

Kelly, R. M., and Strick, P. L. (2004). Macro-architecture of basal ganglia loops with the cerebral cortex: use of rabies virus to reveal multisynaptic circuits. *Prog. Brain Res.* 143, 447–459. doi: 10.1016/S0079-6123(03)43042-2

Khan, S. A, Javed, S., Mooney, L., White, P., Plaha, P., Whone, A., et al. (2012). Clinical outcomes from bilateral versus unilateral stimulation of the pedunculopontine nucleus with and without concomitant caudal zona incerta region stimulation in Parkinson's disease. *Br. J. Neurosurg.* 26, 722–725. doi: 10.3109/02688697.2012.659297

Kobayashi, Y., Inoue, Y., Yamamoto, M., Isa, T., and Aizawa, H. (2004). Pedunculopontine control of visually guided saccades. *Prog. Brain Res.* 143, 447–459. doi: 10.1016/S0079-6123(03)43041-0

Kühn, A. A., Kempf, F, Brücke, C., Doyle, L. G., Martinez-Torres, I., Pogosyan, A., et al. (2008). High-frequency stimulation of the subthalamic nucleus suppresses oscillatory β activity in patients with Parkinson's disease in

parallel with improvement in motor performance. *J. Neurosci.* 28, 6165–6173. doi: 10.1523/JNEUROSCI.0282-08.2008

Kuypers, H. G. , and Lawrence, D. G. (1967). Cortical projections to the red nucleus and the brain stem in the rhesus monkey. *Brain Res.* 4, 151–188. doi: 10.1016/0006-8993(67)90004-2

Lavoie, B., and Parent, A. (1994a). Pedunculopontine nucleus in the squirrel monkey: cholinergic and glutamatergic projections to the substantia nigra. *J. Comp. Neurol.* 344, 232–241.

Lavoie, B., and Parent, A. (1994b). Pedunculopontine nucleus in the squirrel monkey: distribution of cholinergic and monoaminergic neurons in the mesopontine tegmentum with evidence for the presence of glutamate in cholinergic neurons. *J. Comp. Neurol.* 344, 190–209.

Lavoie, B., and Parent, A. (1994c). Pedunculopontine nucleus in the squirrel monkey: projections to the basal ganglia as revealed by anterograde tract-tracing methods. *J. Comp. Neurol.* 344, 210–231.

Lokwan, S. J., Overton, P. G., Berry, M. S., and Clark. (1999). Stimulation of the pedunculopontine tegmental nucleus in the rat produces burst firing in A9 dopaminergic neurons. *Neuroscience* 92, 245–254. doi: 10.1016/S0306-4522(98)00748-9

Martinez-Gonzalez, C., Wang, H. L., Micklem, B. R., Bolam, J. P., and Mena-Segovia, J. (2012). Subpopulations of cholinergic, GABAergic and glutamatergic neurons in the pedunculopontine nucleus contain calcium-binding proteins and are heterogeneously distributed. *Eur. J. Neurosci.* 35, 723–734. doi: 10.1111/j.1460-9568.2012.08002.x

Matsumura, M., Nambu, A., Yamaji, Y., Watanabe, K., Imai, H., Inase, M., et al. (2000). Organization of somatic motor inputs from the frontal lobe to the pedunculopontine tegmental nucleus in the macaque monkey. *Neuroscience* 98, 97–110. doi: 10.1016/S0306-4522(00)00099-3

Matsumura, M., Watanabe, K., and Ohye, C. (1997). Single-unit activity in the primate nucleus tegmenti pedunculopontinus related to voluntary arm movement. *Neurosci. Res.* 28, 155–165. doi: 10.1016/S0168-0102(97)00039-4

Matsuyama, K., and Drew, T. (1997). Organization of the projections from the pericruciate cortex to the pontomedullary brainstem of the cat: a study using the anterograde tracer Phaseolus vulgaris-leucoagglutinin. *J. Comp. Neurol.* 389, 617–641. doi: 10.1002/(SICI)1096-9861(19971229)389:4<617::AID-CNE6>3.0.CO;2-3

McCarley, R. W., and Chokroverty, S. (1994). Neurophysiology of sleep: basic mechanisms underlying control of wakefulness and sleep. *Sleep Disord. Med. Basic Sci. Tech. Consider. Clin. Aspects* 17–36. doi: 10.1016/B978-0-7506-9002-7.50008-2

Mehler, W. R., and Nauta, W. J. (1974). Connections of the basal ganglia and of the cerebellum. *Stereotact. Funct. Neurosurg.* 36 , 205–222. doi: 10.1159/000102797

Mena-Segovia, J., Micklem, B. R., Nair, R. G., Ungless, M. A., and Bolam, J. P. (2009). GABAergic neuron distribution in the pedunculopontine nucleus defines functional subterritories. *J. Comp. Neurol.* 515, 397–408. doi: 10.1002/cne.22065

Mena-Segovia, J., Sims, H. M., Magill, P. J., and Bolam, J. P. (2008a). Cholinergic brainstem neurons modulate cortical gamma activity during slow oscillations. *J. Physiol.* 586, 2947–2960. doi: 10.1113/jphysiol.2008.153874

Mena-Segovia, J., Winn, P., and Bolam, J. P. (2008b). Cholinergic modulation of midbrain dopaminergic systems. *Brain Res. Rev.* 58, 265–271. doi: 10.1016/j.brainresrev.2008.02.003

Mena-Segovia, J., Bolam, J. P., and Magill, P. J. (2004). Pedunculopontine nucleus and basal ganglia: distant relatives or part of the same family? *Trends Neurosci.* 27, 585–588. doi: 10.1016/j.tins.2004.07.009

Mesulam, M. M., Mufson, E. J., Wainer, B. H., and Levey, A. L. (1983). Central cholinergic pathways in the rat: an overview based on an alternative nomenclature (Ch1–Ch6). *Neuroscience* 10, 1185–1201. doi: 10.1016/0306-4522(83)90108-2

Mesulam, M., Geula, C., Bothwell, M. A., and Hersh, L. B. (1989). Human reticular formation: cholinergic neurons of the pedunculopontine and laterodorsal tegmental nuclei and some cytochemical comparisons to forebrain cholinergic neurons. *J. Comp. Neurol.* 283, 611–633. doi: 10.1002/cne.902830414

Mesulam, M., Hersh, L. B., Mash, D. C., and Geula, C. (1992a). Differential cholinergic innervation within functional subdivisions of the human cerebral cortex: a choline acetyltransferase study. *J. Comp. Neurol.* 318, 316–328. doi: 10.1002/cne.903180308

Mesulam, M. M., Mash, D., Hersh, L., Bothwell, M., and Geula, C. (1992b). Cholinergic innervation of the human striatum, globus pallidus, subthalamic nucleus, substantia nigra, and red nucleus. *J. Comp. Neurol.* 323, 252–268. doi: 10.1002/cne.903230209

Middleton, F. A., and Strick, P. L. (2000). Basal ganglia and cerebellar loops: motor and cognitive circuits. *Brain Res. Rev.* 31, 236–250. doi: 10.1016/S0165-0173(99)00040-5

Miller, W. C., and DeLong, M. R. (1987). "Altered tonic activity of neurons in the globus pallidus and subthalamic nucleus in the primate MPTP model of parkinsonism," in *The Basal Ganglia II*, (Springer), 415–427.

Mink, J. W. (1996). The basal ganglia: focused selection and inhibition of competing motor programs. *Prog. Neurobiol.* 50, 381–425. doi: 10.1016/S0301-0082(96)00042-1

Mitani, A., Ito, K., Hallanger, A. E., Wainer, B. H., Kataoka, K., and McCarley, R. W. (1988). Cholinergic projections from the laterodorsal and pedunculopontine tegmental nuclei to the pontine gigantocellular tegmental field in the cat. *Brain Res.* 451, 397–402. doi: 10.1016/0006-8993(88)90792-5

Moonedley, S., and Graybiel, A. M. (1980). "Connections of the nucleus tegmenti pedunculopontinis, pars compacta (TPc) in cat," in *Anatomical Record*, Vol. 196 (New York, NY: John Wiley & Sons Inc., Wiley-Liss), A129–A129.

Morris, M. E., Iansek, R., Matyas, T. A., and Summers, J. J. (1994). The pathogenesis of gait hypokinesia in Parkinson's disease. *Brain* 117, 1169–1181. doi: 10.1093/brain/117.5.1169

Moruzzi, G., and Magoun, H. W. (1949). Brain stem reticular formation and activation of the EEG. *Electroencephalogr. Clin. Neurophysiol.* 1, 455–473. doi: 10.1016/0013-4694(49)90219-9

Muthusamy, K. A., Aravamuthan, B. R., Kringelbach, M. L., Jenkinson, N., Voets, N. L., Johansen-Berg, H., et al. (2007). Connectivity of the human pedunculopontine nucleus region and diffusion tensor imaging in surgical targeting. *J. Neurosurg.* 107, 814–8120. doi: 10.3171/JNS-07/10/0814

Nakamura, Y., Tokuno, H., Moriizumi, T., Kitao, Y., and Kudo, M. (1989). Monosynaptic nigral inputs to the pedunculopontine tegmental nucleus neurons which send their axons to the medial reticular formation in the medulla oblongata. An electron microscopic study in the cat. *Neurosci. Lett.* 103 , 145–150.

Nambu, A., Tokuno, H., and Takada, M. (2002). Functional significance of the cortico–subthalamo–pallidal "hyperdirect" pathway. *Neurosci. Res.* 43, 111–117. doi: 10.1016/S0168-0102(02)00027-5

Nevet, A., Morris, G., Saban, G., Fainstein, N., and Bergman, H. (2004). Discharge rate of substantia nigra pars reticulata neurons is reduced in non-parkinsonian monkeys with apomorphine-induced orofacial dyskinesia. *J. Neurophysiol.* 92, 1973–1981. doi: 10.1152/jn.01036.2003

Nomura, S., Mizuno, N., and Sugimoto, T. (1980). Direct projections from the pedunculopontine tegmental nucleus to the subthalamic nucleus in the cat. *Brain Res.* 196, 223–227. doi: 10.1016/0006-8993(80)90728-3

Olszewski, J., and Baxter, D. (1954). *Cytoarchitecture of the Human Brain Stem*.

Pahapill, P. A., and Lozano, A. M. (2000). The pedunculopontine nucleus and Parkinson's disease. *Brain* 123, 1767–1783. doi: 10.1093/brain/123.9.1767

Pan, W. X., and Hyland, B. I. (2005). Pedunculopontine tegmental nucleus controls conditioned responses of midbrain dopamine neurons in behaving rats. *J. Neurosci.* 25, 4725–4732. doi: 10.1523/JNEUROSCI.0277-05.2005

Pare, D., Smith, Y., Parent, A., and Steriade, M. (1988). Projections of brainstem core cholinergic and non-cholinergic neurons of cat to intralaminar and reticular thalamic nuclei. *Neuroscience* 25, 69–86. doi: 10.1016/0306-4522(88)90007-3

Parent, A., and Hazrati, L. N. (1995). Functional anatomy of the basal ganglia. I. The cortico-basal ganglia-thalamo-cortical loop. *Brain Res. Rev.* 20, 91–127.

Reese, N. B., Garcia-Rill, E., and Skinner, R. D. (1995). The pedunculopontine nucleus—auditory input, arousal and pathophysiology. *Prog. Neurobiol.* 47, 105–133. doi: 10.1016/0301-0082(95)00023-O

Reiner, A., Albin, R. L., Anderson, K. D., D'Amato, C. J., Penney, J. B., and Young, A. B. (1988). Differential loss of striatal projection neurons in Huntington disease. *Proc. Natl. Acad. Sci. U.S.A.* 85, 5733–5737. doi: 10.1073/pnas.85.15.5733

Ros, H., Magill, P. J., Moss, J., Bolam, J. P., and Mena-Segovia, J. (2010). Distinct types of non-cholinergic pedunculopontine neurons are differentially modulated during global brain states. *Neuroscience* 170, 78–91. doi: 10.1016/j.neuroscience.2010.06.068

Rolland, A. S., Tandé, D., Herrero, M. T., Luquin, M. R., Vazquez-Claverie, M., Karachi, C., et al. (2009). Evidence for a dopaminergic innervation of the pedunculopontine nucleus in monkeys, and its drastic reduction after MPTP intoxication. *J. Neurochem.* 110, 1321–1329. doi: 10.1111/j.1471-4159.2009.06220.x

Romo, R., and Schultz, W. (1990). Dopamine neurons of the monkey midbrain, contingencies of responses to active touch during self-initiated arm movements. *J. Neurophysiol.* 63, 592–606. doi: 10.1152/jn.1990.63.3.592

Rossignol, S. (1996). Neural control of stereotypic limb movements. *Compr. Physiol.*

Rye, D. B. (1997). Contributions of the pedunculopontine region to normal and altered REM sleep. *Sleep* 20, 757–788. doi: 10.1093/sleep/20.9.757

Rye, D. B., Johnston, L. H., Watts, R. L., and Bliwise, D. L. (1999). Juvenile Parkinson's disease with REM sleep behavior disorder, sleepiness, and daytime REM onset. *Neurology* 53, 1868–1868.

Rye, D. B., Lee, H. J., Saper, C. B., and Wainer, B. H. (1988). Medullary and spinal efferents of the pedunculopontine tegmental nucleus and adjacent mesopontine tegmentum in the rat. *J. Comp. Neurol.* 269, 315–341. doi: 10.1002/cne.902690302

Rye, D. B., Saper, C. B., Lee, H. J., and Wainer, B. H. (1987). Pedunculopontine tegmental nucleus of the rat: cytoarchitecture, cytochemistry, and some extrapyramidal connections of the mesopontine tegmentum. *J. Comp. Neurol.* 259, 483–528. doi: 10.1002/cne.902590403

Saper, C. B., and Loewy, A. D. (1982). Projections of the pedunculopontine tegmental nucleus in the rat: evidence for additional extrapyramidal circuitry. *Brain Res.* 252, 367–372. doi: 10.1016/0006-8993(82)90404-8

Scarnati, E., and Florio, T. (1997). The pedunculopontine nucleus and related structures: functional organization. *Adv. Neurol.* 74, 97–110.

Scarnati, E., Campana, E., and Pacitti, C. (1984). Pedunculopontine-evoked excitation of substantia nigra neurons in the rat. *Brain Res.* 304, 351–361. doi: 10.1016/0006-8993(84)90339-1

Scarnati, E., Di Loreto, S., Proia, A., and Gallie, G. (1988). The functional role of the pedunculopontine nucleus in the regulation of the electrical activity of entopeduncular neurons in the rat. *Arch. Ital. Biol.* 126, 145–163.

Scarnati, E., Florio, T., Capozzo, A., Confalone, G., and Mazzone, P. (2011). The pedunculopontine tegmental nucleus: implications for a role in modulating spinal cord motoneuron excitability. *J. Neural Transm.* 118, 1409–1421. doi: 10.1007/s00702-010-0532-2

Schultz, W. (1998). Predictive reward signal of dopamine neurons. *J. Neurophysiol.* 80, 1–27. doi: 10.1152/jn.1998.80.1.1

Schultz, W., and Romo, R. (1990). Dopamine neurons of the monkey midbrain: contingencies of responses to stimuli eliciting immediate behavioral reactions. *J. Neurophysiol.* 63, 607–624. doi: 10.1152/jn.1990.63.3.607

Schultz, W., Apicella, P., Scarnati, E., and Ljungberg, T. (1992). Neuronal activity in monkey ventral striatum related to the expectation of reward. *J. Neurosci.* 12, 4595–4610.

Schultz, W., Dayan, P., and Montague, P. R. (1997). A neural substrate of prediction and reward. *Science* 275, 1593–1599.

Semba, K., Reiner, P. B., and Fibiger, H. C. (1990). Single cholinergic mesopontine tegmental neurons project to both the pontine reticular formation and the thalamus in the rat. *Neuroscience* 38, 643–654. doi: 10.1016/0306-4522(90)90058-C

Sims, K. S., and Williams, R. S. (1990). The human amygdaloid complex: a cytologic and histochemical atlas using Nissl, myelin, acetylcholinesterase and nicotinamide adenine dinucleotide phosphate diaphorase staining. *Neuroscience* 36, 449–472. doi: 10.1016/0306-4522(90)90440-F

Skinner, R. D., and Garcia-Rill, E. (1984). The mesencephalic locomotor region (MLR) in the rat. *Brain Res.* 323, 385–389. doi: 10.1016/0006-8993(84)90319-6

Skinner, R. D., Kinjo, N., Henderson, V., and Garcia-Rill, E. (1990). Locomotor projections from the pedunculopontine nucleus to the spinai cord. *Neuroreport* 1, 183–186. doi: 10.1097/00001756-199011000-00001

Spann, B. M., and Grofova, I. (1992). Cholinergic and non-cholinergic neurons in the rat pedunculopontine tegmental nucleus. *Anat. Embryol.* 186, 215–227. doi: 10.1007/BF00174143

Sparks, D. L. (2002). The brainstem control of saccadic eye movements. *Nat. Rev. Neurosci.* 3, 952–964. doi: 10.1038/nrn986

Starr, P. A., Rau, G. M., Davis, V., Marks, W. J., Ostrem, J. L., Simmons, D., et al. (2005). Spontaneous pallidal neuronal activity in human dystonia: comparison with Parkinson's disease and normal macaque. *J. Neurophysiol.* 93 , 3165–3176. doi: 10.1152/jn.00971.2004

Steckler, T., Keith, A. B., and Sahgal, A. (1994). Lesions of the pedunculopontine tegmental nucleus do not alter delayed non-matching to position accuracy. *Behav. Brain Res.* 61, 107–112.

Stein, J. F. (2009). Akinesia, motor oscillations and the pedunculopontine nucleus in rats and men. *Exp. Neurol.* 215, 1–4. doi: 10.1016/j.expneurol.2008.09.022

Steriade, M. (1996). Arousal: revisiting the reticular activating system. *Science* 272:225. doi: 10.1126/science.272.5259.225

Steriade, M. (2004). Acetylcholine systems and rhythmic activities during the waking–sleep cycle. *Prog. Brain Res.* 145, 179–196. doi: 10.1016/S0079-6123(03)45013-9

Steriade, M., and Buzsaki, G. (1990). Parallel activation of thalamic and cortical neurons by brainstem and basal forebrain cholinergic systems. *Brain Cholinergic Syst.* 3–62.

Steriade, M., Paré, D., Parent, A., and Smith, Y. (1988). Projections of cholinergic and non-cholinergic neurons of the brainstem core to relay and associational thalamic nuclei in the cat and macaque monkey. *Neuroscience* 25, 47–67. doi: 10.1016/0306-4522(88)90006-1

Takakusaki, K. (2008). Forebrain control of locomotor behaviors. *Brain Res. Rev.* 57, 192–198. doi: 10.1016/j.brainresrev.2007.06.024

Takakusaki, K., Habaguchi, T., Ohtinata-Sugimoto, J., Saitoh, K., and Sakamoto, T. (2003). Basal ganglia efferents to the brainstem centers controlling postural muscle tone and locomotion: a new concept for understanding motor disorders in basal ganglia dysfunction. *Neuroscience* 119, 293–308. doi: 10.1016/S0306-4522(03)00095-2

Takakusaki, K., Habaguchi, T., Saitoh, K., and Kohyama, J. (2004a). Changes in the excitability of hindlimb motoneurons during muscular atonia induced by stimulating the pedunculopontine tegmental nucleus in cats. *Neuroscience* 124, 467–480. doi: 10.1016/j.neuroscience.2003.12.016

Takakusaki, K., Oohinata-Sugimoto, J., Saitoh, K., and Habaguchi, T. (2004b). Role of basal ganglia–brainstem systems in the control of postural muscle tone and locomotion. *Prog. Brain Res.* 143, 231–237.

Takakusaki, K., Saitoh, K., Harada, H., and Kashiwayanagi, M. (2004c). Role of basal ganglia–brainstem pathways in the control of motor behaviors. *Neurosci. Res.* 50 , 137–151.

Thevathasan, W., Cole, M. H., Graepel, C. L., Cara, C. L., Jonathan, J. A., Jenkinson, J. S., et al. (2012). A spatiotemporal analysis of gait freezing and the impact of pedunculopontine nucleus stimulation. *Brain.* 135 , 1446–1454. doi: 10.1093/brain/aws039

Turner, R. S., and Anderson, M. E. (1997). Pallidal discharge related to the kinematics of reaching movements in two dimensions. *J. Neurophysiol.* 77 , 1051–1074. doi: 10.1152/jn.1997.77.3.1051

Villiger, E., and Piersol, G. A. (1912). *Brain and Spinal Cord; A Manual for the Study of the Morphology and Fibre-Tracts of the Central Nervous System*. Philadelphia, PA; London: J. B. Lippincott.

Vincent, S. R., and Kimura, H. (1992). Histochemical mapping of nitric oxide synthase in the rat brain. *Neuroscience* 46 , 755–784. doi: 10.1016/0306-4522(92)90184-4

Vincent, S. R., Satoh, K., Armstrong, D. M., Panula, P., Vale, W., and Fibiger, H. C. (1986). Neuropeptides and NADPH-diaphorase activity in the ascending cholinergic reticular system of the rat. *Neuroscience* 17 , 167–182. doi: 10.1016/0306-4522(86)90234-4

von Monakow, H., K., Akert, K., and Künzle, H. (1979). Projections of precentral and premotor cortex to the red nucleus and other midbrain areas in Macaca fascicularis. *Experimental brain research* 34 , 91–105. doi: 10.1007/BF00238343

Wallace, M. N., and Fredens, K. (1988). Origin of high acetylcholinesterase activity in the mouse superior colliculus. *Experimental brain research* 72 , 335–346. doi: 10.1007/BF00250255

Wang, H. L., and Morales, M. (2009). Pedunculopontine and laterodorsal tegmental nuclei contain distinct populations of cholinergic, glutamatergic and GABAergic neurons in the rat. *European Journal of Neuroscience* 29 , 340–358. doi: 10.1111/j.1460-9568.2008.06576.x

Waraczynski, M., and Perkins, M. (1998). Lesions of pontomesencephalic cholinergic nuclei do not substantially disrupt the reward value of medial forebrain bundle stimulation. *Brain Res.* 800 , 154–169. doi: 10.1016/S0006-8993(98)00519-8

Whitehouse, P. J., Hedreen, J. C., White, C. L., and Price, D. L. (1983). Basal forebrain neurons in the dementia of Parkinson disease. *Ann. Neurol.* 13 , 243–248. doi: 10.1002/ana.410130304

Wichmann, T., and DeLong, M. R. (1996). Functional and pathophysiological models of the basal ganglia. *Curr. Opin. Neurobiol.* 6 , 751–758. doi: 10.1016/S0959-4388(96)80024-9

Wichmann, T., and DeLong, M. R. (2003). Pathophysiology of Parkinson's disease: the MPTP primate model of the human disorder. *Ann. N. Y. Acad. Sci.* 991 , 199–213. doi: 10.1111/j.1749-6632.2003.tb07477.x

Winn, P. (1998). Frontal syndrome as a consequence of lesions in the pedunculopontine tegmental nucleus: a short theoretical review. *Brain Res. Bull.* 47 , 551–563. doi: 10.1016/S0361-9230(98)00136-1

Winn, P. (2008). Experimental studies of pedunculopontine functions: are they motor, sensory or integrative? *Parkinsonism Relat. Disord.* 14, S194–S198.

Woolf, N. J., and Butcher, L. L. (1986). Cholinergic systems in the rat brain: III. *Projections from the pontomesencephalic tegmentum to the thalamus, tectum, basal ganglia, and basal forebrain. Brain research bulletin* 16 , 603–637.

Yeomans, J. S., Mathur, A., and Tampakeras, M. (1993). Rewarding brain stimulation: role of tegmental cholinergic neurons that activate dopamine neurons. *Behav. Neurosci.* 107, (1077).

Yoshida, M., and Precht, W. (1971). Monosynaptic inhibition of neurons of the substantia nigra by caudatonigral fibers. *Brain Res.* 32 , 225–228. doi: 10.1016/0006-8993(71)90170-3

Zweig, R. M., Whitehouse, P. J., Casanova, M. F., Walker, L. C., Januarykel, W. R., and Price, D. L. (1987). Loss of pedunculopontine neurons in progressive supranuclear palsy. *Annals of neurology 22,* 18–25.

Zweig, R. M., Jankel, W. R., Hedreen, J. C., Mayeux, R., and Price, D. L. (1989). The pedunculopontine nucleus in Parkinson's disease. *Annals of neurology* 26 (1), 41-46. doi: 10.1002/ana.410260106

Conflict of Interest Statement: The authors declare that the research was conducted in the absence of any commercial or financial relationships that could be construed as a potential conflict of interest.

Copyright © 2018 French and Muthusamy. This is an open-access article distributed under the terms of the Creative Commons Attribution License (CC BY). The use, distribution or reproduction in other forums is permitted, provided the original author(s) and the copyright owner are credited and that the original publication in this journal is cited, in accordance with accepted academic practice. No use, distribution or reproduction is permitted which does not comply with these terms.

frontiers in Integrative Neuroscience

ORIGINAL RESEARCH
published: 14 August 2018
doi: 10.3389/fnint.2018.00035

Olfactory Performance as an Indicator for Protective Treatment Effects in an Animal Model of Neurodegeneration

Anja Meyer[1†], Anne Gläser[1,2†], Anja U. Bräuer[1,2,3], Andreas Wree[1], Jörg Strotmann[4], Arndt Rolfs[5] and Martin Witt[1]*

[1] Institute of Anatomy, Rostock University Medical Center, Rostock, Germany, [2] Research Group Anatomy, School of Medicine and Health Sciences, Carl von Ossietzky University Oldenburg, Oldenburg, Germany, [3] Research Center for Neurosensory Science, Carl von Ossietzky University Oldenburg, Oldenburg, Germany, [4] Institute of Physiology, University of Hohenheim, Stuttgart, Germany, [5] Albrecht-Kossel-Institute for Neuroregeneration, Rostock University Medical Center, Rostock, Germany

Background: Neurodegenerative diseases are often accompanied by olfactory deficits. Here we use a rare neurovisceral lipid storage disorder, Niemann–Pick disease C1 (NPC1), to illustrate disease-specific dynamics of olfactory dysfunction and its reaction upon therapy. Previous findings in a transgenic mouse model (*NPC1*$^{-/-}$) showed severe morphological and electrophysiological alterations of the olfactory epithelium (OE) and the olfactory bulb (OB) that ameliorated under therapy with combined 2-hydroxypropyl-ß-cyclodextrin (HPßCD)/allopregnanolone/miglustat or HPßCD alone.

Methods: A buried pellet test was conducted to assess olfactory performance. qPCR for olfactory key markers and several olfactory receptors was applied to determine if their expression was changed under treatment conditions. In order to investigate the cell dynamics of the OB, we determined proliferative and apoptotic activities using a bromodeoxyuridine (BrdU) protocol and caspase-3 (cas-3) activity. Further, we performed immunohistochemistry and western blotting for microglia (Iba1), astroglia (GFAP) and tyrosine hydroxylase (TH).

Results: The buried pellet test revealed a significant olfactory deterioration in *NPC1*$^{-/-}$ mice, which reverted to normal levels after treatment. At the OE level, mRNA for olfactory markers showed no changes; the mRNA level of classical olfactory receptor (ORs) was unaltered, that of unique ORs was reduced. In the OB of untreated *NPC1*$^{-/-}$ mice, BrdU and cas-3 data showed increased proliferation and apoptotic activity, respectively. At the protein level, Iba1 and GFAP in the OB indicated increased microgliosis and astrogliosis, which was prevented by treatment.

Conclusion: Due to the unique plasticity especially of peripheral olfactory components the results show a successful treatment in NPC1 condition with respect to normalization of olfaction. Unchanged mRNA levels for olfactory marker protein and distinct olfactory receptors indicate no effects in the OE in *NPC1*$^{-/-}$ mice. Olfactory deficits are thus likely due to central deficits at the level of the OB. Further studies are needed to examine if

OPEN ACCESS

Edited by:
Lucy Jane Miller,
STAR Institute for Sensory Processing Disorder, United States

Reviewed by:
Juan Andrés De Carlos,
Consejo Superior de Investigaciones Científicas (CSIC), Spain
Michael Leon,
University of California, Irvine, United States

***Correspondence:**
Martin Witt
martin.witt@med.uni-rostock.de

[†] These authors have contributed equally to this work

Received: 04 June 2018
Accepted: 26 July 2018
Published: 14 August 2018

Citation:
Meyer A, Gläser A, Bräuer AU, Wree A, Strotmann J, Rolfs A and Witt M (2018) Olfactory Performance as an Indicator for Protective Treatment Effects in an Animal Model of Neurodegeneration. Front. Integr. Neurosci. 12:35. doi: 10.3389/fnint.2018.00035

olfactory performance can also be changed at a later onset and interrupted treatment of the disease. Taken together, our results demonstrate that olfactory testing in patients with NPC1 may be successfully used as a biomarker during the monitoring of the treatment.

Keywords: Niemann–Pick disease type C1, olfactory receptors, mouse model, astroglia, microglia, olfactory bulb, neurodegeneration, biomarker

INTRODUCTION

Apart from age, the most common physiological reason for neurodegeneration (Doty et al., 1984; Doty, 2018), accelerated neurodegeneration is often accompanied or preceded by olfactory deficits. For example, progressive olfactory deficits constitute early signs of idiopathic Parkinson's disease (IPD), often years before first motor dysfunctions occur (Doty et al., 1988; Mesholam et al., 1998; Hawkes et al., 1999; Haehner et al., 2007; Djordjevic et al., 2008; Ross et al., 2008). After 4 years, 7% of individuals with olfactory loss have developed signs of IPD (Haehner et al., 2007). Patients with IPD, frontotemporal dementia and Alzheimer's disease present elevated numbers of PG dopaminergic neurons (Huisman et al., 2004; Mundinano et al., 2011). Hyposmia has also been reported in several other conditions such as Huntington's disease (Moberg et al., 1987; Barrios et al., 2007), amyotrophic lateral sclerosis (Günther et al., 2018), incidental Lewy body disease (Driver-Dunckley et al., 2014), the neurologic form of Gaucher's disease (McNeill et al., 2012) and numerous more (for reviews see: Attems et al., 2015; Marin et al., 2018).

Olfactory impairment influences the patient's quality of life in an increasingly aging society (Karpa et al., 2010; Croy et al., 2014), but investigations on the significance of olfactory dysfunction in neurodegenerative diseases, such as Niemann–Pick type C1 (NPC1), is usually not in the focus of research.

The exposed location of ORNs and the direct access to the CNS as well as the ability to lifelong adult neurogenesis make the olfactory system a starting point of neuropathologic events (Rey et al., 2018) and thereby an interesting research object. The olfactory system is unique in that it is by far the most proliferative CNS system harboring differentiating progenitor cells, which travel from the subventricular zone via the rostral migratory stream into the OB, where they differentiate into tyrosine hydroxylase (TH+) or GABA(+) interneurons (Alvarez-Buylla and Garcia-Verdugo, 2002; Doetsch, 2003; Lledo et al., 2006). The high central plasticity is accompanied by the high turnover of peripheral ORNs in the OE (Schwob, 2002; Mackay-Sim et al., 2015).

NPC1 is a rare autosomal-recessive lipid storage disease that is characterized by progressive neurodegeneration, inducing ataxia and impairment of intellectual function, as well as hepatosplenomegaly and dystonia (Vanier and Millat, 2003; Garver et al., 2007; Spiegel et al., 2009). The defect is caused by mutations in the *NPC1* gene which leads to disturbances in intracellular lipid trafficking and to accumulation of unesterified cholesterol, glycosphingolipids and other fatty acids in the endosomal/lysosomal system (Carstea et al., 1997). This impaired lipid transport leads particularly to an extensive loss of Purkinje cells in the cerebellum and degeneration of other central nervous compartments (Elleder et al., 1985; Tanaka et al., 1988; Sarna et al., 2003; Maass et al., 2015).

So far, there is no causal therapy of NPC1, though the iminosugar miglustat (Zavesca®) is the only approved drug in Europe used for supporting and symptomatic therapy in NPC1 (Patterson et al., 2007). Miglustat inhibits glucosylceramide synthase, a key enzyme of glycosphingolipid biosynthesis, reducing intracellular accumulation of metabolites, like sphingomyelin and sphingosine (Platt and Jeyakumar, 2008). The therapy results in delayed onset of neurological symptoms with increased lifespan (Patterson et al., 2007; Platt and Jeyakumar, 2008). Another promising therapy results further in prevention of cerebellar Purkinje cell loss, improved motor function and reduced intracellular lipid storage in *NPC1*$^{-/-}$ mice, caused by combination of miglustat, the neurosteroide allopregnanolone and HPßCD, a cyclic oligosaccharide (Davidson et al., 2009, 2016; Hovakimyan et al., 2013a; Maass et al., 2015). Interestingly, the exclusive administration of HPßCD results in reduced cholesterol storage in organs and causes later onset of neurological symptoms, furthermore confirmed by a clinical trial with *NPC1*$^{-/-}$ patients (Liu et al., 2010; Ramirez et al., 2010; Matsuo et al., 2013).

This study focuses on the investigation of the olfactory function in the NPC1 mouse model with different treatment strategies. Sensory malfunctions in NPC1 such as retina degeneration (Claudepierre et al., 2010; Yan et al., 2014) and hearing loss (King et al., 2014) have already been reported in an NPC1 mouse model. Using the same model, we previously reported a severe loss of ORNs in the OE as well as microgliosis and astrogliosis in the first central olfactory relay station, the OB (Hovakimyan et al., 2013b). These alterations can be largely prevented by combined treatment or monotherapy with HPßCD (Meyer et al., 2017).

In this report we show that the earlier observed neurodegeneration and cell proliferation at the peripheral level in NPC1 is also detectable in the OB, albeit at a somewhat lower degree. What is more, NPC1 condition in mice leads to olfactory impairment in a buried pellet test. Olfactory dysfunction is also accompanied by differential regulation in

Abbreviation: Adcy3, Adenylate cyclase 3; Bax, Bcl2-associated X protein; BC, Basal cells; Bcl2, B cell leukemia/lymphoma 2; DK, Cilia/dendritic knobs; EPL, external plexiform layer; GCL, granule cell layer; GL, glomerular layer; HPßCD, 2-hydroxypropyl-ß-cyclodextrin; IPL, internal plexiform layer; LP, Lamina propria; MCL, mitral cell layer; NPC1, Niemann–Pick disease type C1; OB, olfactory bulb; OE, olfactory epithelium; Olfr, olfactory receptor gene; OMP, olfactory marker protein; ONL, olfactory nerve layer; OR, olfactory receptor; ORN, olfactory receptor neuron; PG, Periglomerular; PPIA, Cyclophilin A.

the expression of some olfactory receptors. Since structural and functional parameters tested can be almost completely reconstituted by both therapy arms applied in this study, we suggest that olfactory testing may be regarded as a biomarker during treatment monitoring.

MATERIALS AND METHODS

Animals

Heterozygous breeding pairs of NPC1 mice (BALB/cNctr-Npc1m1N/-J) were obtained from Jackson Laboratories (Bar Harbor, ME, United States) for generating homozygous *NPC1*$^{-/-}$ mutants and *NPC1*$^{+/+}$ control wild type mice. Mice were maintained under standard conditions with free access to food and water with a 12 h day/night cycle, a temperature of 22°C and a relative humidity of 60%. Genotypes were determined until postnatal day P7 by PCR analysis. This study was carried out in accordance with the recommendations of the German legislation on protection of animals and the Committee on the Ethics of Animal Experiments at the University of Rostock. The protocol was approved by the Landesamt für Landwirtschaft, Lebensmittelsicherheit und Fischerei Mecklenburg- Vorpommern (approval IDs: LALLF M-V/ TST/7221.3-1.1-011/16, and LALLF M-V/ TST/7221.3-1.1-030/12).

Genotyping

For genotyping by PCR analysis, 1–2 mm of the tails were clipped at P6 and homogenized in DirectPCR-Tail and 1% proteinase K (Peqlab, Erlangen, Germany) at 55°C with 750 rpm for 16 h overnight on a Thermo Mixer (Eppendorf, Hamburg, Germany). Extracts were centrifuged for 30 s with 6000 rpm and PCR analysis was performed twice with 2 μl of the lysate and two different primer pairs under equal cycling conditions. For detecting the mutant allele (obtained fragment size 475 bp) primers 5′-ggtgctggacagccaagta-3′ and 5′-tgagcccaagcataactt-3′ and for the wild type allele (obtained fragment size 173 bp) 5′-tctcacagccacaagcttcc-3′ and 5′-ctgtagctcatctgccatcg-3′ were used.

Pharmacologic Treatment

The following four groups were systematically evaluated: (1) Sham-treated *NPC1*$^{+/+}$ (wild type) mice; (2) sham-treated *NPC1*$^{-/-}$ mutant mice; (3) *NPC1*$^{-/-}$ mutant mice, which received a combination therapy; (4) *NPC1*$^{-/-}$ mutant mice, which received a HPßCD monotherapy.

We used two different therapeutic schedules for the *NPC1*$^{-/-}$ mutants. The first one was a combination treatment of synergistically working drugs utilizing cyclodextrin, allopregnanolone and miglustat, starting at P7 with an injection of allopregnanolone (Pregnan-3alpha-ol-20-one; 25 mg/kg; Sigma Aldrich, St. Louis, MO, United States) dissolved in cyclodextrin (HPßCD; 2-hydroxypropyl-β-cyclodextrin; 4,000 mg/kg, i.p.; Sigma Aldrich, in Ringer's solution) once a week, as described by Davidson et al. (2009). Additionally, 300 mg/kg miglustat (*N*-butyl-deoxynojirimycin; generous gift of Actelion Pharmaceuticals, Allschwil, Schwitzerland) dissolved in normal saline solution was injected i.p. daily from P10 to P22. Afterward, miglustat powder was administered mixed with food (therapeutic scheme in **Supplementary Figure S1**). For the second treatment schedule, allopregnanolone and miglustat were omitted and only HPßCD was injected weekly (monotherapy). Controls included *NPC1*$^{+/+}$ animals as well as *NPC1*$^{-/-}$ mutants, being untreated or received normal saline solution or Ringer's solution without active substances ("sham-treated"). For a better understanding, sham-treated and untreated mice are designated as "sham-treated" in the following sections of this study, since previous studies did not demonstrate any differences between both groups (Schlegel et al., 2016).

Buried Pellet Test

In order to verify whether the morphological alterations of the *NPC1*$^{-/-}$ mice correlate with impaired olfactory ability we conducted an olfactory behavior test, the buried pellet test according to a protocol of Lehmkuhl et al. (2003). Forty-five *NPC1*$^{-/-}$ and 19 *NPC1*$^{+/+}$ control mice aged between P54-56 were tested. Briefly, mice got accustomed to a piece of sweetened cereal pellet (Honey Bsss Loops, Kellogg, Munich, Germany) 2 days prior to the test and during the fasting period 18–24 h before. On the day of the test mice were habituated to the testing environment for 1 h in a fresh cage with bedding. The testing cage was prepared with ∼ 3 cm bedding and one pellet was buried 0.5 cm below in one corner of the cage. The subject was placed in the test cage and the latency time was measured until the mouse uncovered the pellet. If a mouse did not find the pellet within the predetermined time of 300 s the experiment was terminated and a latency of 5 min was recorded.

Subsequently, the test was repeated using the same scheme but now the pellet was placed on the surface (surface pellet test) to exclude possible motor disorders or alterations in the food motivation (**Supplementary Figure S2**). Latencies are expressed as the mean ± SEM (**Supplementary Table S1**).

5-Bromo-2′-deoxyuridine (BrdU) Injections

BrdU is a thymidine analog, which is incorporated in DNA during the S-phase of DNA synthesis. Consequently, it is a reliable marker for the quantification of the proliferative potential of tissues (Dover and Patel, 1994; Onda et al., 1994; Winner et al., 2002). To label proliferating cells in the OB, 5–7 mice of either group were injected intraperitoneally with BrdU (solubilized in normal saline, 50 mg/kg, Sigma, St. Louis, MO, United States) twice a day from P40 to P46 as described earlier (Meyer et al., 2017). Additionally, a final single dose was given 1 h before perfusion at P55–56 for labeling the dividing cells of the OE (Meyer et al., 2017). Recent studies have noted that conventional dosage of BrdU may lead to considerable destruction of cells (Duque and Rakic, 2011). Thus, we cannot rule out a possible toxic effect upon application of BrdU, however, in our approach this potential error would be a systematic one that applies to all treated animal groups and is likely not to change the relative differences measured between groups.

RNA Extraction and cDNA Synthesis

For qPCR analysis of olfactory receptor genes and olfactory markers, OE was dissected from 16 homozygous *NPC1*$^{-/-}$ mutants and 5 control wild type mice (*NPC1*$^{+/+}$) of both sexes aged to 8 weeks and treated as described in "Pharmacologic Treatment." Mice were deeply anesthetized with pentobarbital (90 mg/kg) and then decapitated. The dissected tissues were frozen in liquid nitrogen and stored at −80°C. TRIzol reagent (Thermo Fisher Scientific, Waltham, MA, United States) was used for homogenization of the tissue, followed by RNA extraction according to the manufacturer's protocol. After precipitation and drying, RNA was resuspended in an aliquot of RNase and DNase-free water quantified by A_{260nm} spectrophotometry (BioSpectrometer® basic, Eppendorf, Hamburg, Germany) and stored at −80°C. cDNA was synthesized with 5 μg of total RNA using the High-Capacity cDNA Reverse Transcription Kit (Thermo Fisher Scientific, Waltham, MA, United States) according to the manufacturer's protocol. Control reactions were performed without MultiScribe Reverse Transcriptase. cDNA was stored at −20°C. The quality of amplified cDNA was controlled using β-*Actin* PCR.

Quantitative Real-Time PCR (qRT-PCR)

Each PCR reaction contained 8 μl RNase and DNase-free water, 10 μl TaqMan® Universal PCR Master Mix (Thermo Fisher Scientific, Waltham, MA, United States), 1 μl cDNA and 1 μl TaqMan Gene Expression Assays for transcripts (listed in **Supplementary Table S2**). mRNA of each sample was normalized relative to *Ppia* and *ß-Actin*, both of them have been proven as useful reference genes for quantitative RT-PCR (**Supplementary Figure S3**) (Kennedy et al., 2013). PCR thermocycling parameters were 95°C for 20 s and 45 cycles of 95°C for 1 s and 60°C for 20 s. For analysis of the relative change in gene expression we used the $2^{-\Delta Ct}$ method. The reactions were run on the CFX96 Touch™ Real-Time PCR Detection System (Bio-Rad Laboratories, Hercules, CA, United States) using Bio-Rad CFX Manager 3.1 Software (Bio-Rad Laboratories, Hercules, CA, United States). Each value is the average of at least three separate experiments.

Lysate Preparation and Western Blot

For the biochemical analysis *NPC1*$^{-/-}$ mutants (n = 3) and *NPC1*$^{+/+}$ wild type controls (n = 2) (of both sexes, aged to 8 weeks, were used for different therapeutic treatment schedules. Protein extracts were prepared from the OB of *NPC1*$^{-/-}$ mutants and *NPC1*$^{+/+}$ control mice (with different treatments as described in Section "Pharmacologic Treatment"). The tissues were frozen in liquid nitrogen and stored at −80°C. Lysate preparation and western blotting were performed according to Vierk et al. (2012) and Velmans et al. (2013) with slight modifications. Tissue was homogenized (POLYTRON®PT 3100 D, Kinematica, Luzern, Switzerland) in TRIzol reagent (Thermo Fisher Scientific, Waltham, MA, United States) followed by extraction of proteins according to the manufacturer's instruction. Protein concentrations were determined with the Biospectrometer basic (Eppendorf, Hamburg, Germany). Homogenates were subjected to 10 or 12% SDS-PAGE under reduced conditions and subsequently transferred to a nitrocellulose membrane (Amersham Protran 0.45 NC, GE Healthcare, Boston, MA, United States). Blots were blocked for 1 h with 5 % BSA (TH, GFAP) or 5% non-fat dry milk (ß-Actin, Iba1) diluted in Tris-buffered saline (TBS) with 0.05% Tween® 20 and incubated overnight at 4°C with the following antibodies: mouse anti-TH (1:1,000, MAB318, Merck, Darmstadt, Germany), mouse anti-GFAP (1:500, MAB360, Merck, Darmstadt, Germany), rabbit anti-Iba1 (1:200, 019-20001, Wako Pure Chemical Industries, Osaka, Japan) and mouse anti-ß-Actin (1:1,000, A5441, Sigma-Aldrich, St. Louis, MO, United States). Secondary antibodies were sheep anti-mouse IgG (1:5,000, GE Healthcare, Boston, MA, United States) and donkey anti-rabbit IgG (1:5,000, GE Healthcare, Boston, MA, United States) conjugated to horseradish peroxidase in 5% non-fat dry milk diluted in TBS with 0.05% Tween® 20. After incubation for 1 h at room temperature proteins were detected using Pierce ECL Plus Western Blotting Substrate (Thermo Fisher Scientific, Waltham, MA, United States) and analyzed by using ImageLab 6.0 software (Bio-Rad Laboratories, Hercules, CA, United States).

Immunohistochemistry

Nineteen *NPC1*$^{-/-}$ mutants and 6 *NPC1*$^{+/+}$ wild type controls of both sexes, aged to 8 weeks, were used for different therapeutic treatment schedules. Mice were deeply anesthetized with a mixture of 50 mg/kg ketamine hydrochloride (Bela-Pharm GmbH & Co KG, Vechta, Germany) and 2 mg/kg body weight of xylazine hydrochloride (Rompun; Bayer HealthCare, Leverkusen, Germany) and then intracardially perfused with normal saline solution, followed by 4% paraformaldehyde (PFA) in 0.1 M phosphate buffered saline (PBS). The animals were then decapitated, skinned, spare tissue was removed and the remaining skull including the nasal turbinates and the whole brain were post-fixed in 4% PFA for 24 h at 4°C. Subsequently, heads were decalcified in 10% EDTA for 5–6 days at 37°C, dehydrated and embedded in paraffin. The heads were serially cut in 10 μm in frontal direction from the tip of the nose to the caudal end of the OB and collected. For orientation, some sections were stained with routine hematoxylin & eosin (H&E).

For the quantification of proliferating cells every 10th section (spaced 100 μm apart) was subjected to anti-BrdU immunohistochemistry. Sections were deparaffinized, rehydrated and pretreated with microwaves in 0.1 M citrate buffer (5 min, 680 W) for antigen retrieval, followed by incubation with 3% hydrogen peroxide (H_2O_2) in PBS to block endogenous peroxidases for 30 min, and 5% normal goat serum (NGS) in PBS for 45 min to block non-specific binding sites. Subsequently, sections were incubated with primary antibody against rat BrdU (1:2,000, #OBT0030G, Abd Serotec, Puchheim, Germany) in 3% NGS/PBS overnight at 4°C. One section of each slide was used for negative control. After washing in PBS, the sections were sequentially incubated for 1 h with the secondary anti-rat IgG (1:200; Vector, Burlingame, CA, United States), the Avidin-biotin-complex (ABC) reagent for 1 h (Vectastain-Elite; Vector, Burlingame, CA, United States) and finally visualized

with H_2O_2 – activated 3,-3′-diaminobenzidine (DAB, Sigma, Munich, Germany). Sections were dehydrated, mounted with DePeX and coverslipped.

In addition, immunohistochemical reactions against Iba1 (1:4,000, #019-19741, Wako, Osaka, Japan) and glial fibrillary acidic protein (GFAP, 1:2,000, #Z0334, Dako, Hamburg, Germany) were analyzed for the evaluation of microglial and astroglial reaction in the OB. For regeneration and plasticity activity of newborn neurons in the OE, we used Growth Associated Protein 43 (GAP43, 1:1,000, #EP890Y, Abcam, Cambridge, England). To observe differentiations in the number of PG interneurons we investigated the immunoreactivity of tyrosine hydroxylase (TH, 1:2,000, #AB1542, Millipore, Temecula, CA, United States). Apoptotic cells were labeled with anti-cleaved caspase-3 (cas-3, 1:500, clone Asp175, #9661, Cell Signaling Technology, Danvers, MA, United States). For controls, primary antisera were omitted. In control sections no reactivity was observed.

Stereology and Quantification

Following Regensburger et al. (2009) and Sui et al. (2012) we quantified BrdU(+) and TH(+) cells of the unilateral OB in 2-7 sections per mouse with an interval of 200 and 100 μm, respectively, using an unbiased stereological method, the optical fractionator. For each group and each genotype 3–9 animals were counted using a computer-aided microscope (Olympus BX-51) and stereology software (Stereo Investigator v7.5, MBF Bioscience, Williston, ND, United States). The whole OB of one hemisphere was first outlined using a 2x or 4x objective lens. Counting was realized at 40x magnification. Cell densities of proliferating cells and TH(+) interneurons per mm^3 of the OB were averaged and the four groups were compared. Therefore, the untreated mutants and untreated *NPC1*$^{+/+}$ mice served as a reference for both, combination treated and HPßCD treated mice. Results are expressed as mean values ± SEM (**Supplementary Table S3**).

Statistical Analysis

Statistical evaluation of the olfactory behavior test, the cell quantifications and the qRT-PCR was done with a non-parametric Mann-Whitney *U*-test by SPSS statistics 22/24 (IBM, Chicago, IL, United States) using genotype and treatment groups as independent variables. Graphs are created using GraphPad Prism 7. $p \leq 0.05$ was considered significant.

RESULTS

Treatment Prevents Smell Loss in *NPC1*$^{-/-}$ Mice

We used the buried pellet test for the evaluation of olfactory performance (**Figure 1** and **Supplementary Table S1**). Sham-treated *NPC1*$^{+/+}$ mice needed on average 53 ± 12 s to uncover the pellet (**Figure 1A**). All sham-treated *NPC1*$^{+/+}$ mice finished the test within the predetermined 5 min, whereby 95% of them finished within the first 60 s. In contrast, sham-treated *NPC1*$^{-/-}$ mice needed significantly longer with an almost threefold latency of 145 ± 27 s (p = 0.003). Also, only 56% of the sham-treated *NPC1*$^{-/-}$ mice finished within the first 60 s and 25% failed completely (**Figure 1B**). The remarkably increased latency of the sham *NPC1*$^{-/-}$ animals was significantly reduced after a combination therapy with miglustat, allopregnanolone and HPßCD (p = 0.028). Combination-treated *NPC1*$^{-/-}$ mice needed 64 ± 12 s to uncover the pellet, 93% finished within the first 120 s and none failed. The combination therapy significantly shortened the latency by 56% (81 s) compared with sham *NPC1*$^{-/-}$ (p = 0.028). However, the latency is still 20% higher than the sham *NPC1*$^{+/+}$ controls but without statistical proof (p = 0.331). HPßCD-treated *NPC1*$^{-/-}$ mice behave similar to combination-treated *NPC1*$^{-/-}$ mice. On average they needed 48 ± 8 s to find the buried pellet. All of them finished within the first 120 s. Consequently, the HPßCD treatment significantly reduced the latency by 68% (98 s) when compared with sham-treated *NPC1*$^{-/-}$ mice (p = 0.007). With only 89% of the latency of the healthy controls, they are only slightly quicker than sham-treated *NPC1*$^{+/+}$ mice (p = 0.898). To exclude motor disorders or alterations in the motivation for foraging of hungry mice, all subjects were tested a second time with the surface pellet test (**Supplementary Figure S2**). All mice of the 4 groups finished the surface pellet test within 60 s. The latency varied from minimum 1 s to a maximum of 47 s with mean values between 5.16 s (sham-treated *NPC1*$^{+/+}$) and 11.07 s (HPßCD-treated *NPC1*$^{-/-}$). Due to the very short latencies of the surface pellet test it can be assumed that the differences result from scattering of the measurements.

Olfactory Receptors Are Differentially Regulated

In order to find possible connections between olfactory impairment in NPC1 disease and molecular events at the level of olfactory sensory neurons, we analyzed expression profiles of olfactory receptor genes (*Olfr)* located in 3 different zones of the mouse turbinate system (**Figure 2**; Nef et al., 1992; Strotmann et al., 1992, 1994; Ressler et al., 1993; Vassar et al., 1993; Sullivan et al., 1996).

Olfr78, located in ciliary membranes of ORNs in the dorsal zone of the OE (Conzelmann et al., 2000) exhibited no differences in sham-treated *NPC1*$^{-/-}$ mice (0.0028 ± 0.0004) compared to *NPC1*$^{+/+}$ mice (0.0029 ± 0.0009) (p = 0.827), but combination (0.0022 ± 0.0004) (p = 0.127) and HPßCD (0.0020 ± 0.0002) (p = 0.275) treatment revealed a slight tendency of decreased expression compared to sham-treated *NPC1*$^{-/-}$ mice (0.0028 ± 0.0004; **Figure 2A**). The expression of *Olfr15*, located in the medial zone of the OE (Kaluza et al., 2004; Strotmann et al., 2004) showed no significant change, though a slightly decreased expression of sham-treated *NPC1*$^{-/-}$ mice (0.0208 ± 0.0075) compared to sham-treated *NPC1*$^{+/+}$ mice (0.0291 ± 0.0022) (p = 0.386) was visible (**Figure 2B**).

Olfr1507 is located in the lateral zone of the OE, showing no differences between *NPC1*$^{+/+}$ (0.0697 ± 0.0174) and sham-treated *NPC1*$^{-/-}$ mice (0.0777 ± 0.0247) (p = 0.773). However, both treatments lead to slightly decreased *Olfr1507* expression

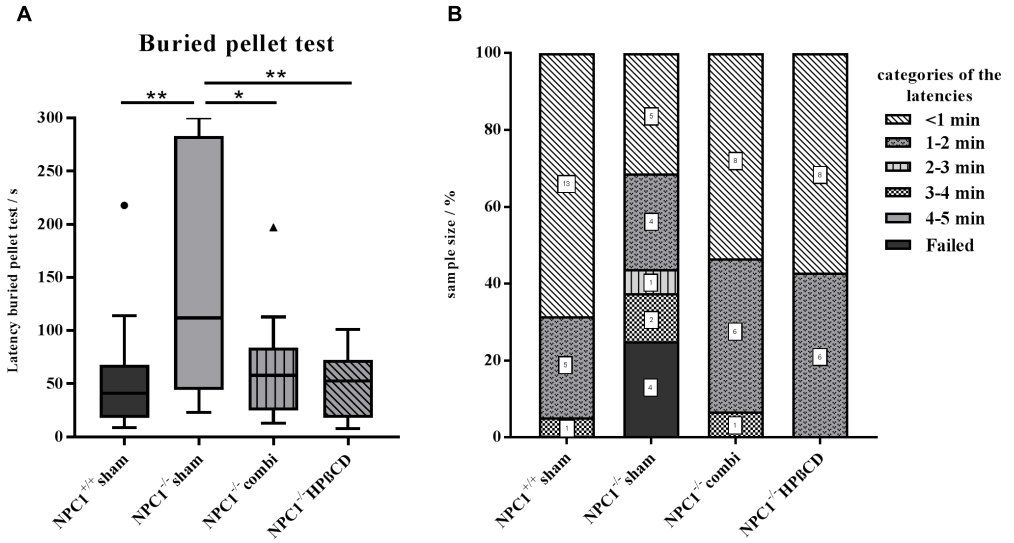

FIGURE 1 | Results of the buried pellet test. Impaired sense of smell in *NPC1*$^{-/-}$ mice is restored after combination treatment and HPßCD monotherapy. **(A)** Performance of *NPC1*$^{+/+}$ and differently treated *NPC1*$^{-/-}$ mice: On average, sham-treated *NPC1*$^{-/-}$ mice needed an almost 3-fold increased latency to find a buried piece of food, demonstrating a drastic loss of olfactory acuity. Both treatments, combination and HPßCD, normalized olfactory ability in *NPC1*$^{-/-}$ mice to the level of *NPC1*$^{+/+}$ controls. Box plot graphs represent the mean ± SEM and depict the median, the upper and lower quartiles, and outliers (circle and triangle). $^{*}p \leq 0.05$, $^{**}p \leq 0.01$ **(B)** Individual latencies of *NPC1*$^{+/+}$ and differently treated *NPC1*$^{-/-}$ mice: Results demonstrate a wide range of latencies. While 95% of the sham-treated *NPC1*$^{+/+}$ mice uncovered the pellet within the first 2 min, only 56% of the sham-treated *NPC1*$^{-/-}$ mice successfully finished within this time span and 25% even failed. After treatment, 93% of the combination and 100% of the HPßCD-treated *NPC1*$^{-/-}$ mice finished within 120 s. Numbers in squares correspond to the number of mice that finished the test within this time span.

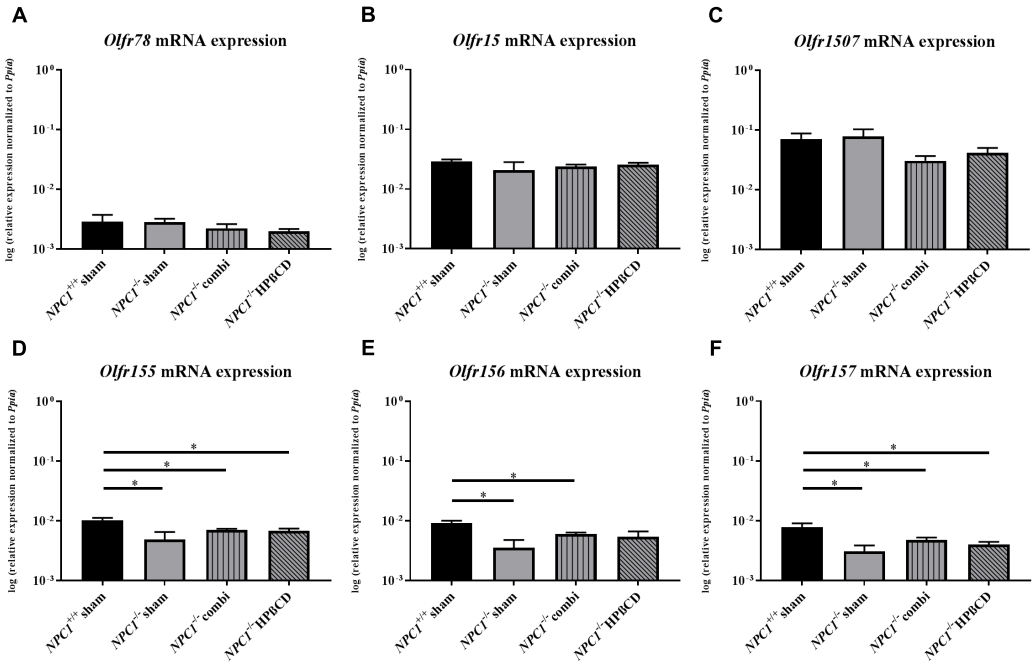

FIGURE 2 | Olfactory receptor expression in the olfactory epithelium (OE) of *NPC1*$^{-/-}$ mutants. Quantitative RT-PCR exhibit no significant changes of the *Olfr78* **(A)**, *Olfr15* **(B),** and *Olfr 1507* **(C)** expression level, in contrast to the *Olfr 155* **(D)**, *Olfr 156* **(E),** and *Olfr 157* **(F)**, showed a significant reduction in sham-treated *NPC1*$^{-/-}$ mice compared to *NPC1*$^{+/+}$ mice. Combination treatment seemed to normalize this effect compared to *NPC1*$^{-/-}$ mice, nevertheless they demonstrated significantly lower expression levels compared to *NPC1*$^{+/+}$ controls. Additionally, *Olfr155* and *Olfr157* showed significantly lower expression levels after HPßCD treatment compared to *NPC1*$^{+/+}$ controls. Data are normalized to *Ppia* and represented as mean ± SEM, n = 3–4. $^{*}p \leq 0.05$.

(combination treatment: 0.0305 ± 0.0061; HPßCD treatment: 0.0415 ± 0.0085) (**Figure 2C**).

Olfr155, 156 and 157, part of the same subfamily (OR37) are not broadly dispersed throughout the OE, but these receptors are concentrated in a small patch in the center of the OE (Strotmann et al., 1992, 1994, 1995, 2009; Kubick et al., 1997; Hoppe et al., 2006). Interestingly, the analysis shows significant changes of expression in the NPC1 mouse model (**Figures 2D–F**). *Olfr155* mRNA level in sham-treated *NPC1*$^{-/-}$ mice was significantly decreased (0.0049 ± 0.0016) compared to *NPC1*$^{+/+}$ mice (0.0103 ± 0.0010) (p = 0.043). Combination (0.0071 ± 0.0003) (p = 0.289) and HPßCD (0.0068 ± 0.0006) (p = 0.480) treatment normalized this decrease slightly, however, it was significantly decreased compared to *NPC1*$^{+/+}$ mice (combination: p = 0.034, HPßCD: p = 0.034). *Olfr156* exhibited similar changes with a significant decrease in sham-treated *NPC1*$^{-/-}$ mice (0.0035 ± 0.0012) compared to *NPC1*$^{+/+}$ mice (0.0092 ± 0.0009) (p = 0.020) that was slightly increased after combination (0.0060 ± 0.0004) (p = 0.289) and HPßCD (0.0054 ± 0.0012) (p = 0.289) treatments compared to *NPC1*$^{-/-}$ mice. Nevertheless, *Olfr156* expression of combination-treated *NPC1*$^{-/-}$ mice (p = 0.032) was significantly reduced compared to *NPC1*$^{+/+}$ mice. *Olfr157* showed similar changes as *Olfr155* and *156*. Sham-treated *NPC1*$^{-/-}$ mice (0.0031 ± 0.0008) exhibited equally decreased *Olfr157* expression compared to *NPC1*$^{+/+}$ mice (0.0078 ± 0.0013) (p = 0.043) that seems to be slightly increased after combination (0.0048 ± 0.0005) (p = 0.149) and HPßCD treatment (0.0040 ± 0.0004) (p = 0.248) compared to *NPC1*$^{-/-}$ mice, however, stayed significantly downregulated compared to *NPC1*$^{+/+}$ mice (combination: p = 0.043, HPßCD: p = 0.043).

Initiation of Neurogenesis in the OE of *NPC1*$^{-/-}$ Mice

In order to investigate the regenerative activity of ingrowing ORN, we performed immunohistochemistry and qPCR for Growth Associated Protein 43 (GAP43), a marker for newborn ORN in the OE (**Figure 3**).

Although not quantified, GAP43 immunohistochemistry did not seem to reveal differences in distribution and density of new ORN in any group investigated. ORN had a cluster-like distribution across the OE and showed a regular anatomy within the OE. However, it seems that GAP43 (+) ORN in *NPC1*$^{-/-}$ mice occupied more nuclei in the middle third of the OE than in each of the remaining groups (**Figure 3B**). Perikarya of GAP43(+) cells being ORN progenitors should be located closer to the basal membrane, as seen in controls and treated animals (**Figures 3A,C,D**).

NPC1$^{-/-}$ mice revealed a slight, but significant increase of *Gap43* mRNA (0.1233 ± 0.0179) compared to *NPC1*$^{+/+}$ mice (0.0911 ± 0.0047) (p = 0.05). This effect was not normalized after HPßCD treatment (0.1297 ± 0.0141) (p = 0.05) (**Figure 3E**). However, combination- treated *NPC1*$^{-/-}$ mice (0.1054 ± 0.0121) showed no significant regulation.

To evaluate the expression level of certain elements of the chemosensory signaling cascade during degeneration, expression of *Omp* was analyzed, albeit with no apparent change (**Figure 3F**). *Adcy3*, a cAMP-generating enzyme involved in the olfactory signal transduction cascade, along with *Omp* was not different between *NPC1*$^{+/+}$ and *NPC1*$^{-/-}$ mice (**Figure 3G**).

Functional Histomorphology of the Olfactory Bulb

To identify possible reasons of impaired olfactory performance, we then studied the distribution of cellular markers at the immunohistochemical level and their expression at the molecular level in the OB.

Coronal sections of the OB were stained with H&E with an interval of 500 μm (**Figure 4**). Light microscopy did not show apparent morphological differences of the OB between any of the 4 groups.

Induction of Proliferation in the Olfactory System of *NPC1*$^{-/-}$ Mice

Earlier investigations of the proliferation activity in the OE of *NPC1*$^{-/-}$ mice proved a notable increase of newly formed cells particularly after therapy (Meyer et al., 2017). Based on these findings, we further evaluated the proliferation activity of the OB. In sham-treated *NPC1*$^{+/+}$ mice, most BrdU(+), proliferating cells were observed in the granular cell layer (GCL), fewer were detectable in the GL, the EPL, the MCL and the IPL (**Figure 5A**). In sham-treated *NPC1*$^{-/-}$ mice an increase in the number of BrdU(+) cells in all layers became evident (**Figure 5B**). This increase seemed reversible after combination treatment (**Figure 5C**) and is contrasted by the outcome in HPßCD-treated *NPC1*$^{-/-}$ mice, where this reconstitution of increased BrdU(+) immunoreactivity could not be observed; the number of BrdU(+) cells in all layers of the OB remained at an increased level (**Figure 5D**).

For a quantitative assessment of the proliferation activity, we counted the BrdU(+) cells in one bulb of each individual (**Figure 5E** and **Supplementary Table S3**). In the OB of sham-treated *NPC1*$^{+/+}$ mice an average density of 77,327 ± 9,109 cells per mm^3 was determined. In sham-treated *NPC1*$^{-/-}$ mice this number increased to 109,557 ± 20,446 BrdU(+) cells per mm^3 (41.7% higher compared to the healthy controls; p = 0.253). Interestingly, in combination-treated *NPC1*$^{-/-}$ mice, a density of 71,779 ± 4,405 cells/ mm^3 was found, a reduction by 34.5% (p = 0.291). With a small deviation of only 7.2% the proliferation went down almost to the normal level of the *NPC1*$^{+/+}$ controls (p = 0.584). Surprisingly, in contrast to the combination therapy, the monotherapy with HPßCD did not lead to a notable decrease in the density of the proliferating cells (118,954 ± 9,298 cells/ mm^3) in *NPC1*$^{-/-}$ mice. In fact, this represents a significant enhancement of 54% when compared to sham-treated *NPC1*$^{+/+}$ mice (p = 0.032) and even a slight, although not significant increase (p = 0.565) compared to combination-treated *NPC1*$^{-/-}$ mice. The difference in the percentage of proliferating cells between combination- and HPßCD-treated *NPC1*$^{-/-}$ mice is highly significant (p = 0.004), with 65.7% less BrdU(+) cells in combination-treated *NPC1*$^{-/-}$, indicating a noticeable difference between both therapies.

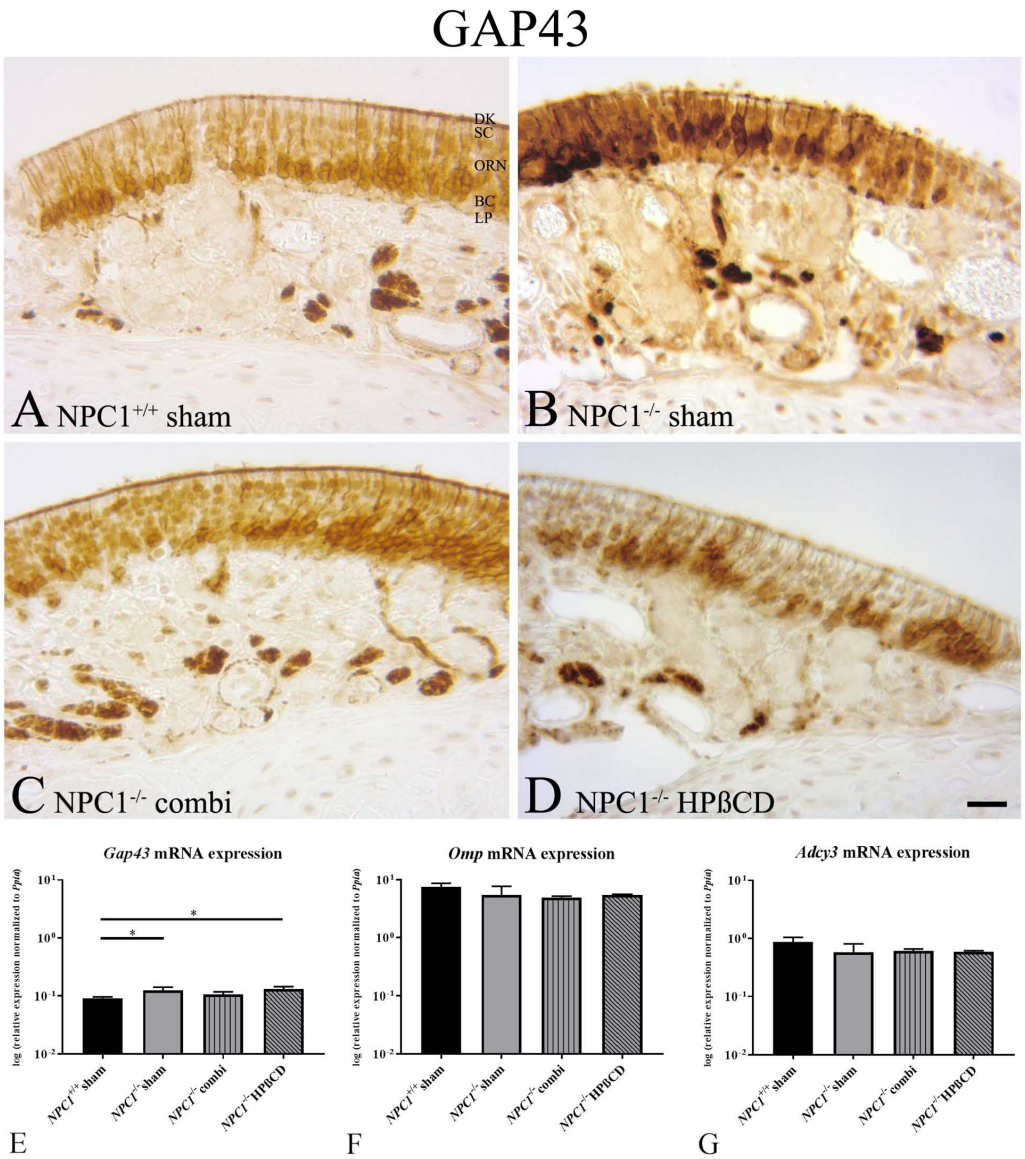

FIGURE 3 | Increased neuronal regeneration in the olfactory epithelium (OE) of sham-treated *NPC1*$^{-/-}$ mice. **(A–D)** Immunohistochemical detection of GAP43 in the olfactory epithelium (OE). Newborn olfactory neurons were regularly distributed across the basal compartment of OE in *NPC1*$^{+/+}$ mice **(A)**, whereas they appeared more cluster-like dispersed in the OE's middle layer of the other groups **(B–D)**. **(E)** Quantitative RT-PCR of the neuronal marker *Gap43* revealed increased expression in sham-treated *NPC1*$^{-/-}$ mice compared to *NPC1*$^{+/+}$ mice (n = 3). *Gap43* expression tended to be normalized in combination-treated *NPC1*$^{-/-}$ mice in contrast to HPßCD treatment that remained still significantly increased compared to sham-treated *NPC1*$^{+/+}$ mice. Expression analysis of *olfactory marker protein* (*Omp*, **F**) and *adenylate cyclase* (*Adcy3*, **G**) in the OE showed no significant changes (n = 3–4). Data are normalized to *Ppia* and represented as mean ± SEM. *$p \leq 0.05$, scale bar in **(D)** = 20 μm.

Based on the above-mentioned results at the cellular level we performed qRT-PCR of the proliferation marker Ki67 (**Figure 5F**). qRT-PCR displayed the total *Ki67* mRNA in the OB normalized to the housekeeping gene *Ppia*. Generally, proliferating cells showed an increase of *Ki67*. Our analysis (n = 4) suggests the tendency of increased *Ki67* expression in sham-treated *NPC1*$^{-/-}$ mice (0.0018 ± 0.0009) compared to *NPC1*$^{+/+}$ mice (0.0007 ± 0.00004) (p = 0.149). Combination treatment of *NPC1*$^{-/-}$ mice showed a slightly reduced *Ki67* expression (0.009 ± 0.00007) (p = 0.564), but still increased compared to *NPC1*$^{+/+}$ mice (p = 0.021). HPßCD treatment (0.0016 ± 0.0007) revealed similar expression as sham-treated *NPC1*$^{-/-}$ mice (p = 1.0) and significantly increased expression compared to *NPC1*$^{+/+}$ mice (p = 0.021). There was no significant difference between HPßCD and combination treatment (p = 1.0), however, the latter seems to be more efficient to decrease mRNA expression. In summary, *Ki67* expression analysis of the OB supports the results of the BrdU quantification. In order to

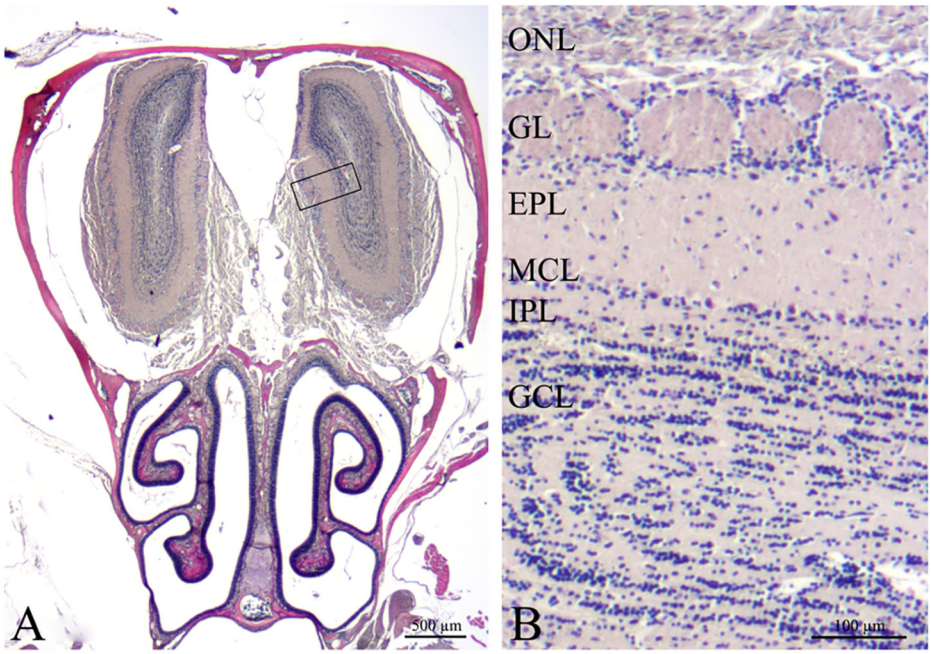

FIGURE 4 | Histological overview of the peripheral and central olfactory structures (H&E). **(A)** Coronal section of the mouse anterior cerebral cavity that houses the olfactory bulbs and the nasal cavity including turbinates and septum with olfactory mucosa. The rectangle delimits the area magnified in **(B)**. Olfactory bulb with 6 layers: ONL, olfactory nerve layer; GL, glomerular layer; EPL, external plexiform layer; MCL, mitral cell layer; IPL, internal plexiform layer; GCL, granular cell layer. Scale bars = 500 µm **(A)**, 100 µm **(B)**.

achieve complimentary data for earlier BrdU analysis of olfactory epithelial cells (Meyer et al., 2017) we also performed a *Ki67* expression analysis of the OE and observed an about 20-fold increase of *Ki67* expression compared to OB (**Figure 5G**). *Ki67* expression in the OE was significantly increased in sham- treated $NPC1^{-/-}$ mice (0.0236 ± 0.0039) compared to $NPC1^{+/+}$ mice (0.0148 ± 0.0012) (p = 0.021). This regulation was enhanced with combination treatment of $NPC1^{-/-}$ mice (0.0322 ± 0.0090) (p = 0.034). HPßCD treatment slightly increased expression (0.0199 ± 0.0023) compared to $NPC1^{+/+}$ mice (p = 0.157). Both, HPßCD (p = 0.048) and combination (p = 0.480) treatments showed no significant change in comparison with sham-treated $NCP1^{-/-}$ mice.

Increased Apoptotic Activity in the OB of $NPC1^{-/-}$ Mice

Caspase-3- positive cells [Cas-3(+)] occurred only rarely in the OB of sham-treated $NPC1^{+/+}$ mice. In contrast, the OB of sham-treated $NPC1^{-/-}$ contained numerous apoptotic cells, mainly in the GCL. Both, combination as well as HPßCD treatments led to a reduction of apoptotic cells in $NPC1^{-/-}$ mice, Cas-3(+) cells were found mainly in the MCL and GL (**Figures 6A–D**).

In order to confirm the results of Cas-3 immunoreactivity we performed expression analysis via qRT-PCR using the apoptotic markers *Bax* and *Bcl2* (**Figure 6E** and **Supplementary Table S4**). *Bax,* an apoptotic activator, increased significantly in $NPC1^{-/-}$ mice (0.0470 ± 0.0030) by 36.7% compared to $NPC1^{+/+}$ mice (0.0344 ± 0.0015) (p = 0.05). Combination treatment (0.0374 ± 0.0023) decreased this apoptotic effect by 27.7% (p = 0.05), whereas HPßCD treatment (0.0256 ± 0.0043) reduced the expression by 62.3% (p = 0.05) compared to sham-treated $NPC1^{-/-}$ mice. The HPßCD treatment reduced the *Bax* expression by 34.5% more than combination treatment that exhibited even a 25.6% less expression than $NPC1^{+/+}$ (p = 0.05).

Expression of *Bcl2,* an apoptotic suppressor, was not significantly changed in any of the groups. Only combination-treated $NPC1^{-/-}$ mice tended to show increased *Bcl2* expression by around 13% compared to $NPC^{+/+}$ and $NPC1^{-/-}$ mice. HPßCD treatment exhibited slightly reduced mRNA expression (7.4%).

The ratio of *Bax* and *Bcl2* serves as an indicator of cell susceptibility to apoptosis and is correlated with the progression of several diseases (Oltvai et al., 1993; Korsmeyer, 1999; Scopa et al., 2001; Salakou et al., 2007). The *Bax/Bcl2* ratio in NPC1 was increased by 34.5% compared to controls. The combination treatment reduced the expression by 38.9%, but only HPßCD treatment decreased the expression in $NCP1^{-/-}$ mice significantly by around 55.4%, which was even 21% less than controls reveal. Summarizing, the *Bax/Bcl2* ratio suggests increased cell susceptibility to apoptosis that may be reduced via HPßCD treatment.

Enhanced Glia Cell Activation in $NPC1^{-/-}$ OB

Iba1, a marker of microglia that is associated with inflammatory processes in neurodegenerative diseases, revealed no reactivity in OB of sham-treated $NPC1^{+/+}$ mice (**Figures 7A–D**). However,

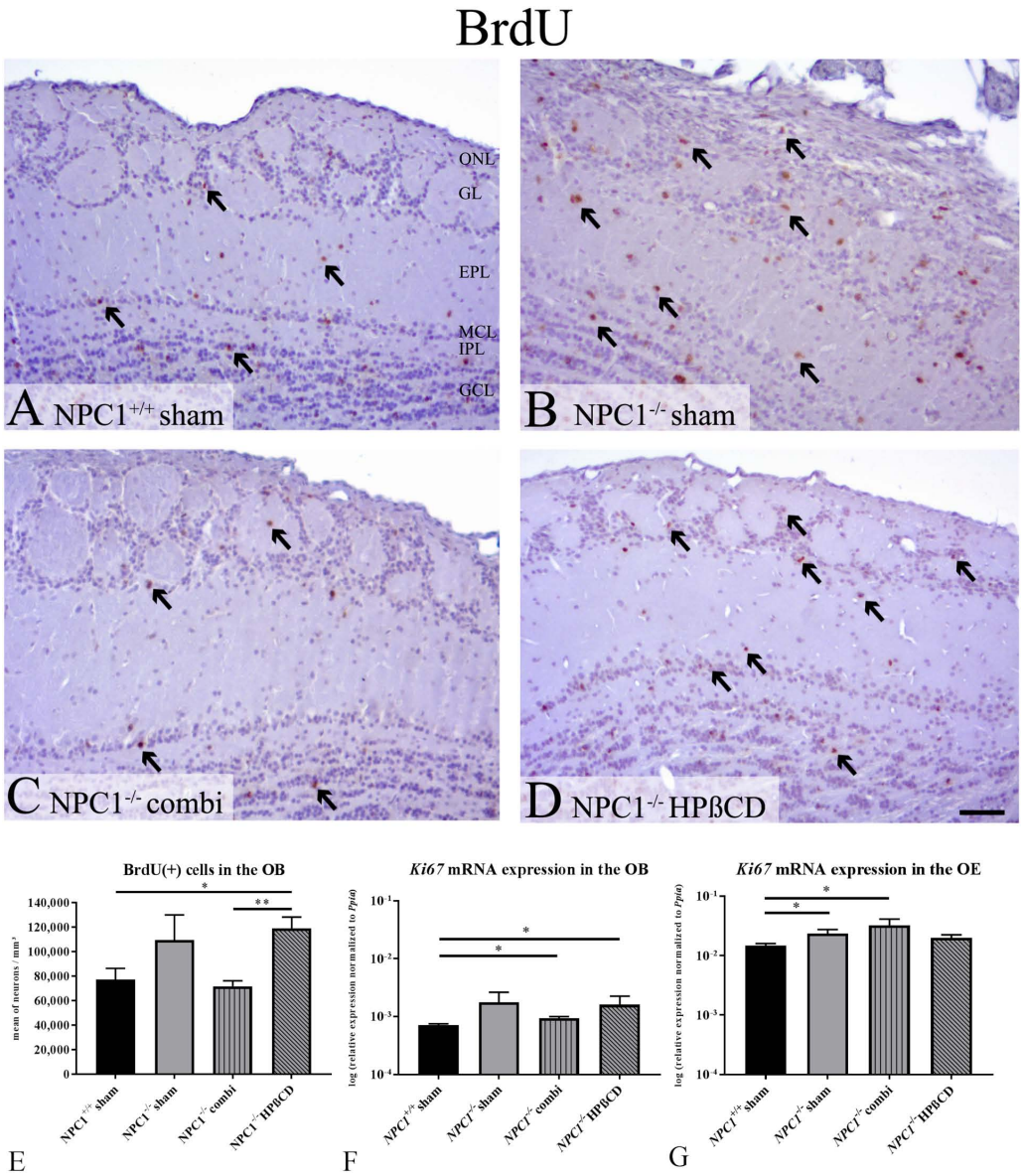

FIGURE 5 | Increased proliferation in the olfactory system of *NPC1*$^{-/-}$ mice with different treatments. **(A–D)** Immunohistochemical reaction of BrdU(+) proliferating cells in the olfactory bulb (OB). **(A)** Sham-treated *NPC1*$^{+/+}$ mice showed many newly formed cells in all layers of the OB. **(B)** The proliferation activity was visibly increased in sham-treated *NPC1*$^{-/-}$ mice. This increase was reversible after combination treatment **(C)**, but not after HPßCD treatment **(D)**. **(E)** Quantification analysis of BrdU(+) cells in the unilateral OB demonstrated a strongly increased number of Brdu(+) cells in sham-treated *NPC1*$^{-/-}$ mice, compared to sham-treated *NPC1*$^{+/+}$ mice. Combination treatment reduced the proliferation activity in *NPC1*$^{-/-}$ to the level of the controls. Surprisingly, HPßCD treatment did not notably decrease the proliferation density in *NPC1*$^{-/-}$. **(F)** Quantitative RT-PCR of differently treated *NPC1*$^{-/-}$ mice in comparison with sham-treated *NPC1*$^{+/+}$ mice revealed an increased *Ki67* mRNA expression in the OB (n = 4) and **(G)** in the OE (n = 3–4). Data are normalized to *Ppia* and represented as mean ± SEM. $^{*}p \leq 0.05$, $^{**}p \leq 0.01$, scale bars **(A–D)** = 50 μm.

sham-treated *NPC1*$^{-/-}$ mice demonstrated a noticeable increase of Iba1(+) cells in the GCL, EPL and GL of the OB. Western blot analysis confirmed the increase of Iba1 in sham-treated *NPC1*$^{-/-}$ OB (**Figure 7E**). The microgliosis was strongly reduced after combination therapy as revealed by immunohistochemistry and western blot. A monotherapy with HPßCD alone had no effect on the microglia immunoreactivity compared to *NPC1*$^{-/-}$ mice (**Figure 7D**).

Preceding studies also revealed an intense immunoreactivity for the astroglial marker GFAP in *NPC1*$^{-/-}$ mice that is, similar to Iba1, involved in neuropathological changes (Hovakimyan et al., 2013b; Meyer et al., 2017). In sham-treated *NPC1*$^{-/-}$ mice, GFAP immunohistochemistry (**Figures 8A–D**) demonstrated a balanced distribution pattern of astrocytes in all layers of the OB, whereby the ONL, GL and the GCL stand out clearly against the EPL. In contrast, sham-treated *NPC1*$^{-/-}$

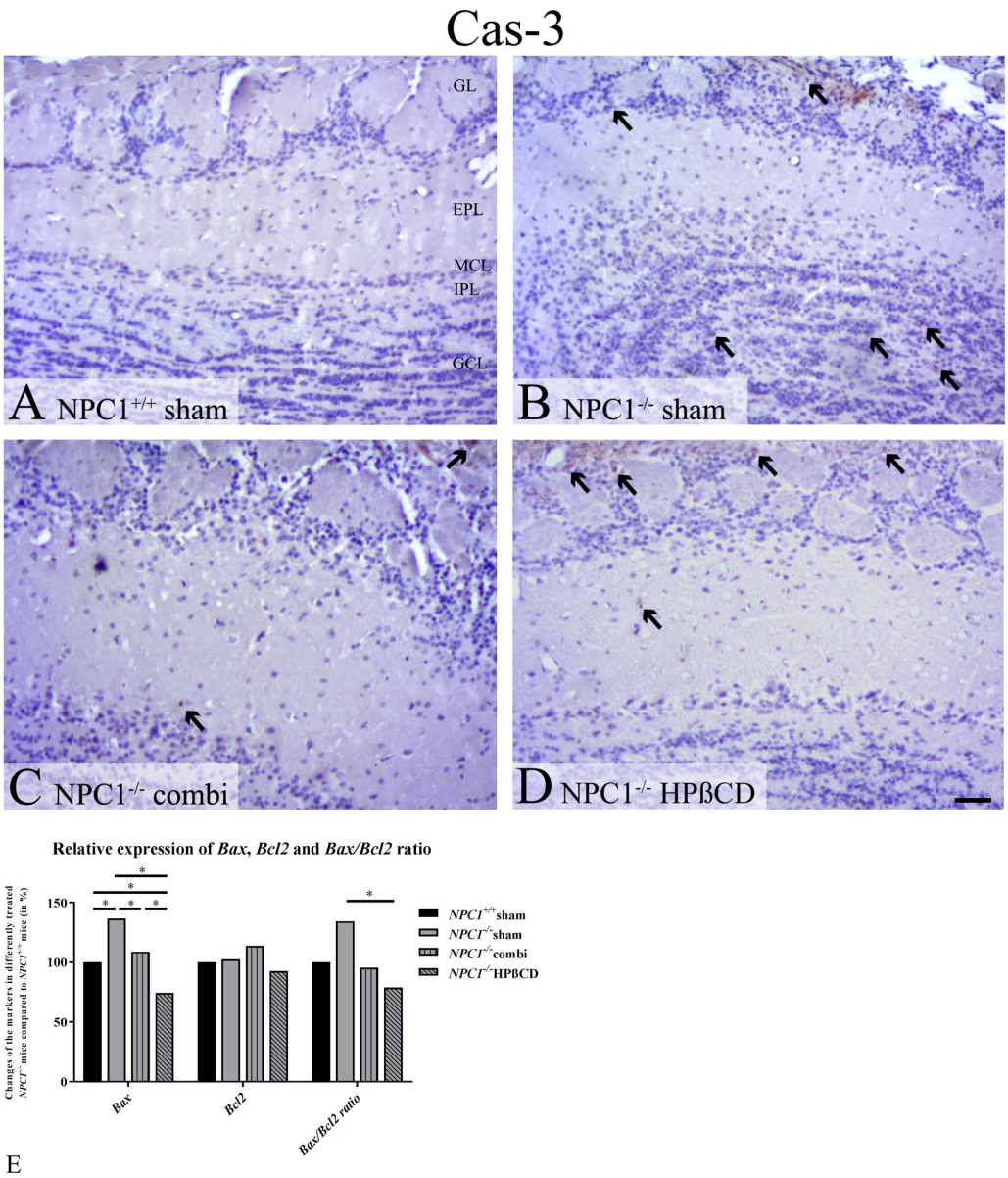

FIGURE 6 | Increased number of apoptotic cells in the olfactory bulb (OB) of *NPC1*$^{-/-}$ mice confirmed by quantitative RT-PCR. **(A–D)** Immunohistochemical reaction of cas-3(+) apoptotic cells in the olfactory bulb (OB). **(A)** Sham-treated *NPC1*$^{+/+}$ mice showed only very few apoptotic cells. **(B)** Sham-treated *NPC1*$^{-/-}$ demonstrated a clear increase of apoptotic cells, mainly in the granular cell layer (GCL). Both, combination **(C)** and HPßCD **(D)** treatments reduced apoptotic activity in *NPC1*$^{-/-}$ mice. **(E)** Changes of *Bax* and *Bcl2* mRNA expression including *Bax/Bcl2* ratio, in the OB (n = 3) of differently treated *NPC1*$^{-/-}$ mice compared to *NPC1*$^{+/+}$ mice. The apoptotic marker *Bax* exhibited a significant upregulation of sham-treated *NPC1*$^{-/-}$ mice compared to *NPC1*$^{+/+}$ mice, that was significantly reduced after combination and HPßCD treatments. Even HPßCD treatment reduced the expression significantly in comparison with *NPC1*$^{+/+}$ mice. Here, expression of *Bcl2*, an anti-apoptotic protein, remained unchanged. The *Bax/Bcl2* ratio showed a significant upregulation in sham-treated *NPC1*$^{-/-}$ mice compared to HPßCD-treated *NPC1*$^{-/-}$ mice. Data (n = 3) are represented as mean (%) compared to sham-treated *NPC1*$^{+/+}$ (set at 100%), $^{*}p \leq 0.05$, scale bars **(A–D)** = 50 μm.

mice showed a pronounced astrogliosis resulting in hardly definable layers of the OB. The distinct increase is confirmed via western blot analysis of sham-treated *NPC1*$^{-/-}$ OB compared to *NPC1*$^{+/+}$ OB (**Figure 8E**). This finding was remarkably reduced after both, combination and HPßCD treatments shown by immunohistochemistry and western blotting.

Tyrosine Hydroxylase Protein Level Is Reduced in *NPC1*$^{-/-}$ OB

Based on the massive loss of ORN in the OE of *NPC1*$^{-/-}$ mice (Meyer et al., 2017), we investigated TH immunoreactivity in dopaminergic PG neurons of the OB (**Figure 9**). Western blot analysis showed a slight decrease of TH in *NPC1*$^{-/-}$ OB

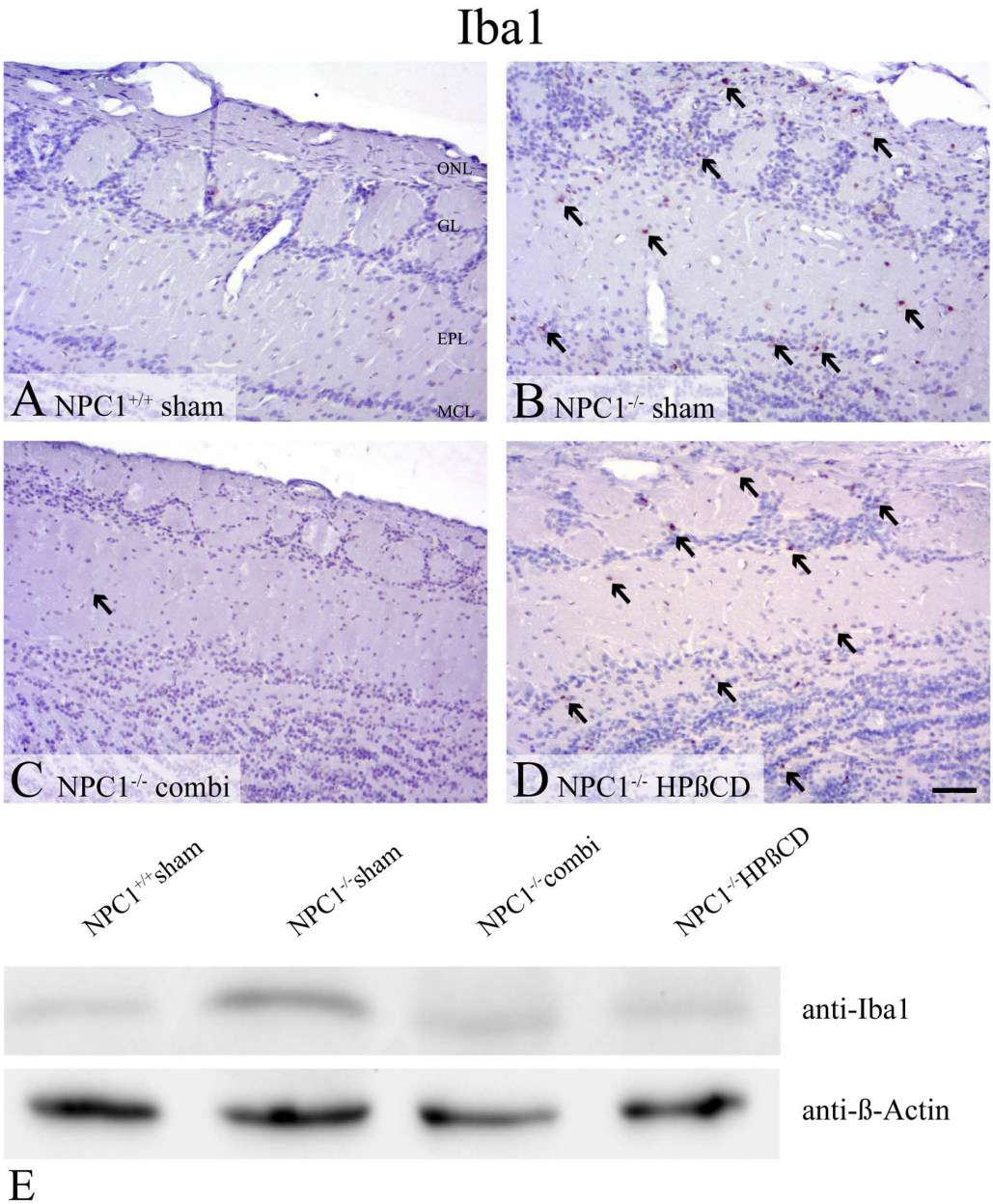

FIGURE 7 | Pronounced microgliosis in the olfactory bulb (OB) of *NPC1*$^{-/-}$ mice, reduced by combination treatment. **(A–D).** Immunohistochemical reaction of Iba1(+) microglial cells in the OB. **(A)** Sham-treated *NPC1*$^{+/+}$ mice revealed no reactivity for Iba1. **(B)** Sham-treated *NPC1*$^{-/-}$ demonstrated a noticeable increase of Iba1(+) cells in the granular cell layer (GCL), external plexiform layer (EPL) and glomerular layer (GL). The microgliosis was reduced after combination treatment in *NPC1*$^{-/-}$ mice **(C)**. However, HPßCD treatment retained an elevated microglial activity in *NPC1*$^{-/-}$ mice **(D)**. Western blot analysis of the OB of differently treated *NPC1*$^{-/-}$ mice compared to sham-treated *NPC1*$^{+/+}$ mice **(E)**. Membrane was probed with an anti-Iba1 antibody and showed a clearly increased Iba1 signal (∼17 kDa) in sham-treated *NPC1*$^{-/-}$ mice compared to *NPC1*$^{+/+}$ mice. The combination and HPßCD treatments revealed reduced microgliosis compared to sham-treated *NPC1*$^{-/-}$ mice. ß-Actin (∼42 kDa) was used as loading control.

compared to the *NPC1*$^{+/+}$ control that seems to be normalized after combination and HPßCD treatment (**Figure 9A**). Determining whether this regulation was induced by an altered number of TH(+) cells we performed a quantitative analysis, counting TH(+) PG cells (**Figure 9B** and **Supplementary Table S3**). In sham-treated *NPC1*$^{+/+}$ mice an average of 88,419 ± 17,605 TH(+) cells/mm^3 was determined. With 87,093 ± 5,202 cells/mm^3 (98.5 %) the number of TH(+) PG cells remained unchanged in sham-treated *NPC1*$^{-/-}$ mice. Compared to the density of sham-treated *NPC1*$^{+/+}$ mice, an increase was found in combination-treated *NPC1*$^{-/-}$ mice (99,714 ± 13,380 TH(+) cells/mm^3; 12.8 %) as well as

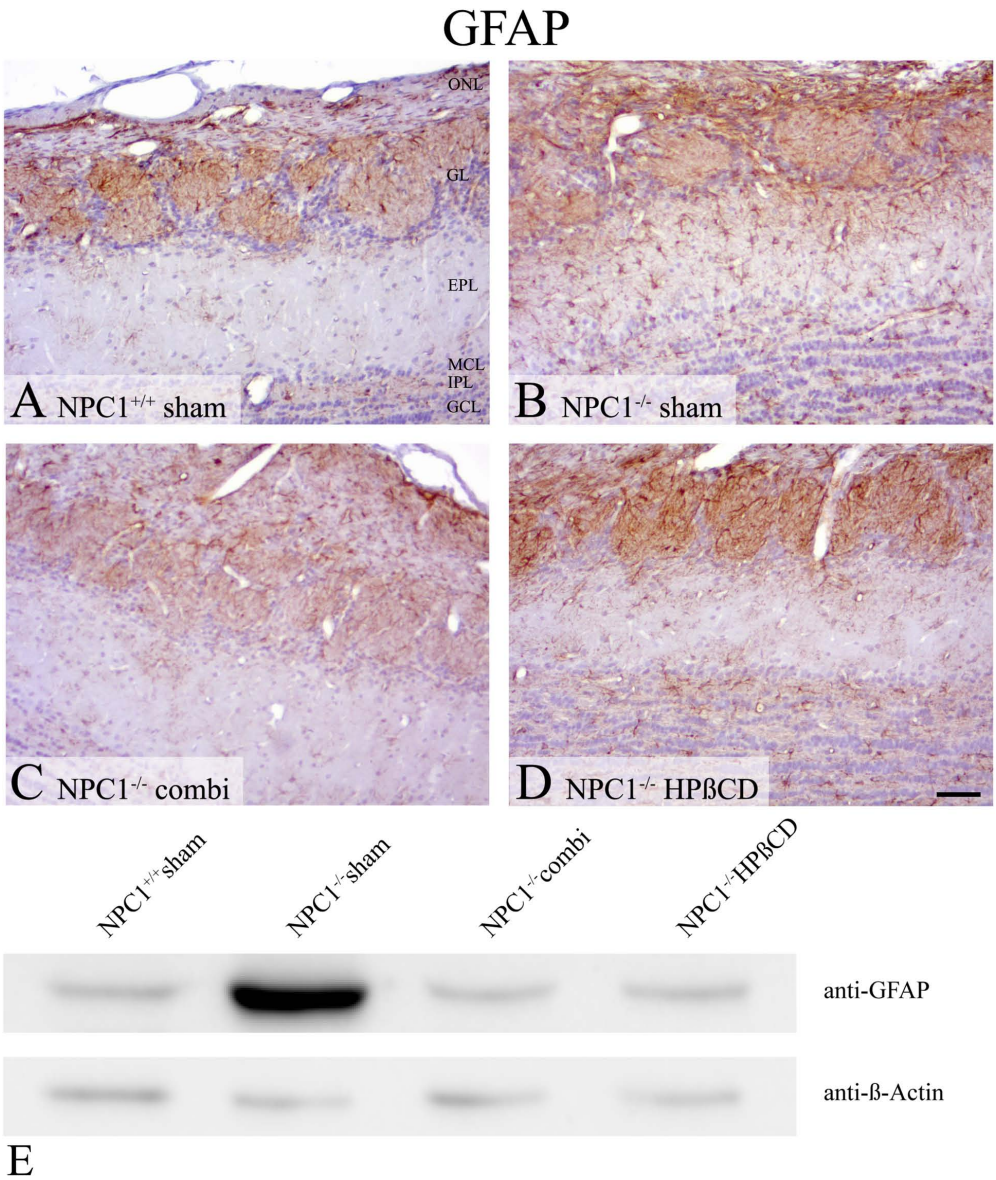

FIGURE 8 | Astrogliosis of sham-treated *NPC1*$^{-/-}$ mice is increased in *NPC1*$^{-/-}$ mice and reduced after combination and HPßCD treatment. **(A–D)** Immunohistochemical reaction of GFAP in the OB. **(A)** Sham-treated *NPC1*$^{+/+}$ mice revealed a balanced distribution pattern of astrocytes in all layers of the OB, mainly in the olfactory nerve layer (ONL), glomerular layer (GL) and granular cell layer (GCL). **(B)** In contrast, sham-treated *NPC1*$^{-/-}$ demonstrated a pronounced astrogliosis that was reduced after combination (combi) **(C)** and HPßCD **(D)** treatments. **(E)** Western blot from total protein lysates of the OB from differently treated *NPC1*$^{-/-}$ mice compared to sham-treated *NPC1*$^{+/+}$ mice. To detect GFAP protein (∼59 kDa) membrane was probed with anti-GFAP antibody that confirms the distinct increase of GFAP(+) cells from sham-treated *NPC1*$^{-/-}$ mice. Combination and HPßCD treatments showed reduced astrogliosis confirming immunohistochemical results. ß-Actin (∼ 42 kDa) was used as loading control.

in HPßCD-treated *NPC1*$^{-/-}$ mice, with 123,253 ± 15,234 cells/mm^3 (39.4%). However, the increased density of TH(+) PG cells after HPßCD treatment of *NPC1*$^{-/-}$ mice was not statistically significant (p = 0.127). Although both therapies contained HPßCD, the combination therapy had a smaller influence on the density of TH(+) interneurons. Thus, these results suggest that the regulation of TH protein in *NPC1*$^{-/-}$ mice (**Figure 9A**) was not induced by alterations in the number of TH(+) cells, but rather by a reduction of TH protein/PG cell.

DISCUSSION

This paper addressed the issue of olfactory performance in a rare neurodegenerative disease, Niemann–Pick Type C1 (NPC1). Earlier investigation of our group has shown that significant olfactory degeneration occurs at the structural level (Hovakimyan et al., 2013b). This is accompanied by a remarkable increase of proliferation in the OE that can both be halted by pharmacologic treatment (Meyer et al., 2017). Therefore,

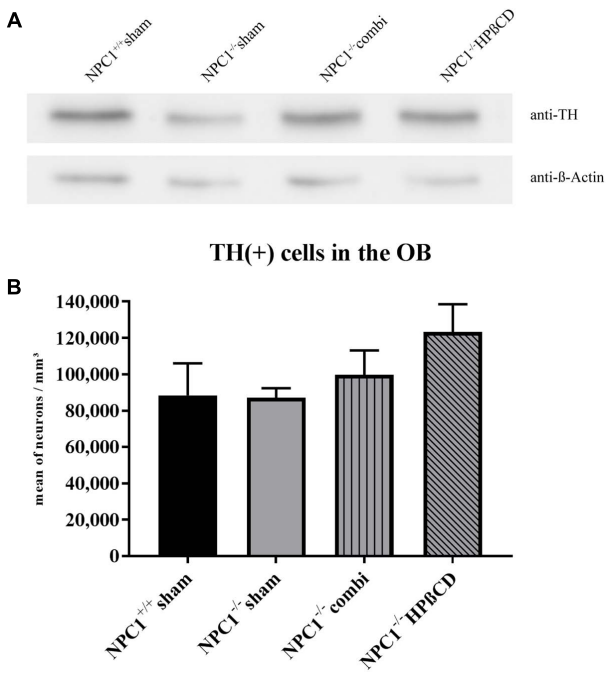

FIGURE 9 | Reduced TH protein in *NPC1*$^{-/-}$ OB is not induced by loss of TH(+) periglomerular neurons (PG). **(A)** Western blot from total protein lysates of the OB from differently treated *NPC1*$^{-/-}$ mice compared to sham-treated *NPC1*$^{+/+}$ mice. To detect the TH protein (∼59 kDa) membrane fraction was probed with anti-TH antibody that showed reduced TH in sham-treated *NPC1*$^{-/-}$ mice compared to *NPC1*$^{+/+}$ mice. Both, combination and HPßCD treatments normalized this reduction. ß-Actin (∼42 kDa) was used as loading control. **(B)** Analysis of TH(+) dopaminergic neurons in the OB. Sham-treated *NPC1*$^{-/-}$ mice showed no alterations in the number of TH(+) periglomerular neurons (PG) when compared to sham-treated *NPC1*$^{+/+}$ control mice. Considering the results of the western blot analysis it suggests a reduction of TH/PG cell. Both treatments, combination and HPßCD, slightly increased the number of TH(+) PG in *NPC1*$^{-/-}$ mice. However, combination therapy had a smaller therapy-induced influence on the TH(+) immunoreactivity in *NPC1*$^{-/-}$ mice. All data represent the mean ± SEM.

the main motivation for this paper was to demonstrate that olfactory testing may be used as a suitable biomarker to evaluate the course of the neurodegenerative signs and symptoms of NPC1. Furthermore, we investigated the impact of the different treatment strategies on structural and physiological functions. Improved olfactory performance during the course of the therapy suggests that early treatment of NPC1 disease rescues olfactory function.

Decreased Olfactory Function in *NPC1*$^{-/-}$ Mice

Using a simple olfactory screening test we showed that *NPC1*$^{-/-}$ mice actually needed significantly more time to find buried pellets in their bedding and that this impairment could be prevented by pharmacologic treatment.

As expected, *NPC1*$^{-/-}$ mice had a severe smell deficit compared to healthy control mice, particularly an almost 3-fold increased latency to find a buried piece of food. The results of the buried pellet test, however, showed a wide range of latencies. While 25% of the sham-treated *NPC1*$^{-/-}$ did not succeed to find the food pellet within a predetermined time of 5 min, 31% were as fast as the mean of sham-treated *NPC1*$^{+/+}$ mice; the results indicate that the severe morphological damages can in some individuals be compensated during the complex process of olfaction. In a control surface pellet test *NPC1*$^{-/-}$ mice had no difficulties finding an exposed piece of food indicating that they most likely have no impairments of motor skills or an altered motivation for foraging. By this, we confirmed and extended the results of Seo et al. (2014) who also demonstrated a poor olfactory performance in *NPC1*$^{-/-}$ mice. Also, our own recent studies using electro-olfactogram recordings from the olfactory mucosa revealed a tendency of decreased odor induced response amplitudes in *NPC1*$^{-/-}$ mice (Hovakimyan et al., 2013b).

Differential Regulation of Olfactory Receptor Genes

The results of our qPCR-experiments regarding olfactory receptor genes revealed that the expression level of genes that are organized in a typical zonal pattern in the OE (*olfr15, 78* and *1507*) was unaltered in *NPC1*$^{-/-}$ mice compared to wildtype individuals. In contrast, a significant reduction of mRNA in *NPC1*$^{-/-}$ mice was found for genes that belong to the OR37 subfamily. Interestingly, neither the treatment with HPßCD nor the combination treatment could rescue this problem completely; thus, regarding these features, the OR37 gene group turned out to be different from classical ORs. The result is consistent with our previous observations that the OR37 genes display unique features, setting them apart from other ORs. They are, for example, expressed by sensory neurons that are clustered in the center of the OE and send their axons to only a single glomerulus in the OB (Strotmann et al., 2000). This is in contrast to the canonical ORs that are expressed by ORNs widely distributed throughout the epithelium and project to two or even more glomeruli. On the next level of organization - the transfer of information to higher brain centers - OR37 projection neurons have been shown not to connect to the typical olfactory cortex, but to nuclei in the amygdala and hypothalamus (Bader et al., 2012a,b), brain regions related to social phenomena or stress. Thus, the OR37 subsystem is supposed to be involved in social communication and may elicit innate reactions in mice (Klein et al., 2015). It is currently not known whether chemosensors in the nose that are involved in social communication are particularly affected in NPC1; the results of our present study indicate, however, that it may be worth addressing this question in future studies.

Massive Glia Activation in the Olfactory Bulb of *NPC1*$^{-/-}$

Interestingly, we found an increase in the density of BrdU(+) proliferating cells as well as a marked enhancement of apoptosis in the OB of sham-treated *NPC1*$^{-/-}$ mice. The increased proliferation activity may be due to the increased number of microglia cells and astrocytes. This is consistent with the observation made by Seo et al. (2014) who demonstrated an

increase of the neurogenic activity in 8 weeks old *NPC1*$^{-/-}$ mice. They found a co-localization of BrdU and Iba1 in 36% of the newly formed cells, implying a 3-fold enhancement of rapidly proliferating microglia in *NPC1*$^{-/-}$ when compared to healthy controls. Further on, they demonstrated that the excessive microgliosis contributed to a progression of olfactory impairment due to a markedly increased apoptosis and inhibited neuronal maturation (Seo et al., 2014). The role of glia in neurodegenerative processes has been controversially discussed. Although there is increasing evidence that glia activation is a result of neuronal death (Suzuki et al., 2003; Chen et al., 2007), it might also be the reason for neurodegeneration (German et al., 2002; Seo et al., 2014, 2016). The elevated numbers of Iba1(+) cells obtained in HPßCD- treated *NPC1*$^{-/-}$ mice seem somewhat inconclusive since the western blot analysis did not reveal an upregulation.

No Loss of Dopaminergic Neurons in *NPC1*$^{-/-}$ Mice

Our previous studies have shown a dramatic loss of ORNs in the OE of *NPC1*$^{-/-}$ mice (Meyer et al., 2017). Several studies described a decline of TH(+) PGs after sensory deprivation or lesion of the OE (Nadi et al., 1981; Stone et al., 1990; Baker et al., 1993; Cho et al., 1996) and thus it seemed reasonable to hypothesize that the number of TH(+) dopaminergic PG is reduced also in *NPC1*$^{-/-}$ mice. Seo et al. (2014) indeed demonstrated a reduction of the TH(+) immunoreactivity by half in the OB of *NPC1*$^{-/-}$ mice. Surprisingly, our quantification revealed reduced numbers of TH(+) neurons compared with *NPC1*$^{+/+}$. However, the TH(+) immunoreactivity exhibited alterations in the TH(+) signal within the glomeruli suggesting a reduction of TH(+) nerve fibers in *NPC1*$^{-/-}$. Western blot results, however, support the findings of Seo et al. (2014) who determined the whole signal intensity rather than the number of TH(+) cells, indicating that the reduction of the TH(+) signal in *NPC1*$^{-/-}$ is caused by a diminution of TH protein in dopaminergic axons and dendrites rather than a destruction of cells.

Reconstitution of Olfactory Function After Combination and HPßCD Treatment

A central finding of the present study is that the treatment of a Niemann–Pick disease mouse model with combination or HPßCD led to a significant improvement of olfactory function. While combination-treated *NPC1*$^{-/-}$ mice needed on average about 20% longer latency time than *NPC1*$^{+/+}$ control mice, HPßCD- treated *NPC1*$^{-/-}$ mice were even minimally faster indicating that both therapies could normalize olfactory function in 8 weeks old *NPC1*$^{-/-}$ mice.

Our mRNA data for *Omp* and *Adcy3* indicated no regulation of surviving ORN in *NPC1*$^{-/-}$ mice. Also, previous electrophysiological recordings of the OE revealed no significant latencies (Hovakimyan et al., 2013b) supporting the notion that OE dynamics such as extremely increased proliferation and generation of new progenitors might compensate for the loss of ORN in sham-treated *NPC1*$^{-/-}$ mice. Therefore, olfactory deficits are likely to be due to central deficits at the level of the OB. After treatment, OB morphology showed less micro- and astrogliosis as well as a decrease of apoptosis even though a complete normalization to the level of *NPC1*$^{+/+}$ mice could not be realized. Former investigations of the cell and tissue dynamics of the OE of *NPC1*$^{-/-}$ revealed a markedly reduced apoptosis and macrophage activity in combination-treated *NPC1*$^{-/-}$ (Meyer et al., 2017).

The monotherapy with HPßCD also revealed a normalization of olfactory function and a visible reduction of apoptosis and astrogliosis in *NPC1*$^{-/-}$mice. Several studies proved the benefit of HPßCD in mice (Liu et al., 2010; Maass et al., 2015; Tanaka et al., 2015) and humans (Ramirez et al., 2010; Maarup et al., 2015). In the *NPC1*$^{-/-}$ OB, proliferation as well as Iba1(+) microglial activity remained unchanged after HPßCD therapy and complied with the profile of sham-treated *NPC1*$^{-/-}$ mice. Surprisingly, both combination and HPßCD treatment did not lead to increased numbers of TH(+) dopaminergic neurons and increased protein levels in the OB, which could otherwise be linked with impaired olfactory acuity (Huisman et al., 2004; Mundinano et al., 2011).

The slight, but not significant increase of TH(+) neurons and simultaneously constant protein content after HPßCD treatment may indicate a reduction of TH protein per cell rather than a substantial change of cell numbers, as reported by Seo et al. (2014, 2016). Also, microglia activity is able to positively influence the survival of TH(+) mesencephalic neurons (Nagata et al., 1993).

CONCLUSION

The present study sheds light on the issue, if easy- to- perform olfactory tests in patients with neurodegenerative diseases may be used as predictive or control tests for the course of a disease, e.g., in dependence of a treatment strategy. Our data in NPC1 show that both treatment approaches prevent neurodegeneration and simultaneously ameliorate olfactory dysfunction.

What is more, these investigations should be expanded to study not only prevention of neurodegenerative symptoms, but also their reversal after a later onset of treatment efforts, which seems more realistic in practice.

AUTHOR CONTRIBUTIONS

AM and MW conceived and designed the experiments. AM and AG performed the experiments. AM, AG, AB, JS, and MW analyzed the data. AM, AG, AB, MW, AR, and AW wrote the paper. All the authors read and approved the last version of the manuscript.

FUNDING

This study was supported by the Verbund Norddeutscher Universitäten to AB and MW.

ACKNOWLEDGMENTS

The authors gratefully thank Actelion Pharmaceuticals (Allschwil, Switzerland) for the gift of miglustat for experimental applications. They are especially thankful to Mathias Lietz, Susann Lehmann, and Anna-Maria Neßlauer for animal care, Robin Piecha for preparing the PCR probes and Teresa Mann, MSc, for critical reading of the manuscript.

SUPPLEMENTARY MATERIAL

The Supplementary Material for this article can be found online at: https://www.frontiersin.org/articles/10.3389/fnint.2018.00035/full#supplementary-material

FIGURE S1 | Scheme of the drug application for the combination treatment. Only mice used for immunohistochemical experiments received BrdU.

FIGURE S2 | Performance of *NPC1*$^{+/+}$ and different treated *NPC1*$^{-/-}$ mice on surface pellet test. Mean values of the latencies vary from minimum 5.16 s (sham-treated *NPC1*$^{+/+}$) to a maximum of 11.07 s (HPßCD-treated *NPC1*$^{-/-}$), indicating that all tested mice most likely have no impairments of motor skills or an altered motivation for foraging. Box plot graphs represent the mean ± SEM and depict the median, the upper and lower quartiles, and outliers (pentagon and circle). $^{*}p \leq 0.05$, $^{**}p \leq 0.01$.

FIGURE S3 | Housekeeping genes *Ppia* and *ß-Actin* were not regulated in the olfactory bulb (OB) and the olfactory epithelium (OE) of *NPC1*$^{-/-}$ mice. Determination of relative expression of certain markers and receptors require normalization to reference genes. The analyses of Cq values (cycle of quantification) resulted in *Ppia* and *ß-Actin* as appropriate housekeeping genes in the OB and OE **(A–D)**. No regulation was present between *NPC1*$^{+/+}$ and *NPC1*$^{-/-}$ mice. Data are represented as mean ± SEM, n = 10–15.

TABLE S1 | Results of the buried and the surface pellet test. Latencies are expressed as the mean values ± SEM in s.

TABLE S2 | FAM-MGB coupled Taqman probes and housekeeping genes used for quantitative RT-PCR.

TABLE S3 | Results of the BrdU(+) and TH(+) quantification of the unilateral OB. Cell densities are expressed as the mean values ± SEM in cells/mm^3.

TABLE S4 | Quantitative RT-PCR displays the relative expression of *Bax* and *Bcl2* mRNA including the *Bax/Bcl2 ratio* in the olfactory bulb (OB) of differently treated *NPC1*$^{-/-}$ mice (n = 3) compared to *NPC1*$^{+/+}$ mice (n = 3). Data are normalized to *Ppia* and represent as mean ± SEM.

REFERENCES

Alvarez-Buylla, A., and Garcia-Verdugo, J. M. (2002). Neurogenesis in adult subventricular zone. *J. Neurosci.* 22, 629–634. doi: 10.1523/JNEUROSCI.22-03-00629.2002

Attems, J., Walker, L., and Jellinger, K. A. (2015). Olfaction and aging: a mini-Review. *Gerontology* 61, 485–490. doi: 10.1159/000381619

Bader, A., Breer, H., and Strotmann, J. (2012a). Untypical connectivity from olfactory sensory neurons expressing OR37 into higher brain centers visualized by genetic tracing. *Histochem. Cell Biol.* 137, 615–628. doi: 10.1007/s00418-012-0919-2

Bader, A., Klein, B., Breer, H., and Strotmann, J. (2012b). Connectivity from OR37 expressing olfactory sensory neurons to distinct cell types in the hypothalamus. *Front. Neural Circuits.* 6:84. doi: 10.3389/fncir.2012.00084

Baker, H., Morel, K., Stone, D. M., and Maruniak, J. A. (1993). Adult naris closure profoundly reduces tyrosine hydroxylase expression in mouse olfactory bulb. *Brain Res.* 1614, 109–116. doi: 10.1016/0006-8993(93)91023-L

Barrios, F. A., Gonzalez, L., Favila, R., Alonso, M. E., Salgado, P. M., Diaz, R., et al. (2007). Olfaction and neurodegeneration in HD. *Neuroreport* 18, 73–76. doi: 10.1097/WNR.0b013e3280102302

Carstea, Morris, J. A., Coleman, K. G., Loftus, S. K., Zhang, D., Cummings, C., et al. (1997). Niemann-Pick C1 disease gene: homology to mediators of cholesterol homeostasis. *Science* 1277, 228–231. doi: 10.1126/science.277.5323.228

Chen, G., Li, H. M., Chen, Y. R., Gu, X. S., and Duan, S. (2007). Decreased estradiol release from astrocytes contributes to the neurodegeneration in a mouse model of niemann-pick disease type C. *Glia* 155, 1509–1518. doi: 10.1002/glia.20563

Cho, J. Y., Min, N., Franzen, L., and Baker, H. (1996). Rapid down-regulation of tyrosine hydroxylase expression in the olfactory bulb of naris-occluded adult rats. *J. Comp. Neurol.* 2369, 264–276. doi: 10.1002/(SICI)1096-9861(19960527)369:2<264::AID-CNE7>3.0.CO;2-1

Claudepierre, T., Paques, M., Simonutti, M., Buard, I., Sahel, J., Maue, R. A., et al. (2010). Lack of niemann-Pick type C1 induces age-related degeneration in the mouse retina. *Mol. Cell Neurosci.* 31, 164–176. doi: 10.1016/j.mcn.2009.10.007

Conzelmann, S., Levai, O., Bode, B., Eisel, U., Raming, K., Breer, H., et al. (2000). Ael brain receptor is expressed in a distinct population of olfactory sensory neurons. *Eur. J. Neurosci.* 12, 3926–3934. doi: 10.1046/j.1460-9568.2000.00286.x

Croy, I., Nordin, S., and Hummel, T. (2014). Olfactory disorders and quality of life–an updated review. *Chem. Senses.* 39, 185–194. doi: 10.1093/chemse/bjt072

Davidson, C. D., Ali, N. F., Micsenyi, M. C., Stephney, G., Renault, S., Dobrenis, K., et al. (2009). Chronic cyclodextrin treatment of murine Niemann-Pick C disease ameliorates neuronal cholesterol and glycosphingolipid storage and disease progression. *PLoS One* 4:e6951. doi: 10.1371/journal.pone.0006951

Davidson, C. D., Fishman, Y. I., Puskas, I., Szeman, J., Sohajda, T., McCauliff, L. A., et al. (2016). Efficacy and ototoxicity of different cyclodextrins in Niemann-Pick C disease. *Ann. Clin. Transl. Neurol.* 3, 366–380. doi: 10.1002/acn3.306

Djordjevic, J., Jones-Gotman, M., De Sousa, K., and Chertkow, H. (2008). Olfaction in patients with mild cognitive impairment and Alzheimer's disease. *Neurobiol. Aging.* 29, 693–706. doi: 10.1016/j.neurobiolaging.2006.11.014

Doetsch, F. (2003). The glial identity of neural stem cells. *Nat. Neurosci.* 6, 1127–1134. doi: 10.1038/nn1144

Doty, R. L. (2018). Age-related deficits in taste and smell. *Otolaryngol. Clin. N. Am.* 51, 815–825. doi: 10.1016/j.otc.2018.03.014

Doty, R. L., Deems, D. A., and Stellar, S. (1988). Olfactory dysfunction in parkinsonism: a general deficit unrelated to neurologic signs, disease stage, or disease duration. *Neurology* 38, 1237–1244. doi: 10.1212/WNL.38.8.1237

Doty, R. L., Shaman, P., Applebaum, S. L., Giberson, R., Siksorski, L., and Rosenberg, L. (1984). Smell identification ability: changes with age. *Science* 2226, 1441–1443. doi: 10.1126/science.6505700

Dover, R., and Patel, K. (1994). Improved methodology for detecting bromodeoxyuridine in cultured cells and tissue sections by immunocytochemistry. *Histochemistry* 102, 383–387. doi: 10.1007/BF00268909

Driver-Dunckley, E., Adler, C. H., Hentz, J. G., Dugger, B. N., Shill, H. A., Caviness, J. N., et al. (2014). Olfactory dysfunction in incidental Lewy body disease and Parkinson's disease. *Parkinsonism Relat. Disord.* 20, 1260–1262. doi: 10.1016/j.parkreldis.2014.08.006

Duque, A., and Rakic, P. (2011). Different effects of BrdU and (3)H-Thymidine incorporation into DNA on cell proliferation, position and fate. *J. Neurosci.* 31, 15205–15217. doi: 10.1523/JNEUROSCI.3092-11.2011

Elleder, M., Jirasek, A., Smid, F., Ledvinova, J., and Besley, G. T. (1985). Niemann-Pick disease type C, study on the nature of the cerebral storage process. *Acta Neuropathol.* 66, 325–336. doi: 10.1007/BF00690966

Garver, W. S., Francis, G. A., Jelinek, D., Shepherd, G., Flynn, J., Castro, G., et al. (2007). The National niemann-Pick C1 disease database: report of clinical features and health problems. *Am. J. Med. Genet. A* 143A, 1204–1211. doi: 10.1002/ajmg.a.31735

German, D. C., Liang, C. L., Song, T., Yazdani, U., Xie, C., and Dietschy, J. M. (2002). Neurodegeneration in the niemann-pick C mouse: glial involvement. *Neuroscience* 109, 437–450. doi: 10.1016/S0306-4522(01)00517-6

Günther, R., Schrempf, W., Hahner, A., Hummel, T., Wolz, M., Storch, A., et al. (2018). Impairment in respiratory function contributes to olfactory impairment

in amyotrophic lateral sclerosis. *Front. Neurol.* 9:79. doi: 10.3389/fneur.2018.00079

Haehner, A., Hummel, T., Hummel, C., Sommer, U., Junghanns, S., and Reichmann, H. (2007). Olfactory loss be a first sign of idiopathic Parkinson's disease. *Mov. Disord.* 322, 839–842. doi: 10.1002/mds.21413

Hawkes, C. H., Shephard, B. C., and Daniel, S. E. (1999). Is Parkinson's disease a primary olfactory disorder? *QJM* 92, 473–480.

Hoppe, R., Breer, H., and Strotmann, J. (2006). Promoter motifs of olfactory receptor genes expressed in distinct topographic patterns. *Genomics* 87, 711–723. doi: 10.1016/j.ygeno.2006.02.005

Hovakimyan, M., Maass, F., Petersen, J., Holzmann, C., Witt, M., Lukas, J., et al. (2013a). Combined therapy with cyclodextrin/allopregnanolone and miglustat improves motor but not cognitive functions in Niemann-Pick Type C1 mice. *Neuroscience* 1252, 201–211. doi: 10.1016/j.neuroscience.2013.08.001

Hovakimyan, M., Meyer, A., Lukas, J., Luo, J., Gudziol, V., Hummel, T., et al. (2013b). Olfactory deficits in niemann-Pick type C1 (NPC1) disease. *PLoS One* 8:e82216. doi: 10.1371/journal.pone.0082216

Huisman, E., Uylings, H. B., and Hoogland, P. V. (2004). A 100% increase of dopaminergic cells in the olfactory bulb explain hyposmia in Parkinson's disease. *Mov. Disord.* 19, 687–692. doi: 10.1002/mds.10713

Kaluza, J. F., Gussing, F., Bohm, S., Breer, H., and Strotmann, J. (2004). Olfactory receptors in the mouse septal organ. *J. Neurosci. Res.* 176, 442–452. doi: 10.1002/jnr.20083

Karpa, M. J., Gopinath, B., Rochtchina, E., Jie Jin, W., Cumming, R. G., Sue, C. M., et al. (2010). Prevalence and neurodegenerative or other associations with olfactory impairment in an older community. *J. Aging Health* 22, 154–168. doi: 10.1177/0898264309353066

Kennedy, B. E., LeBlanc, V. G., Mailman, T. M., Fice, D., Burton, I., Karakach, T. K., et al. (2013). Pre-symptomatic activation of antioxidant responses and alterations in glucose and pyruvate metabolism in niemann-pick type C1-deficient murine brain. *PLoS One* 8:e82685. doi: 10.1371/journal.pone.0082685

King, K. A., Gordon-Salant, S., Pawlowski, K. S., Taylor, A. M., Griffith, A. J., Houser, A., et al. (2014). Hearing loss is an early consequence of Npc1 gene deletion in the mouse model of niemann-pick disease, type C. *J. Assoc. Res. Otolaryngol.*. 15, 529–541. doi: 10.1007/s10162-014-0459-7

Klein, B., Bautze, V., Maier, A. M., Deussing, J., Breer, H., and Strotmann, J. (2015). Activation of the mouse odorant receptor 37 subsystem coincides with a reduction ofel environment-induced activity within the paraventricular nucleus of the hypothalamus. *Eur. J. Neurosci.* 41, 793–801. doi: 10.1111/ejn.12838

Korsmeyer, S. J. (1999). BCL-2 gene family and the regulation of programmed cell death. *Cancer Res.* 59, 1693s–1700s.

Kubick, S., Strotmann, J., Andreini, I., and Breer, H. (1997). Subfamily of olfactory receptors characterized by unique structural features and expression patterns. *J. Neurochem.* 69, 465–475. doi: 10.1046/j.1471-4159.1997.69020465.x

Lehmkuhl, M. J., Normann, R. A., and Maynard, E. M. (2003). High-resolution analysis of the spatio-temporal activity patterns in rat olfactory bulb evoked by enantiomer odors. *Chem. Senses* 1, 499–508. doi: 10.1093/chemse/28.6.499

Liu, B., Ramirez, C. M., Miller, A. M., Repa, J. J., Turley, S. D., and Dietschy, J. M. (2010). Cyclodextrin overcomes the transport defect in nearly every organ of NPC1 mice leading to excretion of sequestered cholesterol as bile acid. *J. Lipid. Res.* 51, 933–944. doi: 10.1194/jlr.M000257

Lledo, P. M., Alonso, M., and Grubb, M. S. (2006). Adult neurogenesis and functional plasticity in neuronal circuits. *Nat. Rev. Neurosci.* 7, 179–193. doi: 10.1038/nrn1867

Maarup, T. J., Chen, A. H., Porter, F. D., Farhat, N. Y., Ory, D. S., Sidhu, R., et al. (2015). Intrathecal 2-hydroxypropyl-beta-cyclodextrin in a single patient with niemann-pick C1. *Mol. Genet. Metab.* 116, 75–79. doi: 10.1016/j.ymgme.2015.07.001

Maass, F., Petersen, J., Hovakimyan, M., Schmitt, O., Witt, M., Hawlitschka, A., et al. (2015). Reduced cerebellar neurodegeneration after combined therapy with cyclodextrin/allopregnanolone and miglustat in NPC1: a mouse model of Niemann-Pick type C1 disease. *J. Neurosci. Res.* 93, 433–442. doi: 10.1002/jnr.23509

Mackay-Sim, A., St John, J., and Schwob, J. E. (2015). "Neurogenesis in the adult olfactory epithelium," in *Handbook of Olfaction and Gustation*, 3rd Edn, ed. R. L. Doty (Hoboken, NJ: John Wiley & Sons), 133–156. doi: 10.1002/9781118971758.ch7

Marin, C., Vilas, D., Langdon, C., Alobid, I., López-Chacón, M., Haehner, A., et al. (2018). Olfactory dysfunction in neurodegenerative diseases. *Curr. Allergy Asthma Rep.* 18:42. doi: 10.1007/s11882-018-0796-4

Matsuo, M., Togawa, M., Hirabaru, K., Mochinaga, S., Narita, A., Adachi, M., et al. (2013). Effects of cyclodextrin in two patients with niemann-pick type C disease. *Mol. Genet. Metab.* 108, 76–81. doi: 10.1016/j.ymgme.2012.11.005

McNeill, A., Duran, R., Proukakis, C., Bras, J., Hughes, D., Mehta, A., et al. (2012). Hyposmia and cognitive impairment in Gaucher disease patients and carriers. *Mov. Disord.* 27, 526–532. doi: 10.1002/mds.24945

Mesholam, R. I., Moberg, P. J., Mahr, R. N., and Doty, R. L. (1998). Olfaction in neurodegenerative disease: a meta-analysis of olfactory functioning in Alzheimer's and Parkinson's diseases. *Arch. Neurol.* 55, 84–90. doi: 10.1001/archneur.55.1.84

Meyer, A., Wree, A., Günther, R., Holzmann, C., Schmitt, O., Rolfs, A., et al. (2017). Increased regenerative capacity of the olfactory epithelium in niemann-pick disease type C1. *Int. J. Mol. Sci.* 18:E777. doi: 10.3390/ijms18040777

Moberg, P. J., Pearlson, G. D., Speedie, L. J., Lipsey, J. R., Strauss, M. E., and Folstein, S. E. (1987). Olfactory recognition: differential impairments in early and late Huntington's and Alzheimer's diseases. *J. Clin. Exp. Neuropsychol.* 9, 650–664. doi: 10.1080/01688638708405208

Mundinano, I. C., Caballero, M. C., Ordonez, C., Hernandez, M., DiCaudo, C., Marcilla, I., et al. (2011). Increased dopaminergic cells and protein aggregates in the olfactory bulb of patients with neurodegenerative disorders. *Acta Neuropathol.* 122, 61–74. doi: 10.1007/s00401-011-0830-2

Nadi, N. S., Head, R., Grillo, M., Hempstead, J., Grannot-Reisfeld, N., and Margolis, F. L. (1981). Chemical deafferentation of the olfactory bulb: plasticity of the levels of tyrosine hydroxylase, dopamine and norepinephrine. *Brain Res.* 213, 365–377. doi: 10.1016/0006-8993(81)90241-9

Nagata, K., Takei, N., Nakajima, K., Saito, H., and Kohsaka, S. (1993). Microglial conditioned medium promotes survival and development of cultured mesencephalic neurons from embryonic rat brain. *J. Neurosci. Res.* 134, 357–363. doi: 10.1002/jnr.490340313

Nef, P., Hermans-Borgmeyer, I., Artieres-Pin, H., Beasley, L., Dionne, V. E., and Heinemann, S. F. (1992). Spatial pattern of receptor expression in the olfactory epithelium. *Proc. Natl. Acad. Sci. U.S.A.* 89, 8948–8952. doi: 10.1073/pnas.89.19.8948

Oltvai, Z. N., Milliman, C. L., and Korsmeyer, S. J. (1993). Bcl-2 heterodimerizes in vivo with a conserved homolog, Bax, that accelerates programmed cell death. *Cell* 274, 609–619. doi: 10.1016/0092-8674(93)90509-O

Onda, K., Davis, R. L., Shibuya, M., Wilson, C. B., and Hoshino, T. (1994). Correlation between the bromodeoxyuridine labeling index and the MIB-1 and Ki-67 proliferating cell indices in cerebral gliomas. *Cancer* 074, 1921–1926. doi: 10.1002/1097-0142(19941001)74:7<1921::AID-CNCR2820740716>3.0.CO;2-9

Patterson, M. C., Vecchio, D., Prady, H., Abel, L., and Wraith, J. E. (2007). Miglustat for treatment of niemann-pick C disease: a randomised controlled study. *Lancet Neurol.* 6, 765–772. doi: 10.1016/S1474-4422(07)70194-1

Platt, F. M., and Jeyakumar, M. (2008). Substrate reduction therapy. *Acta Paediatr. Suppl.* 97, 88–93. doi: 10.1111/j.1651-2227.2008.00656.x

Ramirez, C. M., Liu, B., Taylor, A. M., Repa, J. J., Burns, D. K., Weinberg, A. G., et al. (2010). Weekly cyclodextrin administration normalizes cholesterol metabolism in nearly every organ of the niemann-pick type C1 mouse and markedly prolongs life. *Pediatr. Res.* 68, 309–315. doi: 10.1203/00006450-201011001-00604

Regensburger, M., Kohl, Z., Grundmann, K., Winner, B., Riess, O., and Winkler, J. (2009). Adult neural precursor cells unaffected in animal models of DYT1 dystonia. *Neuroreport* 220, 1529–1533. doi: 10.1097/WNR.0b013e328331c761

Ressler, K. J., Sullivan, S. L., and Buck, L. B. (1993). A zonal organization of odorant receptor gene expression in the olfactory epithelium. *Cell* 73, 597–609. doi: 10.1016/0092-8674(93)90145-G

Rey, N. L., Wesson, D. W., and Brundin, P. (2018). The olfactory bulb as the entry site for prion-like propagation in neurodegenerative diseases. *Neurobiol. Dis.* 109, 226–248. doi: 10.1016/j.nbd.2016.12.013

Ross, G. W., Petrovitch, H., Abbott, R. D., Tanner, C. M., Popper, J., Masaki, K., et al. (2008). Association of olfactory dysfunction with risk for future Parkinson's disease. *Ann. Neurol.* 63, 167–173. doi: 10.1002/ana.21291

Salakou, S., Kardamakis, D., Tsamandas, A. C., Zolota, V., Apostolakis, E., Tzelepi, V., et al. (2007). Increased Bax/Bcl-2 ratio up-regulates caspase-3 and

increases apoptosis in the thymus of patients with myasthenia gravis. *In Vivo.* 21, 123–132.

Sarna, J. R., Larouche, M., Marzban, H., Sillitoe, R. V., Rancourt, D. E., and Hawkes, R. (2003). Patterned Purkinje cell degeneration in mouse models of niemann-pick type C disease. *J. Comp. Neurol.* 1456, 279–291. doi: 10.1002/cne.10522

Schlegel, V., Thieme, M., Holzmann, C., Witt, M., Grittner, U., Rolfs, A., et al. (2016). Pharmacologic treatment assigned for niemann pick type C1 disease partly changes behavioral traits in wild-type mice. *Int. J. Mol. Sci.* 17:E1866. doi: 10.3390/ijms17111866

Schwob, J. E. (2002). Neural regeneration and the peripheral olfactory system. *Anat. Rec.* 269, 33–49. doi: 10.1002/ar.10047

Scopa, C. D., Vagianos, C., Kardamakis, D., Kourelis, T. G., Kalofonos, H. P., and Tsamandas, A. C. (2001). bcl-2/bax ratio as a predictive marker for therapeutic response to radiotherapy in patients with rectal cancer. *Appl. Immunohistochem. Mol. Morphol.* 9, 329–334. doi: 10.1097/00129039-200112000-00007

Seo, Y., Kim, H. S., Kang, I., Choi, S. W., Shin, T. H., Shin, J. H., et al. (2016). Cathepsin S contributes to microglia-mediated olfactory dysfunction through the regulation of Cx3cl1-Cx3cr1 axis in a Niemann-Pick disease type C1 model. *Glia* 64, 2291–2305. doi: 10.1002/glia.23077

Seo, Y., Kim, H.-S., Shin, Y., Kang, I., Choi, S. W., Yu, K.-R., et al. (2014). Excessive microglial activation aggravates olfactory dysfunction by impeding the survival of newborn neurons in the olfactory bulb of niemann–pick disease type C1 mice. *Biochim. Biophys. Acta (BBA) – Mol. Basis Dis.* 1842, 2193–2203. doi: 10.1016/j.bbadis.2014.08.005

Spiegel, R., Raas-Rothschild, A., Reish, O., Regev, M., Meiner, V., Bargal, R., et al. (2009). The clinical spectrum of fetal niemann-pick type C. *Am. J. Med. Genet. A* 149A, 446–450. doi: 10.1002/ajmg.a.32642

Stone, D. M., Wessel, T., Joh, T. H., and Baker, H. (1990). Decrease in tyrosine hydroxylase, but not aromatic L-amino acid decarboxylase, messenger RNA in rat olfactory bulb following neonatal, unilateral odor deprivation. *Brain Res. Mol. Brain Res.* 8, 291–300. doi: 10.1016/0169-328X(90)90042-C

Strotmann, J., Bader, A., Luche, H., Fehling, H. J., and Breer, H. (2009). The patch-like pattern of OR37 receptors is formed by turning off gene expression in non-appropriate areas. *Mol. Cell Neurosci.* 41, 474–485. doi: 10.1016/j.mcn.2009.05.005

Strotmann, J., Conzelmann, S., Beck, A., Feinstein, P., Breer, H., and Mombaerts, P. (2000). Local permutations in the glomerular array of the mouse olfactory bulb. *J. Neurosci.* 120, 6927–6938. doi: 10.1523/JNEUROSCI.20-18-06927.2000

Strotmann, J., Levai, O., Fleischer, J., Schwarzenbacher, K., and Breer, H. (2004). Olfactory receptor proteins in axonal processes of chemosensory neurons. *J. Neurosci.* 24, 7754–7761. doi: 10.1523/JNEUROSCI.2588-04.2004

Strotmann, J., Wanner, I., Helfrich, T., Beck, A., Meinken, C., Kubick, S., et al. (1994). Olfactory neurones expressing distinct odorant receptor subtypes are spatially segregated in the nasal neuroepithelium. *Cell Tissue Res.* 276, 429–438. doi: 10.1007/BF00343941

Strotmann, J., Wanner, I., Helfrich, T., and Breer, H. (1995). Receptor expression in olfactory neurons during rat development: in situ hybridization studies. *Eur. J. Neurosci.* 7, 492–500. doi: 10.1111/j.1460-9568.1995.tb00345.x

Strotmann, J., Wanner, I., Krieger, J., Raming, K., and Breer, H. (1992). Expression of odorant receptors in spatially restricted subsets of chemosensory neurones. *Neuroreport* 3, 1053–1056. doi: 10.1097/00001756-199212000-00005

Sui, Y., Horne, M. K., and Stanic, D. (2012). Reduced proliferation in the adult mouse subventricular zone increases survival of olfactory bulb interneurons. *PLoS One* 7:e31549. doi: 10.1371/journal.pone.0031549

Sullivan, S. L., Adamson, M. C., Ressler, K. J., Kozak, C. A., and Buck, L. B. (1996). The chromosomal distribution of mouse odorant receptor genes. *Proc. Natl. Acad. Sci. U.S.A.* 293, 884–888. doi: 10.1073/pnas.93.2.884

Suzuki, H., Sakiyama, T., Harada, N., Abe, M., and Tadokoro, M. (2003). Pathologic changes of glial cells in murine model of niemann-pick disease type C: immunohistochemical, lectin-histochemical and ultrastructural observations. *Pediatr. Int.* 45, 1–4. doi: 10.1046/j.1442-200X.2003.01651.x

Tanaka, J., Nakamura, H., and Miyawaki, S. (1988). Cerebellar involvement in murine sphingomyelinosis: a new model of niemann-pick disease. *J. Neuropathol. Exp. Neurol.* 47, 291–300. doi: 10.1097/00005072-198805000-00008

Tanaka, Y., Yamada, Y., Ishitsuka, Y., Matsuo, M., Shiraishi, K., Wada, K., et al. (2015). Efficacy of 2-hydroxypropyl-beta-cyclodextrin in niemann-pick disease type C model mice and its pharmacokinetic analysis in a patient with the disease. *Biol. Pharm. Bull.* 38, 844–851. doi: 10.1248/bpb.b14-00726

Vanier, M. T., and Millat, G. (2003). Niemann-pick disease type C. *Clin. Genet.* 64, 269–281. doi: 10.1034/j.1399-0004.2003.00147.x

Vassar, R., Ngai, J., and Axel, R. (1993). Spatial segregation of odorant receptor expression in the mammalian olfactory epithelium. *Cell* 374, 309–318. doi: 10.1016/0092-8674(93)90422-M

Velmans, T., Battefeld, A., Geist, B., Farres, A. S., Strauss, U., and Brauer, A. U. (2013). Plasticity-related gene 3 promotes neurite shaft protrusion. *BMC Neurosci.* 114:36. doi: 10.1186/1471-2202-14-36

Vierk, R., Glassmeier, G., Zhou, L., Brandt, N., Fester, L., Dudzinski, D., et al. (2012). Aromatase inhibition abolishes LTP generation in female but not in male mice. *J. Neurosci.* 132, 8116–8126. doi: 10.1523/JNEUROSCI.5319-11.2012

Winner, B., Cooper-Kuhn, C. M., Aigner, R., Winkler, J., and Kuhn, H. G. (2002). Long-term survival and cell death of newly generated neurons in the adult rat olfactory bulb. *Eur. J. Neurosci.* 16, 1681–1689. doi: 10.1046/j.1460-9568.2002.02238.x

Yan, X., Ma, L., Hovakimyan, M., Lukas, J., Wree, A., Frank, M., et al. (2014). Defects in the retina of niemann-pick type C 1 mutant mice. *BMC Neurosci.* 215:126. doi: 10.1186/s12868-014-0126-2

Conflict of Interest Statement: The authors declare that the research was conducted in the absence of any commercial or financial relationships that could be construed as a potential conflict of interest.

Copyright © 2018 Meyer, Gläser, Bräuer, Wree, Strotmann, Rolfs and Witt. This is an open-access article distributed under the terms of the Creative Commons Attribution License (CC BY). The use, distribution or reproduction in other forums is permitted, provided the original author(s) and the copyright owner(s) are credited and that the original publication in this journal is cited, in accordance with accepted academic practice. No use, distribution or reproduction is permitted which does not comply with these terms.

frontiers in Behavioral Neuroscience

ORIGINAL RESEARCH
published: 27 August 2018
doi: 10.3389/fnbeh.2018.00185

Optogenetic Stimulation of GABAergic Neurons in the Globus Pallidus Produces Hyperkinesia

*Jun Tian[1], Yaping Yan[1], Wang Xi[2], Rui Zhou[2], Huifang Lou[2], Shumin Duan[2], Jiang Fan Chen[3] and Baorong Zhang[1]**

[1] Second Affiliated Hospital, Zhejiang University School of Medicine, Hangzhou, China, [2] Department of Neurobiology, School of Medicine, Zhejiang University, Hangzhou, China, [3] School of Ophthalmology and Optometry, Wenzhou Medical University, Wenzhou, China

The globus pallidus (GP) is emerging as a critical locus of basal ganglia control of motor activity, but the exact role of GABAergic GP neurons remain to be defined. By targeted expression of channelrhodopsin 2 (ChR2) in GABAergic neurons using the VGAT-ChR2-EYFP transgenic mice, we showed that optogenetic stimulation of GABAergic neurons in the right GP produced hyperkinesia. Optogenetic stimulation of GABAergic GP neurons increased c-Fos-positive cells in GP, M1 cortex, and caudate-putamen (CPu), and decreased c-Fos-positive cells in entopeduncular nucleus (EPN), compared to the contralateral hemisphere. In agreement with the canonical basal ganglia model. Furthermore, we delivered AAV-CaMKIIα-ChR2-mCherry virus to the excitatory neurons of the subthalamic nucleus (STN) and selectively stimulated glutamatergic afferent fibers from the STN onto the GP. This optogenetic stimulation produced abnormal movements, similar to the behaviors that observed in the VGAT-ChR2-EYFP transgenic mice. Meanwhile, we found that the c-Fos expression pattern in the GP, M1, STN, EPN, and CPu produced by optogenetic activation of glutamatergic afferent fibers from the STN in GP was similar to the c-Fos expression pattern in the VGAT-ChR2-EYFP transgenic mice. Taken together, our results suggest that excess GP GABAergic neurons activity could be the neural substrate of abnormal involuntary movements in hyperkinetic movement disorders. The neural circuitry underlying the abnormal involuntary movements is associated with excessive GP, M1, CPu activity, and reduced EPN activity. Inhibition of GP GABAergic neurons represents new treatment targets for hyperkinetic movement disorder.

Keywords: optogenetic stimulation, GABAergic neurons, hyperkinesia, movement disorders, globus pallidus

OPEN ACCESS

Edited by:
Caroline Whyatt, Rutgers University, The State University of New Jersey, United States

Reviewed by:
Masahiko Takada, Kyoto University, Japan
Jose Bargas, Universidad Nacional Autónoma de México, Mexico
Yasuyuki Ishikawa, Maebashi Institute of Technology, Japan
Zhimin Song, Emory University, United States

***Correspondence:**
Baorong Zhang
brzhang@zju.edu.cn

Received: *27 August 2017*
Accepted: *02 August 2018*
Published: *27 August 2018*

Citation:
Tian J, Yan Y, Xi W, Zhou R, Lou H, Duan S, Chen JF and Zhang B (2018) Optogenetic Stimulation of GABAergic Neurons in the Globus Pallidus Produces Hyperkinesia. Front. Behav. Neurosci. 12:185. doi: 10.3389/fnbeh.2018.00185

INTRODUCTION

The basal ganglia (BG), consisting of the striatum; the internal and external globus pallidus (GPi and GPe), which are also referred to as the globus pallidus (GP) and the entopeduncular nucleus (EPN) in rodents; the subthalamic nucleus (STN) and the substantianigra (SN), receives and processes cortical inputs and in return regulates cortical activity (Albin et al., 1989). The BG plays an important role in motor control through the direct and indirect pathways with ~~the~~ coordinated activity but often opposite effects on movement; the direct pathway selects

specific motor programs/actions to facilitate movement, whereas the indirect pathway suppresses undesired motor programs (Albin et al., 1989; Chevalier and Deniau, 1990; Hikosaka, 2007; Gerfen and Surmeier, 2011; Rothwell, 2011). Consistent with the classical model of the basal ganglia, optogenetic activation of the striatal media spiny neurons (MSNs) in the direct pathway increases ambulation, while activation of the striatal MSNs in the indirect pathway decreases ambulation (Kravitz et al., 2010). The GP is traditionally considered as a homogeneous relay component of the "indirect pathway" (Albin et al., 1989; Gittis et al., 2014), but it is increasingly recognized as the central "hub" (Qiu et al., 2010, 2016; Goldberg and Bergman, 2011; Gittis et al., 2014) for its centrally placed structure in the basal ganglia that receives inputs from and projects to all major BG components (Grillner et al., 2005; Nambu, 2008; Goldberg and Bergman, 2011). The GP receives major GABAergic input through the afferent fibers from the striatopallidal projection neurons and glutamatergic input from the afferent fibers from the STN (Kita, 2007). The critical role of the GP in the control of movement is illustrated by the abnormal activity of GP neurons in movement disorders, including the increased firing rates in the GP in Huntington's disease (Starr et al., 2008) and beta oscillations of the GP neurons in Parkinson's disease (PD) (Mallet et al., 2008). Consistent with the critical role of the GP in basal ganglia circuits and behavior, quinolinic acid lesion of the GP leads to a decrease in spontaneous movement (Hauber et al., 1998) and activation of GP neurons by the microinjection of the GABAA receptor antagonist bicuculline (Matsumura et al., 1995) into the GP induces spontaneous movement (Grabli et al., 2004) and dyskinesia in primates (Crossman et al., 1984; Bronfeld et al., 2010).

However, the GP control of motor activity is complex since motor suppression has been associated with either electrophysiological pause (Kita and Kita, 2011), increased firing rate (Starr et al., 2008), or beta-oscillation (Pavlides et al., 2012). The firing rates of pallidal neurons are similar in Huntington's (with the increased abnormal movements) and PD patients (with reduced motor activity) (Tang et al., 2005). Studies with neurotoxin lesion and pharmacological activation have also produced results that are not consistent with the model. For example, GP lesion in rats increases (rather than decreases) spontaneous movement (Norton, 1976; Joel et al., 1998; Qiu et al., 2016). These mixed results, in part, reflect the complex neuronal connections of the GP with other structures of the basal ganglia and the molecular and functional diversity of GP neurons that contribute to motor and non-motor features of behavior (Mallet et al., 2012; Gittis et al., 2014; Mastro et al., 2014). The exact function of the GP in motor control largely remains to be defined.

The difficulty in defining GP function is, in part, due to technical limitations in selectively manipulating defined elements of the GP circuit in freely moving animals. The GP has heterogeneous neuronal populations; a majority of GP neurons (∼95%) are GABAergic neurons, while a minority of GP neurons (∼5%) are cholinergic neurons (Hegeman et al., 2016). GP GABAergic neurons can be divided into two classes based on their firing patterns, which are termed ~~as~~ "prototypical" neurons and "arkypallidal" neurons (Mallet et al., 2008; Abdi et al., 2015; Dodson et al., 2015). The prototypical and arkypallidal neurons project to distinct targets. The prototypical neurons project to STN and EPN, whereas arkypallidal neurons only project to the striatum (Mallet et al., 2012). The two populations of GABAergic GP neurons express different sets of transcription factors and have different roles (Abdi et al., 2015; Bahuguna et al., 2017; Lindahl and HellgrenKotaleski, 2017). A recent study found that activation of arkypallidal neurons suppressed motor output (Glajch et al., 2016). The exact role of GABAergic GP neurons in motor control is still unclear. Using the recently developed optogenetics (Boyden et al., 2005; Zhang et al., 2010) for manipulating the intrinsic GABAergic neurons in GP and glutamatergic afferents from STN in freely moving mice, we investigate the role of GABAergic GP neurons in the control of movement.

MATERIALS AND METHODS

Animals

The experiments were performed on 8- to 10-week-old mice. The VGAT-ChR2-EYFP mice were obtained from MinminLuo's laboratory at Beijing University, China (Zhao et al., 2011). In these mice, channelrhodopsin-2 (ChR2) was expressed in neurons under control of the vesicular GABA transporter (VGAT) promoter. VGAT was expressed by GABAergic neurons (Zhao et al., 2011) so that optical stimulation in these mice selectively stimulated GABAergic neurons. In addition, because the ChR2 was fused to EYFP, EYFP fluorescence was used to visualize the cellular localization of ChR2 (Henderson et al., 2014). All procedures were performed in accordance with the guidelines of the Zhejiang University Animal Experimentation Committee. This committee approved the experiments.

Surgery

The mice were anesthetized with pentobarbital sodium (80 mg/kg, Sigma-Aldrich) and fixed to a stereotaxic apparatus (Stoelting). The guide cannula (RWD Life Science) was unilaterally implanted into the right GP [(Anterior–Posterior (AP): −0.3 mm, Medial–Lateral (ML): +1.9 mm, Dorsal-Ventral (DV): 2.6 mm) (according to the mouse brain in Stereotaxic Coordinates; Paxinos and Franklin, 2001)]. Four skull screw holes were drilled, and tightly fitting screws were driven through the skull until the surface of the dura was reached. Both the cannula and the stainless steel anchoring screws were fixed to the skull with dental cement. After the surgical procedures, the animals were allowed to recover in individual chambers for at least 7 days. During experimentation, each animal was transferred to a chamber and connected to an optical fiber.

EEG Recording

The animals were also implanted with a custom-made electroencephalogram (EEG) unit, which was placed on the rear of the skull, posterior to the site of cannula implantation. EEG signals were recorded from electrodes placed on the M1 cortex (AP: +2.1 mm, ML: +2.0 mm). The EEG signals from the implanted electrodes were monitored using the headstage of an

EEG recording system (RM6240). Fast Fourier Transform (FFT) analyses were performed to determine the frequency spectrum.

Virus Injections

The AAV-CaMKIIα-ChR2-mCherry virus, which expressed ChR2 fused to the mCherry fluorescent protein under the control of the CaMKIIα promoter, was purchased from Shanghai SBO Medical Biotechnology. The virus was stereotaxically injected into eight C57/BL6 mice. The virus (0.3 μl) was injected into the right STN (AP: −1.8 mm, ML: +1.8 mm, DV: 3.6 mm) using Quintessential Stereotaxic Injector (Stoelting) at 40 nl/min. The mice were allowed to recover from the injection for 2 weeks for maximal virus expression prior to behavioral assessments.

In vivo Optical Stimulation and Behavioral Tests

The optical fiber (0.2 mm in diameter) was inserted into the implanted cannula, and pulse trains of light (473 nm, 5–12 mW, 5 ms pulses at 20 Hz for 30 s) were delivered. The behavioral activities of the mice in response to optical stimulation were continuously observed and analyzed in the home cages. Eight types of behaviors were evaluated during the 30-s period that preceded optical stimulation, as well as during optical stimulation. The behaviors were defined as follows: (1) resting (awake without movements); (2) grooming; (3) exploration (moving in the cage); (4) licking; (5) chewing; (6) torsion spasms; (7) turning left; and (8) turning right. The duration of each behavior was quantified. Detailed behavioral analyses were performed offline using the recorded video. The analysis was made independently by two members of the laboratory who were blind to the treatments (none of the authors). Eight VGAT-ChR2-EYFP mice and eight mice infected with AAV-CaMKIIα-ChR2-mCherry were used to do the behavioral tests.

Immunohistochemistry

To verify the targeted expression of the ChR2-expressing neurons in the GP and STN and their projections in the GP, the mice were anesthetized with pentobarbital sodium (160 mg/kg, Sigma-Aldrich) and transcardially perfused with physiological saline, followed by 4% paraformaldehyde. The brains were post-fixed in 4% paraformaldehyde overnight at 4°C. Coronal sections (30 μm) were treated with 0.3% Triton X-100 and placed in a PBS blocking solution containing 5% bovine serum albumin for 1 h at room temperature. The sections were then incubated with primary antibodies (mouse anti-GAD67, 1:1,000, millipore; goat anti-CaMKIIα, 1:500, abcam) in blocking solution for 1 day at 4°C. The sections were then washed in PBS three times for 5 min each and incubated for 2 h at room temperature with FITC-, Cy3-, or Cy5-conjugated secondary antibodies (1:1,000, SIGMA). To determine c-Fos immunoreactivity in the basal ganglia and cortex, the mice were continuously stimulated (5-ms pulses at 20 Hz) for 10 min and transcardially perfused 90 min later. After the sectioning and blocking procedures described above were completed, the sections were incubated with the primary antibody (rabbit anti-c-Fos, 1:500, calbiochem) for 1 day at 4°C. Then, the sections were washed in PBS three times for 5 min each and incubated for 2 h at room temperature with the Cy3-conjugated or Alexa 448-conjugated secondary antibody (1:1,000, SIGMA). The sections were then rinsed in 90% glycerol and coverslipped, and the immunostained neurons were analyzed. Ten VGAT-ChR2-EYFP mice, 10 wild-type mice, and eight mice infected with AAV-CaMKIIα-ChR2-mCherry were used for c-Fos immunohistochemistry. Three brain sections containing the GP (at −0.3 mm bregma), M1 (at 2.1 mm bregma), EPN (at −1.3 mm bregma), STN (at −1.8 mm bregma), and dorsal striatum (caudate-putamen, CPu) (at +0.3 mm bregma) per mouse were selected to count c-Fos-positive neurons. For each brain section, the total number of c-Fos-positive neurons in a given brain structure was counted and divided by the area occupied by this structure (in square millimeters) to obtain a density (number of c-Fos-positive neurons/area in square millimeters). c-Fos-positive neuron counts were performed at 20X magnification by an observer who was blind to the experimental treatment. Three sections for each area per mouse were analyzed. The resulting values were averaged for each area per mouse, and these averages were compared across groups.

Statistical Analysis

Behavioral studies were analyzed using a paired, two-tailed *t*-test. The paired, two-tailed *t*-test was performed both prior to and during optical stimulation. For c-Fos expression data, another paired, two-tailed *t*-test was performed between the sides ipsilateral and contralateral to the optical stimulation of mice transfected with AAV-CaMKIIa-ChR2 in STN. A two-way ANOVA, followed by *post-hoc* Tukey's test, was performed among three groups of VGAT-ChR2-EYFP transgenic mice and wild-type control mice. Statistical analysis was performed with SPSS version 17. $P < 0.05$ was taken to be statistically significant. The specific tests used were noted in the text and figure legends.

RESULTS

Optical Stimulation of GABaergic Neurons in the Right GP Produced Hyperkinesia

We first verified that ChR2 expression was restricted to GABAergic neurons under control of VGAT promoter, which directed the selective expression of ChR2 in GABAergic and glycinergic neurons (Chaudhry et al., 1998) in the VGAT-ChR2-EYFP transgenic mice (Zhao et al., 2011). Consistent with the previous report (Zhao et al., 2011), we found that ChR2 was selectively expressed in GP GABAergic neurons as indicated by the co-localization of ChR2 and GAD67 (a marker for GABAergic neurons) in GP in the VGAT-ChR2-EYFP transgenic mice (**Figure 1A**). Thus, we employed the VGAT-ChR2-EYFP transgenic mouse line to manipulate the activity of GABAergic neurons for studying the behavioral response to light (ChR2) stimulation.

We applied 5-ms pulses of photostimulation at 20 Hz for 10–30 s to activate ChR2 in the GP GABAergic neurons and found that the mice developed dystonia-like, hyperkinetic motor symptoms (dystonia-like posture, repetitive grooming, licking, chewing, and circling left) in response to ChR2

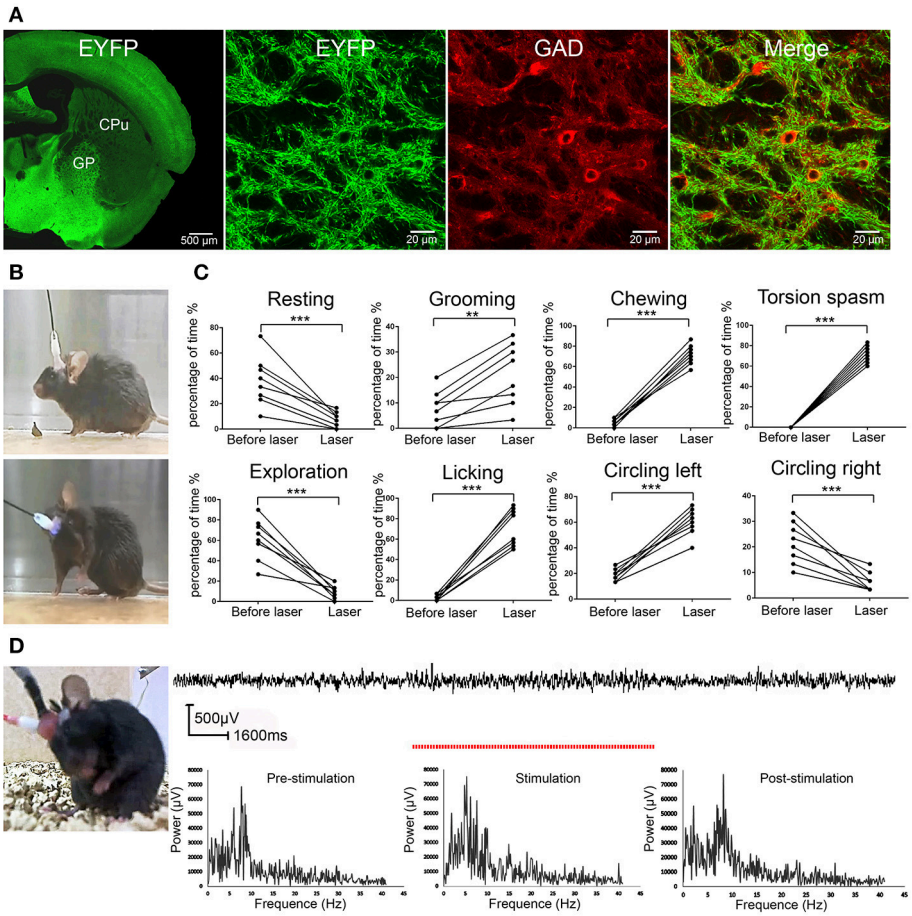

FIGURE 1 | ChR2 activation of the GP GABAergic neurons induced dystonia-like behaviors in VGAT-ChR2-EYFP transgenic mice. **(A)** Specific expression of ChR2 in GP GABAergic neurons in VGAT-ChR2-EYFP transgenic mice. The confocal images show that GP GABAergic neurons expressed ChR2-EYFP and were co-stained with GAD67. **(B)** The mouse did not show any abnormal performance before light stimulation (upper panel) and showed torsion of the neck and forelimb after light stimulation of the right GP (lower panel). The symptoms could be seen more clearly in the video (**Video S1**). **(C)** The percentage of the 30-s period the animal spent engaging in each behavior. During optical stimulation of the right GP, the VGAT-ChR2-EYFP transgenic mice displayed more grooming, licking, chewing, dystonia-like behaviors (torsion of the neck and left forelimb) and circling left, and displayed less resting, exploration and circling right, compared to that prior to light stimulation [$^{**}p < 0.01$, $^{***}p < 0.001$, $n = 8$, using a paired, two-tailed *t*-test; grooming: $t_{(7)} = -4.989$, $p = 0.002$; licking: $t_{(7)} = -10.728$, $p < 0.001$; chewing: $t_{(7)} = -18.466$, $p < 0.001$; torsion spasm: $t_{(7)} = -24.826$, $p < 0.001$; circling left: $t_{(7)} = -10.458$, $p < 0.001$; resting: $t_{(7)} = 5.255$, $p = 0.001$; exploration: $t_{(7)} = 6.844$, $p < 0.001$; circling right; $t_{(7)} = 5.624$, $p = 0.001$]. **(D)** EEG recording in the M1 cortex from a mouse that developed dystonia-like behaviors. The EEG signal in the M1 cortex did not show any sign of epileptic activity. The red dashed line represents the time of optical stimulation. Power spectrum of EEG signals recorded before, during, and after stimulus are depicted. There was no apparent increased power for the frequency range from 0.5 to 40 Hz during the stimulus.

stimulation (**Figure 1B**; **Video S1**). To quantify the abnormal behaviors produced by ChR2 stimulation, we adapted the following behavioral rating system: 1. resting (awake without movement); 2. grooming (cleaning its whiskers with its forelimbs); 3. exploration; 4. licking; 5. chewing; 6. torsion spasm; 7. circling left; and 8. circling right. The duration of the eight types of behavior was quantified in 30-s segments during ChR2 stimulation and over a 30-s control period before ChR2 stimulation. Under normal conditions, the mice primarily displayed resting, explorative, and grooming behaviors. During optical stimulation of the right GP, the VGAT-ChR2-EYFP transgenic mice displayed more stereotyped movements (grooming, licking, and chewing), as well as dystonia-like behaviors (torsion of the neck and left forelimb) and circling left, and displayed less resting, exploration and circling right, compared to that prior to light stimulation [$^{**}p < 0.01$; $^{***}p < 0.001$; $n = 8$, using a paired, two-tailed *t*-test; grooming: $t_{(7)} = -4.989$, $p = 0.002$; licking: $t_{(7)} = -10.728$, $p < 0.001$; chewing: $t_{(7)} = -18.466$, $p < 0.001$; torsion spasm: $t_{(7)} = -24.826$, $p < 0.001$; circling left: $t_{(7)} = -10.458$, $p < 0.001$; resting: $t_{(7)} = 5.255$, $p = 0.001$; exploration: $t_{(7)} = 6.844$, $p < 0.001$; circling right; $t_{(7)} = 5.624$, $p = 0.001$] (**Figure 1C**). To exclude the possible epileptic effect of ChR2 stimulation in GP GABAergic neurons, we also simultaneously recorded EEGs from M1 cortex in the mice ($n = 8$) that developed dystonia-like behaviors under ChR2 stimulation. When the mice displayed dystonia-like behaviors, the EEG from M1 showed no sign of epileptic activities, indicating that the dystonia-like behaviors were not

caused by seizures. We also performed FFT analyses on original EEG signals to determine the frequency spectra. There was no apparent increased power for the frequency range from 0.5 to 40 Hz during the stimulus. An example of EEG recordings is represented in **Figure 1D**.

ChR2 Stimulation of the GP GABaergic Neurons Produced the Network Level Changes of the Basal Ganglia Circuit, as Indicated by c-Fos Expression in the GP, M1, EPN, STN, and CPu

Next, we used c-Fos as a marker for neuronal activity to determine the influence of GP GABAergic neuron activation on the basal ganglia network level activities. The right GP was optically stimulated, and c-Fos expression in the GP, EPN, M1, STN, and CPu was determined and compared between the two hemispheres of the VGAT-ChR2-EYFP transgenic mice and the light-exposed hemisphere of wild-type mice (control). The c-Fos-expressing neurons in the GP were all GAD67-positive neurons (**Figures 2A,B**), indicating that optical stimulation activated GP GABAergic neurons. ChR2 stimulation of right side GP GABAergic neurons increased the c-Fos-positive neurons in the ipsilateral GP, M1 and CPu, and decreased the c-Fos-positive neurons in the ipsilateral EPN, compared to the contralateral side. There was no statistically significant difference between the c-Fos-positive neurons in the ipsilateral STN and contralateral side ($n = 10$, two-way ANOVA followed by *post-hoc* Tukey's test). There was a significant effect of ChR2 stimulation [$F_{(2,18)} = 20.377$, $p < 0.001$] and brain region effect [$F_{(4,36)} = 54.76$, $p < 0.001$]. A ChR2 stimulation–brain region interaction [$F_{(8,72)} = 28.22$, $p < 0.001$] occurred. *Post-hoc* comparison: GP (right hemisphere light vs. left hemisphere): $^{***}p < 0.001$; M1 (right hemisphere light vs. left hemisphere): $^{***}p < 0.001$; EPN (right hemisphere light vs. left hemisphere): $^{***}p < 0.001$; CPu (right hemisphere light vs. left hemisphere): $^{***}p < 0.001$; STN (right hemisphere light vs. left hemisphere): $P = 0.9980$ (**Figure 2C**). These results indicated that excessive GP activity reduced EPN activity and increased M1 and CPu activity.

ChR2 Stimulation of Glutamatergic Afferent Fibers From the STN in the GP Produced Similar Abnormal Movements

The GP primarily receives glutamatergic afferent fibers from the STN (Kita, 2007). To assess the effect of stimulating glutamatergic afferent fibers from the STN in the GP, we injected AAV-CaMKIIα-ChR2-mCherry virus into the right STN. We confirmed that ChR2-mCherry was selectively expressed in the STN but not in other nearby regions (**Figure 3A**). We also found that ChR2-mCherry was expressed in the two other remote brain regions: the ipsilateral GP and EPN, but not in the ipsilateral M1 (**Figure 3A**). The selected schematics were adapted from the mouse brain in Stereotaxic Coordinates (Paxinos and Franklin, 2001). The results were consistent with the notion that the GP and EPN are the targets of STN, except for M1 (Hamani et al., 2004). The ChR2-mCherry expression STN neurons were all CaMKIIα positive (**Figure 3B**). We verified that ChR2 was expressed in the glutamatergic afferent fibers from the STN in the GP. According to current knowledge, one of the distinct advantages of the optogenetic approach is the ability to selectively manipulate basal ganglia projections to define its role in the control of motor and motivation and emotional behavior (Deisseroth, 2014). We implanted the fiber guide cannula above the right GP to selectively stimulate the glutamatergic afferent fibers from the STN in the GP (**Figure 3C**). Following ChR2 stimulation of the STN axons in the GP (but not the EPN), the mice displayed more stereotyped movements (grooming) and dystonia-like behaviors (torsion of the neck and left forelimb), and displayed less resting and exploration, similar to the behaviors produced by ChR2 stimulation of GABAergic neurons in the right GP in the VGAT-ChR2-EYFP transgenic mice. The mice did not display chewing and licking. The mice rotated in the opposite direction, compared to the VGAT-ChR2-EYFP transgenic mice [$^{**}p < 0.01$, $^{***}p < 0.001$, $n = 8$, using a paired, two-tailed *t*-test; grooming: $t_{(7)} = -6.859$, $p < 0.001$; torsion spasm: $t_{(7)} = -15.317$, $p < 0.001$; resting: $t_{(7)} = 8.793$, $p < 0.001$; exploration: $t_{(7)} = 10.604$, $p < 0.001$; circling left: $t_{(7)} = 4.660$, $p = 0.002$; circling right: $t_{(7)} = -10.817$, $p < 0.001$; chewing: $t_{(7)} = -0.261$, $p = 0.802$; licking: $t_{(7)} = -0.475$, $p = 0.649$; **Figure 3D**].

ChR2 Stimulation of Glutamatergic Afferent Fibers From the STN in the GP Produced Similar Network Level Changes of Basal Ganglia Circuit as Indicated by c-Fos Expression in the GP, M1, STN, EPN, and CPu

We further investigated the effect of ChR2 stimulation of glutamatergic afferent fibers from the STN in the GP on the expression of c-Fos in the GP, M1, STN, EPN, and CPu. We found that ChR2 stimulation of glutamatergic afferent fibers from the STN in the GP increased the c-Fos-positive neurons in the ipsilateral GP, M1, and CPu, and decreased the c-Fos-positive neurons in the ipsilateral EPN, compared to the contralateral side, similar to the ChR2 stimulation of GP GABAergic neurons in the VGAT-ChR2-EYFP transgenic mice. There was no statistically significant difference between the c-Fos-positive neurons in the ipsilateral STN and contralateral side [$^{***}p < 0.001$; $n = 8$, using a paired, two-tailed *t*-test; GP: $t_{(7)} = 11.143$, $p < 0.001$; M1: $t_{(7)} = 14.697$, $p < 0.001$; CPu: $t_{(7)} = 13.353$, $p < 0.001$; EPN: $t_{(7)} = -16.253$, $p < 0.001$; STN: $t_{(7)} = 0.607$, $p = 0.563$; **Figure 4**].

DISCUSSION

There are few studies directly addressing the effect of optogenetic stimulation of GP neurons on motor activity. Here we used the recently developed optogenetics for manipulating the intrinsic GABAergic neurons in GP and glutamatergic afferents from STN in freely moving mice to study the exact role of GP neurons in the control of movement. We found that the light activation of ChR2-expressing GP neurons in the VGAT-ChR2-EYFP transgenic mice produced dystonia-like behaviors (e.g., torsion spasm of

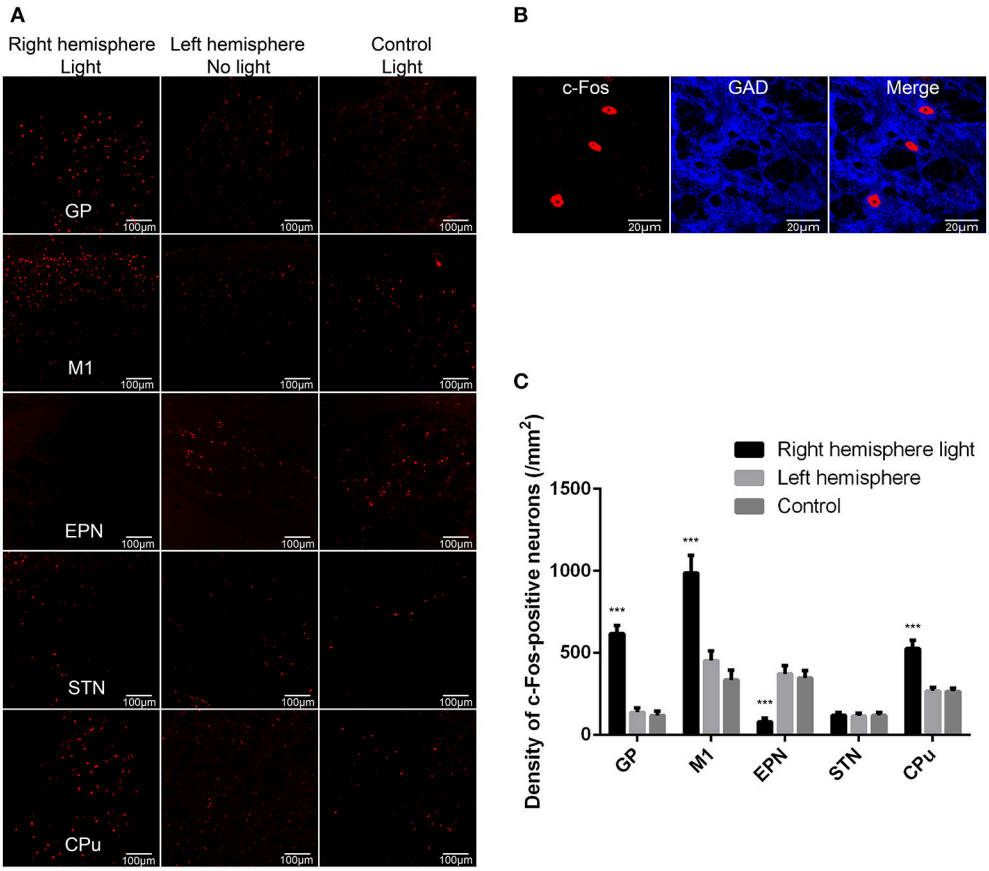

FIGURE 2 | ChR2 stimulation of the GP GABAergic neurons produced the network level changes of basal ganglia circuit as indicated by c-Fos expression in the GP, M1, EPN, STN, and CPu. **(A)** We detected c-Fos immunoreactivity in the light-exposed ipsilateral and contralateral hemispheres of VGAT-ChR2-EYFP transgenic mice, as well as in the light-exposed hemisphere of wild-type mice (control). **(B)** The c-Fos-positive neurons in the GP were all GAD67-positive neurons. **(C)** A bar graph of c-Fos-positive cell counts in the GP, M1, EPN, STN, and CPu. Asterisks indicate significant difference between the c-Fos-positive cells in ipsilateral hemispheres and contralateral hemispheres to optical stimulation {$n = 10$, two-way ANOVA followed by *post-hoc* Tukey's test. There was a significant effect of ChR2 stimulation [$F_{(2,18)} = 20.377$, $p < 0.001$], and brain region effect [$F_{(4,36)} = 54.76$, $p < 0.001$]. A ChR2 stimulation–brain region interaction [$F_{(8,72)} = 28.22$, $p < 0.001$] occurred. *Post-hoc* comparison: GP (right hemisphere light vs. left hemisphere): $^{***}p < 0.001$; M1 (right hemisphere light vs. left hemisphere): $^{***}p < 0.001$; EPN (right hemisphere light vs. left hemisphere): $^{***}p < 0.001$; CPu (right hemisphere light vs. left hemisphere): $^{***}p < 0.001$}.

the neck and abnormal forelimb posture) and stereotyped movements (repeated grooming, chewing, and licking). This is due to the fact that all ChR2-expressing GABAergic neurons that have an axon passing through or projecting into the GP could be activated in this way. Therefore, it is not quite certain whether the dystonia-like behaviors were caused by excessive activity of the intrinsic GABAergic neurons in the GP. Then, we indirectly drove the firing of GP neurons through activation of their excitatory inputs from the STN by injection of AAV virus containing ChR2 in STN and light stimulation in the GP. Following ChR2 stimulation of the STN axons in the GP (but not the EPN), the mice displayed stereotyped movements (grooming) and dystonia-like behaviors (torsion of the neck and left forelimb) similar to the behaviors produced by ChR2 stimulation of GABAergic neurons in the right GP in the VGAT-ChR2-EYFP transgenic mice. We also noticed that the mice did not display chewing and licking and rotated in the opposite direction compared to the VGAT-ChR2-EYFP transgenic mice. We considered that the dystonia-like behaviors could be mainly caused by excessive activity of the intrinsic GABAergic neurons in the GP. As we know, stimulation of STN axons in the GP mainly drove GP neurons, but the effects of antidromic stimulation also needed to be taken into account. Stimulation of STN axons in the GP likely drives all the other basal ganglia synaptic targets of STN neurons. It was possible that the different behaviors in the two experimental conditions were caused by the wide-spread excitatory effects evoked by STN stimulation. Our finding of the induction of abnormal involuntary movements by optogenetic activation of GABAergic GP neurons collaborates with previous pharmacological, lesioning, and electrophysiology studies (Grabli et al., 2004; Reiner, 2004; Starr et al., 2008), providing new support for the critical role of the GP in the control of motor activity. For example, in primates, local microinjection of the GABAA antagonist bicuculline into the

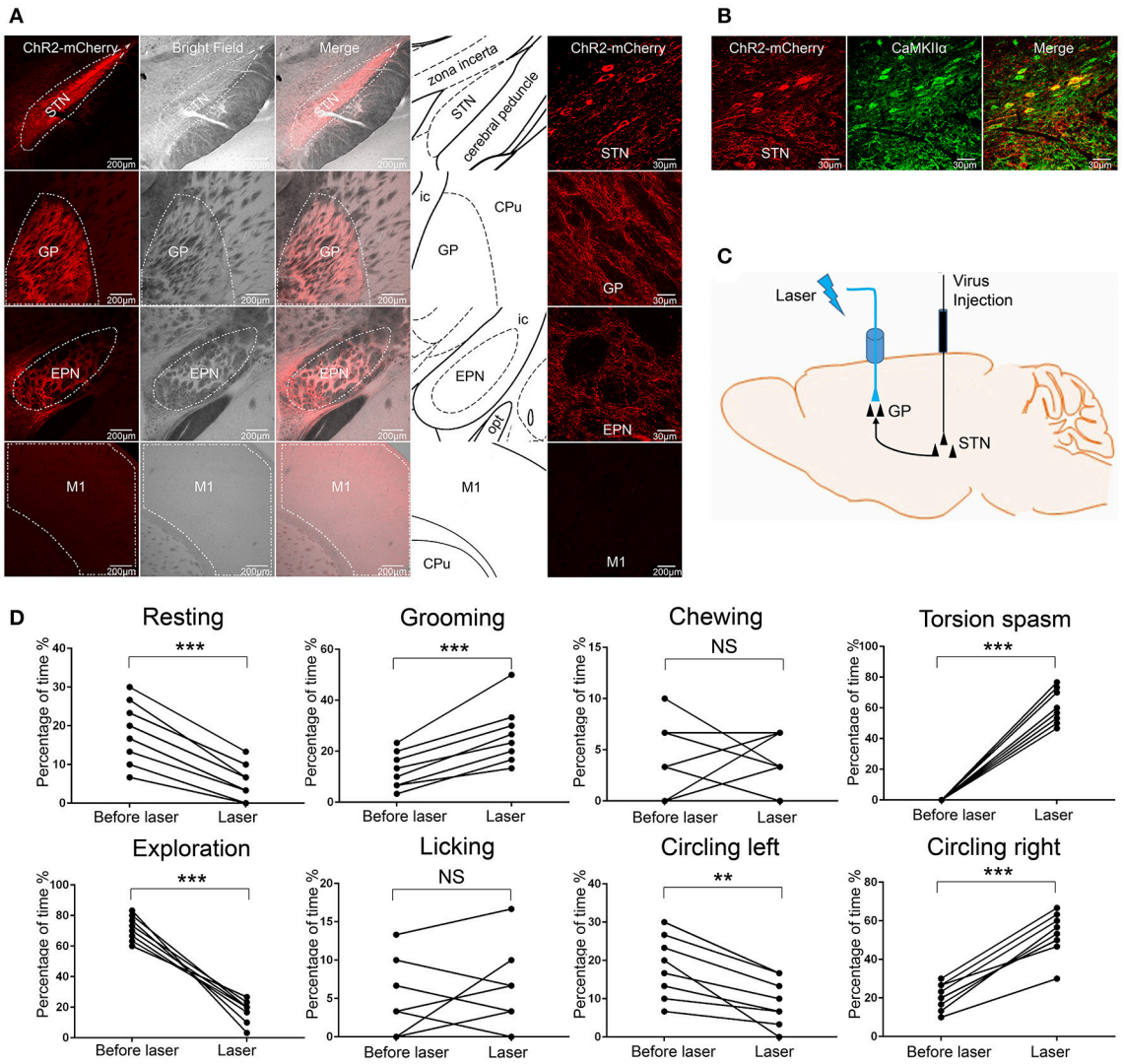

FIGURE 3 | ChR2 stimulation of glutamatergic afferent fibers from the STN in the GP produced similar abnormal movements. **(A)** ChR2-mCherry was selectively expressed in the STN but not in other nearby regions. ChR2-mCherry was also expressed in the two other remote brain regions: GP and EPN, but not in the M1. The selected schematics were adapted from the mouse brain in Stereotaxic Coordinates (Paxinos and Franklin, 2001). **(B)** ChR2-mCherry-expressing STN neurons co-stained with the excitatory neuron-specific marker CaMKIIα. **(C)** Schematic of the optical stimulation of glutamatergic afferent fibers from the STN in the GP. **(D)** The percentage of the 30-s period the animal spent engaging in each behavior. During optical stimulation of the right GP, the mice displayed more grooming, dystonia-like behaviors (torsion of the neck and left forelimb) and circling right, and displayed less resting and exploration [$^{**}p < 0.01$, $^{***}p < 0.001$, $n = 8$, using a paired, two-tailed t-test; grooming: $t_{(7)} = -6.859$, $p < 0.001$; torsion spasm: $t_{(7)} = 15.317$, $p < 0.001$; resting: $t_{(7)} = 8.793$, $p < 0.001$; exploration: $t_{(7)} = 10.604$, $p < 0.001$; circling left: $t_{(7)} = 4.660$, $p = 0.002$; circling right: $t_{(7)} = -10.817$, $p < 0.001$; chewing: $t_{(7)} = -0.261$, $p = 0.802$; licking: $t_{(7)} = -0.475$, $p = 0.649$].

GP induced abnormal involuntary movements (Grabli et al., 2004), while lesioning of the GP with quinolinic acid decreased spontaneous movement (Ayalon et al., 2004). To the best of our knowledge, the present study is the first time to selectively manipulate GABAergic GP neurons in freely moving animals to investigate the critical role of the GP in the control of motor activity.

Additionally, the expression patterns of c-Fos (a marker of neuronal activation) (Sagar et al., 1988) in the five basal ganglia structures (GP, M1, STN, EPN, and CPu) in response to ChR2 activation of the GABAergic GP neurons suggest that the neural circuitry underlying the abnormal involuntary movements is associated with excessive GP, M1, CPu activity and reduced EPN activity. GP GABAergic neurons can be divided into two classes based on their firing patterns, which are termed as "prototypical" neurons and "arkypallidal" neurons. The prototypical and arkypallidal neurons project to distinct targets. Arkypallidal neurons are the major GP cell type input to the striatum, while almost all prototypical neurons innervate STN (Abdi et al., 2015). The activation of arkypallidal neurons was supposed to decrease the c-Fos expression in the striatum. However, in our study we found that the c-Fos-positive neurons in the ipsilateral CPu were

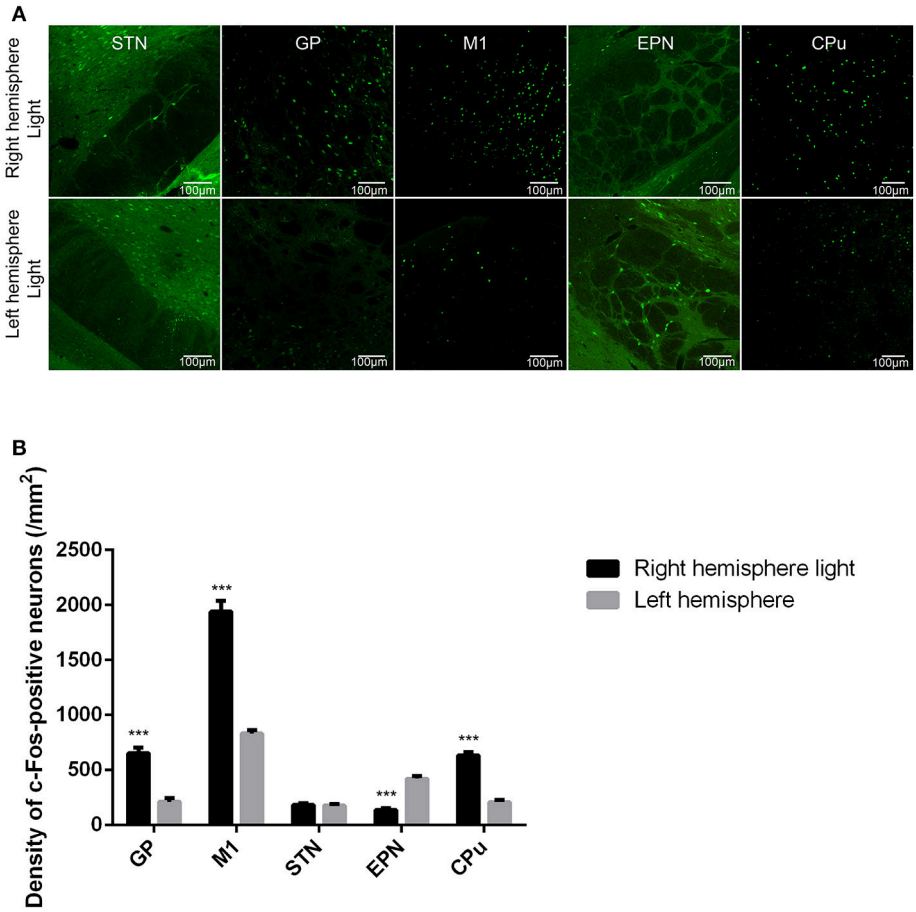

FIGURE 4 | ChR2 stimulation of glutamatergic afferent fibers from the STN in the GP produced similar changes in c-Fos expression in the GP, M1, STN, EPN, and CPu as ChR2 stimulation of GABAergic neurons in the GP. **(A)** c-Fos expression in the light-exposed (right) and contralateral (left) hemisphere of the mouse after ChR2 stimulation of glutamatergic afferent fibers from the STN in the GP. c-Fos expression was detected in the GP, M1, STN, EPN, and CPu. **(B)** Quantitative analysis of c-Fos-positive cell counts in the GP, M1, STN, EPN, and CPu are presented in a bar graph. Asterisks indicate significant differences between the ipsilateral hemisphere and contralateral hemisphere to optical stimulation [***$p < 0.001$; $n = 8$, using a paired, two-tailed t-test; GP: $t_{(7)} = 11.143$, $p < 0.001$; M1: $t_{(7)} = 14.697$, $p < 0.001$; CPu: $t_{(7)} = 13.353$, $p < 0.001$; EPN: $t_{(7)} = -16.253$, $p < 0.001$; STN: $t_{(7)} = 0.607$, $p = 0.563$].

increased after the ChR2 stimulation of GP GABAergic neurons. We had to take into account the activation of prototypical neurons. The activation of prototypical neurons will inhibit the EPN through an indirect motor pathway (GP—STN—EPN). We did find the predominant decrease of the c-Fos-positive neurons in the ENP. The ENP is the major inhibitory output nuclei of the BG. The decreased ENP activity will lead to increased cortex activity. Then the increased excitatory input to the CPu from the cortex will lead to increased CPu activity, aligned with the findings in our study. So the reason for c-Fos increases in the CPu could be related to the activation of prototypical neurons in our study. Then, we inferred that prototypical neurons could be more influential in obtaining our results. Recently, Glajch showed that specific activation of arkypallidal neurons suppressed movement (Glajch et al., 2016). Our results are consistent with Glajch's study. Since the arkypallidal neurons suppress movement, the prototypical neurons possibly play different and even opposing roles in motor control, producing hyperkinesia, as shown in our study. This finding is needed to study the exact role of prototypical neurons in movement control in the future.

Another noteworthy observation is that no significant activity decrease was observed in the STN (the major output target of the GP) in response to ChR2 activation of the GABAergic GP neurons. The most likely reason for this is the complex organization of the STN. The STN is also the target of the cortex, thalamus and brainstem, not only the target of the GP (Hamani et al., 2004). We need to take into account the excitatory input to the STN from the cortex. The relationship between STN activity and motor symptoms is complicated. It is reported that both optogenetic excitation and inhibition of STN neurons did not change the PD rats' motor symptoms (Gradinaru et al., 2009). Meanwhile, we found that the c-Fos expression pattern in the GP, M1, STN, EPN, and CPu produced by optogenetic activation of glutamatergic afferent fibers from the STN in the GP was similar to the c-Fos expression pattern produced by optogenetic activation of GABAergic neurons in the GP. Here, although

the STN processes were stimulated directly, the c-Fos-positive neurons in the STN did not increase. The most likely reason for this is that STN activity could be affected by other afferent projections, such as GABAergic afferent projections from the GP. These findings support that optogenetic activation of GABAergic neurons in the GP and glutamatergic afferent fibers from the STN in the GP produced similar motor behaviors, which were caused by similar network changes of the basal ganglia circuit. The exact role of the STN in the basal ganglia needs for study in future experiments. Of course, the c-Fos expression is not directly related to neuronal activity. It is still not clear whether the stimulation increased firing rate of GP neurons or promoted synchronization within the GP. In the future, quantifying the light stimulation effect on the electrical activity of GP neurons will be more accurate.

Recently, optogenetic stimulation of intrinsic GP neurons has been shown to increase total sleep by 66% (rather than arousal or motor activity; Qiu et al., 2016), a finding consistent with the early report that lesioning of the GP by kainate produces a huge (45%) increase in arousal (Qiu et al., 2010). The different GP neuronal populations stimulated by ChR2 in Qiu's study (i.e., GABAergic and ChAT neurons in the GP) and ours (GABAergic neurons only under control of VGAT promoter) may account for this difference. The current study failed to address distinct effects of different types of GP GABAergic neurons with distinct molecular identities, firing patterns and complex connections, with likely distinct behavioral responses. However, we speculate that the prototypical neuronal population is the most probable GP GABAergic neuronal population to cause our results. Future studies are needed to address the specific contribution of prototypical GP GABAergic neurons to motor control.

The hyperkinesia that characterizes Huntington Disease (HD) (Ross et al., 2014) is postulated to be related to preferential loss of the indirect pathway neurons that project to the GP (Albin et al., 1990). Because the indirect pathway neurons are GABAergic neurons, this pathology may result in excessive GP activity (GP disinhibition), which could be the neural substrate of HD. Previous studies have also suggested that a reduction in the striatal-GP activity and an increase in the EPN inhibition mediated by GP efferent contribute to dystonia (Hantraye et al., 1990). Also, the neuropathological basis of Tourette's syndrome (TS) has been attributed to the disruption of local inhibitory circuits within the striatum-GP circuit, which would lead to the aberrant activation of the cortical-basal ganglia loop, resulting in abnormal tic-like movements (Albin and Mink, 2006; Felling and Singer, 2011; Bronfeld and Bar-Gad, 2013). Our findings that optogenetic stimulation of the intrinsic GP GABAergic neurons or the STN-GP glutamatergic projections in the GP produced abnormal movements support the view that excessive GP activity could be the neural substrate of the abnormal involuntary movements found in movement disorders such as Huntington's disease and dystonia. Because the prototypical neuron population is the most probable GP GABAergic neuronal population to cause our results, we speculate that excessive prototypical neurons activity could be the neural substrate of the abnormal involuntary movements. Inhibition of GP GABAergic neurons, mainly prototypical neurons through surgical means, deep brain stimulation (DBS) or drug-based interventions, represent new treatment targets for hyperkinetic movement disorder. Of high importance is to understand the functional role of different types of GP neurons in the basal ganglia. Certainly, there is much more to be discovered.

CONCLUSION

To our knowledge, there are few studies directly addressing the effect of optogenetic stimulation of GP neurons on motor activity. Here, we found that optogenetic stimulation of GABAergic neurons in the GP or glutamatergic afferent fibers from the STN in the GP, produced hyperkinesia. Our data supported the important role of the GABAergic GP neurons, mainly prototypical neurons, in the control of movement. Albeit, there are still a lot of questions ahead of us. Future studies are needed to address the specific contribution of prototypical GABAeregic GP neurons to motor control.

AUTHOR CONTRIBUTIONS

JT designed and performed the study. JT and JC contributed to the major writing of manuscript. YY analyzed the data. WX was engaged in EEG recordings. RZ provided help in mice surgery. HL did some mice behavioral tests. All authors have reviewed and edited the manuscript. SD, JC, and BZ supervised the study. BZ is designated correspondence on the manuscript.

ACKNOWLEDGMENTS

This study is funded by National Natural Science Foundation of China (81271248 and 81500967), and the Zhejiang Provincial Natural Science Foundation of China (LY15H090008).

SUPPLEMENTARY MATERIAL

The Supplementary Material for this article can be found online at: https://www.frontiersin.org/articles/10.3389/fnbeh.2018.00185/full#supplementary-material

REFERENCES

Abdi, A., Mallet, N., Mohamed, F. Y., Sharott, A., Dodson, P. D., Nakamura, K. C., et al. (2015). Prototypic and arkypallidal neurons in the dopamine-intact external globuspallidus. *J. Neurosci.* 35, 6667–6688. doi: 10.1523/JNEUROSCI.4662-14.2015

Albin, R. L., and Mink, J. W. (2006). Recent advances in Tourette syndrome research. *Trends Neurosci.* 29, 175–182. doi: 10.1016/j.tins.2006.01.001

Albin, R. L., Reiner, A., Anderson, K. D., Penney, J. B., and Young, A. B., (1990). Striatal and nigral neuron subpopulations in rigid Huntington's disease: implications for the functional anatomy of chorea and rigidity-akinesia. *Ann. Neurol.* 27, 357–365. doi: 10.1002/ana.410270403

Albin, R. L., Young, A. B., and Penney, J. B., (1989). The functional anatomy of basal ganglia disorders. *Trends Neurosci.* 12, 366–375. doi: 10.1016/0166-2236(89)90074-X

Ayalon, L., Doron, R., Weiner, I., and Joel, D., (2004). Amelioration of behavioral deficits in a rat model of Huntington's disease by an excitotoxic lesion to the globuspallidus. *Exp. Neurol.* 186, 46–58. doi: 10.1016/S0014-4886(03)00312-1

Bahuguna, J., Tetzlaff, T., Kumar, A., HellgrenKotaleski, J., and Morrison, A., (2017). Homologous basal ganglia network models in physiological and parkinsonian conditions. *Front. Comput. Neurosci.* 11:79. doi: 10.3389/fncom.2017.00079

Boyden, E. S., Zhang, F., Bamberg, E., Nagel, G., and Deisseroth, K., (2005). Millisecond-timescale, genetically targeted optical control of neural activity. *Nat. Neurol. Sci.* 8, 1263–1268. doi: 10.1038/nn1525

Bronfeld, M., and Bar-Gad, I. (2013). Tic disorders: what happens in the basal ganglia? *Neuroscientist* 19, 101–108. doi: 10.1177/10738584124 44466

Bronfeld, M., Belelovsky, K., Erez, Y., Bugaysen, J., Korngreen, A., and Bar-Gad, I., (2010). Bicuculline-induced chorea manifests in focal rather than globalized abnormalities in the activation of the external and internal globuspallidus. *J. Neurophysiol.* 104, 3261–3275. doi: 10.1152/jn.00093.2010

Chaudhry, F. A., Reimer, R. J., Bellocchio, E. E., Danbolt, N. C., Osen, K. K., Edwards, R. H., et al. (1998). The vesicular GABA transporter, VGAT, localizes to synaptic vesicles in sets of glycinergic as well as GABAergic neurons. *J. Neurosci.* 18, 9733–9750. doi: 10.1523/JNEUROSCI.18-23-09733.1998

Chevalier, G., and Deniau, J. M. (1990). Disinhibition as a basic process in the expression of striatal functions. *Trends Neurosci.* 13, 277–280. doi: 10.1016/0166-2236(90)90109-N

Crossman, A. R., Sambrook, M. A., and Jackson, A., (1984). Experimental hemichorea/hemiballismus in the monkey. Studies on the intracerebral site of action in a drug-induced dyskinesia. *Brain* 107, 579–596. doi: 10.1093/brain/107.2.579

Deisseroth, K. (2014). Circuit dynamics of adaptive and maladaptive behaviour.*Nature* 505, 309–317. doi: 10.1038/nature12982

Dodson, P. D., Larvin, J. T., Duffell, J. M., Garas, F. N., Doig, N. M., Kessaris, N., et al. (2015). Distinct developmental origins manifest in the specialized encoding of movement by adult neurons of the external globuspallidus. *Neuron* 86, 501–513. doi: 10.1016/j.neuron.2015.03.007

Felling, R. J., and Singer, H. S., (2011). Neurobiology of tourette syndrome: current status and need for further investigation. *J. Neurosci.* 31, 12387–12395. doi: 10.1523/JNEUROSCI.0150-11.2011

Gerfen, C. R., and Surmeier, D. J. (2011). Modulation of striatal projection systems by dopamine. *Annu. Rev. Neurosci.* 34, 441–466. doi: 10.1146/annurev-neuro-061010-113641

Gittis, A. H., Berke, J. D., Bevan, M. D., Chan, C. S., Mallet, N., Morrow, M. M., et al. (2014). New roles for the external globuspallidus in basal ganglia circuits and behavior. *J. Neurosci.* 34, 15178–15183. doi: 10.1523/JNEUROSCI.3252-14.2014

Glajch, K. E., Kelver, D. A., Hegeman, D. J., Cui, Q., Xenias, H. S., Augustine, E. C., et al. (2016). Npas1+ pallidal neurons target striatal projection neurons. *J. Neurosci.* 36, 5472–5488. doi: 10.1523/JNEUROSCI.1720-15.2016

Goldberg, J. A., and Bergman, H., (2011). Computational physiology of the neural networks of the primate globuspallidus: function and dysfunction. *Neuroscience* 198, 171–192. doi: 10.1016/j.neuroscience.2011.08.068

Grabli, D., McCairn, K., Hirsch, E. C., Agid, Y., Feger, J., Francois, C., et al. (2004). Behavioural disorders induced by external globuspallidus dysfunction in primates: I. behavioural study. *Brain* 127, 2039–2054. doi: 10.1093/brain/awh220

Gradinaru, V., Mogri, M., Thompson, K. R., Henderson, J. M., and Deisseroth, K. (2009). Optical deconstruction of parkinsonian neural circuitry.*Science* 324, 354–359. doi: 10.1126/science.1167093

Grillner, S., Hellgren, J., Ménard, A., Saitoh, K., and Wikström, M. A. (2005). Mechanisms for selection of basic motor programs–roles for the striatum and pallidum. *Trends Neurosci.* 28, 364–370. doi: 10.1016/j.tins.2005.05.004

Hamani, C., Saint-Cyr, J. A., Fraser, J., Kaplitt, M., and Lozano, A. M. (2004). The subthalamic nucleus in the context of movement disorders. *Brain* 127, 4–20. doi: 10.1093/brain/awh029

Hantraye, P., Riche, D., Maziere, M., and Isacson, O. (1990). A primate model of Huntington's disease: behavioral and anatomical studies of unilateral excitotoxic lesions of the caudate-putamen in the baboon. *Exp. Neurol.* 108, 91–104. doi: 10.1016/0014-4886(90)90014-J

Hauber, W., Lutz, S., and Münkle, M., (1998). The effects of globuspallidus lesions on dopamine-dependent motor behaviour in rats. *Neuroscience* 86, 147–157. doi: 10.1016/S0306-4522(98)00009-8

Hegeman, D. J., Hong, E. S., Hernández, V. M., and Chan, C. S., (2016). The external globuspallidus: progress and perspectives. *Eur. J. Neurosci.* 43, 1239–1265. doi: 10.1111/ejn.13196

Henderson, K. W., Gupta, J., Tagliatela, S., Litvina, E., Zheng, X., Van Zandt, M. A., et al. (2014). Long-term seizure suppression and optogenetic analyses of synaptic connectivity in epileptic mice with hippocampal grafts of GABAergic interneurons. *J. Neurosci.* 34, 13492–13504. doi: 10.1523/JNEUROSCI.0005-14.2014

Hikosaka, O. (2007). GABAergic output of the basal ganglia. *Prog. Brain Res.* 160, 209–226. doi: 10.1016/S0079-6123(06)60012-5

Joel, D., Ayalon, L., Tarrasch, R., Veenman, L., Feldon, J., and Weiner, I. (1998). Electrolytic lesion of globus pallidus ameliorates the behavioral and neurodegenerative effects of quinolinic acid lesion of the striatum: a potential novel treatment in a rat model of Huntington's disease. *Brain Res.* 787, 143–148. doi: 10.1016/S0006-8993(97)01428-5

Kita, H. (2007). Globus pallidus external segment. *Prog. Brain Res.* 160, 111–133. doi: 10.1016/S0079-6123(06)60007-1

Kita, H., and Kita, T. (2011). Role of striatum in the pause and burst generation in the globus pallidus of 6-OHDA-treated rats. *Front. Syst. Neurosci.* 5:42. doi: 10.3389/fnsys.2011.00042

Kravitz, A. V., Freeze, B. S., Parker, P. R., Kay, K., Thwin, M. T., Deisseroth, K., et al. (2010). Regulation of parkinsonian motor behaviours by optogenetic control of basal ganglia circuitry. *Nature* 466, 622–626. doi: 10.1038/nature09159

Lindahl, M., and HellgrenKotaleski, J., (2017). Untangling basal ganglia network dynamics and function: role of dopamine depletion and inhibition investigated in a spiking network model. *eNeuro* 3:e0156-16.2016. doi: 10.1523%2FENEURO.0156-16.2016

Mallet, N., Micklem, B. R., Henny, P., Brown, M. T., Williams, C., Bolam, J. P., et al. (2012). Dichotomous organization of the external globuspallidus. *Neuron* 74, 1075–1086. doi: 10.1016/j.neuron.2012.04.027

Mallet, N., Pogosyan, A., Márton, L. F., Bolam, J. P., Brown, P., and Magill, P. J. (2008). Parkinsonian beta oscillations in the external globuspallidus and their relationship with subthalamic nucleus activity. *J. Neurosci.* 28, 14245–14258. doi: 10.1523/JNEUROSCI.4199-08.2008

Mastro, K. J., Bouchard, R. S., Holt, H. A., and Gittis, A. H. (2014). Transgenic mouse lines subdivide external segment of the globuspallidus (GPe) neurons and reveal distinct GPe output pathways. *J. Neurosci.* 34, 2087–2099. doi: 10.1523/JNEUROSCI.4646-13.2014

Matsumura, M., Tremblay, L., Richard, H., and Filion, M. (1995). Activity of pallidal neurons in the monkey during dyskinesia induced by injection of bicuculline in the external pallidum. *Neuroscience* 65, 59–70. doi: 10.1016/0306-4522(94)00484-M

Nambu, A. (2008). Seven problems on the basal ganglia.*Curr. Opin. Neurobiol.* 18, 595–604. doi: 10.1016/j.conb.2008.11.001

Norton, S. (1976). Hyperactive behavior of rats after lesions of the globuspallidus. *Brain Res. Bull.* 1, 193–202. doi: 10.1016/0361-9230(76)90069-1

Pavlides, A., Hogan, S. J., and Bogacz, R. (2012). Improved conditions for the generation of beta oscillations in the subthalamic nucleus–globuspallidus network. *Eur. J. Neurosci.* 36, 2229–2239. doi: 10.1111/j.1460-9568.2012.08105.x

Paxinos, G. F., and Franklin, K. (2001). *The Mouse Brain in Stereotaxic Coordinates*. San Diego, CA: Elsevier Academic Press.

Qiu, M. H., Vetrivelan, R., Fuller, P. M., and Lu, J., (2010). Basal ganglia control of sleep-wake behavior and cortical activation. *Eur. J. Neurosci.* 31, 499–507. doi: 10.1111/j.1460-9568.2009.07062.x

Qiu, M. H., Yao, Q. L., Vetrivelan, R., Chen, M. C., and Lu, J., (2016). Nigrostriatal dopamine acting on globus pallidus regulates sleep. *Cereb. Cortex* 26, 1430–1439. doi: 10.1093/cercor/bhu241

Reiner, A., (2004). Can lesions of GPe correct HD deficits? *Exp. Neurol.* 186, 1–5. doi: 10.1016/j.expneurol.2003.11.002

Ross, C. A., Aylward, E. H., Wild, E. J., Langbehn, D. R., Long, J. D., Warner, J. H., et al. (2014). Huntington disease: natural history, biomarkers and prospects for therapeutics. *Nat. Rev. Neurol.* 10, 204–216. doi: 10.1038/nrneurol.2014.24

Rothwell, J. C. (2011). The motor functions of the basal ganglia. *J. Integr. Neurosci.* 10, 303–315. doi: 10.1142/S0219635211002798

Sagar, S. M., Sharp, F. R., and Curran, T. (1988). Expression of c-fos protein in brain: metabolic mapping at the cellular level. *Science* 240, 1328–1331. doi: 10.1126/science.3131879

Starr, P. A., Kang, G. A., Heath, S., Shimamoto, S., and Turner, R. S. (2008). Pallidal neuronal discharge in Huntington's disease: support for selective loss of striatal cells originating the indirect pathway. *Exp. Neurol.* 211, 227–233. doi: 10.1016/j.expneurol.2008.01.023

Tang, J. K., Moro, E., Lozano, A. M., Lang, A. E., Hutchison, W. D., Mahant, N., et al. (2005). Firing rates of pallidal neurons are similar in Huntington's and Parkinson's disease patients. *Exp. Brain Res.* 166, 230–236. doi: 10.1007/s00221-005-2359-x

Zhang, F., Gradinaru, V., Adamantidis, A. R., Durand, R., Airan, R. D., de Lecea, L., et al. (2010). Optogenetic interrogation of neural circuits: technology for probing mammalian brain structures. *Nat. Protoc.* 5, 439–456. doi: 10.1038/nprot.2009.226

Zhao, S., Ting, J. T., Atallah, H. E., Qiu, L., Tan, J., Gloss, B., et al. (2011). Cell type-specific channelrhodopsin-2 transgenic mice for optogenetic dissection of neural circuitry function. *Nat. Methods* 8, 745–752. doi: 10.1038/nmeth.1668

Conflict of Interest Statement: The authors declare that the research was conducted in the absence of any commercial or financial relationships that could be construed as a potential conflict of interest.

Copyright © 2018 Tian, Yan, Xi, Zhou, Lou, Duan, Chen and Zhang. This is an open-access article distributed under the terms of the Creative Commons Attribution License (CC BY). The use, distribution or reproduction in other forums is permitted, provided the original author(s) and the copyright owner(s) are credited and that the original publication in this journal is cited, in accordance with accepted academic practice. No use, distribution or reproduction is permitted which does not comply with these terms.

frontiers in Human Neuroscience

ORIGINAL RESEARCH
published: 26 September 2018
doi: 10.3389/fnhum.2018.00367

Motor Sequence Learning Is Associated With Hippocampal Subfield Volume in Humans With Medial Temporal Lobe Epilepsy

Jinyi Long[1]†, Yanyun Feng[2]†, HongPeng Liao[3], Quan Zhou[4] and M. A. Urbin[5]*

[1]College of Information Science and Technology, Jinan University, Guangzhou, China, [2]Department of Radiology, The First People's Hospital of Foshan, Foshan, China, [3]School of Automation Science and Engineering, South China University of Technology, Guangzhou, China, [4]Department of Neurology, The First People's Hospital of Foshan, Foshan, China, [5]Department of Physical Medicine and Rehabilitation, University of Pittsburgh, Pittsburgh, PA, United States

Objectives: Medial temporal lobe epilepsy (mTLE) is characterized by decreased hippocampal volume, which results in motor memory consolidation impairments. However, the extent to which motor memory acquisition are affected in humans with mTLE remains poorly understood. We therefore examined the extent to which learning of a motor tapping sequence task is affected by mTLE.

Methods: MRI volumetric analysis was performed using a T1-weighted three-dimensional gradient echo sequence in 15 patients with right mTLE and 15 control subjects. Subjects trained on a motor sequence tapping task with the left hand in right mTLE and non-dominant hand in neurologically-intact controls.

Results: The number of correct sequences performed by the mTLE patient group increased after training, albeit to a lesser extent than the control group. Although hippocampal subfield volume was reduced in mTLE relative to controls, no differences were observed in the volumes of other brain areas including thalamus, caudate, putamen and amygdala. Correlations between hippocampal subfield volumes and the change in pre- to post-training performance indicated that the volume of hippocampal subfield CA2–3 was associated with motor sequence learning in patients with mTLE.

Significance: These results provide evidence that individuals with mTLE exhibit learning on a motor sequence task. Learning is linked to the volume of hippocampal subfield CA2–3, supporting a role of the hippocampus in motor memory acquisition.

Highlights

- Humans with mTLE exhibit learning on a motor tapping sequence task but not to the same extent as neurologically-intact controls.
- Hippocampal subfield volumes are significantly reduced after mTLE. Surrounding brain area volumes do not show abnormalities.
- Hippocampal subfield CA2–3 volume is associated with motor sequence learning in humans with mTLE.

Keywords: epilepsy, motor sequence learning, medial temporal lobe, hippocampus, MRI

OPEN ACCESS

Edited by:
Elizabeth B. Torres, Rutgers University, The State University of New Jersey, United States

Reviewed by:
David L. Wright, Texas A&M University, United States
Juan Pablo Princich, Garrahan Hospital, Argentina

Correspondence:
Jinyi Long
jinyil@jnu.edu.cn

†These authors have contributed equally to this work

Received: *26 March 2018*
Accepted: *28 August 2018*
Published: *26 September 2018*

Citation:
Long J, Feng Y, Liao H, Zhou Q and Urbin MA (2018) Motor Sequence Learning Is Associated With Hippocampal Subfield Volume in Humans With Medial Temporal Lobe Epilepsy. Front. Hum. Neurosci. 12:367. doi: 10.3389/fnhum.2018.00367

INTRODUCTION

The hippocampus is involved in procedural memory, a type of memory necessary for motor sequence learning (Albouy et al., 2013). During a serial reaction time task, amnesic patients have been shown to outperform controls by repeating the sequence of key presses to the location of the stimulus through increasingly rapid performance. However, these same patients exhibit an impaired ability to recognize the sequence (Reber and Squire, 1998). Medial temporal lobe epilepsy (mTLE) is characterized by seizures originating in mesial temporal lobe structures. Decreased hippocampal volume ipsilateral to the epileptogenic temporal lobe has been reported in this patient population (Marsh et al., 1997). At present, it is not known whether motor sequence learning is preserved in humans with mTLE.

Neural correlates of motor sequence learning have been characterized in neurologically-intact controls and include the cerebellum, basal ganglia, supplementary motor area, as well as primary motor and premotor cortices (Willingham et al., 2002; Doyon et al., 2003). However, the role of hippocampus during motor sequence learning is still controversial. Most prior work has not implicated the hippocampus in motor sequence learning (Curran, 1997; Clark and Squire, 1998; Chun and Phelps, 1999; Poldrack et al., 2001), but other findings suggest that the hippocampus is necessary irrespective of whether knowledge of the sequence was implicitly or explicitly acquired (Grafton et al., 1995; Schendan et al., 2003). The hippocampus is thought to support motor sequence learning by encoding temporally discontiguous but structured information and events (Schendan et al., 2003; Eichenbaum, 2004; Albouy et al., 2008).

Hippocampus is composed of several histologically distinct subfields: subiculum, cornu ammonis sectors (CA)1–4, and dentate gyrus (DG). There is evidence that histological differences influence functional characteristics of each subfield. Animal studies suggest a selective role for CA1 pyramidal cells in intermediate and long-terms patial learning or memory consolidation, but not in short-term acquisition or encoding (Blum et al., 1999; Remondes and Schuman, 2004; Vago et al., 2007). Rather, CA2–3 is thought to be responsible for encoding and early retrieval (Hasselmo, 2005; Acsády and Káli, 2007). In addition, there is evidence that CA1 pyramidal cells are less critically involved in declarative memory compared to DG granule cells or CA4 pyramidal cells in humans with TLE (Coras et al., 2014).

The goal of our study was to examine the effect of mTLE on motor sequence learning. Considering the spatial recall demands of a motor tapping sequence, we hypothesized that mTLE patients will exhibit a reduced ability to learn a motor sequence task. To test this hypothesis, 15 patients with right mTLE and 15 controls trained on a motor sequence tapping task, and MRI volumetric analysis was performed using a T1-weighted three-dimensional gradient echo sequence.

MATERIALS AND METHODS

Subjects

We recruited patients with unilateral mTLE from the First People's Hospital of Foshan. First, each patient underwent non-invasive neurophysiologic evaluation via interictal EEG recordings and extensive video-EEG monitoring to record seizures. Next, two examiners independently obtained the evaluation of ictal semiology and defined the cerebral structures impacted by epileptic activity according to clinical and EEG features of the seizures. In addition, 3-T MRI was performed to investigate temporal lobe structures in detail for all patients. The presence of medial temporal sclerosis was evaluated qualitatively by visual inspection of structure MRI. Raters were blind to motor sequence learning results. Patients with epileptic paroxysms in extra-temporal regions on EEG were excluded. A total of 15 mTLE patients (seven males, 29.9 $\pm$ 7.8 years of age) with right (onset) unilateral seizures were enrolled. Demographics and clinical information of patients are provided in **Table 1**. All subjects with TLE exhibited MRI evidence of right hippocampal sclerosis. We also recruited 15 healthy adults (nine males, 29.1 $\pm$ 9.1 years of age) to serve as controls. Musicians were excluded from the sample. All subjects were right-handed. All subjects gave their written informed consent prior to the study, which was in accordance with the Declaration of Helsinki and approved by the local ethics committee at the Jinan University and the First People's Hospital of Foshan.

MRI Data Acquisition

A 3-T MR imaging system (General Electric) was used for scanning. A high resolution three-dimensional T1-weighted image was acquired via a 3D-fast spoiled gradient recall sequence with the following parameters: IR = 450 ms, flip angle = 15°, and FOV = 24 $\times$ 24 cm^2. One hundred and forty-six slices with a slice thickness of 1 mm were acquired to construct a 256 $\times$ 228 data matrix.

Structural Volume Evaluation

The volumetric segmentation was performed with experimental software (Freesurfer package v5.1[1]), which provided fully automatic cortical parcellation and segmentation of subcortical structures. The program calculates brain sub-volumes by assigning a neuro-anatomical label to each voxel based on probabilistic information estimated automatically from a manually labeled training set. Briefly, this process includes motion correction, removal of non-brain tissue using a hybrid watershed/surface deformation procedure, multiple intensity and spatial normalization, Talairach transformation, segmentation of the subcortical white matter and deep gray matter structures (Fisch et al., 2004; Ségonne et al., 2004). Details regarding the process and analysis pipeline has been described elsewhere[1]. Finally, 12 hippocampal sub-regions in the left or right hemisphere were automatically obtained: fimbria, CA1, CA2-CA3, CA4-DG, subiculum and presubiculum. All sub-regions from each participant were visually inspected to detect visible

[1]https://surfer.nmr.mgh.harvard.edu/

TABLE 1 | Demographic and clinical characteristics (Mean ± SD).

	mTLE	Control	*p*-value
Sample size	15	15	–
Sex (male/female)	7/8	9/6	0.74[a]
Age (years)	29.9 ± 7.8	29.1 ± 9.1	0.67[b]
Education (years)	11.2 ± 3.8	13.6 ± 3.5	0.51[b]
Epilepsy duration (years)	12.5 ± 10.8	–	
Age at epilepsy onset	10.7 ± 9.1	–	
Frequency (times/year)	22.3 ± 31.7	–	

[a]*Chi-square test;* [b]*two-sample t-test.*

errors in segmentation. The whole hippocampus volume was obtained by adding all hippocampal subfields. In addition to hippocampal subfields, we also calculated the volumes of surrounding brain areas that served as references for volumes outside of the hippocampus. These reference areas included thalamus, caudate, putamen and amygdala in the right hemisphere. The total intracranial volume (TIV) was also automatically calculated by FreeSurfer software. Volumes of the hippocampal subfields and surrounding brain areas were adjusted for TIV using the following formula (Buckner et al., 2004):

$$\mathrm{Volume}_{\mathrm{adj}} = \mathrm{Volume}_{\mathrm{observed}} - \beta\left(\mathrm{TIV}_{\mathrm{observed}} - \mathrm{TIV}_{\mathrm{sample\ mean}}\right) \quad (1)$$

where, β is the slope of the regional volume regression on $\mathrm{TIV}_{\mathrm{observed}}$.

The volumetric segmentation was also performed with experimental software of Freesurfer package v6.0 (Iglesias et al., 2015). Finally, 12 hippocampal sub-regions in the left or right hemisphere were automatically obtained including hippocampal tail, subiculum, CA1, hippocampal fissure, presubiculum, parasubiculum, molecular layer, granule cell layer of DG (GC-DG), CA2-CA3, CA4, fimbria and hippocampus-amygdala-transition-area (HATA). The TIV was also automatically calculated. Volumes of the hippocampal subfields were adjusted for TIV using the formula as described above.

Motor Sequence Learning Task

Subjects performed a finger-tapping task in a particular sequence during a pre-training performance test, a training protocol, and a post-training performance test (**Figure 1**; Korman et al., 2003; Walker et al., 2003). During motor sequence learning task, the seizures were not monitored. Note that the post-test was performed immediately following training on the motor sequence. T1 images were acquired upon enrollment in the study and before behavioral testing. Participants were instructed to press four numeric keys on a standard computer keyboard with the fingers of the left-hand in right mTLE and finger of the non-dominant, left hand in controls. Each trial of the task involved repeating the same five-element sequence (4-1-3-2-4) as quickly and accurately as possible during a 30-s interval, followed by 30 s of rest. Subjects were instructed to not correct for errors and to continue tapping without pause as smoothly as possible. During a trial, the sequence was displayed on a monitor in front of the subject. Each key press produced a dot on the monitor. Pre- and post-training tests consisted of three, 30-s trials with 30-s rest periods between each trial. Performance was measured as the total number of correct sequences completed and the number of errors in a trial. The training protocol consisted of 12, 30-s trials with 30-s rest periods between trials, lasting a total of 12 min.

Statistical Analysis

Normal distribution was tested by the Shapiro–Wilk's test and Mauchly's test was used to test for sphericity. Data were log transformed when not normally distributed. When sphericity could not be assumed, the Greenhouse–Geisser correction statistic was used. Two-way analysis of variance (ANOVA) was performed to determine the effect of GROUP (mTLE and controls) and TIME (pre-training and post-training) on the numbers of errors and correct sequences. One-way ANOVAs were performed to determine the effect of GROUP on the volume size of hippocampal subfields and reference brain areas (i.e., thalamus, caudate, putamen and amygdala). In the above ANOVA analysis, age, gender and years of education (log transformed) were modeled as nuisance variables. Bonferroni *post hoc* analysis was used to test for pairwise comparisons. Partial correlation analyses (corrected for log of years of education) were used to assess the relative importance of each subfield within left and right hippocampus in predicting motor sequence learning. The threshold for significance was set at $P < 0.008$ (Bonferroni correction based on six hippocampal subfields) to control for multiple comparisons. To test the possible impact of epilepsy history and disease load (age at onset, duration, epilepsy frequency) on volume size of hippocampal subfields and motor sequence learning, nonparametric statistics (Spearman correlations) were used. We also examined the possible impact of the time between seizures and the moments of behavioral testing on motor sequence learning with spearman correlations. Significance was set at $P < 0.05$. Group data are presented as mean ± SD in the text.

RESULTS

Behavioral Results

Figure 2 illustrates pre- and post-training performance (numbers of errors and correct sequences completed) during the motor sequence tapping task in mTLE and control groups. A two-way ANOVA showed a significant effect of GROUP ($F_{(1,56)} = 21.3$,

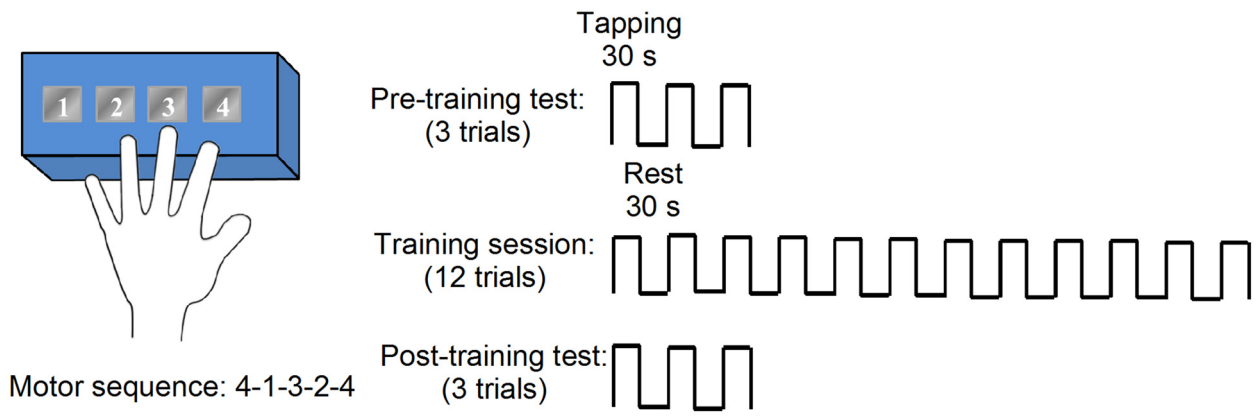

FIGURE 1 | Motor sequence task consisted of blocks of multiple trials, with each trial consisting of an active tapping period (30 s) and a rest period (30 s). Tapping periods required subjects to repeatedly tap a five-element numerical sequence (e.g., 4-1-3-2-4) on a numbered button box. Pre- and post-training performance tests were comprised of three trials, while training involved 12 trials.

$P < 0.001$), TIME ($F_{(1,56)} = 12.4$, $P < 0.001$) and in their interaction ($F_{(1,56)} = 10.1$, $P < 0.001$) on the number of correct sequences completed (**Figure 2A**). *Post hoc* tests showed that the number of correct sequences was greater at post-training compared with pre-training in control ($p < 0.01$) and mTLE groups ($p < 0.01$). However, the increase in the number of correct sequences was greater in controls relative to the mTLE group ($p < 0.001$, **Figure 2B**). There was no difference of the baseline performance between groups ($p > 0.05$). A two-way ANOVA showed no significant effect of GROUP ($F_{(1,56)} = 1.2$, $P = 0.13$), TIME ($F_{(1,56)} = 0.85$, $P = 0.32$) and in their interaction ($F_{(1,56)} = 1.8$, $P = 0.11$) on the number of errors (**Figures 2C,D**).

Volumetric Results

Figure 3 shows volume size of hippocampal subfields (**Figure 3A**) and reference brain areas (i.e., thalamus, caudate, putamen and amygdala; **Figure 3B**) in mTLE and control groups by FreeSurfer v5.1. The ANOVA for hippocampal subfields and reference brain areas showed a significant effect of GROUP on volume size ($F_{(1,19)} = 15.23$, $P = 0.006$). *Post hoc* tests indicated that volume size of all hippocampal subfields was less in the mTLE group compared to the control group: fimbria ($F_{(1,15)} = 11.7$, $P < 0.001$), CA1 ($F_{(1,15)} = 12.4$, $P < 0.001$), CA2-CA3 ($F_{(1,15)} = 15.3$, $P < 0.001$), CA4-DG ($F_{(1,15)} = 8.1$, $P < 0.001$), subiculum ($F_{(1,15)} = 7.8$, $P < 0.001$), and presubiculum ($F_{(1,15)} = 10.5$, $P < 0.001$). However, volume size of specific reference brain areas was not different between groups: thalamus ($F_{(1,15)} = 0.61$, $P = 0.42$), caudate ($F_{(1,15)} = 0.35$, $P = 0.56$), putamen ($F_{(1,15)} = 1.5$, $P = 0.26$) and amygdala ($F_{(1,15)} = 2.01$, $P = 0.18$).

Table 2 presents volume size of hippocampal subfields in mTLE and control groups by FreeSurfer v6.0. The ANOVA for hippocampal subfields in the right hemisphere showed a significant effect of GROUP on volume size ($F_{(1,11)} = 20.1$, $P < 0.001$). *Post hoc* tests indicated that volume size of all hippocampal subfields but the hippocampal fissure in the right hemisphere was less in the mTLE group compared to the control group. In addition, volume size of the hippocampal subfields in the left hemisphere was not different between groups.

Behavior-Volumetric Correlations

Figure 4 illustrates the association between motor sequence learning (i.e., the percentage increase of correct sequences post-training relative to pre-training) and hippocampal subfield volumes in mTLE subjects by FreeSurfer v5.1. Right hippocampal subfield CA2–3 volume was significantly correlated with motor sequence learning in mTLE subjects ($p < 0.008$; **Figure 4**). No other right hippocampal subfield volumes were correlated with motor sequence learning. Right hippocampal subfield volumes were not correlated with motor tapping performance at either pre-training or post-training ($p > 0.05$) nor with seizure frequency, duration of epilepsy, and epilepsy onset ($p > 0.05$). In addition, left hippocampal subfield volumes were not correlated with motor sequence learning ($p > 0.05$). Seizure history and seizure load were not correlated with motor sequence learning ($p > 0.05$). The time between seizures and the moments of behavioral testing were also not correlated with motor sequence learning ($p > 0.05$).

To test the reproducibility of our results, we also calculated the association between motor sequence learning and both sides of hippocampal subfield volumes in mTLE subjects by FreeSurfer v6. The results were similar with that using FreeSurfer v5.1. Only right hippocampal subfield CA2–3 volume was significantly correlated with motor sequence learning in mTLE subjects ($p < 0.001$). No other right or left hippocampal subfield volumes were correlated with motor sequence learning ($p > 0.05$).

DISCUSSION

The current study investigated the effect of mTLE on motor sequence learning. Findings indicate that patients with mTLE can learn a motor sequence tapping task, albeit to a lesser extent than neurologically-intact controls. Although

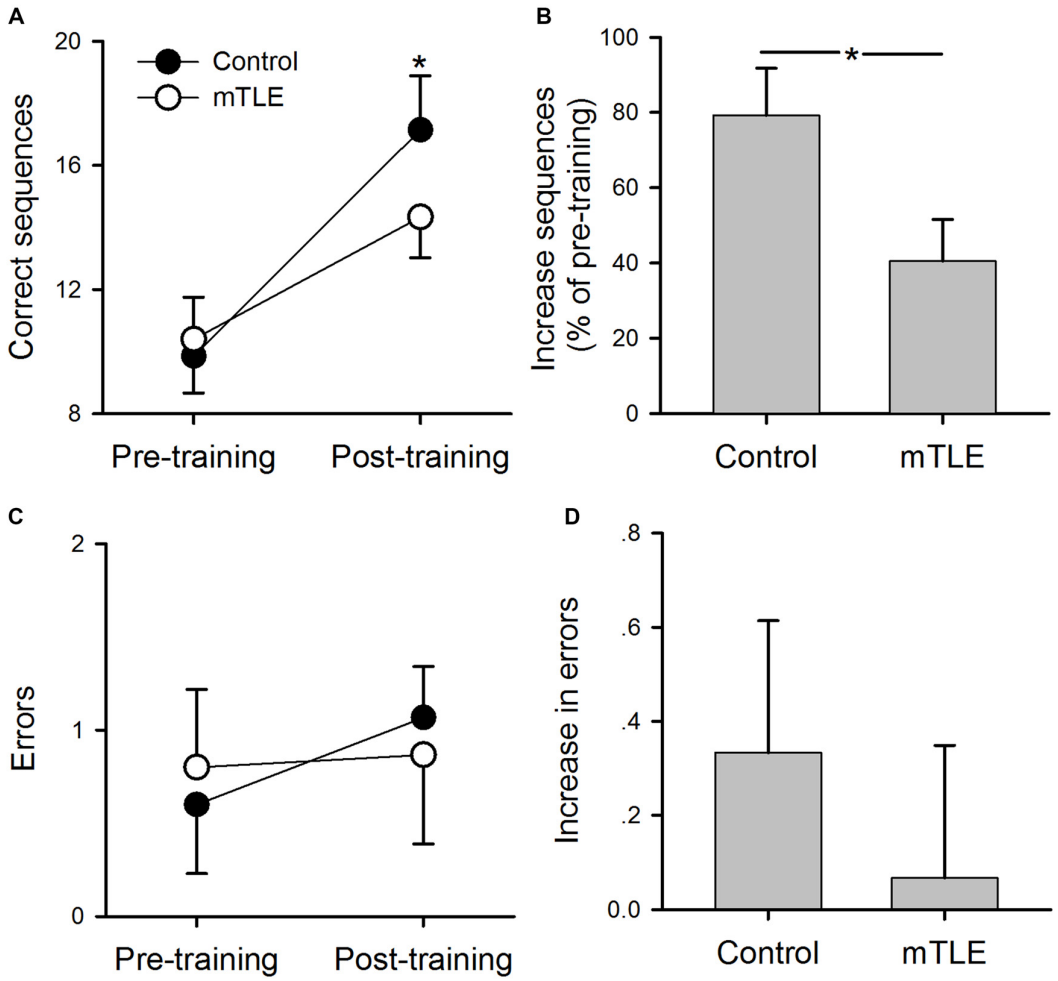

FIGURE 2 | Performance on the motor sequence task. **(A)** Mean number of correct sequences completed during pre- and post-training sessions in control and medial temporal lobe epilepsy (mTLE) groups. **(B)** Percent increase in correct sequences completed from pre- to post-training in control and mTLE groups. **(C)** Mean number of errors during pre- and post-training sessions in control and mTLE groups. **(D)** Percent increase in errors from pre- to post-training sessions in control and mTLE groups. Error bars indicate SDs. $^*P < 0.05$.

all hippocampal subfield volumes were decreased in mTLE patients, CA2–3 volume was associated with motor sequence learning. Thus, results demonstrate that patients with mTLE have impairments in motor memory acquisition. However, these impairments do not preclude some degree of motor sequence learning, which is associated with the volume of hippocampal subfield CA2–3.

Contributions of Hippocampus to Motor Sequence Learning

Consistent with previous work, we found that performance increased after training on a sequence tapping task (Korman et al., 2003; Walker et al., 2003). Since hippocampus is thought to be involved in motor sequence learning (Albouy et al., 2013), it is plausible that structural abnormalities influence learning of such a task even after practice. Previous work has shown that hippocampus is critical for encoding temporally discontiguous but structured information and events (Schendan et al., 2003; Eichenbaum, 2004). If hippocampus contributes to motor sequence learning processes, then disease states such as mTLE would likely alter neuronal interactions critical for learning in this regard. It was therefore unexpected that mTLE patients exhibited sequence learning. The percentage change in performance, however, was significantly reduced relative to controls, suggesting that learning was adversely impacted by hippocampal abnormalities. It should be noted that baseline performance was not different than controls (**Figure 2A**), indicating that individuals in the mTLE group did not have impairments in motor function or were otherwise unable to perform at the same level as participants in the control group. These findings align with previous work showing that amnesic patients outperform controls through intensive training on a serial reaction time task but show an impaired ability to explicitly recognize the sequence of stimuli location (Reber and Squire, 1998). Taken together, motor memory acquisition appears to be supported by medial temporal lobe structures.

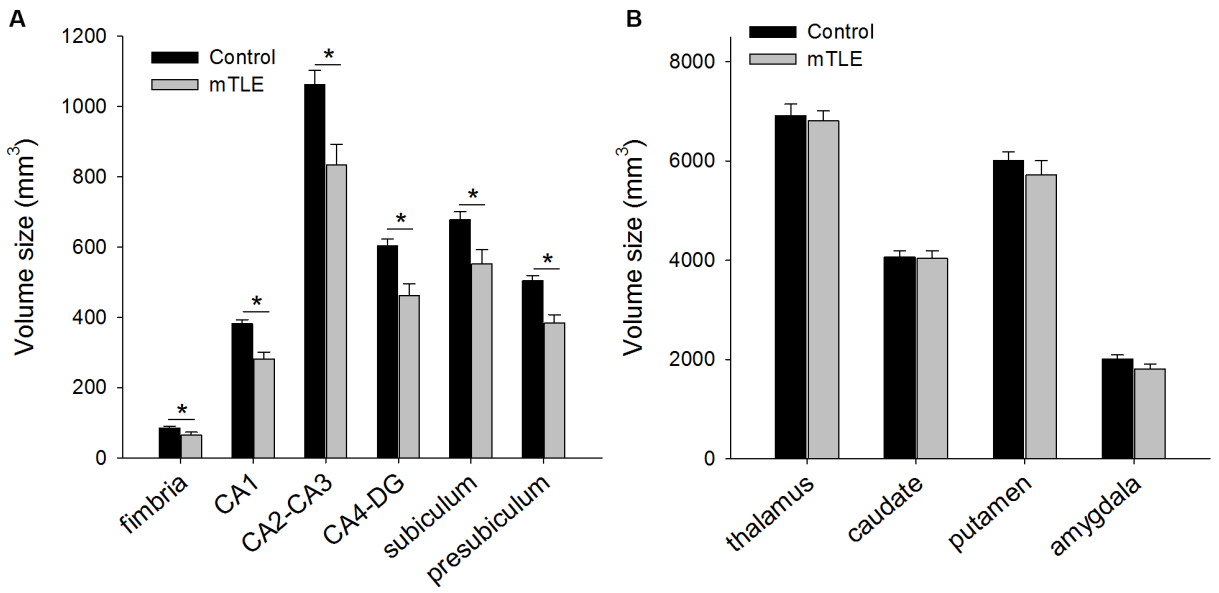

FIGURE 3 | (A) Mean volume size of hippocampus subfields and **(B)** reference brain areas in control and mTLE groups. Error bars indicate SDs. $^*P < 0.05$.

Volume Size in Hippocampal Subfields and Surrounding Brain Areas

mTLE patients had reduced hippocampal subfield volumes, a finding that is consistent with postmortem examination and other cross-sectional studies of this population (Duncan, 1997; Keller and Roberts, 2008; Mueller et al., 2012). The lack of unchanged volumes in other areas such as caudate, putamen, and amygdala for mTLE are generally in agreement previous work (Bernasconi et al., 2004; Keller and Roberts, 2008). However, patients in this study did not exhibit reductions in volume size of the thalamus, which runs counter to prior findings (Bernasconi et al., 2004). The discrepancy

TABLE 2 | Hippocampal subfield volumes calculated by FreeSurfer ver.6.0 (Mean ± SD).

	mTLE (*n* = 15)	Control (*n* = 15)	*p*-value
Left hemisphere			
Hippocampal_tail	568.6 ± 53.2	587.1 ± 71.8	0.38
Subiculum	431.4 ± 52.3	446.3 ± 46.7	0.62
CA1	667.2 ± 75.8	681.9 ± 67.2	0.49
Presubiculum	302.7 ± 22.5	316.8 ± 36.7	0.54
Parasubiculum	52.9 ± 10.8	55.7 ± 13.1	0.68
Molecular_layer	556.3 ± 51.2	556.3 ± 51.2	0.42
GC-DG	310.8 ± 39.2	318.2 ± 35.7	0.48
CA2-CA3	195.8 ± 26.7	203.4 ± 22.4	0.71
CA4	254.9 ± 30.6	261.4 ± 27.8	0.68
Fimbria	93.3 ± 23.8	106.7 ± 27.2	0.52
HATA	61.5 ± 8.3	60.6 ± 10.6	0.76
Hippocampal_fissure	151.4 ± 25.9	156.1 ± 28.7	0.63
Right hemisphere			
Hippocampal_tail	391.7 ± 90.1	562.3 ± 64.9	0.38
Subiculum	305.8 ± 56.4	452.1 ± 49.5	0.62
CA1	462.3 ± 86.4	667.8 ± 62.1	0.49
Presubiculum	215.3 ± 30.6	320.1 ± 28.9	0.54
Parasubiculum	40.2 ± 8.5	58.3 ± 11.4	0.68
Molecular_layer	382.4 ± 49.1	571.3 ± 52.3	0.42
GC-DG	205.3 ± 34.5	305.7 ± 37.1	0.48
CA2-CA3	126.7 ± 27.1	221.8 ± 32.8	0.71
CA4	162.7 ± 33.2	278.1 ± 30.2	0.68
Fimbria	59.6 ± 18.2	95.5 ± 20.4	0.52
HATA	51.7 ± 10.2	61.5 ± 9.2	0.76
Hippocampal_fissure	141.7 ± 28.3	150.2 ± 23.6	0.63

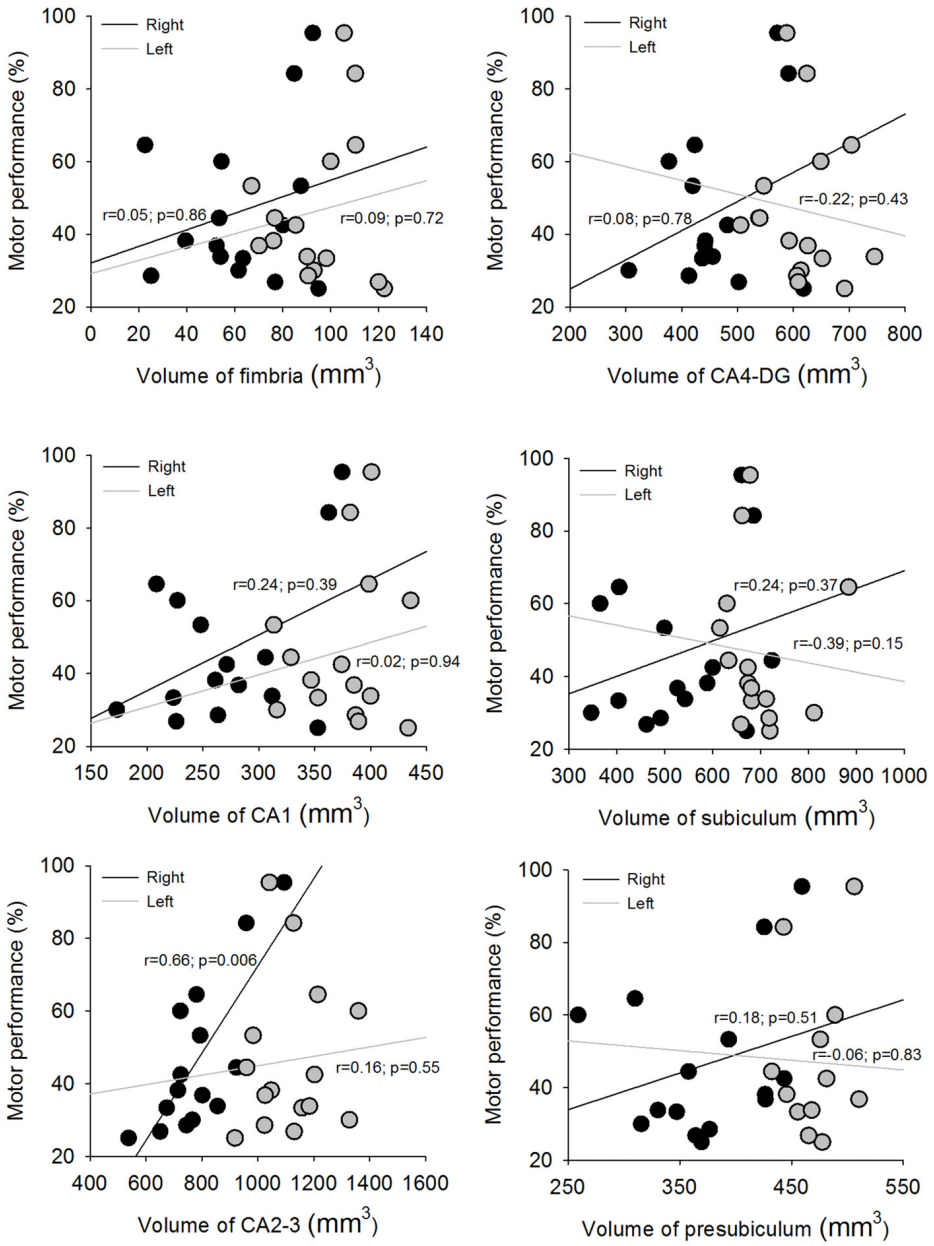

FIGURE 4 | Scatter plots depicting the association between motor sequence learning and the hippocampus subfields in right and left hemispheres.

may be because mTLE patients in the current study did not have a history of febrile convulsions (Dreifuss et al., 2001).

CA2–3 Contributions to Motor Sequence Learning

We found that subfield CA2–3 was the only hippocampal subfield associated with motor sequence learning in the mTLE group. There is evidence showing that sub-region CA3 plays a significant role in short-term spatial memory acquisition and encoding processes, while sub-region CA1 contributes to intermediate/long-term spatial memory and consolidation (O'Reilly and McClelland, 1994; Treves and Rolls, 1994; Kesner et al., 2004; Remondes and Schuman, 2004; Daumas et al., 2005). Within a given day, encoding of information acquired in a Hebb-Williams maze or in contextual fear conditioning is impaired by targeted lesions to the CA3 and DG sub-regions, but not from targeted lesions to the CA1 sub-region. In contrast, retention and retrieval is disrupted following lesions to CA1 across days, but not following lesions to CA3 or DG (Lee and Kesner, 2004a,b; Jerman et al., 2006). Impairments have also been demonstrated in delay-dependent retrieval without

impairing immediate recall or encoding of spatial information after infusing glutamatergic antagonists (Lee and Kesner, 2002), or cyclooxygenase-2 inhibitors (Sharifzadeh et al., 2006) into the CA1 sub-region, but not when infused into the CA3 sub-region. Findings from the current study are in agreement with those of previous work and demonstrate that the integrity of the CA2–3 hippocampal subfield was correlated with motor sequence learning.

Limitations

Aside from a small sample size, there are at least four important limitations of our study. First, the current cross-sectional study is limited in that it does not capture long-term hippocampal volume loss. Understanding the evolution of change in volume of hippocampus and its individual subfields would provide unique insights into the relationship between volumetric reductions due to mTLE and the extent of impairments in motor sequence learning. Second, motor sequence learning was only related to initial motor memory acquisition in the current study. Future studies should examine other hippocampal-dependent tasks associated with other types of memory (e.g., non-motor sequence learning), which will provide greater insight into the role of specific sub-parts of the hippocampus. Third, we only investigated initial motor memory acquisition. Whether long-term memory or consolidation of the motor sequence is impacted by mTLE is an important consideration. Accordingly, future work should focus on how memories are sufficiently strengthened to be behaviorally salient, thus, allowing further insight into the role of specific hippocampal regions. Finally, since mTLE may be a heterogeneous group with varying hippocampal subfield anomalies difficult to identify solely based on MRI, future work can expand on the current findings by including a histopathology report according to the International League Against Epilepsy (ILAE) classification of Hippocampal sclerosis (Blümcke et al., 2013).

DISCLOSURE

We confirm that we have read the Journal's position on issues involved in ethical publication and affirm that this report is consistent with those guidelines.

AUTHOR CONTRIBUTIONS

All authors reviewed and approved the manuscript content.

FUNDING

This work was partly supported by the funding from the National Natural Science Foundation of China (Grant No. 61403147 and 61773179), and Guangdong Provincial Natural Science Foundation of China (Program No. 2014A030313233).

REFERENCES

Acsády, L., and Káli, S. (2007). Models, structure, function: the transformation of cortical signals in the dentate gyrus. *Prog. Brain Res.* 163, 577–599. doi: 10.1016/s0079-6123(07)63031-3

Albouy, G., King, B. R., Maquet, P., and Doyon, J. (2013). Hippocampus and striatum: dynamics and interaction during acquisition and sleep-related motor sequence memory consolidation. *Hippocampus* 23, 985–1004. doi: 10.1002/hipo.22183

Albouy, G., Sterpenich, V., Balteau, E., Vandewalle, G., Desseilles, M., Dang-Vu, T., et al. (2008). Both the hippocampus and striatum are involved in consolidation of motor sequence memory. *Neuron* 58, 261–272. doi: 10.1016/j.neuron.2008.02.008

Bernasconi, N., Duchesne, S., Janke, A., Lerch, J., Collins, D. L., and Bernasconi, A. (2004). Whole-brain voxel-based statistical analysis of gray matter and white matter in temporal lobe epilepsy. *Neuroimage* 23, 717–723. doi: 10.1016/j.neuroimage.2004.06.015

Blümcke, I., Thom, M., Aronica, E., Armstrong, D. D., Bartolomei, F., Bernasconi, A., et al. (2013). International consensus classification of hippocampal sclerosis in temporal lobe epilepsy: a Task Force report from the ILAE commission on diagnostic methods. *Epilepsia* 54, 1315–1329. doi: 10.1111/epi.12220

Blum, S., Moore, A. N., Adams, F., and Dash, P. K. (1999). A mitogen-activated protein kinase cascade in the CA1/CA2 subfield of the dorsal hippocampus is essential for long-term spatial memory. *J. Neurosci.* 19, 3535–3544. doi: 10.1523/JNEUROSCI.19-09-03535.1999

Buckner, R. L., Head, D., Parker, J., Fotenos, A. F., Marcus, D., Morris, J. C., et al. (2004). A unified approach for morphometric and functional data analysis in young, old, and demented adults using automated atlas-based head size normalization: reliability and validation against manual measurement of total intracranial volume. *Neuroimage* 23, 724–738. doi: 10.1016/j.neuroimage.2004.06.018

Chun, M. M., and Phelps, E. A. (1999). Memory deficits for implicit contextual information in amnesic subjects with hippocampal damage. *Nat. Neurosci.* 2, 844–847. doi: 10.1038/12222

Clark, R. E., and Squire, L. R. (1998). Classical conditioning and brain systems: the role of awareness. *Science* 280, 77–81. doi: 10.1126/science.280.5360.77

Coras, R., Pauli, E., Li, J., Schwarz, M., Rössler, K., Buchfelder, M., et al. (2014). Differential influence of hippocampal subfields to memory formation: insights from patients with temporal lobe epilepsy. *Brain* 137, 1945–1957. doi: 10.1093/brain/awu100

Curran, T. (1997). Higher-order associative learning in amnesia: evidence from the serial reaction time task. *J. Cogn. Neurosci.* 9, 522–533. doi: 10.1162/jocn.1997.9.4.522

Daumas, S., Halley, H., Francés, B., and Lassalle, J. M. (2005). Encoding, consolidation, and retrieval of contextual memory: differential involvement of dorsal CA3 and CA1 hippocampal subregions. *Learn. Mem.* 12, 375–382. doi: 10.1101/lm.81905

Doyon, J., Penhune, V., and Ungerleider, L. G. (2003). Distinct contribution of the cortico-striatal and cortico-cerebellar systems to motor skill learning. *Neuropsychologia* 41, 252–262. doi: 10.1016/s0028-3932(02)00158-6

Dreifuss, S., Vingerhoets, F. J., Lazeyras, F., Andino, S. G., Spinelli, L., Delavelle, J., et al. (2001). Volumetric measurements of subcortical nuclei in patients with temporal lobe epilepsy. *Neurology* 57, 1636–1641. doi: 10.1212/WNL.57.9.1636

Duncan, J. S. (1997). Imaging and epilepsy. *Brain* 120, 339–377. doi: 10.1093/brain/120.2.339

Eichenbaum, H. (2004). Hippocampus: cognitive processes and neural representations that underlie declarative memory. *Neuron* 44, 109–120. doi: 10.1016/j.neuron.2004.08.028

Fisch, B., Salat, D. H., van der Kouwe, A. J., Makris, N., Ségonne, F., Quinn, B. T., et al. (2004). Sequence-independent segmentation of magnetic resonance images. *Neuroimage* 23, S69–S84. doi: 10.1016/j.neuroimage.2004.07.016

Grafton, S. T., Hazeltine, E., and Ivry, R. (1995). Functional mapping of sequence learning in normal humans. *J. Cogn. Neurosci.* 7, 497–510. doi: 10.1162/jocn.1995.7.4.497

Hasselmo, M. E. (2005). The role of hippocampal CA3 and CA1 in matching entorhinal input with retrieval of associations between objects and context: theoretical comment on Lee et al. (2005). *Behav. Neurosci.* 119, 342–345. doi: 10.1037/0735-7044.119.1.342

Iglesias, J. E., Augustinack, J. C., Nguyen, K., Player, C. M., Player, A., Wright, M., et al. (2015). A computational atlas of the hippocampal formation using ex vivo, ultra-high resolution MRI: application to adaptive segmentation of *in vivo* MRI. *Neuroimage* 115, 117–137. doi: 10.1016/j.neuroimage.2015.04.042

Jerman, T., Kesner, R. P., and Hunsaker, M. R. (2006). Disconnection analysis ofCA3 and DG in mediating encoding but not retrieval in a spatial maze learning task. *Learn. Mem.* 13, 458–464. doi: 10.1101/lm.246906

Keller, S. S., and Roberts, N. (2008). Voxel-based morphometry of temporal lobe epilepsy: an introduction and review of the literature. *Epilepsia* 49, 741–757. doi: 10.1111/j.1528-1167.2007.01485.x

Kesner, R. P., Lee, I., and Gilbert, P. (2004). A behavioral assessment of hippocampal function based on a subregional analysis. *Rev. Neurosci.* 15, 333–351. doi: 10.1515/revneuro.2004.15.5.333

Korman, M., Raz, N., Flash, T., and Karni, A. (2003). Multiple shifts in the representation of a motor sequence during the acquisition of skilled performance. *Proc. Natl. Acad. Sci. U S A* 100, 12492–12497. doi: 10.1073/pnas.2035019100

Lee, I., and Kesner, R. P. (2002). Differential contribution of NMDA receptors in hippocampal subregions to spatial working memory. *Nat. Neurosci.* 5, 162–168. doi: 10.1038/nn790

Lee, I., and Kesner, R. P. (2004a). Differential contributions of dorsal hippocampal subregions to memory acquisition and retrieval in contextual fear-conditioning. *Hippocampus* 14, 301–310. doi: 10.1002/hipo.10177

Lee, I., and Kesner, R. P. (2004b). Encoding versus retrieval of spatial memory: double dissociation between the dentate gyrus and the perforant path inputs into CA3 in the dorsal hippocampus. *Hippocampus* 14, 66–76. doi: 10.1002/hipo.10167

Marsh, L., Morrell, M. J., Shear, P. K., Sullivan, E. V., Freeman, H., Marie, A., et al. (1997). Cortical and hippocampal volume deficits in temporal lobe epilepsy. *Epilepsia* 38, 576–587. doi: 10.1111/j.1528-1157.1997.tb01143.x

Mueller, S. G., Laxer, K. D., Scanlon, C., Garcia, P., McMullen, W. J., Loring, D. W., et al. (2012). Different structural correlates for verbal memory impairment in temporal lobe epilepsy with and without mesial temporal lobe sclerosis. *Hum. Brain Mapp.* 33, 489–499. doi: 10.1002/hbm.21226

O'Reilly, R. C., and McClelland, J. L. (1994). Hippocampal conjunctive encoding, storage, and recall: avoiding a trade-off. *Hippocampus* 4, 661–682. doi: 10.1002/hipo.450040605

Poldrack, R. A., Clark, J., Paré-Blagoev, E. J., Shohamy, D., Creso Moyano, J., Myers, C., et al. (2001). Interactive memory systems in the human brain. *Nature* 414, 546–550. doi: 10.1038/35107080

Reber, P. J., and Squire, L. R. (1998). Encapsulation of implicit and explicit memory in sequence learning. *J. Cogn. Neurosci.* 10, 248–263. doi: 10.1162/089892998562681

Remondes, M., and Schuman, E. M. (2004). Role for a cortical input to hippocampal area CA1 in the consolidation of a long-term memory. *Nature* 431, 699–703. doi: 10.1038/nature02965

Ségonne, F., Dale, A. M., Busa, E., Glessner, M., Salat, D., Hahn, H. K., et al. (2004). A hybrid approach to the skull stripping problem in MRI. *Neuroimage* 22, 1060–1075. doi: 10.1016/j.neuroimage.2004.03.032

Schendan, H. E., Searl, M. M., Melrose, R. J., and Stern, C. E. (2003). An FMRI study of the role of the medial temporal lobe in implicit and explicit sequence learning. *Neuron* 37, 1013–1025. doi: 10.1016/s0896-6273(03)00123-5

Sharifzadeh, M., Tavasoli, M., Soodi, M., Mohammadi-Eraghi, S., Ghahremani, M. H., and Roghani, A. (2006). A time course analysis of cyclooxygenase-2 suggests a role in spatial memory retrieval in rats. *Neurosci. Res.* 54, 171–179. doi: 10.1016/j.neures.2005.11.004

Treves, A., and Rolls, E. T. (1994). Computational analysis of the role of the hippocampus in memory. *Hippocampus* 4, 374–391. doi: 10.1002/hipo.450040319

Vago, D. R., Bevan, A., and Kesner, R. P. (2007). The role of the direct perforant path input to the CA1 subregion of the dorsal hippocampus in memory retention and retrieval. *Hippocampus* 17, 977–987. doi: 10.1002/hipo.20329

Walker, M. P., Brakefield, T., Hobson, J. A., and Stickgold, R. (2003). Dissociable stages of human memory consolidation and reconsolidation. *Nature* 425, 616–620. doi: 10.1038/nature01930

Willingham, D. B., Salidis, J., and Gabrieli, J. D. (2002). Direct comparison of neural systems mediating conscious and unconscious skill learning. *J. Neurophysiol.* 88, 1451–1460. doi: 10.1152/jn.2002.88.3.1451

Conflict of Interest Statement: The authors declare that the research was conducted in the absence of any commercial or financial relationships that could be construed as a potential conflict of interest.

Copyright © 2018 Long, Feng, Liao, Zhou and Urbin. This is an open-access article distributed under the terms of the Creative Commons Attribution License (CC BY). The use, distribution or reproduction in other forums is permitted, provided the original author(s) and the copyright owner(s) are credited and that the original publication in this journal is cited, in accordance with accepted academic practice. No use, distribution or reproduction is permitted which does not comply with these terms.

frontiers in Behavioral Neuroscience

ORIGINAL RESEARCH
published: 02 October 2018
doi: 10.3389/fnbeh.2018.00226

Impaired Performance of the Q175 Mouse Model of Huntington's Disease in the Touch Screen Paired Associates Learning Task

*Tuukka O. Piiponniemi[1†], Teija Parkkari[1], Taneli Heikkinen[1], Jukka Puoliväli[1], Larry C. Park[2], Roger Cachope[2] and Maksym V. Kopanitsa[1,3]**

[1]Charles River Discovery Services, Kuopio, Finland, [2]CHDI Management/CHDI Foundation, Los Angeles, CA, United States, [3]UK Dementia Research Institute at Imperial College London, Division of Brain Sciences, Department of Medicine, Imperial College London, London, United Kingdom

Cognitive disturbances often predate characteristic motor dysfunction in individuals with Huntington's disease (HD) and place an increasing burden on the HD patients and caregivers with the progression of the disorder. Therefore, application of maximally translational cognitive tests to animal models of HD is imperative for the development of treatments that could alleviate cognitive decline in human patients. Here, we examined the performance of the Q175 mouse knock-in model of HD in the touch screen version of the paired associates learning (PAL) task. We found that 10–11-month-old heterozygous Q175 mice had severely attenuated learning curve in the PAL task, which was conceptually similar to previously documented impaired performance of individuals with HD in the PAL task of the Cambridge Neuropsychological Test Automated Battery (CANTAB). Besides high rate of errors in PAL task, Q175 mice exhibited considerably lower responding rate than age-matched wild-type (WT) animals. Our examination of effortful operant responding during fixed ratio (FR) and progressive ratio (PR) reinforcement schedules in a separate cohort of similar age confirmed slower and unselective performance of mutant animals, as observed during PAL task, but suggested that motivation to work for nutritional reward in the touch screen setting was similar in Q175 and WT mice. We also demonstrated that pronounced sensorimotor disturbances in Q175 mice can be detected at early touch screen testing stages, (e.g., during "Punish Incorrect" phase of operant pretraining), so we propose that shorter test routines may be utilised for more expedient studies of treatments aimed at the rescue of HD-related phenotype.

Keywords: Huntington's disease, visuospatial, touch screen, paired associates learning, reinforcement, progressive ratio, motivation, mouse

OPEN ACCESS

Edited by:
Caroline Whyatt, University of Hertfordshire, United Kingdom

Reviewed by:
Xavier Xifró, University of Girona, Spain
Maud Gratuze, Washington University in St. Louis, United States

****Correspondence:***
Maksym V. Kopanitsa
m.kopanitsa@imperial.ac.uk

†Present address:
Tuukka O. Piiponniemi, Faculty of Medicine, Tartu University, Tartu, Estonia

Received: *09 July 2018*
Accepted: *10 September 2018*
Published: *02 October 2018*

Citation:
Piiponniemi TO, Parkkari T, Heikkinen T, Puoliväli J, Park LC, Cachope R and Kopanitsa MV (2018) Impaired Performance of the Q175 Mouse Model of Huntington's Disease in the Touch Screen Paired Associates Learning Task. Front. Behav. Neurosci. 12:226. doi: 10.3389/fnbeh.2018.00226

INTRODUCTION

Huntington's disease (HD) is a late-onset neurological condition characterised by progressive cognitive impairment and motor disturbances (McColgan and Tabrizi, 2018). The prevalence of HD is approximately 1 in 10,000 in individuals of Western European descent, whereas in Asian populations, the incidence is much lower (Baig et al., 2016). HD arises due to

autosomal dominantly inherited expansion of CAG trinucleotide repeats in the huntingtin (*HTT*) gene on chromosome 4, which results in the production of mutant HTT protein with abnormally long polyglutamine track at the N-terminus (MacDonald et al., 1993). Aggregation of mutated HTT negatively impacts multiple cellular processes, including transcription, translation, proteostasis and mitochondrial function (Jimenez-Sanchez et al., 2017). Axonal transport and synaptic function deficits are prominent in neurones affected by HD with striatal medium spiny neurones being particularly sensitive (Bunner and Rebec, 2016). HD is usually diagnosed in middle age (35–45 years of age), when first motor symptoms begin to appear, followed by fatal outcome within 20 years. Despite a well-established genetic underpinning of HD, the currently approved treatments are all symptomatic and as such, do not modify the disease progression (Mrzljak and Munoz-Sanjuan, 2015; Wyant et al., 2017).

To understand the mechanisms of HD pathogenesis and to establish experimental platforms for drug discovery, multiple lines of genetically altered mice have been generated that can be classified into three groups: (a) mice expressing truncated human *HTT* fragments, e.g., R6 lines; (b) mice expressing full-length human *HTT* modified by the insertion of variable numbers of CAG repeats, e.g., YAC128 or BACHD lines; and (c) knock-in models, in which CAG repeats are inserted into the endogenous mouse *Htt* gene, e.g., Hdh^{Q92} line (Menalled and Chesselet, 2002; Chang et al., 2015). There are several reasons to use knock-in models of HD. First, the placement of abnormally expanded CAG repeats into the endogenous mouse *Htt* gene context avoids overexpression artefacts. Second, although the phenotype in knock-in mice takes longer to develop and is relatively mild, this circumstance may be advantageous for designing longitudinal experiments and is mechanistically reminiscent of the late HD onset in humans.

The knock-in Q175 model derives from Hdh^{Q140} line and has a spontaneous expansion of the CAG copy number in exon 1 of *Htt* (Menalled et al., 2012). Despite both heterozygous and homozygous Q175 mice generally have less aggressive phenotype than some other HD mouse models, they nonetheless recapitulate main manifestations of HD in humans, such as progressive accumulation of mutant huntingtin aggregates in striatal and cortical neurones, synapse loss, striatal and cortical atrophy, altered brain metabolic profile, decreased body weight and motor impairments (Oakeshott et al., 2011; Heikkinen et al., 2012; Menalled et al., 2012; Peng et al., 2016). Cognitive behaviour of Q175 mice was assessed by using two-choice swimming test, T-maze, and simple instrumental tasks that used lever presses and nosepokes to obtain nutritional reinforcement (Oakeshott et al., 2011, 2013; Heikkinen et al., 2012; Menalled et al., 2012; Whittaker et al., 2017). To make the results of behavioural evaluations of mouse models of HD more relevant to the clinical setting, it would be advantageous to apply testing techniques that have greater similarity to cognitive examinations of humans. Touch screen-based approach has a high translational value as unlike some more forceful techniques to assess cognitive functions in rodents, it is based on interactions with a touch-sensitive screen prompted by visual stimuli and nutritional rewards for correct responses (Bussey et al., 2012; Hvoslef-Eide et al., 2016). Q175 mice, as well as other HD mouse models, such as R6/2 and BACHD, were recently tested in touch screen chambers and found to exhibit age-dependent deficits in the acquisition of pairwise visual discrimination skills and in the reversal of visual discrimination learning (Morton et al., 2006; Farrar et al., 2014; Skillings et al., 2014; Curtin et al., 2015; Glynn et al., 2016). From the instrumental point of view, the touch screen-based setting is analogous to the one used for clinical assessment of cognitive impairment in humans, e.g., by the Cambridge Neuropsychological Test Automated Battery (CANTAB; Nithianantharajah and Grant, 2013). Many studies have utilised the paired associates learning (PAL) CANTAB task to evaluate cognitive functions in individuals affected by neurodegenerative diseases. In that task, during encoding phase, the participant has to memorise the locations on the screen of initially one and gradually up to eight unique patterns and then, during the retrieval, touch the correct white boxes, where each stimulus, now presented in the centre of the screen, was shown during encoding (Barnett et al., 2016). PAL task performance was found to be impaired in HD patients (Lange et al., 1995; Lawrence et al., 1996; Begeti et al., 2016). In the rodent version of the task (Talpos et al., 2009; Horner et al., 2013), animals demonstrate learning of the similar object-location relationship by selectively touching one (correct) out of two simultaneously presented images on the basis of its location on the screen (**Figure 1A**). Common neural basis of performance in rodents and humans has been inferred from lesion, pharmacological and genetic studies in the former and brain imaging studies in the latter (Barnett et al., 2016). This circumstance facilitates the translation of PAL results obtained in preclinical models to the clinical setting as it indicates similarity of behavioural processing strategies in humans and rodents. In the present study, we examined whether Q175 mice had deficits in the mouse version of PAL task. In addition, because performance of Q175 mice during PAL routine suggested altered motivation to perform food-rewarded touch screen tasks, we also compared the rates of sustained repetitive responding of Q175 and litter-matched wild-type (WT) mice in fixed ratio (FR) and progressive ratio (PR) operant tasks recently implemented in the touch screen chamber setting (**Figure 1B**; Heath et al., 2015, 2016).

MATERIALS AND METHODS

Animals

All animal experiments were performed as specified in the licence authorised by the National Animal Experiment Board of Finland (Eläinkoelautakunta, ELLA) and according to the National Institutes of Health (Bethesda, MD, USA) guidelines for the care and use of laboratory animals.

Given that homozygosity for the extended CAG repeat is extremely rare in humans, we sought to assess cognitive phenotypes in mice heterozygous for the mutant knock-in allele. As it has been shown that cognitive performance in heterozygous

Q175 mice progressively decreases with age (Curtin et al., 2015; Southwell et al., 2016), to maximise the chance to reveal phenotypes in touch screen tests, we chose to work with 10–11-month-old animals.

In the PAL experiment, the selected cohort comprised 14 male 10-month old Q175 mice heterozygous for the mutant *Htt*^{tm1Mfc} allele harbouring 185–210 CAG repeats (Menalled et al., 2012) and 15 age-matched male WT mice. We will henceforth refer to this subset of mutants by their original name, zQ175.

In the course of testing, one mutant mouse failed to complete the last pretraining stage and another mutant mouse acquired PAL very slowly, so it had to be excluded from the final PAL analysis. Thus, PAL performance was analysed for 15 WT and 12 zQ175 mice.

For the FR/PR test, we used a separate cohort of 12 male 11-month-old Q175FΔ*neo* mice (Southwell et al., 2016) and 11 WT littermates that were housed at 2–3 animals per cage. These animals had the floxed *neo* cassette upstream of exon 1 removed, whereas zQ175 mice used in the PAL test retained it[1]. We used this subtype of Q175 mice because during the allocated slot for FR/PR tests, only Q175FΔ*neo* mice were available that had age and sex comparable to those in the above described zQ175 cohort from the PAL test. Moreover, it has been shown that the phenotype of Q175FΔ*neo* mice is similar to that of the mutants retaining the *neo* cassette, although the changes become manifested at a slightly earlier age (Southwell et al., 2016; Heikkinen et al., 2017). In the end of the experiments, tail samples were sent to Laragen Inc. for genotype and CAG repeat number confirmation.

Animals were kept in a temperature- and humidity-controlled environment under a 13:11 h light/dark cycle (lights on at 07:00 am and off at 8:00 pm) at 22 ± 1°C. Cages (IVC type II, Allentown Inc., Allentown, NJ, USA) were kept at negative pressure and furnished with corn cob-derived bedding (The Andersons, Maumee, OH, USA), nesting material (aspen wool, Tapvei Oy, Kortteinen, Finland), a tinted polycarbonate tunnel (Datesand, Manchester, UK) and a petite green gumabone (BioServ, Flemington, NJ, USA). During the experiment, mice were kept on a restricted diet (Purina Lab Diet 5001) at 85%–90% of their free-feeding weight in order to maintain motivation for the task, with water *ad libitum*.

For the PAL test, mice received one 60-min long training session per day, whereas in the FR/PR test, animals were tested for up to 120 min daily. For both tests, testing proceeded in the afternoon hours, starting between 4:30 pm and 6:30 pm, 5–7 days per week.

Food Deprivation

Before the start of the experiments, animals were gently handled and weighed. Access to food was gradually restricted, so that each animal was within 85%–90% of their free feeding weight. In addition, a small quantity of Valio Profeel strawberry-flavoured milk drink (Valio, Helsinki, Finland) was provided initially into the cages to accustom the animals with the flavour and taste of the reward to be used during testing. To maintain the weight of mice in the 85%–90% range throughout testing period, the animals received a rationed amount (typically 2.5–3.5 g) of standard lab pellets daily immediately after testing.

Equipment

Touchscreen testing was performed in 24 Bussey-Saksida mouse touch screen operant chambers (Campden Instruments, Loughborough, UK) essentially as described (Horner et al., 2013; Heath et al., 2016). For the PAL and FR/PR tasks, the 3- and 5-window masks were used in front of the touch sensitive screen, respectively (Campden Instruments).

Activity Assessment

On the first day of testing, after a 3-day gradual food deprivation period, the naïve mice were placed individually into Campden Instruments Ltd. touchscreen chambers for 30 min, with no rewards available. The total numbers of beam breaks (combined front and rear), traversals (number of

[1]http://www.informatics.jax.org/allele/key/24931

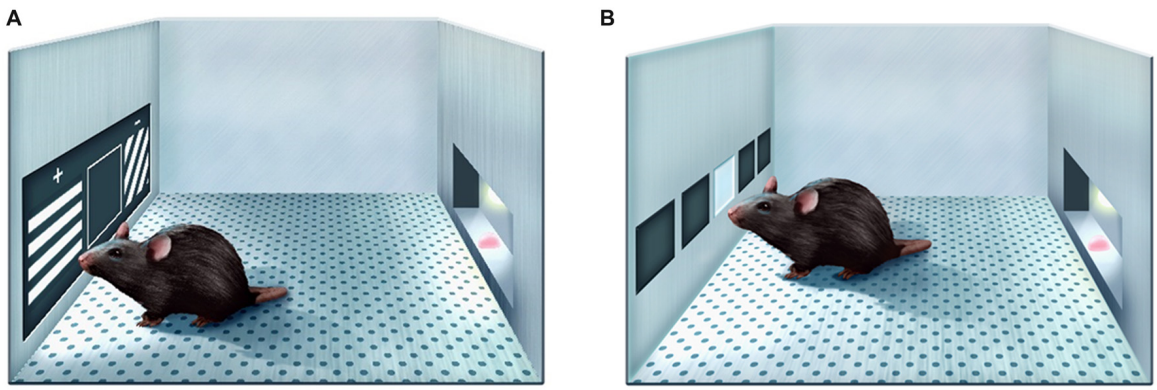

FIGURE 1 | Schematic illustration of the paired associates learning (PAL) task **(A)** and Fixed/Progressive Ratio (FR/PR) task **(B)** in Bussey-Saksida touch screen operant chambers.

times the mouse "traversed" the chamber, defined as a rear beam break followed by a front beam break), screen touches and nose pokes into the food magazine in 30 min were recorded.

Pre-training for the PAL Task

Prior to the PAL test, the mice were trained on basic touchscreen task requirements, which were introduced gradually, as described previously (Horner et al., 2013, 2018). Following activity assessment, mice were first tested in a Pavlovian task ("Initial Touch" stage) that introduced several aspects of the touchscreen testing, including the relationship between visual stimulus presentation and reward availability. One out of 40 variously shaped images was presented randomly in one of the three response windows for 30 s. When the image disappeared, the magazine light turned on and a drop reward was delivered with a tone. If the mouse touched the image, it disappeared immediately and the mouse was rewarded with a larger reward portion concomitantly with a tone and magazine illumination. After a 20-s inter-trial interval (ITI), the next trial commenced. This stage was considered complete when 30 trials were completed in 1 h and all rewards were consumed.

At the next stage of pre-training ("Must Touch" stage), a visual stimulus was presented randomly in one of the three locations on the screen, and remained there until touched, introducing the requirement for mice to touch (nose-poke) the image on the screen. Doing so was rewarded (milkshake, tone, magazine light on). A 20-s ITI (magazine inactive, no image presented) occurred after the collection of the reward pellet, after which a new trial began with a presentation of the next image. This stage was considered complete when 30 trials are completed in 1 h.

Thereafter, the requirement to initiate trials was introduced ("Must Initiate" stage); sessions progressed as in the previous phase, but after the ITI, the magazine light was turned on, and mice had to nose poke into it to start the next trial. Successful initiation (here and in all subsequent task phases) was indicated by the extinction of the magazine light and appearance of an image on the screen. Again, this stage was considered complete when the mouse finished 30 trials in 1 h.

Finally, a "punishment" was introduced for touching the empty (plain black) location instead of the image providing a cue that signalled incorrect responses ("Punish Incorrect" stage). Sessions progressed as in the previous stage, except that if a mouse touched the empty location, it was "punished" with a 5 s "time out" (image disappeared, house light switched on, no reward). Following this, a 5 s correction ITI started after which mice could initiate a correction trial, to begin a correction procedure. In the correction procedure, the trial was repeated with the same stimuli in the same location until the mouse made the correct response. A correct response was rewarded in the usual way, the correction procedure ended, and after a standard 20 s ITI, mice were able to initiate a normal trial. After reaching a performance criterion of at least 75% of the 36 trials in a session correct (not including correction trials) and with 36 trials completed in under 60 min in two consecutive sessions, mice were moved on to the actual PAL task.

PAL Task

During the PAL task, each daily 36-trial (or maximum 60-min long) session commenced with the requirement to initiate, as during pretraining. Doing so triggered presentation of a pair of images, one in two of the three windows (left, middle or right). The third window remained blank and non-responsive. There were three possible visual stimuli ("Lines Grid-Right," "Lines Grid-Left" and "Vertical lines") with dark and light lines going in different directions (**Figure 1A**). On each trial, the correct (S+) stimulus was determined by a combination of stimulus shape (the "object") and its location, e.g., "Vertical lines" image was correct in the left location, "Grid-Right" image—in the middle, and "Grid-left image"—on the right. On each trial, one image was presented in its correct location along with one of the two alternative images in its incorrect location (S−), giving a total of 6 possible trial types. Visual stimuli remained on the screen until S+ or S− was touched, and were removed immediately following a touch to either. Touches to the blank inactive location were ignored. Response to S+ was rewarded (tone, reward drop of milkshake delivered, magazine light on, no "time out"); response to the S− was "punished" (house light on for a 5 s "time out," no milkshake delivery). Incorrect responses to S− were followed by a correction procedure as described above. The task ITI was normally 20 s, but only 5 s prior to correction trials. No trial type was presented more than three times consecutively.

Mice were tested for 50 compound sessions, and their performance was analysed in blocks of five sessions ($36 \times 5 = 180$ trials in total). The minimal possible duration of PAL testing was 53 days, because the first and second of the 50 sessions were deliberately split into 3 and 2 days (3×12 trials and 2×18 trials), respectively, to introduce the animals gradually to the PAL task. It should be noted that the precise definition of the PAL "session" in this study was the total time needed for the mouse to complete 36 trials: because many animals failed to complete the usually required 36 daily trials (Horner et al., 2018) for multiple days, particularly during the early stages of the PAL task, additional training days were given as required to ensure all mice were presented with exactly 1,800 trials in total.

Performance score (number of correct responses out of 36 trials in each session) was converted to a percentage correct score for each mouse, and these were averaged across 180 trials (i.e., blocks of five sessions). The numbers of correction touches, touches to the blank area, as well as response times and reward collection latencies were also recorded and analysed across blocks of five sessions.

FR Training

Following activity assessment and completion of "Initial Touch" pre-training, identical to that used for mice in the PAL group, the animals in the *FR/PR* group underwent FR training during which animals learned to nose-poke the image initially once and then several times in a row to receive the reward (Heath et al., 2015, 2016). Animals were permitted a maximum of

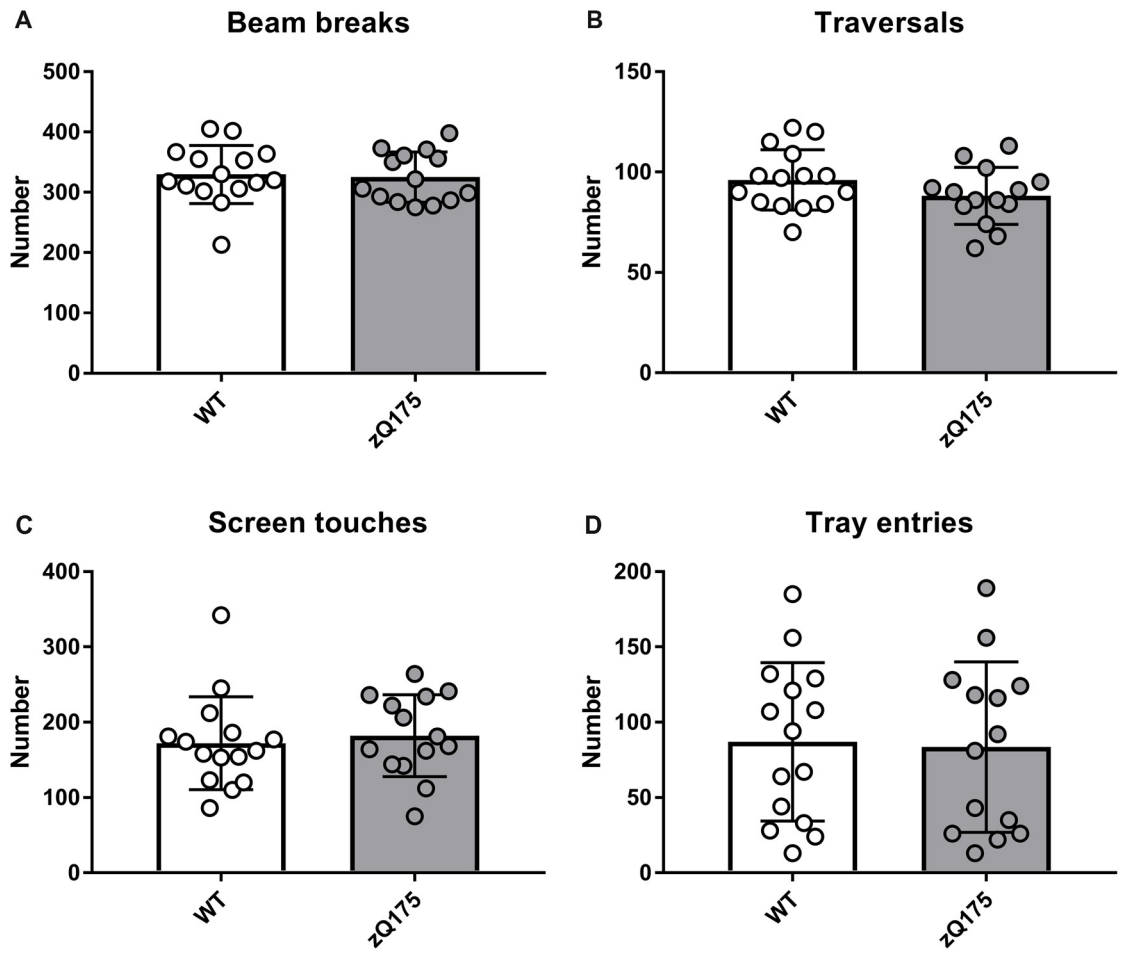

FIGURE 2 | Locomotor activity of zQ175 and wild-type (WT) mice of the PAL cohort. Numbers of infrared beam breaks **(A)** chamber traversals **(B)** screen touches **(C)** and food magazine entries **(D)** made by animals of the two genotypes were not statistically different ($P > 0.05$; Student's *t*-test or Mann-Whitney U-test, as appropriate). Data are presented as the mean ± standard deviation. Here and in other Figures, circles represent individual mouse data. $N_{zQ175} = 14$; $N_{WT} = 15$.

60 min to complete 30 trials of FR training schedule. A single trial consisted of the presentation of a 4 × 4-cm white square stimulus in the central screen response location indefinitely (**Figure 1B**). Animals were required to touch the stimulus, which was then removed from the screen. A single reward was then delivered coincident with magazine illumination and tone delivery (1 s, 3 kHz). Animals were required to collect the reward from the magazine before the next trial would commence after a 4.5-s ITI. As one operant response was required to elicit a single reward, this schedule is referred to as FR1. To move to the next FR stage, animals had to complete 30 trials in a single session and consume all earned rewards.

Animals that fulfilled FR1 performance criterion were advanced to FR2 training. The FR2 schedule required producing two operant screen responses to earn a single reward. Repeated responding was reinforced by brief (500-ms) removal of the stimulus following successful screen contact and delivery of a distinct "chirp" tone (10 ms, 3 kHz). As with FR1 training, the criterion for advancement to the next stage required animals to complete 30 trials in a single session and consume all earned rewards.

Upon completion of FR2 performance criteria, animals were advanced to FR3 training that required emission of three operant screen responses to earn a single reward. Similarly, the criterion for advancement to the next, FR5 stage required animals to complete 30 trials in a single session and consume all earned rewards.

During FR5 stage, in addition to the requirement to complete 30 trials in a single session, mice are usually expected to demonstrate specificity of interaction with the target screen location over the other four never illuminated locations. For example, a target:blank touch ratio of at least 3:1 is recommended, which can be quickly achieved in young C57Bl/6J mice (Heath et al., 2015, 2016). However, in our pilot experiments, we found that some Q175Δ*neo* mice have difficulty achieving that level of specificity even after 15 daily sessions, whereas many WT mice attained it quicker. Therefore, to avoid large differences in the number of days spent on

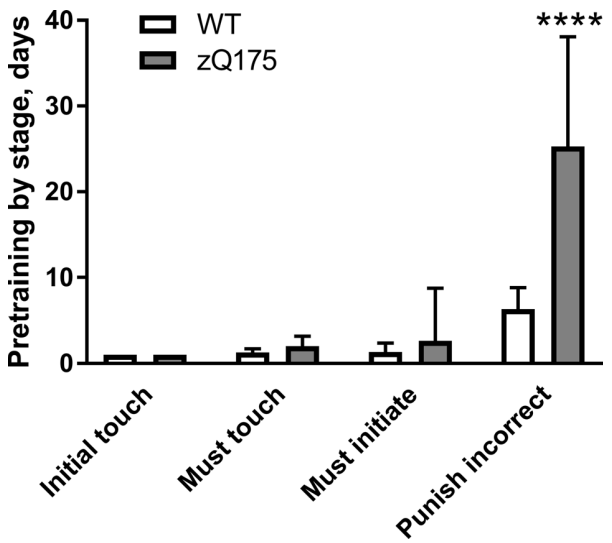

FIGURE 3 | Duration of touch screen pretraining stages in zQ175 and WT mice (PAL cohort). Data are presented as the mean ± standard deviation. For the zQ175 mouse that failed to achieve Punish incorrect criterion within 50 daily sessions, the number of days at that stage was capped at 50. Statistical significance of differences is indicated as follows: ****$P < 0.0001$ (Student's *t*-test with Welch's correction). $N_{zQ175} = 14$; $N_{WT} = 15$.

FR5 training between genotypes, we adopted more relaxed criteria for FR5 stage completion before advancing animals to PR testing: (i) all animals received at least five FR5 daily sessions; (ii) additional FR5 sessions were given after 5 days if the mice did not complete all 30 trials on three last consecutive days; and (iii) the total number of FR5 sessions was capped at 10.

Throughout FR training schedules, mice were left in the touchscreen chambers for 45–60 min, even if they completed the required number of trials within a shorter period. This was done to accustom animals to spending longer times in the chamber, as would be required during the subsequent PR testing. To assess performance during the last FR5 session in detail, we analysed schedule length, target and blank touch rates, target/blank touch ratio, post-reinforcement pause (time between head exit from food magazine after reward collection and the first touch on the next ratio), inter-touch interval, reward collection latency, as well as screen (front) and magazine (rear) infrared beam break rates.

PR Testing

PR test is an effort-based task that allows determining in quantitative terms the motivation of the animal to expend physical effort to receive reinforcing stimulus, typically of nutritional nature (Markou et al., 2013). During PR schedule, the requirement to perform a certain number of elementary physical acts, e.g., lever presses in the original PR task (Hodos, 1961) or nose pokes to a touch-sensitive screen (Heath et al., 2015), gradually increases during the session. As a result, when the required effort becomes too high, cost/benefit calculations prompt the animal to cease responding, and the number of responses following the last rewarded response ratio, known as "breakpoint," is used as a measure of perseveration.

In our experiments, animals were permitted a maximum of 120 min per session to complete as many trials as possible. The first trial of all PR sessions required a single operant screen response after which a single reward was delivered coincident with magazine illumination and tone delivery (1 s, 3 kHz). Animals were required to collect the reward from the magazine before the next trial commenced after a 4.5 s ITI. The response requirement was increased in all subsequent trials according to a linear ramp of 8 (1, 9, 17, 25. . .n + 8; PR8) with repeated touches supported by brief 500-ms removal of the screen stimulus following successful screen contact and delivery of a "chirp" tone (10 ms, 3 kHz). PR8 schedule ended if animals failed to make a screen touch or visit food magazine following reward delivery for 5 min or after 120 min, whichever was sooner.

Testing on PR8 schedule proceeded for seven consecutive days. In addition to breakpoint, the classical measure of PR task performance, we also analysed schedule length, target and blank touch rates, target/blank touch ratio, post-reinforcement pause, inter-touch interval, reward collection latency and front and rear infrared beam break rates.

Statistical Analysis

Pairwise comparisons in groups with normally distributed values were done by the Student's independent samples *t*-test, applying Welch's correction for groups with unequal variances if necessary. In groups for which the assumption of normality was rejected by the D'Agostino-Pearson test, the non-parametric Mann-Whitney U-test was used for pairwise comparisons. One-sample *t*-test was used to assess the difference of the group mean from a theoretical value. In our previous study (Piiponniemi et al., 2017) we noticed that within-session reaction times and reward collection latencies were right-skewed even after log10 or square root transformations. Therefore, for between-genotype comparisons, session median rather than session mean values of these parameters from individual mice were used, because they were more robust to the effect of outliers and more representative as central tendency measures for each session. Datasets of repeated measurements were analysed by the two-way analysis of variance (ANOVA; within-subject factor—day/session; between-subject factor—genotype). In the case of statistically significant genotype × session interactions, *post hoc* Holm-Šidák multiple comparisons test was used to determine at which sessions (or blocks thereof) the difference between genotypes was significant. All statistical analyses were conducted with a significance level of 0.05 by using GraphPad Prism 7 (GraphPad Software Inc., La Jolla, CA, USA). Throughout the text, data are presented as the mean ± standard deviation.

RESULTS

PAL Experiment

At the start of testing, zQ175 and WT mice in the PAL cohort were 306 ± 7.0 and 300.6 ± 4.9 days old, so the

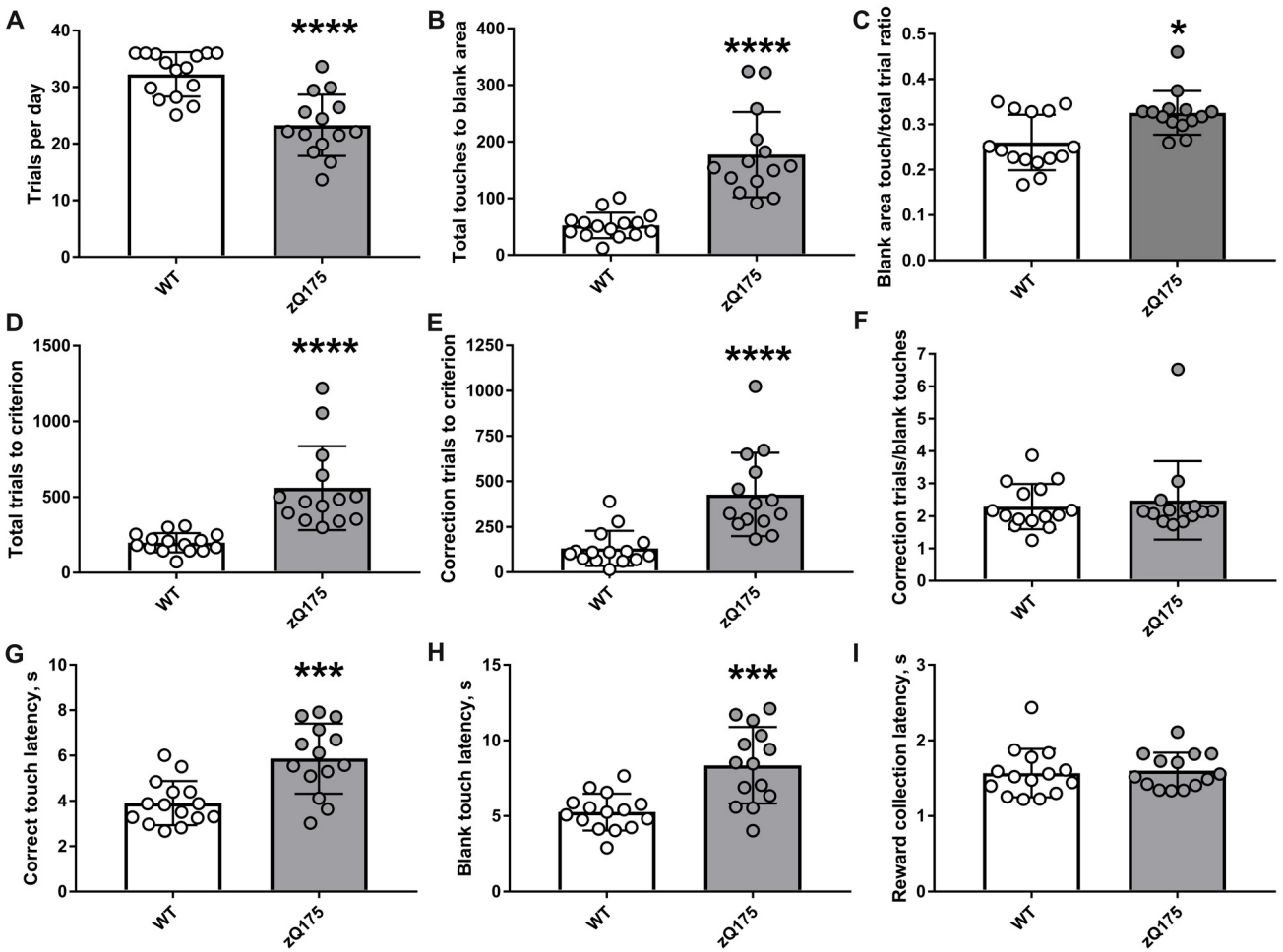

FIGURE 4 | Detailed analysis of performance during Punish incorrect stage of touch screen pretraining in zQ175 and WT mice. **(A)** Average number of Punish incorrect trials per day. **(B)** Total number of touches to blank area made until reaching the stage criterion. **(C)** The ratio of touches to blank area to the total number of trials. **(D)** Total number of trials to criterion. **(E)** Total number of correction trials to criterion. **(F)** The ratio of correction trials to the total number of touches to blank area. **(G)** Median latency to do correct (image) touch. **(H)** Median latency to do blank area touch. **(I)** Median latency to collect the reward from food magazine. Data are presented as the mean ± standard deviation. Statistical significance of differences is indicated as follows: $^{*}P < 0.05$; $^{***}P < 0.001$; $^{****}P < 0.0001$ (Student's *t*-test, Student's *t*-test with Welch's correction, or Mann-Whitney test, as appropriate). $N_{zQ175} = 14$; $N_{WT} = 15$.

mutants were slightly but significantly older ($P = 0.0456$, Mann-Whitney test). Before the start of food restriction, the free-feeding mutant animals were lighter than WT animals (28.7 ± 2.09 g vs. 32.7 ± 1.65 g, respectively; $P < 0.0001$, Student's *t*-test). The latter observation was in accordance with previously reported weight loss in zQ175 mice (Heikkinen et al., 2012).

Activity in PAL Cohort

Overall locomotor activity of zQ175 mice did not differ from that of WT mice as they made a similar number of beam breaks and traversals during their first 30-min exposure to touchscreen chamber (**Figures 2A,B**). In addition, zQ175 and WT mice made similar numbers of screen touches and entries to the food tray (**Figures 2C,D**). Therefore, we concluded that at the age of 10 months, zQ175 mice did not exhibit major locomotor and anxiety phenotypes, which could nonspecifically affect their learning of the touch screen routine.

Pretraining for PAL Touch Screen Task

Sequential introduction of basic operant learning steps during pretraining for PAL touch screen task showed that zQ175 mice performed comparably to WT counterparts during "Initial touch," "Must touch" and "Must initiate" pretraining stages ($P > 0.05$ in all cases; **Figure 3**). However during the "Punish incorrect" stage, zQ175 mice required fourfold larger number of days than WT animals to achieve the criterion: 25.3 ± 12.6 vs. 6.3 ± 2.5 days, respectively ($P < 0.0001$, Student's *t*-test with Welch's correction; **Figure 3**). Moreover, one zQ175 mouse failed to achieve the criterion for "Punish incorrect" stage even after 50 days, whereupon it was excluded from further testing.

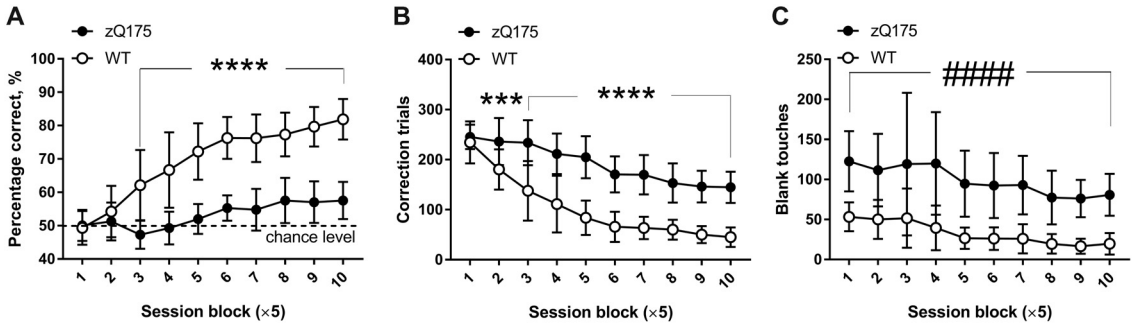

FIGURE 5 | Main parameters of PAL task performance in zQ175 and WT mice. **(A)** Percentage of correct responses during 50 consecutive PAL sessions pooled across 10 blocks of five sessions each. In some cases, especially during early stages of PAL task, the 36 session trials had to be given across several days (see "Materials and Methods" section for detailed explanation). **(B)** Total number of correction trials across 10 blocks of five PAL sessions each. **(C)** Total number of touches to blank area across 10 blocks of five PAL sessions each. Data are presented as the mean ± standard deviation. Data were analysed by the two-way ANOVA (within-subject factor—session block; between-subject factor— genotype). In the case of statistically significant genotype × session interactions, *post hoc* Holm-Šidák multiple comparisons test was used to determine at which blocks of sessions the difference between genotypes was significant ($^{***}P < 0.001$; $^{****}P < 0.0001$). If genotype × session interaction was not significant, main genotype effect was indicated as follows: $^{\#\#\#\#}P < 0.0001$. $N_{zQ175} = 12$; $N_{WT} = 15$.

Protracted attainment of the "Punish incorrect" stage criterion by zQ175 mice stemmed from two principal causes (**Figure 4**). First, during "Punish incorrect" stage of pretraining, zQ175 mice more frequently failed to complete the required number of trials per day. Second, mutant animals poked into the image with insufficient selectivity, making an unacceptably high number of touches to the blank parts of the screen while an image was present in one of the three windows). In particular, we found that although each animal was given a chance to complete 36 trials per day during pretraining, zQ175 mice completed on average only 23.3 ± 5.4 "Punish incorrect" trials daily (**Figure 4A**), which was a significantly lower trial rate than that of WT animals (32.3 ± 3.9; $P < 0.0001$, Student's *t*-test). Furthermore, zQ175 mice made significantly more touches to blank area than WT animals (**Figure 4B**). Because mutant mice had to complete more trials due to relatively lower operant responding, we also compared blank area touch rates, i.e., the ratio of blank area touches to total trials and found that zQ175 mice exhibited a higher relative blank touch rate than did WT animals (**Figure 4C**). The combination of lower daily trial rate and reduced accuracy of responding led to a significantly higher number of total trials (image touch trials + blank touch trials) by zQ175 mice to complete "Punish incorrect" stage (**Figure 4D**). In addition, zQ175 mice received more correction trials, i.e., when following a blank area touch, the trial was repeated with the same stimuli in the same location until the mouse made the touch to the image (**Figure 4E**). The difference in correction trials could be explained by the higher number of initial blank area touches as well as by repeated poking into unilluminated parts of the screen during several correction trials in a row. We found that zQ175 mice unlikely had a strong preference for unilluminated parts of the screen (or, in other words, aversion to the lit part of the screen), because the ratio of total correction trials to total number of blank touches in mutant mice was comparable to that in WT animals (**Figure 4F**).

We also analysed latencies of several behavioural reactions in zQ175 and WT mice during the "Punish incorrect" stage and found that mutants were slower to poke both into the image (correct response, **Figure 4G**) and into the blank area of the screen (incorrect response, **Figure 4H**) after the image had appeared. At the same time, zQ175 and WT mice collected reward with similar latencies (**Figure 4I**).

PAL Task Performance

During pretraining for the PAL task, mice learned to poke into the window displaying a random image and to suppress poking into the remaining blank, non-illuminated two windows. Therefore, when the animals were progressed to the actual PAL task (**Figure 1A**), their initial performance fluctuated around 50% correct (chance) level because they poked randomly into one of the two simultaneously displayed images, only one of which was in the correct location. In the course of the 50 PAL sessions, WT mice demonstrated clear improvement of their object-location associative learning from chance level in the beginning of testing to over 80% correct response rate during the last five sessions (**Figure 5A**). In contrast, zQ175 mice showed deficient acquisition of the PAL task, as their performance, even at later stages, was only slightly higher than chance level (10th session block: 58.0 ± 5.6%, $P = 0.0007$, one-sample *t*-test against theoretical mean of 50%) and much lower than the percentage of correct responses of WT animals (**Figure 5A**). There was a significant interaction between the effects of genotype and session on the percentage of correct response ($F_{(9,225)} = 20.36$, $P < 0.0001$, mixed model repeated measures ANOVA) with the values being significantly different between genotypes at session blocks 3–10 (**Figure 5A**; $P < 0.0001$, *post hoc* Holm-Šidák multiple comparisons test). Furthermore, zQ175 mice received more correction trials following touches to "S−" (**Figure 5B**). As during the "Punish incorrect" pretraining stage, mutant mice touched blank window more frequently than did WT mice (**Figure 5C**; main effect of genotype $F_{(1,25)} = 69.7$; $P < 0.0001$, mixed model repeated measures ANOVA).

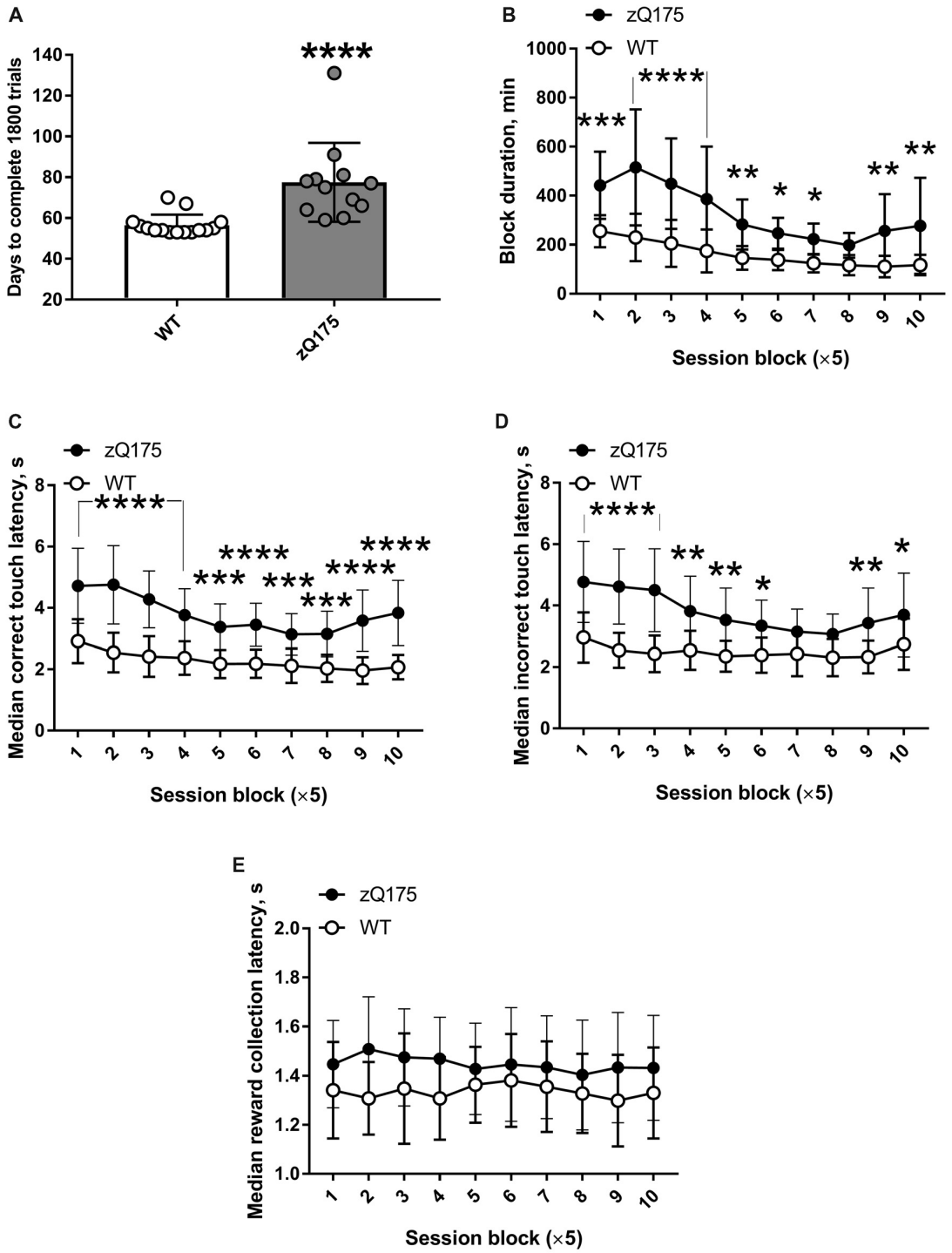

FIGURE 6 | Decelerated performance of PAL task by zQ175 mice. **(A)** Number of days required to complete the 1,800 PAL trials (50 sessions of 36 trials each). **(B)** Duration of the block of five sessions at different stages of PAL task. **(C)** Median latency to touch the correct image. **(D)** Median latency to touch the incorrect image. **(E)** Median latency to collect the reward from food magazine. Data are presented as the mean ± standard deviation. Statistical significance of differences is indicated as follows: *$P < 0.05$; **$P < 0.01$; ***$P < 0.001$; ****$P < 0.0001$ (Mann-Whitney test **(A)** or *post hoc* Holm-Šidák multiple comparisons test after significant genotype × session interactions were revealed by two-way repeated measures ANOVA **(B–D)**). N_{zQ175}s = 12; N_{WT} = 15.

zQ175 mice required significantly longer time to complete the PAL task than did WT mice (**Figure 6A**). The shortest possible duration of PAL testing was 53 days, because the first and second of the 50 sessions were deliberately split into 3 and

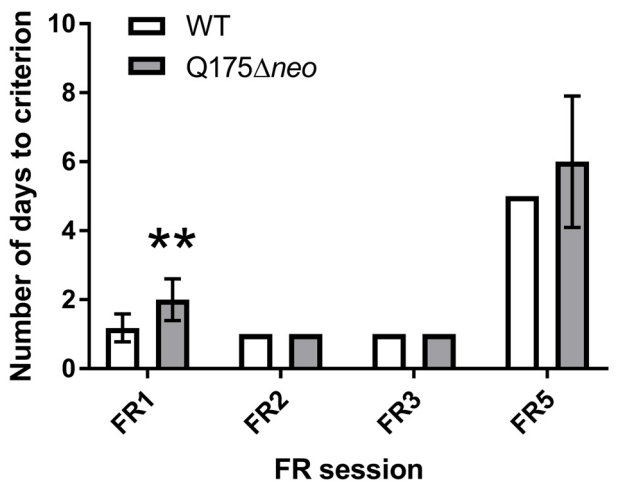

FIGURE 7 | Performance of Q175Δ*neo* and WT mice during FR schedules. Data are presented as the mean ± standard deviation. Q175 dataset includes data from two mutant mice that failed to consistently complete 30 FR5 trials and the number of their FR5 sessions was capped at 10. Statistical significance of differences is indicated as follows: $^{**}P < 0.01$ (Mann-Whitney test). $N_{Q175\Delta neo} = 12$; $N_{WT} = 11$.

2 days (3 × 12 trials and 2 × 18 trials), respectively, to introduce the more demanding requirement to associate images with a particular location more gradually. Whereas only two out of 15 WT mice required more than 60 days to complete 50 sessions (36 trials each), only two out of 14 zQ175 mice completed it within 60 days (**Figure 6A**). One zQ175 animal required more than 3 days on average to complete a session, i.e., it was doing less than 12 trials per day. Experiments with that mouse were stopped when it had completed about half of the required sessions, and these data were not used in PAL analysis. zQ175 mice had significantly longer PAL sessions at all experimental stages, except for session block 8 (genotype × session block interaction: $F_{(9,225)} = 5.557$, $P < 0.0001$; **Figure 6B**). Mutant animals displayed consistently longer latencies to touch the correct visual stimulus (genotype × session block interaction: $F_{(9,225)} = 3.364$, $P = 0.0007$; **Figure 6C**). Similarly, the latencies of the first touch to the incorrect image in a pair were also longer in zQ175 mice during all sessions except for session blocks 7 and 8 (genotype × session block interaction: $F_{(9,225)} = 3.764$, $P = 0.0002$; **Figure 6D**). At the same time, neither genotype ($F_{(1,25)} = 3.086$, $P = 0.0912$) nor session block ($F_{(9,25)} = 0.695$, $P = 0.714$) significantly affected the latency to collect the reward (**Figure 6E**). The latter finding suggested that longer image touch latencies of zQ175 mice were task-specific deficits and not a consequence of some generalised motor impairment.

FR/PR Experiment

The slower rate of responding and frequent failure to complete the required moderate number of trials during pretraining and during actual PAL task in zQ175 mice could reflect deficient reinforcement learning and/or lower motivation. The latter construct can be more selectively (i.e., without the confound of the learning deficit) assessed in effort-based tasks, using, for example, FR and PR schedules (Hodos, 1961; Markou et al., 2013). Therefore, using a separate cohort of 11-month-old related Q175Δ*neo* mice and their WT littermates, we examined their performance in the recently developed touch screen version of FR and PR tasks (Heath et al., 2015, 2016).

At the start of this experiment, litter-matched Q175Δ*neo* and WT mice in the FR/PR cohort were 329 days old on average. Before the start of food restriction, the free-feeding weight of Q175Δ*neo* mice in this cohort was lighter than that of WT littermates (29.0 ± 1.4 g vs. 34.0 ± 2.0 g, respectively; $P < 0.0001$, Student's *t*-test). This phenotype has been also observed in the original article about Q175FΔ*neo* mice (Southwell et al., 2016). As in the case of the PAL cohort (**Figure 2**), no significant differences were found between Q175Δ*neo* and WT mice in any of the activity parameters measured during the first exposure to touch screen chamber ($P > 0.05$ for all four measures, data not shown).

FR Test Performance

The majority of WT mice achieved FR1 criterion in 1 day, whereas most Q175Δ*neo* mice required at least 2 days for that (**Figure 7**). All mice, irrespective of the genotype, completed FR2 and FR3 task criteria within 1 day. Mutant animals required nominally more days to achieve FR5 criterion. However, the difference did not achieve statistical significance ($P = 0.093$, Mann-Whitney U-test). Partly, it was because we capped the maximum number of FR5 sessions to 10: 2 out of 12 Q175Δ*neo* mice still failed to complete all 30 trials during 60 min of FR5 testing on FR5 days 8–10. There were numerous differences in the dynamics and specificity of FR schedule responding between Q175Δ*neo* and WT mice and to illustrate them, we analysed the performance of mice during the last FR5 session, whereupon the animals were moved to PR testing. Last FR5 session length was significantly longer in mutant animals (**Figure 8A**). The protracted performance was due to longer post-reinforcement pause (the period between head exit from the food magazine following reward collection and the first touch in the next trial) and slower responding during the trial evidenced by longer inter-response intervals (times between the images being touched; **Figures 8B,C**).

Target touch rate was significantly lower in Q175Δ*neo* mice, whereas blank touch rate was similar between genotypes (**Figures 8D,E**). However, as the session length was considerably longer in Q175Δ*neo* mice, they made significantly more blank touches over the course of the whole session (161 ± 62 vs. 78 ± 49, $P = 0.001$, Mann-Whitney U-test). Thus, target/blank touch ratio for the whole session was significantly lower in Q175Δ*neo* mice (**Figure 8F**). These data suggested that Q175Δ*neo* mice exhibited lower specificity of the interaction with the relevant part of the touch screen, making relatively fewer target touches per given time.

Whereas the activity near the screen during the last FR5 session was similar between genotypes, rear IR beam break rate was relatively slower in Q175Δ*neo* mice (**Figures 8G,H**). It is unlikely that the latter difference was associated with decreased

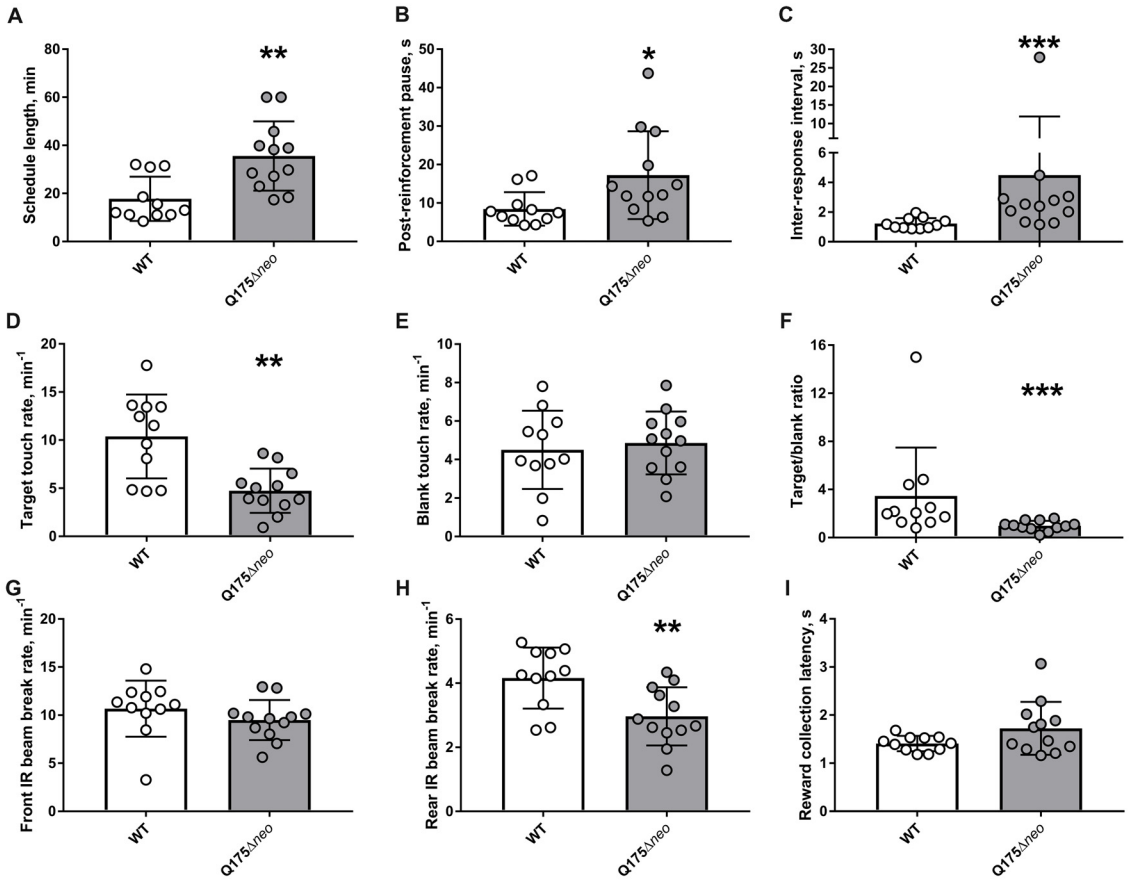

FIGURE 8 | Detailed analysis of performance during the last FR5 session. **(A)** Last FR5 session length. **(B)** Median post-reinforcement pause. **(C)** Median inter-response interval. Y-axis was split for better illustration of all individual values. **(D)** Target touch rate. **(E)** Blank touch rate. **(F)** The ratio of the number of target touches to the number of touches to blank area. **(G)** Front infrared (IR) beam break rate. **(H)** Rear IR beam break rate. **(I)** Median latency to collect the reward from food magazine. Data are presented as the mean ± standard deviation. Statistical significance of differences is indicated as follows: $^{*}P < 0.05$; $^{**}P < 0.01$; $^{***}P < 0.001$; Student's *t*-test, Student's *t*-test with Welch's correction, or Mann-Whitney test, as appropriate. $N_{Q175\Delta neo} = 12$; $N_{WT} = 11$.

motivation to work for reward: mutant and WT animals collected the reward with very similar latencies (**Figure 8I**). Moreover, the rates of empty magazine entries were similar in Q175Δ*neo* mice and in WT littermates (0.88 min^{-1} vs. 1.00 min^{-1}, $P = 0.45$, Mann-Whitney U-test), indicating that mutants actively sought the nutritional reward.

To verify if the above described differences were not considerably distorted by the data from the two Q175Δ*neo* mice that failed to complete all 30 trials during their last three FR5 sessions, we also carried out the same comparisons having excluded those two animals. All the statistically significant genotype effects with the exception of the longer post-reinforcement pause in Q175 mice remained significant (data not shown), so we advanced all mutant animals to the PR schedule.

PR Test Performance

Both Q175Δ*neo* and WT mice vigorously emitted operant responses during PR8 sessions. Whereas there was a significant effect of session on breakpoint value ($F_{(6,126)} = 5.054$, $P = 0.0001$), genotype did not affect breakpoints (**Figure 9A**). Genotype, session number or interaction of these factors did not significantly affect the length of daily sessions that were stopped after 5 min of inactivity in most cases (**Figure 9B**). One Q175Δ*neo* mouse kept responding for 2 h on the first day of PR8 schedule, so its session length was capped at this value for analysis. Post-reinforcement pauses before the start of new ratios were similar in both genotypes (**Figure 9C**), but median inter-touch intervals were slightly but significantly longer in Q175Δ*neo* mice ($P = 0.046$, main genotype effect, **Figure 9D**). As was the case during FR5 sessions, target touch rate was slower in mutant animals (genotype effect: $F_{(1,21)} = 11.19$, $P = 0.0031$; session effect: $F_{(6,126)} = 10.46$, $P < 0.0001$; **Figure 9E**), whereas neither genotype nor session affected blank touch rates (**Figure 9F**). Target/blank touch ratio was gradually decreasing in the course of testing on PR8 schedule (session effect: $F_{(6,126)} = 3.681$, $P = 0.0021$) and overall lower in Q175Δ*neo* mice (genotype effect: $F_{(1,21)} = 10.84$, $P = 0.0035$; **Figure 9G**). Neither front beam nor rear beam rates were affected by genotype or PR8 session

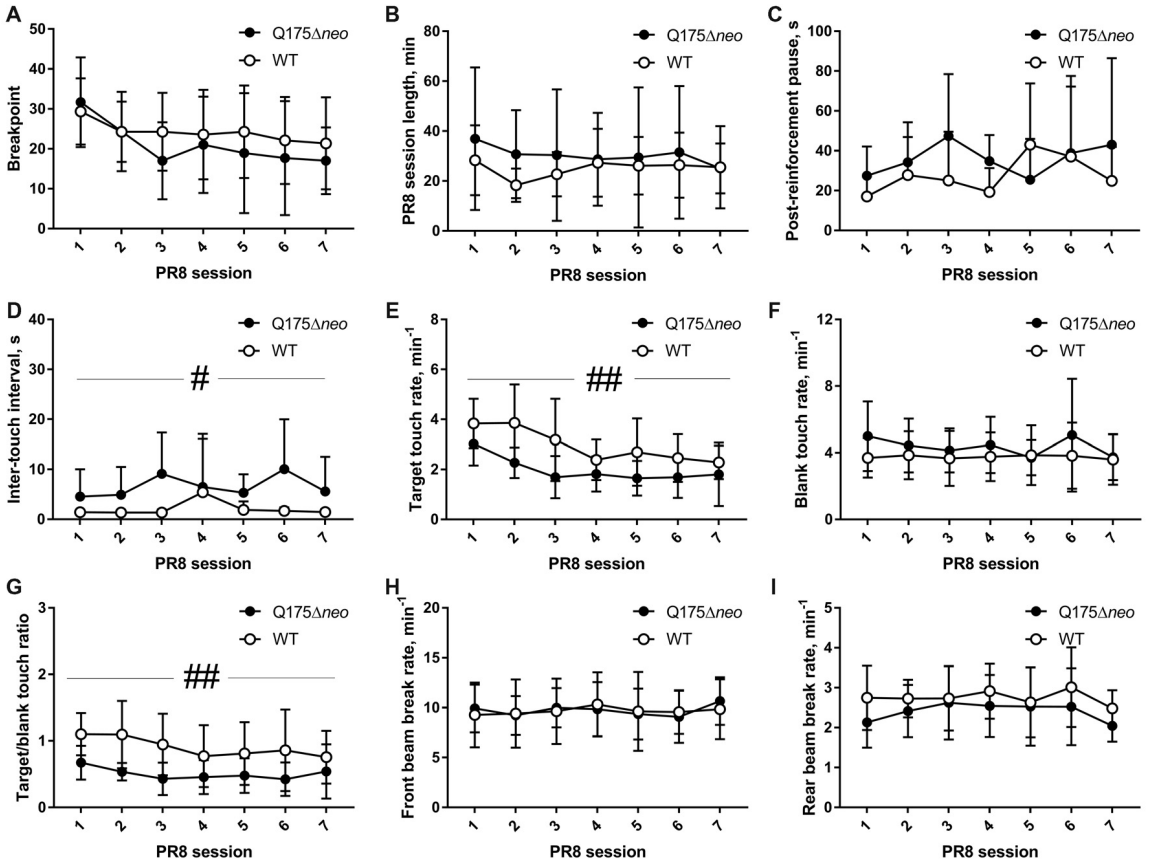

FIGURE 9 | Performance of Q175Δ*neo* and WT mice during consecutive daily PR sessions on PR8 schedule. **(A)** Breakpoints. **(B)** Lengths of daily sessions. **(C)** Median post-reinforcement pause values. **(D)** Median inter-response intervals. **(E)** Target touch rates. **(F)** Blank touch rates. **(G)** Target/blank touch ratio values. **(H)** Front infrared (IR) beam break rates. **(I)** Rear IR beam break rates. Data are presented as the mean ± standard deviation (in **(C,D)** due to large variability, only the upper part of standard deviation range is provided for clarity). Genotype × session interactions were not significant. Main genotype effect is indicated as follows: $^{\#}P < 0.05$; $^{\#\#}P < 0.01$. For **(A,B, E–I)** $N_{Q175}\Delta neo = 12$; $N_{WT} = 11$. For analyses in **(C,D)** $N_{Q175}\Delta neo = 8$; $N_{WT} = 10$, as data from mice that completed less than two ratios in any of the seven PR schedule days were excluded.

(**Figures 9H,I**). We also analysed directional behaviour toward reward magazine and found no differences in reward collection latency (genotype effect: $F_{(1,20)} = 2.109$, $P = 0.162$; session effect: $F_{(6,120)} = 1.06$, $P = 0.39$; data from one Q175Δ*neo* mouse were excluded as on 1 day, it did not collect the reward). Furthermore, neither genotype nor session significantly affected the rate of empty food magazine visits (genotype effect: $F_{(1,21)} = 2.099$, $P = 0.1621$; session effect: $F_{(6,126)} = 1.847$, $P = 0.095$).

DISCUSSION

In the present study, we show a pronounced deficit in object location/PAL in 10–11-month-old heterozygous zQ175 mice, an animal model of HD. Besides high rate of errors, we also noted considerably lower responding rate in mutants during the last stage of pretraining and during the PAL task itself. Our examination of effortful operant responding during FR and PR reinforcement schedules in closely related Q175Δ*neo* mice of similar age confirmed slower and unselective performance of mutant animals observed during the PAL task but suggested that motivation to work for nutritional reward in Q175Δ*neo* and WT mice was similar.

Visuospatial deficits have been extensively documented in HD patients (Mohr et al., 1991; Lawrence et al., 2000; Dumas et al., 2013; Pirogovsky et al., 2015; Corey-Bloom et al., 2016). These findings have been conceptually recapitulated in animal models of HD. Deficient spatial learning in Morris water maze has been noted in R6/1 (Brooks et al., 2012), R6/2 (Lione et al., 1999), YAC128 (Brooks et al., 2012a), HdhQ92 (Brooks et al., 2012c), HdhQ111 (Giralt et al., 2012), HdhQ150 (Brooks et al., 2012b) HD mouse models and in transgenic HD rats (Kirch et al., 2013), whereas individuals with HD perform poorly in the human versions of the water maze (Majerová et al., 2012; Begeti et al., 2016). Learning of delayed matching to position and delayed non-matching to position tasks was deficient in HdhQ111 and zQ175 mice (Curtin et al., 2015; Yhnell et al., 2016b) as well as in transgenic HD monkey (Chan et al., 2014), mirroring deficits in similar tests in symptomatic HD patients (Lange et al., 1995; Lawrence et al., 2000).

However, differences in preclinical animal and clinical test settings often preclude straightforward comparisons of the changes observed in rodents and individuals with HD. For example, learning in Morris water maze is driven by the negative reinforcement (such as stress), which may adversely affect the performance and is incompatible with assessing cognition in humans. Application of touch screen technology for testing cognition in rodents and other species facilitates such cross-species evaluations: touch screen tests have been used for diagnosing cognitive dysfunction in humans for decades, although it should be remembered that they were partly inspired by the desire to utilise cognitive testing routines originally developed in rodents and monkeys (Barnett et al., 2016). Recent refinement of touch screen-based techniques enabled successful replication of human cognitive phenotypes in mice with homologous mutations and even permitted reverse, mouse-to-human, translation (Nithianantharajah et al., 2013, 2015).

Here, for the first time, we applied touch screen PAL task to a mouse model of HD. Impaired performance of zQ175 mice in this task (**Figure 5**) has important translational parallels, as disruptions of verbal and pattern-location associative learning in HD patients have been demonstrated in various tests, including CANTAB (Lange et al., 1995; Sprengelmeyer et al., 1995; Rich et al., 1997; Lawrence et al., 2000; Begeti et al., 2016). In human CANTAB PAL task, the performance of individuals is usually assessed by the number of trials required to correctly locate all patterns, the number of errors made and the memory score, representing the overall number of patterns correctly located after the first presentation (Lawrence et al., 2000). Compared to healthy control subjects, HD patients use more trials, commit more errors and demonstrate lower memory score, typically experiencing considerable difficulty at the six- and eight-pattern stages of the task (Lange et al., 1995; Lawrence et al., 2000; Begeti et al., 2016). These deficits are directly comparable to the significantly lower number of correct responses and higher number of correction trials observed in zQ175 mice compared to those in WT counterparts (**Figure 5**). Persistently low percentage of correct responses of zQ175 mice in the course of PAL task was likely caused by disturbances in multiple cognitive domains. As discussed by Lawrence et al. (2000), visuospatial tasks require several distinct processes: (1) attendance to and discrimination between the stimuli; (2) acquisition of the learning rule, including the realisation that correct responses are associated with reward, and memory of the rule throughout testing; (3) matching the available set of stimuli to the sample in memory; and (4) appropriate response selection. Furthermore, successful performance in positively reinforced visuospatial tasks ultimately depends on inherent motivation to work for corresponding reward.

Impaired ability to discriminate between two visual images in touch screen chambers had been noted in 26-week old but, surprisingly, not in 48-week old zQ175 mice (Farrar et al., 2014; Curtin et al., 2015). In R6/2 mice, age- and CAG repeat number-dependent impairments in pairwise visual discrimination have been shown (Morton et al., 2006; Glynn et al., 2016). These mouse phenotypes are reminiscent of compromised perception of visual stimuli in HD patients (Büttner et al., 1994; Jacobs et al., 1995; O'Donnell et al., 2008). However, as argued by Lawrence et al. (2000), it is unlikely that HD patients have a generalised perceptual deficit as their poor performance in perceptual tests, e.g., in simultaneous matching-to-sample, might be due to attentional deficits.

In our experiments, longer latencies to touch correct and incorrect images in PAL task in zQ175 mice (**Figures 6C,D**) as well as longer post-reinforcement pause in FR5 task in Q175Δ*neo* mice (**Figure 8B**) suggest that decreased attention may also contribute to impaired acquisition of PAL. Deficits in rapid attention to visual stimuli in other knock-in HD mouse models were also demonstrated by using 5-choice serial reaction time task (Trueman et al., 2009, 2012; Yhnell et al., 2016a,c). These data are in accord with reduced attentional capacity of HD patients (Finke et al., 2007; Georgiou-Karistianis et al., 2012; Hart et al., 2015).

Notably, post-reinforcement pauses were not significantly different between WT and Q175Δ*neo* mice during testing on PR8 schedule (**Figure 9C**), which could reflect eventual recovery of this deficit upon continuous training. Positive effects of training on the discriminatory ability and attention of Q175 and R6/2 mice have been reported previously (Curtin et al., 2015; Yhnell et al., 2016c).

Poor rule learning likely was also a factor in deficient performance of zQ175 mice in PAL task. Pronounced deficits in operant responding of mutants were already evident at the last "Punish incorrect" stage of pretraining for PAL task (**Figures 3**, **4**): mutant mice required many more trials to learn to selectively touch the image, while withholding interactions with blank windows. This deficit may be explained by impaired proactive selective stopping, a process that involves activation of striatal, pallidal and frontal areas in humans, which is disturbed in HD patients (Majid et al., 2013). Similar deficit has not been reported during instrumental pretraining of zQ175 and R6/2 HD mice for the pairwise discrimination touch screen task, likely because the "Punish incorrect" step was not used (Morton et al., 2006; Farrar et al., 2014; Curtin et al., 2015). Acquisition of the simple nose poke response (akin to "Must Touch" pretraining stage used here) was impaired slightly in 53-week and 74-week old heterozygous zQ175 mice and nearly completely abrogated in homozygous mutants (Oakeshott et al., 2011). Furthermore, zQ175, R6/2 and BAC HD mice exhibited deficits in a simple visual Go/No-Go task that required animals to nose-poke into a recess for food reward in the presence of light, but to withhold responding in the absence of the reinforcer (Oakeshott et al., 2013). In addition, impaired operant rule learning in delayed alternation task has been reported in HdhQ92 mouse model of HD (Trueman et al., 2009). These findings are in accord with numerous reports on deficient rule learning in individuals with HD (Knopman and Nissen, 1991; Lange et al., 1995; Filoteo et al., 2001).

Our data on the performance of Q175Δ*neo* mice in FR and PR tasks were somewhat unexpected. On the one hand, protracted execution of FR task (**Figures 8A,B**) and longer inter-touch intervals during both FR and PR schedules (**Figures 8C**, **9D**) were in line with decelerated performance of similar mutants in the PAL task (**Figure 6**). Psychomotor slowing in zQ175 mice

was also noted in touch screen visual discrimination task (Farrar et al., 2014), so these data collectively demonstrate that Q175 mouse lines can be used for modelling HD-related bradykinesia (Thompson et al., 1988; Sánchez-Pernaute et al., 2000). On the other hand, indices related to the motivation, such as breakpoint, the rate of empty food magazine visits, or reward collection latency, were similar between genotypes (**Figures 8I**, **9A**), despite an earlier study of zQ175 mice, which utilised a lever-equipped apparatus, revealed lower breakpoints in 30-week old mutants (Covey et al., 2016). In a similar setting, 27–33-month-old zQ175 mice showed slower response rates and reduced number of earned reinforcements on PR schedules (Oakeshott et al., 2012; Curtin et al., 2015). In the latter studies, in the absence of clear breakpoints, those measures were deemed to reflect lower motivation. Lower response (target touch) rate in Q175Δ*neo* mice was noted also in our experiments (**Figures 8D**, **9E**), however, the breakpoints, which correlate with the number of earned rewards, were similar in WT and mutant animals (**Figure 9A**). Lower breakpoint values were also described in HdhQ111 mice (Yhnell et al., 2016a; Minnig et al., 2018).

The discrepancies between breakpoint data in this study and published reports likely stem from a differential setting (touch screen chambers vs. lever-equipped operant boxes or operant buckets) and steeper, PR8, reinforcement schedule than those employed in other studies in which breakpoints were achieved (Covey et al., 2016; Yhnell et al., 2016a; Minnig et al., 2018). Also, there was a subtle genetic difference between Q175Δ*neo* mice in our experiments and zQ175 mice used in published studies. Generally, mice emitted relatively fewer responses in the touch screen version of PR task (compare breakpoints in **Figure 9A** per 120 min of testing with Figure 1A of Covey et al. (2016)), which implies that touch screen testing was more strenuous. However, it is then unclear why this circumstance did not make detection of phenotype in Q175Δ*neo* mice easier. It must be noted though that the strategies to achieve similar breakpoint values in WT and Q175Δ*neo* mice were different, as mutants made target touches relatively less frequently. Nonetheless, our results suggest that modelling apathetic behaviour in Q175 mouse lines by testing them on PR schedules in touch screen chambers is less optimal than using lever-equipped chambers.

Despite similar breakpoints were observed during testing on PR8 schedule in a related Q175 line (**Figure 9A**), motivational deficits may still have affected the performance of zQ175 mice during the PAL task. Because mutants made more errors and their learning rate was low (**Figure 5A**), the rewards were relatively less frequent than in WT counterparts, which could add to the demotivation of zQ175 mice during PAL testing. At the same time, the effect of gross locomotor disturbances, another important confound in HD mouse models, on the performance in PAL and FR/PR tasks may probably be excluded: although we tested fairly mature animals, initial locomotor activity (**Figure 2**), reward collection latencies, and front beam break rates were similar. The rate of rear infrared beam break was lower in Q175Δ*neo* mice during the last FR5 session (**Figure 8H**), but it was similar to that in WT mice during the subsequent PR sessions (**Figure 9I**).

In summary, we have expanded the list of known cognitive deficits in the knock-in zQ175 mouse model of HD by showing a drastic impairment of their object location associative memory in the PAL task. Normal performance of this touch screen task is thought to be dependent on the integrity of the hippocampus, dorsal striatum and prefrontal cortex (Owen et al., 1995; Talpos et al., 2009; Delotterie et al., 2015; Kim et al., 2015), i.e., the areas known to be affected by degeneration or biochemical and physiological disturbances in zQ175 mice (Heikkinen et al., 2012; Smith et al., 2014; Rothe et al., 2015; Covey et al., 2016; Peng et al., 2016; Sebastianutto et al., 2017) in correspondence to similar deficits in HD patients. Although the advantage of the highly translational, touch screen-based approach in the case of PAL is weakened by relatively long time needed to complete the test, using younger animals may potentially decrease the overall test duration. In addition, a recently reported more intensive training regimen for PAL task may be applied to shorten the duration of the experiment (Kim et al., 2016). We also demonstrated that pronounced sensorimotor disturbances in Q175 mouse lines can be detected at early touch screen testing stages, e.g., during "Punish incorrect" stage of pretraining for the PAL task or during FR schedule. Therefore, these shorter routines may be utilised for more expedient studies of pharmacological treatments and other strategies aimed at the rescue of HD-related phenotype.

AUTHOR CONTRIBUTIONS

MK, TP, LP and RC designed the study. TOP and MK conducted the experiments. TH and JP provided the resources and advised on experimental design. MK and TOP analysed the data. MK wrote the manuscript.

FUNDING

This work was supported by CHDI Foundation. During the analysis of experimental data and manuscript preparation, MK was supported by the UK Dementia Research Institute at Imperial College London.

REFERENCES

Baig, S. S., Strong, M., and Quarrell, O. W. (2016). The global prevalence of Huntington's disease: a systematic review and discussion. *Neurodegener. Dis. Manag.* 6, 331–343. doi: 10.2217/nmt-2016-0008

Barnett, J. H., Blackwell, A. D., Sahakian, B. J., and Robbins, T. W. (2016). The paired associates learning (PAL) test: 30 years of cantab translational neuroscience from laboratory to bedside in dementia research. *Curr. Top. Behav. Neurosci.* 28, 449–474. doi: 10.1007/7854_2015_5001

Begeti, F., Schwab, L. C., Mason, S. L., and Barker, R. A. (2016). Hippocampal dysfunction defines disease onset in Huntington's disease. *J. Neurol. Neurosurg. Psychiatry* 87, 975–981. doi: 10.1136/jnnp-2015-312413

Brooks, S., Higgs, G., Janghra, N., Jones, L., and Dunnett, S. B. (2012a). Longitudinal analysis of the behavioural phenotype in YAC128 (C57BL/6J) Huntington's disease transgenic mice. *Brain Res. Bull.* 88, 113–120. doi: 10.1016/j.brainresbull.2010.05.005

Brooks, S., Higgs, G., Jones, L., and Dunnett, S. B. (2012b). Longitudinal analysis of the behavioural phenotype in $^{Hdh(CAG)150}$ Huntington's disease knock-in mice. *Brain Res. Bull.* 88, 182–188. doi: 10.1016/j.brainresbull.2010.05.004

Brooks, S., Higgs, G., Jones, L., and Dunnett, S. B. (2012c). Longitudinal analysis of the behavioural phenotype in Hdh^{Q92} Huntington's disease knock-in mice. *Brain Res. Bull.* 88, 148–155. doi: 10.1016/j.brainresbull.2010.05.003

Brooks, S. P., Janghra, N., Workman, V. L., Bayram-Weston, Z., Jones, L., and Dunnett, S. B. (2012). Longitudinal analysis of the behavioural phenotype in R6/1 (C57BL/6J) Huntington's disease transgenic mice. *Brain Res. Bull.* 88, 94–103. doi: 10.1016/j.brainresbull.2011.01.010

Bunner, K. D., and Rebec, G. V. (2016). Corticostriatal dysfunction in Huntington's disease: the basics. *Front. Hum. Neurosci.* 10:317. doi: 10.3389/fnhum.2016.00317

Bussey, T. J., Holmes, A., Lyon, L., Mar, A. C., Mcallister, K. A., Nithianantharajah, J., et al. (2012). New translational assays for preclinical modelling of cognition in schizophrenia: the touchscreen testing method for mice and rats. *Neuropharmacology* 62, 1191–1203. doi: 10.1016/j.neuropharm.2011.04.011

Büttner, T., Schulz, S., Kuhn, W., Blumenschein, A., and Przuntek, H. (1994). Impaired colour discrimination in Huntington's disease. *Eur. J. Neurol.* 1, 153–157. doi: 10.1111/j.1468-1331.1994.tb00064.x

Chan, A. W., Xu, Y., Jiang, J., Rahim, T., Zhao, D., Kocerha, J., et al. (2014). A two years longitudinal study of a transgenic Huntington disease monkey. *BMC Neurosci.* 15:36. doi: 10.1186/1471-2202-15-36

Chang, R., Liu, X., Li, S., and Li, X. J. (2015). Transgenic animal models for study of the pathogenesis of Huntington's disease and therapy. *Drug Des. Devel. Ther.* 9, 2179–2188. doi: 10.2147/dddt.s58470

Corey-Bloom, J., Gluhm, S., Herndon, A., Haque, A. S., Park, S., and Gilbert, P. E. (2016). Benton judgment of line orientation (JoLO) test: a brief and useful measure for assessing visuospatial abilities in manifest, but not premanifest, Huntington's disease. *J. Huntingtons Dis.* 5, 91–96. doi: 10.3233/jhd-150175

Covey, D. P., Dantrassy, H. M., Zlebnik, N. E., Gildish, I., and Cheer, J. F. (2016). Compromised dopaminergic encoding of reward accompanying suppressed willingness to overcome high effort costs is a prominent prodromal characteristic of the Q175 mouse model of Huntington's disease. *J. Neurosci.* 36, 4993–5002. doi: 10.1523/jneurosci.0135-16.2016

Curtin, P. C., Farrar, A. M., Oakeshott, S., Sutphen, J., Berger, J., Mazzella, M., et al. (2015). Cognitive training at a young age attenuates deficits in the zQ175 mouse model of HD. *Front. Behav. Neurosci.* 9:361. doi: 10.3389/fnbeh.2015.00361

Delotterie, D. F., Mathis, C., Cassel, J. C., Rosenbrock, H., Dorner-Ciossek, C., and Marti, A. (2015). Touchscreen tasks in mice to demonstrate differences between hippocampal and striatal functions. *Neurobiol. Learn. Mem.* 120, 16–27. doi: 10.1016/j.nlm.2015.02.007

Dumas, E. M., van den Bogaard, S. J., Middelkoop, H. A., and Roos, R. A. (2013). A review of cognition in Huntington's disease. *Front. Biosci.* 5, 1–18. doi: 10.2741/S355

Farrar, A. M., Murphy, C. A., Paterson, N. E., Oakeshott, S., He, D., Alosio, W., et al. (2014). Cognitive deficits in transgenic and knock-in HTT mice parallel those in Huntington's disease. *J. Huntingtons Dis.* 3, 145–158. doi: 10.3233/JHD-130061

Filoteo, J. V., Maddox, W. T., and Davis, J. D. (2001). A possible role of the striatum in linear and nonlinear category learning: evidence from patients with Huntington's disease. *Behav. Neurosci.* 115, 786–798. doi: 10.1037/0735-7044.115.4.786

Finke, K., Schneider, W. X., Redel, P., Dose, M., Kerkhoff, G., Muller, H. J., et al. (2007). The capacity of attention and simultaneous perception of objects: a group study of Huntington's disease patients. *Neuropsychologia* 45, 3272–3284. doi: 10.1016/j.neuropsychologia.2007.06.006

Georgiou-Karistianis, N., Farrow, M., Wilson-Ching, M., Churchyard, A., Bradshaw, J. L., and Sheppard, D. M. (2012). Deficits in selective attention in symptomatic Huntington disease: assessment using an attentional blink paradigm. *Cogn. Behav. Neurol.* 25, 1–6. doi: 10.1097/wnn.0b013e318248c503

Giralt, A., Puigdellivol, M., Carreton, O., Paoletti, P., Valero, J., Parra-Damas, A., et al. (2012). Long-term memory deficits in Huntington's disease are associated with reduced CBP histone acetylase activity. *Hum. Mol. Genet.* 21, 1203–1216. doi: 10.1093/hmg/ddr552

Glynn, D., Skillings, E. A., and Morton, A. J. (2016). A comparison of discrimination learning in touchscreen and 2-choice swim tank using an allelic series of Huntington's disease mice. *J. Neurosci. Methods* 265, 56–71. doi: 10.1016/j.jneumeth.2015.07.016

Hart, E. P., Dumas, E. M., Van Zwet, E. W., Van Der Hiele, K., Jurgens, C. K., Middelkoop, H. A., et al. (2015). Longitudinal pilot-study of sustained attention to response Task and P300 in manifest and pre-manifest Huntington's disease. *J. Neuropsychol.* 9, 10–20. doi: 10.1111/jnp.12031

Heath, C. J., Bussey, T. J., and Saksida, L. M. (2015). Motivational assessment of mice using the touchscreen operant testing system: effects of dopaminergic drugs. *Psychopharmacology* 232, 4043–4057. doi: 10.1007/s00213-015-4009-8

Heath, C. J., Phillips, B. U., Bussey, T. J., and Saksida, L. M. (2016). Measuring motivation and reward-related decision making in the rodent operant touchscreen system. *Curr. Protoc. Neurosci.* 74, 8.34.1–8.34.20. doi: 10.1002/0471142301.ns0834s74

Heikkinen, T., Bragge, T., Lehtimäki, K., Parkkari, T., Puoliväli, J., Howland, D., et al. (2017). "Characterization of behavioral changes, MRI brain volumetry and MR spectroscopy in ZQ175 knock-in delta neo minus mouse model of Huntington's disease," in *Society for Neuroscience Annual Meeting, Program No. 575.04/V19* (Washington, DC).

Heikkinen, T., Lehtimaki, K., Vartiainen, N., Puoliväli, J., Hendricks, S. J., Glaser, J. R., et al. (2012). Characterization of neurophysiological and behavioral changes, MRI brain volumetry and ^{1}H MRS in zQ175 knock-in mouse model of Huntington's disease. *PLoS One* 7:e50717. doi: 10.1371/journal.pone.0050717

Hodos, W. (1961). Progressive ratio as a measure of reward strength. *Science* 134, 943–944. doi: 10.1126/science.134.3483.943

Horner, A. E., Heath, C. J., Hvoslef-Eide, M., Kent, B. A., Kim, C. H., Nilsson, S. R., et al. (2013). The touchscreen operant platform for testing learning and memory in rats and mice. *Nat. Protoc.* 8, 1961–1984. doi: 10.1038/nprot.2013.122

Horner, A. E., McLaughlin, C. L., Afinowi, N. O., Bussey, T. J., Saksida, L. M., Komiyama, N. H., et al. (2018). Enhanced cognition and dysregulated hippocampal synaptic physiology in mice with a heterozygous deletion of PSD-95. *Eur. J. Neurosci.* 47, 164–176. doi: 10.1111/ejn.13792

Hvoslef-Eide, M., Nilsson, S. R., Saksida, L. M., and Bussey, T. J. (2016). Cognitive translation using the rodent touchscreen testing approach. *Curr. Top. Behav. Neurosci.* 28, 423–447. doi: 10.1007/7854_2015_5007

Jacobs, D. H., Shuren, J., and Heilman, K. M. (1995). Impaired perception of facial identity and facial affect in Huntington's disease. *Neurology* 45, 1217–1218. doi: 10.1212/wnl.45.6.1217

Jimenez-Sanchez, M., Licitra, F., Underwood, B. R., and Rubinsztein, D. C. (2017). Huntington's disease: mechanisms of pathogenesis and therapeutic strategies. *Cold Spring Harb. Perspect. Med* 7:a024240. doi: 10.1101/cshperspect.a024240

Kim, C. H., Heath, C. J., Kent, B. A., Bussey, T. J., and Saksida, L. M. (2015). The role of the dorsal hippocampus in two versions of the touchscreen automated paired associates learning (PAL) task for mice. *Psychopharmacology* 232, 3899–3910. doi: 10.1007/s00213-015-4025-8

Kim, M., Kwak, C., Yu, N.-K., and Kaang, B.-K. (2016). Optimization of the touchscreen paired-associate learning (PAL) task for mice and its dorsal hippocampal dependency. *Anim. Cells Syst.* 20, 229–236. doi: 10.1080/19768354.2016.1221855

Kirch, R. D., Meyer, P. T., Geisler, S., Braun, F., Gehrig, S., Langen, K. J., et al. (2013). Early deficits in declarative and procedural memory dependent behavioral function in a transgenic rat model of Huntington's disease. *Behav. Brain Res.* 239, 15–26. doi: 10.1016/j.bbr.2012.10.048

Knopman, D., and Nissen, M. J. (1991). Procedural learning is impaired in Huntington's disease: evidence from the serial reaction time task. *Neuropsychologia* 29, 245–254. doi: 10.1016/0028-3932(91)90085-m

Lange, K. W., Sahakian, B. J., Quinn, N. P., Marsden, C. D., and Robbins, T. W. (1995). Comparison of executive and visuospatial memory function in Huntington's disease and dementia of Alzheimer type matched for degree of dementia. *J. Neurol. Neurosurg. Psychiatry* 58, 598–606. doi: 10.1136/jnnp.58.5.598

Lawrence, A. D., Sahakian, B. J., Hodges, J. R., Rosser, A. E., Lange, K. W., and Robbins, T. W. (1996). Executive and mnemonic functions in early Huntington's disease. *Brain* 119, 1633–1645. doi: 10.1093/brain/119.5.1633

Lawrence, A. D., Watkins, L. H., Sahakian, B. J., Hodges, J. R., and Robbins, T. W. (2000). Visual object and visuospatial cognition in Huntington's disease: implications for information processing in corticostriatal circuits. *Brain* 123, 1349–1364. doi: 10.1093/brain/123.7.1349

Lione, L. A., Carter, R. J., Hunt, M. J., Bates, G. P., Morton, A. J., and Dunnett, S. B. (1999). Selective discrimination learning impairments in mice expressing the human Huntington's disease mutation. *J. Neurosci.* 19, 10428–10437. doi: 10.1523/jneurosci.19-23-10428.1999

MacDonald, M. E., Ambrose, C. M., Duyao, M. P., Myers, R. H., Lin, C., Srinidhi, L., et al. (1993). A novel gene containing a trinucleotide repeat that is expanded and unstable on Huntington's disease chromosomes. *Cell* 72, 971–983. doi: 10.1016/0092-8674(93)90585-e

Majerová, V., Kalinčík, T., Laczó, J., Vyhnálek, M., Hort, J., Bojar, M., et al. (2012). Disturbance of real space navigation in moderately advanced but not in early Huntington's disease. *J. Neurol. Sci.* 312, 86–91. doi: 10.1016/j.jns.2011.08.016

Majid, D. S., Cai, W., Corey-Bloom, J., and Aron, A. R. (2013). Proactive selective response suppression is implemented via the basal ganglia. *J. Neurosci.* 33, 13259–13269. doi: 10.1523/jneurosci.5651-12.2013

Markou, A., Salamone, J. D., Bussey, T. J., Mar, A. C., Brunner, D., Gilmour, G., et al. (2013). Measuring reinforcement learning and motivation constructs in experimental animals: relevance to the negative symptoms of schizophrenia. *Neurosci. Biobehav. Rev.* 37, 2149–2165. doi: 10.1016/j.neubiorev.2013.08.007

McColgan, P., and Tabrizi, S. J. (2018). Huntington's disease: a clinical review. *Eur. J. Neurol.* 25, 24–34. doi: 10.1111/ene.13413

Menalled, L. B., and Chesselet, M. F. (2002). Mouse models of Huntington's disease. *Trends Pharmacol. Sci.* 23, 32–39. doi: 10.1016/S0165-6147(00)01884-8

Menalled, L. B., Kudwa, A. E., Miller, S., Fitzpatrick, J., Watson-Johnson, J., Keating, N., et al. (2012). Comprehensive behavioral and molecular characterization of a new knock-in mouse model of Huntington's disease: zQ175. *PLoS One* 7:e49838. doi: 10.1371/journal.pone.0148839

Minnig, S., Bragg, R. M., Tiwana, H. S., Solem, W. T., Hovander, W. S., Vik, E. S., et al. (2018). Early detection of apathetic phenotypes in Huntington's disease knock-in mice using open source tools. *Sci. Rep.* 8:2304. doi: 10.1038/s41598-018-20607-7

Mohr, E., Brouwers, P., Claus, J. J., Mann, U. M., Fedio, P., and Chase, T. N. (1991). Visuospatial cognition in Huntington's disease. *Mov. Disord.* 6, 127–132. doi: 10.1002/mds.870060207

Morton, A. J., Skillings, E., Bussey, T. J., and Saksida, L. M. (2006). Measuring cognitive deficits in disabled mice using an automated interactive touchscreen system. *Nat. Methods* 3:767. doi: 10.1038/nmeth1006-767

Mrzljak, L., and Munoz-Sanjuan, I. (2015). Therapeutic strategies for Huntington's disease. *Curr. Top. Behav. Neurosci.* 22, 161–201. doi: 10.1007/7854_2013_250

Nithianantharajah, J., and Grant, S. G. (2013). Cognitive components in mice and humans: combining genetics and touchscreens for medical translation. *Neurobiol. Learn. Mem.* 105, 13–19. doi: 10.1016/j.nlm.2013.06.006

Nithianantharajah, J., Komiyama, N. H., McKechanie, A., Johnstone, M., Blackwood, D. H., St Clair, D., et al. (2013). Synaptic scaffold evolution generated components of vertebrate cognitive complexity. *Nat. Neurosci.* 16, 16–24. doi: 10.1038/nn.3276

Nithianantharajah, J., McKechanie, A. G., Stewart, T. J., Johnstone, M., Blackwood, D. H., St Clair, D., et al. (2015). Bridging the translational divide: identical cognitive touchscreen testing in mice and humans carrying mutations in a disease-relevant homologous gene. *Sci. Rep.* 5:14613. doi: 10.1038/srep14613

Oakeshott, S., Farrar, A., Port, R., Cummins-Sutphen, J., Berger, J., Watson-Johnson, J., et al. (2013). Deficits in a simple visual Go/No-go discrimination task in two mouse models of Huntington's disease. *PLoS Curr.* 5:ecurrents.hd.fe74c94bdd446a0470f6f905a30b5dd1. doi: 10.1371/currents.hd.fe74c94bdd446a0470f6f905a30b5dd1

Oakeshott, S., Port, R., Cummins-Sutphen, J., Berger, J., Watson-Johnson, J., Ramboz, S., et al. (2012). A mixed fixed ratio/progressive ratio procedure reveals an apathy phenotype in the BAC HD and the z_Q175 KI mouse models of Huntington's disease. *PLoS Curr.* 4:e4f972cffe82c0. doi: 10.1371/4f972cffe82c0

Oakeshott, S., Port, R. G., Cummins-Sutphen, J., Watson-Johnson, J., Ramboz, S., Park, L., et al. (2011). HD mouse models reveal clear deficits in learning to perform a simple instrumental response. *PLoS Curr.* 3:Rrn1282. doi: 10.1371/currents.rrn1282

O'Donnell, B. F., Blekher, T. M., Weaver, M., White, K. M., Marshall, J., Beristain, X., et al. (2008). Visual perception in prediagnostic and early stage Huntington's disease. *J. Int. Neuropsychol. Soc.* 14, 446–453. doi: 10.1017/s1355617708080405

Owen, A. M., Sahakian, B. J., Semple, J., Polkey, C. E., and Robbins, T. W. (1995). Visuo-spatial short-term recognition memory and learning after temporal lobe excisions, frontal lobe excisions or amygdalo-hippocampectomy in man. *Neuropsychologia* 33, 1–24. doi: 10.1016/0028-3932(94)00098-a

Peng, Q., Wu, B., Jiang, M., Jin, J., Hou, Z., Zheng, J., et al. (2016). Characterization of behavioral, neuropathological, brain metabolic and key molecular changes in zQ175 knock-in mouse model of Huntington's disease. *PLoS One* 11:e0148839. doi: 10.1371/journal.pone.0148839

Piiponniemi, T. O., Bragge, T., Vauhkonen, E. E., Vartiainen, P., Puoliväli, J. T., Sweeney, P. J., et al. (2017). Acquisition and reversal of visual discrimination learning in APPSwDI/Nos2$^{-/-}$ (CVN) mice. *Neurosci. Lett.* 650, 126–133. doi: 10.1016/j.neulet.2017.04.049

Pirogovsky, E., Nicoll, D. R., Challener, D. M., Breen, E., Gluhm, S., Corey-Bloom, J., et al. (2015). The visual spatial learning test: differential impairment during the premanifest and manifest stages of Huntington's disease. *J. Neuropsychol.* 9, 77–86. doi: 10.1111/jnp.12036

Rich, J. B., Campodonico, J. R., Rothlind, J., Bylsma, F. W., and Brandt, J. (1997). Perseverations during paired-associate learning in Huntington's disease. *J. Clin. Exp. Neuropsychol.* 19, 191–203. doi: 10.1080/01688639708403850

Rothe, T., Deliano, M., Wojtowicz, A. M., Dvorzhak, A., Harnack, D., Paul, S., et al. (2015). Pathological gamma oscillations, impaired dopamine release, synapse loss and reduced dynamic range of unitary glutamatergic synaptic transmission in the striatum of hypokinetic Q175 Huntington mice. *Neuroscience* 311, 519–538. doi: 10.1016/j.neuroscience.2015.10.039

Sánchez-Pernaute, R., Kunig, G., Del Barrio Alba, A., De Yebenes, J. G., Vontobel, P., and Leenders, K. L. (2000). Bradykinesia in early Huntington's disease. *Neurology* 54, 119–125. doi: 10.1212/wnl.54.1.119

Sebastianutto, I., Cenci, M. A., and Fieblinger, T. (2017). Alterations of striatal indirect pathway neurons precede motor deficits in two mouse models of Huntington's disease. *Neurobiol. Dis.* 105, 117–131. doi: 10.1016/j.nbd.2017.05.011

Skillings, E. A., Wood, N. I., and Morton, A. J. (2014). Beneficial effects of environmental enrichment and food entrainment in the R6/2 mouse model of Huntington's disease. *Brain Behav.* 4, 675–686. doi: 10.1002/brb3.235

Smith, G. A., Rocha, E. M., Mclean, J. R., Hayes, M. A., Izen, S. C., Isacson, O., et al. (2014). Progressive axonal transport and synaptic protein changes correlate with behavioral and neuropathological abnormalities in the heterozygous Q175 KI mouse model of Huntington's disease. *Hum. Mol. Genet.* 23, 4510–4527. doi: 10.1093/hmg/ddu166

Southwell, A. L., Smith-Dijak, A., Kay, C., Sepers, M., Villanueva, E. B., Parsons, M. P., et al. (2016). An enhanced Q175 knock-in mouse model of Huntington disease with higher mutant huntingtin levels and accelerated disease phenotypes. *Hum. Mol. Genet.* 25, 3654–3675. doi: 10.1093/hmg/ddw212

Sprengelmeyer, R., Canavan, A. G., Lange, H. W., and Homberg, V. (1995). Associative learning in degenerative neostriatal disorders: contrasts in explicit and implicit remembering between Parkinson's and Huntington's diseases. *Mov. Disord.* 10, 51–65. doi: 10.1002/mds.870100110

Talpos, J. C., Winters, B. D., Dias, R., Saksida, L. M., and Bussey, T. J. (2009). A novel touchscreen-automated paired-associate learning (PAL) task sensitive to pharmacological manipulation of the hippocampus: a translational rodent model of cognitive impairments in neurodegenerative disease. *Psychopharmacology* 205, 157–168. doi: 10.1007/s00213-009-1526-3

Thompson, P. D., Berardelli, A., Rothwell, J. C., Day, B. L., Dick, J. P., Benecke, R., et al. (1988). The coexistence of bradykinesia and chorea in Huntington's disease and its implications for theories of basal ganglia control of movement. *Brain* 111, 223–244. doi: 10.1093/brain/111.2.223

Trueman, R. C., Brooks, S. P., Jones, L., and Dunnett, S. B. (2009). Rule learning, visuospatial function and motor performance in the Hdh^{Q92} knock-in mouse model of Huntington's disease. *Behav. Brain Res.* 203, 215–222. doi: 10.1016/j.bbr.2009.05.006

Trueman, R. C., Dunnett, S. B., Jones, L., and Brooks, S. P. (2012). Five choice serial reaction time performance in the Hdh^{Q92} mouse model of Huntington's disease. *Brain Res. Bull.* 88, 163–170. doi: 10.1016/j.brainresbull.2011.10.019

Whittaker, D. S., Wang, H. B., Loh, D. H., Cachope, R., and Colwell, C. S. (2017). Possible use of a H3R antagonist for the management of nonmotor symptoms

in the Q175 mouse model of Huntington's disease. *Pharmacol. Res. Perspect.* 5:e00344. doi: 10.1002/prp2.344

Wyant, K. J., Ridder, A. J., and Dayalu, P. (2017). Huntington's disease-update on treatments. *Curr. Neurol. Neurosci. Rep.* 17:33. doi: 10.1007/s11910-017-0739-9

Yhnell, E., Dunnett, S. B., and Brooks, S. P. (2016a). A longitudinal operant assessment of cognitive and behavioural changes in the *Hdh*^{Q111} mouse model of Huntington's disease. *PLoS One* 11:e0164072. doi: 10.1371/journal.pone.0164072

Yhnell, E., Dunnett, S. B., and Brooks, S. P. (2016b). The utilisation of operant delayed matching and non-matching to position for probing cognitive flexibility and working memory in mouse models of Huntington's disease. *J. Neurosci. Methods* 265, 72–80. doi: 10.1016/j.jneumeth.2015.08.022

Yhnell, E., Lelos, M. J., Dunnett, S. B., and Brooks, S. P. (2016c). Cognitive training modifies disease symptoms in a mouse model of Huntington's disease. *Exp. Neurol.* 282, 19–26. doi: 10.1016/j.expneurol.2016.05.008

Conflict of Interest Statement: All research was conceptualised, planned and directed by scientific staff at CHDI and Charles River Discovery. CHDI is a not-for-profit biomedical research organisation exclusively dedicated to discovering and developing therapeutics that slow the progression of Huntington's disease. Charles River Discovery Services Finland Oy is a contract research organisation that conducted part of the study through a fee-for-service agreement for CHDI Foundation. At the time of the study, LP and RC were employed by CHDI Management, Inc., as advisors to CHDI Foundation, Inc., whereas TOP, TP, TH, JP and MK were employed by Charles River Discovery Services Finland Oy.

Copyright © 2018 Piiponniemi, Parkkari, Heikkinen, Puoliväli, Park, Cachope and Kopanitsa. This is an open-access article distributed under the terms of the Creative Commons Attribution License (CC BY). The use, distribution or reproduction in other forums is permitted, provided the original author(s) and the copyright owner(s) are credited and that the original publication in this journal is cited, in accordance with accepted academic practice. No use, distribution or reproduction is permitted which does not comply with these terms.

frontiers in Behavioral Neuroscience

ORIGINAL RESEARCH
published: 11 December 2018
doi: 10.3389/fnbeh.2018.00296

The Role of Premotor Areas in Dual Tasking in Healthy Controls and Persons With Multiple Sclerosis: An fNIRS Imaging Study

Soha Saleh[1,2], Brian M. Sandroff[3], Tyler Vitiello[1], Oyindamola Owoeye[4], Armand Hoxha[1], Patrick Hake[5], Yael Goverover[5,6], Glenn Wylie[7], Guang Yue[1,2] and John DeLuca[2,5]*

[1]Human Performance and Engineering Research, Kessler Foundation, West Orange, NJ, United States, [2]Rutgers New Jersey Medical School, Newark, NJ, United States, [3]Department of Physical Therapy, University of Alabama at Birmingham, Birmingham, AL, United States, [4]Department of Biomedical Engineering, New Jersey Institute of Technology, Newark, NJ, United States, [5]Neuropsychology and Neuroscience Research, Kessler Foundation, East Hanover, NJ, United States, [6]Department of Occupational Therapy, New York University, New York, NY, United States, [7]Rocco Ortenzio Neuroimaging Center, Kessler Foundation, West Orange, NJ, United States

Persons with multiple sclerosis (pwMS) experience declines in physical and cognitive abilities and are challenged by dual-tasks. Dual-tasking causes a drop in performance, or what is known as dual-task cost (DTC). This study examined DTC of walking speed (WS) and cognitive performance (CP) in pwMS and healthy controls (HCs) and the effect of dual-tasking on cortical activation of bilateral premotor cortices (PMC) and bilateral supplementary motor area (SMA). Fourteen pwMS and 14 HCs performed three experimental tasks: (1) single cognitive task while standing (SingCog); (2) single walking task (SingWalk); and (3) dual-task (DualT) that included concurrent performance of the SingCog and SingWalk. Six trials were collected for each condition and included measures of cortical activation, WS and CP. WS of pwMS was significantly lower than HC, but neuropsychological (NP) measures were not significantly different. pwMS and HC groups had similar DTC of WS, while DTC of CP was only significant in the MS group; processing speed and visual memory predicted 55% of this DTC. DualT vs. SingWalk recruited more right-PMC activation only in HCs and was associated with better processing speed. DualT vs. SingCog recruited more right-PMC activation and bilateral-SMA activation in both HC and pwMS. Lower baseline WS and worse processing speed measures in pwMS predicted higher recruitment of right-SMA (rSMA) activation suggesting maladaptive recruitment. Lack of significant difference in NP measures between groups does not rule out the influence of cognitive factors on dual-tasking performance and cortical activations in pwMS, which might have a negative impact on quality of life.

Keywords: multiple sclerosis, dual-task cost, fNIRS, premotor cortex, SMA, neuropsychology measures

OPEN ACCESS

Edited by:
Elizabeth B. Torres, Rutgers University, The State University of New Jersey, United States

Reviewed by:
Pierfilippo De Sanctis, Albert Einstein College of Medicine, United States
Martina Mancini, Oregon Health & Science University, United States

****Correspondence:***
Soha Saleh
ssaleh@kesslerfoundation.org

Received: *10 July 2018*
Accepted: *16 November 2018*
Published: *11 December 2018*

Citation:
Saleh S, Sandroff BM, Vitiello T, Owoeye O, Hoxha A, Hake P, Goverover Y, Wylie G, Yue G and DeLuca J (2018) The Role of Premotor Areas in Dual Tasking in Healthy Controls and Persons With Multiple Sclerosis: An fNIRS Imaging Study. Front. Behav. Neurosci. 12:296. doi: 10.3389/fnbeh.2018.00296

INTRODUCTION

One of the hallmarks, burdensome features of multiple sclerosis (MS) involves the interrelated deterioration of both physical and cognitive performance (CP), perhaps based on co-occurring damage in neural regions that are important for those functions (Benedict et al., 2011; Motl et al., 2016; Cattaneo et al., 2017). For example, walking is a motor activity that

often requires executive function and attention, especially in processing external and internal cues, so it is likely that deficits in cognitive processing contribute to gait deficits (Amboni et al., 2013). Importantly, walking in the real-word rarely occurs in isolation. That is, real-world walking is often accompanied by increased attentional demands based on performing simultaneous tasks (i.e., walking while thinking [dual-tasking] Holtzer et al., 2011). The increased attentional demands associated with dual-tasking during walking can lead to increased rate of error and consequently put persons with MS (pwMS) at an elevated risk of falling or getting injured (Wajda et al., 2013). One recent meta-analytic study reported that complex dual-tasking has negative effects on postural stability in pwMS, posing an elevated fall risk (Ghai et al., 2017). By extension, such an elevated fall risk further reduces the quality of life, ability to perform activities of daily living, and sustaining stable employment (Raggi et al., 2016). As such, quantifying the impact of dual-tasking during walking in pwMS is paramount.

Dual-tasking during walking can be measured using a variety of different paradigms. For example, paradigms that have been included in studies involving pwMS include walking while talking (e.g., alternate-letter alphabet task Learmonth et al., 2014) or mathematical calculations like subtracting by 7's), among others to measure cognitive-motor interference (CMI). Of note, CMI is rarely expressed in terms of CP in this population, which has been acknowledged as a major limitation of the field (Leone et al., 2015; Goverover et al., 2018). Nevertheless, studies in MS samples have reported a decline in gait performance in response to adding a cognitive load vs. walking alone (Sosnoff et al., 2011; Doi et al., 2013; Learmonth et al., 2014; Downer et al., 2016). Indeed, such declines might be a product of cognitive problems associated with MS (Diamond et al., 1997; DeLuca et al., 2004a,b; Beckmann et al., 2005; Lengenfelder et al., 2006; Dobryakova et al., 2016), given that successful dual-tasking requires divided attention and the ability to process information simultaneously from multiple internal or external sources. Yet, there is equivocal evidence regarding the association between the dual-task cost of walking (DTCW; i.e., the reduction in walking performance under single- vs. dual-task conditions) and cognition in MS (Motl et al., 2014; Sosnoff et al., 2014; Kirkland et al., 2015; Sandroff et al., 2015a).

The lack of consistent associations between the DTCW and cognition in pwMS is not consistent with literature in other populations whereby the DTCW is consistently and robustly associated with aspects of information processing (Holtzer et al., 2014). Given the importance of executive functioning during walking, neuroimaging studies have focused on the role of the prefrontal cortex (PFC) during dual-tasking compared with walking alone using mobile imaging technologies like functional near-infrared spectroscopy (fNIRS), since it is not feasible to study actual walking behavior in an MRI scanner. Evidence suggests that PFC activity is elevated during dual-tasking in pwMS (Holtzer et al., 2011; Chaparro et al., 2017) as well as in healthy individuals (Mirelman et al., 2014) compared with walking alone. In addition to the PFC, premotor areas (premotor cortices (PMC) and supplementary motor area (SMA)) play an important role in executive functioning and working memory (Alvarez and Emory, 2006; Harding et al., 2015; Ptak et al., 2017), the cortical control of walking (Koenraadt et al., 2014), and in coupling cues to motor acts and in the guidance of movement (Moisa et al., 2012). Taken together, this suggests that premotor areas might play an important role in dual-tasking, which might be particularly challenged in pwMS. One recent mobile imaging study (Lu et al., 2015) reported large correlations between increased activation in these regions and a decline in gait performance while dual-tasking in healthy young adults; however, there are no published neuroimaging studies examining the roles of the PMC during dual-tasking in pwMS. Such an investigation would provide critical information for a better understanding of the neural underpinnings and potential impact of cognitive-motor interactions in this population.

The present study examined activation of bilateral premotor areas and SMA during dual-tasking (DualT), walking alone (i.e., single walking task, SingWalk) and performance of a cognitive task alone (i.e., single cognitive task, SingCog) in pwMS and healthy controls (HCs) using fNIRS. We hypothesized that relative to HCs, pwMS would demonstrate a pattern of higher premotor activation during dual-tasking relative to single tasks based on previous results from functional neuroimaging studies (Hillary et al., 2003; Rocca et al., 2009, 2012). This hypothesis is also based on the assumption that pwMS likely allocate more neural resources than HCs during dual-tasking to maximize safety by avoiding injury/falls (Sandroff et al., 2015a). We further hypothesized that in pwMS, patterns of PMC activation and behavioral DTC outcomes would be associated with measures of walking speed (WS) and neurocognitive performance.

MATERIALS AND METHODS

Subjects

Participants with MS and HCs were recruited from local communities in NJ. Inclusion criteria for all subjects included age between 18 years and 64 years and no history of major depression, schizophrenia, bipolar disorder, or substance abuse disorders, and not taking any medications that may affect cognition and ambulation. Inclusion criteria for pwMS were: (a) clinical definite MS diagnosis (McDonald et al., 2001); (b) relapse-free for the past 30 days; and (c) ability to walk with or without a cane, but not a walker/rollator. HC participants were recruited such that each matched one of the participants with MS based on age, sex and education. A total of 270 participants were contacted, and 32 were enrolled. The final sample of participants consisted of 14 persons (2 M, 12 F) with relapsing-remitting MS and 14 age, gender and education level matched, HC participants.

Setup and Procedure

Experiment Procedure

Participants were enrolled in two testing sessions, separated by a minimum of 2 days. In the 1st session, subjects were screened for eligibility and enrolled in the study after providing written informed consent approved by the Kessler Foundation Institutional Review Board, and with the 1964 Helsinki declaration and its later amendments or comparable

ethical standards. Following the provision of informed consent, participants completed a set of tests to evaluate ambulation and cognition by trained personnel. Neuropsychological (NP) assessment utilized the Brief International Cognitive Assessment for MS (BICAMS; Langdon et al., 2012) battery of tests that included the following: the Symbol Digit Modalities Test (SDMT; Smith et al., 1982) as a measure of information processing speed; the second edition of California Verbal Learning Test (CVLT-II; Delis et al., 2000), as a measure of verbal learning and memory, and the Brief Visuospatial Memory Test-Revised (BVMT-R; Benedict, 1997) as a measure of visuospatial learning and memory. NP measures were administered and scored in accordance with standard published procedures (Langdon, 2015). Ambulation was measured using the timed 25-foot walk test (T25FW) based on standard procedures (Motl et al., 2017). The primary outcome from the T25FW was WS expressed as feet/second (ft/s).

Table 1 summarizes participant demographics in both groups and average of WS and BICAMS measures. T25FW WS was slower for pwMS than HC (4 ft/s vs. 4.9 ft/s, $F = 6.01$, $p = 0.021$, $d = 0.93$), while scores of BICAMS tests were not different between groups. There was also a positive correlation between WS and SDMT scores in the MS group ($r = 0.72$, $Z = 3.01$, $p = 0.003$, $r^2 = 0.52$), indicating cognitive-motor coupling (Benedict et al., 2011).

TABLE 1 | Demographics of participants in both groups.

Measure	Group	
	MS	HC
Age (years)	50 ± 8 years old	50 ± 9 years
Education (years)	15.5 ± 1.8	16.1 ± 1.6
T25FW walking speed (ft/s)*	3.99 ± 1.21	4.89 ± 0.65
BVMT-R raw score	3.14 ± 1.96	4.07 ± 2.05
CVLT-II	52.2 ± 9.26	55.86 ± 8.8
SDMT	53.2 ± 12.4	57.7 ± 5.77
WS and BVMT-R correlation	−0.15	−0.18
WS and CVLT-II correlation	0.36	−0.12
WS and SDMT correlation	0.72**	0.06

*Denotes statistically significant difference between groups ($p < 0.05$). **Denotes statistically significant correlation. T25FW, 25-foot walk test; SDMT, Symbol Digit Modalities Test; CVLT-II, California Verbal Learning Test; BVMT-R, Brief Visuospatial Memory Test-Revised; WS, walking speed in the T25FW test.*

fNIRS

fNIRS technology has been successfully used in recording brain activity during ambulation (Lu et al., 2015; Chaparro et al., 2017), especially using advanced wearable multi-channel systems (Piper et al., 2014). In the present study, fNIRS (NIRSport^{TM}, NIRX, Germany) was used to collect hemodynamic activity in bilateral PMC and SMA areas. NIRSport is a wearable fNIRS system specifically designed to maximize the signal-to-noise ratio in a mobile setting (Piper et al., 2014). The optical detectors include photo-electrical receivers enclosed within a circuitry that includes a trans-impedance amplifier with a fixed 10 MΩ feedback resistor. This design provides a higher signal to noise ratio where the signal is amplified at the optode site before being transmitted to the main amplifier and data acquisition system (DAQ) and being contaminated with more motion artifacts. In the current study, six sources and six detectors were used and assembled in a montage similar to a montage used in (Lu et al., 2015) resulting in 12 total channels. Channels were arranged based on the international 10-5 system to collect data from four regions of interest (ROIs): left and right PMC (lPMC and rPMC), and left and right SMA (lSMA and rSMA; see **Figure 1**). NIRstar software and NIRSlab Matlab toolbox

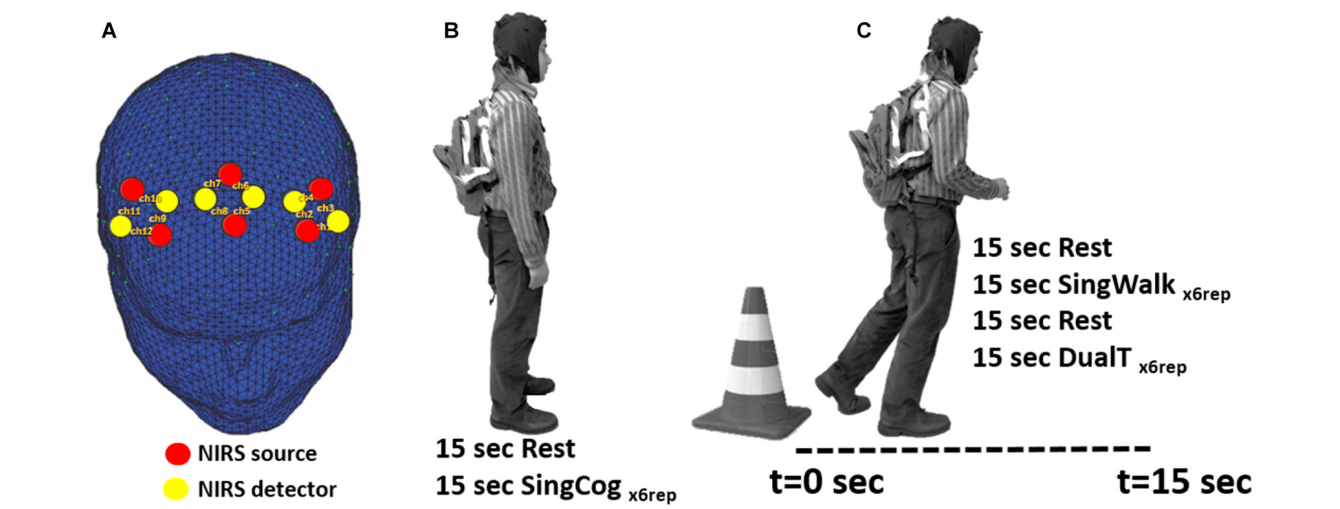

FIGURE 1 | (A) Location of functional near-infrared spectroscopy (fNIRS) sources, detectors and channels. Location of sources and detectors are shown in red and yellow dots, respectively. The six sources and six detectors are arranged in pairs to give 12 channels that cover bilateral premotor cortices (PMC) and bilateral supplementary motor area (SMA) regions. **(B)** SingCog task, subjects were in a standing position and rested for 15 s before performing a serial 7's mathematical calculation task for six repetitions. **(C)** Subjects were instructed to stand next to a traffic cone for 15 s; then at the Go cue, they were instructed to walk in a comfortable speed for 15 s while the researcher recorded the distance they traveled. In the SingWalk condition, they were asked to simply walk straight in a long hallway. In the DualT task, they were asked to perform the serial 7's task as fast as they could while walking.

(Piper et al., 2014) were used to set up the probe locations and montages. Each of the light emitting diodes (LEDs) in this system emits dual-wavelength light (760 nm and 850 nm), and the sampling rate is 6.25 Hz.

In the second session, subjects were fitted with the fNIRS system and performed three experimental conditions: (1) single cognitive task (SingCog) while standing; (2) single walking task (SingWalk); and (3) dual-task (DualT, walking while performing the cognitive task). The cognitive task in both SingCog and DualT was a conventional paradigm that requires subtracting serial 7's from a given number between 70 and 100, randomly chosen by the investigators (SingCog task; Leone et al., 2015), and reporting the results of subtractions verbally and aloud. Subjects carried a backpack during the SingCog, SingWalk and DualT tasks that included the data acquisition hardware of NIRsport system. The backpack weighted around 2 lb that did not result in any complaints about its weight.

Each experimental condition (SingWalk, SingCog, DualT) was repeated six times (six trials); task duration of each trial was 15 s, preceded by 15 s of rest (baseline condition) to allow the hemodynamic signal to reach a stable baseline (total 30 s × 6 trials of data per condition). The order of these conditions was randomized and counterbalanced to avoid any confounds in results related to physical or cognitive fatigue, or adaptation to the cognitive task. Behavioral measures included responses to the cognitive tasks (SingCog and DualT) as well as walking distance over the 15-s walking trials (SingWalk and DualT). Importantly, under the DualT condition, participants were explicitly asked to prioritize both walking and cognitive tasks equally.

Data Analysis

Behavioral Measures

Cognitive-Motor Interference (CMI) during the walking trials was evaluated based on the change in speed (Sandroff et al., 2015a) and on the change in behavioral performance on the cognitive task across experimental conditions. DTC of WS (DTCW) was calculated as % change in WS (i.e., ((DualT − SingWalk)/(SingWalk))*100), with more negative values indicating larger reductions in WS under the DualT condition relative to the SingWalk condition. Similarly, DTC on cognitive task performance (DTCC) was calculated based on the total number of correct answers in the 15-s duration of task execution in comparison to SingCog task (i.e., ((DualT − SingCog)/(SingCog))*100).

Neurophysiology Measures

Preprocessing

fNIRS data were analyzed using NIRSlab Matlab toolbox (2017 release, Matlab2013b). Estimation of oxyhemoglobin (HbO) and deoxyhemoglobin (HbR) signals was done using Beer-Lambert Law, fitting the data to Differential Path Factor (PDF) values of 7.25 and 6.38 for 760 nm and 850 nm wavelengths, respectively (Essenpreis et al., 1993). The coefficient of variation (CV) of each channel was calculated by multiplying the standard deviation of the channel's data by 100 and dividing it by the mean. Channels with CV >15% were considered bad channels and rejected before further processing of fNIRS data to reduce the effect of physical artifacts (Piper et al., 2014). Discontinuities and spike artifacts were removed followed by 0.01–0.14 Hz bandpass filter to exclude irrelevant frequency bands and to eliminate the effects of heartbeat, respiration and low-frequency signal drifts for each wavelength. After the rejection of channels with CV% >15, the HbO and HbR were averaged over the six trials for each condition to improve signal-to-noise ratio. Next, an average of HbO and HbR signals were calculated for the channels representing each ROI, resulting in a time series of data for four ROIs instead data of 12 channels data. The time series included data of the 15 s baseline (rest) and 15 s task for each condition. The relative changes in HbO and HbR during the 15 s tasks relative to 15 s baseline was calculated using a customized Matlab script. Then, the index of hemoglobin differential (HbDiff = Δ(HbO − HbR)) was calculated and used to evaluate brain activations in each experimental condition (i.e., SingCog, SingWalk, DualT). HbDiff was used as a parameter of cortical activation where a more positive HbO and more negative HbR results in higher HbDiff during the task period compared to baseline. An alternative to using HbDiff as a measure of brain activation was to use both ΔHbO and ΔHbR; HbDiff was chosen instead in order to simplify the analysis. This approach further has been adopted in previous fNIRS studies (Lassnigg et al., 1999; Lu et al., 2015).

Group Average

ANCOVA was used to compare the difference between groups in DTCC, i.e., the percent change in the number of correct answers in the DualT condition vs. SingCog, and DTCW, measured as percent change in WS in DualT condition vs. SignWalk condition. Single task behavioral data were used as covariates. A General Linear model was used to perform repeated measures Analysis of Variance (2 × 3 × 4 rANOVA) on cortical activation. Condition (SingCog, SingWalk, DualT) and ROI (bilateral PMC and SMA) were included as within-subjects factors, and group (MS vs. HC) was included as a between-subjects factor. To decompose any significant group by condition by ROI interactions from the rANOVA, we further performed follow-up 2 × 2 ANOVA comparisons between groups and (1) SingCog and DualT to understand the effect of walking in a dual-task on cortical activation; and (2) SingWalk and DualT to understand the effect of cognitive effort in a dual-task on cortical activation within ROI. Significance was set to $\alpha = 0.05$ corrected for multiple comparisons when necessary. Bonferroni correction for multiple comparisons was performed using the family-wise error rate divided by the number of comparisons (c) as the significance threshold (modified $\alpha_m = \alpha_{FW}/c$). The family-wise type I error rate was calculated assuming $\alpha_{FW} = 1 - (1 - \alpha)^c$ (Keppel and Wickens, 2004), So, to account for performing 2 × 2 ANOVA comparisons for the four ROIs, the α_{FW} was set to 0.185 and the significance threshold was set to $\alpha_m = 0.046$.

Regression Analysis

Stepwise Hierarchical Regression analysis was performed to test the possible influences of baseline measures of T25FW WS

and BICAMS tests scores on DTCW and DTCC. Similarly, we studied if these baseline measures predicted the change in cortical activation due to walking effort (WalkE) and cognitive effort (CogE). The change in activation due to walking effort was calculated by subtracting cortical activation in SingCog from DualT condition (WalkE = DualT − SingCog). Similarly, the change in activation due to the cognitive effort was calculated by subtracting cortical activation in SingWalk from DualT condition (CogE = DualT − SingWalk). We tested if T25FW WS or the three NP measures predicted the amplitude of these contrasts. Matlab ("stepwiselm" function) was used in this analysis, this function uses forward and backward stepwise regression to determine the final model; it uses a p-value of an F-statistic to test models with and without a potential term at each step and it stops when no single step improves the model. Similar to the ANOVA comparisons, the significance threshold was corrected for a total of 20 comparisons (eight regression tests for the eight contrasts per group and four predictors in each test), with $\alpha_m = \alpha_{FW}/c = 0.64/20 = 0.032$.

Correlation Between Cortical Activation and Measures of Gait and Cognitive Performance During Dual-Tasking

Bivariate correlation analysis was used to test the relationship between cortical activations and gait performance (WS) and CP (number of answers in the serial 7's tasks) during dual-tasks. Since a total of 8 tests were done in each group, the significance threshold was corrected similarly to the other statistical analysis tests in this manuscript with $\alpha_m = \alpha_{FW}/c = 0.56/16 = 0.035$.

RESULTS

DTCW and DTCC

As shown in **Figure 2**, DTCW was similar in both groups; WS dropped by 16.8% (±15.7%) in the MS group, and by 12.5% (±11.3%) in the HC group. DTCC, i.e., number of serial 7's answers, dropped by 19.3% (±30%) in the MS group and increased by 11% (±39%) in the HC group, where the HC group participants performed better under dual-task condition compared to SingCog ($F = 5.8$, $p = 0.023$, $\eta_p^2 = 0.21$). This indicates that MS had no effect on DTCW but had a significant effect on DTCC. Despite, the similar DTCW in both groups, higher DTCW (more negative values) in the MS group was predicted by a better (higher) BVMT-R score ($R^2 = 0.33$, $F = 5.89$, $p = 0.032$, $\eta_p^2 = 0.3$). On the other hand, higher DTC of serial 7's performance (higher deterioration in CP) in the MS group was predicted by worse BVMT-R ($F = 5.7$, $p = 0.034$, $\eta_p^2 = 0.3$) and SDMT scores ($F = 5.3$, $p = 0.036$, $\eta_p^2 = 0.29$). Together BVMT-R and SDMT explained approximately 55% of variance in DTCC ($R^2 = 0.55$, $F = 6.8$,

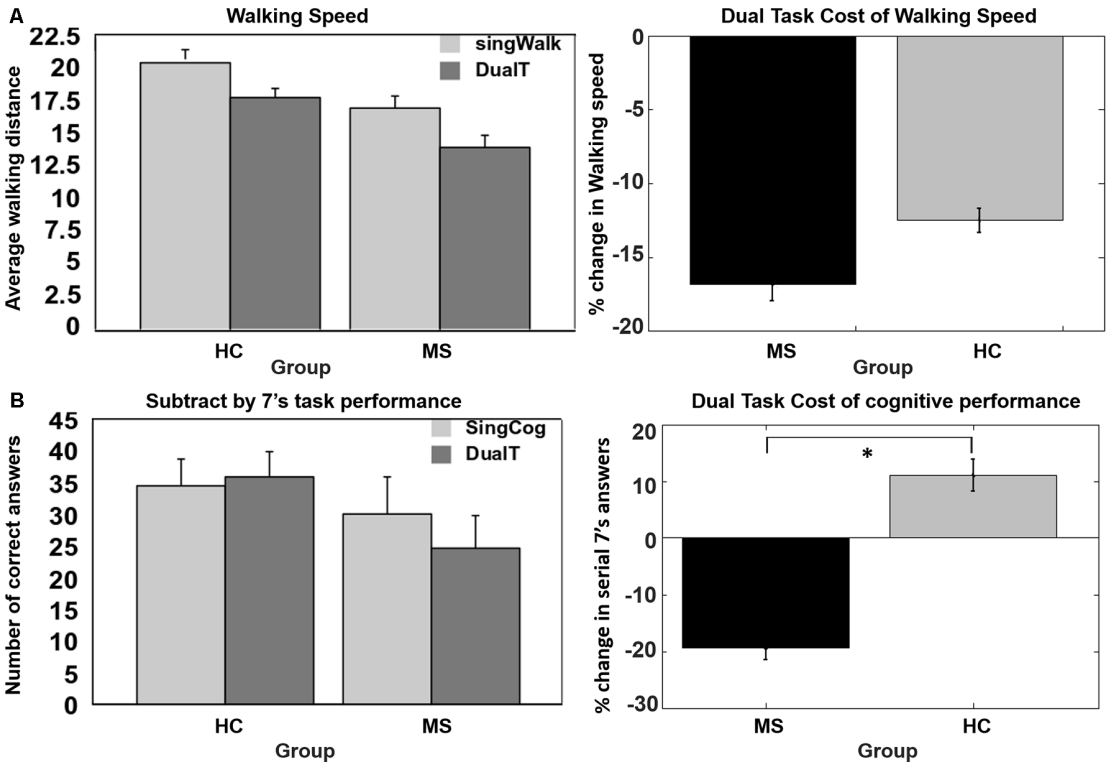

FIGURE 2 | (A) No group difference in dual-task cost (DTC) of walking speed (WS). **(B)** Significant difference in DTC of serial 7's cognitive task performance, decrease in performance in multiple sclerosis (MS) group and no change or improvement in performance in the healthy control (HC) group. *Denotes statistical significance ($p < 0.05$). Error bar denotes standard errors.

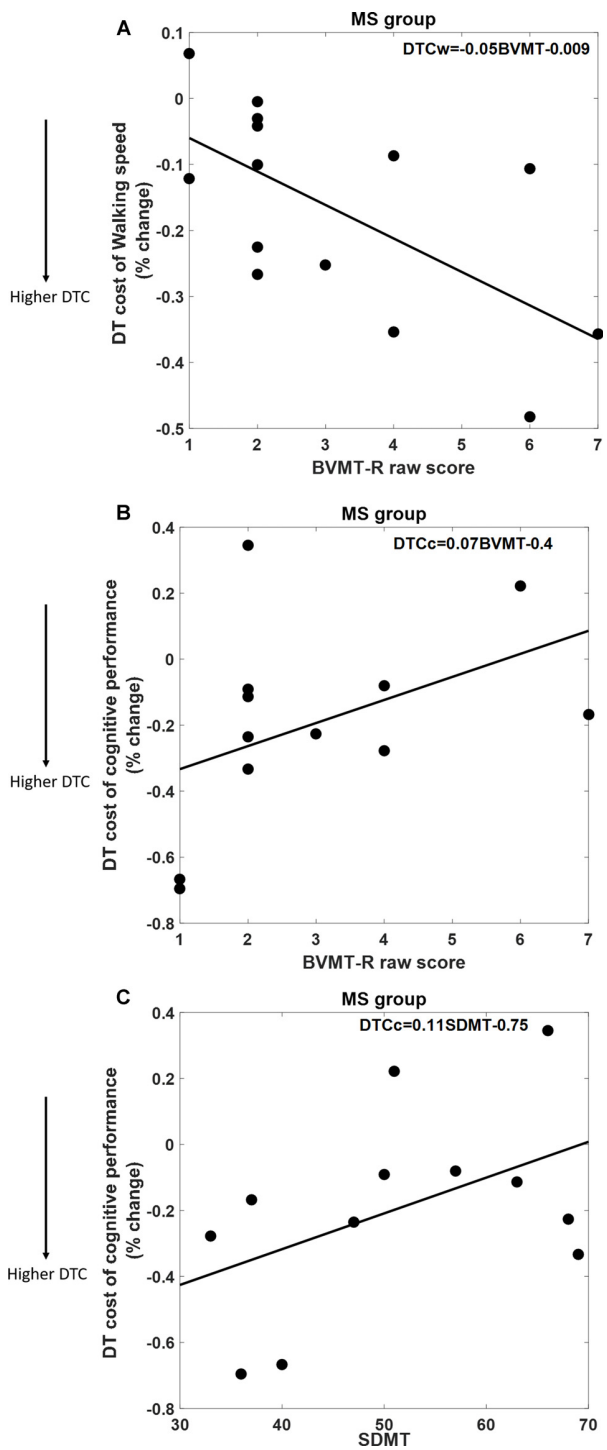

FIGURE 3 | (A) Better Brief Visuospatial Memory Test-Revised (BVMT-R) score predicts 33% of DTC of WS. **(B,C)** Both BVMT-R and Symbol Digit Modalities Test (SDMT) scores predict 55% of DTC of cognitive performance in the serial 7's mathematical calculations task; better BVMT-R and SDMT scores are associated with lower DTC of CP.

$p = 0.01$, $\eta_p^2 = 0.55$; see **Figure 3**). Collectively, this indicates that during the dual-task, MS participants with better information processing and visual memory focused more on the cognitive task and demonstrated higher DTC of WS and lower DTC of CP.

Dual Task Effect on Brain Activations

Overall three-way condition by ROI by group comparison revealed significant differences between conditions (SingCog, SingWalk, DualT, $F = 6.7$, $p = 0.003$, $\eta_p^2 = 0.34$), and ROIs (lPMC, rPMC, lSMA, rSMA, $F = 3.7$, $p = 0.016$, $\eta_p^2 = 0.22$; see **Figures 4A,B**) and no difference between groups. There was a two-way ROI by group interaction ($F = 2.9$, $p = 0.041$, $\eta_p^2 = 0.18$) such that across conditions, left PMC activation was higher in the MS group (see **Figure 4C**). There was also an ROI by condition interaction such that the right PMC activation was higher in the DualT condition ($F = 2.35$, $p = 0.033$, $\eta_p^2 = 0.15$; see **Figure 4D**). To further understand the dual-task vs. single task effect on cortical activation in the four ROIs, we performed a 2 × 2 ANOVA to compare between groups (MS vs. HC) and DualT vs. SingWalk within each ROI. A second 2 × 2 ANOVA was done to compare between groups and DualT vs. SingCog within each ROI. The results are presented below.

DualT vs. SingWalk

There was a statistically significant condition (DualT vs. SingWalk) by group (MS vs. HC) interaction ($F = 5.1$, $p = 0.03$, $\eta_p^2 = 0.16$) on rPMC activation only. *Post hoc* test within rPMC showed that HC recruited higher rPMC activation ($F = 6.02$, $p = 0.029$, $\eta_p^2 = 0.19$) under DualT conditions relative to singWalk condition while there was no change in rPMC activation in the pwMS group. The results of the regression analysis showed that the higher the information processing speed (higher SDMT score), the greater was the dual-tasking vs. single walking task effect on cortical activation in the HC group ($R^2 = 0.59$, $F = 17.3$, $p = 0.001$; see **Figure 5**). This suggests that rPMC plays an important role in maintaining similar CP across conditions, which did not significantly change in the HC group.

DualT vs. SingCog

There was a main effect of condition (DualT vs. SingCog) on activation in rPMC ($F = 12.2$, $p = 0.002$, $\eta_p^2 = 0.32$), lSMA ($F = 6.5$, $p = 0.016$, $\eta_p^2 = 0.2$), and rSMA ($F = 9.5$, $p = 0.005$, $\eta_p^2 = 0.27$) regions, where the activation was higher during dual-tasking in these ROIs (see **Figure 6**). There was no main effect of group in any ROI. However, there was a marginal effect, such that an increase in left PMC activation in the MS group with moderate effect size (lPMC; $F = 3.7$, $p = 0.066$, $\eta_p^2 = 0.125$). There was no statistically significant condition by group interaction on cortical activation in any ROI. Regression analysis showed that higher rPMC activation in DualT vs. SingCog in the HC group was predicted by better SDMT score ($R^2 = 0.36$, $F = 6.77$, $p = 0.023$; see **Figure 7A**). Within the MS group, the effect of DualT on rPMC activation was not predicted by ambulation or NP measures. However, DualT effect on rSMA activation was associated with slower WS ($R^2 = 0.65$, $F = 22.4$, $p = 0.0005$), and lower information processing speed (SDMT score; $R^2 = 0.31$, $F = 5.5$, $p = 0.037$),

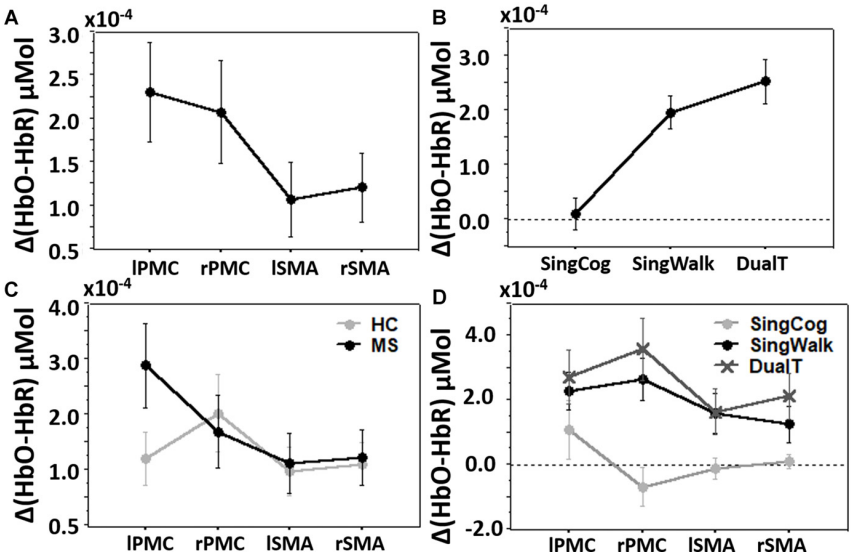

FIGURE 4 | (A) Cortical activation in the four regions of interest (ROIs). **(B)** Cortical activation in the three conditions. **(C)** Cortical activation in the four ROIs and two groups showing ROI by group interaction driven by higher left PMC (lPMC) activation in the MS group. **(D)** Cortical activation in the four ROIs and three conditions showing ROI by condition interaction driven by higher right PMC (rPMC) and right SMA (rSMA) in the DualT condition. Error bar denotes standard errors.

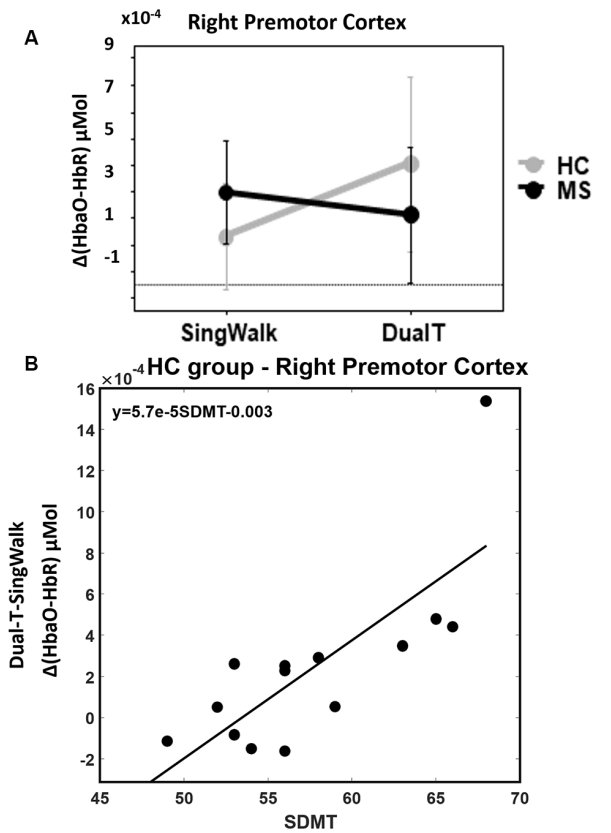

FIGURE 5 | (A) Interaction between groups and condition (walking alone and dual-task), higher rPMC activation during dual-tasking vs. walking alone in the HC group, and no difference in the MS group. Error bar denotes standard errors. **(B)** Better SDMT scores predict higher cortical activation in dual-tasking vs. single walking task.

which was marginally significant with Bonferroni correction (see **Figures 7B,C**).

Relationship Between Cortical Activation and Performance During Dual-Tasking

Correlational analysis was performed to examine the relationship between cortical activation and DualT performance (see **Table 2**). In the MS group, lSMA and rSMA increased activation correlated with slower WS. This suggests that these regions were associated with gait adjustments during dual-tasking in pwMS. A similar relationship was not found in the HC group, and there was no significant correlation between cortical activation in the DualT and the number of answers in the serial 7's task in the four ROIs in both groups.

DISCUSSION

To our knowledge, this is the first examination of DTC of CP and bilateral PMC and SMA modulations of dual-tasking during dynamic tasks in pwMS vs. HC. Results showed a slowdown in speed in both groups during dual-tasking, but a deterioration in CP only in the MS group. This was observed despite the fact that the MS participants were not impaired based on traditional NP tests (i.e., BICAMS). While the MS subjects had higher DTC of CP, this was associated with the need for increased right SMA activation. This effect was greater in pwMS with lower SDMT scores (i.e., processing speed) than those with higher SDMT scores. The following sections discuss each of the primary study results within the context of how dual-tasking influences behavior and cortical activation in ambulatory and cognitive domains of functioning.

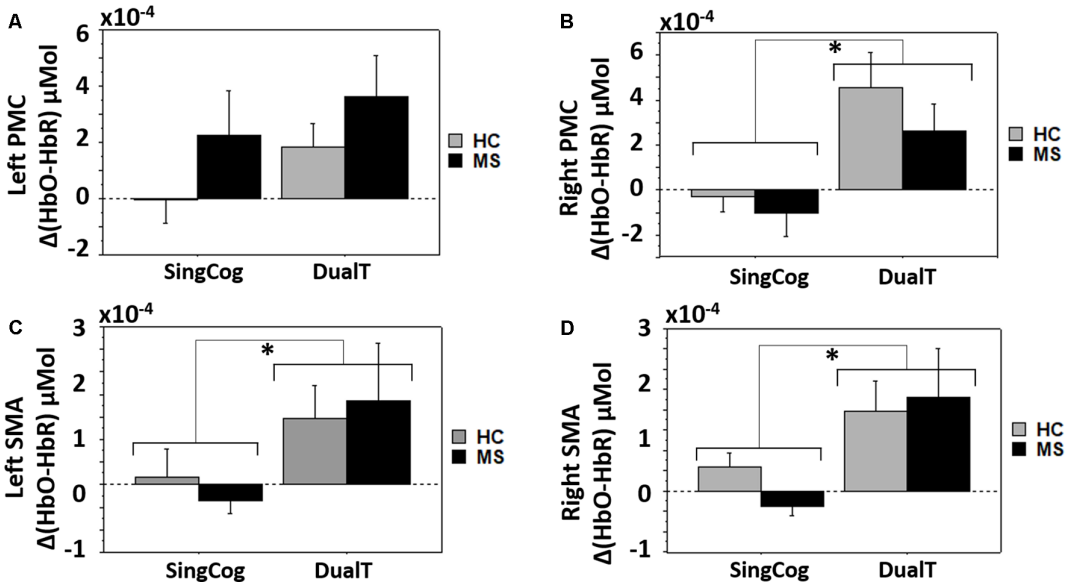

FIGURE 6 | (A) Cortical activation in the dual-task vs. single cognitive task in lPMC in both groups. **(B–D)** Higher cortical activation in the dual-task vs. single cognitive task in rPMC, lSMA and rSMA in both groups. *Denotes statistical significance ($p < 0.046$). Error bar denotes standard errors.

Dual-Tasking Influence on Behavioral Performance

For both pwMS and HC groups, dual-tasking reduced WS to a similar magnitude relative to walking alone in the two groups, despite pwMS walked slower than HC in general. This finding is consistent with previous studies that have similarly reported slowing in ambulation during dual-tasking (Leone et al., 2015) relative to walking alone. The observed lack of differences in DTCW between groups is also consistent with the high-level evidence that although pwMS walk slower than HCs for both single- and dual-task walking, respectively, the DTCW is not different between persons with MS and HCs overall (Learmonth et al., 2017). By comparison, dual-tasking did affect CP (i.e., the number of correct answers in the cognitive task) relative to performing the cognitive task in isolation, where MS subjects, but not HC, performed worse in the DualT vs. SingCog condition. Despite the non-significant difference in NP (i.e., BICAMS) measures between groups, higher (better) performance in BVMT-R and SDMT correlated with lower DTCC in MS group, and higher (better) performance in BVMT-R predicted higher DTC of WS. These results suggest that individuals with MS who demonstrated better cognitive function implicitly prioritized performing the cognitive task successfully by slowing down and focusing their attention on the cognitive task.

Taken together, these findings show that even in the absence of cognitive impairment as assessed by NP testing (i.e., BICAMS), when faced with a dual-task, persons with MS can show a decline in CP. This DTC in otherwise cognitively intact persons with MS might have a negative impact on community ambulation and physical activity in pwMS (Sandroff et al., 2012, 2015b).

Dual-Tasking Influence on Cortical Activations

Comparison of cortical activation during dual-tasking vs. SingWalk and SingCog demonstrated difference in cortical activation between the HC and MS groups. This difference in activation was in both PMC and SMA regions, and it was partially associated with cognitive function in MS group, despite similar performance as HC group on BICAMS.

PMC Activation

Higher rPMC activation in DualT vs. both single tasks, SingWalk and SingCog, in the HC group suggests that this cortical region is involved in both walking and cognition as single tasks, but its recruitment increases linearly with increased DTC relative to both SingWalk and SingCog. On the other hand, cortical activation did not change during the dual-tasking vs. single walking task conditions in the MS group, suggesting that the role of rPMC is altered in pwMS under these conditions. In the MS group, Group × ROI interaction showed higher left PMC activation in all the three conditions, including the SingCog task. Unlike HC, MS participants required bilateral PMC activation even to perform the single cognitive task, suggesting the need for increased recruitment to perform the cognitive task alone. This could be consistent with studies showing compensation in pwMS who are not cognitively impaired (Audoin et al., 2003; Mainero et al., 2004).

SMA Activation

DualT vs. SingCog task resulted in higher activation of rPMC, rSMA and lSMA regions showing no group by condition interaction. More interestingly, higher activation in rSMA in pwMS was predicted by slower WS and slower information processing speed (SDMT score). In addition, higher activation

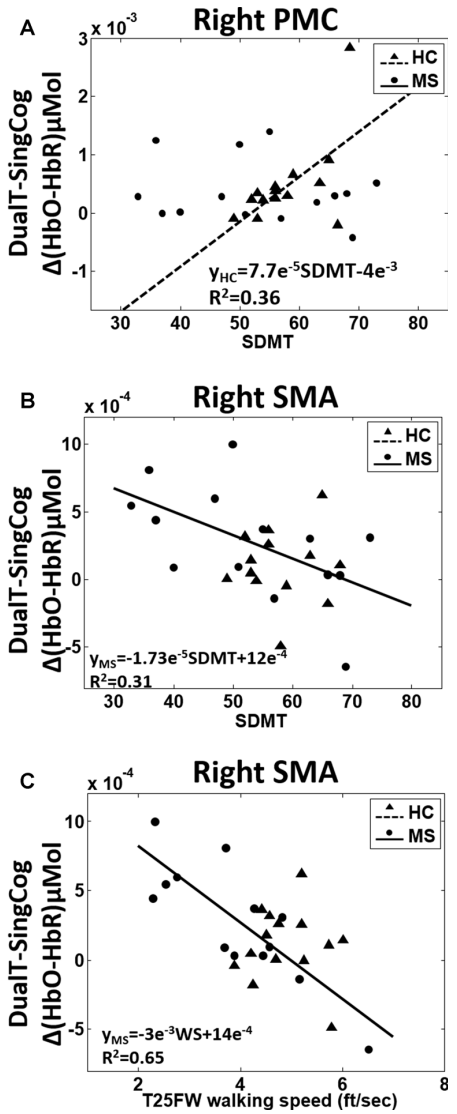

FIGURE 7 | (A) Higher SDMT score predicts higher rPMC cortical activation in dual-tasking vs. single cognitive task in the HC group (black dotted line). **(B)** Better SDMT predicts weaker or negative difference in rSMA activation in dual-task vs. single cognitive task in the MS group (black solid line). **(C)** Faster WS predicts weaker or negative difference in rSMA activation in dual-task vs. single cognitive task in the MS group (black solid line).

of both lSMA and rSMA during dual-tasking correlated with slower WS. SMA is a key premotor region that is involved in the control of several motor activities, including walking, so the results suggest that individuals with lower WS and SDMT score require higher activation of rSMA region to process gait performance in a dual-task vs. single cognitive task in the MS group, and to compensate for the DTC on cognition.

Relationship Between Cortical Activation and Behavioral Performance

Interestingly, MS group showed a correlation between higher bilateral SMA activations and lower WS during dual-tasking.

TABLE 2 | Correlational analysis between cortical activations and performance during dual-tasks.

Group	Condition		lPMC	rPMC	lSMA	rSMA
MS	Walking		$r = -0.51$	$r = -0.38$	$r = -0.72$*	$r = -0.6$*
	Speed		$p = 0.06$	$p = 0.18$	$p = 0.004$	$p = 0.02$
	Serial	7's	$r = -0.25$	$r = -0.15$	$r = -0.21$	$r = -0.28$
	Answers		$p = 0.38$	$p = 0.6$	$p = 0.46$	$p = 0.33$
HC	Walking		$r = -0.14$	$r = 0.007$	$r = -0.12$	$r = -0.29$
	Speed		$p = 0.6$	$p = 0.98$	$p = 0.68$	$p = 0.31$
	Serial	7's	$r = 0.01$	$r = -0.1$	$r = 0.228$	$r = 0.05$
	Answers		$p = 0.74$	$p = 0.73$	$p = 0.43$	$p = 0.86$

*Denotes statistically significant correlation ($\alpha_m < 0.035$).

Similar relationship was not found in the HC group. This is inconsistent with the relationship reported in healthy young population tested in a similar dual-task experiment design (Lu et al., 2015). Lu et al. (2015) reported a correlation between higher rSMA activity and higher WS, claiming that higher brain activation contributes to maintaining gait performance. This difference in findings could be attributed to the difference in age between older HC in this study and younger HC in Lu et al. (2015) study, and it could suggest that this relationship is modulated in pwMS. More research is required to understand this relationship.

Study Limitations

Several limitations in the design and analyses warrant acknowledgment. All the MS participants had a relapsing-remitting clinical disease course, so the present results may not generalize to participants with MS with progressive disease presentations. There is a need to explore this relationship in a larger sample that includes subjects with a wider range of MS phenotypes and impairment levels to better understand the dual-tasking effect on brain activation. Finally, although the cognitive task was relatively simple, it required delivery of quick answers within a short period of time and was selected to challenge components of information processing that are affected by MS during walking (Lengenfelder et al., 2006; Genova et al., 2012; Sandroff et al., 2014). Indeed, deficits in these aspects of information processing probably represent the primary cognitive deficit in MS (DeLuca et al., 2004a). However, a different type of cognitive task might have a different effect on brain activation (Stojanovic-Radic et al., 2014) and others (Patel et al., 2014; Kirkland et al., 2015). In addition to addressing these limitations, it is important to design dual-tasking using a non-verbal cognitive task in future studies and to investigate the role of regions in the frontoparietal network, which might be significant in processing dual-tasking and might be challenged by MS.

CONCLUSION

This investigation introduces novel findings related to dual-tasking cost and the role of PMC in processing dual-tasking in pwMS and HCs. When faced with a dual-task (cognitive and motor), even MS patients with intact cognitive ability show a decline in CP. This reduction in CP while performing a dual task was associated with a different pattern of cortical activation,

where left PMC was active in SingCog condition only in the MS group, and higher right SMA activation during dual-tasking correlated with worse motor and cognitive function. Further investigation is needed to delineate the roles of these regions, and other sensorimotor and fronto-parietal regions in dual-tasking, to examine the interaction between physical and cognitive tasks and the neural correlates of these behaviors, and to understand the brain mechanisms of interrelated cognitive and physical deficits in MS. Such a line of research is furtherly important for the design and implementation of targeted and optimized clinical interventions for mitigating the burden of these highly prevalent MS-related consequences (Johansson et al., 2007; Oliver et al., 2007; Motl et al., 2016).

AUTHOR CONTRIBUTIONS

Experiment design was performed by authors SS, BS, YG and JDL, with helpful feedback from GW and GY. Data were collected by SS, TV, OO, AH and PH. Data were analyzed by SS, OO and TV. Dissemination of findings was done by SS, BS and JDL. All authors contributed to writing the manuscript.

FUNDING

This study was funded in part by National Multiple Sclerosis Society grant CA 1069-A-7 (GY and JDL).

REFERENCES

Alvarez, J. A., and Emory, E. (2006). Executive function and the frontal lobes: a meta-analytic review. *Neuropsychol. Rev.* 16, 17–42. doi: 10.1007/s11065-006-9002-x

Amboni, M., Barone, P., and Hausdorff, J. M. (2013). Cognitive contributions to gait and falls: evidence and implications. *Mov. Disord.* 28, 1520–1533. doi: 10.1002/mds.25674

Audoin, B., Ibarrola, D., Philippe, J. P., Confort-Gouny, S., Malikova, I., Ali-Chérif, A., et al. (2003). Compensatory cortical activation observed by fMRI during a cognitive task at the earliest stage of MS. *Hum. Brain Mapp.* 20, 51–58. doi: 10.1002/hbm.10128

Beckmann, C. F., DeLuca, M., Devlin, J. T., and Smith, S. M. (2005). Investigations into resting-state connectivity using independent component analysis. *Philos. Trans. R. Soc. Lond. B Biol. Sci.* 360, 1001–1013. doi: 10.1098/rstb.2005.1634

Benedict, R. H. B. (1997). The brief visuospatial memory test—revised. *Psychol. Assess.* 2, 145–153.

Benedict, R. H. B., Holtzer, R., Motl, R. W., Foley, F. W., Kaur, S., Hojnacki, D., et al. (2011). Upper and lower extremity motor function and cognitive impairment in multiple sclerosis. *J. Int. Neuropsychol. Soc.* 17, 643–653. doi: 10.1017/s1355617711000403

Cattaneo, D., Lamers, I., Bertoni, R., Feys, P., and Jonsdottir, J. (2017). Participation restriction in people with multiple sclerosis: prevalence and correlations with cognitive, walking, balance, and upper limb impairments. *Arch. Phys. Med. Rehabil.* 98, 1308–1315. doi: 10.1016/j.apmr.2017.02.015

Chaparro, G., Balto, J. M., Sandroff, B. M., Holtzer, R., Izzetoglu, M., Motl, R. W., et al. (2017). Frontal brain activation changes due to dual-tasking under partial body weight support conditions in older adults with multiple sclerosis. *J. Neuroeng. Rehabil.* 14:65. doi: 10.1186/s12984-017-0280-8

Delis, D. C., Kramer, J. H., Kaplan, E., and Ober, B. A. (2000). *California Verbal Learning Test—Second Edition. Adult Version.* San Antonio, TX: The Psychological Corporation.

DeLuca, J., Chelune, G. J., Tulsky, D. S., Lengenfelder, J., and Chiaravalloti, N. D. (2004a). Is speed of processing or working memory the primary information processing deficit in multiple sclerosis? *Front. Neurol.* 26, 550–562. doi: 10.1080/13803390490496641

DeLuca, J., Christodoulou, C., Diamond, B. J., Rosenstein, E. D., Kramer, N., and Natelson, B. H. (2004b). Working memory deficits in chronic fatigue syndrome: differentiating between speed and accuracy of information processing. *J. Int. Neuropsychol. Soc.* 10, 101–109. doi: 10.1017/s1355617704101124

Diamond, B. J., DeLuca, J., Kim, H., and Kelley, S. M. (1997). The question of disproportionate impairments in visual and auditory information processing in multiple sclerosis. *J. Clin. Exp. Neuropsychol.* 19, 34–42. doi: 10.1080/01688639708403834

Dobryakova, E., Costa, S. L., Wylie, G. R., DeLuca, J., and Genova, H. M. (2016). Altered effective connectivity during a processing speed task in individuals with multiple sclerosis. *J. Int. Neuropsychol. Soc.* 22, 216–224. doi: 10.1017/s1355617715001034

Doi, T., Makizako, H., Shimada, H., Park, H., Tsutsumimoto, K., Uemura, K., et al. (2013). Brain activation during dual-task walking and executive function among older adults with mild cognitive impairment: a FNIRS study. *Aging Clin. Exp. Res.* 25, 539–544. doi: 10.1007/s40520-013-0119-5

Downer, M. B., Kirkland, M. C., Wallack, E. M., and Ploughman, M. (2016). Walking impairs cognitive performance among people with multiple sclerosis but not controls. *Hum. Mov. Sci.* 49, 124–131. doi: 10.1016/j.humov.2016.06.010

Essenpreis, M., Elwell, C. E., Cope, M., van der Zee, P., Arridge, S. R., and Delpy, D. T. (1993). Spectral dependence of temporal point spread functions in human tissues. *Appl. Opt.* 32, 418–425. doi: 10.1364/ao.32.000418

Genova, H. M., Lengenfelder, J., Chiaravalloti, N. D., Moore, N. B., and DeLuca, J. (2012). Processing speed versus working memory: contributions to an information-processing task in multiple sclerosis. *Appl. Neuropsychol.* 19, 132–140. doi: 10.1080/09084282.2011.643951

Ghai, S., Ghai, I., and Effenberg, A. O. (2017). Effects of dual tasks and dual-task training on postural stability: a systematic review and meta-analysis. *Clin. Interv. Aging* 12, 557–577. doi: 10.2147/cia.s125201

Goverover, Y., Sandroff, B. M., and DeLuca, J. (2018). Dual task of fine motor skill and problem solving in individuals with multiple sclerosis: a pilot study. *Arch. Phys. Med. Rehabil.* 99, 635–640. doi: 10.1016/j.apmr.2017.10.012

Harding, I. H., Yücel, M., Harrison, B. J., Pantelis, C., and Breakspear, M. (2015). Effective connectivity within the frontoparietal control network differentiates cognitive control and working memory. *Neuroimage* 106, 144–153. doi: 10.1016/j.neuroimage.2014.11.039

Hillary, F. G., Chiaravalloti, N. D., Ricker, J. H., Steffener, J., Bly, B. M., Lange, G., et al. (2003). An investigation of working memory rehearsal in multiple sclerosis using fMRI. *J. Clin. Exp. Neuropsychol.* 25, 965–978. doi: 10.1076/jcen.25.7.965.16490

Holtzer, R., Mahoney, J., and Verghese, J. (2014). Intraindividual variability in executive functions but not speed of processing or conflict resolution predicts performance differences in gait speed in older adults. *J. Gerontol. A Biol. Sci. Med. Sci.* 69, 980–986. doi: 10.1093/gerona/glt180

Holtzer, R., Mahoney, J. R., Izzetoglu, M., Izzetoglu, K., Onaral, B., and Verghese, J. (2011). FNIRS study of walking and walking while talking in young and old individuals. *J. Gerontol. A Biol. Sci. Med. Sci.* 66A, 879–887. doi: 10.1093/gerona/glr068

Johansson, S., Ytterberg, C., Claesson, I. M., Lindberg, J., Hillert, J., Andersson, M., et al. (2007). High concurrent presence of disability in multiple sclerosis: associations with perceived health. *J. Neurol.* 254, 767–773. doi: 10.1007/s00415-006-0431-5

Keppel, G., and Wickens, T. D. (2004). *Design and Analysis: A Researcher's Handbook.* London: Pearson.

Kirkland, M. C., Wallack, E. M., Rancourt, S. N., and Ploughman, M. (2015). Comparing three dual-task methods and the relationship to physical and cognitive impairment in people with multiple sclerosis and controls. *Mult. Scler. Int.* 2015:650645. doi: 10.1155/2015/650645

Koenraadt, K. L. M., Roelofsen, E. G. J., Duysens, J., and Keijsers, N. L. W. (2014). Cortical control of normal gait and precision stepping: an FNIRS study. *Neuroimage* 85, 415–422. doi: 10.1016/j.neuroimage.2013.04.070

Langdon, D. W., Amato, M. P., Boringa, J., Brochet, B., Foley, F., Fredrikson, S., et al. (2012). Recommendations for a brief international cognitive

assessment for multiple sclerosis (BICAMS). *Mult. Scler.* 18, 891–898. doi: 10.1177/1352458511431076

Langdon, D. (2015). BICAMS (Www.BICAMS.Net). *Multiple Sclerosis* 23, 37–38. Available online at: http://ovidsp.ovid.com/ovidweb.cgi?T=JS%7B&%7DPAGE=reference%7B&%7DD=emed17%7B&%7DNEWS=N%7B&%7DAN=72057877%5Cn, http://journals.sagepub.com.proxy1.lib.uwo.ca/doi/pdf/10.1177/1352458515602640

Lassnigg, A., Hiesmayr, M., Keznickl, P., Müllner, T., Ehrlich, M., and Grubhofer, G. (1999). Cerebral oxygenation during cardiopulmonary bypass measured by near- infrared spectroscopy: effects of hemodilution, temperature and flow. *J. Cardiothorac. Vasc. Anesth.* 13, 544–548. doi: 10.1016/s1053-0770(99)90005-8

Learmonth, Y. C., Ensari, I., and Motl, R. W. (2017). Cognitive motor interference in multiple sclerosis: insights from a systematic quantitative review. *Arch. Phys. Med. Rehabil.* 98, 1229–1240. doi: 10.1016/j.apmr.2016.07.018

Learmonth, Y. C., Sandroff, B. M., Pilutti, L. A., Klaren, R. E., Ensari, I., Riskin, B. J., et al. (2014). Cognitive motor interference during walking in multiple sclerosis using an alternate-letter alphabet task. *Arch. Phys. Med. Rehabil.* 95, 1498–1503. doi: 10.1016/j.apmr.2014.03.007

Lengenfelder, J., Bryant, D., Diamond, B. J., Kalmar, J. H., Moore, N. B., and DeLuca, J. (2006). Processing speed interacts with working memory efficiency in multiple sclerosis. *Arch. Clin. Neuropsychol.* 21, 229–238. doi: 10.1016/j.acn.2005.12.001

Leone, C., Patti, F., and Feys, P. (2015). Measuring the cost of cognitive-motor dual tasking during walking in multiple sclerosis. *Mult. Scler.* 21, 123–131. doi: 10.1177/1352458514547408

Lu, C. F., Liu, Y. C., Yang, Y. R., Wu, Y. T., and Wang, R. Y. (2015). Maintaining gait performance by cortical activation during dual-task interference: a functional near-infrared spectroscopy study. *PLoS One* 10:e0129390. doi: 10.1371/journal.pone.0129390

Mainero, C., Caramia, F., Pozzilli, C., Pisani, A., Pestalozza, I., Borriello, G., et al. (2004). fMRI evidence of brain reorganization during attention and memory tasks in multiple sclerosis. *Neuroimage* 21, 858–867. doi: 10.1016/j.neuroimage.2003.10.004

McDonald, W. I., Compston, A., Edan, G., Goodkin, D., Hartung, H. P., Lublin, F. D., et al. (2001). Recommended diagnostic criteria for multiple sclerosis: guidelines from the international panel on the diagnosis of multiple sclerosis. *Ann. Neurol.* 50, 121–127. doi: 10.1097/00041327-200206000-00041

Mirelman, A., Maidan, I., Bernad-Elazari, H., Nieuwhof, F., Reelick, M., Giladi, N., et al. (2014). Increased frontal brain activation during walking while dual tasking: an FNIRS study in healthy young adults. *J. Neuroeng. Rehabil.* 11:85. doi: 10.1186/1743-0003-11-85

Moisa, M., Siebner, H. R., Pohmann, R., and Thielscher, A. (2012). Uncovering a context-specific connectional fingerprint of human dorsal premotor cortex. *J. Neurosci.* 32, 7244–7252. doi: 10.1523/JNEUROSCI.2757-11.2012

Motl, R. W., Sandroff, B. M., and DeLuca, J. (2016). Exercise training and cognitive rehabilitation: a symbiotic approach for rehabilitating walking and cognitive functions in multiple sclerosis? *Neurorehabil. Neural Repair* 30, 499–511. doi: 10.1177/1545968315606993

Motl, R. W., Sosnoff, J. J., Dlugonski, D., Pilutti, L. A., Klaren, R., and Sandroff, B. M. (2014). Walking and cognition, but not symptoms, correlate with dual task cost of walking in multiple sclerosis. *Gait Posture* 39, 870–874. doi: 10.1016/j.gaitpost.2013.11.023

Motl, R. W., Cohen, J. A., Benedict, R., Phillips, G., LaRocca, N., Hudson, L. D., et al. (2017). Validity of the timed 25-foot walk as an ambulatory performance outcome measure for multiple sclerosis. *Mult. Scler.* 23, 704–710. doi: 10.1177/1352458517690823

Oliver, D., Connelly, J. B., Victor, C. R., Shaw, F. E., Whitehead, A., Genc, Y., et al. (2007). Strategies to prevent falls and fractures in hospitals and care homes and effect of cognitive impairment: systematic review and meta-analyses. *BMJ* 334:82. doi: 10.1136/bmj.39049.706493.55

Patel, P., Lamar, M., and Bhatt, T. (2014). Effect of type of cognitive task and walking speed on cognitive-motor interference during dual-task walking. *Neuroscience* 260, 140–148. doi: 10.1016/j.neuroscience.2013.12.016

Piper, S. K., Krueger, A., Koch, S. P., Mehnert, J., Habermehl, C., Steinbrink, J., et al. (2014). A wearable multi-channel FNIRS system for brain imaging in freely moving subjects. *Neuroimage* 85, 64–71. doi: 10.1016/j.neuroimage.2013.06.062

Ptak, R., Schnider, A., and Fellrath, J. (2017). The dorsal frontoparietal network: a core system for emulated action. *Trends Cogn. Sci.* 21, 589–599. doi: 10.1016/j.tics.2017.05.002

Raggi, A., Covelli, V., Schiavolin, S., Scaratti, C., Leonardi, M., and Willems, M. (2016). Work-related problems in multiple sclerosis: a literature review on its associates and determinants. *Disabil. Rehabil.* 38, 936–944. doi: 10.3109/09638288.2015.1070295

Rocca, M. A., Valsasina, P., Ceccarelli, A., Absinta, M., Ghezzi, A., Riccitelli, G., et al. (2009). Structural and functional MRI correlates of stroop control in benign MS. *Hum. Brain Mapp.* 30, 276–290. doi: 10.1002/hbm.20504

Rocca, M. A., Valsasina, P., Martinelli, V., Misci, P., Falini, A., Comi, G., et al. (2012). Large-scle neuronal network dysfunction in relapsing-remitting multiple sclerosis. *Neurology* 79, 1449–1458. doi: 10.1212/wnl.0b013e31826d5f10

Sandroff, B. M., Benedict, R. H., and Motl, R. W. (2015a). Nonsignificant associations between measures of inhibitory control and walking while thinking in persons with multiple sclerosis. *Arch. Phys. Med. Rehabil.* 96, 1518–1524. doi: 10.1016/j.apmr.2015.04.015

Sandroff, B. M., Klaren, R. E., and Motl, R. W. (2015b). Relationships among physical inactivity, deconditioning, and walking impairment in persons with multiple sclerosis. *J. Neurol. Phys. Ther.* 39, 103–110. doi: 10.1097/npt.0000000000000087

Sandroff, B. M., Dlugonski, D., Pilutti, L. A., Pula, J. H., Benedict, R. H. B., and Motl, R. W. (2014). Physical activity is associated with cognitive processing speed in persons with multiple sclerosis. *Mult. Scler. Relat. Disord.* 3, 123–128. doi: 10.1016/j.msard.2013.04.003

Sandroff, B. M., Dlugonski, D., Weikert, M., Suh, Y., Balantrapu, S., and Motl, R. W. (2012). Physical activity and multiple sclerosis: new insights regarding inactivity. *Acta Neurol. Scand.* 126, 256–262. doi: 10.1111/j.1600-0404.2011.01634.x

Smith A., Aaron, and Western Psychological Services (Firm) (1982). *Symbol Digit Modalities Test: Manual.* Los Angeles, CA: Western Psychological Corporation.

Sosnoff, J. J., Boes, M. K., Sandroff, B. M., Socie, M. J., Pula, J. H., and Motl, R. W. (2011). Walking and thinking in persons with multiple sclerosis who vary in disability. *Arch. Phys. Med. Rehabil.* 92, 2028–2033. doi: 10.1016/j.apmr.2011.07.004

Sosnoff, J. J., Socie, M. J., Sandroff, B. M., Balantrapu, S., Suh, Y., Pula, J. H., et al. (2014). Mobility and cognitive correlates of dual task cost of walking in persons with multiple sclerosis. *Disabil. Rehabil.* 36, 205–209. doi: 10.3109/09638288.2013.782361

Stojanovic-Radic, J., Wylie, G., Voelbel, G., Chiaravalloti, N., and DeLuca, J. (2014). Neuroimaging and cognition using functional near infrared spectroscopy (FNIRS) in multiple sclerosis. *Brain Imaging Behav.* 9, 302–311. doi: 10.1007/s11682-014-9307-y

Wajda, D. A., Motl, R. W., and Sosnoff, J. J. (2013). Dual task cost of walking is related to fall risk in persons with multiple sclerosis. *J. Neurol. Sci.* 335, 160–163. doi: 10.1016/j.jns.2013.09.021

Conflict of Interest Statement: The authors declare that the research was conducted in the absence of any commercial or financial relationships that could be construed as a potential conflict of interest.

Copyright © 2018 Saleh, Sandroff, Vitiello, Owoeye, Hoxha, Hake, Goverover, Wylie, Yue and DeLuca. This is an open-access article distributed under the terms of the Creative Commons Attribution License (CC BY). The use, distribution or reproduction in other forums is permitted, provided the original author(s) and the copyright owner(s) are credited and that the original publication in this journal is cited, in accordance with accepted academic practice. No use, distribution or reproduction is permitted which does not comply with these terms.

frontiers in Human Neuroscience

BRIEF RESEARCH REPORT
published: 12 March 2019
doi: 10.3389/fnhum.2019.00084

Balance Training With a Vibrotactile Biofeedback System Affects the Dynamical Structure of the Center of Pressure Trajectories in Chronic Stroke Patients

Kentaro Kodama[1†], *Kazuhiro Yasuda*[2*†], *Nikita A. Kuznetsov*[3], *Yuki Hayashi*[4] *and Hiroyasu Iwata*[4]

[1] Department of Economics, Kanagawa University, Yokohama, Japan, [2] Research Institute for Science and Engineering, Waseda University, Tokyo, Japan, [3] School of Kinesiology, Louisiana State University, Baton Rouge, LA, United States, [4] Graduate School of Creative Science and Engineering, Waseda University, Tokyo, Japan

Haptic-based vibrotactile biofeedback (BF) is a promising technique to improve rehabilitation of balance in stroke patients. However, the extent to which BF training changes temporal structure of the center of pressure (CoP) trajectories remains unknown. This study aimed to investigate the effect of vibrotactile BF training on the temporal structure of CoP during quiet stance in chronic stroke patients using detrended fluctuation analysis (DFA). Nine chronic stroke patients (age; 81.56 ± 44 months post-stroke) received a balance training regimen using a vibrotactile BF system twice a week over 4 weeks. A Wii Balance board was used to record five 30 s trials of quiet stance pre- and post-training at 50 Hz. DFA revealed presence of two linear scaling regions in CoP indicating presence of fast- and slow-scale fluctuations. Averaged across all trials, fast-scale fluctuations showed persistent dynamics ($\alpha = 1.05 \pm 0.08$ for ML and $\alpha = 0.99 \pm 0.17$ for AP) and slow-scale fluctuations were anti-persistent ($\alpha = 0.35 \pm 0.05$ for ML and $\alpha = 0.32 \pm 0.05$ for AP). The slow-scale dynamics of ML CoP in stroke patients decreased from pre-training to post-BF training ($\alpha = 0.40 \pm 0.13$ vs. 0.31 ± 0.09). These results suggest that the vibrotactile BF training affects postural control strategy used by chronic stroke patients in the ML direction. Results of the DFA are further discussed in the context of balance training using vibrotactile BF and interpreted from the perspective of intermittent control of upright stance.

Keywords: stroke, postural control, haptic biofeedback, balance rehabilitation, detrended fluctuation analysis (DFA)

OPEN ACCESS

Edited by:
Elizabeth B. Torres, Rutgers University, The State University of New Jersey, United States

Reviewed by:
Sonia Julia-Sanchez, Ministerio de Educación Cultura y Deporte, Spain
Luc Berthouze, University of Sussex, United Kingdom

****Correspondence:***
Kazuhiro Yasuda
kazuhiro-yasuda@aoni.waseda.jp

† These authors have contributed equally to this work

Received: *14 June 2018*
Accepted: *18 February 2019*
Published: *12 March 2019*

Citation:
Kodama K, Yasuda K, Kuznetsov NA, Hayashi Y and Iwata H (2019) Balance Training With a Vibrotactile Biofeedback System Affects the Dynamical Structure of the Center of Pressure Trajectories in Chronic Stroke Patients. Front. Hum. Neurosci. 13:84. doi: 10.3389/fnhum.2019.00084

INTRODUCTION

Following a stroke, a complex interplay of sensory, motor, and cognitive impairments may interfere with balance (de Haart et al., 2004). Stroke patients commonly show increased postural sway and asymmetric weight distribution while standing (Mansfield et al., 2013; Hendrickson et al., 2014). Impaired balance decreases mobility and increases fall risk in elderly stroke patients (Lamb et al., 2003). Vibrotactile biofeedback (BF) application to the trunk is a promising method for restoring

balance ability (e.g., Dozza et al., 2007; Bechly et al., 2013). However, we previously found that a 4 week vibrotactile BF training did not induce significant changes on several center of pressure (CoP) measures (i.e., sway area, path length) in chronic stroke patients (Yasuda et al., 2018).

In this report, we apply *detrended fluctuation analysis* (DFA; Peng et al., 1994) to characterize the effects of this BF training in stroke patients. DFA offers an additional perspective on postural control dynamics in comparison to traditional CoP metrics because it examines control processes across multiple time scales (Eke et al., 2002; Seuront, 2009). DFA can evaluate presence of temporal correlations across a range of window sizes (Brown and Liebovitch, 2010). Fractal processes can be categorized in two families: *fractional Gaussian noise* (fGn) and *fractional Brownian motions* (fBm). The scaling exponent, DFA α, is interpreted as an indicator of temporal correlation pattern: If $0 < \alpha < 1$ (fGn) with anti-persistent ($\alpha < 0.5$), random ($\alpha = 0.5$), or persistent dynamics ($\alpha > 0.5$). If $1 < \alpha < 2$ (fBm) with under-diffusive (a < 1.5), Brownian ($\alpha = 1.5$), hyper-diffusive dynamics ($\alpha > 1.5$) (Delignières et al., 2011).

Previous studies have indicated that DFA can identify differences in postural control strategy between young and elderly adults (Amoud et al., 2007; Duarte and Sternad, 2008). Roerdink et al. (2006) applied DFA to CoP data to compare stroke patients with healthy elderly and showed that the CoP trajectories of both the healthy elderly and stroke patients exhibited temporally correlated patterns rather than random noise (Roerdink et al., 2006).

The dynamical structure of CoP during quiet stance is characterized by presence of multiple scaling regions (Minamisawa et al., 2009; Teresa Blázquez et al., 2009; Kuznetsov et al., 2013). Kuznetsov et al. (2013) reported three scaling regions in a sample of healthy young adults. Presence of multiple scaling regions may be indicative of intermittent control strategy (Loram et al., 2011) or continuous open- and closed-loop control strategy (Collins and De Luca, 1995).

The effect of vibrotactile BF on the dynamics across multiple-scales for postural control remains unknown however. Postural control strategy used by stroke patients may differ from the strategies used by younger adults or healthy elderly due to freezing, asymmetrical weight distribution, and sensory input alterations. We hypothesized that intensive balance training using vibrotactile BF would affect the dynamical structure of CoP trajectories in chronic stroke patients.

MATERIALS AND METHODS

Participants

We recruited 9 participants with chronic hemiparetic stroke from the Department of Physical Medicine and Rehabilitation, Tokyo General Hospital (**Table 1**). Inclusion criteria were positive history of chronic unilateral ischemic or hemorrhagic stroke, age 50–80 years, stroke >6 months ago, completion of conventional therapy, and ability to stand unsupported for 10 min and sense BF system vibrations. Prior to the study, all participants underwent conventional balance rehabilitation with a physical therapist twice a week.

BF System Overview

The vibrotactile BF device consisted of a Nintendo Wii balance board (Nintendo Co., Ltd., Kyoto, Japan) and a personal computer with custom software (Visual Studio; Microsoft Corp., Redmond, WA, USA). CoP position data were measured in both the ML and AP directions at 50 Hz. The system uses vibration motors attached to the belt at the level of the pelvic girdle (bilaterally attached at the anterior superior iliac and posterior superior iliac spine) to convey information about body sway (**Figure 1**).

Protocol and Postural Task

Participants underwent 45 min of BF training 2 times per week for 2 weeks. The training consisted of two task-oriented balance training exercises used as part of the conventional rehabilitation (Teasell et al., 2008).

Two balance training exercises were used: (1) standing on a rubber foam mat (balance mat, Sanwa Kako Co. Ltd, Japan): participants stood barefoot on the mat with their eyes open and were instructed to use the BF information to stabilize their postural sway (i.e., they were instructed to stay within the predefined threshold area using BF information) and (2) weight-shifting to the paralyzed limb: participants were instructed to move their paralyzed lower limb forward and then put their weight on that limb. While doing so, participants used the BF information to help maintain a stable standing position. Each training session comprised 10 repetitions of the balance task (1 min per repetition, 10 min total) with a short interval between repetitions. The BF threshold setting was reset on each day of training before implementing tasks (1) and (2). We determined the circular threshold as a 95% confidence circle area (Yasuda et al., 2017) during the 30 s stance. Target area was defined as 90% of the pre-measured 95% confidence circle area. The BF vibrators were activated when the CoP exceeded this threshold (Yasuda et al., 2017).

Analysis

Traditionally, DFA requires integration of the signal if it is similar to an fGn process. COP variability is non-stationary and is therefore not like an fGn—a stationary process. Hence, COP fluctuations are already more similar to fBm and do not require integration prior to DFA. The range of scales considered ranged from 0.12 s to 10.86 s. The evaluated scales were generated as $Scale = 2^w/F_s$, where $F_s = 50$ Hz and w ranged from $\log_2$(6 samples) to $\log_2$(750 samples) in increments of 0.5 on $\log_2$ scale (e.g., $w = 2.585, 3.085, 3.585, \ldots, 9.085$) for a total of 14 scales in the range (F_s: sampling frequency). Using these scales allowed us to have equal logarithmic distance between the windows on the DFA plot (see **Figure 2** for an illustration).

CoP was filtered using the Savitzky-Golay filter (order 3, length 7) to minimize distortions associated with linear filtering techniques (Gao et al., 2011). A linearity test was performed comparing fit of multiple models to the DFA plots (Ton and Daffertshofer, 2015). The results showed that a linear model with a single scaling exponent was not a good fit for our data. However, automated fits suggested a range of models: quadratic, cubic, exponential, and 2- and 3-region linear models in different individual trials.

TABLE 1 | Participants' demographic data ($n = 9$).

Participant	Gender	Age	Type of stroke	Time since stroke	Hemiplegic side	Brs (L/E)	Superficial sensation (L/E)
1	M	75–80	Infarcted	2 years 1 month	L	V	Mild
2	F	75–80	Infarcted	10 years 7 months	R	IV	Mild
3	M	55–60	Hemorrhagic	4 years	R	V	Moderate
4	M	55–60	Hemorrhagic	4 years 8 months	L	IV	Mild
5	M	50–55	Hemorrhagic	8 years	R	IV	Mild
6	M	75–80	Infarcted	7 years	L	IV	Moderate
7	M	55–60	Hemorrhagic	8 years 5 months	R	IV	Moderate
8	F	65–70	Hemorrhagic	13 years 5 months	R	III	Severe
9	M	65–70	Infarcted	3 years	L	V	Mild

Brs, Brunnstrom recovery stage; L/E, lower extremity; M, male; F, female.

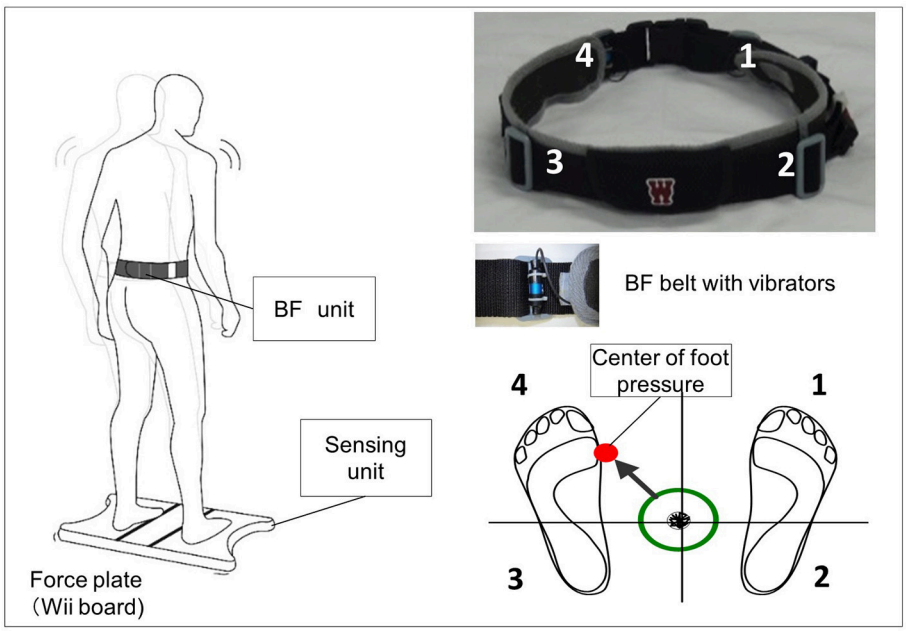

FIGURE 1 | Biofeedback system overview. Vibrators on the pelvic belts worn by the participants vibrated in the corresponding direction when the center of pressure (CoP) exceeded the predefined threshold (e.g., if CoP shifts to the back left, the back left vibrator is activated).

Based on preliminary visual inspection of all DFA plots of all COP recordings, we made the assumption that the multi-scale dynamics could be adequately characterized using a two-region linear model. We chose to fit a linear (vs. polynomial or exponential) model because it allows to interpret DFA slopes based on the fBm/fGn model (persistent, anti-persistent, random). We chose a 2-region (vs. 3-region) model because previous work has identified 2 scaling regions in COP (Collins and De Luca, 1995 and Kuznetsov et al., 2013; see their results when downsampled to 50 Hz).

We identified the cross-over point between the two regions based on visual inspection of each DFA plot. For the AP signals Region 1 ranged from 0.12 s to 1.37 s (fast-scale fluctuations) and Region 2 ranged from 1.37 to 10.86 s (slow-scale fluctuations). For the ML signals region 1 ranged from 0.12 s to 1.79 s and Region 2 is ranged from 1.79 to 10.86 s.

Scaling exponents were calculated for each region and a paired *t*-test was used to compare pre- and post-BF training in the ML and in the AP directions.

RESULTS

To examine whether vibrotactile BF training affect the CoP dynamics in chronic stroke patients, the DFA was applied to CoP trajectories data in the ML and AP directions. **Figure 2** shows a representative DFA plots in a single trial. **Table 2** presents the average DFA scaling exponents for each participant. **Figure 3** shows the mean and standard error of the DFA scaling exponents for fast and slow-scales in the ML and AP directions.

ML COP: There was no significant difference between the DFA scaling exponents in the pre- and post-training in Region 1 ($p = 0.56$), while the scaling exponent was lower post-training (α

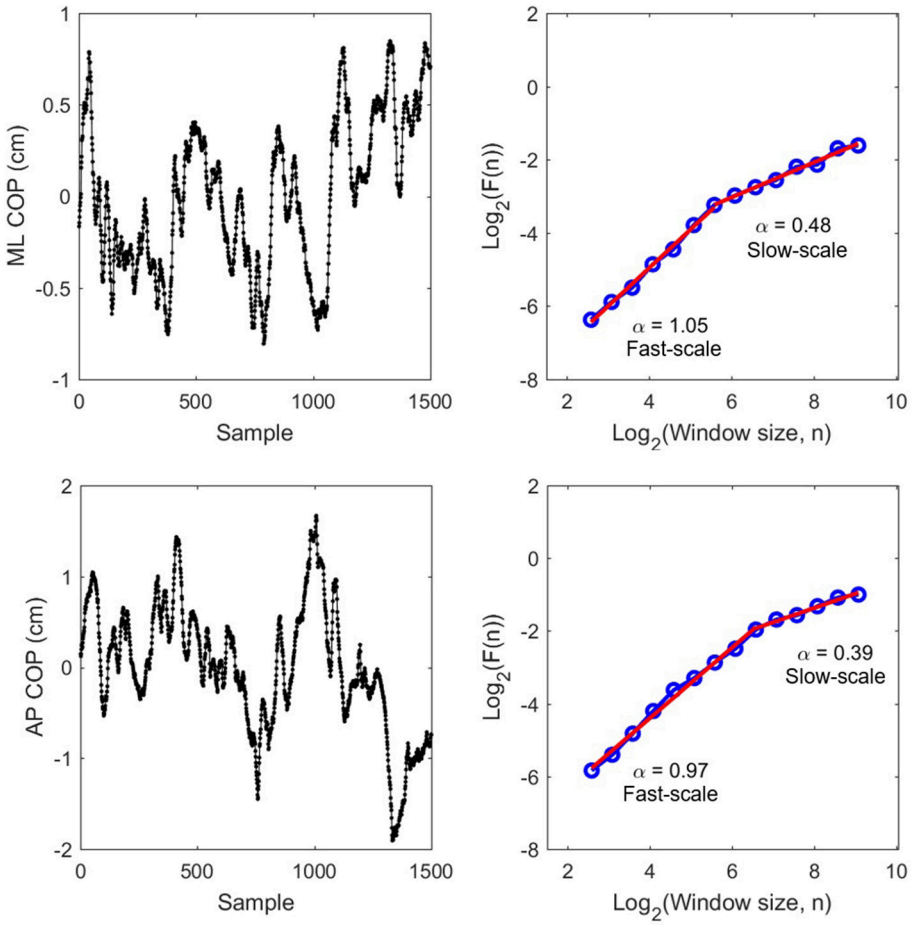

FIGURE 2 | Raw COP data **(Left)** for ML and AP and their corresponding DFA plots **(Right)** from P8 pre-test trial 2. Red slopes indicate estimated scaling exponents α for fast-scale and slow-scale fluctuations.

$= 0.31 \pm 0.09$) compared to pre-training ($\alpha = 0.40 \pm 0.13$) in Region 2, $t_{(8)} = 3.06$, $p = 0.015$ (see **Figure 3**).

AP COP: There were no significant differences between pre- and post-training in both Region 1 and 2 ($p = 0.62$ and $p = 0.75$, respectively).

DISCUSSION

To the best of our knowledge, this is the first study to describe changes in the dynamical structure of CoP trajectories resulting from vibrotactile feedback training. Our results showed that CoP variability during quiet stance is characterized by two linear scaling regions in chronic stroke patients. The first scaling region captures relatively fast-scale CoP dynamics that range from 0.12 to 1.37 s for AP CoP and from 0.12 to 1.79 s for ML CoP. The second region captures relatively slow-scale dynamics ranging from 1.37 to 10.86 s for AP and from 1.79 to 10.86 s for ML. DFA scaling exponents indicate that the fast-scale region is characterized by persistent CoP fluctuations, while the slow-scale region is characterized by anti-persistent CoP fluctuations.

Such dynamics can be interpreted from the perspective of intermittent control (Loram et al., 2011), where the position of the center of gravity is allowed to drift with only intermittent corrections as long as it remains within the boundaries of the base of support (BOS). This kind of control strategy would account for the observation of persistent fluctuations at the fast time scales (drifting toward the boundary) and anti-persistent fluctuations at slow scales (intermittent correction away from the boundary). This is also consistent with the rambling-trembling hypothesis of postural control (Zatsiorsky and Duarte, 2000). According to this hypothesis, CNS controls upright posture using two hierarchical levels: a reference position for maintaining equilibrium is specified at one level, and the lower level maintains balance around that reference position by negating deviations ("trembling") from it. The set point for equilibrium migrates ("rambles") during quiet stance. The fast-scale persistent region in our results may be capturing the trembling component while the anti-persistent slow-scale region may be indexing changes in the rambling dynamics.

Taken from this perspective, our results indicate that the BF training induced a change in the error correction strategy in ML CoP because the slow-scale scaling exponent suggested stronger anti-persistent dynamics in post-training compared to pre-training. We interpret reduction as tighter control over body

TABLE 2 | DFA scaling exponent α for two scaling regions.

	ML				AP			
	Region 1		Region 2		Region 1		Region 2	
Participant	Pre	Post	Pre	Post	Pre	Post	Pre	Post
1	1.10	1.10	0.57	0.40	1.06	0.99	0.40	0.24
2	1.22	1.19	0.25	0.21	0.96	1.07	0.17	0.29
3	1.01	1.09	0.36	0.35	1.23	1.01	0.38	0.29
4	1.04	0.94	0.58	0.36	0.79	0.77	0.40	0.36
5	1.07	1.11	0.48	0.30	1.11	1.04	0.50	0.31
6	0.96	1.05	0.35	0.33	0.86	1.00	0.31	0.28
7	0.99	1.02	0.23	0.18	1.35	1.27	0.34	0.45
8	1.01	0.91	0.31	0.25	0.96	0.84	0.31	0.29
9	1.00	1.14	0.43	0.43	0.76	0.90	0.18	0.36
Mean	1.04	1.06	0.40	0.31	1.01	0.99	0.33	0.32
SD	0.08	0.09	0.13	0.09	0.20	0.14	0.11	0.06

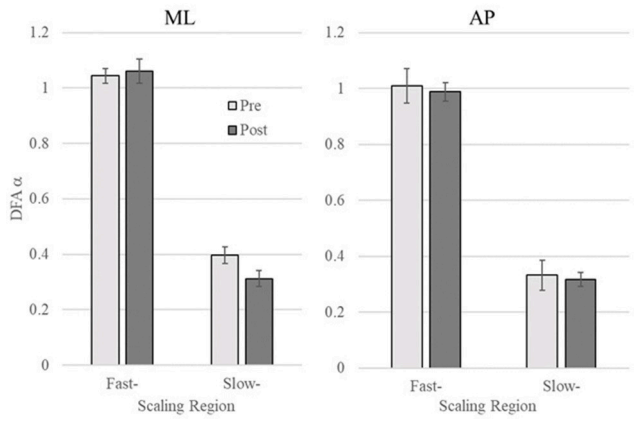

FIGURE 3 | DFA scaling exponent of pre- and post-training in the mediolateral (ML) and anteroposterior (AP) directions **(Left** and **Right**, respectively). Error bars indicate standard error of the mean.

sway as it gets closer to the BOS limits. For stroke patients it is often difficult to maintain postural balance, particularly in the ML direction because of hemiplegia. This can cause asymmetric balancing referred to as the weight-bearing asymmetry (WBA), destabilizing coordination between the left and right limbs, and large variations in CoP. During quiet stance, a substantial amount of WBA in favor of the non-paretic leg is commonly observed. Therefore, we speculate that intensive balance exercise might show stronger effects particularly in the ML direction rather than that in the AP direction.

Roerdink et al. (2006) reported that the scaling exponent was not affected by standard rehabilitation. In contrast, our results suggest that the BF training can affect the scaling exponent in slow-scale region of the CoP trajectories of stroke patients in the ML direction. These results may suggest that the BF training has a potential to lead the change in the CoP dynamics beyond that of typical rehabilitation.

We previously found that 4 week vibrotactile BF training did not induce significant changes in traditional CoP measures (i.e., sway area, mean velocity) in chronic stroke patients (Yasuda et al., 2018). Thus, it is possible that vibrotactile BF may affect only the temporal structure of CoP trajectories. This possibility is worth considering in clinical settings because it is important to evaluate the effect of BF devices on the CoP dynamics. Although the underlying mechanism remains unclear, we speculated that intensive subtle coordination of the CoP within the BF circular threshold may influence the CoP dynamics. Further experimental studies (e.g., comparison of the different sizes of the threshold area) are warranted to specifically describe the expected effect of the BF system.

Although these results should be interpreted cautiously, the present report has important implications because the results describe the specific influence of BF devices by applying dynamical methods (e.g., DFA). Importantly, persistent dynamics in the fast scaling region do not signify presence of long-range correlations in these data—a much longer durations of trials are required to establish long-range correlations (Duarte and Zatsiorsky, 2001). One limitation of the study is the lack of a control group. However, the internal validity was strengthened by excluding participants who had experienced a stroke <6 months before the study. Therefore, the results may have been biased by the learning effects. Further studies should be assessed with more rigorous methodology or randomized study designs.

ETHICS STATEMENT

All participants provided informed consent. All procedures were approved by the Ethics Committee for Human Research, Waseda University.

AUTHOR CONTRIBUTIONS

KY designed this study, acquired and analyzed the data, and drafted the manuscript. KK and NK substantially contributed to data analysis and manuscript drafting. YH contributed to data acquisition and analysis. HI helped conceive the BF system and design the study. All authors have read and approved the final manuscript. No one who qualifies for authorship has been omitted from the list.

FUNDING

This study was supported by the Japan Society for the Promotion of Science (JSPS), Grant-in-Aid for Scientific Research (C) No. 17K01875, Grant-in-Aid for Junior Researchers, Research Institute for Science and Engineering, Waseda University, and the Global Robot Academia Institute, Waseda University [FY2018].

ACKNOWLEDGMENTS

We thank the staff of the Tokyo General Hospital for assisting in participant recruitment and screening. We would also like to thank Zenyu Ogawa for his support in designing the hardware.

REFERENCES

Amoud, H., Abadi, M., Hewson, D. J., Michel-Pellegrino, V., Doussot, M., and Duchêne, J. (2007). Fractal time series analysis of postural stability in elderly and control subjects. *J. Neuroeng. Rehabil.* 4:12. doi: 10.1186/1743-0003-4-12

Bechly, K. E., Carender, W. J., Myles, J. D., and Sienko, K. H. (2013). Determining the preferred modality for real-time biofeedback during balance training. *Gait Posture* 37, 391–396. doi: 10.1016/j.gaitpost.2012.08.007

Brown, C. T., and Liebovitch, L. S. (2010). *Fractal Analysis*. London: SAGE Publications. Available online: https://uk.sagepub.com/en-gb/asi/fractal-analysis/book233383

Collins, J. J., and De Luca, C. J. (1995). The effects of visual input on open-loop and closed-loop postural control mechanisms. *Exp. Brain Res.* 103, 151–163. doi: 10.1007/BF00241972

de Haart, M., Geurts, A. C., Huidekoper, S. C., Fasotti, L., and van Limbeek, J. (2004). Recovery of standing balance in postacute stroke patients: a rehabilitation cohort study11No commercial party having a direct financial interest in the results of the research supporting this article has or will confer a benefit upon the authors(s) or upon any organization with which the author(s) is/are associated. *Arch. Phys. Med. Rehabil.* 85, 886–895. doi: 10.1016/j.apmr.2003.05.012

Delignières, D., Torre, K., and Bernard, P.-L. (2011). Transition from persistent to anti-persistent correlations in postural sway indicates velocity-based control. *PLoS Comput. Biol.* 7:e1001089. doi: 10.1371/journal.pcbi.1001089

Dozza, M., Wall, C., Peterka, R. J., Chiari, L., Horak, F. B., and Horak, F. B. (2007). Effects of practicing tandem gait with and without vibrotactile biofeedback in subjects with unilateral vestibular loss. *J. Vestib. Res.* 17, 195–204.

Duarte, M., and Sternad, D. (2008). Complexity of human postural control in young and older adults during prolonged standing. *Exp. Brain Res.* 191, 265–276. doi: 10.1007/s00221-008-1521-7

Duarte, M., and Zatsiorsky, V. M. (2001). Long-range correlations in human standing. *Phys. Lett. A* 283, 124–128. doi: 10.1016/S0375-9601(01)00188-8

Eke, A., Herman, P., Kocsis, L., and Kozak, L. R. (2002). Fractal characterization of complexity in temporal physiological signals. *Physiol. Meas.* 23, R1–R38. doi: 10.1088/0967-3334/23/1/201

Gao, J., Hu, J., and Tung, W. (2011). Facilitating joint chaos and fractal analysis of biosignals through nonlinear adaptive filtering. *PLoS ONE* 6:e24331. doi: 10.1115/DSCC2011-6083

Hendrickson, J., Patterson, K. K., Inness, E. L., McIlroy, W. E., and Mansfield, A. (2014). Relationship between asymmetry of quiet standing balance control and walking post-stroke. *Gait Posture* 39, 177–181. doi: 10.1016/j.gaitpost.2013.06.022

Kuznetsov, N. A., Bonnette, S., Gao, J., and Riley, M. A. (2013). Adaptive fractal analysis reveals limits to fractal scaling in center of pressure trajectories. *Ann. Biomed. Eng.* 41, 1646–1660. doi: 10.1007/s10439-012-0646-9

Lamb, S. E., Ferrucci, L., Volapto, S., Fried, L. P., and Guralnik, J. M. (2003). Risk factors for falling in home-dwelling older women with stroke. *Stroke* 34, 494–501. doi: 10.1161/01.STR.0000053444.00582.B7

Loram, I. D., Gollee, H., Lakie, M., and Gawthrop, P. J. (2011). Human control of an inverted pendulum: is continuous control necessary? Is intermittent control effective? Is intermittent control physiological? *J. Physiol.* 589, 307–324. doi: 10.1113/jphysiol.2010.194712

Mansfield, A., Danells, C. J., Zettel, J. L., Black, S. E., and McIlroy, W. E. (2013). Determinants and consequences for standing balance of spontaneous weight-bearing on the paretic side among individuals with chronic stroke. *Gait Posture* 38, 428–432. doi: 10.1016/j.gaitpost.2013.01.005

Minamisawa, T., Takakura, K., and Yamaguchi, T. (2009). Detrended fluctuation analysis of temporal variation of the Center of Pressure (COP) during quiet standing in Parkinsonian patients. *J. Phys. Ther. Sci.* 21, 287–292. doi: 10.1589/jpts.21.287

Peng, C. K., Buldyrev, S. V., Havlin, S., Simons, M., Stanley, H. E., and Goldberger, A. L. (1994). Mosaic organization of DNA nucleotides. *Phys. Rev. E* 49, 1685–1689.

Roerdink, M., De Haart, M., Daffertshofer, A., Donker, S. F., Geurts, A. C. H., and Beek, P. J. (2006). Dynamical structure of center-of-pressure trajectories in patients recovering from stroke. *Exp. Brain Res.* 174, 256–269. doi: 10.1007/s00221-006-0441-7

Seuront, L. (2009). *Fractals and Multifractals in Ecology and Aquatic Science*. Boca Raton, FL: CRC Press.

Teasell, R. W., Foley, N. C., Salter, K. L., and Jutai, J. W. (2008). A blueprint for transforming stroke rehabilitation care in canada: the case for change. *Arch. Phys. Med. Rehabil.* 89, 575–578. doi: 10.1016/j.apmr.2007.08.164

Teresa Blázquez, M., Anguiano, M., de Saavedra, F. A., Lallena, A. M., and Carpena, P. (2009). Study of the human postural control system during quiet standing using detrended fluctuation analysis. *Phys. A Stat. Mech. Appl.* 388, 1857–1866. doi: 10.1016/j.physa.2009.01.001

Ton, R., and Daffertshofer, A. (2015). Model selection for identifying power-law scaling. *Neuroimage* 136, 215–226. doi: 10.1016/j.neuroimage.2016.01.008

Yasuda, K., Kaibuki, N., Harashima, H., and Iwata, H. (2017). The effect of a haptic biofeedback system on postural control in patients with stroke: an experimental pilot study. *Somatosens. Motor Res.* 34, 65–71. doi: 10.1080/08990220.2017.1292236

Yasuda, K., Saichi, K., Kaibuki, N., Harashima, H., and Iwata, H. (2018). Haptic-based perception-empathy biofeedback system for balance rehabilitation in patients with chronic stroke: concepts and initial feasibility study. *Gait Posture* 62, 484–489. doi: 10.1016/j.gaitpost.2018.04.013

Zatsiorsky, V. M., and Duarte, M. (2000). Rambling and trembling in quiet standing. *Motor Control* 4, 185–200. doi: 10.1123/mcj.4.2.185

Conflict of Interest Statement: The authors declare that the research was conducted in the absence of any commercial or financial relationships that could be construed as a potential conflict of interest.

Copyright © 2019 Kodama, Yasuda, Kuznetsov, Hayashi and Iwata. This is an open-access article distributed under the terms of the Creative Commons Attribution License (CC BY). The use, distribution or reproduction in other forums is permitted, provided the original author(s) and the copyright owner(s) are credited and that the original publication in this journal is cited, in accordance with accepted academic practice. No use, distribution or reproduction is permitted which does not comply with these terms.

APPENDIX

Brunnstrom stages of stroke recovery.

Lower extremity function:

Stage I: Flaccidity.

Stage II: Minimal voluntary movements.

Stage III: Hip flexion, knee flexion, and ankle dorsiflexion performed as a combined motion while sitting and standing.

Stage IV: While sitting: knee flexion beyond 90°; ankle dorsiflexion with the heel on the floor.

Stage V: While standing: isolated knee flexion with hip extended; isolated ankle dorsiflexion with knee extended.

frontiers in Integrative Neuroscience

REVIEW
published: 22 May 2019
doi: 10.3389/fnint.2019.00016

Putting the "Sensory" Into Sensorimotor Control: The Role of Sensorimotor Integration in Goal-Directed Hand Movements After Stroke

Lauren L. Edwards[1†], Erin M. King[1†], Cathrin M. Buetefisch[2,3,4] and Michael R. Borich[2]*

[1]Neuroscience Graduate Program, Graduate Division of Biological and Biomedical Sciences, Emory University, Atlanta, GA, United States, [2]Department of Rehabilitation Medicine, Laney Graduate School, Emory University, Atlanta, GA, United States, [3]Department of Neurology, Emory University, Atlanta, GA, United States, [4]Department of Radiology and Imaging Sciences, School of Medicine, Emory University, Atlanta, GA, United States

Integration of sensory and motor information is one-step, among others, that underlies the successful production of goal-directed hand movements necessary for interacting with our environment. Disruption of sensorimotor integration is prevalent in many neurologic disorders, including stroke. In most stroke survivors, persistent paresis of the hand reduces function and overall quality of life. Current rehabilitative methods are based on neuroplastic principles to promote motor learning that focuses on regaining motor function lost due to paresis, but the sensory contributions to motor control and learning are often overlooked and currently understudied. There is a need to evaluate and understand the contribution of both sensory and motor function in the rehabilitation of skilled hand movements after stroke. Here, we will highlight the importance of integration of sensory and motor information to produce skilled hand movements in healthy individuals and individuals after stroke. We will then discuss how compromised sensorimotor integration influences relearning of skilled hand movements after stroke. Finally, we will propose an approach to target sensorimotor integration through manipulation of sensory input and motor output that may have therapeutic implications.

Keywords: sensorimotor integration, motor learning, motor control, stroke, sensation

OPEN ACCESS

Edited by:
Elizabeth B. Torres, Rutgers University, The State University of New Jersey, United States

Reviewed by:
Limor Avivi-Arber, University of Toronto, Canada
Barry Sessle, University of Toronto, Canada

***Correspondence:**
Michael R. Borich
michael.borich@emory.edu

†These authors have contributed equally to this work

Received: *28 January 2019*
Accepted: *03 May 2019*
Published: *22 May 2019*

Citation:
Edwards LL, King EM, Buetefisch CM and Borich MR (2019) Putting the "Sensory" Into Sensorimotor Control: The Role of Sensorimotor Integration in Goal-Directed Hand Movements After Stroke. Front. Integr. Neurosci. 13:16. doi: 10.3389/fnint.2019.00016

INTRODUCTION

Goal-directed movements of the hand are required to perform most tasks of daily living, such as tying a shoe, buttoning a shirt, and typing, among others. These highly coordinated voluntary movements involve interacting with and manipulating objects in the environment and rely on sensorimotor integration. Sensorimotor integration is the ability to incorporate sensory inputs that provide information about one's body and the external environment to inform and shape motor output (Wolpert et al., 1998). More specifically, sensory inputs for goal-directed hand movements provide information in an egocentric reference frame detailing location, size, weight, and shape of an object. In addition, kinematic information

about the hand and upper extremity, including the trajectory needed to interact with the object, is provided. Successful integration of information contributes to generating the most efficient motor plan to execute a given task. Additionally, ongoing sensory feedback during motor performance refines the motor plan to optimize current and future performance. This process of sensorimotor integration is often disrupted in neurological disorders, such as stroke.

Stroke is defined as infarction of central nervous system tissue attributable to ischemia, based on neuropathological, neuroimaging, and/or clinical evidence of permanent injury (Sacco et al., 2013). Stroke is the fourth leading cause of death and remains the number one leading cause of long-term adult disability (Benjamin et al., 2017). Furthermore, the loss of productivity after stroke currently costs the United States an average of $33.9 billion per year and is expected to reach $56 billion by 2030 (Ovbiagele et al., 2013), making stroke a public health crisis. A primary contributor to persistent disability after stroke is incomplete motor recovery (Lai et al., 2002). Spontaneous biological recovery of motor function occurs during the first months after stroke (Cramer, 2008), underlying a current emphasis on intensive early intervention, although results are often mixed and complex (Bernhardt et al., 2017a). Despite intensive therapy, upper extremity impairment resolves up to 70% of baseline function for a given patient with some patients showing even less recovery than predicted (Winters et al., 2015). Most stroke survivors are left with a limited ability to perform skilled hand movements necessary for daily functioning (Lang et al., 2013). To reduce disability after stroke, there is a need to improve our understanding of the neuronal network physiology necessary to regain skilled functional hand use.

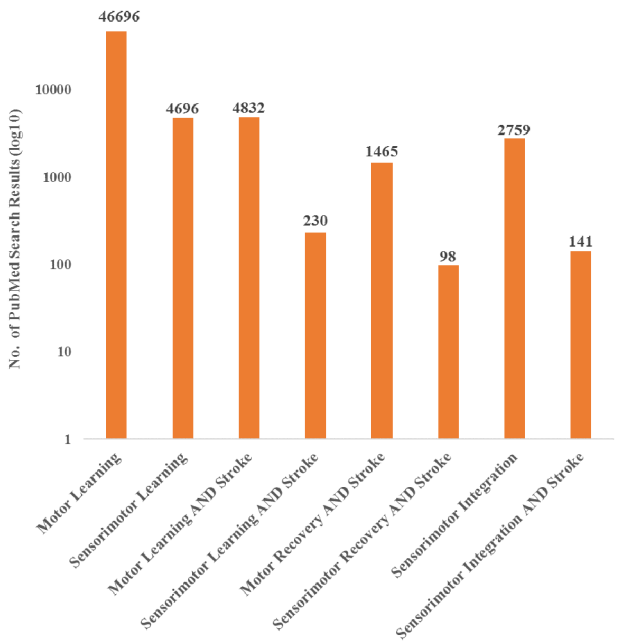

FIGURE 1 | PubMed search results for both motor and sensorimotor aspects of learning and stroke recovery. More publications focused on motor learning and recovery than on both motor and sensory components of learning and recovery. Furthermore, there were a relatively small number of publications involving sensorimotor integration and stroke compared to sensorimotor integration overall. "Sensorimotor," "Sensori-motor," and "Sensory motor" were all used to ensure differences in terminology did not affect the search results. Additionally, "Sensory motor" and "Sensory-motor" produced the same search results.

Currently, the field has primarily investigated motor deficits and motor learning with limited consideration of the role of sensory information, even though it is recognized that integration of sensory information is a critical component of motor control (Borich et al., 2015; Bolognini et al., 2016). Furthermore, evidence has shown that sensory input is important for recovery after stroke. In a systematic review, Meyer et al. found that across six studies, the extent of deficits in proprioception and light touch of the arm and hand were significantly related to recovery after stroke (Meyer et al., 2014). Despite evidence that sensory input is a critical component to motor execution, research nomenclature has been primarily focused on motor characteristics post-stroke and has therefore not capitalized fully on the information a sensorimotor perspective could provide. This observation is supported by a literature search showing an emphasis towards motor recovery and learning after stroke, over sensorimotor recovery and learning, with limited focus on sensorimotor integration (**Figure 1**). While it is possible that authors may use these terms interchangeably, the literature search terminology suggests that there is potential bias towards motor contributions. Therefore, there is an important gap in our understanding of the contributions of sensorimotor integration to recovery.

In the following brief review, we will highlight the importance of processing and integrating sensory and motor information that underlies skill performance and learning with an emphasis on skilled hand movements in stroke. We will focus primarily on three cortical regions: primary motor cortex (M1), posterior parietal cortex (PPC) and primary somatosensory cortex (S1) while briefly mentioning other cortical and subcortical brain areas also involved in sensorimotor integration. These brain regions are highlighted due to our focus on the integration of sensory and motor information at the level of the cortex, but also because these cortical areas receive blood supply from the middle cerebral artery (MCA), which is the most common type of stroke (Walcott et al., 2014). Furthermore, all three brain regions contribute to the corticospinal tract (CST) that provide necessary contributions to executing and controlling skilled hand movements routinely used in daily life. It should be noted that strokes occur in other brain regions but usually have less of an impact on sensorimotor integration underlying goal-directed, skilled hand movements and are outside the primary scope of this review article.

In the first section of this review article, we will discuss the role of sensorimotor integration *via* M1, PPC, and S1 in normal, skilled hand movements. We will then discuss how sensorimotor integration is affected by stroke and how impaired sensorimotor integration can impact relearning of skilled hand movements. Last, we propose an approach to target sensorimotor integration

by manipulating sensory input and restricting motor output that may have therapeutic implications for stroke recovery.

THE ROLE OF M1 IN GOAL-DIRECTED HAND MOVEMENTS

M1 Involvement in Movement Execution

The M1 has a critical role in the execution of voluntary movements. Upper extremity movement execution is particularly dependent on descending output from M1 through the spinal cord to upper limb muscles. Pyramidal neurons in layer 5 have axons that are bundled together as a significant portion of the CST, where 85%–90% of the fibers decussate in the pyramids to provide control to the hand contralateral to the hemisphere of the M1 (Rosenzweig et al., 2009). The remaining fibers, approximately 10%–15%, maintain ipsilateral projections that have a minor role in distal extremity motor control (Zaaimi et al., 2012). Of the neurons terminating in the spinal cord, some neurons will indirectly influence movements by synapsing onto interneurons in the intermediate zone (Rathelot and Strick, 2009) whereas direct control arises from the cortico-motoneuronal (CM) cells that terminate monosynaptically on α-motoneurons in the ventral horn of the spinal cord (Lemon et al., 1986). These α-motoneurons innervate skeletal muscle to control contralateral muscle contractions, and subsequently, voluntary movements (Rathelot and Strick, 2009; Schieber, 2011). The most abundant projections from M1 are to motor neurons that innervate hand muscles allowing for direct and individualized control of fingers required for complex and skilled hand movements (Dum and Strick, 1996). A lesion to these CST axonal fibers is the leading cause of motor disability and specifically causes loss in individualized finger function (Lawrence and Kuypers, 1968; Lemon, 2008), reiterating the importance of this connection from M1 to the α-motoneurons innervating muscles of the hand. While CST is the largest contributor to skilled hand movement, there are other pathways, such as the reticulospinal tract, that offer additional contributions to certain aspects of hand function (for review, see Baker, 2011). The topographical organization of M1 demonstrates a larger spatial representation for the hand reflecting the relative importance of the output from CM cells to the hand (Penfield and Boldrey, 1937). The populations of CM cells in M1 fire differentially to allow for a variety of functional uses of the hand (Griffin et al., 2015). Within these populations, individual neurons can be tuned to preferentially code for single or multiple fingers or more proximal joints (Kirsch et al., 2014), and the kinematics of a movement, such as direction, force, and speed are also encoded (Georgopoulos et al., 1982, 1992; Mahan and Georgopoulos, 2013). This level of specification in M1 neuronal tuning allows for the execution of an extensive repertoire of complex hand movements.

As mentioned previously, the execution of skilled hand movements by M1 requires sensory information. Representations of the external environment must be generated from visual, proprioceptive, and tactile input (Makino et al., 2016), and these representations are combined with internal representations of the motor system, such as hand position, to create an internal model (Blakemore et al., 1998). Both external and internal representations have inherent variability that can be reduced by incorporating input from multiple sensory modalities (Körding and Wolpert, 2004).

Successful multisensory integration contributes to execution of a motor command that results in the desired movement outcome. For instance, if the goal is to button a shirt, the internal model should include the position of the button and buttonhole and starting position of the hand. These positions are determined by visual, proprioceptive, and tactile information that will be processed through PPC [visual (Kaas et al., 2011)] and S1 [proprioceptive, tactile (Kim et al., 2015), and nociceptive (Liang et al., 2011)], Sensory information associated with manipulation of the button will also be provided. The relevant sensory information is then relayed to M1, where a motor command is generated. This internal model will also be influenced by prior motor execution that contributes to development of an efference copy of the motor output (von Holst and Mittelstaedt, 1950). Using this information, an internal model includes predictions about expected sensory feedback resulting from the generated movement (Flanagan et al., 2006). In this example, if the button is not at the correct angle required for it to go through the button hole, or if the hand is in the incorrect starting position, the sensory reafferent information occurring in response to movement will not align with the predicted feedback generated from the efference copy (von Holst and Mittelstaedt, 1950). Therefore, the predicted sensory consequence will be updated, the model adapted, and subsequently, the error will be corrected by adjusting the motor command (Shadmehr et al., 2010).

There are several brain regions involved in sensorimotor integration for goal-directed hand movements (**Figure 2**). Non-cortical structures contributing to sensorimotor integration include the: basal ganglia (Nagy et al., 2006), cerebellum (Proville et al., 2014), and thalamus (Mo and Sherman, 2019). In rodents and primates, it has been shown that distinct subdivisions of the thalamus receive input from the basal ganglia and cerebellar nuclei and project to M1 (Bosch-Bouju et al., 2013; Bopp et al., 2017). The ventroanterior and ventromedial nuclei receive information from the basal ganglia, typically through GABAergic projections. The ventrolateral nucleus receives glutamatergic projections from cerebellar nuclei. In addition to these motor thalamic regions, there has been evidence from rodent models to suggest that sensory thalamic regions, such as the posterior medial nucleus, project directly to M1 (Ohno et al., 2012; Hooks et al., 2013, 2015). However, it is unclear whether these specific pathways are present in humans and non-human primates.

Here, our main focus is on sensory signals from PPC and S1 that convey pertinent information about somatosensation, proprioception, and visuomotor transformations to M1. The ability to transform visual and proprioceptive information about the location and space of the internal and external world is important to inform motor commands (Burnod et al., 1992). M1 neurons fire in response to both visual and proprioceptive stimuli (for review, see Hatsopoulos and Suminski, 2011). The M1 hand area is separated into caudal (M1c) and rostral (M1r) subregions: CM cells primarily arise from M1c and

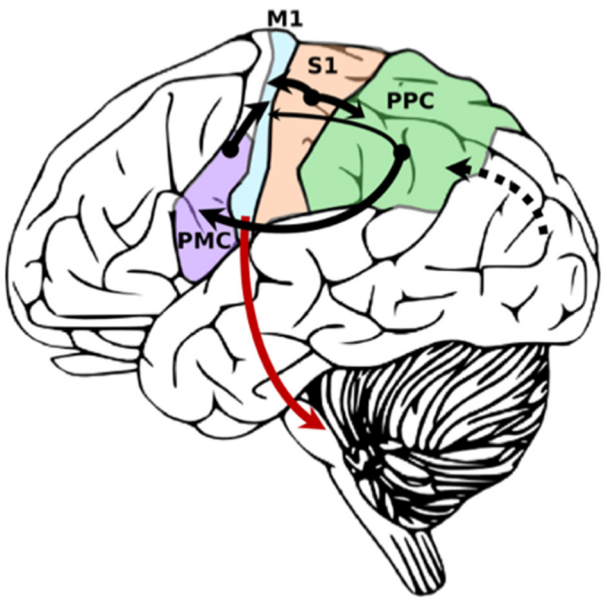

FIGURE 2 | Simplified diagram demonstrating primary sensory inputs to primary motor cortex. Cortico-cortical connections are black. Cortico-fugal projections from M1 are red. Width of arrow denotes strength of connection. Dotted line denotes primary visual input from visual cortex into posterior parietal cortex (PPC) for multimodal integration.

provide direct control of movements of the hand and distal forearm, whereas neurons in M1r influence motor control indirectly using interneurons in the spinal cord (Rathelot and Strick, 2009). Recent work suggests that this rostral and caudal subdivision of the M1 hand area also exists in humans and maintains differences in function (Viganò et al., 2019). S1 has strong reciprocal connections with M1c, whereas PPC has comparatively weaker connections to M1r (Stepniewska et al., 1993). Lesions made independently to M1c and M1r in adult squirrel monkeys produced different deficits, where M1c lesions resulted in cutaneous sensory deficits, and M1r lesions produced errors in aiming of the hand (Friel et al., 2005). These results are not only consistent with the sensory inputs that are expected to arise from PPC and S1 but show the importance of sensorimotor integration such that different regions of M1 specialize in integrating the unique sensory information provided by PPC and S1. Furthermore, proprioceptive and visual inputs to input to M1 will be weighted differently depending on the goal of the task (Sober and Sabes, 2003) further attesting to the dynamic nature of sensorimotor integration in M1.

M1 Plasticity and Sensorimotor Learning

In addition to the role of M1 in the production of movement, M1 also undergoes substantial plasticity, which has a critical role for learning skilled movements. Here, we define "motor learning" as an improvement in motor skill beyond baseline performance leading to a reduction in performance error that is retained over time (Shmuelof et al., 2012). Given that an error signal is inherently tied to sensory feedback and therefore needed for the learning of motor skills guided by sensory information (for review, see Seidler et al., 2013), we refer to motor learning as sensorimotor learning. Sensorimotor learning has been shown to induce functional and structural changes in M1 in rodents (Kleim et al., 1998) and non-human primates (Nudo et al., 1996a). In rodents, compared to practicing an unskilled lever-pressing task, practicing a skilled task that required specific paw manipulations to retrieve food pellets resulted in larger changes in M1 motor map representation of the forelimb, demonstrating that sensorimotor learning induces M1 plasticity (Kleim et al., 1998). M1 plasticity is defined as lasting changes in the morphological and/or functional properties of M1 (Sanes and Donoghue, 2000); experience-dependent plasticity is when these changes occur in response to life experiences, such as stroke (Kleim and Jones, 2008). In the rodent M1, plasticity underlying sensorimotor learning occurs through mechanisms of synaptic long-term potentiation (LTP) and long-term depression (LTD; Rioult-Pedotti et al., 2000). Similar to these results from rodent studies, the involvement of an LTP-like mechanism has been also demonstrated in plastic changes of M1 when adult humans practice ballistic thumb movements (Bütefisch et al., 2000). Importantly, in non-human primates, changes in M1 motor map representation of the distal forelimb were specific to skilled motor learning, whereas performing repetitive unskilled movements alone was not sufficient to induce changes in motor representations (Plautz et al., 2000). Additionally, disrupting M1 activity in humans with transcranial magnetic stimulation (TMS) immediately after motor practice can disrupt memory consolidation for that skill (Muellbacher et al., 2002b; Robertson, 2004) resulting in reduced learning, indicating the importance of M1 in the early consolidation of motor learning. The role of M1 plasticity in sensorimotor learning has also been demonstrated in the orofacial representations in humans (Arima et al., 2011) and nonhuman primates (Arce-McShane et al., 2014).

LTP in M1 is considered a primary synaptic process involved in the experience-dependent plasticity that underlies sensorimotor learning (Kleim et al., 1998; Bütefisch et al., 2000; Sanes and Donoghue, 2000; Ziemann et al., 2004; Nudo, 2013). At the synaptic level, a bidirectional range of dynamic modifiability exists, such that a synapse experiences a limited amount of synaptic strengthening (LTP) or reduction in strength (LTD; Rioult-Pedotti et al., 2000). The ability of a synapse to maintain a target range of modifiability to prevent over- or under-excitation of the neural circuit is referred to as homeostatic metaplasticity (Whitt et al., 2014). Evidence of synaptic metaplasticity suggests that prior history of synaptic plasticity influences the degree of future synaptic modification (Abraham and Bear, 1996). For instance, a synapse that is close to the upper limit of synaptic modifiability would not experience the same degree of LTP induction as a synapse farther away from its upper limit (**Figure 3**). Previous electrophysiological evidence from *in vitro* studies suggests that inducing LTD at a synapse, bringing it farther from its upper limit of modifiability, enhances the capacity for subsequent LTP induction (Rioult-Pedotti et al., 2000). This same principle has been demonstrated at the systems

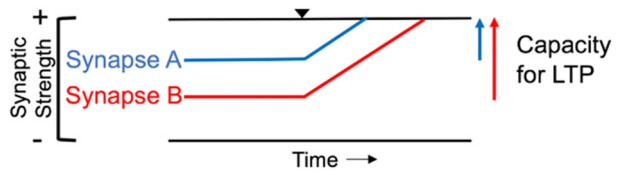

FIGURE 3 | Homeostatic range of synaptic modifiability. In the illustration, *Synapse A* begins closer to its upper limit of modifiability (top black line) and has less capacity for long-term potentiation (LTP) than *Synapse B*. Black triangle denotes induction of LTP. *Synapse B* is further from the upper limit of synaptic strength, resulting in a greater capacity for LTP induction compared to *Synapse A*.

level (Ziemann et al., 2004). It was shown that sensorimotor learning reduced the capacity for subsequent LTP but enhanced the capacity for LTD in human M1. Additionally, the degree to which further LTP is blocked has been correlated with the magnitude of motor memory retention after sensorimotor learning (Cantarero et al., 2013a,b). Taken together, these results highlight the importance of experience-dependent plasticity in sensorimotor learning. LTP is largely mediated by glutamate, the primary excitatory neurotransmitter in the brain, and its interaction with the *N*-methyl-D-aspartate (NMDA) receptor throughout the cortex (Lüscher and Malenka, 2012). Functional inactivation of the NMDA receptor in M1 abolished the capacity for LTP induction *in vivo*, suggesting that these glutamatergic receptors are necessary for LTP to occur (Hasan et al., 2013). In addition to glutamatergic synapse contributions to experience-dependent plasticity, gamma-aminobuytric acid (GABA) synaptic modifiability is another important contributor to plasticity. GABA is the main inhibitory neurotransmitter in the brain (Blicher et al., 2015), and transient reductions in GABAergic inhibition have been shown to be necessary for LTP induction in M1 (Hess et al., 1996; Blicher et al., 2015; Kida et al., 2016).

In subsequent sections, we will review the importance of sensory inputs in shaping experience-dependent plasticity underlying sensorimotor learning under normal conditions and after stroke.

THE ROLE OF SENSORY REGIONS IN GOAL-DIRECTED HAND MOVEMENTS

Posterior Parietal Cortex (PPC) as a Sensorimotor Integration Hub

The PPC is comprised of Brodmann Area (BA) 5, 7, 39 and 40 in the human brain and is anatomically connected to motor areas M1 and premotor cortex (PMC) *via* the superior longitudinal fasciculus (SLF; Makris et al., 2005; Koch et al., 2010). Although the PPC is not traditionally considered a primary part of the cortical motor network, it is involved in motor execution with populations of neurons that are motor dominant, in addition to populations that are visually dominant, or a combination of the two (Sakata et al., 1995). Non-human primate studies have demonstrated dense reciprocal PPC-M1 connections between the rostral strip of PPC and the medial lateral portion of M1 (Fang et al., 2005). Furthermore, regions of the PPC have distinct and direct pathways and networks with prefrontal motor cortical regions organized in functional zones (Gharbawie et al., 2011), which demonstrates the level of specific information the PPC can provide to the motor network. While PPC has been speculated to primarily influence M1 through polysynaptic connections with the PMC (Chao et al., 2015), support has been shown for monosynaptic projections from PPC to M1 (Karabanov et al., 2012). Additionally, in non-human primates, it has been shown that PPC has disynaptic connections with hand motoneurons in the dorsal horn and intermediate zone of the spinal cord (Rathelot et al., 2017), further suggesting potential contributions of PPC to the control of hand movements *via* the motor and sensory information PPC provides.

The PPC is a multisensory association area functioning to integrate different sensory modalities from visual, somatosensory, prefrontal and auditory inputs (Whitlock, 2017). The PPC has abundant reciprocal connections with sensory areas and is functionally parcellated such that the rostral portion of PPC is connected to somatosensory and motor regions, and the caudal portion of PPC has connections with visual and auditory regions (Stepniewska et al., 2009). The necessary inputs to PPC for sensorimotor processing needed for skilled hand movements include direct reciprocal inputs from the dorsomedial visual area that allows for continuous visual motion analysis necessary for interacting with the environment (Beck and Kaas, 1998; Kaskan and Kaas, 2007; Rosa et al., 2009; for review, see Kaas et al., 2011). Sensory inputs to BA 5 primarily come from somatosensory area S2 and the parietal ventral area, along with weaker inputs from S1 (Stepniewska et al., 2009). All three regions provide pertinent sensory information to PPC about proprioceptive and tactile activity of hand movements (Cohen et al., 1994; Prud'homme and Kalaska, 1994) that are important for sensorimotor integration used in hand exploration and object discrimination (Hinkley et al., 2007). Inputs to BA 5 are important as BA 5 is responsible for visuomotor transformations (Kalaska, 1996), making the PPC-M1 connection important for visuomotor control and visual-spatial processing (Binkofski et al., 1998; Mutha et al., 2011). PPC combines sensory signals about visual and kinematic reference frames into complex sensorimotor representations that are relayed to M1 to optimize motor commands (Sabes, 2011). PPC neurons are not only involved in control and error correction of a movement once initiated but are important for movement planning to achieve a motor goal (Mulliken et al., 2008; Aflalo et al., 2015), as neuronal firing also encodes movement intention (Snyder et al., 1997). Lesions in the rostral portion of PPC result in difficulty with shaping the fingers prior to grasping an object (Binkofski et al., 1998), further demonstrating an important role for PPC during the sensorimotor integration required for successfully performing goal-directed hand movements.

Primary Somatosensory Cortex Involvement in Sensorimotor Integration

In the human brain, S1 is comprised of BA 3a, 3b, 1, and 2 and receives direct somatosensory input from thalamus

(Kaneko et al., 1994a). Somatosensory information is relayed from the periphery to the thalamus from the medial lemniscus (Boivie, 1978) *via* the spinothalamic tract (Boivie, 1979). Additionally, the posterior medial nucleus of the thalamus connects to inhibitory neurons in layer 1 (L1) of S1 that synapse onto the apical dendrites of neurons from other cortical layers (Castejon et al., 2016). Peripheral sensory information that is task-irrelevant can be filtered out through inhibition of afferent pathways *via* a process known as sensory gating (Eguibar et al., 1994). The thalamic relay nuclei are important for sensory gating, and lesions to the thalamus result in sensory gating impairments (Staines et al., 2002). This ascending sensory information can be modulated or gated by corticofugal descending projections from S1 to the dorsal column nuclei (Jabbur and Towe, 1961; Martinez-Lorenzana et al., 2001). Both S1 and M1 demonstrate somatotopic organization with representation of body regions localized to specific cortical cell columns (Kuehn et al., 2017). Furthermore, while M1 was previously thought to be agranular, it is now known that M1 shares the same structure as other primary cortical areas (Barbas and Garcia-Cabezas, 2015). The L4 in M1 is not cytoarchitecturally distinguishable, but electrophysiological studies have demonstrated it has traditional input/output proprieties: L4 receives excitatory input from the thalamus, has excitatory unidirectional outputs to L2/3, and weaker long-range corticortical connections (Yamawaki et al., 2014). However, there are distinct differences in that M1 has approximately half the amount of synapses that are exclusively excitatory whereas in S1, there are more synapses formed with both excitatory and inhibitory neurons (Bopp et al., 2017). It is proposed that M1 likely receives its feedforward inhibition through thalamacortical projections to L1 instead of L4 (Kuramoto et al., 2009; Bopp et al., 2017). In addition to connections from the thalamus, S1 also has direct projections to M1 that are important for the integration of somatosensory and motor information (Cash et al., 2015). In rodents, reciprocal projections connect the sensory representation in S1 to the corresponding motor representation in M1, creating a glutamatergic M1-S1 loop that connects L2/3 and 5a in S1 with L2/3 and 5a in M1 (**Figure 4**; Mao et al., 2011; Hooks et al., 2013). S1 relays somatosensory information through monosynaptic and polysynaptic connections to M1 (Kaneko et al., 1994a), and ongoing sensory input is used to refine and update descending motor commands (Rosenkranz and Rothwell, 2012). L2/3 neurons in M1 are able to directly excite pyramidal output neurons within the same cortical area (Kaneko et al., 1994b). At the network level, S1 activity has both excitatory (Rocco-Donovan et al., 2011) and inhibitory (Borich et al., 2015) effects on M1 at the network level. However, only excitatory projections from S1 to M1 have been characterized at the synaptic level (Papale and Hooks, 2018). The connectivity of inhibitory interneurons within M1 and how they are affected by sensory input have not been well studied. These S1-M1 connections provide an infrastructure for highly complex information integration that has the potential to be shaped and targeted for sensorimotor control and learning.

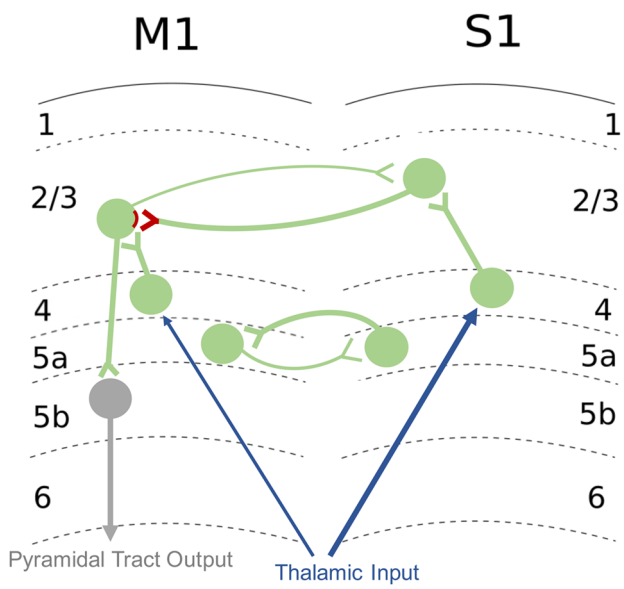

FIGURE 4 | Excitatory M1-S1 connections. Sensory input from thalamus is relayed to layer 4 (L4) then to L2/3 of S1. S1 sends glutamatergic projections onto excitatory neurons in L2/3 of M1, and these synapses are sites of LTP and long-term depression (LTD) plasticity of connections involved in sensorimotor integration (denoted in red). Reciprocal connections of the M1-S1 loop are also shown. Pyramidal neurons from L2/3 of M1 project to output neurons in L5b of M1. Afferent inputs are shown in blue, intracortical connections are in green, and efferent outputs are shown in gray. Circles denote populations of neurons. Additional inputs and outputs are not shown. Refer to text for additional detail regarding M1-S1 connections.

The ability of S1 to influence synaptic plasticity in M1 depends on sensorimotor synapses in L2/3 of M1. Synapses between S1 and M1 undergo plasticity that is driven by sensory input and results in the alteration of motor output (Kaneko et al., 1994a,b). These synapses are a main site of LTP and LTD in M1 (Kaneko et al., 1994a) and send excitatory projections to the pyramidal output neurons of M1 (Kaneko et al., 1994b; Huber et al., 2012). These connections allow for sensory feedback to shape motor output both in the short-term (immediate to minutes) and long-term (hours or longer). The ability for sensory input to influence motor output is specific to the connections between primary sensorimotor areas. Tetanic stimulation of S1, but not the ventrolateral nucleus of the thalamus, has been shown to produce LTP in L2/3 synapses of M1 (Iriki et al., 1989; Kaneko et al., 1994a). Tetanic stimulation of sensory thalamus only resulted in LTP in thalamocortical synapses with concurrent stimulation of S1 (Kaneko et al., 1994a). The S1-M1 connection has also been implicated in sensorimotor learning *in vivo* and is thought to be a main site of synaptic modifiability in response to motor skill learning (Papale and Hooks, 2018). These direct projections have been hypothesized to be a site of integration of sensory input and motor output and have an important role in guiding motor activity in response to sensory input (Hasan et al., 2013). One study in non-human primates demonstrated that ablation of S1 impaired the acquisition of motor skill but did not impair performance of the particular motor skill that had

been learned previously, possibly due to intact thalamo-cortical connections that had been strengthened during skill training (Pavlides et al., 1993). Additionally, temporary inhibition of S1 in rodents has been shown to impair the ability to adapt motor performance based on changes in sensory input; however, basic motor patterns and motor commands that had learned previously were not affected (Mathis et al., 2017). Therefore, there is evidence to suggest that S1 is important for the ability to learn skilled movement and adjust motor plans to sensory input but may be less important for performance of overlearned or stereotyped movements in the upper limb. It should be noted, however, that ablation of other areas of S1, such as the face area, can lead to deficits in basic motor function, and previously learned motor tasks (Lin et al., 1993; Hiraba et al., 2000; Yao et al., 2002). In addition to connections between S1 and the ipsilateral M1, interhemispheric inhibitory connections between S1 s exist in humans (Ragert et al., 2011) and have been shown to influence plasticity in M1. For example, Conde et al. (2013) demonstrated that LTP-like plasticity in M1 induced by paired TMS and peripheral stimulation of the contralateral upper extremity switched to LTD-like plasticity when peripheral stimulation was applied to the upper limb ipsilateral to the TMS. These results demonstrate that the cortical sensorimotor circuitry that contributes to plasticity is not limited to one hemisphere, and interhemispheric network connectivity likely influences sensorimotor learning. However, the specific involvement of S1 in motor performance will depend on the characteristics of the task including the importance of sensory information for skilled performance.

IMPACT OF STROKE ON SENSORIMOTOR INTEGRATION AND LEARNING

Sensorimotor Deficits After Stroke

The impact of stroke on sensorimotor integration depends on the location of the stroke. Because the MCA supplies both the motor and sensory regions and is the most common type of stroke (Walcott et al., 2014), stroke in this vascular territory has a great likelihood of affecting sensorimotor integration. Therefore, our discussion is primarily focused on MCA strokes affecting the sensorimotor cortex although strokes in other vascular territories may also impact sensorimotor integration (Staines et al., 2002). There are dynamic processes post-stroke that change as a function of time and affect the neurophysiology of sensorimotor integration. Time post-stroke is defined in phases: hyper-acute (0–24 h); acute (1–7 days); early subacute (7 days–3 months); late subacute (3–6 months); and chronic (>6 months; Bernhardt et al., 2017b). Initial neuronal cell death in the lesion core leads to both structural and functional disconnection with brain regions outside the primary area of infarct (Carrera and Tononi, 2014). Motor recovery occurs in part from spontaneous biological repair (SBR) that transitions from a state of cell death and inflammation to a state of increased neuronal excitability and experience-dependent plasticity lasting ∼3 months post-stroke (Cramer, 2008). Most recovery post-stroke occurs rapidly in the early sub-acute phase and the magnitude of improvement slows down in the late sub-acute phase (Lee et al., 2015). In the chronic phase post-stroke, patients have reached a stable, though modifiable plateau in motor recovery (Jørgensen et al., 1995) with less than 20% of patients experiencing full recovery of upper extremity motor function (Kwakkel et al., 2003).

Upper extremity paresis is the most predominant motor impairment after MCA stroke, which results from a lesion involving the CST that is also necessary for skilled hand movements (Lang and Schieber, 2003). Paresis can contribute to deficits in both the initiation and termination of voluntary movement of the wrist (Chae et al., 2002). Other motor deficits include spasticity and impaired motor control (Raghavan, 2015), with 85% of patients in the chronic phase post-stroke still possessing residual motor deficits (Lee et al., 2015).

Common somatosensory modalities affected after stroke are tactile sensation, proprioception, and stereognosis (Connell et al., 2008). It has been recently reported that 62% of acute stroke patients demonstrated deficits in their ability to locate their hand and arm in space (Findlater et al., 2016). Deficits in proprioception have direct implications as information about the arm and hand are necessary for proper movement and important for improving sensorimotor function after stroke (Aman et al., 2014). Due to the reliance of the motor system on sensory information for movement optimization, sensory impairment is expected to have motor repercussions. Similarly, sensory deficits can occur even when there are ischemic lesions specifically in the M1 motor pathway and not in somatosensory afferents (Nudo et al., 2000), suggesting that sensory integration can be disrupted even in the absence of a lesion present in sensory afferent pathways. Clinically, sensorimotor deficits are usually discussed in terms of sensory deficits and motor deficits assessed separately. Sensory and/or motor deficits after stroke have been routinely measured using observer-based clinical scales either focused on measuring level of impairment, with scales such as the Fugl-Meyer Assessment (Fugl-Meyer et al., 1975) and Nottingham Sensory Assessment (Lincoln et al., 1998), or focused on measuring level of function with the Wolf Motor Function Test (Wolf et al., 2001) and the Jebsen Taylor Hand Test (Jebsen et al., 1969). However, there are several limitations of standard observer-based clinical assessments including: decreased reliability and sensitivity compared to objective assessments, lack of precision with non-continuous data, and greater susceptibility to floor and ceiling effects of performance (Scott and Dukelow, 2011). Therefore, there is a need for objective assessments to better characterize post-stroke sensorimotor deficits.

Assessment of Sensorimotor Integration After Stroke

In addition to the need for objective assessments of sensorimotor deficits, it is important to examine the impact of stroke on sensorimotor integration to better understand the relationship between sensory and motor deficits. As defined earlier, sensorimotor integration is the ability to incorporate sensory inputs to shape motor output (Wolpert et al., 1998). Therefore, examining the effects of manipulating sensory information on motor output can be employed to evaluate

sensorimotor integration. For a detailed review of various measurement techniques, see Riemann et al. (2002). One approach utilizes robotic-based technologies during visually guided upper extremity tasks to quantify aspects of sensorimotor control. Coderre et al. (2010) examined the characteristics of feed-forward control and feedback control of stroke patients in the early sub-acute recovery period. It was observed that most patients with deficits initiating movement also had deficits with adjusting movement from sensory feedback, emphasizing that movement difficulties were not solely due to motor impairments but also due to an inefficiency with integration of sensory modalities. Using another robotic-based assessment, it was shown that kinesthetic impairments post-stroke were not resolved with the addition of visual information indicating the location of the arm in space (Semrau et al., 2018). This observation was unique to stroke patients in comparison to healthy controls and the impairment was attributed, in part, to damage to the PPC. Studies have previously shown that sensorimotor abnormalities during motor control are related to parietal lesions (Desmurget et al., 1999; Findlater et al., 2016), signifying the important role of PPC in sensorimotor integration.

In addition to robotic-based assessments, sensorimotor integration has also been probed using non-invasive stimulation in humans. Combining a peripheral sensory stimulus with non-invasive brain stimulation using TMS can measure the effects of afferent sensory input on the magnitude of TMS-evoked motor output. One example assessment is short-latency afferent inhibition (SAI) where somatosensory input from peripheral stimulation of the median nerve can inhibit motor output to hand muscles (Tokimura et al., 2000). In the acute phase post-stroke, patients have reduced SAI compared to healthy controls (Di Lazzaro et al., 2012), that seems to normalize in the chronic phase where there is no significant difference in SAI between patients and controls (Brown et al., 2018). Sensorimotor integration may be disrupted shortly after stroke but this reduction was correlated with improved outcome in the chronic phase (Di Lazzaro et al., 2012) This suggests that while decreased SAI may be beneficial acutely, it must normalize chronically for improved motor function. Previous work has also shown that the integration of S1 afferent input to M1 decreased acutely but was more comparable to healthy controls at 6 months post-stroke; this finding also paralleled improvement in sensation (Bannister et al., 2015). Sensorimotor integration has also been assessed using a vibration-based sensory stimulus of the muscle belly preceding TMS. It was found sensorimotor integration was abnormal in chronic stroke patients and greater abnormality was associated with greater magnitude of motor impairment and dysfunction (Brown et al., 2018). Taken together, these studies demonstrate that sensorimotor integration is impacted differentially depending on time post-stroke and the type of sensory information provided, but overall is an important process during recovery.

Plasticity and Sensorimotor Learning After Stroke

Many cellular and synaptic processes contribute to plasticity after stroke. In the acute phase after stroke, LTP is facilitated in the perilesional areas, suggesting an amplification of network plasticity that influences cortical reorganization (Hagemann et al., 1998). Neuroplasticity is enhanced through processes such as axonal sprouting and GABA receptor downregulation (Carmichael, 2016). Additionally, functional recovery is most rapid during this early time period, occurring in the first 3 months for humans and roughly 1 month for rodents (Caleo, 2015). Plasticity subsequently plateaus in the chronic stage of recovery (Hendricks et al., 2002; Hara, 2015). Rehabilitative interventions have been shown to be most effective when initiated early after stroke and become less effective with time post-stroke (Biernaskie et al., 2004). Despite the plateau in neuroplasticity during the chronic phase of recovery, it is currently unclear whether this level differs from that of matched healthy controls. In a study by Zeiler et al. (2016) in a rodent model of chronic stroke, the induction of a second stroke enhanced plasticity and response to skilled motor training, indicating that it is possible to reopen this window of enhanced plasticity during the later stages of recovery. Increasing the capacity for neuroplasticity during the chronic stage of recovery has the potential to enhance recovery of function for stroke survivors with persistent motor-related disability.

As mentioned previously, GABAergic activity is strongly related to synaptic plasticity in healthy individuals. In rodent models of cerebral ischemia, GABAergic inhibition has been shown to be elevated within minutes (Globus et al., 1991), a potentially neuroprotective mechanism to counteract excitotoxicity caused by excess glutamate release (Pellegrini-Giampietro, 2003). GABA levels return to baseline within an hour of reoxygenation (Schwartz-Bloom and Sah, 2001). Reductions in GABAergic inhibition continue during the acute phase after stroke, and this process has been related to functional motor recovery in mice (Clarkson et al., 2010). It has been suggested that this reduction in GABAergic activity serves to facilitate neuroplasticity in M1 through unmasking of existing, inactive synaptic connections (Paik and Yang, 2014), the development of new connections (Murphy and Corbett, 2009), or the induction of LTP (Hess et al., 1996; Sanes and Donoghue, 2000). While GABAergic activity has been shown to be an important contributor to plasticity after stroke, other mechanisms, such as brain derived neurotrophic factor (BDNF) and neuromodulin signaling, have been implicated as well. For in-depth reviews of cellular and synaptic mechanisms of plasticity after stroke, see Murphy and Corbett (2009) and Alia et al. (2017). Given that similar mechanisms are thought to underlie neuroplasticity and functional recovery after stroke (Kleim and Jones, 2008), therapeutic strategies that optimally promote neuroplasticity hold promise for improving the rate and magnitude of functional recovery after stroke.

As discussed earlier, motor skill learning has been shown to induce structural and functional changes in M1 that underpin sensorimotor learning in rodents (Kleim et al., 1998), non-human primates (Nudo, 2013), and healthy humans (Bütefisch et al., 2000; Sanes and Donoghue, 2000; Ziemann et al., 2004). It has also been shown that motor skill learning underlies recovery of function after stroke in humans (Krakauer, 2006) and non-human primates (Nudo et al., 1996b). One mechanism

underlying recovery is the preservation or expansion of the M1 representation of the affected hand. Skilled motor training after stroke in non-human primates prevented the reduction of the affected distal upper extremity representation in M1 that occurred after an equivalent period of no training (Nudo et al., 1996b). In some cases, the hand representation expanded into representations for adjacent body parts after training, and this reorganization of M1 corresponded to better recovery of skilled hand function. It has also been shown that S1 activity contributes to sensorimotor learning and recovery after stroke in humans and non-human primates. Nudo et al. (2000) demonstrated that impairments in sensory inputs to M1 after stroke in non-human primates contributed to motor deficits in a task that required skilled hand movements. In humans, continuous theta burst stimulation (cTBS), a TMS paradigm that can decrease excitability of the stimulated area, delivered over contralesional S1 in order to reduce transcallosal inhibition on ipsilesional S1 was shown to enhance motor recovery after stroke (Meehan et al., 2011). Another study by Brodie et al. (2014) demonstrated that excitatory rTMS to the ipsilesional S1 paired with motor skill training increased sensorimotor learning compared to stimulation or skill training in isolation. Therefore, attempting to enhance S1 excitability and/or sensorimotor integration may offer an effective approach to improve sensorimotor learning and functional recovery after stroke.

STRATEGIES TO MODULATE SENSORIMOTOR INTEGRATION AND POTENTIAL THERAPEUTIC EFFECTS AFTER STROKE

Current Therapeutic Interventions

Sensorimotor integration occurs across the neuraxis and therefore provides multiple potential targets for therapeutic intervention. Several experimental procedures have been developed to modulate afferent input to M1, and therefore sensorimotor integration, in humans. Peripheral vibration is a neuromodulation approach that increases afferent input that is thought to modulate M1 excitability by regulating the activity of cortical inhibitory interneurons that are involved in motor output (Rosenkranz and Rothwell, 2006). This increase in afferent input is thought to change the response of M1 to sensory input and therefore influence sensorimotor integration in the cortex. Both focal (Celletti et al., 2017) and whole-body vibration (Boo et al., 2016) have shown promise in improving upper extremity function in individuals with stroke. However, across studies, the effectiveness of vibration to improve post-stroke motor function remains unclear (Liao et al., 2014; Park et al., 2018).

In contrast to increasing afferent input to M1, models of temporary deafferentation have shown promise in targeting sensorimotor integration by reducing sensory input to modulate motor output. In rodents, transection of the facial nerve leads to a rapid expansion of the adjacent forelimb representation in M1, likely due to rapid removal of GABAergic inhibition (Sanes et al., 1988; Huntley, 1997). This concept has been applied non-invasively in humans by temporarily reducing afferent input from a portion of the upper extremity to M1 with the goal of reducing GABAergic inhibition to adjacent areas of the limb. It is thought that rapid unmasking of horizontal connections leads to an expansion of the cortical representation. Targeting this mechanism, several temporary deafferentation strategies have been studied in humans with the goal of increasing M1 representation of the affected limb to improve functional outcomes after stroke. Ischemic nerve block (INB) of the arm is one method that serves as a model of transient segmental deafferentation in humans. Using a pneumatic tourniquet at the elbow, afferent sensory inputs from the distal forearm to the sensorimotor cortex are restricted, leading to an increase in excitability of cortical representations of muscles immediately proximal to the deafferented forearm (Brasil-Neto et al., 1993). However, this form of INB may be less applicable for individuals with stroke, as a main goal of stroke rehabilitation is to improve hand function, and it appears that INB effects more proximal parts of the arm (Lang et al., 2013). A different approach that has been shown to increase motor function after stroke is the application of anesthesia to areas proximal to the hand, such as the brachial plexus (Muellbacher et al., 2002a) or forearm (Sens et al., 2012, 2013), simulating deafferentation of the upper or lower arm, respectively. After applying anesthesia to the brachial plexus of the affected arm, Muellbacher et al. (2002a) demonstrated an improvement in motor skill after training in individuals with chronic stroke compared to training without anesthesia. Additionally, there was an increase in motor output in response to TMS application with no change in motor threshold, suggesting a rapid cortical reorganization and reduction in inhibition. Application of anesthetic cream to the forearm, another region proximal to the hand, improved somatosensory and motor function distal to the site of application in individuals with chronic stroke (Sens et al., 2013). Blood flow restriction (BFR) is another technique that uses a pneumatic cuff applied to the arm to reduce blood flow to a target level that is maintained during exercise (Yasuda et al., 2014). Brandner et al. (2015) showed that BFR during resistance exercise increases corticomotor excitability, and this effect is thought to be mediated by the reduction in cortical afferent input. A primary concern for the use of INB and BFR in a rehabilitation setting is that the use of a tourniquet or arm cuff poses a risk for individuals with sensory impairments and/or cardiovascular irregularities, such as individuals with stroke (Spranger et al., 2015). Therefore, individuals with stroke may benefit from a method of temporary deafferentation with fewer potential risks.

Future Directions for Therapeutic Interventions

Short-term immobilization of the arm is a safe, low-cost approach for the transient modulation of sensorimotor cortical function in healthy individuals. In humans and animals, prolonged immobilization or disuse of a limb can occur after neurological insult that induces maladaptive plasticity, such as reduction in cortical representations of the limb (Pons et al., 1991; Langer et al., 2012; Milliken et al., 2013; Viaro et al., 2014), which can contribute to "learned nonuse" and a compensatory

reliance on the unaffected limb (Wolf, 2007). While learned nonuse and its effects on cortical organization have been examined, short-term immobilization has been less well-studied. Short-term arm immobilization (typically 8 h) reduces sensory input to, and motor output from, the contralateral sensorimotor cortex resulting in transiently decreased M1 and S1 cortical excitability following immobilization in healthy individuals (Huber et al., 2006; Rosenkranz et al., 2014). This decrease in excitability is thought to be driven by LTD-like processes (Huber et al., 2006). Allen et al. (2003) demonstrated that whisker deprivation in rodents induced LTD-like effects in sensorimotor areas that occluded further LTD induction but enhanced LTP induction in slice preparations, consistent with the model of homeostatic metaplasticity. Short-term immobilization of the arm has been proposed as a strategy to induce LTD-like plasticity and enhance the capacity for LTP induction in the human motor cortex. Indeed, a single short bout (8 h) of immobilization temporarily reduced TMS-based measures of cortical excitability; however, the capacity for synaptic strengthening was significantly enhanced (Rosenkranz et al., 2014). However, the behavioral effects of this enhanced synaptic strengthening are currently unclear.

Given that short-term immobilization modulates excitability of S1 and M1, it is likely that immobilization impacts the integration of sensory and motor information that underlies experience-dependent plasticity. Therefore, short-term immobilization could potentially modulate neural processes underlying sensorimotor learning. However, the effects of immobilization on sensorimotor learning have not been well studied in humans. To our knowledge, only one study has examined sensorimotor learning after short-term arm immobilization (Opie et al., 2016) and did not show a clear effect of immobilization on sensorimotor learning. The lack of effect could be due, in part, to the high number of individuals with the BDNF Val66Met polymorphism that is associated with reduced use-dependent plasticity in sensorimotor areas (Kleim et al., 2006). Given the relationship between neural plasticity and sensorimotor learning, further examination of the effect of short-term arm immobilization on sensorimotor learning is warranted. Short-term arm immobilization could show promise as a rehabilitative intervention to increase post-stroke sensorimotor recovery by enhancing the capacity for neuroplasticity leading to better training-related increases in motor function. More broadly, given its demonstrated role in motor control, promotion of sensorimotor integration plasticity has potential as a therapeutic strategy post-stroke.

CONCLUSION

Skilled hand movements are necessary for normal function in daily life but are frequently impaired after stroke. Goal-directed functional movements rely on accurate integration sensory information and when sensorimotor integration is compromised, movement ability is compromised. Despite the importance of sensory contributions to normal and abnormal movement, research has predominantly focused on motor aspects of stroke recovery. Given that sensorimotor integration has been shown to be negatively impacted after stroke and correlated with level of recovery, there is an increasing need to focus future research efforts towards comprehensive characterization of the neural mechanisms of sensorimotor integration and their contributions to functional movements in both health and disease. Furthermore, an increased understanding of contributions of sensorimotor integration and sensorimotor learning to skilled hand movements post-stroke will likely offer new rehabilitative targets to increase the recovery of function after stroke.

AUTHOR CONTRIBUTIONS

LE and EK planned, drafted, and edited the manuscript. CB and MB planned and edited the manuscript.

FUNDING

The authors would like to acknowledge their funding sources. LE is supported by R01NS090677-04S1. EK is supported by 2T32HD071845-06. CB is partially supported by R01NS090677, R21NS092385, StrokeNet U24NS107234. MB is supported by NIH NCMRR, K12HD055931, P2CCHD086844 and a Research Grant from the Foundation for Physical Therapy. The funding for open access publication fee for this article were provided by the Emory University Department of Rehabilitation Medicine.

REFERENCES

Abraham, W. C., and Bear, M. F. (1996). Metaplasticity: the plasticity of synaptic plasticity. *Trends Neurosci.* 19, 126–130. doi: 10.1016/s0166-2236(96)80018-x

Aflalo, T., Kellis, S., Klaes, C., Lee, B., Shi, Y., Pejsa, K., et al. (2015). Neurophysiology. Decoding motor imagery from the posterior parietal cortex of a tetraplegic human. *Science* 348, 906–910. doi: 10.1126/science.aaa5417

Alia, C., Spalletti, C., Lai, S., Panarese, A., Lamola, G., Bertolucci, F., et al. (2017). Neuroplastic changes following brain ischemia and their contribution to stroke recovery: novel approaches in neurorehabilitation. *Front. Cell. Neurosci.* 11:76. doi: 10.3389/fncel.2017.00076

Allen, C. B., Celikel, T., and Feldman, D. E. (2003). Long-term depression induced by sensory deprivation during cortical map plasticity *in vivo*. *Nat. Neurosci.* 6, 291–299. doi: 10.1038/nn1012

Aman, J. E., Elangovan, N., Yeh, I. L., and Konczak, J. (2014). The effectiveness of proprioceptive training for improving motor function: a systematic review. *Front. Hum. Neurosci.* 8:1075. doi: 10.3389/fnhum.2014.01075

Arce-McShane, F. I., Hatsopoulos, N. G., Lee, J. C., Ross, C. F., and Sessle, B. J. (2014). Modulation dynamics in the orofacial sensorimotor cortex during motor skill acquisition. *J. Neurosci.* 34, 5985–5997. doi: 10.1523/jneurosci.4367-13.2014

Arima, T., Yanagi, Y., Niddam, D. M., Ohata, N., Arendt-Nielsen, L., Minagi, S., et al. (2011). Corticomotor plasticity induced by tongue-task training in humans: a longitudinal fMRI study. *Exp. Brain Res.* 212, 199–212. doi: 10.1007/s00221-011-2719-7

Baker, S. N. (2011). The primate reticulospinal tract, hand function and functional recovery. *J. Physiol.* 589, 5603–5612. doi: 10.1113/jphysiol.2011.215160

Bannister, L. C., Crewther, S. G., Gavrilescu, M., and Carey, L. M. (2015). Improvement in touch sensation after stroke is associated with resting functional connectivity changes. *Front. Neurol.* 6:165. doi: 10.3389/fneur.2015.00165

Barbas, H., and Garcia-Cabezas, M. A. (2015). Motor cortex layer 4: less is more. *Trends Neurosci.* 38, 259–261. doi: 10.1016/j.tins.2015.03.005

Beck, P. D., and Kaas, J. H. (1998). Cortical connections of the dorsomedial visual area in prosimian primates. *J. Comp. Neurol.* 398, 162–178. doi: 10.1002/(sici)1096-9861(19980824)398:2<162::aid-cne2>3.0.co;2-z

Benjamin, E. J., Blaha, M. J., Chiuve, S. E., Cushman, M., Das, S. R., Deo, R., et al. (2017). Heart disease and stroke statistics-2017 update: a report from the american heart association. *Circulation* 135, e146–e603. doi: 10.1161/CIR.0000000000000485

Bernhardt, J., Godecke, E., Johnson, L., and Langhorne, P. (2017a). Early rehabilitation after stroke. *Curr. Opin. Neurol.* 30, 48–54. doi: 10.1097/WCO.0000000000000404

Bernhardt, J., Hayward, K. S., Kwakkel, G., Ward, N. S., Wolf, S. L., Borschmann, K., et al. (2017b). Agreed definitions and a shared vision for new standards in stroke recovery research: the stroke recovery and rehabilitation roundtable taskforce. *Neurorehabil. Neural Repair* 31, 793–799. doi: 10.1177/1545968317732668

Biernaskie, J., Chernenko, G., and Corbett, D. (2004). Efficacy of rehabilitative experience declines with time after focal ischemic brain injury. *J. Neurosci.* 24, 1245–1254. doi: 10.1523/JNEUROSCI.3834-03.2004

Binkofski, F., Dohle, C., Posse, S., Stephan, K. M., Hefter, H., Seitz, R. J., et al. (1998). Human anterior intraparietal area subserves prehension: a combined lesion and functional MRI activation study. *Neurology* 50, 1253–1259. doi: 10.1212/wnl.50.5.1253

Blakemore, S. J., Goodbody, S. J., and Wolpert, D. M. (1998). Predicting the consequences of our own actions: the role of sensorimotor context estimation. *J. Neurosci.* 18, 7511–7518. doi: 10.1523/jneurosci.18-18-07511.1998

Blicher, J. U., Near, J., Naess-Schmidt, E., Stagg, C. J., Johansen-Berg, H., Nielsen, J. F., et al. (2015). GABA levels are decreased after stroke and GABA changes during rehabilitation correlate with motor improvement. *Neurorehabil. Neural Repair* 29, 278–286. doi: 10.1177/1545968314543652

Boivie, J. (1978). Anatomical observations on the dorsal column nuclei, their thalamic projection and the cytoarchitecture of some somatosensory thalamic nuclei in the monkey. *J. Comp. Neurol.* 178, 17–48. doi: 10.1002/cne.901780103

Boivie, J. (1979). An anatomical reinvestigation of the termination of the spinothalamic tract in the monkey. *J. Comp. Neurol.* 186, 343–369. doi: 10.1002/cne.901860304

Bolognini, N., Russo, C., and Edwards, D. J. (2016). The sensory side of post-stroke motor rehabilitation. *Restor. Neurol. Neurosci.* 34, 571–586. doi: 10.3233/rnn-150606

Boo, J. A., Moon, S. H., Lee, S. M., Choi, J. H., and Park, S. E. (2016). Effect of whole-body vibration exercise in a sitting position prior to therapy on muscle tone and upper extremity function in stroke patients. *J. Phys. Ther. Sci.* 28, 558–562. doi: 10.1589/jpts.28.558

Bopp, R., Holler-Rickauer, S., Martin, K. A., and Schuhknecht, G. F. (2017). An ultrastructural study of the thalamic input to layer 4 of primary motor and primary somatosensory cortex in the mouse. *J. Neurosci.* 37, 2435–2448. doi: 10.1523/jneurosci.2557-16.2017

Borich, M. R., Brodie, S. M., Gray, W. A., Ionta, S., and Boyd, L. A. (2015). Understanding the role of the primary somatosensory cortex: opportunities for rehabilitation. *Neuropsychologia* 79, 246–255. doi: 10.1016/j.neuropsychologia.2015.07.007

Bosch-Bouju, C., Hyland, B. I., and Parr-Brownlie, L. C. (2013). Motor thalamus integration of cortical, cerebellar and basal ganglia information: implications for normal and parkinsonian conditions. *Front. Comput. Neurosci.* 7:163. doi: 10.3389/fncom.2013.00163

Brandner, C. R., Warmington, S. A., and Kidgell, D. J. (2015). Corticomotor excitability is increased following an acute bout of blood flow restriction resistance exercise. *Front. Hum. Neurosci.* 9:652. doi: 10.3389/fnhum.2015.00652

Brasil-Neto, J. P., Valls-Solé, J., Pascual-Leone, A., Cammarota, A., Amassian, V. E., Cracco, R., et al. (1993). Rapid modulation of human cortical motor outputs following ischaemic nerve block. *Brain* 116, 511–525. doi: 10.1093/brain/116.3.511

Brodie, S. M., Meehan, S., Borich, M. R., and Boyd, L. A. (2014). 5 Hz repetitive transcranial magnetic stimulation over the ipsilesional sensory cortex enhances motor learning after stroke. *Front. Hum. Neurosci.* 8:143. doi: 10.3389/fnhum.2014.00143

Brown, K. E., Neva, J. L., Feldman, S. J., Staines, W. R., and Boyd, L. A. (2018). Sensorimotor integration in chronic stroke: baseline differences and response to sensory training. *Restor. Neurol. Neurosci.* 36, 245–259. doi: 10.3233/RNN-170790

Burnod, Y., Grandguillaume, P., Otto, I., Ferraina, S., Johnson, P. B., and Caminiti, R. (1992). Visuomotor transformations underlying arm movements toward visual targets: a neural network model of cerebral cortical operations. *J. Neurosci.* 12, 1435–1453. doi: 10.1523/jneurosci.12-04-01435.1992

Bütefisch, C. M., Davis, B. C., Wise, S. P., Sawaki, L., Kopylev, L., Classen, J., et al. (2000). Mechanisms of use-dependent plasticity in the human motor cortex. *Proc. Natl. Acad. Sci. U S A* 97, 3661–3665. doi: 10.1073/pnas.050350297

Caleo, M. (2015). Rehabilitation and plasticity following stroke: insights from rodent models. *Neuroscience* 311, 180–194. doi: 10.1016/j.neuroscience.2015.10.029

Cantarero, G., Lloyd, A., and Celnik, P. (2013a). Reversal of long-term potentiation-like plasticity processes after motor learning disrupts skill retention. *J. Neurosci.* 33, 12862–12869. doi: 10.1523/jneurosci.1399-13.2013

Cantarero, G., Tang, B., O'Malley, R., Salas, R., and Celnik, P. (2013b). Motor learning interference is proportional to occlusion of LTP-like plasticity. *J. Neurosci.* 33, 4634–4641. doi: 10.1523/jneurosci.4706-12.2013

Carmichael, S. T. (2016). The 3 Rs of stroke biology: radial, relayed and regenerative. *Neurotherapeutics* 13, 348–359. doi: 10.1007/s13311-015-0408-0

Carrera, E., and Tononi, G. (2014). Diaschisis: past, present, future. *Brain* 137, 2408–2422. doi: 10.1093/brain/awu101

Cash, R. F., Isayama, R., Gunraj, C. A., Ni, Z., and Chen, R. (2015). The influence of sensory afferent input on local motor cortical excitatory circuitry in humans. *J. Physiol.* 593, 1667–1684. doi: 10.1113/jphysiol.2014.286245

Castejon, C., Barros-Zulaica, N., and Nunez, A. (2016). Control of somatosensory cortical processing by thalamic posterior medial nucleus: a new role of thalamus in cortical function. *PLoS One* 11:e0148169. doi: 10.1371/journal.pone.0148169

Celletti, C., Sinibaldi, E., Pierelli, F., Monari, G., and Camerota, F. (2017). Focal muscle vibration and progressive modular rebalancing with neurokinetic facilitations in post- stroke recovery of upper limb. *Clin. Ter.* 168, e33–e36. doi: 10.7417/CT.2017.1979

Chae, J., Yang, G., Park, B. K., and Labatia, I. (2002). Delay in initiation and termination of muscle contraction, motor impairment and physical disability in upper limb hemiparesis. *Muscle Nerve* 25, 568–575. doi: 10.1002/mus.10061

Chao, C. C., Karabanov, A. N., Paine, R., Carolina De Campos, A., Kukke, S. N., Wu, T., et al. (2015). Induction of motor associative plasticity in the posterior parietal cortex-primary motor network. *Cereb. Cortex* 25, 365–373. doi: 10.1093/cercor/bht230

Clarkson, A. N., Huang, B. S., Macisaac, S. E., Mody, I., and Carmichael, S. T. (2010). Reducing excessive GABA-mediated tonic inhibition promotes functional recovery after stroke. *Nature* 468, 305–309. doi: 10.1038/nature09511

Coderre, A. M., Zeid, A. A., Dukelow, S. P., Demmer, M. J., Moore, K. D., Demers, M. J., et al. (2010). Assessment of upper-limb sensorimotor function of subacute stroke patients using visually guided reaching. *Neurorehabil. Neural Repair* 24, 528–541. doi: 10.1177/1545968309356091

Cohen, D. A., Prud'homme, M. J., and Kalaska, J. F. (1994). Tactile activity in primate primary somatosensory cortex during active arm movements: correlation with receptive field properties. *J. Neurophysiol.* 71, 161–172. doi: 10.1152/jn.1994.71.1.161

Conde, V., Vollmann, H., Taubert, M., Sehm, B., Cohen, L. G., Villringer, A., et al. (2013). Reversed timing-dependent associative plasticity in the human brain through interhemispheric interactions. *J. Neurophysiol.* 109, 2260–2271. doi: 10.1152/jn.01004.2012

Connell, L. A., Lincoln, N. B., and Radford, K. A. (2008). Somatosensory impairment after stroke: frequency of different deficits and their recovery. *Clin. Rehabil.* 22, 758–767. doi: 10.1177/0269215508090674

Cramer, S. C. (2008). Repairing the human brain after stroke: I. Mechanisms of spontaneous recovery. *Ann. Neurol.* 63, 272–287. doi: 10.1002/ana.21393

Desmurget, M., Epstein, C. M., Turner, R. S., Prablanc, C., Alexander, G. E., and Grafton, S. T. (1999). Role of the posterior parietal cortex in updating reaching movements to a visual target. *Nat. Neurosci.* 2, 563–567. doi: 10.1038/9219

Di Lazzaro, V., Profice, P., Pilato, F., Capone, F., Ranieri, F., Florio, L., et al. (2012). The level of cortical afferent inhibition in acute stroke correlates with long-term functional recovery in humans. *Stroke* 43, 250–252. doi: 10.1161/STROKEAHA.111.631085

Dum, R. P., and Strick, P. L. (1996). Spinal cord terminations of the medial wall motor areas in macaque monkeys. *J. Neurosci.* 16, 6513–6525. doi: 10.1523/jneurosci.16-20-06513.1996

Eguibar, J. R., Quevedo, J., Jiménez, I., and Rudomin, P. (1994). Selective cortical control of information flow through different intraspinal collaterals of the same muscle afferent fiber. *Brain Res.* 643, 328–333. doi: 10.1016/0006-8993(94)90042-6

Fang, P. C., Stepniewska, I., and Kaas, J. H. (2005). Ipsilateral cortical connections of motor, premotor, frontal eye and posterior parietal fields in a prosimian primate, Otolemur garnetti. *J. Comp. Neurol.* 490, 305–333. doi: 10.1002/cne.20665

Findlater, S. E., Desai, J. A., Semrau, J. A., Kenzie, J. M., Rorden, C., Herter, T. M., et al. (2016). Central perception of position sense involves a distributed neural network - evidence from lesion-behavior analyses. *Cortex* 79, 42–56. doi: 10.1016/j.cortex.2016.03.008

Flanagan, J. R., Bowman, M. C., and Johansson, R. S. (2006). Control strategies in object manipulation tasks. *Curr. Opin. Neurobiol.* 16, 650–659. doi: 10.1016/j.conb.2006.10.005

Friel, K. M., Barbay, S., Frost, S. B., Plautz, E. J., Hutchinson, D. M., Stowe, A. M., et al. (2005). Dissociation of sensorimotor deficits after rostral versus caudal lesions in the primary motor cortex hand representation. *J. Neurophysiol.* 94, 1312–1324. doi: 10.1152/jn.01251.2004

Fugl-Meyer, A. R., Jääskö, L., Leyman, I., Olsson, S., and Steglind, S. (1975). The post-stroke hemiplegic patient. 1. A method for evaluation of physical performance. *Scand. J. Rehabil. Med.* 7, 13–31.

Georgopoulos, A. P., Ashe, J., Smyrnis, N., and Taira, M. (1992). The motor cortex and the coding of force. *Science* 256, 1692–1695. doi: 10.1126/science.256.5064.1692

Georgopoulos, A. P., Kalaska, J. F., Caminiti, R., and Massey, J. T. (1982). On the relations between the direction of two-dimensional arm movements and cell discharge in primate motor cortex. *J. Neurosci.* 2, 1527–1537. doi: 10.1523/jneurosci.02-11-01527.1982

Gharbawie, O. A., Stepniewska, I., and Kaas, J. H. (2011). Cortical connections of functional zones in posterior parietal cortex and frontal cortex motor regions in new world monkeys. *Cereb. Cortex* 21, 1981–2002. doi: 10.1093/cercor/bhq260

Globus, M. Y., Busto, R., Martinez, E., Valdes, I., Dietrich, W. D., and Ginsberg, M. D. (1991). Comparative effect of transient global ischemia on extracellular levels of glutamate, glycine and γ-aminobutyric acid in vulnerable and nonvulnerable brain regions in the rat. *J. Neurochem.* 57, 470–478. doi: 10.1111/j.1471-4159.1991.tb03775.x

Griffin, D. M., Hoffman, D. S., and Strick, P. L. (2015). Corticomotoneuronal cells are "functionally tuned". *Science* 350, 667–670. doi: 10.1126/science.aaa8035

Hagemann, G., Redecker, C., Neumann-Haefelin, T., Freund, H. J., and Witte, O. W. (1998). Increased long-term potentiation in the surround of experimentally induced focal cortical infarction. *Ann. Neurol.* 44, 255–258. doi: 10.1002/ana.410440217

Hara, Y. (2015). Brain plasticity and rehabilitation in stroke patients. *J. Nippon Med. Sch.* 82, 4–13. doi: 10.1272/jnms.82.4

Hasan, M. T., Hernández-González, S., Dogbevia, G., Trevino, M., Bertocchi, I., Gruart, A., et al. (2013). Role of motor cortex NMDA receptors in learning-dependent synaptic plasticity of behaving mice. *Nat. Commun.* 4:2258. doi: 10.1038/ncomms3258

Hatsopoulos, N. G., and Suminski, A. J. (2011). Sensing with the motor cortex. *Neuron* 72, 477–487. doi: 10.1016/j.neuron.2011.10.020

Hendricks, H. T., Van Limbeek, J., Geurts, A. C., and Zwarts, M. J. (2002). Motor recovery after stroke: a systematic review of the literature. *Arch. Phys. Med. Rehabil.* 83, 1629–1637. doi: 10.1053/apmr.2002.35473

Hess, G., Aizenman, C. D., and Donoghue, J. P. (1996). Conditions for the induction of long-term potentiation in layer II/III horizontal connections of the rat motor cortex. *J. Neurophysiol.* 75, 1765–1778. doi: 10.1152/jn.1996.75.5.1765

Hinkley, L. B., Krubitzer, L. A., Nagarajan, S. S., and Disbrow, E. A. (2007). Sensorimotor integration in S2, PV, and parietal rostroventral areas of the human sylvian fissure. *J. Neurophysiol.* 97, 1288–1297. doi: 10.1152/jn.00733.2006

Hiraba, H., Yamaguchi, Y., Satoh, H., Ishibashi, Y., and Iwamura, Y. (2000). Deficits of masticatory movements caused by lesions in the orofacial somatosensory cortex of the awake cat. *Somatosens. Mot. Res.* 17, 361–372. doi: 10.1080/089902002000202239

Hooks, B. M., Lin, J. Y., Guo, C., and Svoboda, K. (2015). Dual-channel circuit mapping reveals sensorimotor convergence in the primary motor cortex. *J. Neurosci.* 35, 4418–4426. doi: 10.1523/jneurosci.3741-14.2015

Hooks, B. M., Mao, T., Gutnisky, D. A., Yamawaki, N., Svoboda, K., and Shepherd, G. M. (2013). Organization of cortical and thalamic input to pyramidal neurons in mouse motor cortex. *J. Neurosci.* 33, 748–760. doi: 10.1523/JNEUROSCI.4338-12.2013

Huber, D., Gutnisky, D. A., Peron, S., O'Connor, D. H., Wiegert, J. S., Tian, L., et al. (2012). Multiple dynamic representations in the motor cortex during sensorimotor learning. *Nature* 484, 473–478. doi: 10.1038/nature11039

Huber, R., Ghilardi, M. F., Massimini, M., Ferrarelli, F., Riedner, B. A., Peterson, M. J., et al. (2006). Arm immobilization causes cortical plastic changes and locally decreases sleep slow wave activity. *Nat. Neurosci.* 9, 1169–1176. doi: 10.1038/nn1758

Huntley, G. W. (1997). Correlation between patterns of horizontal connectivity and the extend of short-term representational plasticity in rat motor cortex. *Cereb. Cortex* 7, 143–156. doi: 10.1093/cercor/7.2.143

Iriki, A., Pavlides, C., Keller, A., and Asanuma, H. (1989). Long-term potentiation in the motor cortex. *Science* 245, 1385–1387. doi: 10.1126/science.2551038

Jabbur, S. J., and Towe, A. L. (1961). Cortical excitation of neurons in dorsal column nuclei of cat, including an analysis of pathways. *J. Neurophysiol.* 24, 499–509. doi: 10.1152/jn.1961.24.5.499

Jebsen, R. H., Taylor, N., Trieschmann, R. B., Trotter, M. J., and Howard, L. A. (1969). An objective and standardized test of hand function. *Arch. Phys. Med. Rehabil.* 50, 311–319.

Jørgensen, H. S., Nakayama, H., Raaschou, H. O., Vive-Larsen, J., Støier, M., and Olsen, T. S. (1995). Outcome and time course of recovery in stroke. Part II: time course of recovery. The copenhagen stroke study. *Arch. Phys. Med. Rehabil.* 76, 406–412. doi: 10.1016/s0003-9993(95)80568-0

Kaas, J. H., Gharbawie, O. A., and Stepniewska, I. (2011). The organization and evolution of dorsal stream multisensory motor pathways in primates. *Front. Neuroanat.* 5:34. doi: 10.3389/fnana.2011.00034

Kalaska, J. F. (1996). Parietal cortex area 5 and visuomotor behavior. *Can. J. Physiol. Pharmacol.* 74, 483–498. doi: 10.1139/y96-040

Kaneko, T., Caria, M. A., and Asanuma, H. (1994a). Information processing within the motor cortex. I. Responses of morphologically identified motor cortical cells to stimulation of the somatosensory cortex. *J. Comp. Neurol.* 345, 161–171. doi: 10.1002/cne.903450202

Kaneko, T., Caria, M. A., and Asanuma, H. (1994b). Information processing within the motor cortex. II. Intracortical connections between neurons receiving somatosensory cortical input and motor output neurons of the cortex. *J. Comp. Neurol.* 345, 172–184. doi: 10.1002/cne.903450203

Karabanov, A., Jin, S. H., Joutsen, A., Poston, B., Aizen, J., Ellenstein, A., et al. (2012). Timing-dependent modulation of the posterior parietal cortex-primary motor cortex pathway by sensorimotor training. *J. Neurophysiol.* 107, 3190–3199. doi: 10.1152/jn.01049.2011

Kaskan, P. M., and Kaas, J. H. (2007). Cortical connections of the middle temporal and the middle temporal crescent visual areas in prosimian galagos (*Otolemur garnetti*). *Anat. Rec.* 290, 349–366. doi: 10.1002/ar.20440

Kida, H., Tsuda, Y., Ito, N., Yamamoto, Y., Owada, Y., Kamiya, Y., et al. (2016). Motor training promotes both synaptic and intrinsic plasticity of layer ii/iii pyramidal neurons in the primary motor cortex. *Cereb. Cortex* 26, 3494–3507. doi: 10.1093/cercor/bhw134

Kim, S. S., Gomez-Ramirez, M., Thakur, P. H., and Hsiao, S. S. (2015). Multimodal interactions between proprioceptive and cutaneous signals in primary somatosensory cortex. *Neuron* 86, 555–566. doi: 10.1016/j.neuron.2015.03.020

Kirsch, E., Rivlis, G., and Schieber, M. H. (2014). Primary motor cortex neurons during individuated finger and wrist movements: correlation of spike firing rates with the motion of individual digits versus their principal components. *Front. Neurol.* 5:70. doi: 10.3389/fneur.2014.00070

Kleim, J. A., Barbay, S., and Nudo, R. J. (1998). Functional reorganization of the rat motor cortex following motor skill learning. *J. Neurophysiol.* 80, 3321–3325. doi: 10.1152/jn.1998.80.6.3321

Kleim, J. A., Chan, S., Pringle, E., Schallert, K., Procaccio, V., Jimenez, R., et al. (2006). BDNF val66met polymorphism is associated with modified experience-dependent plasticity in human motor cortex. *Nat. Neurosci.* 9, 735–737. doi: 10.1038/nn1699

Kleim, J. A., and Jones, T. A. (2008). Principles of experience-dependent neural plasticity: implications for rehabilitation after brain damage. *J. Speech Lang. Hear. Res.* 51, S225–S239. doi: 10.1044/1092-4388(2008/018)

Koch, G., Cercignani, M., Pecchioli, C., Versace, V., Oliveri, M., Caltagirone, C., et al. (2010). *In vivo* definition of parieto-motor connections involved in planning of grasping movements. *Neuroimage* 51, 300–312. doi: 10.1016/j.neuroimage.2010.02.022

Körding, K. P., and Wolpert, D. M. (2004). Bayesian integration in sensorimotor learning. *Nature* 427, 244–247. doi: 10.1038/nature02169

Krakauer, J. W. (2006). Motor learning: its relevance to stroke recovery and neurorehabilitation. *Curr. Opin. Neurol.* 19, 84–90. doi: 10.1097/01.wco.0000200544.29915.cc

Kuehn, E., Dinse, J., Jakobsen, E., Long, X., Schafer, A., Bazin, P. L., et al. (2017). Body topography parcellates human sensory and motor cortex. *Cereb. Cortex* 27, 3790–3805. doi: 10.1093/cercor/bhx026

Kuramoto, E., Furuta, T., Nakamura, K. C., Unzai, T., Hioki, H., and Kaneko, T. (2009). Two types of thalamocortical projections from the motor thalamic nuclei of the rat: a single neuron-tracing study using viral vectors. *Cereb. Cortex* 19, 2065–2077. doi: 10.1093/cercor/bhn231

Kwakkel, G., Kollen, B. J., van der Grond, J., and Prevo, A. J. (2003). Probability of regaining dexterity in the flaccid upper limb: impact of severity of paresis and time since onset in acute stroke. *Stroke* 34, 2181–2186. doi: 10.1161/01.STR.0000087172.16305.CD

Lai, S. M., Studenski, S., Duncan, P. W., and Perera, S. (2002). Persisting consequences of stroke measured by the stroke impact scale. *Stroke* 33, 1840–1844. doi: 10.1161/01.str.0000019289.15440.f2

Lang, C. E., Bland, M. D., Bailey, R. R., Schaefer, S. Y., and Birkenmeier, R. L. (2013). Assessment of upper extremity impairment, function and activity after stroke: foundations for clinical decision making. *J. Hand Ther.* 26, 104–114. doi: 10.1016/j.jht.2012.06.005

Lang, C. E., and Schieber, M. H. (2003). Differential impairment of individuated finger movements in humans after damage to the motor cortex or the corticospinal tract. *J. Neuroinflammation* 90, 1160–1170. doi: 10.1152/jn.00130.2003

Langer, N., Hänggi, J., Müller, N. A., Simmen, H. P., and Jäncke, L. (2012). Effects of limb immobilization on brain plasticity. *Neurology* 78, 182–188. doi: 10.1212/WNL.0b013e31823fcd9c

Lawrence, D. G., and Kuypers, H. G. (1968). The functional organization of the motor system in the monkey. I. The effects of bilateral pyramidal lesions. *Brain* 91, 1–14. doi: 10.1093/brain/91.1.1

Lee, K. B., Lim, S. H., Kim, K. H., Kim, K. J., Kim, Y. R., Chang, W. N., et al. (2015). Six-month functional recovery of stroke patients: a multi-time-point study. *Int. J. Rehabil. Res.* 38, 173–180. doi: 10.1097/MRR.0000000000000108

Lemon, R. N. (2008). Descending pathways in motor control. *Annu. Rev. Neurosci.* 31, 195–218. doi: 10.1146/annurev.neuro.31.060407.125547

Lemon, R. N., Mantel, G. W., and Muir, R. B. (1986). Corticospinal facilitation of hand muscles during voluntary movement in the conscious monkey. *J. Physiol.* 381, 497–527. doi: 10.1113/jphysiol.1986.sp016341

Liang, M., Mouraux, A., and Iannetti, G. D. (2011). Parallel processing of nociceptive and non-nociceptive somatosensory information in the human primary and secondary somatosensory cortices: evidence from dynamic causal modeling of functional magnetic resonance imaging data. *J. Neurosci.* 31, 8976–8985. doi: 10.1523/jneurosci.6207-10.2011

Liao, L. R., Huang, M., Lam, F. M., and Pang, M. Y. (2014). Effects of whole-body vibration therapy on body functions and structures, activity and participation poststroke: a systematic review. *Phys. Ther.* 94, 1232–1251. doi: 10.2522/ptj.20130366

Lin, L. D., Murray, G. M., and Sessle, B. J. (1993). The effect of bilateral cold block of the primate face primary somatosensory cortex on the performance of trained tongue-protrusion task and biting tasks. *J. Neurophysiol.* 70, 985–996. doi: 10.1152/jn.1993.70.3.985

Lincoln, N. B., Jackson, J. M., and Adams, S. A. (1998). Reliability and revision of the nottingham sensory assessment for stroke patients. *Physiotherapy* 84, 358–365. doi: 10.1016/s0031-9406(05)61454-x

Lüscher, C., and Malenka, R. C. (2012). NMDA receptor-dependent long-term potentiation and long-term depression (LTP/LTD). *Cold Spring Harb. Perspect. Biol.* 4:a005710. doi: 10.1101/cshperspect.a005710

Mahan, M. Y., and Georgopoulos, A. P. (2013). Motor directional tuning across brain areas: directional resonance and the role of inhibition for directional accuracy. *Front. Neural. Circuits* 7:92. doi: 10.3389/fncir.2013.00092

Makino, H., Hwang, E. J., Hedrick, N. G., and Komiyama, T. (2016). Circuit mechanisms of sensorimotor learning. *Neuron* 92, 705–721. doi: 10.1016/j.neuron.2016.10.029

Makris, N., Kennedy, D. N., Mcinerney, S., Sorensen, A. G., Wang, R., Caviness, V. S. Jr., et al. (2005). Segmentation of subcomponents within the superior longitudinal fascicle in humans: a quantitative, *in vivo*, DT-MRI study. *Cereb. Cortex* 15, 854–869. doi: 10.1093/cercor/bhh186

Mao, T., Kusefoglu, D., Hooks, B. M., Huber, D., Petreanu, L., and Svoboda, K. (2011). Long-range neuronal circuits underlying the interaction between sensory and motor cortex. *Neuron* 72, 111–123. doi: 10.1016/j.neuron.2011.07.029

Martinez-Lorenzana, G., Machín, R., and Avendaño, C. (2001). Definite segregation of cortical neurons projecting to the dorsal column nuclei in the rat. *Neuroreport* 12, 413–416. doi: 10.1097/00001756-200102120-00044

Mathis, M. W., Mathis, A., and Uchida, N. (2017). Somatosensory cortex plays an essential role in forelimb motor adaptation in mice. *Neuron* 93, 1493.e6–1503.e6. doi: 10.1016/j.neuron.2017.02.049

Meehan, S. K., Dao, E., Linsdell, M. A., and Boyd, L. A. (2011). Continuous theta burst stimulation over the contralesional sensory and motor cortex enhances motor learning post-stroke. *Neurosci. Lett.* 500, 26–30. doi: 10.1016/j.neulet.2011.05.237

Meyer, S., Karttunen, A. H., Thijs, V., Feys, H., and Verheyden, G. (2014). How do somatosensory deficits in the arm and hand relate to upper limb impairment, activity, and participation problems after stroke? A systematic review. *Phys. Ther.* 94, 1220–1231. doi: 10.2522/ptj.20130271

Milliken, G. W., Plautz, E. J., and Nudo, R. J. (2013). Distal forelimb representations in primary motor cortex are redistributed after forelimb restriction: a longitudinal study in adult squirrel monkeys. *J. Neurophysiol.* 109, 1268–1282. doi: 10.1152/jn.00044.2012

Mo, C., and Sherman, S. M. (2019). A sensorimotor pathway via higher-order thalamus. *J. Neurosci.* 39, 692–704. doi: 10.1523/JNEUROSCI.1467-18.2018

Muellbacher, W., Richards, C., Ziemann, U., Wittenberg, G., Weltz, D., Boroojerdi, B., et al. (2002a). Improving hand function in chronic stroke. *Arch. Neurol.* 59, 1278–1282. doi: 10.1001/archneur.59.8.1278

Muellbacher, W., Ziemann, U., Wissel, J., Dang, N., Kofler, M., Facchini, S., et al. (2002b). Early consolidation in human primary motor cortex. *Nature* 415, 640–644. doi: 10.1038/nature712

Mulliken, G. H., Musallam, S., and Andersen, R. A. (2008). Forward estimation of movement state in posterior parietal cortex. *Proc. Natl. Acad. Sci. U S A* 105, 8170–8177. doi: 10.1073/pnas.0802602105

Murphy, T. H., and Corbett, D. (2009). Plasticity during stroke recovery: from synapse to behaviour. *Nat. Rev. Neurosci.* 10, 861–872. doi: 10.1038/nrn2735

Mutha, P. K., Sainburg, R. L., and Haaland, K. Y. (2011). Left parietal regions are critical for adaptive visuomotor control. *J. Neurosci.* 31, 6972–6981. doi: 10.1523/JNEUROSCI.6432-10.2011

Nagy, A., Eördegh, G., Paróczy, Z., Márkus, Z., and Benedek, G. (2006). Multisensory integration in the basal ganglia. *Eur. J. Neurosci.* 24, 917–924. doi: 10.1111/j.1460-9568.2006.04942.x

Nudo, R. J. (2013). Recovery after brain injury: mechanisms and principles. *Front. Hum. Neurosci.* 7:887. doi: 10.3389/fnhum.2013.00887

Nudo, R. J., Friel, K. M., and Delia, S. W. (2000). Role of sensory deficits in motor impairments after injury to primary motor cortex. *Neuropharmacology* 39, 733–742. doi: 10.1016/s0028-3908(99)00254-3

Nudo, R. J., Milliken, G. W., Jenkins, W. M., and Merzenich, M. M. (1996a). Use-dependent alterations of movement representations in primary motor cortex of adult squirrel monkeys. *J. Neurosci.* 16, 785–807. doi: 10.1523/JNEUROSCI.16-02-00785.1996

Nudo, R. J., Wise, B. M., SiFuentes, F., and Milliken, G. W. (1996b). Neural substrates for the effects of rehabilitative training on motor recovery after ischemic infarct. *Science* 272, 1791–1794. doi: 10.1126/science.272.5269.1791

Ohno, S., Kuramoto, E., Furuta, T., Hioki, H., Tanaka, Y. R., Fujiyama, F., et al. (2012). A morphological analysis of thalamocortical axon fibers of rat posterior thalamic nuclei: a single neuron tracing study with viral vectors. *Cereb. Cortex* 22, 2840–2857. doi: 10.1093/cercor/bhr356

Opie, G. M., Evans, A., Ridding, M. C., and Semmler, J. G. (2016). Short-term immobilization influences use-dependent cortical plasticity and fine motor performance. *Neuroscience* 330, 247–256. doi: 10.1016/j.neuroscience.2016.06.002

Ovbiagele, B., Goldstein, L. B., Higashida, R. T., Howard, V. J., Johnston, S. C., Khavjou, O. A., et al. (2013). Forecasting the future of stroke in the United States: a policy statement from the American Heart Association and American Stroke Association. *Stroke* 44, 2361–2375. doi: 10.1161/STR.0b013e318297734f2

Paik, N. J., and Yang, E. (2014). Role of GABA plasticity in stroke recovery. *Neural Regen. Res.* 9, 2026–2028. doi: 10.4103/1673-5374.147920

Papale, A. E., and Hooks, B. M. (2018). Circuit changes in motor cortex during motor skill learning. *Neuroscience* 368, 283–297. doi: 10.1016/j.neuroscience.2017.09.010

Park, Y. J., Park, S. W., and Lee, H. S. (2018). Comparison of the effectiveness of whole body vibration in stroke patients: a meta-analysis. *Biomed. Res. Int.* 2018:5083634. doi: 10.1155/2018/5083634

Pavlides, C., Miyashita, E., and Asanuma, H. (1993). Projection from the sensory to the motor cortex is important in learning motor skills in the monkey. *J. Neurophysiol.* 70, 733–741. doi: 10.1152/jn.1993.70.2.733

Pellegrini-Giampietro, D. E. (2003). The distinct role of mGlu1 receptors in post-ischemic neuronal death. *Trends Pharmacol. Sci.* 24, 461–470. doi: 10.1016/s0165-6147(03)00231-1

Penfield, W., and Boldrey, E. (1937). Somatic motor and sensory representation in thecerebral cortex of man as studied by electrical stimulation. *Brain* 60, 389–443. doi: 10.1093/brain/60.4.389

Plautz, E. J., Milliken, G. W., and Nudo, R. J. (2000). Effects of repetitive motor training on movement representations in adult squirrel monkeys: role of use versus learning. *Neurobiol. Learn. Mem.* 74, 27–55. doi: 10.1006/nlme.1999.3934

Pons, T. P., Garraghty, P. E., Ommaya, A. K., Kaas, J. H., Taub, E., and Mishkin, M. (1991). Massive cortical reorganization after sensory deafferentation in adult macaques. *Science* 252, 1857–1860. doi: 10.1126/science.1843843

Proville, R. D., Spolidoro, M., Guyon, N., Dugué, G. P., Selimi, F., Isope, P., et al. (2014). Cerebellum involvement in cortical sensorimotor circuits for the control of voluntary movements. *Nat. Neurosci.* 17, 1233–1239. doi: 10.1038/nn.3773

Prud'homme, M. J., and Kalaska, J. F. (1994). Proprioceptive activity in primate primary somatosensory cortex during active arm reaching movements. *J. Neurophysiol.* 72, 2280–2301. doi: 10.1152/jn.1994.72.5.2280

Ragert, P., Nierhaus, T., Cohen, L. G., and Villringer, A. (2011). Interhemispheric interactions between the human primary somatosensory cortices. *PLoS One* 6:e16150. doi: 10.1371/journal.pone.0016150

Raghavan, P. (2015). Upper limb motor impairment after stroke. *Phys. Med. Rehabil. Clin. N. Am.* 26, 599–610. doi: 10.1016/j.pmr.2015.06.008

Rathelot, J. A., and Strick, P. L. (2009). Subdivisions of primary motor cortex based on cortico-motoneuronal cells. *Proc. Natl. Acad. Sci. U S A* 106, 918–923. doi: 10.1073/pnas.0808362106

Rathelot, J. A., Dum, R. P., and Strick, P. L. (2017). Posterior parietal cortex contains a command apparatus for hand movements. *Proc. Natl. Acad. Sci. U S A* 114, 4255–4260. doi: 10.1073/pnas.1608132114

Riemann, B. L., Myers, J. B., and Lephart, S. M. (2002). Sensorimotor system measurement techniques. *J. Athl. Train.* 37, 85–98.

Rioult-Pedotti, M. S., Friedman, D., and Donoghue, J. P. (2000). Learning-induced LTP in neocortex. *Science* 290, 533–536. doi: 10.1126/science.290.5491.533

Robertson, E. M. (2004). Skill learning: putting procedural consolidation in context. *Curr. Biol.* 14, R1061–R1063. doi: 10.1016/j.cub.2004.11.048

Rocco-Donovan, M., Ramos, R. L., Giraldo, S., and Brumberg, J. C. (2011). Characteristics of synaptic connections between rodent primary somatosensory and motor cortices. *Somatosens. Mot. Res.* 28, 63–72. doi: 10.3109/08990220.2011.606660

Rosa, M. G., Palmer, S. M., Gamberini, M., Burman, K. J., Yu, H. H., Reser, D. H., et al. (2009). Connections of the dorsomedial visual area: pathways for early integration of dorsal and ventral streams in extrastriate cortex. *J. Neurosci.* 29, 4548–4563. doi: 10.1523/JNEUROSCI.0529-09.2009

Rosenkranz, K., and Rothwell, J. C. (2006). Differences between the effects of three plasticity inducing protocols on the organization of the human motor cortex. *Eur. J. Neurosci.* 23, 822–829. doi: 10.1111/j.1460-9568.2006.04605.x

Rosenkranz, K., and Rothwell, J. C. (2012). Modulation of proprioceptive integration in the motor cortex shapes human motor learning. *J. Neurosci.* 32, 9000–9006. doi: 10.1523/JNEUROSCI.0120-12.2012

Rosenkranz, K., Seibel, J., Kacar, A., and Rothwell, J. (2014). Sensorimotor deprivation induces interdependent changes in excitability and plasticity of the human hand motor cortex. *J. Neurosci.* 34, 7375–7382. doi: 10.1523/JNEUROSCI.5139-13.2014

Rosenzweig, E. S., Brock, J. H., Culbertson, M. D., Lu, P., Moseanko, R., Edgerton, V. R., et al. (2009). Extensive spinal decussation and bilateral termination of cervical corticospinal projections in rhesus monkeys. *J. Comp. Neurol.* 513, 151–163. doi: 10.1002/cne.21940

Sabes, P. N. (2011). Sensory integration for reaching: models of optimality in the context of behavior and the underlying neural circuits. *Prog. Brain Res.* 191, 195–209. doi: 10.1016/B978-0-444-53752-2.00004-7

Sacco, R. L., Kasner, S. E., Broderick, J. P., Caplan, L. R., Connors, J. J., Culebras, A., et al. (2013). An updated definition of stroke for the 21st century: a statement for healthcare professionals from the American Heart Association/American Stroke Association. *Stroke* 44, 2064–2089. doi: 10.1161/STR.0b013e318296aeca

Sakata, H., Taira, M., Murata, A., and Mine, S. (1995). Neural mechanisms of visual guidance of hand action in the parietal cortex of the monkey. *Cereb. Cortex* 5, 429–438. doi: 10.1093/cercor/5.5.429

Sanes, J. N., and Donoghue, J. P. (2000). Plasticity and primary motor cortex. *Annu. Rev. Neurosci.* 23, 393–415. doi: 10.1146/annurev.neuro.23.1.393

Sanes, J. N., Suner, S., Lando, J. F., and Donoghue, J. P. (1988). Rapid reorganization of adult rat motor cortex somatic representation patterns after motor nerve injury. *Proc. Natl. Acad. Sci. U S A* 85, 2003–2007. doi: 10.1073/pnas.85.6.2003

Schieber, M. H. (2011). Dissociating motor cortex from the motor. *J. Physiol.* 589, 5613–5624. doi: 10.1113/jphysiol.2011.215814

Schwartz-Bloom, R. D., and Sah, R. (2001). γ-Aminobutyric acid$_A$ neurotransmission and cerebral ischemia. *J. Neurochem.* 77, 353–371. doi: 10.1046/j.1471-4159.2001.00274.x

Scott, S. H., and Dukelow, S. P. (2011). Potential of robots as next-generation technology for clinical assessment of neurological disorders and upper-limb therapy. *J. Rehabil. Res. Dev.* 48, 335–353. doi: 10.1682/jrrd.2010.04.0057

Seidler, R. D., Kwak, Y., Fling, B. W., and Bernard, J. A. (2013). Neurocognitive mechanisms of error-based motor learning. *Adv. Exp. Med. Biol.* 782, 39–60. doi: 10.1007/978-1-4614-5465-6_3

Semrau, J. A., Herter, T. M., Scott, S. H., and Dukelow, S. P. (2018). Vision of the upper limb fails to compensate for kinesthetic impairments in subacute stroke. *Cortex* 109, 245–259. doi: 10.1016/j.cortex.2018.09.022

Sens, E., Knorr, C., Preul, C., Meissner, W., Witte, O. W., Miltner, W. H., et al. (2013). Differences in somatosensory and motor improvement during temporary functional deafferentation in stroke patients and healthy subjects. *Behav. Brain Res.* 252, 110–116. doi: 10.1016/j.bbr.2013.05.048

Sens, E., Teschner, U., Meissner, W., Preul, C., Huonker, R., Witte, O. W., et al. (2012). Effects of temporary functional deafferentation on the brain, sensation, and behavior of stroke patients. *J. Neurosci.* 32, 11773–11779. doi: 10.1523/JNEUROSCI.5912-11.2012

Shadmehr, R., Smith, M. A., and Krakauer, J. W. (2010). Error correction, sensory prediction, and adaptation in motor control. *Annu. Rev. Neurosci.* 33, 89–108. doi: 10.1146/annurev-neuro-060909-153135

Shmuelof, L., Krakauer, J. W., and Mazzoni, P. (2012). How is a motor skill learned? Change and invariance at the levels of task success and trajectory control. *J. Neurophysiol.* 108, 578–594. doi: 10.1152/jn.00856.2011

Snyder, L. H., Batista, A. P., and Andersen, R. A. (1997). Coding of intention in the posterior parietal cortex. *Nature* 386, 167–170. doi: 10.1038/386167a0

Sober, S. J., and Sabes, P. N. (2003). Multisensory integration during motor planning. *J. Neurosci.* 23, 6982–6992. doi: 10.1523/JNEUROSCI.23-18-06982.2003

Spranger, M. D., Krishnan, A. C., Levy, P. D., O'Leary, D. S., and Smith, S. A. (2015). Blood flow restriction training and the exercise pressor reflex: a call for concern. *Am. J. Physiol. Heart Circ. Physiol.* 309, H1440–H1452. doi: 10.1152/ajpheart.00208.2015

Staines, W. R., Black, S. E., Graham, S. J., and McIlroy, W. E. (2002). Somatosensory gating and recovery from stroke involving the thalamus. *Stroke* 33, 2642–2651. doi: 10.1161/01.str.0000032552.40405.40

Stepniewska, I., Cerkevich, C. M., Fang, P. C., and Kaas, J. H. (2009). Organization of the posterior parietal cortex in galagos: II. Ipsilateral cortical connections of physiologically identified zones within anterior sensorimotor region. *J. Comp. Neurol.* 517, 783–807. doi: 10.1002/cne.22190

Stepniewska, I., Preuss, T. M., and Kaas, J. H. (1993). Architectonics, somatotopic organization, and ipsilateral cortical connections of the primary motor area (M1) of owl monkeys. *J. Comp. Neurol.* 330, 238–271. doi: 10.1002/cne.903300207

Tokimura, H., Di Lazzaro, V., Tokimura, Y., Oliviero, A., Profice, P., Insola, A., et al. (2000). Short latency inhibition of human hand motor cortex by somatosensory input from the hand. *J. Physiol.* 523, 503–513. doi: 10.1111/j.1469-7793.2000.t01-1-00503.x

Viaro, R., Budri, M., Parmiani, P., and Franchi, G. (2014). Adaptive changes in the motor cortex during and after longterm forelimb immobilization in adult rats. *J. Physiol.* 592, 2137–2152. doi: 10.1113/jphysiol.2013.268821

Viganò, L., Fornia, L., Rossi, M., Howells, H., Leonetti, A., Puglisi, G., et al. (2019). Anatomo-functional characterisation of the human "hand-knob": a direct electrophysiological study. *Cortex* 113, 239–254. doi: 10.1016/j.cortex.2018.12.011

von Holst, E., and Mittelstaedt, H. (1950). The reafference principle: interaction between the cnetral nervous system and the periphery. *Die Naturwissenschaften* 37, 464–476. doi: 10.1007/BF00622503

Walcott, B. P., Miller, J. C., Kwon, C. S., Sheth, S. A., Hiller, M., Cronin, C. A., et al. (2014). Outcomes in severe middle cerebral artery ischemic stroke. *Neurocrit. Care* 21, 20–26. doi: 10.1007/s12028-013-9838-x

Whitlock, J. R. (2017). Posterior parietal cortex. *Curr. Biol.* 27, R691–R695. doi: 10.1016/j.cub.2017.06.007

Whitt, J. L., Petrus, E., and Lee, H. K. (2014). Experience-dependent homeostatic synaptic plasticity in neocortex. *Neuropharmacology* 78, 45–54. doi: 10.1016/j.neuropharm.2013.02.016

Winters, C., van Wegen, E. E., Daffertshofer, A., and Kwakkel, G. (2015). Generalizability of the proportional recovery model for the upper extremity after an ischemic stroke. *Neurorehabil. Neural Repair* 29, 614–622. doi: 10.1177/1545968314562115

Wolf, S. L. (2007). Revisiting constraint-induced movement therapy: are we too smitten with the mitten? Is all nonuse "learned"? and other quandaries. *Phys. Ther.* 87, 1212–1223. doi: 10.2522/ptj.20060355

Wolf, S. L., Catlin, P. A., Ellis, M., Archer, A. L., Morgan, B., and Piacentino, A. (2001). Assessing Wolf motor function test as outcome measure for research in patients after stroke. *Stroke* 32, 1635–1639. doi: 10.1161/01.str.32.7.1635

Wolpert, D. M., Goodbody, S. J., and Husain, M. (1998). Maintaining internal representations: the role of the human superior parietal lobe. *Nat. Neurosci.* 1, 529–533. doi: 10.1038/2245

Yamawaki, N., Borges, K., Suter, B. A., Harris, K. D., and Shepherd, G. M. (2014). A genuine layer 4 in motor cortex with prototypical synaptic circuit connectivity. *Elife* 3:e05422. doi: 10.7554/elife.05422

Yao, D., Yamamura, K., Narita, N., Murray, G. M., and Sessle, B. J. (2002). Effects of reversible cold block of face primary somatosensory cortex on orofacial movements and related face primary motor cortex neuronal activity. *Somatosens. Mot. Res.* 19, 261–271. doi: 10.1080/08990220210000037728

Yasuda, T., Fukumura, K., Fukuda, T., Iida, H., Imuta, H., Sato, Y., et al. (2014). Effects of low-intensity, elastic band resistance exercise combined with blood flow restriction on muscle activation. *Scand. J. Med. Sci. Sports* 24, 55–61. doi: 10.1111/j.1600-0838.2012.01489.x

Zaaimi, B., Edgley, S. A., Soteropoulos, D. S., and Baker, S. N. (2012). Changes in descending motor pathway connectivity after corticospinal tract lesion in macaque monkey. *Brain* 135, 2277–2289. doi: 10.1093/brain/aws115

Zeiler, S. R., Hubbard, R., Gibson, E. M., Zheng, T., Ng, K., O'Brien, R., et al. (2016). Paradoxical motor recovery from a first stroke after induction of a second stroke: reopening a postischemic sensitive period. *Neurorehabil. Neural Repair* 30, 794–800. doi: 10.1177/1545968315624783

Ziemann, U., Ilić, T. V., Pauli, C., Meintzschel, F., and Ruge, D. (2004). Learning modifies subsequent induction of long-term potentiation-like and long-term depression-like plasticity in human motor cortex. *J. Neurosci.* 24, 1666–1672. doi: 10.1523/JNEUROSCI.5016-03.2004

Conflict of Interest Statement: The authors declare that the research was conducted in the absence of any commercial or financial relationships that could be construed as a potential conflict of interest.

Copyright © 2019 Edwards, King, Buetefisch and Borich. This is an open-access article distributed under the terms of the Creative Commons Attribution License (CC BY). The use, distribution or reproduction in other forums is permitted, provided the original author(s) and the copyright owner(s) are credited and that the original publication in this journal is cited, in accordance with accepted academic practice. No use, distribution or reproduction is permitted which does not comply with these terms.

frontiers in Human Neuroscience

ORIGINAL RESEARCH
published: 04 June 2019
doi: 10.3389/fnhum.2019.00179

Ecological Momentary Assessment of Head Motion: Toward Normative Data of Head Stabilization

Peter Hausamann[1,2,3,4]*, *Martin Daumer*[1,3], *Paul R. MacNeilage*[4,5] *and Stefan Glasauer*[2,4]

[1] Chair for Data Processing, Department of Electrical and Computer Engineering, Technical University of Munich, Munich, Germany, [2] Chair for Computational Neuroscience, Institute for Medical Technology, Brandenburg University of Technology Cottbus-Senftenberg, Senftenberg, Germany, [3] The Human Motion Institute, Sylvia Lawry Center for Multiple Sclerosis Research e.V., Munich, Germany, [4] Bernstein Center for Computational Neuroscience, Ludwig-Maximilians-Universität München, Munich, Germany, [5] Department of Psychology, University of Nevada, Reno, NV, United States

Head stabilization is fundamental for balance during locomotion but can be impaired in elderly or diseased populations. Previous studies have identified several parameters of head stability with possible diagnostic value in a laboratory setting. Recently, the ecological validity of measures obtained in such controlled contexts has been called into question. The aim of this study was to investigate the ecological validity of previously described parameters of head stabilization in a real-world setting. Ten healthy subjects participated in the study. Head and trunk movements of each subject were recorded with inertial measurement units (IMUs) for a period of at least 10 h. Periods of locomotion were extracted from the measurements and predominant frequencies, root mean squares (RMSs) and bout lengths were estimated. As parameters of head stabilization, attenuation coefficients (ACs), harmonic ratios (HRs), coherences, and phase differences were computed. Predominant frequencies were distributed tightly around 2 Hz and ACs, HRs, and coherences exhibited the highest values in this frequency range. All head stability parameters exhibited characteristics consistent with previous reports, although higher variances were observed. These results suggest that head stabilization is tuned to the 2 Hz fundamental frequency of locomotion and that previously described measures of head stability could generalize to a real-world setting. This is the first study to address the ecological validity of these measures, highlighting the potential use of head stability parameters as diagnostic tools or outcome measures for clinical trials. The low cost and ease of use of the IMU technology used in this study could additionally be of benefit for a clinical application.

Keywords: head stabilization, accelerometry, motion sensors, gait, balance

OPEN ACCESS

Edited by:
Jonathan T. Delafield-Butt, University of Strathclyde, United Kingdom

Reviewed by:
Eric Anson, University of Rochester, United States
Jerome Carriot, McGill University, Canada
Faisal Karmali, Harvard Medical School, United States

***Correspondence:**
Peter Hausamann
peter.hausamann@tum.de

Received: *31 January 2019*
Accepted: *17 May 2019*
Published: *04 June 2019*

Citation:
Hausamann P, Daumer M, MacNeilage PR and Glasauer S (2019) Ecological Momentary Assessment of Head Motion: Toward Normative Data of Head Stabilization. Front. Hum. Neurosci. 13:179. doi: 10.3389/fnhum.2019.00179

1. INTRODUCTION

During locomotion, reflexive head movements operate to minimize horizontal head translation (Cromwell et al., 2001a; Mazzà et al., 2009) and simultaneously compensate for vertical translation by pitching the head (Pozzo et al., 1990; Hirasaki et al., 1999). These stabilization behaviors are thought to be crucial for effective control of both balance and locomotion because they reduce undesired variability of vestibular and visual sensory inputs (Pozzo et al., 1990). In elderly

individuals, head stabilization is compromised during both steady-state walking (Cromwell et al., 2001b) and gait initiation (Laudani et al., 2006; Maslivec et al., 2018). Impaired head stabilization has also been associated with disorders such as Parkinson's disease (PD) (Latt et al., 2009; Buckley et al., 2015), multiple sclerosis (MS) (Psarakis et al., 2018) and bilateral vestibular defects (Pozzo et al., 1991).

Motion capture and accelerometry are widely used in the analysis of head stabilization during human locomotion (Pozzo et al., 1990; Hirasaki et al., 1999; Kavanagh and Menz, 2008). However, studies using motion capture systems are usually constrained to a laboratory setting by design. Similarly, previous studies using wearable sensors have been limited by the need to instruct and supervise subjects and faithfully annotate periods of locomotion. Several recent studies have questioned the ecological validity of measurements obtained in such controlled contexts, i.e., how well these measurements generalize to real world conditions (Stellmann et al., 2015; Brodie et al., 2017). An alternative approach, known as ecological momentary assessment (EMA) (Shiffman et al., 2008), advocates the sampling of clinically relevant parameters in a subject's natural environment rather than a clinical setting.

In support of EMA, researchers have observed that clinical measures such as 10 m walk test times do not significantly correlate with more objective outcomes such as fall risk, raising doubts concerning the clinical relevance of these measures (Brodie et al., 2017). The frequently used 6 min walking test has been challenged by the fact that in many diseased or elderly populations, 6 min of uninterrupted walking rarely occur during daily life (Stellmann et al., 2015). While there are some clinical tests whose results correlate with objective outcomes (such as clinical assessment of gait speed, Albrecht et al., 2001), these examples highlight the need to validate standardized measures in a real-world context.

Wearable accelerometry devices have been suggested for sampling human motion during daily life (Motl et al., 2012) and can be used as a way to assess head stabilization performance in the spirit of EMA. Compared with clinical tests, they provide a cost-effective and straightforward method of recording ecologically valid measures. Previous studies of vestibular stimulation have used these kinds of sensors to address head and whole body motion in more realistic contexts, but were either constrained to pre-defined activities (Carriot et al., 2014, 2017) or lacked measurements of angular velocity (MacDougall, 2005).

In order to assess whether they are indicative of real-life locomotor function, previously established measures of head stability (Hirasaki et al., 1999; Mazzà et al., 2009; Bellanca et al., 2013) need to be evaluated with respect to their ecological validity. Results obtained from a sample of healthy individuals could then be used as a normative baseline for future studies involving populations with balance, gait or neurological disorders.

Therefore, the aims of this study were: (i) to record a dataset of real-world human motion of trunk and head with wearable sensors, (ii) to compute previously described parameters of head stabilization from this data, and (iii) to compare the computed parameters with previous results obtained in controlled environments.

2. MATERIALS AND METHODS

2.1. Subjects

A convenience sample of ten healthy human subjects (five male, five female, age 21–28, most of them students participating in lecture "Clinical Applications of Computational Medicine" at the Technical university of Munich) with no history of balance or gait disorders participated in the experiment. All subjects signed an informed consent form compliant with the European General Data Protection Regulation and gave explicit consent to the publication of the recorded data. The study protocol was approved by the institutional review board of the Sylvia Lawry Center for Multiple Sclerosis Research.

2.2. Sensor Devices

We used a small, self-contained IMU to record both linear acceleration and angular velocity of the human head and trunk. The device (Actigraph GT9X Link) was chosen for its ability to continuously record accelerometer and gyroscope data at a sampling rate of 100 Hz for 24 h. To record head motion, the sensor unit was firmly attached to the inside of a baseball cap that was worn by the subjects. To record trunk motion, an IMU of the same model was attached to a specialized neoprene belt (actibelt flex-belt, Trium Analysis Online GmbH, Munich, Germany) worn at the waist under the clothing. The actibelt system itself is frequently used in clinical accelerometry studies, but was not used in this study because in its current version it is not equipped with a gyroscope.

2.3. Data Acquisition

Subjects were outfitted with the recording equipment in the morning of a typical work/university day and instructed to wear the equipment for at least 10 h. They were instructed to take note of periods during which they took off either sensor unit and these periods were subsequently excluded from analysis. The recording equipment was returned the next morning.

The IMUs were synchronized by knocking both devices against each other at the beginning and the end of each recording. This created clearly visible peaks in the accelerometer measurement that were used to correct timing offsets and drifts between the devices. All subjects performed a calibration routine for both sensor units in order to align the sensor coordinates with head- and trunk-fixed reference frames. For the head device, they first held their heads in a slightly forward-pitched position that aligned Reidâ's plane (MacNeilage and Glasauer, 2017) with an earth-horizontal plane. Afterwards, they nodded their heads five times around the pitch axis. This yields a unique transformation that rotates the acceleration due to gravity to be purely vertical and rotates the angular velocity to be purely around the medial/lateral axis for this calibration routine (resulting in a head-fixed reference frame as shown in **Figure 1A**). A similar routine was performed for the trunk device which was calibrated such that the acceleration due to gravity was purely vertical when the subjects stood up straight.

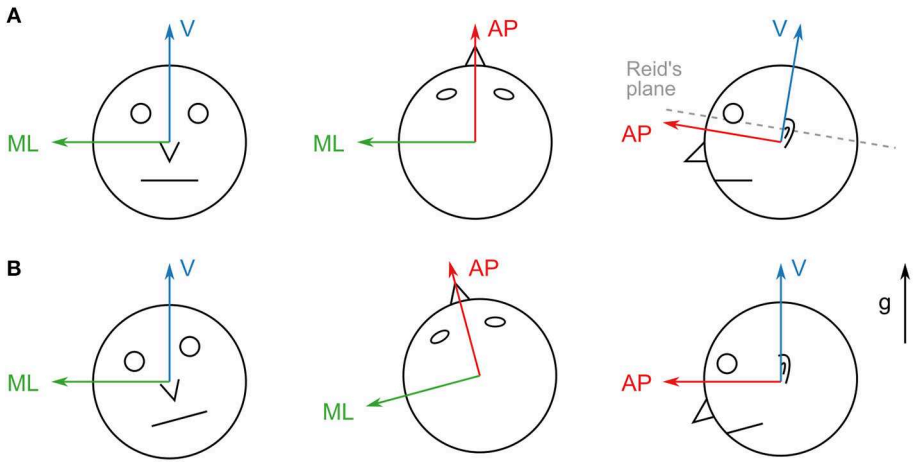

FIGURE 1 | (A) Axes of the head sensor coordinate system. The vertical axis is adjusted to be perpendicular to Reid's plane. This coordinate system remains head-fixed during all translations and rotations. **(B)** Axes of the aligned coordinate system. The vertical axis points in the direction of gravity (g). The system remains world-fixed during roll and pitch rotations (left and right) but remains head-fixed during yaw rotations (middle) and translations.

2.4. Coordinate Frame Transformations

The IMUs used for this study record linear acceleration and angular velocity, but provide no direct information about the orientation of the device in world coordinates. The calibration approach outlined in the previous section yields a head/trunk-fixed coordinate system (**Figure 1A**). However, for comparability with previously reported results obtained in laboratory settings (Hirasaki et al., 1999; Menz et al., 2003; Mazzà et al., 2009) it is necessary to transform the measurements into a frame of reference whose vertical axis remains parallel to the direction of gravity. Reference frames in these studies are defined as right-handed coordinate systems with the vertical axis pointing upwards in the direction of gravity, the anterior/posterior axis pointing in the direction of the subject's motion and the medial/lateral axis pointing to the left of the motion direction (**Figure 1B**).

2.5. Estimation of the Direction of Gravity From IMU Data

Gravitational acceleration g is linked to linear acceleration a and angular velocity through the following equations (Glasauer, 1992):

$$g = a - i \tag{1}$$

$$\frac{\partial g}{\partial t} = \omega \times g \tag{2}$$

where i denotes the inertial acceleration of the device. Various filters are described in the literature that combine the linear acceleration and angular velocity measurements to produce an estimate of orientation. We propose a basic sensor fusion approach (**Table 1**) that we show to be sufficiently accurate for typical trajectories occurring during human locomotion.

The angular velocity was high-passed at 0.1 Hz with a 5th-order Butterworth filter to remove errors due to gyroscope drift. The linear acceleration was low-passed with the same type of filter to reduce the influence of transient accelerations on the estimate. The estimates of orientation and acceleration due to gravity from the filter could then be used to transform the raw acceleration measured by the sensor into net inertial acceleration in aligned coordinates:

$$i_A = rot(q^{-1}, a - g) \tag{3}$$

TABLE 1 | Description of the gravity filter algorithm for estimating gravity direction from IMU data.

Inputs	Linear acceleration in sensor coordinates $a(t)$
	Angular velocity in sensor coordinates $\omega(t)$
	Correction factor α
	Acceleration due to gravity in world coordinates g_W
Outputs	Estimate of acceleration due to gravity in sensor coordinates $g(t)$
	Quaternion representing sensor orientation in aligned coordinates $q(t)$
Description	Start with initial estimate $g(0) = g_W$, for all $t \in 1..T$: 1. Compute estimate of angular displacement: $\phi(t) = \omega(t)\Delta t$ 2. Compute estimate of gravity: $g(t) = \phi(t) \times g(t-1)$ 3. Update estimate with linear acceleration: $g(t) = g(t) + (1-\alpha)a(t)$ 4. Normalize estimate $g(t) = g(t)/\lvert g(t)\rvert$ 5. Compute $q(t)$ as the quaternion transforming $g(t)$ into g_W: a. Normalized axis of rotation: $n = g_W \times g(t)$, $n = n/\lvert n\rvert$ b. Angle of rotation: $= \cos^{-1}(< g_W, g(t) >)$ c. Quaternion from axis-angle representation: $q(t) = R(n, \theta)$

The correction factor $\alpha \in [0, 1]$ determines the weight of ω in the final estimate; an α of 0 means that ω is not used at all, while an α of 1 means that the linear acceleration is ignored. T is the number of samples and Δt is the time difference between two samples, corresponding to 10 ms at a sampling rate of 100 Hz. $< g_W, g(t) >$ denotes the inner product between g_W and $g(t)$ and $R(n, \theta)$ computes the quaternion from the axis-angle representation of the rotation:
$R(n, \theta) = (cos(\theta/2), n_x sin(\theta/2), n_y sin(\theta/2), n_z sin(\theta/2))$.

where $rot(q, v)$ denotes the rotation of the vector v by the quaternion q. It should be noted that step 5 of **Table 1** ensures that the transformation has no yaw rotation component since $q(t)$ is computed from a rotation around the axis n which is always perpendicular to g_W. For consistency with previously reported results (Hirasaki et al., 1999) where translations were described in a world-fixed, but rotations were described in a head/trunk-fixed frame, we did not transform the angular velocity into the aligned coordinate system.

We recorded a short dataset of one subject wearing one IMU attached to a baseball cap on the head. The sensor was mounted facing upwards on a plastic plate equipped with four optical markers for a motion capture system (8 Qualisys Oqus 100 cameras and Qualisys Track Manager software, version 2.9, Qualisys AB, Göteborg, Sweden). The subject performed different locomotor activities (walking, running) as well as spontaneous head movements while sitting for about 8 min. Afterwards, the sensor apparatus was removed from the baseball cap and rapidly swung around, creating high accelerations, and rapid orientation changes of the device for about 1 min. The motion capture data was used as a gold standard for evaluating the accuracy of the orientation estimate as well as finding the optimal parametrization of the algorithm.

We investigated the influence of the low-pass cut-off frequency of the linear acceleration (f_{LP}) as well as the correction factor α on the estimate quality and compared our approach with a previously described complementary filter method (Wetzstein, 2017). The accuracy was measured with the geodesic distance from the estimated quaternion q to the gold standard quaternion q_{GS} (corresponding to the angle of the shortest arc between the two orientations, Huynh, 2009):

$$d = \cos^{-1}\left(2 < q, q_{GS} >^2 -1\right) \tag{4}$$

Both filter algorithms were implemented in Python 3.6 using the just-in-time compilation tools of the `numba` library (version 0.42) to greatly enhance execution speed. Run times were compared on an Intel Core i7-7700K CPU in single-threaded execution at a clock rate of 4.2 GHz. Based on the results of this analysis (see **Supplementary Material**), accelerometer and gyroscope data were transformed to the respective reference frames before further processing.

2.6. Step Detection

In order to isolate periods of locomotion for analysis, we used a step detection method based on the inertial acceleration of the trunk sensor in aligned coordinates. We recorded a dataset of one subject wearing the trunk sensor, performing different locomotor activities at different speeds, including walking, running, stair walking, and cycling. This data was used to parametrize a peak detector for extracting possible steps as well as to determine discriminative features that distinguish cycling from other types of motion.

Peaks were detected in the vertical axis component with a minimum height of 0.2 g, prominence of 0.4 g and distance of 20 ms (corresponding to a maximum detectable step frequency of 5 Hz, Schimpl et al., 2011). For each peak, we computed the short-time power spectrum $S(f)$ of the linear acceleration in all three spatial axes with a segment length of 1,024 samples centered around the peak, weighted with a Blackman window function. The power spectrum was used to determine predominant frequency in each axis, i.e., the frequency with the highest spectral power. We investigated the distribution of RMS vertical accelerations as well as the difference between predominant frequencies in the vertical (V) and medial/lateral (ML) direction and used the results as criteria for the exclusion of cycling periods (see **Supplementary Material**).

The step detection method was applied to the trunk sensor data for each of the 10 subjects. Since we limited our analysis to frequencies above 1 Hz (see results), detected steps were grouped together as bouts if the time difference between two consecutive steps was smaller than 1 s. Bouts of single steps, i.e., where no other steps where detected within 1 s before and afterwards, were subsequently excluded from further analysis.

2.7. Predominant Frequency as a Proxy for Walking Speed

We determined the predominant frequencies of head and trunk accelerations for each step in all three spatial axes using the same short-time power spectrum approach as described above, albeit with a segment length of 512 samples. We used a shorter segment length than in the step detection procedure as it increased the temporal resolution at the expense of frequency resolution, yielding more accurate results for short bouts. We also calculated the magnitude of accelerations using the RMS for each step segment in all three directions. Furthermore, means and standard deviations of trunk predominant frequency in the V direction were calculated for each bout.

In Hirasaki et al. (1999), the authors showed a strong link between walking velocity and predominant frequency of vertical head translation. While we did not validate the exact correspondence for our data, predominant frequency of vertical head acceleration was used as a proxy measure for gait speed, allowing qualitative comparisons between previously published results and ours. In the following, we use the term "predominant frequency" as a shorthand for predominant frequency of vertical head acceleration.

2.8. Assessment of Head Stabilization During Locomotion

2.8.1. Attenuation Coefficient

The reduction of linear accelerations through the upper body was quantified for each step segment using the AC between trunk and head. Segments consisted of 512 samples centered around the peak and were weighted using a Blackman window function in order to decrease the influence of non-locomotor accelerations for short bouts. ACs were calculated in the anterior/posterior (AP), ML, and V directions using the RMS values of head (A_H) and trunk acceleration (A_T) (Mazzà et al., 2009) as:

$$AC = 1 - \frac{A_H}{A_T} \tag{5}$$

Positive values indicate an attenuation of head accelerations with respect to trunk accelerations whereas negative values correspond to increased accelerations at the head when compared to the trunk.

2.8.2. Harmonic Ratio

Regularity and smoothness of motion was quantified using the HR for both head and trunk accelerations. In the AP and V directions, the HR was calculated as the total spectral power of the even harmonics divided by the total spectral power of the odd harmonics of the predominant frequency:

$$HR = \frac{\sum_k^N S\left(2kf_{dom}\right)}{\sum_k^N S\left(2(k+1)f_{dom}\right)} \tag{6}$$

where f_{dom} denotes the predominant frequency of the segment in the respective direction and $N = 10$ is the number of harmonics we considered. Because of the biphasic nature of accelerations within strides (two steps), high values indicate that acceleration patterns remain in phase across stride cycles and are associated with stable gait (Menz et al., 2003). In the ML direction, the HR was calculated inversely due to the fact that lateral motion is monophasic within one stride (left and right step, Lowry et al., 2012):

$$HR = \frac{\sum_k^N S\left(2(k+1)f_{dom}\right)}{\sum_k^N S\left(2kf_{dom}\right)} \tag{7}$$

2.8.3. Coherence

We quantified head-trunk coordination and compensatory head motion during locomotion using the coherence (Hirasaki et al., 1999):

$$K_{xy}^2(f) = \frac{S_{xy}(f)^2}{S_{xx}(f)S_{yy}(f)} \tag{8}$$

where $S_{xy}(f)$ denotes the cross-power spectrum of signals x and y, $S_{xx}(f)$ is the power spectrum of signal x, and $S_{yy}(f)$ is the power spectrum of signal y. Coherence values were computed between head pitch velocity and vertical head acceleration and between head pitch velocity and trunk pitch velocity.

As the coherence for the power spectrum of a single segment is ill-defined, we used an extended segment length of 1,024 samples centered around every step. Each segment was divided into 5 sub-segments of 512 samples with an overlap of 128 samples. This approach guaranteed a well-defined coherence measure for each segment with the same frequency resolution as in the rest of the experiments.

2.8.4. Phase Difference

As another measure of head stabilization we used the phase difference between two signals x and y (Hirasaki et al., 1999). This was calculated by determining the peak of the cross-correlation between x and y, in segments of 512 samples centered around each detected step. The time-lag of this peak was then transformed into a phase difference by dividing by the period length of signal x, estimated via auto-correlation. Phases differences were calculated between vertical head acceleration and head pitch velocity and between vertical head acceleration and trunk pitch velocity.

Since we computed phases differences between acceleration and pitch velocity, we corrected the resulting differences to be comparable with previously reported results that compared vertical displacement and pitch angle (Hirasaki et al., 1999). Pitch angle is obtained from pitch velocity by integrating once (taking into account some initial value) and translation is obtained from acceleration by integrating twice. Since the integration of a sinusoidal signal introduces a phase shift of $-\frac{\pi}{2}$, the overall phase correction for the difference is $2\left(-\frac{\pi}{2}\right) - \left(-\frac{\pi}{2}\right) = -\frac{\pi}{2}$.

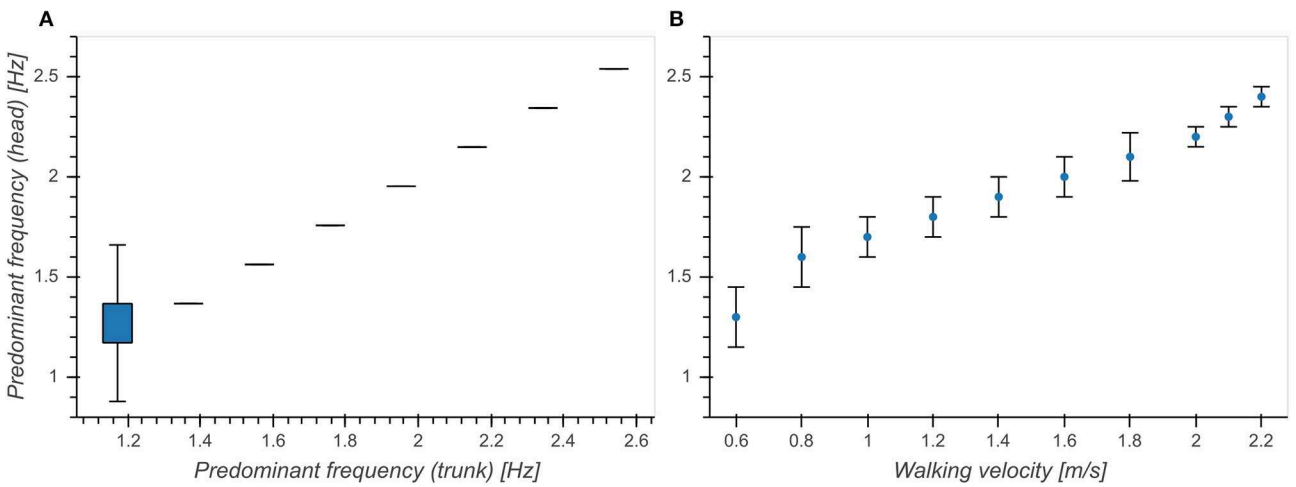

FIGURE 2 | Relationship between predominant frequency of vertical head acceleration and **(A)** predominant frequency of vertical trunk acceleration. **(B)** walking velocity (Figure 8B from Hirasaki et al., 1999). Boxes above 1.2 Hz in **(A)** are not visible because all of the samples between the first and third quartile had the same value.

2.9. Statistical Analysis

The influence of the predominant frequency on the calculated measures was estimated with a Kruskal-Wallis test by calculating an effect size as follows (Tomczak and Tomczak, 2014):

$$\eta^2 = \frac{H - k + 1}{n - k} \tag{9}$$

where H is the Kruskal-Wallis statistic, k is the number of predominant frequency groups and n is the number of samples. Effect sizes were considered small for $\eta^2 < 0.04$, intermediate for $0.04 < \eta^2 < 0.11$ and large for $\eta^2 > 0.11$ (Cohen, 1988). For pairwise comparisons between independent samples (e.g., between previously reported results and ours), Welch's two-sample t-test was used. Pairwise comparisons between dependent samples (e.g., between different spatial directions) were performed with a paired t-test. For each test, we reported p-values and considered results to be significant if $p < 0.01$. However, since this was an exploratory study, statistical power of these tests might be limited.

Statistical analysis was performed with the `stats` module of the `scipy` library (version 1.2.0) in Python 3.6. Results of our analyses were plotted as a function of predominant frequency using boxplots. Boxes indicated the range from the first to the third quartile and the band indicated the median. Whiskers were plotted from the lowest sample within 1.5 times the interquartile range (IQR) of the lower quartile to the highest sample within 1.5 times the IQR of the upper quartile. Due to the large amount of samples, outliers were not plotted. The number of samples was $n = 34455$, the number of steps that fell within the analyzed predominant frequency range (93.74% of all detected steps, see results and **Supplementary Material**).

3. RESULTS

Predominant frequency of vertical trunk acceleration was strongly correlated with predominant frequency of vertical

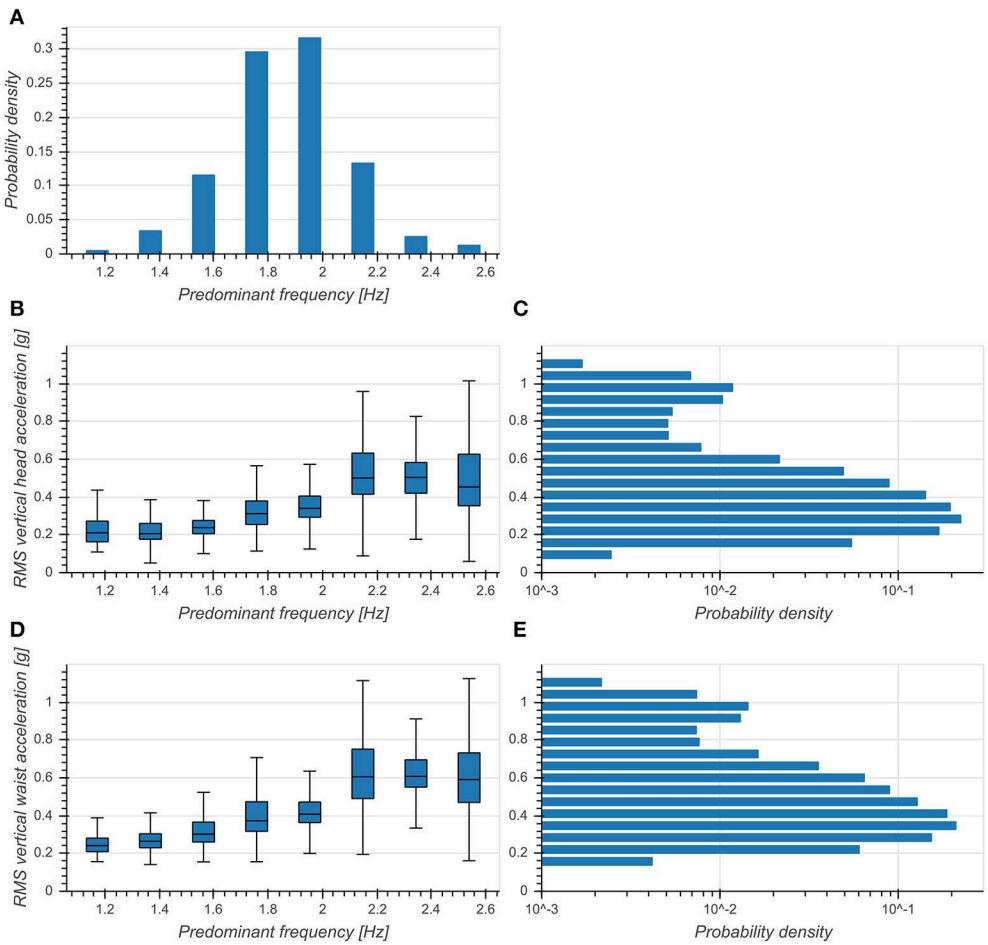

FIGURE 3 | (A) Distribution of predominant frequency of vertical head acceleration. **(B)** Boxplot of RMS vertical head accelerations as a function of predominant frequency. **(C)** Distribution of RMS vertical head accelerations (logarithmic scale). **(D)** Boxplot of RMS vertical trunk accelerations as a function of predominant frequency. **(E)** Distribution of RMS vertical trunk accelerations (logarithmic scale).

head acceleration between 1 and 2.6 Hz ($\eta^2 = 0.887$, $p < 0.001$, **Figure 2A**). **Figure 2B** shows a re-plot of Figure 8B from Hirasaki et al. (1999), showing the relationship between walking velocity and predominant frequency of vertical head acceleration. In order to make our results comparable to previously published results, we limited our analysis to segments with head predominant frequencies between 1 and 2.6 Hz, corresponding to the range of frequencies associated with walking speeds between 0.6 and 2.2 m/s determined in Hirasaki et al. (1999).

Predominant frequency of vertical head acceleration was approximately normally distributed around 1.86 Hz with a standard deviation of 0.23 Hz (**Figure 3A**). RMS vertical accelerations exhibited a distribution skewed toward higher RMS values with a peak at 0.3 g for both head and trunk (**Figures 3C,E**). RMS accelerations increased with predominant frequency for both head ($\eta^2 = 0.375$, $p < 0.001$, **Figure 3B**) and trunk ($\eta^2 = 0.377$, $p < 0.001$, **Figure 5D**) and exhibited broader distributions with higher frequencies. This indicated a strong preference of subjects to move with a fundamental frequency close to 2 Hz and maintaining moderate accelerations of both head and trunk.

Distribution of bout lengths decreased logarithmically with the logarithm of bout length (**Figure 4A**). The effect of bout length on per-bout mean predominant frequencies was small ($\eta^2 = 0.022$, $p < 0.001$), although the median seemed to increase with larger bout lengths and they exhibited broader distributions for shorter bouts (**Figure 4B**). Standard deviations of predominant frequencies showed an intermediate dependence on bout length ($\eta^2 = 0.101$, $p < 0.001$) and exhibited smaller variances above 100 steps (**Figure 4C**). This showed a clear preference of subjects toward walking short bouts while longer bouts seemed to be connected to an increase of predominant frequency and a simultaneous decrease of variability.

The effect of predominant frequency on ACs in V direction was small ($\eta^2 = 0.039$, $p < 0.001$, **Figure 5A**). However, ACs increased with predominant frequency up to 2 Hz and afterwards decreased with higher frequencies in both AP ($\eta^2 = 0.165$, $p < 0.001$) and ML ($\eta^2 = 0.144$, $p < 0.001$) directions (**Figure 5A**). Pairwise comparisons between directions revealed significant differences between each pair of directions ($p < 0.001$), with ACs in V direction being lower than those in AP and ML directions. These differences were especially evident around 2 Hz, corresponding to the frequency range containing the highest number of samples (see also **Figure 3A**). ACs in V and AP direction differed significantly ($p < 0.001$) from those reported by Mazzà et al. (2009), but not in the ML ($p = 0.043$) direction (**Figure 5B**). We found the most substantial difference in the V direction where we observed higher values, indicating that real-world vertical accelerations of the head are more strongly attenuated than previously reported.

The influence of predominant frequency on HRs was small across all directions for both head and trunk ($\eta^2 < 0.04$, $p < 0.001$), although we observed higher standard deviations between 2 and 2.4 Hz, especially in the AP and V directions (**Figures 6A,C**). Distributions differed significantly between each pair of directions ($p < 0.001$). Statistical testing revealed no significant differences between our results and those reported by (Menz et al., 2003) except for the head in the ML direction ($p < 0.001$), but we saw higher standard deviations for all axes and both sensor locations (**Figures 6B,D**). The high values of HRs measured around 2 Hz are an indication of highly regular and stable gait in this frequency range.

There was an intermediate effect of predominant frequency on coherence both between vertical head acceleration and head pitch velocity ($\eta^2 = 0.109$, $p < 0.001$, **Figure 7A**) and between head and trunk pitch velocity ($\eta^2 = 0.084$, $p < 0.001$, **Figure 7C**). We observed an increase of mean coherence value around 2.15

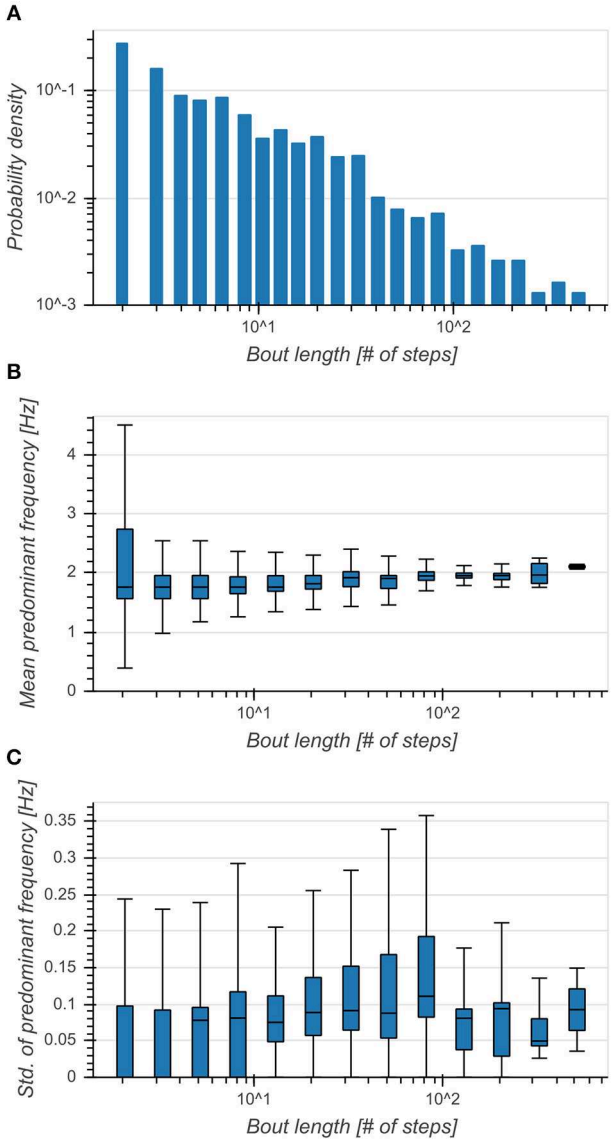

FIGURE 4 | (A) Distribution of bout lengths (logarithmic scale). **(B)** Boxplot of mean predominant frequency for each bout as a function of bout length. Broader distributions indicated a higher variance of predominant frequencies between bouts. **(C)** Boxplot of standard deviation of predominant frequency for each bout as a function of bout length. Higher values indicated a higher variance of predominant frequencies within bouts.

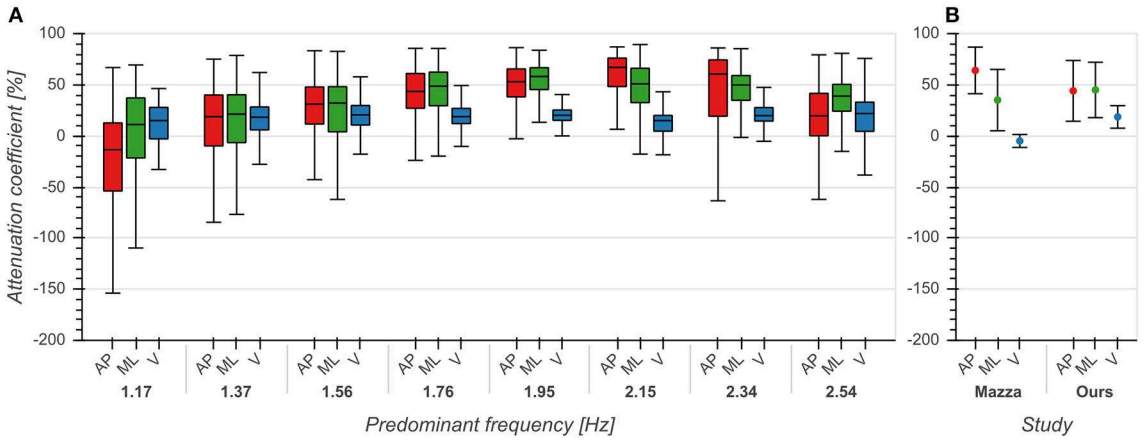

FIGURE 5 | Attenuation coefficients of accelerations between trunk and head in anterior/posterior (AP), medial/lateral (ML) and vertical (V) directions. **(A)** Attenuation coefficients as a function of predominant frequency. **(B)** Comparison between mean +/– std attenuation coefficients from Mazzà et al. (2009) and our data. Means for Mazzà et al. (2009) were computed as the average of the means of the two groups (male, female). Standard deviations were estimated by multiplying the reported standard error of the mean by the square root of the sample size and then computing the square root of the sum of squares of the groups. See also first row of Figure 2 from Mazzà et al. (2009) for comparison .

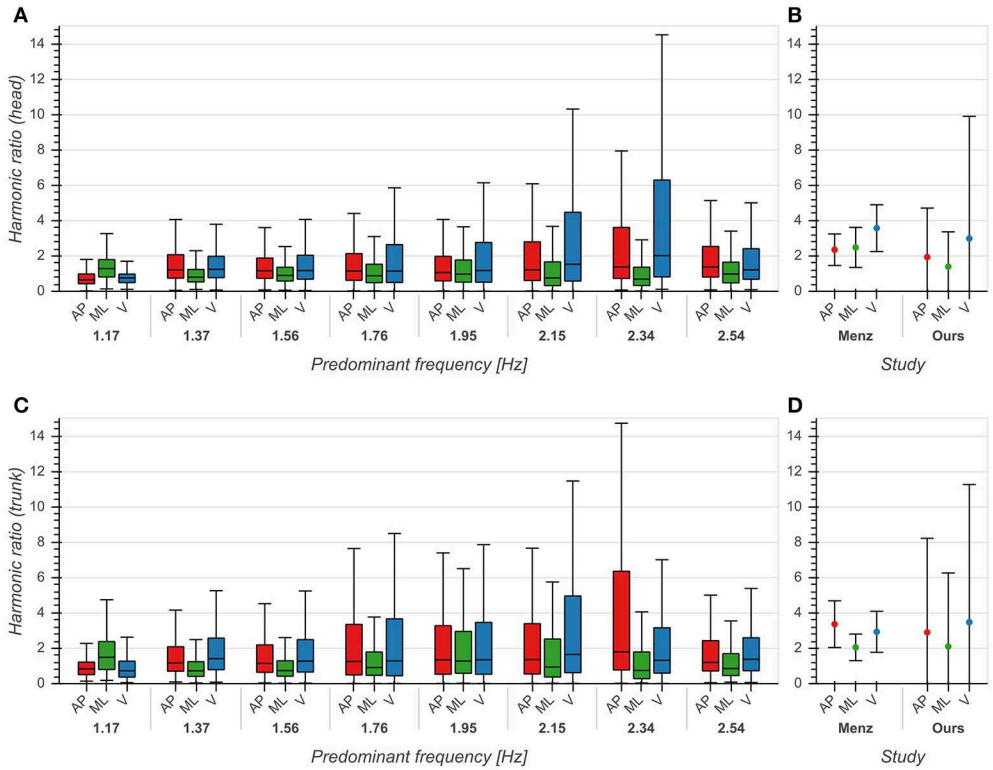

FIGURE 6 | Harmonic ratios of accelerations in anterior/posterior (AP), medial/lateral (ML) and vertical (V) directions. **(A)** Boxplot of harmonic ratios of head accelerations as a function of predominant frequency. **(B)** Comparison between mean ± std harmonic ratios (head) from Menz et al. (2003) and our data. **(C)** Boxplot of harmonic ratios of trunk accelerations as a function of predominant frequency. **(D)** Comparison between mean ± std harmonic ratios (trunk) from Menz et al. (2003) and our data. See also Figure 6 from Menz et al. (2003) for comparison .

Hz as well as a decrease of standard deviation. Coherence values differed significantly between head and trunk in the predominant frequency range from 1.37 to 2.34 Hz. These results are consistent with those reported in Hirasaki et al. (1999) (**Figures 7B,D**), although it should be noted that they obtained values for vertical displacement and pitch angle instead of vertical acceleration and pitch velocity. However, since the coherence measures the similarity between signals at the predominant frequency, a mere

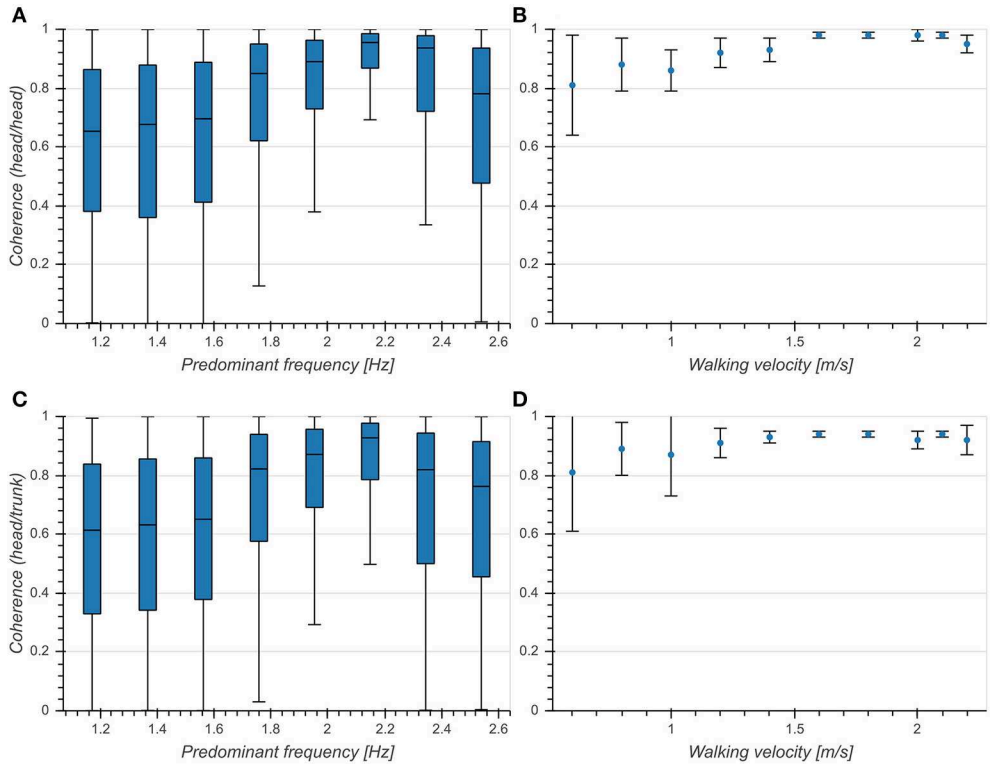

FIGURE 7 | Coherence at predominant frequency. **(A)** Boxplot of coherence between vertical head acceleration and head pitch velocity as a function of predominant frequency. **(B)** Coherence between vertical head displacement and head pitch angle as a function of walking velocity [Figure 9A from Hirasaki et al. (1999)]. **(C)** Boxplot of coherence between head pitch velocity and trunk pitch velocity as a function of predominant frequency. **(D)** Coherence between head pitch angle and trunk pitch angle as a function of walking velocity [Figure 9B from Hirasaki et al. (1999)] .

phase shift as introduced by the integration of a sinusoidal signal component should not alter the value of the coherence function. These results demonstrate a tight coupling between both head pitch and vertical head translation as well as head and trunk pitch around the preferred predominant frequency of 2 Hz.

Predominant frequency had a small effect on phase differences for both head ($\eta^2 = 0.006$, $p < 0.001$, **Figure 8A**) and trunk ($\eta^2 = 0.022$, $p < 0.001$, **Figure 8C**). There was a significant difference between head and trunk for the whole analyzed range of predominant frequencies except for 1.17, 1.37, and 2.15 Hz. While the overall mean phase differences were comparable to those reported in Hirasaki et al. (1999), we did not observe a dependence on predominant frequency (**Figures 8B,D**). This indicates a phase lock between vertical head displacement and head/trunk pitch angle, independent of predominant frequency.

4. DISCUSSION

Due to the limited ecological validity of measurements obtained in a controlled laboratory setting (Motl et al., 2012; Brodie et al., 2017), there is a need for methods to measure and analyze head stabilization and head-trunk coordination in real-world scenarios. For clinical applications, it is first necessary to obtain normative data from healthy individuals as a baseline for possible diagnostic use. In this study, we measured head and trunk motion in an ecologically valid context and calculated several derivative measures of head stabilization performance. These measures were chosen based on those reported in the literature, and they evaluate horizontal head stabilization as well as head motion that compensates for vertical translation. Overall, our measures based on real-world accelerometry data agree quite well with similar measures derived from laboratory-based data, suggesting that these methods for quantifying head stabilization performance could generalize. However, we noticed some important differences and in general we observed larger variances in the distribution of these measures.

Predominant frequencies of motion were tightly coupled between trunk and head (**Figure 2**) and exhibited a narrow distribution around 2 Hz (**Figure 3**). Incidence of bout lengths decreased strongly toward longer bouts, but means and standard deviations of predominant frequencies did not strongly depend on bout length, showing only a small increase of means and simultaneous decrease of standard deviations toward longer bouts (**Figure 4**). These findings seem to confirm previous reports (MacDougall, 2005) which identified 2 Hz as the fundamental frequency of human locomotion across a wide range of activities. The observed changes in predominant frequency distribution as a function of bout length indicate a tendency of subjects toward more goal-directed and stable walking for

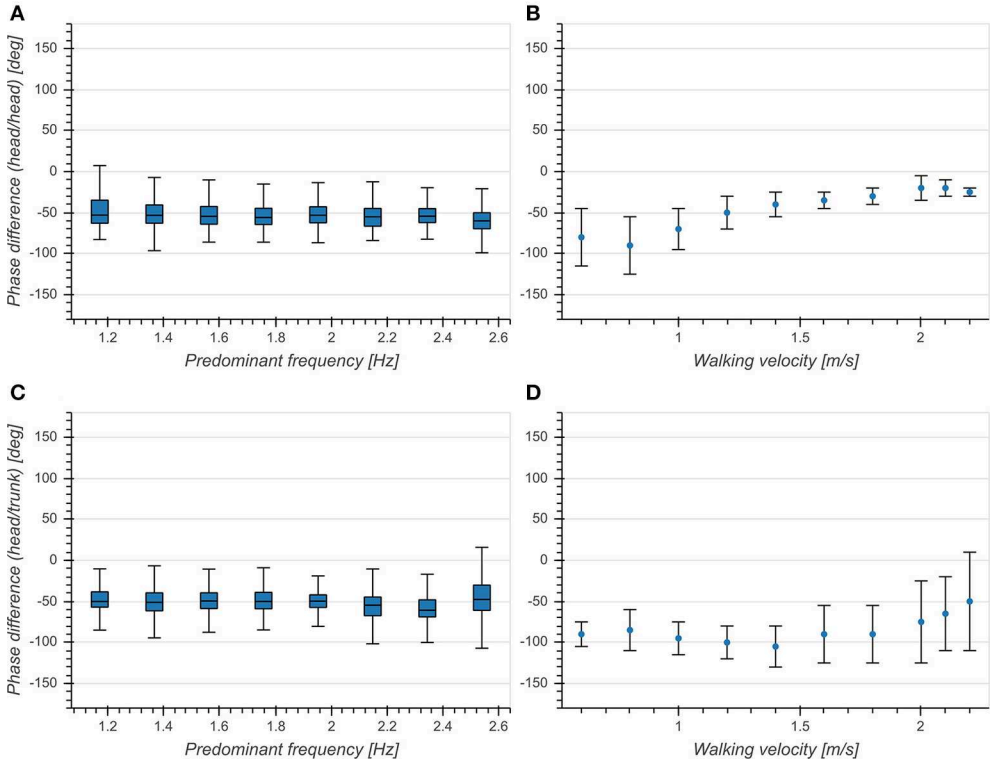

FIGURE 8 | (A) Boxplot of corrected phase difference between vertical head acceleration and head pitch velocity as a function of predominant frequency. **(B)** Phase difference between vertical head displacement and head pitch angle as a function of walking velocity [Figure 5C from Hirasaki et al. (1999)]. **(C)** Boxplot of corrected phase difference between vertical head acceleration and trunk pitch velocity as a function of predominant frequency. **(D)** Phase difference between vertical head displacement and trunk pitch angle as a function of walking velocity [Figure 5B from Hirasaki et al. (1999)].

longer distances. However, the observed differences for short bouts could also have other causes: On the one hand, these bouts could consist of false positive steps detected during cycling. With a larger annotated dataset it should be possible to develop a more refined step detection approach, possibly involving machine learning techniques or GPS data. Special care needs to be taken in order to faithfully detect slow or asymmetric gaits if the goal is to develop a diagnostic tool. On the other hand, it is possible that this in an artifact of the spectral analysis used for determining predominant frequency, which analyses segments of 5 s length in order to achieve the desirable frequency resolution. This choice arguably influenced the analysis of very short bouts as non-locomotion data was included in the transform window. Yet, for the analysis of elderly people and pathological gaits, short bouts are of paramount importance, as they make up most of the daily walking activity (Schimpl et al., 2011). Special frequency analysis techniques for non-stationary data such as the empirical mode decomposition Huang et al., 1998 could help circumvent this issue.

Attenuation of accelerations from trunk to head was stronger in AP and ML directions than in the V direction (**Figure 5**), consistent with previous reports (Kavanagh et al., 2005; Mazzà et al., 2009). The reason for this is that the kinematic chain of the upper body aims at minimizing horizontal accelerations in order to stabilize the head in space. Compared with the results of Mazzà et al. (2009) we observed stronger attenuation in the V direction; this could be due to characteristics of our uncontrolled environment such as inclusion of stair walking. Buckley et al. (2015) observed that attenuation of accelerations in the ML direction was significantly lower in patients with Parkinson's disease when compared with healthy controls. This deterioration in patients seems to indicate that attenuation of lateral accelerations is due to active stabilization and not simply biomechanical constraints of the head-trunk chain. Attenuation strengths in AP and ML directions also showed a dependence on predominant frequency, exhibiting the highest values around 2 Hz. To the best of our knowledge, this is the first time that ACs were characterized as a function of predominant frequency. These results suggest that the attenuation of horizontal head accelerations is tuned to the fundamental frequency of locomotion and that the quantification of this attenuation could be used as an ecologically valid objective measure of head stability.

Regularity of motion as measured by the HR was consistent with previous reports (Menz et al., 2003), although we found higher variances in all directions of motion (**Figure 6**). This could be explained by the fact that a significant effect of environmental factors such as walking on uneven surfaces (Menz et al., 2003) or unilateral limb loading (Bellanca et al., 2013) on the measured HRs has been observed. Previous studies found significantly

lower HRs at both trunk and head between patients with MS (Psarakis et al., 2018) or PD (Latt et al., 2009; Lowry et al., 2009) and healthy controls, although there have been differing reports in the case of PD (Buckley et al., 2015). We observed an increase in HRs with predominant frequencies above 2 Hz, most prominently in the AP and V directions, in accordance with earlier reports (Menz et al., 2003). Based on these findings, we conclude that the HR might be a suitable measure of head stabilization in a real-world context.

The similarity between vertical head acceleration and head pitch and between head pitch and trunk pitch as measured by the coherence was maximal at predominant frequencies around 2.2 Hz (**Figure 7**). This is in line with previous reports (Hirasaki et al., 1999) which observed the highest coherence values at walking speeds above the most common gait velocity of 1.4 m/s. Compared to their results, we measured lower means and higher standard deviations of coherence values across the entire range of analyzed predominant frequencies. These differences can be explained by the fact that Hirasaki et al., 1999 analyzed steady-state walking on a treadmill with a target for gaze fixation. High coherences are associated with compensatory head motion aimed at maintaining gaze stability (Hirasaki et al., 1999). In a real-world setting, often characterized by intermittent walking and frequent gaze shifts, it is not surprising that overall lower coherence values are observed. Lower coherences have also been linked to vestibular deficits (Pozzo et al., 1991), suggesting a possible applicability of this measure in a clinical context.

Phase differences between vertical head acceleration and head/trunk pitch were distributed around -50° across the entire analyzed range of predominant frequencies (**Figure 8**). This is partly consistent with previous studies (Hirasaki et al., 1999), however these studies reported an effect of walking velocity on the phase difference which we did not observe. Similar to the coherence, we hypothesize that the observed differences are due to our measurement scenario lacking a target for gaze fixation. We are not aware of any studies investigating phase differences of subjects with gait, balance or neurological disorders.

With the exception of phase differences, all analyzed metrics indicated strongest head stabilization around 2 Hz, corresponding to the preferred walking speed of the participants. We also observed the lowest variances of these measures in this range, in line with previous reports by Wuehr et al. (2013) who showed that coefficients of variation of gait parameters such as stride time and stride length are lowest at self-selected walking speeds. Additionally, they measured higher variances in patients with cerebellar ataxia, especially outside of the range of preferred speeds, raising the question whether similar effects could occur for parameters of head stability.

Another disorder characterized by movement deficits is autism spectrum disorder (ASD) (Trevarthen and Delafield-Butt, 2013). Children diagnosed with ASD exhibit atypical motor patterns that can be identified using machine learning techniques with great accuracy (Anzulewicz et al., 2016). Computer-vision based tracking of head motion revealed that magnitude and velocity of head turning as well as velocity of head inclination are greater in children with ASD than in healthy controls (Cassell et al., 2018). This difference was especially evident when subjects watched video of social stimuli. Therefore, assessment of head motion during real-world social interactions could be a valuable tool for ASD diagnosis and research.

It should be noted that the size and makeup of our sample of participants is a possible source for bias. The sample included exclusively young subjects which facilitated comparison with previously reported results. In contrast, a normative dataset for comparison with diseased populations will likely have to include older subjects. A longer measurement period (at least one week) could also be helpful in increasing the significance of findings. Furthermore, neither the gravity estimation nor the step detection algorithm have been independently validated and we did not control for movement of the sensors relative to head or trunk. However, all analyses performed in the aligned coordinate system are largely robust to small shifts in sensor position. The other concerns can be addressed in the study design of future studies.

In conclusion, we have shown that several previously described head stability parameters, when measured in an ecologically valid context, exhibited characteristics similar to those obtained in a laboratory setting. We have also characterized these parameters in function of predominant frequency as a proxy for walking speed (**Figures 5–8**). Nevertheless, we found some critical differences that could be attributed to features unique to the real-world context. Real-world measurements of attenuation coefficients were comparable to those previously obtained in a laboratory setting (Mazzà et al., 2009), as were measurements of harmonic ratios (Menz et al., 2003). We could also replicate previously reported characteristics of coherences and phase differences (Hirasaki et al., 1999). Most of these measures have been shown to have value for diagnostic purposes or as endpoints for clinical trials. Our results indicate that the evaluated parameters are largely robust to characteristics that are usually absent in a laboratory context, such as frequent and large shifts of gaze and attention, dual tasking or walking with a companion. The data recorded in this study could serve as a model for collecting normative reference data of healthy individuals. Future studies will have to address the direct comparison of ecologically valid head stabilization parameters between healthy controls and patients with gait, balance, or neurological disorders. This way, mobile accelerometry could serve as a cheap and easy method to gain clinically relevant insights.

ETHICS STATEMENT

This study was carried out in accordance with the recommendations of the institutional review board of the Sylvia Lawry Center for Multiple Sclerosis Research in accordance with written informed consent from all subjects. All subjects gave written informed consent in accordance with the Declaration of Helsinki and the European General Data Protection Regulation. The protocol was approved by the institutional review board of the Sylvia Lawry Center for Multiple Sclerosis Research.

AUTHOR CONTRIBUTIONS

PH, MD, PM, and SG conceived and designed the experiments, contributed materials and analysis tools, wrote the paper and developed algorithms. PH performed the experiments and analyzed the data.

FUNDING

This work was supported by German Research Foundation (DFG) grant MA 6233/1-1 and Federal Ministry of Education and Research (BMBF) grants 01GQ1004A and 01GQ1004B as well as the DFG and the Technical University of Munich (TUM) in the framework of the Open Access Publishing Program supported under grant code NIH P20GM103650.

ACKNOWLEDGMENTS

The authors would like to thank Alexander Knorr for his help with the motion capture system used for tuning the orientation estimation filter and Marcello Grassi for his help with the statistical analysis and also like to thank the developers and maintainers of several open source Python libraries used for analysis and plotting, namely numpy, pandas, xarray, scipy, and bokeh.

SUPPLEMENTARY MATERIAL

The Supplementary Material for this article can be found online at: https://www.frontiersin.org/articles/10.3389/fnhum.2019.00179/full#supplementary-material

REFERENCES

Albrecht, H., Wötzel, C., Erasmus, L. P., Kleinpeter, M., König, N., and Pöllmann, W. (2001). Day-to-day variability of maximum walking distance in MS patients can mislead to relevant changes in the expanded disability status scale (EDSS): average walking speed is a more constant parameter. *Mult. Scleros.* 7, 105–109. doi: 10.1191/135245801678227621

Anzulewicz, A., Sobota, K., and Delafield-Butt, J. T. (2016). Toward the autism motor signature: gesture patterns during smart tablet gameplay identify children with autism. *Sci. Rep.* 6, 1–13. doi: 10.1038/srep31107

Bellanca, J. L., Lowry, K. A., VanSwearingen, J. M., Brach, J. S., and Redfern, M. S. (2013). Harmonic ratios: a quantification of step to step symmetry. *J. Biomechan.* 46, 828–831. doi: 10.1016/j.jbiomech.2012.12.008

Brodie, M. A., Coppens, M. J., Ejupi, A., Gschwind, Y. J., Annegarn, J., Schoene, D., et al. (2017). Comparison between clinical gait and daily-life gait assessments of fall risk in older people. *Geriat. Gerontol. Int.* 17, 2274–2282. doi: 10.1111/ggi.12979

Buckley, C., Galna, B., Rochester, L., and Mazzà, C. (2015). Attenuation of upper body accelerations during gait: piloting an innovative assessment tool for Parkinson's disease. *BioMed Res. Int.* 2015, 1–6. doi: 10.1155/2015/865873

Carriot, J., Jamali, M., Chacron, M. J., and Cullen, K. E. (2014). Statistics of the vestibular input experienced during natural self-motion: implications for neural processing. *J. Neurosci.* 34, 8347–8357. doi: 10.1523/JNEUROSCI.0692-14.2014

Carriot, J., Jamali, M., Cullen, K. E., and Chacron, M. J. (2017). Envelope statistics of self-motion signals experienced by human subjects during everyday activities: implications for vestibular processing. *PLoS ONE* 12:e0178664. doi: 10.1371/journal.pone.0178664

Cassell, J., Cohn, J. F., Britton, J. C., Martin, K. B., Ren, G., Hammal, Z., et al. (2018). Objective measurement of head movement differences in children with and without autism spectrum disorder. *Mol. Aut.* 9, 1–10. doi: 10.1186/s13229-018-0198-4

Cohen, J. (1988). *Statistical Power Analysis for the Behavioral Sciences, 2nd Edn.* New York, NY: Taylor & Francis Inc. doi: 10.4324/9780203771587

Cromwell, R. L., Newton, R. A., and Carlton, L. G. (2001a). Horizontal plane head stabilization during locomotor tasks. *J. Motor Behav.* 33, 49–58. doi: 10.1080/00222890109601902

Cromwell, R. L., Newton, R. A., and Forrest, G. (2001b). Head stability in older adults during walking with and without visual input. *J. Vestib. Res.* 11, 105–114.

Glasauer, S. (1992). Interaction of semicircular canals and otoliths in the processing structure of the subjective Zenith. *Ann. N. Y. Acad. Sci.* 656, 847–849. doi: 10.1111/j.1749-6632.1992.tb25272.x

Hirasaki, E., Moore, S. T., Raphan, T., and Cohen, B. (1999). Effects of walking velocity on vertical head and body movements during locomotion. *Exp. Brain Res.* 127, 117–130. doi: 10.1007/s002210050781

Huang, N. E., Shen, Z., Long, S. R., Wu, M.-L. C., Snin, H. H., Zheng, Q., et al. (1998). The empirical mode decomposition and the Hilbert spectrum for nonlinear and non-stationary time series analysis. *Proc. R. Soc. A Math. Phys. Eng. Sci.* 454, 903–995. doi: 10.1098/rspa.1998.0193

Huynh, D. Q. (2009). Metrics for 3D rotations: comparison and analysis. *J. Math. Imag. Vision* 35, 155–164. doi: 10.1007/s10851-009-0161-2

Kavanagh, J. J., and Menz, H. B. (2008). Accelerometry: a technique for quantifying movement patterns during walking. *Gait Post.* 28, 1–15. doi: 10.1016/j.gaitpost.2007.10.010

Kavanagh, J. J., Morrison, S., and Barrett, R. S. (2005). Coordination of head and trunk accelerations during walking. *Eur. J. Appl. Phys.* 94, 468–475. doi: 10.1007/s00421-005-1328-1

Latt, M. D., Menz, H. B., Fung, V. S., and Lord, S. R. (2009). Acceleration patterns of the head and pelvis during gait in older people with Parkinson's disease: a comparison of fallers and nonfallers. *J. Gerontol. Ser. A Biol. Sci. Med. Sci.* 64, 700–706. doi: 10.1093/gerona/glp009

Laudani, L., Casabona, A., Perciavalle, V., and Macaluso, A. (2006). Control of head stability during gait initiation in young and older women. *J. Electromyogr. Kinesiol.* 16, 603–610. doi: 10.1016/j.jelekin.2006.08.001

Lowry, K. A., Lokenvitz, N., and Smiley-Oyen, A. L. (2012). Age- and speed-related differences in harmonic ratios during walking. *Gait Post.* 35, 272–276. doi: 10.1016/j.gaitpost.2011.09.019

Lowry, K. A., Smiley-Oyen, A. L., Carrel, A. J., and Kerr, J. P. (2009). Walking stability using harmonic ratios in Parkinson's disease. *Move. Disorder.* 24, 261–267. doi: 10.1002/mds.22352

MacDougall, H. G. (2005). Marching to the beat of the same drummer: the spontaneous tempo of human locomotion. *J. Appl. Physiol.* 99, 1164–1173. doi: 10.1152/japplphysiol.00138.2005

MacNeilage, P. R., and Glasauer, S. (2017). Quantification of head movement predictability and implications for suppression of vestibular input during locomotion. *Front. Comput. Neurosci.* 11:47. doi: 10.3389/fncom.2017.00047

Maslivec, A., Bampouras, T. M., Dewhurst, S., Vannozzi, G., Macaluso, A., and Laudani, L. (2018). Mechanisms of head stability during gait initiation in young and older women: a neuro-mechanical analysis. *J. Electromyogr. Kinesiol.* 38, 103–110. doi: 10.1016/j.jelekin.2017.11.010

Mazzà, C., Iosa, M., Picerno, P., and Cappozzo, A. (2009). Gender differences in the control of the upper body accelerations during level walking. *Gait Post.* 29, 300–303. doi: 10.1016/j.gaitpost.2008.09.013

Menz, H. B., Lord, S. R., and Fitzpatrick, R. C. (2003). Acceleration patterns of the head and pelvis when walking on level and irregular surfaces. *Gait Post.* 18, 35–46. doi: 10.1016/S0966-6362(02)00159-5

Motl, R. W., Sandroff, B. M., and Sosnoff, J. J. (2012). Commercially available accelerometry as an ecologically valid measure of ambulation in

individuals with multiple sclerosis. *Exp. Rev. Neurotherapeut.* 12, 1079–1088. doi: 10.1586/ern.12.74

Pozzo, T., Berthoz, A., and Lefort, L. (1990). Head stabilization during various locomotor tasks in humans. I. Normal subjects. *Exp. Brain Res.* 82, 97–106.

Pozzo, T., Berthoz, A., Lefort, L., and Vitte, E. (1991). Head stabilization during various locomotor tasks in humans. II. Patients with bilateral peripheral vestibular deficits. *Exp. Brain Res.* 85, 208–17.

Psarakis, M., Greene, D. A., Cole, M. H., Lord, S. R., Hoang, P., and Brodie, M. (2018). Wearable technology reveals gait compensations, unstable walking patterns and fatigue in people with multiple sclerosis. *Physiol. Measure.* 39:075004. doi: 10.1088/1361-6579/aac0a3

Schimpl, M., Moore, C., Lederer, C., Neuhaus, A., Sambrook, J., Danesh, J., et al. (2011). Association between walking speed and age in healthy, free-living individuals using mobile accelerometry-a cross-sectional study. *PLoS ONE* 6:e23299. doi: 10.1371/journal.pone.0023299

Shiffman, S., Stone, A. A., and Hufford, M. R. (2008). Ecological momentary assessment. *Ann. Rev. Clin. Psychol.* 4, 1–32. doi: 10.1146/annurev.clinpsy.3.022806.091415

Stellmann, J. P., Neuhaus, A., Götze, N., Briken, S., Lederer, C., Schimpl, M., et al. (2015). Ecological validity of walking capacity tests in multiple sclerosis. *PLoS ONE* 10:e123822. doi: 10.1371/journal.pone.0123822

Tomczak, M., and Tomczak, E. (2014). The need to report effect size estimates revisited. An overview of some recommended measures of effect size. *Trends Sport Sci.* 1, 19–25.

Trevarthen, C., and Delafield-Butt, J. T. (2013). Autism as a developmental disorder in intentional movement and affective engagement. *Front. Int. Neurosci.* 7:49. doi: 10.3389/fnint.2013.00049

Wetzstein, G. (2017). *EE 267 Virtual Reality Course Notes : Orientation Tracking with IMUs*. Technical Report 2, Stanford University, California.

Wuehr, M., Schniepp, R., Ilmberger, J., Brandt, T., and Jahn, K. (2013). Speed-dependent temporospatial gait variability and long-range correlations in cerebellar ataxia. *Gait Post.* 37, 214–218. doi: 10.1016/j.gaitpost.2012.07.003

Conflict of Interest Statement: MD is the Director of the Sylvia Lawry Center for MS Research. He is managing director of Trium Analysis Online GmbH (50 % ownership). Trium is a manufacturer of CTG monitoring systems. He is an Academic Editor for PeerJ and has invented the "free heel running pad."

MD has served on the scientific advisory board for the EPOSA study; has received funding for travel from ECTRIMS; serves on the editorial board of MedNous; is co-author with Michael Scholz on patents re: Apparatus for measuring activity (Trium Analysis Online GmbH), method and device for detecting a movement pattern (Trium Analysis Online GmbH), device and method to measure the activity of a person (Trium Analysis Online GmbH), co-author with Christian Lederer of device and method to determine the fetal heart rate from ultrasound signals (Trium Analysis Online GmbH), author of method and device for detecting drifts, jumps and/or outliers of measurement values, coauthor of patent applications with Michael Scholz of device and method to determine the global alarm state of a patient monitoring system, method of communication of units in a patient monitoring system, and system and method for patient monitoring; serves as a consultant for University of Oxford, Imperial College London, University of Southampton, Charité Berlin, University of Vienna, Greencoat Ltd, Biopartners, Biogen Idec, Bayer Schering Pharma, Roche, and Novartis; and receives/has received research support from the EU-FP7, BMBF, BWiMi, and Hertie Foundation.

PH is an employee of the Sylvia Lawry Centre for MS Research.

The remaining authors declare that the research was conducted in the absence of any commercial or financial relationships that could be construed as a potential conflict of interest.

Copyright © 2019 Hausamann, Daumer, MacNeilage and Glasauer. This is an open-access article distributed under the terms of the Creative Commons Attribution License (CC BY). The use, distribution or reproduction in other forums is permitted, provided the original author(s) and the copyright owner(s) are credited and that the original publication in this journal is cited, in accordance with accepted academic practice. No use, distribution or reproduction is permitted which does not comply with these terms.

frontiers in Integrative Neuroscience

REVIEW
published: 18 July 2019
doi: 10.3389/fnint.2019.00027

Sensory Modulation Disorder (SMD) and Pain: A New Perspective

Tami Bar-Shalita[1,2†], *Yelena Granovsky*[3†], *Shula Parush*[4] *and Irit Weissman-Fogel*[5*†]

[1]Department of Occupational Therapy, School of Health Professions, Sackler Faculty of Medicine, Tel Aviv University, Tel Aviv, Israel, [2]Sagol School of Neuroscience, Tel Aviv University, Tel Aviv, Israel, [3]Laboratory of Clinical Neurophysiology, Department of Neurology, Faculty of Medicine, Technion—Israel Institute of Technology, Rambam Health Care Campus, Haifa, Israel, [4]School of Occupational Therapy, Faculty of Medicine of Hadassah, Hebrew University of Jerusalem, Jerusalem, Israel, [5]Physical Therapy Department, Faculty of Social Welfare and Health Sciences, University of Haifa, Haifa, Israel

Sensory modulation disorder (SMD) affects sensory processing across single or multiple sensory systems. The sensory over-responsivity (SOR) subtype of SMD is manifested clinically as a condition in which non-painful stimuli are perceived as abnormally irritating, unpleasant, or even painful. Moreover, SOR interferes with participation in daily routines and activities (Dunn, 2007; Bar-Shalita et al., 2008; Chien et al., 2016), co-occurs with daily pain hyper-sensitivity, and reduces quality of life due to bodily pain. Laboratory behavioral studies have confirmed abnormal pain perception, as demonstrated by hyperalgesia and an enhanced lingering painful sensation, in children and adults with SMD. Advanced quantitative sensory testing (QST) has revealed the mechanisms of altered pain processing in SOR whereby despite the existence of normal peripheral sensory processing, there is enhanced facilitation of pain-transmitting pathways along with preserved but delayed inhibitory pain modulation. These findings point to central nervous system (CNS) involvement as the underlying mechanism of pain hypersensitivity in SOR. Based on the mutual central processing of both non-painful and painful sensory stimuli, we suggest shared mechanisms such as cortical hyper-excitation, an excitatory-inhibitory neuronal imbalance, and sensory modulation alterations. This is supported by novel findings indicating that SOR is a risk factor and comorbidity of chronic non-neuropathic pain disorders. This is the first review to summarize current empirical knowledge investigating SMD and pain, a sensory modality not yet part of the official SMD realm. We propose a neurophysiological mechanism-based model for the interrelation between pain and SMD. Embracing the pain domain could significantly contribute to the understanding of this condition's pathogenesis and how it manifests in daily life, as well as suggesting the basis for future potential mechanism-based therapies.

Keywords: sensory modulation disorder (SMD), pain perception and modulation, sensory over-responsivity (SOR), excitatory/inhibitory imbalance, sensory systems

OPEN ACCESS

Edited by:
Elizabeth B. Torres, Rutgers University, The State University of New Jersey, United States

Reviewed by:
Anthony H. Dickenson, Independent Researcher, London, United Kingdom
Guilherme Lucas, University of São Paulo, Brazil

***Correspondence:**
Irit Weissman-Fogel
ifogel@univ.haifa.ac.il

†These authors have contributed equally to this work

***Received:** 08 March 2019*
***Accepted:** 01 July 2019*
***Published:** 18 July 2019*

Citation:
Bar-Shalita T, Granovsky Y, Parush S and Weissman-Fogel I (2019) Sensory Modulation Disorder (SMD) and Pain: A New Perspective. Front. Integr. Neurosci. 13:27. doi: 10.3389/fnint.2019.00027

A PRO-NOCICEPTIVE STATE IN SENSORY MODULATION DISORDER (SMD)

Tactile over-responsiveness was characterized some decades ago as consisting of defensive-protective behaviors which are accompanied by stress responses to nociceptive qualities of sensory stimuli (Ayres, 1972; Fisher and Dunn, 1983). Specifically, non-painful sensory stimuli are often experienced by individuals with this disorder as aversive, bothersome (Kinnealey et al., 1995) and lingering (Miller et al., 2007). Despite these reports, the pain sensory system has been neglected in both the Sensory modulation disorder (SMD) clinical and research domains. Interestingly, *allodynia*, a clinical term not implying a mechanism, refers to pain due to a stimulus that does not normally provoke pain [International Association of the Study of Pain (IASP), 2017]. Consequently, allodynia represents a condition where the response mode differs from the stimulus mode [International Association of the Study of Pain (IASP), 2017], the latter of which may be induced by various non-painful stimuli such as light touch, cool or warm stimuli (Price, 1994; Zeilhofer, 2008). Therefore, we suggest allodynia to mirror sensory over-responsivity (SOR), a subtype of SMD, by perceiving non-painful sensations as irritating, unpleasant or painful (Miller et al., 2007). According to the International Association for the Study of Pain [International Association of the Study of Pain (IASP), 2017], pain is "an unpleasant sensory and emotional experience associated with actual or potential tissue damage or described in terms of such damage." This definition of pain has led our research efforts for the past decade, where we have endeavored to further our understanding of the SOR phenomenon, by studying its phenotype as well as its underlying mechanisms.

Pain and other sensory systems are measured in the laboratory setting by performing quantitative sensory testing (QST), a standardized method to test for and characterize sensory sensitivity. QST measures the perceived intensity of a given stimulus (i.e., the subjective experience) while controlling the intensity of the stimulus (Dyck et al., 1993; McGrath and Brown, 2006; Hansson et al., 2007; Arendt-Nielsen and Yarnitsky, 2009). Moreover, it is used to indirectly evaluate the underlying sensory functioning by testing a spectrum of peripheral nerve system functions, as well as revealing abnormalities related to disorders of the central nervous system (CNS; Bartlett et al., 1998; Hagander et al., 2000; Arendt-Nielsen and Yarnitsky, 2009). Previous studies in our lab have used QST to evaluate somatosensory *detection thresholds* [i.e., the minimum intensity levels at which 50% of stimuli are recognized; International Association of the Study of Pain (IASP), 2017], including those of light touch, vibration, warm and cool sensations. We found no differences between individuals with SOR and those without, neither in children nor in adults. Furthermore, when measuring heat and cold *pain thresholds* [i.e., the minimum intensity levels of a stimulus that are perceived as painful; International Association of the Study of Pain (IASP), 2017], again, no such group differences were found (Bar-Shalita et al., 2009, 2012). In light of these findings, we showed that somatosensory detection and pain thresholds are not impacted in SOR. Intact sensory detection thresholds denote the absence of peripheral nerve system lesions. However, when we investigated laboratory-induced suprathreshold stimuli to measure the perceived pain intensity, we found group differences in both children and adults; individuals with SOR rated heat and mechanical painful stimuli as more painful than those without SMD, demonstrating hyperalgesia in the former group (Bar-Shalita et al., 2009, 2012; Weissman-Fogel et al., 2018). *Hyperalgesia* denotes abnormally increased pain from a stimulus that normally provokes pain, and like allodynia, it is a clinical term rather than a mechanism [International Association of the Study of Pain (IASP), 2017]. Furthermore, we revealed that in individuals with SOR the evoked pain sensation is higher in intensity and lingers for a longer duration after stimulus termination vs. non-SMD subjects who showed an expected gradual reduction in pain intensity that reached a level of no-pain within a 5–6 min time period (Bar-Shalita et al., 2009, 2012, 2014; Weissman-Fogel et al., 2018). This lingering sensation, termed *after-sensation*, validates the clinical symptoms reported by clients and could explain the accumulation of aversive sensations experienced by individuals with SMD throughout the day (Kinnealey et al., 2015).

After-sensation and hyperalgesia are both excitatory signs indicating central-sensitization that impacts pain perception (Andersen et al., 1996; Woolf and Salter, 2000; Woolf and Max, 2001; Gottrup et al., 2003; D'Mello and Dickenson, 2008). In SOR, we were the first to report the existence of a pro-nociceptive state resulting in pain amplification (Weissman-Fogel et al., 2018). Searching for this pro-nociceptive state underlying mechanism, we found inhibitory mechanisms which did not differ from non-SMD controls, though clearly presented a delayed process of inhibition. This emerged when testing the conditioned pain modulation (CPM) neurophysiological phenomenon, where one painful stimulus, the "conditioning stimulus," inhibits a concomitant or subsequent painful "test stimulus" (Weissman-Fogel et al., 2018). Thus, individuals with SOR have central sensitization which is expressed as a pro-nociceptive state due to over excitation rather than reduced inhibition. Incoming sensory stimuli from the peripersonal space ("the spatial region surrounding the body that a person regards as theirs psychologically"; Senkowski et al., 2014) are experienced by an individual with SOR as painful (allodynia) and therefore require greater recruitment of top-down inhibitory mechanisms to support survival. In children and adults with SOR, their survival efforts are expressed by defensive-protecting behaviors when confronted with sensory stimuli intruding their peripersonal space. Indeed, quality of life is reduced in individuals with SOR, specifically due to bodily pain.

ABNORMAL CENTRAL SENSORY PROCESSING IN SMD

Current neurophysiological methods such as electroencephalography (EEG) have been used to define the neural origins of SMD. It has been found that the behavioral

phenotype of SMD is due to atypical neural processing of both single *non-painful* sensory stimulus (i.e., somatosensory or auditory) and integration of simultaneous multi-sensory stimulation (i.e., somatosensory and auditory), This has been manifested by greater (Parush et al., 1997, 2007) and prolonged (Zlotnik et al., 2018) early event-related potentials (ERPs; a brain response to a specific external event) in response to tactile and auditory stimuli, respectively, along with smaller (Gavin et al., 2011) or greater (Davies et al., 2010) amplitudes of late auditory ERPs. This abnormally intense processing and lingering of sensory stimuli may result in individuals with SMD feeling overwhelmed when facing everyday sensory experiences. On top of this, adaptation deficiency to repetitive stimuli has been evident in ERPs (Kisley et al., 2004; Davies and Gavin, 2007; Brett-Green et al., 2010; i.e., ERP amplitude inhibition in response to repetitive paired-click stimulation), indicating a deficiency in pain inhibition probably due to an inefficient gating process. Moreover, atypical (neural integration of simultaneous multisensory stimulation (i.e., multisensory integration) has been indicated by spatio-temporal distribution of ERP responses to dual auditory and somatosensory stimuli (Brett-Green et al., 2010). Specifically, while in typically developing children multisensory integration occurs in central and post-central scalp regions during both early and later stages of sensory information processing (Brett-Green et al., 2008), those with SMD demonstrate a fronto-central distribution (Brett-Green et al., 2010). Accordingly, we have recently found (Granovsky et al., 2019) that subjects with SOR have different topographical dispersions of resting state EEG activity within the alpha band; while non-SMD individuals demonstrated increased activity toward parietal sites, those with SOR did not show this topographical distribution. Finally, novel findings from our lab point at an abnormal basic neurophysiological activity under a task-free condition in SOR individuals whereby there was a global reduction of cortical activity in theta, alpha and beta bands, most prominently in the alpha band, compared to non-SMD individuals. Thus, individuals with SOR demonstrate a neurophysiological state of a "non-resting" brain, which may partly explain their reported ongoing daily alertness to peripersonal stimuli. Furthermore, based on the "Gating by Inhibition" theory (Jensen and Mazaheri, 2010), alpha activity in higher-order cortical areas is mandatory for inhibiting task-irrelevant input. Thus, reduced alpha activity may consequently result in excessive sensory input processing which may contribute or result in SOR.

Studies have found associations between neurophysiological measures and behavioral manifestations of SMD, based on self- and caregiver reports of daily experience of sensory stimuli and functional performance on sensory tasks (Kisley et al., 2004; Gavin et al., 2011; Zlotnik et al., 2018). Namely, more sensory responsive or more avoiding behavior was correlated with higher amplitudes and more prolonged latencies of sensory response ERPs. This may reflect the major resources needed to process daily sensory stimuli among people with SMD. Moreover, such brain responses to sensory stimuli have correctly distinguished children with SMD from typically developing children and adults with 77%–96% accuracy (Davies and Gavin, 2007; Davies et al., 2010; Gavin et al., 2011). We, therefore, suggest that these neurophysiological differences may serve as characteristic markers of SMD that are underpinned by the anatomical abnormalities in sensory pathways (Owen et al., 2013) and which may contribute to the sensitive and/or avoidance behavior. This experience-induced neural plasticity may further mark its footprint in a sensory signature and thereby contribute to the sensory symptoms and daily life challenges experienced by individuals with SMD. Whether such a neurophysiological anomaly in individuals with SMD is nature or nurture, there is no doubt it reduces their successful social and functional participation in their home, school and community environments.

AN EXCITATORY/INHIBITORY (E/I) IMBALANCE AS A SHARED MECHANISM FOR SMD AND PAIN

The neurophysiological studies described above which investigated the central processes in response to external non-painful stimuli suggest an imbalance between excitatory and inhibitory processes in the brain. A balanced excitatory (glutamatergic) and inhibitory [γ-aminobutyric acid (GABA)ergic and glycinergic] ratio is essential for the brain to work appropriately in response to different sensory inputs. In adults, the tightly regulated E/I balance is achieved by homeostatic control of the strength and weight of transmissions in response to external stimuli. An increased E/I ratio can lead to a prolonged neocortical activity which may be associated with abnormal sensory processing such as hypersensitivity to different sensory stimuli (Zhang and Sun, 2011).

The E/I balance is one of the fundamental elements required for a normal sensory threshold and for regulating supra-threshold stimuli that originate from different sensory organs. In her early work, Ayres (Ayres, 1972) described the interrelationship of excitatory and inhibitory processes as modulation. Sufficient modulation occurs when the two processes work in harmony. Dunn (1997, 2001) developed a model of sensory modulation to explain the relationship between behavior and neurophysiological responses. Based on Dunn's model of sensory processing, the nervous system's functionality is represented by neurological thresholds whereby a "high threshold" requires a greater sensory input for activation while a "low threshold" requires lower stimulation for activation of sensory processing (Dunn, 1999). Behaviorally, individuals with low thresholds notice and respond to sensory stimuli more readily than the typical individuals, and thus represent a sensory profile that is sensory sensitive and sensory avoiding, defined as SOR (Miller et al., 2007). It is suggested by both Dunn (2001) and Miller et al. (2007) that individual sensory profiles are grouped based on psychophysiological measures, such as sensory thresholds and responses to supra-threshold stimuli, rather than by responses to specific sensory modalities. This, therefore, suggests that there are neurophysiological mechanisms common to more than

one sensory system including the pain, auditory, tactile, and visual systems.

The hypersensitivity and lingering in response to experimental pain observed in individuals with SOR (Bar-Shalita et al., 2009, 2012, 2014; Weissman-Fogel et al., 2018) despite efficient habituation and inhibition capabilities (Weissman-Fogel et al., 2018) indicates increased neuronal excitation in the pain-transmitting pathways with no inhibition deficiency. We, therefore, suggest that the enhanced activity of pain-facilitatory pathways with preserved pain-inhibitory mechanisms in SMD may be related to an E/I imbalance (Weissman-Fogel et al., 2018). Glutamate, the main excitatory neurotransmitter, and GABA, the main inhibitory transmitter within the CNS play key roles in central pain processing. Specifically, glutamate plays an important role in pain transmission and modulation (see review: Goudet et al., 2009). The glutamate receptors are widely distributed throughout the CNS where they regulate cell excitability and synaptic transmission at different levels of the pain matrix. Expression of glutamate receptors have been reported in the thalamus (Lourenço Neto et al., 2000), amygdala (Neugebauer, 2007), and the midbrain periaqueductal gray region (PAG; Marabese et al., 2005) and generally serve a pro-nociceptive role (Goudet et al., 2009). The ascending dorsal horn nociceptive neurons project toward all these brain areas with the PAG being an important center for the processing of nociceptive information and descending modulatory circuitry. Glutamate receptors that have also been detected in glial cells which are active regulators and protectors of nervous system and therefore play a role in pain. On the other hand, GABA receptors have an important anti-nociceptive role in acute and chronic pain. At the supra-spinal level, they depress ascending adrenergic and dopaminergic input to the brainstem, and facilitate the descending noradrenergic input to the spinal cord dorsal horn (Goudet et al., 2009). Importantly, elevated brain glutamate levels (Harris et al., 2009; Prescot et al., 2009; Petrou et al., 2012) and lower levels of GABA (Foerster et al., 2012; Petrou et al., 2012) have been reported in chronic pain conditions. This neurotransmitter imbalance is manifested by neuronal hyperexcitability, which can be alleviated by anticonvulsants. Anticonvulsants inhibit neuronal hyperexcitability by multiple mechanisms including direct or indirect enhancement of inhibitory GABAergic neurotransmission, or inhibition of glutamatergic neurotransmission (Sullivan and Robinson, 2006).

The coupling between SOR to daily non-painful stimuli and enhanced pain facilitation suggests a common brain mechanism that is due to an E/I imbalance. This shared mechanism in SMD individuals who are pain-free may further serve as a predisposing factor for the development of pain disorders. Indeed, we recently found SMD to be a contributing factor for having complex regional pain syndrome (CRPS). CRPS is a chronic pain syndrome of unknown pathophysiology that develops after limb surgery or injury in 4%–7% of patients (Harden et al., 2010; Bruehl, 2015). Though the origin and progress of CRPS varies, it usually evokes a severe state of disablement in the affected limb, which robustly reduces function and quality of life (Lohnberg and Altmaier, 2013; van Velzen et al., 2014; Bean et al., 2016). No specific clinical sign or symptom has been found as a risk factor for CRPS onset (Pons et al., 2015). Yet, early identification of those at risk for CRPS is linked to enhanced outcomes (Li et al., 2010; Wertli et al., 2013). Our findings revealed that for a person with SMD the risk of CRPS is 2.68–8.21 times higher than for a person without SMD. Consequently, including the SMD domain as a risk factor in the CRPS clinical discussion prior to intervention may allow for an early diagnosis and a significant prognostic improvement.

MULTI-SENSORY PROCESSING SHAPING THE PAIN EXPERIENCE IN SMD

Applying a nociceptive stimulus to the skin evokes activity imaged in a large network of brain regions which is referred to as the "pain matrix." The pain matrix comprises the primary (S1) and secondary (S2) somatosensory cortices, the insula, and the anterior cingulate cortex (ACC; Treede et al., 1999; Peyron et al., 2002; Apkarian et al., 2005). However, Mouraux et al.'s (2011) findings challenge this model and suggest that the pain matrix regions are equally involved in processing non-nociceptive and nociceptive stimuli. Moreover, they postulate that most parts of the pain matrix are likely involved in cognitive brain processes that detect and process salient multisensory stimuli. Based on the hypothesis that most of the neocortex is multisensory (Ghazanfar and Schroeder, 2006), Senkowski et al. (2014) argue that pain-related neural responses at all processing stages can be shaped by non-painful stimuli. Different factors, such as stimulus intensity and valence, affect the way other sensory stimuli shape the pain perception. Specifically, painful stimuli accompanied by environmental input from other sensory modalities can impact not only the pain perception but also the processing of these stimuli. Other sensory modality stimuli may draw attention away and subsequently reduce the perceived pain intensity, or conversely, these stimuli can amplify the saliency of the painful stimuli and evoke an augmented pain experience. This suggests that non-painful stimuli in the peripersonal space have an important role in shaping the pain experience. Exploring this association, we found that the correlation between daily pain sensitivity and hyper-responsiveness tripled in individuals with SOR compared to non-SMD individuals (Bar-Shalita et al., 2015). Moreover, an unpleasant sensation intruding the peripersonal space usually evokes a defense response (Senkowski et al., 2014). Indeed, children and adults with SOR demonstrate and report protective responses to non-painful stimuli (Miller et al., 2007), which may be explained similarly to the main function of pain, warning of danger and preventing future tissue damage (Crombez et al., 2005; Dowman, 2011; Senkowski et al., 2014). Taken together, research on the multisensory shaping of pain has definite clinical implications (e.g., Senkowski and Heinz, 2016), but also offers an important novel understanding of the mechanisms as well as the relevance of multisensory processing to pain processing.

CLINICAL MANIFESTATION OF SOR IN CHRONIC PAIN CONDITIONS

Increased sensitivity to non-painful sensory stimuli is widely described for many chronic pain states. For example, in migraine, lower sensory thresholds, enhanced psychophysical and neurophysiological responses, and reduced adaptation and habituation to a specific sensory modality (usually visual or auditory) have all been reported including during the inter-ictal state (Harriott and Schwedt, 2014; Demarquay and Mauguière, 2016). Furthermore, many migraineurs report inter-ictal discomfort to everyday stimuli such as odors, light and sound, which may even trigger or worsen headache intensity (Vanagaite et al., 1997; Martin et al., 2006; Borini et al., 2008; Friedman and De Ver Dye, 2009; Noseda and Burstein, 2013; Schwedt, 2013). Thus, this multi-sensory hypersensitivity may point to an abnormal central multisensory integration in migraine (Schwedt, 2013).

Similar to the suggested SMD pathophysiology, the underlying neurophysiological mechanisms of increased sensitivity in inter-ictal migraine suggest alterations in the cortical circuits and neurotransmitters which maintain the E/I balance (Pietrobon and Moskowitz, 2013; Demarquay and Mauguière, 2016). Moreover, the results of our recent study have revealed that 45% of migraine patients are diagnosed with SMD (Granovsky et al., 2018), an incidence far above the ∼10% SMD incidence (range 5%–16%) among pain-free healthy pediatric and adult populations (Ahn et al., 2004; Ben-Sasson et al., 2009; Bar-Shalita et al., 2015). The association of SOR with migraine pain symptoms such as having sensory aura, a higher frequency of monthly attacks, and an enhanced activity of pain facilitatory pathways (Granovsky et al., 2018) further support the inter-relation between non-painful sensory and pain transmitting pathways (Schwedt, 2013). An example of this is a study reporting that experimentally-evoked trigeminal pain further enhances the cortical hyperexcitability and the lack of habituation to light in migraine patients (Boulloche et al., 2010). This phenomenon can be related to the anatomical integration of pain and visual processing in thalamic nuclei (Noseda and Burstein, 2013) that project to cortical areas involved in the processing of pain and visual perception. We can only hypothesize about a similarity of the central neuroanatomical integration alterations in sensory and pain-transmitting pathways to that described in migraine.

Another chronic pain state characterized by a global disturbance in sensory responsiveness is fibromyalgia (FM). Many studies have reported on greater sensitivity to various non-painful sensory experimental stimuli (tactile, thermal, electrical, auditory) in FM (Lautenbacher et al., 1994; Montoya et al., 2006; Geisser et al., 2008; Hollins et al., 2009). Similar to migraine, FM patients have also enhanced sensory responses to everyday real-life stimuli such as auditory stimuli (Geisser et al., 2008) and cutaneous sensations (Borg et al., 2015). This greater sensitivity is known as a "generalized hypervigilance" and is considered as one of the pathophysiological mechanisms of FM (McDermid et al., 1996; Rollman, 2009). Some authors also refer to heightened affective, sensory and pain responses as an abnormality of the interoceptive system in FM (Lovero et al., 2009; Seth and Friston, 2016; Duschek et al., 2017; Valenzuela-Moguillansky et al., 2017; Martínez et al., 2018). Along with the widely reported pro-nociceptive pattern of psychophysical and neurophysiological responses (Staud and Spaeth, 2008; Staud, 2011; O'Brien et al., 2018), sensory over-responsiveness in FM can point to a decrease in inhibitory and/or an increase in facilitatory activity in the CNS.

Since pain is a multidimensional and complex experience composed of sensory, affective-motivational, cognitive-evaluative components (Melzack and Casey, 1968), we propose the SMD as another factor that may shape the pain experience.

ABNORMAL EEG RESPONSES AS A SHARED MECHANISM FOR SMD AND PAIN

In migraine and FM, along with enhanced pain psychophysical responses, cortical activity has been repeatedly shown to be abnormal. More specifically, reports from many studies have pointed to higher amplitudes of early (A-delta mediated) pain-evoked ERPs (Gibson et al., 1994; Lorenz et al., 1996; Lev et al., 2010; de Tommaso et al., 2011; Truini et al., 2015), along with deficient habituation of these and other neurophysiological responses (Valeriani et al., 2003; Lev et al., 2010; de Tommaso et al., 2014, 2015; Harriott and Schwedt, 2014). Similarly, research in SMD has also indicated higher (Parush et al., 1997, 2007) and prolonged (Zlotnik et al., 2018) early ERPs in response to non-painful sensory stimuli along with an adaptation deficiency (Kisley et al., 2004; Davies and Gavin, 2007; Brett-Green et al., 2010). These neurophysiological markers again suggest a shared mechanism in SMD and chronic pain, namely, enhanced cortical activity and deficient inhibition.

Though brain imaging studies in SMD are yet to come, we can deduce from a standardized low resolution brain electromagnetic tomography (sLORETA) study in migraine that these neurophysiological markers may be linked with enhanced activity of S1 and reduced activity of the orbitofrontal cortex (the part of the prefrontal cortex associated with initiation of pain inhibition; Lev et al., 2010). In migraine, these neurophysiological activity patterns are observed in painful as well as non-painful stimuli (de Tommaso et al., 2013) and moreover are correlated with the clinical characteristics (Lev et al., 2013).

An abnormal pattern of EEG responses in chronic pain patients is also reported in resting-state conditions. The most consistent reported findings refer to the abnormal alpha, theta or beta activity in migraine and FM. More specifically in migraine, increased alpha power has been recorded in posterior brain regions, while activity in the frontal lobe has revealed decreased activity in alpha generators (Clemens et al., 2008; Cao et al., 2018). Other studies have also reported on a global inter-ictal decrease of EEG activity

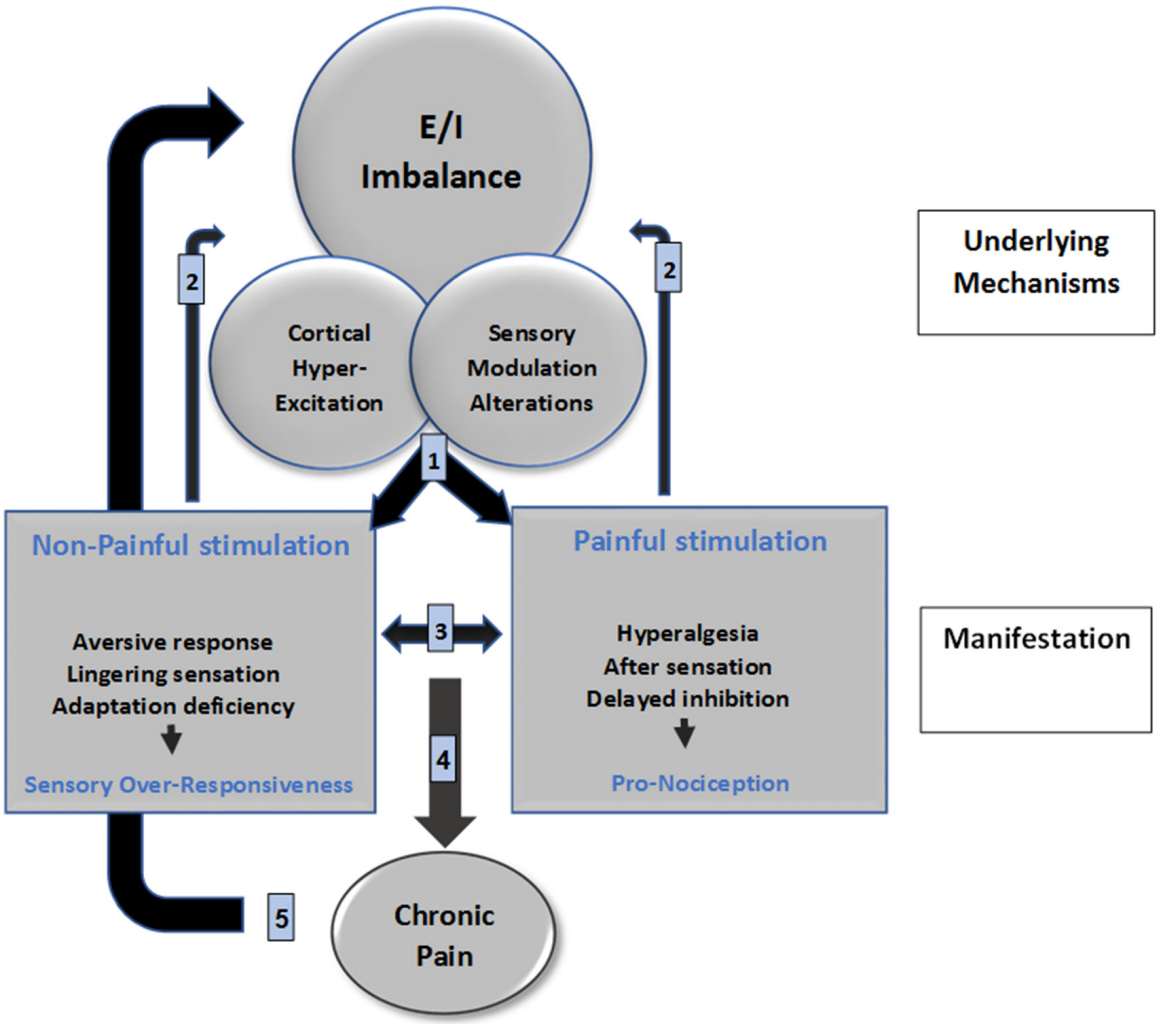

FIGURE 1 | SMDolor model depicts a neurophysiological mechanism-based model for the interrelation between pain and SMD. The numbers represents the putative processes that manifest clinically: SOR, and pro-nociceptive state expressions of central alteration (1); both conditions elicit stimuli processing impact on brain mechanisms due to brain plasticity (2); and also create a bi-directional impact on the sensory perception (3); which may accumulate to develop chronic pain as a consequence of pro-nociception (4); which then nurtures the brain mechanisms alterations via brain plasticity (5).

(Tsounis and Varfis, 1992; Cao et al., 2016) and on an association between slower alpha activity and greater disease and attack durations (Bjørk et al., 2009). Whereas in FM, decreased alpha, increased beta (Vanneste et al., 2017) and augmented theta activity (Fallon et al., 2018) have been found in different cortical areas and have also been reported to positively correlate with clinical symptoms. Interestingly, abnormal alpha activity and a global reduction of cortical activity in theta, alpha and beta bands has also been observed in SMD (Granovsky et al., 2019).

Further validation for the suggested link between chronic pain and SMD is evident in our recent unpublished data on migraineurs (article in preparation). Our research has indicated that lower connectivity values in the theta band at centro-parietal region are correlated with higher scores in SOR.

SENSORY MODULATION ALTERATIONS AS A SHARED MECHANISM FOR CHRONIC PAIN AND SMD

The assessment of pain modulation is performed by using various stimulation protocols which include a combination of different stimulus modalities and psychophysical tests. The latter selectively engage the pain facilitatory bottom-up or pain inhibitory top-down pathways and are believed to reflect the "real-life" modulation process exerted by patients when exposed to clinical pain. One of the most studied mechanisms of the supraspinally-mediated descending pain inhibitory system is the diffuse noxious inhibitory control (DNIC). DNIC engages the activation of the endogenous analgesia system, where upon arrival of data to the brainstem the

ascending pain activates descending pain inhibitory pathways, exerting effects on incoming nociceptive inputs (Le Bars, 2002). The pain alleviating efficiency of DNIC relates on the balance between the anti-nociceptive effect of noradrenergic neurotransmission, and pro- or anti-nociceptive effect of serotonergic neurotransmission, that depends on the type of serotonin receptor (Bannister and Dickenson, 2016). The neurophysiological mechanism for the activation of bottom-up facilitatory pathways is associated with the glutamate-mediated windup of second-order neurons and reflects the state of central neuronal sensitization (Woolf and Thompson, 1991). Moreover, imbalance between the excited pain facilitatory systems, and the reduced activity in pain inhibitory pathways, including reduced functional connectivity with the brain regions associated with pain inhibition and/or enhanced connectivity with the brain regions associated with pain facilitation (Wang et al., 2016; Harper et al., 2018) point on a pro-nociceptive pain modulation profile as reported in many chronic pain states (Granovsky and Yarnitsky, 2013; Yarnitsky et al., 2014; Yarnitsky, 2015), including migraine and FM. Despite the still open chicken-and-egg question on the causality of the interrelations between the modulation state and the presence of the various pain syndromes, it is believed that a pre-existing facilitatory state of the CNS leads to the establishment of a pro-nociceptive profile and the acquisition of chronic pain syndromes. This causative relation was found in a longitudinal study on pain-free pre-thoracotomy patients, demonstrating that those with less-efficient endogenous pain inhibition had a higher incidence and intensity of chronic post-operative pain (Yarnitsky et al., 2008). These results were later reproduced for cesarean section and major abdominal surgery patients, respectively (Landau et al., 2010; Wilder-Smith et al., 2010). All the above findings taken together demonstrate that SMD is a pro-nociceptive condition (Weissman-Fogel et al., 2018). We propose that SOR is a predisposing factor or risk factor for chronic pain.

SUMMARY

We propose a neurophysiological mechanism-based model for the interrelation between pain and SMD, namely the SMDolor Model (**Figure 1**; the numbers guide the following explanation). Shared central neural mechanisms between SOR and pain, E/I imbalance; cortical hyper-excitation and sensory modulation alterations, are the cornerstone of this proposed model. These shared mechanisms are behaviorally expressed (1) as SOR in sensory systems processing non-painful stimuli, and as a pro-nociceptive state when processing painful stimuli. Daily life events require a multi-sensory integration for adaptive responding. This warrants a convergence of sensory stimuli from different modalities including pain which in turn causes pain to be influenced by these other sensory stimuli and vice versa (3), consequently, daily life events are experienced as aversive, irritating, and painful by individuals with SOR. These experiences induce neuronal plasticity (2) that may further result in a sensory signature which strengthens the abnormal shared mechanisms, contributing to the sensory symptoms that shape the daily life challenges experienced by individuals with SOR. These loop reactions may in some cases accumulate up to the point of developing a chronic pain condition (4). Chronic pain may then further nurture the shared central neural mechanisms (5).

AUTHOR CONTRIBUTIONS

All authors listed have made a substantial, direct and intellectual contribution to the work, and approved it for publication.

REFERENCES

Ahn, R. R., Miller, L. J., Milberger, S., and Mcintosh, D. N. (2004). Prevalence of parents' perceptions of sensory processing disorders among kindergarten children. *Am. J. Occup. Ther.* 58, 287–293. doi: 10.5014/ajot.58.3.287

Andersen, O. K., Felsby, S., Nicolaisen, L., Bjerring, P., Jensen, T. S., and Arendt-Nielsen, L. (1996). The effect of Ketamine on stimulation of primary and secondary hyperalgesic areas induced by capsaicin—a double-blind, placebo-controlled, human experimental study. *Pain* 66, 51–62. doi: 10.1016/0304-3959(96)02995-8

Apkarian, A. V., Bushnell, M. C., Treede, R.-D., and Zubieta, J.-K. (2005). Human brain mechanisms of pain perception and regulation in health and disease. *Eur. J. Pain* 9, 463–484. doi: 10.1016/j.ejpain.2004.11.001

Arendt-Nielsen, L., and Yarnitsky, D. (2009). Experimental and clinical applications of quantitative sensory testing applied to skin, muscles and viscera. *J. Pain* 10, 556–572. doi: 10.1016/j.jpain.2009.02.002

Ayres, A. J. (1972). *Sensory Integration and Learning Disorders.* Los Angeles, CA: Western Psychological Services.

Bannister, K., and Dickenson, A. H. (2016). What the brain tells the spinal cord. *Pain* 157, 2148–2151. doi: 10.1097/j.pain.0000000000000568

Bar-Shalita, T., Deutsch, L., Honigman, L., and Weissman-Fogel, I. (2015). Ecological aspects of pain in sensory modulation disorder. *Res. Dev. Disabil.* 45–46, 157–167. doi: 10.1016/j.ridd.2015.07.028

Bar-Shalita, T., Vatine, J. J., and Parush, S. (2008). Sensory modulation disorder: a risk factor for participation in daily life activities. *Dev. Med. Child Neurol.* 50, 932–937. doi: 10.1111/j.1469-8749.2008.03095.x

Bar-Shalita, T., Vatine, J. J., Parush, S., Deutsch, L., and Seltzer, Z. (2012). Psychophysical correlates in adults with sensory modulation disorder. *Disabil. Rehabil.* 34, 943–950. doi: 10.3109/09638288.2011.629711

Bar-Shalita, T., Vatine, J.-J., Seltzer, Z. E., and Parush, S. (2009). Psychophysical correlates in children with sensory modulation disorder (SMD). *Physiol. Behav.* 98, 631–639. doi: 10.1016/j.physbeh.2009.09.020

Bar-Shalita, T., Vatine, J. J., Yarnitsky, D., Parush, S., and Weissman-Fogel, I. (2014). Atypical central pain processing in sensory modulation disorder: absence of temporal summation and higher after-sensation. *Exp. Brain Res.* 232, 587–595. doi: 10.1007/s00221-013-3767-y

Bartlett, G., Stewart, J. D., Tamblyn, R., and Abrahamowicz, M. (1998). Normal distributions of thermal and vibration sensory thresholds. *Muscle Nerve* 21, 367–374. doi: 10.1002/(sici)1097-4598(199803)21:3<367::aid-mus11>3.0.co;2-x

Bean, D. J., Johnson, M. H., Heiss-Dunlop, W., and Kydd, R. R. (2016). Extent of recovery in the first 12 months of complex regional pain syndrome type-1: a prospective study. *Eur. J. Pain* 20, 884–894. doi: 10.1002/ejp.813

Ben-Sasson, A., Carter, A. S., and Briggs-Gowan, M. J. (2009). Sensory over-responsivity in elementary school: prevalence and social-emotional correlates. *J. Abnorm. Child Psychol.* 37, 705–716. doi: 10.1007/s10802-008-9295-8

Bjørk, M., Stovner, L., Nilsen, B., Stjern, M., Hagen, K., and Sand, T. (2009). The occipital α rhythm related to the "migraine cycle" and headache burden: a blinded, controlled longitudinal study. *Clin. Neurophysiol.* 120, 464–471. doi: 10.1016/j.clinph.2008.11.018

Borg, C., Emond, F. C., Colson, D., Laurent, B., and Michael, G. A. (2015). Attentional focus on subjective interoceptive experience in patients with fibromyalgia. *Brain Cogn.* 101, 35–43. doi: 10.1016/j.bandc.2015.10.002

Borini, C. A., Gatti, F. R., Grezos, R. M. L., and Fragoso, Y. D. (2008). Odors as triggering and worsening factors in migraine. *Anxiety* 76:53.

Boulloche, N., Denuelle, M., Payoux, P., Fabre, N., Trotter, Y., and Géraud, G. (2010). Photophobia in migraine: an interictal PET study of cortical hyperexcitability and its modulation by pain. *J. Neurol. Neurosurg. Psychiatry* 81, 978–984. doi: 10.1136/jnnp.2009.190223

Brett-Green, B. A., Miller, L. J., Gavin, W. J., and Davies, P. L. (2008). Multisensory integration in children: a preliminary ERP study. *Brain Res.* 1242, 283–290. doi: 10.1016/j.brainres.2008.03.090

Brett-Green, B. A., Miller, L. J., Schoen, S. A., and Nielsen, D. M. (2010). An exploratory event-related potential study of multisensory integration in sensory over-responsive children. *Brain Res.* 1321, 67–77. doi: 10.1016/j.brainres.2010.01.043

Bruehl, S. (2015). Complex regional pain syndrome. *BMJ* 351:h2730. doi: 10.1136/bmj.h2730

Cao, Z., Lai, K.-L., Lin, C.-T., Chuang, C.-H., Chou, C.-C., and Wang, S.-J. (2018). Exploring resting-state EEG complexity before migraine attacks. *Cephalalgia* 38, 1296–1306. doi: 10.1177/0333102417733953

Cao, Z., Lin, C.-T., Chuang, C.-H., Lai, K.-L., Yang, A. C., Fuh, J.-L., et al. (2016). Resting-state EEG power and coherence vary between migraine phases. *J. Headache Pain* 17:102. doi: 10.1186/s10194-016-0697-7

Chien, C.-W., Rodger, S., Copley, J., Branjerdporn, G., and Taggart, C. (2016). Sensory processing and its relationship with children's daily life participation. *Phys. Occup. Ther. Pediatr.* 36, 73–87. doi: 10.3109/01942638.2015.1040573

Clemens, B., Bánk, J., Piros, P., Bessenyei, M., Vető, S., Tóth, M., et al. (2008). Three-dimensional localization of abnormal EEG activity in migraine. *Brain Topogr.* 21, 36–42. doi: 10.1007/s10548-008-0061-6

Crombez, G., Van Damme, S., and Eccleston, C. (2005). Hypervigilance to pain: an experimental and clinical analysis. *Pain* 116, 4–7. doi: 10.1016/j.pain.2005.03.035

Davies, P. L., Chang, W. P., and Gavin, W. J. (2010). Middle and late latency erp components discriminate between adults, typical children, and children with sensory processing disorders. *Front. Integr. Neurosci.* 4:16. doi: 10.3389/fnint.2010.00016

Davies, P. L., and Gavin, W. J. (2007). Validating the diagnosis of sensory processing disorders using EEG technology. *Am. J. Occup. Ther.* 61, 176–189. doi: 10.5014/ajot.61.2.176

de Tommaso, M., Federici, A., Santostasi, R., Calabrese, R., Vecchio, E., Lapadula, G., et al. (2011). Laser-evoked potentials habituation in fibromyalgia. *J. Pain* 12, 116–124. doi: 10.1016/j.jpain.2010.06.004

de Tommaso, M., Nolano, M., Iannone, F., Vecchio, E., Ricci, K., Lorenzo, M., et al. (2014). Update on laser-evoked potential findings in fibromyalgia patients in light of clinical and skin biopsy features. *J. Neurol.* 261, 461–472. doi: 10.1007/s00415-013-7211-9

de Tommaso, M., Stramaglia, S., Marinazzo, D., Trotta, G., and Pellicoro, M. (2013). Functional and effective connectivity in EEG α and β bands during intermittent flash stimulation in migraine with and without aura. *Cephalalgia* 33, 938–947. doi: 10.1177/0333102413477741

de Tommaso, M., Trotta, G., Vecchio, E., Ricci, K., Van De Steen, F., Montemurno, A., et al. (2015). Functional connectivity of EEG signals under laser stimulation in migraine. *Front. Hum. Neurosci.* 9:640. doi: 10.3389/fnhum.2015.00640

Demarquay, G., and Mauguière, F. (2016). Central nervous system underpinnings of sensory hypersensitivity in migraine: insights from neuroimaging and electrophysiological studies. *Headache* 56, 1418–1438. doi: 10.1111/head.12651

D'Mello, R., and Dickenson, A. H. (2008). Spinal cord mechanisms of pain. *Br. J. Anaesth.* 101, 8–16. doi: 10.1093/bja/aen088

Dowman, R. (2011). The role of somatic threat feature detectors in the attentional bias toward pain: effects of spatial attention. *Psychophysiology* 48, 397–409. doi: 10.1111/j.1469-8986.2010.01068.x

Dunn, W. (1997). The impact of sensory processing abilities on the daily lives of young children and their families: a conceptual model. *Infants Young Child.* 9, 23–35. doi: 10.1097/00001163-199704000-00005

Dunn, W. (1999). *Sensory Profile: User's Manual.* San Antonio, TX: Psychological Corporation.

Dunn, W. (2001). The sensations of everyday life: empirical, theoretical, and pragmatic considerations. *Am. J. Occup. Ther.* 55, 608–620. doi: 10.5014/ajot.55.6.608

Dunn, W. (2007). Supporting children to participate succesfully in everyday life by using sensory processing knowledge. *Infants Young Child.* 20, 84–101. doi: 10.1097/01.iyc.0000264477.05076.5d

Duschek, S., Montoro, C. I., and Reyes Del Paso, G. A. (2017). Diminished interoceptive awareness in fibromyalgia syndrome. *Behav. Med.* 43, 100–107. doi: 10.1080/08964289.2015.1094442

Dyck, P. J., Zimmerman, I., Gillen, D., Johnson, D., Karnes, J., and O'Brien, P. (1993). Cool, warm, and heat-pain detection thresholds Testing methods and inferences about anatomic distribution of receptors. *Neurology* 43, 1500–1508. doi: 10.1212/wnl.43.8.1500

Fallon, N., Chiu, Y., Nurmikko, T., and Stancak, A. (2018). Altered theta oscillations in resting EEG of fibromyalgia syndrome patients. *Eur. J. Pain* 22, 49–57. doi: 10.1002/ejp.1076

Fisher, A. G., and Dunn, W. (1983). Tactile defensiveness: historical perspectives, new research- a theory grows. *Sens. Integr. Spec. Interest Sec. Newsl.* 6, 1–2.

Foerster, B. P., Edden, M., Sundgren, R., Schmidt-Wilcke, P., Lowe, T., and Harte, S. E. (2012). Reduced insular γ-aminobutyric acid in fibromyalgia. *Arthritis Rheum.* 64, 579–583. doi: 10.1002/art.33339

Friedman, D. I., and De Ver Dye, T. (2009). Migraine and the environment. *Headache* 49, 941–952. doi: 10.1111/j.1526-4610.2009.01443.x

Gavin, W. J., Dotseth, A., Roush, K. K., Smith, C. A., Spain, H. D., and Davies, P. L. (2011). Electroencephalography in children with and without sensory processing disorders during auditory perception. *Am. J. Occup. Ther.* 65, 370–377. doi: 10.5014/ajot.2011.002055

Geisser, M. E., Glass, J. M., Rajcevska, L. D., Clauw, D. J., Williams, D. A., Kileny, P. R., et al. (2008). A psychophysical study of auditory and pressure sensitivity in patients with fibromyalgia and healthy controls. *J. Pain* 9, 417–422. doi: 10.1016/j.jpain.2007.12.006

Ghazanfar, A. A., and Schroeder, C. E. (2006). Is neocortex essentially multisensory? *Trends Cogn. Sci.* 10, 278–285. doi: 10.1016/j.tics.2006.04.008

Gibson, S., Littlejohn, G., Gorman, M., Helme, R., and Granges, G. (1994). Altered heat pain thresholds and cerebral event-related potentials following painful CO_2 laser stimulation in subjects with fibromyalgia syndrome. *Pain* 58, 185–193. doi: 10.1016/0304-3959(94)90198-8

Gottrup, H., Kristensen, A., Bach, F., and Jensen, T. (2003). Aftersensations in experimental and clinical hypersensitivity. *Pain* 103, 57–64. doi: 10.1016/s0304-3959(02)00415-3

Goudet, C., Magnaghi, V., Landry, M., Nagy, F., Gereau Iv, R. W., and Pin, J.-P. (2009). Metabotropic receptors for glutamate and GABA in pain. *Brain Res. Rev.* 60, 43–56. doi: 10.1016/j.brainresrev.2008.12.007

Granovsky, Y., Shor, M., Shifrin, A., Sprecher, E., Yarnitsky, D., and Bar-Shalita, T. (2018). Assessment of responsiveness to everyday non-noxious stimuli in pain-free migraineurs with versus without aura. *J. Pain* 19, 943–951. doi: 10.1016/j.jpain.2018.03.008

Granovsky, Y., Weissman-Fogel, I., and Bar-Shalita, T. (2019). Resting-state electroencephalography in participants with sensory overresponsiveness: an exploratory study. *Am. J. Occup. Ther.* 73, 7301205100p1–7301205100p11. doi: 10.5014/ajot.2019.029231

Granovsky, Y., and Yarnitsky, D. (2013). Personalized pain medicine: the clinical value of psychophysical assessment of pain modulation profile. *Rambam Maimonides Med. J.* 4:e0024. doi: 10.5041/rmmj.10131

Hagander, L. G., Midani, H. A., Kuskowski, M. A., and Parry, G. J. (2000). Quantitative sensory testing: effect of site and skin temperature on thermal thresholds. *Clin. Neurophysiol.* 111, 17–22. doi: 10.1016/s1388-2457(99)00192-3

Hansson, P., Backonja, M., and Bouhassira, D. (2007). Usefulness and limitations of quantitative sensory testing: clinical and research application in neuropathic pain states. *Pain* 129, 256–259. doi: 10.1016/j.pain.2007.03.030

Harden, R. N., Bruehl, S., Perez, R. S., Birklein, F., Marinus, J., Maihofner, C., et al. (2010). Validation of proposed diagnostic criteria (the "Budapest Criteria") for

complex regional pain syndrome. *Pain* 150, 268–274. doi: 10.1016/j.pain.2010.04.030

Harper, D. E., Ichesco, E., Schrepf, A., Hampson, J. P., Clauw, D. J., Schmidt-Wilcke, T., et al. (2018). Resting functional connectivity of the periaqueductal gray is associated with normal inhibition and pathological facilitation in conditioned pain modulation. *J. Pain* 19, 635.e1–635.e15. doi: 10.1016/j.jpain.2018.01.001

Harriott, A. M., and Schwedt, T. J. (2014). Migraine is associated with altered processing of sensory stimuli. *Curr. Pain Headache Rep.* 18:458. doi: 10.1007/s11916-014-0458-8

Harris, R. E., Sundgren, P. C., Craig, A., Kirshenbaum, E., Sen, A., Napadow, V., et al. (2009). Elevated insular glutamate in fibromyalgia is associated with experimental pain. *Arthritis Rheum.* 60, 3146–3152. doi: 10.1002/art.24849

Hollins, M., Harper, D., Gallagher, S., Owings, E. W., Lim, P. F., Miller, V., et al. (2009). Perceived intensity and unpleasantness of cutaneous and auditory stimuli: an evaluation of the generalized hypervigilance hypothesis. *Pain* 141, 215–221. doi: 10.1016/j.pain.2008.10.003

International Association of the Study of Pain (IASP). (2017). IASP Terminology. Available online at: https://www.iasp-pain.org/Education/Content.aspx?ItemNumber=1698#Pain

Jensen, O., and Mazaheri, A. (2010). Shaping functional architecture by oscillatory α activity: gating by inhibition. *Front. Hum. Neurosci.* 4:186. doi: 10.3389/fnhum.2010.00186

Kinnealey, M., Oliver, B., and Wilbarger, P. (1995). A phenomenological study of sensory defensiveness in adults. *Am. J. Occup. Ther.* 49, 444–451. doi: 10.5014/ajot.49.5.444

Kinnealey, M., Riuli, V., and Smith, S. (2015). Case study of an adult with sensory modulation disorder. *Sens. Integr. Spec. Interest Sec. Q.* 38, 1–4.

Kisley, M. A., Noecker, T. L., and Guinther, P. M. (2004). Comparison of sensory gating to mismatch negativity and self-reported perceptual phenomena in healthy adults. *Psychophysiology* 41, 604–612. doi: 10.1111/j.1469-8986.2004.00191.x

Landau, R., Kraft, J. C., Flint, L. Y., Carvalho, B., Richebé, P., Cardoso, M., et al. (2010). An experimental paradigm for the prediction of Post-Operative Pain (PPOP). *J. Vis. Exp.* 35:1671. doi: 10.3791/1671

Lautenbacher, S., Rollman, G. B., and McCain, G. (1994). Multi-method assessment of experimental and clinical pain in patients with fibromyalgia. *Pain* 59, 45–53. doi: 10.1016/0304-3959(94)90046-9

Le Bars, D. (2002). The whole body receptive field of dorsal horn multireceptive neurones. *Brain Res. Rev.* 40, 29–44. doi: 10.1016/s0165-0173(02)00186-8

Lev, R., Granovsky, Y., and Yarnitsky, D. (2010). Orbitofrontal disinhibition of pain in migraine with aura: an interictal EEG-mapping study. *Cephalalgia* 30, 910–918. doi: 10.1177/0333102409357249

Lev, R., Granovsky, Y., and Yarnitsky, D. (2013). Enhanced pain expectation in migraine: EEG-based evidence for impaired prefrontal function. *Headache* 53, 1054–1070. doi: 10.1111/j.1526-4610.2012.02297.x

Li, Z., Smith, B. P., Tuohy, C., Smith, T. L., and Koman, L. A. (2010). Complex regional pain syndrome after hand surgery. *Hand Clin.* 26, 281–289. doi: 10.1016/j.hcl.2009.11.001

Lohnberg, J. A., and Altmaier, E. M. (2013). A review of psychosocial factors in complex regional pain syndrome. *J. Clin. Psychol. Med. Settings* 20, 247–254. doi: 10.1007/s10880-012-9322-3

Lorenz, J., Grasedyck, K., and Bromm, B. (1996). Middle and long latency somatosensory evoked potentials after painful laser stimulation in patients with fibromyalgia syndrome. *Electroencephalogr. Clin. Neurophysiol.* 100, 165–168. doi: 10.1016/0013-4694(95)00259-6

Lourenço Neto, F., Schadrack, J., Berthele, A., Zieglgänsberger, W., Tölle, T. R., and Castro-Lopes, J. M. (2000). Differential distribution of metabotropic glutamate receptor subtype mRNAs in the thalamus of the rat. *Brain Res.* 854, 93–105. doi: 10.1016/s0006-8993(99)02326-4

Lovero, K. L., Simmons, A. N., Aron, J. L., and Paulus, M. P. (2009). Anterior insular cortex anticipates impending stimulus significance. *Neuroimage* 45, 976–983. doi: 10.1016/j.neuroimage.2008.12.070

Marabese, I., De Novellis, V., Palazzo, E., Mariani, L., Siniscalco, D., Rodella, L., et al. (2005). Differential roles of mGlu8 receptors in the regulation of glutamate and γ-aminobutyric acid release at periaqueductal grey level. *Neuropharmacology* 49, 157–166. doi: 10.1016/j.neuropharm.2005.02.006

Martin, P. R., Reece, J., and Forsyth, M. (2006). Noise as a trigger for headaches: relationship between exposure and sensitivity. *Headache* 46, 962–972. doi: 10.1111/j.1526-4610.2006.00468.x

Martínez, E., Aira, Z., Buesa, I., Aizpurua, I., Rada, D., and Azkue, J. J. (2018). Embodied pain in fibromyalgia: disturbed somatorepresentations and increased plasticity of the body schema. *PLoS One* 13:e0194534. doi: 10.1371/journal.pone.0194534

McDermid, A. J., Rollman, G. B., and Mccain, G. A. (1996). Generalized hypervigilance in fibromyalgia: evidence of perceptual amplification. *Pain* 66, 133–144. doi: 10.1016/0304-3959(96)03059-x

McGrath, P. A., and Brown, S. C. (2006). Quantitative sensory testing in children: practical considerations for research and clinical practice. *Pain* 123, 1–2. doi: 10.1016/j.pain.2006.03.024

Melzack, R., and Casey, K. L. (1968). "Sensory, motivational, and central control determinants of pain: a new conceptual model," in *International Symposium On the Skin Sense*, ed. Kenshalo (Springfield: C.C. Thomas), 423–435.

Miller, L. J., Anzalone, M. E., Lane, S. J., Cermak, S. A., and Osten, E. T. (2007). Concept evolution in sensory integration: a proposed nosology for diagnosis. *Am. J. Occup. Ther.* 61, 135–140. doi: 10.5014/ajot.61.2.135

Montoya, P., Sitges, C., García-Herrera, M., Rodríguez-Cotes, A., Izquierdo, R., Truyols, M., et al. (2006). Reduced brain habituation to somatosensory stimulation in patients with fibromyalgia. *Arthritis Rheum.* 54, 1995–2003. doi: 10.1002/art.21910

Mouraux, A., Diukova, A., Lee, M. C., Wise, R. G., and Iannetti, G. D. (2011). A multisensory investigation of the functional significance of the "pain matrix". *Neuroimage* 54, 2237–2249. doi: 10.1016/j.neuroimage.2010.09.084

Neugebauer, V. (2007). The amygdala: different pains, different mechanisms. *Pain* 127, 1–2. doi: 10.1016/j.pain.2006.10.004

Noseda, R., and Burstein, R. (2013). Migraine pathophysiology: anatomy of the trigeminovascular pathway and associated neurological symptoms, cortical spreading depression, sensitization, and modulation of pain. *Pain* 154, S44–S53. doi: 10.1016/j.pain.2013.07.021

O'Brien, A. T., Deitos, A., Pego, Y. T., Fregni, F., and Carrillo-de-la-Peña, M. T. (2018). Defective endogenous pain modulation in fibromyalgia: a meta-analysis of temporal summation and conditioned pain modulation paradigms. *J. Pain* 19, 819–836. doi: 10.1016/j.jpain.2018.01.010

Owen, J. P., Marco, E. J., Desai, S., Fourie, E., Harris, J., Hill, S. S., et al. (2013). Abnormal white matter microstructure in children with sensory processing disorders. *Neuroimage Clin.* 2, 844–853. doi: 10.1016/j.nicl.2013.06.009

Parush, S., Sohmer, H., Steinberg, A., and Kaitz, M. (1997). Somatosensory functioning in children with attention deficit hyperactivity disorder. *Dev. Med. Child Neurol.* 39, 464–468. doi: 10.1111/j.1469-8749.1997.tb07466.x

Parush, S., Sohmer, H., Steinberg, A., and Kaitz, M. (2007). Somatosensory function in boys with ADHD and tactile defensiveness. *Physiol. Behav.* 90, 553–558. doi: 10.1016/j.physbeh.2006.11.004

Petrou, M., Pop-Busui, R., Foerster, B. R., Edden, R. A., Callaghan, B. C., Harte, S. E., et al. (2012). Altered excitation-inhibition balance in the brain of patients with diabetic neuropathy. *Acad. Radiol.* 19, 607–612. doi: 10.1016/j.acra.2012.02.004

Peyron, R., Frot, M., Schneider, F., Garcia-Larrea, L., Mertens, P., Barral, F., et al. (2002). Role of operculoinsular cortices in human pain processing: converging evidence from PET, fMRI, dipole modeling, and intracerebral recordings of evoked potentials. *Neuroimage* 17, 1336–1346. doi: 10.1006/nimg.2002.1315

Pietrobon, D., and Moskowitz, M. A. (2013). Pathophysiology of migraine. *Annu. Rev. Physiol.* 75, 365–391. doi: 10.1146/annurev-physiol-030212-183717

Pons, T., Shipton, E. A., Williman, J., and Mulder, R. T. (2015). Potential risk factors for the onset of complex regional pain syndrome type 1: a systematic literature review. *Anesthesiol. Res. Pract.* 2015:956539. doi: 10.1155/2015/956539

Prescot, A., Becerra, L., Pendse, G., Tully, S., Jensen, E., Hargreaves, R., et al. (2009). Excitatory neurotransmitters in brain regions in interictal migraine patients. *Mol. Pain* 5:34. doi: 10.1186/1744-8069-5-34

Price, D. D. (1994). "Psychophysical measurement of normal and abnormal pain processing," in *Touch, Temperature, and Pain in Health and Disease: Mechanisms and Assessments*, eds J. Boivie, P. Hansson and U. Lindblom (Seattle, WA: IASP Press), 3–27.

Rollman, G. B. (2009). Perspectives on hypervigilance. *Pain* 141, 183–184. doi: 10.1016/j.pain.2008.12.030

Schwedt, T. J. (2013). Multisensory integration in migraine. *Curr. Opin. Neurol.* 26, 248–253. doi: 10.1097/WCO.0b013e328360edb1

Senkowski, D., and Heinz, A. (2016). Chronic pain and distorted body image: implications for multisensory feedback interventions. *Neurosci. Biobehav. Rev.* 69, 252–259. doi: 10.1016/j.neubiorev.2016.08.009

Senkowski, D., Hofle, M., and Engel, A. K. (2014). Crossmodal shaping of pain: a multisensory approach to nociception. *Trends Cogn. Sci.* 18, 319–327. doi: 10.1016/j.tics.2014.03.005

Seth, A. K., and Friston, K. J. (2016). Active interoceptive inference and the emotional brain. *Philos. Trans. R. Soc. B Biol. Sci.* 371:20160007. doi: 10.1098/rstb.2016.0007

Staud, R. (2011). Brain imaging in fibromyalgia syndrome. *Clin. Exp. Rheumatol.* 29, S109–S117.

Staud, R., and Spaeth, M. (2008). Psychophysical and neurochemical abnormalities of pain processing in fibromyalgia. *CNS Spectr.* 13, 12–17. doi: 10.1017/s109285290002678x

Sullivan, M. D., and Robinson, J. P. (2006). Antidepressant and anticonvulsant medication for chronic pain. *Phys. Med. Rehabil. Clin. N. Am.* 17, 381–400. doi: 10.1016/j.pmr.2005.12.006

Treede, R.-D., Kenshalo, D. R., Gracely, R. H., and Jones, A. K. (1999). The cortical representation of pain. *Pain* 79, 105–111. doi: 10.1016/s0304-3959(98)00184-5

Truini, A., Gerardi, M., Di Stefano, G., La Cesa, S., Iannuccelli, C., Pepe, A., et al. (2015). Hyperexcitability in pain matrices in patients with fibromyalgia. *Clin. Exp. Rheumatol.* 33, s68–s72.

Tsounis, S., and Varfis, G. (1992). α rhythm power and the effect of photic stimulation in migraine with brain mapping. *Clin. Electroencephalogr.* 23, 1–6. doi: 10.1177/155005949202300103

Valenzuela-Moguillansky, C., Reyes-Reyes, A., and Gaete, M. I. (2017). Exteroceptive and interoceptive body-self awareness in fibromyalgia patients. *Front. Hum. Neurosci.* 11:117. doi: 10.3389/fnhum.2017.00117

Valeriani, M., de Tommaso, M., Restuccia, D., Le Pera, D., Guido, M., Iannetti, G., et al. (2003). Reduced habituation to experimental pain in migraine patients: a CO2 laser evoked potential study. *Pain* 105, 57–64. doi: 10.1016/s0304-3959(03)00137-4

van Velzen, G. A., Perez, R. S., van Gestel, M. A., Huygen, F. J., van Kleef, M., van Eijs, F., et al. (2014). Health-related quality of life in 975 patients with complex regional pain syndrome type 1. *Pain* 155, 629–634. doi: 10.1016/j.pain.2013.12.017

Vanagaite, J., Pareja, J., Støren, O., White, L., Sanc, T., and Stovner, L. (1997). Light-induced discomfort and pain in migraine. *Cephalalgia* 17, 733–741. doi: 10.1046/j.1468-2982.1997.1707733.x

Vanneste, S., Ost, J., Van Havenbergh, T., and De Ridder, D. (2017). Resting state electrical brain activity and connectivity in fibromyalgia. *PLoS One* 12:e0178516. doi: 10.1371/journal.pone.0178516

Wang, T., Zhan, W., Chen, Q., Chen, N., Zhang, J., Liu, Q., et al. (2016). Altered resting-state ascending/descending pathways associated with the posterior thalamus in migraine without aura. *Neuroreport* 27, 257–263. doi: 10.1097/wnr.0000000000000529

Weissman-Fogel, I., Granovsky, Y., and Bar-Shalita, T. (2018). Sensory over-responsiveness among healthy subjects is associated with a pronociceptive state. *Pain Pract.* 18, 473–486. doi: 10.1111/papr.12619

Wertli, M., Bachmann, L. M., Weiner, S. S., and Brunner, F. (2013). Prognostic factors in complex regional pain syndrome 1: a systematic review. *J. Rehabil. Med.* 45, 225–231. doi: 10.2340/16501977-1103

Wilder-Smith, O. H., Schreyer, T., Scheffer, G. J., and Arendt-Nielsen, L. (2010). Patients with chronic pain after abdominal surgery show less preoperative endogenous pain inhibition and more postoperative hyperalgesia: a pilot study. *J. Pain Palliat. Care Pharmacother.* 24, 119–128. doi: 10.3109/15360281003706069

Woolf, C. J., and Max, M. B. (2001). Mechanism-based pain diagnosis: issues for analgesic drug development. *Anesthesiology* 95, 241–249. doi: 10.1097/00000542-200107000-00034

Woolf, C. J., and Salter, M. W. (2000). Neuronal plasticity: increasing the gain in pain. *Science* 288, 1765–1769. doi: 10.1126/science.288.5472.1765

Woolf, C. J., and Thompson, S. W. (1991). The induction and maintenance of central sensitization is dependent on N-methyl-D-aspartic acid receptor activation; implications for the treatment of post-injury pain hypersensitivity states. *Pain* 44, 293–299. doi: 10.1016/0304-3959(91)90100-c

Yarnitsky, D. (2015). Role of endogenous pain modulation in chronic pain mechanisms and treatment. *Pain* 156, S24–S31. doi: 10.1097/01.j.pain.0000460343.46847.58

Yarnitsky, D., Crispel, Y., Eisenberg, E., Granovsky, Y., Ben-Nun, A., Sprecher, E., et al. (2008). Prediction of chronic post-operative pain: pre-operative DNIC testing identifies patients at risk. *Pain* 138, 22–28. doi: 10.1016/j.pain.2007.10.033

Yarnitsky, D., Granot, M., and Granovsky, Y. (2014). Pain modulation profile and pain therapy: between pro-and antinociception. *Pain* 155, 663–665. doi: 10.1016/j.pain.2013.11.005

Zeilhofer, H. U. (2008). Loss of glycinergic and GABAergic inhibition in chronic pain—contributions of inflammation and microglia. *Int. Immunopharmacol.* 8, 182–187. doi: 10.1016/j.intimp.2007.07.009

Zhang, Z., and Sun, Q.-Q. (2011). The balance between excitation and inhibition and functional sensory processing in the somatosensory cortex. *Int. Rev. Neurobiol.* 97, 305–333. doi: 10.1016/b978-0-12-385198-7.00012-6

Zlotnik, S., Attias, J., Pratt, H., and Engel-Yeger, B. (2018). Neurophysiological manifestations of auditory hypersensitivity correlate with daily life experiences. *Neurosci. Med.* 9, 29–45. doi: 10.4236/nm.2018.91005

Conflict of Interest Statement: The authors declare that the research was conducted in the absence of any commercial or financial relationships that could be construed as a potential conflict of interest.

Copyright © 2019 Bar-Shalita, Granovsky, Parush and Weissman-Fogel. This is an open-access article distributed under the terms of the Creative Commons Attribution License (CC BY). The use, distribution or reproduction in other forums is permitted, provided the original author(s) and the copyright owner(s) are credited and that the original publication in this journal is cited, in accordance with accepted academic practice. No use, distribution or reproduction is permitted which does not comply with these terms.

frontiers in Integrative Neuroscience

REVIEW
published: 06 September 2019
doi: 10.3389/fnint.2019.00040

Sensory Over-Responsivity as an Added Dimension in ADHD

Shelly J. Lane[1,2]* *and Stacey Reynolds*[3]*

[1] Department of Occupational Therapy, College of Health and Human Science, Colorado State University, Fort Collins, CO, United States, [2] Faculty of Health and Medicine, School of Health Sciences, University of Newcastle, Callaghan, NSW, Australia, [3] Department of Occupational Therapy, Kathryn Lawrence Dragas Sensory Processing and Stress Evaluation Laboratory, Virginia Commonwealth University, Richmond, VA, United States

Years of research have added to our understanding of Attention Deficit Hyperactivity Disorder (ADHD). None-the-less there is still much that is poorly understood. There is a need for, and ongoing interest in, developing a deeper understanding of this disorder to optimally identify risk and better inform treatment. Here, we present a compilation of findings examining ADHD both behaviorally and using neurophysiologic markers. Drawing on early work of McIntosh and co-investigators, we examined response to sensory challenge in children with ADHD, measuring HPA activity and electrodermal response (EDR) secondary to sensory stressors. In addition, we have examined the relationship between these physiologic measures, and reports of behavioral sensory over-responsivity and anxiety. Findings suggest that sensory responsivity differentiates among children with ADHD and warrants consideration. We link these findings with research conducted both prior to and after our own work and emphasize that there a growing knowledge supporting a relationship between ADHD and sensory over-responsivity, but more research is needed. Given the call from the National Institute of Health to move toward a more dimensional diagnostic process for mental health concerns, and away from the more routine categorical diagnostic process, we suggest sensory over-responsivity as a dimension in the diagnostic process for children with ADHD.

Keywords: sensory over-responsivity, ADHD, anxiety, cortisol, children

OPEN ACCESS

Edited by:
Elizabeth B. Torres, Rutgers University, The State University of New Jersey, United States

Reviewed by:
Antonio Pereira, Federal University of Pará, Brazil
Beth Pfeiffer, Temple University, United States

Correspondence:
Shelly J. Lane
shelly.lane@colostate.edu
Stacey Reynolds
reynoldsse3@vcu.edu

Received: *28 January 2019*
Accepted: *02 August 2019*
Published: *06 September 2019*

Citation:
Lane SJ and Reynolds S (2019) Sensory Over-Responsivity as an Added Dimension in ADHD. Front. Integr. Neurosci. 13:40. doi: 10.3389/fnint.2019.00040

INTRODUCTION

Attention Deficit Hyperactivity Disorder (ADHD), is a neurodevelopmental disorder characterized by ongoing patterns of inattention and/or hyperactivity and impulsivity that impacts an individual's functioning across multiple environments. Despite being the most commonly diagnosed mental disorder in children in the United States (Centers for Disease Control and Prevention, 2018), ADHD remains a heterogeneous disorder that is not fully understood (or agreed upon) within the medical and scientific communities. None-the-less, in the United States and other countries, ADHD diagnosis is based upon evaluation by a licensed medical professional using the Diagnostic and Statistical Manual, 5th edition (DSM-5, American Psychiatric Association, 2013) "yes/no" approach to symptom presentation. Three sub-types of ADHD were introduced with the

publication of the DSM-IV and these presentations were retained in the 5th edition. These classifications are (1) Predominantly Inattentive, (2) Predominately Hyperactive/Impulsive, and (3) Combined Type. A key criticism to the current approach to the diagnosis of ADHD is a failure to recognize the condition as dimensional disorder that may contain different sub-classifications, comorbidity patterns, symptom trajectories, and neurobiological correlates (Epstein and Loren, 2013). As noted by Epstein and Loren (2013) the "DSM-5 continues to place everyone meeting diagnostic criteria into a single category which does not capture the dimensionality of underlying constructs" (p. 3). The current subtyping strategies of the DSM have also been called into question, due to both the "capricious" nature by which they are assigned and the lack of studies supporting an underlying neurobiological basis for the divisions (Valor and Tannock, 2010, p. 749; Epstein and Loren, 2013).

Researchers have sought to understand the complex features more fully associated with childhood ADHD and have begun to examine qualitative and quantitative variables that impacted the expression, or predicted outcomes, of ADHD. Diagnostic moderators such as comorbid anxiety disorder, symptom severity, and child intellectual level were all identified in the ADHD population as part of a large multimodal treatment study (March et al., 2000; Owens et al., 2003; Hinshaw, 2007). In addition, neurobiological mechanisms associated with arousal and stress responsivity have begun to gain attention within the ADHD literature. Response differences within the hypothalamic-pituitary-adrenal (HPA) axis that may be related to an altered threshold for detection of stressors has emerged as a potential feature of ADHD (Kariyawasam et al., 2002). Specifically, several investigators identified a blunted cortisol response to stress in ADHD, especially in those individuals with the combined subtype of the disorder or more severe behavioral comorbidities (King et al., 1998; Maldonado et al., 2009; Van West et al., 2009). However, in a smaller sample of studies investigators also found that some children with ADHD showed higher cortisol levels following stressors (Hong et al., 2003; White and Mulligan, 2005) and yet still other studies have found no differences between ADHD and control populations (Lackschewitz et al., 2008; Hirvikoski et al., 2009). Heterogeneity in these outcomes is likely due to a variety of factors including variability in diagnostic process, cortisol collection methods used, stressors (e.g., social threat, academic task), composition of the diagnostic group, and control for comorbidities. Interestingly, anxiety disorder was noted to be a potential moderating factor in cortisol release in both ADHD and non-ADHD populations (Greaves-Lord et al., 2007; Hastings et al., 2009), suggesting the particular importance of considering co-morbidities in ADHD research.

In parallel to the work described above, but in a separate body of research, investigators began to focus on the presence of atypical sensory responsivity in children with ADHD. While a variety of terms have been used in the literature to reflect atypical sensory responsivity, sensory modulation disorders (SMD) may best describe this group of behaviors as a type underlying sensory processing dysfunction. SMDs are characterized by an inability to respond to environmental stimuli in a way that matches the demands of the stimulus (Lane, 2019). Individuals characterized as having sensory over-responsiveness (SOR) experience sensations more intensely or for a longer duration than is normal, often resulting in "fight or flight" behaviors. For those with the sensory under-responsive (SUR) subtype of SMD, sensory stimuli in the environment are disregarded, or not responded to, resulting in the child seeming to lack initial awareness. This group may appear apathetic or lacking motivation (Miller et al., 2007). As a whole, the SOR characterization has been more widely studied in the literature and is the better established subtype (Reynolds and Lane, 2008).

Multiple investigators have established that children with ADHD have difficulties in sensory processing and regulating emotional responses to sensation based on parent report questionnaires (Dunn and Bennett, 2002; Kalpogianni, 2002; Yochman et al., 2004). These studies are limited by methodology; many of the questions on the SMD parent-report tools include behaviors that overlap with the diagnostic features associated with ADHD (e.g., emotional and social responses, activity levels). Studies using objective physiological measures to record responses to sensory stimuli began to emerge in the ADHD literature, but with inconsistent findings. Mangeot et al. (2001) used electrodermal reactivity, reflecting sympathetic nervous system activity, to measure responses to sensory stimuli in children with and without ADHD. They found that children with ADHD had greater sympathetic responses to sensory stimuli upon initial presentation compared to typical children. However, other researchers using similar electrodermal measures found no differences in responsivity between ADHD and non-ADHD groups (Herpertz et al., 2003). Prior to 2009, a single published study was identified investigating SOR as a moderating variable for electrophysiological measurement in children with ADHD. Using EEG measures, Parush et al. (2007) indicated that children with ADHD and a specific form of SOR, tactile over-responsivity or defensiveness, showed different central processing of somatosensory input relative to children with ADHD without tactile-over-responsivity. Parush et al. (2007) indicated that there was a need to further investigate SOR in children with ADHD, examining children with and without SOR using neurophysiological outcomes.

Importantly, while the research published in the first decade of the 21st century expanded the scientific community's knowledge of ADHD, associated symptoms, and neurological processes, these studies were generally conducted in isolation. That is to say, anxiety in ADHD was studied separately from stress responsivity in ADHD, and separately from sensory responsivity in ADHD. Building from these studies, our work in the Kathryn Lawrence Dragas Sensory Processing and Stress Evaluation (SPASE) lab began a trajectory of work, considering the potential relationships between and among these constructs (i.e., sensation, anxiety, and stress responses), using a more dimensional approach. We will review this work, published between 2009 and 2012, in the proceeding section, followed by an update on the current literature to provide an understanding of this area to date.

The overall purpose of this review is to summarize the current state of understanding related to ADHD and sensory processing as well as to provide a direction for future research.

Ultimately, we will suggest that atypical sensory processing is an important and often overlooked dimension in the diagnosis and classification of ADHD.

ADHD, CORTISOL, ELECTRODERMAL RESPONSE, AND ANXIETY: FINDINGS FROM THE SPASE LAB

Study 1 (Reynolds and Lane, 2009): SOR and Anxiety in Children With ADHD

Our initial work investigated the co-existence of SOR and anxiety in children with ADHD (n = 24) and without ADHD (n = 24) (Reynolds and Lane, 2009). SOR in this investigation was identified using a research version [version 1.4; (V1.4)] of the Sensory Over-Responsivity Inventory (SensOR; Miller, unpublished). The SensOR had been designed as one component of a larger tool, providing parent report of sensory responses within the range of sensory domains. V1.4 was the outgrowth of content validity, field testing, and item analysis completed on earlier versions. This version was shown to have high internal consistency (Cronbach's α = 0.65 to 0.88) and strong construct validity, distinguishing between SOR and typical responsiveness within each sensory domain ($p < 0.001$ for each domain; Schoen et al., 2008). Items on this tool addressed sensory responses across tactile, auditory, visual, olfactory, gustatory, and movement-proprioceptive sensory domains. While still in development at the time of its use, this tool was considered optimal for that study because of the focus on the over-responsive type of sensory modulation dysfunction. Established sensory-processing tools at that point in time failed to clearly distinguish between over-responsiveness and under-responsiveness. Koziol and Budding (2012) had identified this shortcoming as problematic. Scores across sensory category, and the total SensOR score were compared with scores obtained from a typical sample.

The Revised Children's Manifest Anxiety Scale (RCMAS; Reynolds and Richmond, 2005), a behavioral measure of anxiety, was used to assess anxiety in Study 1. The RCMAS is a 37-item self-report tool appropriate for use with children ages 6 to 19. This tool provides scores across three subscales, physiological anxiety, worry/oversensitive, and social concerns/concentration, and a total score. Each subscale and the total score have been shown to have moderate to high internal consistency (α = 0.69, 0.84, 0.72, and 0.89, respectively) (Muris et al., 2002). There are 28-items measuring anxiety, and an additional nine items making up a lie or social desirability score. High RCMAS scores are consistent with greater anxiety. High lie scale scores are interpreted to reflect inconsistent, inaccurate, or other problematic responding styles from the child. There is no overlap between RCMAS items and SensOR items, but some overlap exists between RCMAS items and diagnostic symptoms of ADHD (e.g., RCMAS items "It is hard for me to keep my mind on my school work" and "I wiggle in my seat a lot" share features of both inattention and increased activity that parallel ADHD diagnostic items). Higher scores on the RCMAS indicate greater levels of anxiety. Six-month test–retest reliability indicates stability in scores for all subscales (rs = 0.52 to 0.68, $p \leq 0.01$; Turgeon and Chartrand, 2003). Our approach with this tool was to have parents read aloud the items to their child, and have the child circle a "yes" or "no" to reflect their response.

Our findings in this study supported the work of Parush et al. (2007) in documenting that children with ADHD could be differentiated based on their response to sensation. Parush et al. (2007) focused their study on tactile defensiveness, suggesting that their findings indicated atypical central processing of somatosensation possibly related to disruptions in central nervous system inhibitory systems. Like Parush et al. (2007), we identified two sub-groups of children with ADHD: those with ADHD and SOR (ADHDs) and those with ADHD but no SOR (ADHDt). Further, we found that children with ADHDs more frequently exhibited anxiety within a clinically significant range than did children with ADHDt (Reynolds and Lane, 2009). If atypical neural inhibitory mechanisms play a role in tactile defensiveness, as suggested, it is possible that faulty inhibitory mechanisms are at play for both the SOR and high anxiety we identified in our work. In a systematic review, Levy had suggested that the anxiety identified in some children with ADHD might be explained by faulty prefrontal cortex and hippocampal gating, or inhibition, of amygdalar activity (Levy, 2004). Our work adds support to this possibility. Interestingly, reductions in the inhibitory neurotransmitter GABA have been identified in cortical regions that include the somatosensory and motor cortices, in children with ADHD (Edden et al., 2012). It is possible that GABA plays a role in the combination of SOR and anxiety we found in children with ADHD. Unfortunately, we were not able to assess these neurobiologic possibilities. However, our identification of a relationship between SOR and anxiety in children with ADHD had not been previously identified, and we suggested that SOR should be considered as an additional dimension within the diagnosis of ADHD.

Study 2 (Reynolds et al., 2010): Moderating Role of SOR

Subsequently we studied the same sample of children with and without ADHD (n = 48) based on their response to sensory challenge, measuring sensory responsivity, electrodermal response (EDR) to sensory challenge, and cortisol at baseline and following the sensory challenge (Reynolds et al., 2010). In this study we used a version of the Sensory Challenge Protocol developed by McIntosh et al. (1999), and described in detail elsewhere (McIntosh et al., 1999). As an overview, the protocol provided stimuli within auditory, visual, smell, touch, and movement domains. Eight stimuli within one sensory domain were presented in series, using variable inter-stimulus intervals (10–15 s). Following each set of eight stimuli the protocol moved to the next sensory domain. Overall the protocol required approximately 20 min to administer. To adequately compare changes in cortisol pre- and post-exposure to sensory stimuli, we collected two salivary cortisol samples, 5-min apart, before the sensory protocol began (baseline), and seven cortisol samples post-protocol, each 5 min apart. Salivary cortisol samples were collected by placing a plain (non-citric acid) cotton

Salivette (Sarstedt, Newton, NC, United States) under the child's tongue for 60 s prior to and following the sensory challenge. Children rested and watched a silent cartoon during the post-protocol period.

Our findings pointed to SOR as a moderator variable for the HPA response to sensory challenge, reflecting a pre-existing condition/status of the participant. We proposed that children with SOR were predisposed to respond differently to the sensory stimuli in this protocol. Interestingly, we found that the subgroup of children, those with ADHDs, showed typical cortisol responses, while children with ADHDt had the expected blunted cortisol response. These findings lead us to suggest that children with ADHD might be better understood by also examining sensory responsivity (Reynolds et al., 2010). A blunted cortisol response, such as we identified in the ADHDt children, had been identified by previously in children with ADHD as a whole, and within a population of children with ADHD and behavioral co-morbidities (King et al., 1998; Maldonado et al., 2009; Van West et al., 2009). However, these findings are quite inconsistent across studies (Kamradt et al., 2018). Kamradt et al. (2018) indicate that a link between the HPA axis and ADHD had been found for children with severe externalizing behaviors, and that these behaviors might be the driver of this relationship. Our findings of sensory responsivity as a distinguishing feature indicates a need to examine further this characteristic in children with ADHD. While we did not find severe externalizing behaviors, the behaviors associated with avoidance of sensation seen in some children with SOR might be interpreted as significant externalizing behavior. We further proposed that this different sensory responsiveness might influence optimal interventions; perhaps children with both ADHD and SOR would best respond to a dual approach to treatment, addressing both the characteristics of ADHD and those of SOR. This will require additional research.

Study 3 (Lane et al., 2010): Differentiating SOR and ADHD

Considering that the relationship between anxiety, neuroendocrine, electrodermal, and behavioral characteristics of children with ADHD might support a unique dimensional perspective on ADHD, we further examined our data, to determine if we could predict group membership among 84 6–12-year-old children with ADHDs, ADHDt, and children with no diagnosis (typicals; TYP) (Lane et al., 2010). As before, we used the RCMAS (Reynolds and Richmond, 2005) to document anxiety and SOR was identified using the SensOR (Schoen et al., 2008).

The Sensory Challenge Protocol provided the sensory stressor and we examined EDR and cortisol measures to address our question. EDR reflects the sympathetic nervous system reaction to sensation, the stressor in this study. Our protocol included a 3-min baseline and ongoing EDR measurement during the sensory challenge protocol and for a 3-min recovery at the end of the sensory challenge protocol. EDR measurement used procedures we had successfully used in other studies (Reynolds et al., 2010), and followed the recommendations of Fowles et al. (1981). Variables of interest included average tonic electrodermal activity during baseline and recovery, and mean EDR magnitude within each sensory domain to examine sensory reactivity. Not surprisingly, it was necessary to log transform the data prior to analysis as raw data were positively skewed; this is typical of EDR data (Dawson et al., 1990, 2007; Boucsein, 1992). As noted earlier, cortisol was sampled twice at baseline and for seven 5-min intervals following completion of the sensory challenge protocol.

Using stepwise discriminative analysis we found that anxiety variables were the strongest predictors, although the overall model was further strengthened using EDR variables. The combination of these variables allowed us to correctly classify 85.6% of our total sample into groups that included ADHDs, ADHDt, TYP, and TYPs. We were able to cross validate this discriminative function, correctly classifying nearly 45% of all children. In interpreting these findings we suggested that SOR be considered a steady state characteristic, driving the child's response to environmental sensation. Nigg (2006) had described the hyperactive/impulsive characteristics of ADHD as related to reactive control and low level neural responses that are stimulus driven. We had hypothesized that the sensory responsivity we see with SOR in children with ADHD may also be related to poor reactive control. Nigg et al. (2005) both related these behaviors to meso-limbic dopamine system. While we did not investigate this, it remains a possibility. Additional consideration of the role of anxiety, it is also possible that these children experience a prefrontal/hippocampal gating deficit, such as that suggested by Levy (2004). Additional research is required.

Study 4 (Lane et al., 2012): SOR and Anxiety in ADHD – Cause or Co-existence?

Green and Ben-Sasson (2010) had suggested that over-responsiveness to environmental sensation may become associated with other contextual features such as specific objects and events that surround the sensory stressor. They further hypothesized that this association, and the individual's interpretation of it as both unpredictable and uncontrollable, could result in general anxiety due to the development of phobias or avoidance, hypervigilance, hyperarousal (Lane et al., 2012). Green and Ben-Sasson (2010) termed this the primary SOR model. Our study utilized a combined data set of children with ADHD and children with Autism Spectrum Disorder (ASD) to achieve a large enough sample size (n = 131) to conduct a path analysis examining the primary SOR model. As reported above, we used the SensOR (Schoen et al., 2008) to identify SOR in children with ADHD. The Sensory Profile (SP; Dunn, 1999) was used for children with ASD. This tool is also a parent report tool that identifies the child's response to everyday sensation. There are 125 items on the SP, grouped into sensory domains and factors. Scoring identifies sensory quadrants into which children "fit," reflecting the interface between neural threshold and self-regulation/responsiveness. Cronbach's alpha for quadrant groupings are moderate to strong (r = 0.87 to 0.93; Dunn, 2006). For this study, which focused

on the construct of over- responsivity, we used only the Sensory Sensitivity and Sensation Avoiding quadrant scores of the Sensory Profile.

To examine the primary SOR hypothesis we used path analysis (Wright, 1921). Path analysis is an approach that represents general linear models as paths; latent variables are used in the analysis. This approach allowed us to examine mediation models in which the effect of one variable (the predictor) on an outcome variable depends on a third, or mediator, variable (MacKinnon, 2008). As such we investigated our hypothesis that response to sensory challenge would mediate the relationship between our predictor and outcome variables. We used scores from the SP or the SensOR Inventory, representing SOR, and baseline physiological variables reflecting tonic arousal at the start of the sensory challenge protocol (electrodermal activity and cortisol) as predictors, and mean EDR magnitude as the mediating variable. We included recovery electrodermal activity and total anxiety score as outcome variables reflecting both recovery from potentially altered arousal levels and generalized anxiety.

We substantiated a link between SOR and anxiety in our TYP group of children. While there is ongoing controversy relative to the presence of SOR in children and adults without another diagnosis, several investigative groups have identified individuals with SOR and no additional diagnosis (Kinnealey and Oliver, 1995; McIntosh et al., 1999; Reynolds and Lane, 2008; Van Hulle et al., 2012). We also substantiated a previously described relationship between SOR and anxiety in children with ADHD (Reynolds and Lane, 2009; Lane et al., 2010). Thus, initial findings offered a degree of confirmation of the primary SOR model proposed by Green and Ben-Sasson (2010), indicating that the presence of SOR may in fact be one cause of child anxiety.

Beyond these initial findings, our path analysis confirmed a relationship between SOR and anxiety in TYP children and children with ADHD. The EDR to sensory challenge fully mediated the relationship between baseline sympathetic activity and total anxiety scores. In addition, the EDR partially accounted for a relationship between skin conductance at baseline and at recovery. We did not find mediation between baseline measures (cortisol and SOR) and outcome measures (total anxiety and skin conductance at recovery). Thus, our path model indicated that the strength of the child's response to sensory stimuli, as seen using the sensory challenge protocol, mediates the relationship between baseline measures of arousal and attention, and anxiety and sympathetic nervous system recovery. This too supports the primary SOR model proposed by Green and Ben-Sasson (2010) indicating that SOR may be an underlying cause of child anxiety (Lane et al., 2012). A recent paper by Amos et al. (2019), also examined this relationship in a group of children with ASD. These investigators substantiated the primary SOR model, indicating that SOR and stress were mediators between autistic traits in the general population and anxiety.

Limitations

There are of course limitations to this body of work. Our sample sizes were small, with recruitment challenged by our desire to include children with ADHD but not co-morbid behavioral or psychological conditions (e.g., ASD, Oppositional Defiant Disorder). These smaller sample sizes limited our ability to distinguish between ADHD presentations (that is primarily inattentive, primarily hyperactive, or combination), as well as our ability to examine gender differences. Our sample was also self-referred, and inherent in this is potential selection bias. Our work in the SPASE lab has been globally focused on sensory processing, and our interest in sensory processing may have attracted a unique sample of children. An additional study limitation was our use of parent report measures to assess sensory responsivity. While there is support for the validity of parent report (Diamond and Squires, 1993; Greenfield et al., 2004), there are also notable problems with this manner of data collection for some types of behaviors (Ben-Sasson et al., 2009; Woodard et al., 2012). Additional assessment limitations relate to the ADHD diagnosis; we did not include tests of attention or repeat the diagnostic process for children with a prior diagnosis of ADHD. As these studies were designed to develop a greater understanding of the dimensions of ADHD, we did not have a comparison group with only SOR. In spite of the limitations, our findings lead us to suggest that SOR is a promising dimension, but that more research is needed to clarify and substantiate the relationships we have proposed between sensory processing, anxiety, and stress responsivity in ADHD.

RESEARCH DEVELOPMENTS IN ADHD WITH LINKS TO SENSORY RESPONSIVITY

Research examining the constructs of sensory responsiveness, anxiety and physiological stress responsivity have continued to emerge in the ADHD literature, and results have filled in some of the gaps left by our original work. The purpose of this section is to succinctly review recent progress in the area of ADHD and sensory responsivity.

Multiple studies have been conducted replicating earlier findings that individuals with ADHD have a higher prevalence of atypical sensory responsivity compared to those without ADHD (Shimizu et al., 2014; Pfeiffer et al., 2015; Bijlenga et al., 2017; Panagiotidi et al., 2018). Shimizu et al. (2014) looked at correlations between sensory processing and modulation problems (as measured by the Brazilian version of the Sensory Profile) and behavioral symptomatology in children with and without ADHD (n = 37 per group). In addition to finding that children with ADHD had a greater prevalence of atypical sensory modulation and nearly all other sensory processing problems, these authors also found strong correlations between a variety of sensory processing and modulation impairments and inappropriate behavior and learning responses in children with ADHD. Although sensory-based sub-groups were not used in this study, the authors did examine differences in SP scores between ADHD subtypes (primarily inattentive, primarily sensory processing domain and ADHD-combined), but no significant differences were identified. These findings support the work of Engel-Yeger and Ziv-On (2011) who also found no significant differences between ADHD subtypes

using an abbreviated version of the SP in a population of 58 boys with ADHD.

Pfeiffer et al. (2014) sought to determine if the response to specific sensory domain inputs was associated with inattention and hyperactivity/impulsivity (core ADHD symptoms) in children ages 5–10 years. These investigators used the Sensory Processing Measure-Home Form; a parent report tool that assesses response to sensation across the range of sensory domains, social participation and motor planning (Parham and Ecker, 2007). Similar to other reports, Pfeiffer and colleagues found greater sensory modulation concerns across all sensory domains in children with ADHD relative to age-matched controls. Interestingly, they identified no significant relationships between sensory modulation scores within visual, auditory, tactile, proprioceptive, and vestibular domains and inattention or hyperactivity/impulsivity. These results were concordant with Ghanizadeh (2011) who summarized the literature in this area and concluded that DSM-based ADHD subtypes are not distinct disorders with regard to atypical sensory processing.

While the majority of research investigating atypical sensory processing and ADHD has been conducted in children, Bijlenga et al. (2017) investigated the prevalence of sensory over and under responsivity in adults with and without ADHD. In this study, 116 adults completed an Adult/Adolescent Sensory Profile (Brown and Dunn, 2002) along with an ADHD self-rating scale. As expected, the ADHD group had more sensory symptoms across all areas of the Sensory Profile and those scores correlated significantly with ADHD symptom scores. Interestingly, 43% of adult females had sensory over and/or under responsivity compared to 22% of adult males, with SOR being more prevalent in females (32%).

Panagiotidi et al. (2018) also investigated the relationship between atypical sensory processing and ADHD traits in adults, using self-report. These investigators collected responses from two online questionnaires (Glasgow Sensory Questionnaire, Adult ADHD Self-Report Scale) in a general adult population (n = 234). Similar to what had already been found in diagnostic samples, these investigators found an association between ADHD traits and a higher frequency of sensory difficulties in all sensory systems (e.g., visual, tactile, and auditory). In this investigation they found this relationship for both over and under responsivity. A shortcoming of this study was that no statistical methods were used to assess gender differences or potential sensory-based subtypes. Panagiotidi's work was in part based on earlier work by Overton (2008) and Panagiotidi et al. (2017). These investigators had proposed that one potential neural locus linking ADHD, attentional concerns, and sensory over-responsivity was atypical multi-sensory integration in the superior colliculus. Overton (2008) put forth a strong argument indicating that the superior colliculus was itself over-responsive to sensory input. This structure drives our response to phasic sensory changes in the environment and leads us to turn both head and eyes toward the novel stimulus. Research in both animals and humans indicates that lesions of the superior colliculus, or disconnecting it from the prefrontal cortex, produces distractibility. Panagiotidi et al. (2017) further identified that individuals with ADHD characteristics showed poor multisensory integration (auditory and visual), quite possibly in the superior colliculus, resulting in each stimulus being perceived independently, and potentially resulting in distractibility. These investigators acknowledged that the superior colliculus was only one structure among a network of cortical and subcortical structures also linked to multisensory integration and detection of stimulus synchrony and asynchrony.

Similar to the study by Panagiotidi and Colleagues, Ben-Sasson et al. (2014) used a large normative population to study ADHD and sensory symptomatology on a continuous scale. In this study, 922 children were followed from infancy to school age. Measures included the SensOR (Schoen et al., 2008) and the ADHD scale on the Child Behavior Checklist (Achenbach and Rescorla, 2001). The authors used a dimensional clustering approach to characterize children based on ADHD and SOR symptoms. Study findings supported prior findings indicating that SOR and ADHD are often seen together in a normative sample. Ben-Sasson et al. indicated that nearly half of their sample with elevated ADHD symptoms also evidenced SOR. Similarly, of the sample with SOR, 50% also evidenced symptoms of ADHD. These rates are similar to those found by Bijlenga et al. (2017) the adult ADHD population and in our previous studies with school age children (Lane et al., 2010). An intriguing new finding from this work was that ADHD and SOR identified in early childhood continued to present into school age; this relationship appears to be stable across several developmental years. While it is fairly well established that both ADHD and SOR are conditions that do not simply resolve with age (Rasmussen and Gillberg, 2000; Ben-Sasson et al., 2010; Van Hulle et al., 2015), the stability of their co-occurrence over time specifically suggests stability in the sensory dimension of ADHD.

Another interesting finding from the Ben-Sasson (2014) study was that girls with ADHD appeared to be at a unique risk for having tactile over-responsivity. Previous findings in children had been somewhat mixed, with some investigators indicating that girls with ADHD more frequently show tactile defensiveness (Goldsmith et al., 2006; Bröring et al., 2008), and others finding no difference between boys and girls (Cheung and Siu, 2009). Interestingly, Bijlenga et al. (2017) had also found that adult women with ADHD were more likely than men with ADHD to show sensory responsivity differences, and within those differences were more likely to experience SOR.

Given that there is over-lap between behaviors associated with poor sensory processing and ADHD, there has been some effort put toward understanding how these behaviors may change or manifest over time and how they might be better distinguished from one another. For instance, Yochman et al. (2013) documented that children with SMD could be distinguished from children with ADHD using an early form of the SPM, the Evaluation of Sensory Processing (Johnson-Ecker and Parham, 2000; Parham and Johnson-Ecker, 2002) and additional psychophysical tools. Somewhat in contrast to our findings, these investigators contended that response to sensation was in fact a means of separating children with ADHD from children with SMD. Looking at change over the developmental trajectory, Ben-Sasson et al. (2014) found that children with ADHD only, SOR only, and Combined ADHD +SOR all showed

patterns of over- activity and inattention in early childhood (24–48 months). The SOR-only group displayed a decline in these symptoms throughout childhood while the ADHD and ADHD+SOR groups did not. This parallels evidence suggesting that adults with SMD do not display core deficits in attentional tasks (Mazor-Karsenty et al., 2015). One explanation for this trend is that infants who later present only with SOR may display difficulties with attention and activity levels early on due to constant over-arousal and hypervigilance toward sensory stimuli (Ben-Sasson et al., 2014). Another explanation, offered by Mazor-Karsenty et al. (2015), is that inattention and high activity levels may be a stable characteristic (trait) of those with ADHD, while individuals with SOR only may experience transient states of inattention or altered activity levels under specific sensory conditions.

Both ADHD and SOR have been shown to have a genetic link. For ADHD heritability is high (Faraone et al., 2005). There has been limited investigation into the heritability of SOR, but Goldsmith et al. (2006) and Van Hulle et al. (2012) indicate that mothers of children with SOR might pass on genes related to either SOR or psychopathology. These investigators reported that SOR exists independent of other childhood psychopathology, but also commonly alongside childhood psychopathology. Interestingly they found stronger correlations between SOR symptomatology and internalizing symptoms (including anxiety) than with externalizing symptoms (including characteristics of ADHD).

Brain imaging studies might also offer some insights. While they have produced some inconsistencies for children with ADHD, looking across these investigations and the few available on children with sensory processing disorders uncovers some interesting overlaps. For instance, Owen and colleagues found, in children with sensory processing disorders, decreases of fractional anisotropy in several regions, but of interest is the superior longitudinal fascicle. Individuals with both sensory processing disorder (Owen et al., 2013) and ADHD (Liston et al., 2011) show differences in this region. Examining these tracks in individuals with both sensory processing disorders and ADHD could prove to be fruitful.

Since our initial work examining links between sensory processing, anxiety, and stress responsivity, no other studies could be identified that have examined these constructs simultaneously in children or adults with ADHD. Researchers of HPA functioning in the ADHD population have continued using a variety of methods for inducing stress and producing variable results (e.g., Corominas-Roso et al., 2015; Raz and Leykin, 2015). Kamradt et al. (2018), using meta-analysis, indicated that no consistent significant association between ADHD and cortisol reactivity could be found. However, an identified limitation was a lack of differentiation among symptom presentations and co-morbidities in the selected studies. In contradiction to this finding, Corominas-Roso et al. (2015) found a blunted cortisol response following a social challenge in those individuals with the ADHD combined subtype, but not in those with the inattentive subtype. In our preliminary work we had identified a blunted cortisol response in those children with ADHD but only in the absence of concomitant SOR. Thus, there are multiple conflicting findings relative to HPA responses in adults and children with ADHD, suggesting a need for additional research both to explore DSM-based ADHD classifications and sensory-based subgrouping schemes.

Finally, the overlap between symptoms of anxiety and ADHD has been widely studied in recent years; and research suggests that approximately 25% of adults with ADHD also meet the criteria for generalized anxiety disorder (GAD) and that approximately 25% of adults with GAD also meet the criteria for ADHD (Van Ameringen et al., 2011; Piñeiro-Dieguez et al., 2016; Reimherr et al., 2017). In adult populations, higher anxiety has been associated with both the combined type ADHD presentation as well as with greater ADHD symptomatology (for review see Reimherr et al., 2017). In children, the rates of overlap may be even higher, with some studies estimating that 30–40% of clinically referred children with ADHD have internalizing disorders such as anxiety (Jensen et al., 2001; Tannock, 2009). In both the pediatric and adult populations, the combined presence of ADHD symptoms and anxiety is thought to lead to a more complicated behavioral manifestation with greater functional impairments. Differential diagnosis between ADHD and anxiety disorders is an ongoing challenge in clinical settings (Grogan et al., 2018) and some researchers have even suggested a distinct ADHD-Anxiety clinical subtype (Jensen et al., 2001; Reimherr et al., 2017). Interestingly, both adults and children have demonstrated a reduction in anxiety symptoms when taking medications traditionally prescribed for ADHD (i.e., methylphenidate, atomoxetine), suggesting a potential common neurobiology of the symptoms comprising each disorder (Snicova et al., 2016; Reimherr et al., 2017).

Our previous work established a link between SOR and anxiety (Reynolds and Lane, 2009; Lane et al., 2012) in children with ADHD, and this link has been well substantiated in other diagnostic groups of children and adults, particularly those with ASD (Bart et al., 2017; Carpenter et al., 2018; Syu and Lin, 2018). Within the ASD literature, testable models have been proposed that link SOR, anxiety, and autistic traits as well as aspects of physiological and behavioral stress (Green and Ben-Sasson, 2010; Amos et al., 2019). As noted earlier, Amos et al. (2019), found that SOR and stress mediated the relationship between autistic traits and anxiety, in that the relationship between autistic traits and anxiety became non-significant after accounting for the effects of SOR and stress. While no specific models have been proposed and tested outlining these relationships in the ADHD population, similar mediating relationships likely exist and warrant further study in the ADHD field.

DISCUSSION

Years of research have added greatly to our understanding of ADHD. None-the-less there is a need for, and ongoing interest in, developing a deeper understanding of this disorder, to optimally identify risk and better inform treatment. This is consistent with the intent of the Research Domain Criteria

(RDoC) delineated by the National Institute of Mental Health (NIMH) which are designed to support a better understanding of mental health and ill-health using multiple dimensions (Morris and Cuthbert, 2012). Here, we have presented a compilation of findings from our laboratory, examining ADHD behaviorally and using neurophysiologic markers. Drawing on early work of McIntosh and co- investigators, we examined response to sensory challenge in children with ADHD, measuring HPA activity and EDR secondary to sensory stressors. In addition, we have examined the relationship between these physiologic measures, and reports of behavioral sensory over-responsivity and anxiety. Together our findings suggest that sensory responsivity is not ubiquitously present in children with ADHD, and they offer a different perspective on the variability of ADHD. The co-existence of atypical sensory processing and ADHD has been documented by a number of other investigators (Pfeiffer et al., 2014; Shimizu et al., 2014; Bijlenga et al., 2017; Panagiotidi et al., 2018), providing support for our findings. Given the call from the NIMH to move toward a more dimensional diagnostic process for mental health concerns, and away from the more routine categorical diagnostic process, we suggest sensory over-responsivity as a dimension in the diagnostic process.

Our collected findings are of interest. Not all children with ADHD show SOR, but when they do, the SOR influences other aspects of behavior. In addition, we have documented that the presence of SOR moderates the stress response to sensory challenge for both typical children and children with ADHD. That is when children identified as having SOR they release cortisol in response to threat (in this case, sensory challenge) regardless of the presence or absence of the ADHD diagnosis. In contrast, children with ADHDt showed a blunted cortisol response, a finding reported by at least some other investigators (King et al., 1998; Maldonado et al., 2009; Van West et al., 2009). Further, although anxiety has been widely reported to accompany ADHD (Jensen et al., 2001; Tannock, 2009), in our work we show that anxiety that is clinically significant is not seen in children without SOR, whether they have ADHD or not. Finally, we have shown that response to perceived sensory threat influences the ability of the child with SOR to restore levels of arousal and attention to baseline, suggesting that the influence of response to this threat may itself challenge the child's ability to regulate his or her behavior.

An important aspect of the co-occurrence of ADHD and sensory responsivity comes in the form of an impact on activity and participation. The three cases presented in our early work (Reynolds and Lane, 2008) indicated that difficulties with sensory processing, particularly sensory over-responsivity, impacted participation in routine, everyday activities. The negative impact on activity and participation has been shown by several other investigators, in association with no diagnosis other than a sensory processing deficit (c.f. Bar-Shalita et al., 2008; Cosbey et al., 2010; Ismael et al., 2015; Chien et al., 2016) in children with ASD (c.f. Provost et al., 2009; Hochhauser and Engel-Yeger, 2010; Reynolds et al., 2011a; Little et al., 2015; Piller and Pfeiffer, 2016), in children with ADHD (c.f. Engel-Yeger and Ziv-On, 2011; Reynolds et al., 2011b; Yochman et al., 2013; Pfeiffer et al., 2014), and to some extent in adults (c.f. Meredith et al., 2016).

The RDoC encourages investigators to use multiple methodologies to understand defined constructs, and we have moved toward this goal with our work. The findings reported here reflect parameters most closely related to the arousal and regulatory systems domain of function in the RDoC, although anxiety and perceived threat also reflect the negative valence systems domain. As units of analysis we have used physiologic, behavioral, and informant-report tools that reflect and relate to sensory processing in children with ADHD. Based on our work we have suggested that sensory responsivity may be an important factor to consider beyond the DSM V diagnosis of ADHD presentation.

Future Directions

There are several directions that could be taken to develop a dimensional understanding of ADHD. Two of these more closely examine anxiety and SOR in children with ADHD. The first involves more thoroughly embedding our understanding of these features of ADHD within the context of daily life. As noted above, this process has begun. Investigations have been conducted examining the impact of atypical sensory responsivity in children with ADHD on their participation in the activities of daily life. Examining the role played by anxiety has not been undertaken relative to occupation and participation, and links between anxiety, SOR, ADHD, and engagement in the occupations of childhood have yet to be addressed.

The second direction involves embedding this work within a neurodevelopmental trajectory. This has been done to some extent in children with SOR and no other diagnosis (Ben-Sasson et al., 2010), and to a much greater extent in children with SOR and ASD (c.f. Green et al., 2012; McCormick et al., 2015; Baranek et al., 2018; Williams et al., 2018). No longitudinal studies could be found examining sensory over-responsivity, or sensory processing deficits, in children with ADHD.

Overall there is greater depth and breadth in investigations of sensory processing concerns and their relationship with the diagnosis of ASD. This is to be expected as sensory responsivity differences form one component of the DSM V diagnostic criteria for this disorder. This body of literature is vast, and it is beyond the intent of this paper to summarize the work that has been done. However, it may be important to look to that literature and consider its application in understanding the dimension of atypical sensory responsivity in children with ADHD. In doing so we may gain a better understanding of specific neural systems and networks underlying both atypical sensory responsivity and ADHD. In fact, Koziol et al. (2011) have hypothesized that interactions between the neocortex (sensory processing, motor programming), basal ganglia (selection of appropriate perceptions and motor programs), and cerebellum (sensory and motor modulation) may underlie both atypical sensory responsiveness and ADHD. Imaging studies, such as

those conducted by Marco et al. (2013) with children with sensory processing concerns and autism (Owen et al., 2013; Chang et al., 2014) would provide evidence of the relationship between the behavioral features and neural connectivity, to support or negate the hypotheses proposed by Koziol et al. (2011).

CONCLUSION

In conclusion, it is time to take a dimensional perspective in understanding ADHD and its various manifestations. There is general agreement that it is, in fact, a dimensional disorder (Epstein and Loren, 2013), and that through considering ADHD from a dimensional perspective we will gain an understanding of the impact on function and optimize intervention. We may also gain a deeper understanding of neurobiological differences in this population. Anxiety has been proposed as one dimension to consider, and we propose that the atypical sensory modulation is another dimension that can add to our understanding of this disorder.

AUTHOR CONTRIBUTIONS

Both authors listed have made a substantial, direct and intellectual contribution to the work, and approved it for publication.

FUNDING

This work was partially funded by the Wallace Research Foundation. Additional funding was provided by the Virginia Commonwealth University.

ACKNOWLEDGMENTS

We are deeply appreciative to the families who took time to participate in our research. We extend our thanks to Lucy Jane Miller for her ongoing support and encouragement before, during, and through these investigations.

REFERENCES

Achenbach, T. M., and Rescorla, L. A. (2001). *Manual for the ASEBA School-Age Forms & Profiles*. Burlington, VT: University of Vermont.

American Psychiatric Association (2013). "Attention-deficit and disruptive behavior disorders," in *Diagnostic and Statistical Manual of Mental Disorders*, 5th Edn, ed. R. Spitzer (Arlington, VA: American Psychiatric Association).

Amos, G. A., Byrne, G., Chouinard, P. A., and Godber, T. (2019). Autism traits, sensory over-responsivity, anxiety and stress: a test of explanatory models. *J. Autism Dev. Disord.* 49, 98–112. doi: 10.1007/s10803-018-3695-6

Baranek, G. T., Carlson, M., Sideris, J., Kirby, A. V., Watson, L. R., Williams, K. L., et al. (2018). Longitudinal assessment of stability of sensory features in children with autism spectrum disorder or other developmental disabilities. *Autism Res.* 12, 100–111. doi: 10.1002/aur.2008

Bar-Shalita, T., Vatine, J.-J. J., and Parush, S. (2008). Sensory modulation disorder: a risk factor for participation in daily life activities. *Dev. Med. Child Neurol.* 50, 932–937. doi: 10.1111/j.1469-8749.2008.03095.x

Bart, O., Bar-Shalita, T., Mansour, H., and Dar, R. (2017). Relationships among sensory responsiveness, anxiety, and ritual behaviors in children with and without atypical sensory responsiveness. *Phys. Occup. Ther. Pediatr.* 37, 322–331. doi: 10.1080/01942638.2016.11855

Ben-Sasson, A., Carter, A. S., and Briggs-Gowan, M. J. (2010). The development of sensory over-responsivity from infancy to elementary school. *J. Abnorm. Child Psychol.* 38, 1193–1202. doi: 10.1007/s10802-010-9435-9

Ben-Sasson, A., Hen, L., Fluss, R., Cermak, S. A., Engel-Yeger, B., and Gal, E. (2009). A meta-analysis of sensory modulation symptoms in individuals with autism spectrum disorders. *J. Autism Dev. Disord.* 39, 1–11. doi: 10.1007/s10803-008-0593-3

Ben-Sasson, A., Soto, T. W., Heberle, A. E., Carter, A. S., and Briggs-Gowan, M. J. (2014). Early and concurrent features of ADHD and sensory over-responsivity symptom clusters. *J. Atten. Disord.* 21, 835–845. doi: 10.1177/1087054714543495

Bijlenga, D., Tjon-Ka-Jie, J. Y. M., Schuijers, F., and Kooij, J. J. S. (2017). Atypical sensory profiles as core features of adult ADHD, irrespective of autistic symptoms. *Eur. Psychiatry* 43, 51–57. doi: 10.1016/j.eurpsy.2017.02.481

Boucsein, W. (1992). *Electrodermal Activity*. New York, NY: Plenum Press.

Bröring, T., Rommelse, N., Sergeant, J., and Scherder, E. (2008). Sex differences in tactile defensiveness in children with ADHD and their siblings. *Dev. Med. Child Neurol.* 50, 129–133. doi: 10.1111/j.1469-8749.2007.02024.x

Brown, C. E., and Dunn, W. (2002). *Adult/Adolescent Sensory Profile: User's Manual*. San Antonio, TX: The Psychological Corporation.

Carpenter, K. L. H., Baranek, G. T., Copeland, W. E., Compton, S., Zucker, N., Dawson, G., et al. (2018). Sensory over-responsivity: an early risk factor for anxiety and behavioral challenges in young children. *J. Abnorm. Child Psychol.* 47, 1075–1088. doi: 10.1007/s10802-018-0502-y

Centers for Disease Control and Prevention (2018). *Facts About Mental Disorders in U.S. Children*. Available at: www.cdc.gov/childrensmentalhealth/data.html (accessed January 3, 2019).

Chang, Y.-S., Owen, J. P., Desai, S. S., Hill, S. S., Arnett, A. B., Harris, J., et al. (2014). Autism and Sensory processing disorders: shared white matter disruption in sensory pathways but divergent connectivity in social-emotional pathways. *PloS One* 9:e103038. doi: 10.1371/journal.pone.0103038

Cheung, P. P. P., and Siu, A. M. H. (2009). A comparison of patterns of sensory processing in children with and without developmental disabilities. *Res. Dev. Disabil.* 30, 1468–1480. doi: 10.1016/j.ridd.2009.07.009

Chien, C.-W., Rodger, S., Copley, J., Branjerdporn, G., and Taggart, C. (2016). Sensory processing and its relationship with children's daily life participation. *Phys. Occup. Ther. Pediatr.* 36, 73–87. doi: 10.3109/01942638.2015.1040573

Corominas-Roso, M., Palomar, G., Ferrer, R., Real, A., Nogueira, M., Corrales, M., et al. (2015). Cortisol response to stress in adults with attention deficit hyperactivity disorder. *Int. J. Neuropsychopharmacol.* 18, 1–10. doi: 10.1093/ijnp/pyv027

Cosbey, J., Johnston, S. S., and Dunn, M. L. (2010). Sensory processing disorders and social participation. *Am. J. Occup. Ther.* 64, 462–473. doi: 10.5014/ajot.2010.09076

Dawson, M. E., Schell, A. M., and Filion, D. L. (1990). "The electrodermal system," in *Principles of Psychophysiology: Physical, Social, and Inferential Elements*, eds J. T. Cacioppo and L. G. Tassinary (New York, NY: Cambridge University press), 294–324.

Dawson, M. E., Schell, A. M., and Filion, D. L. (2007). "The electrodermal system," in *Handbook of Psychophysiology*, 3rd Edn, eds J. T. Cacioppo, L. G. Tassinary, and G. G. Berntson (New York, NY: Cambridge University Press), 159–181.

Diamond, K. E., and Squires, J. (1993). The role of parental report in the screening and assessment of young children. *J. Early Interv.* 17, 107–115. doi: 10.1177/105381519301700203

Dunn, W. (1999). *Sensory Profile User's Manual*. San Antonio, TX: Psychological Corporation.

Dunn, W. (2006). *Sensory Profile Supplement: User's Manual*. San Antonio, TX: Pearson.

Dunn, W., and Bennett, D. (2002). Patterns of sensory processing in children with Attention Deficit Hyperactivity Disorder (ADHD). *Occup. Ther. J. Res.* 22, 4–15.

Edden, R. A. E., Crocetti, D., Zhu, H., Gilbert, D. L., and Mostofsky, S. H. (2012). Reduced GABA concentration in Attention-Deficit/Hyperactivity Disorder. *Arch. Gen. Psychiatry* 69, 750–753. doi: 10.1001/archgenpsychiatry.2011.2280

Engel-Yeger, B., and Ziv-On, D. (2011). The relationship between sensory processing difficulties and leisure activity preference of children with different types of ADHD. *Res. Dev. Disabil.* 32, 1154–1162. doi: 10.1016/j.ridd.2011.01.008

Epstein, J. N., and Loren, R. E. A. (2013). Changes in the definition of ADHD in DSM-5: subtle but important. *Neuropsychiatry* 3, 455–458. doi: 10.2217/npy.13.59

Faraone, S. V., Perlis, R. H., Doyle, A. E., Smoller, J. W., Goralnick, J. J., Holmgren, M. A., et al. (2005). Molecular genetics of attention-deficit/hyperactivity disorder. *Biol. Psychiatry* 57, 1313–1323.

Fowles, D. C., Christie, M. J., Edelberg, R., Grings, W. W., Lykken, D. T., and Venables, P. H. (1981). Committee report: publication recommendations for electrodermal measurements. *Psychophysiology* 18, 232–239. doi: 10.1111/j.1469-8986.1981.tb03024.x

Ghanizadeh, A. (2011). Sensory processing problems in children with ADHD, a systematic review. *Psychiatry Investig.* 8, 89–94. doi: 10.4306/pi.2011.8.2.89

Goldsmith, H. H., Van Hulle, C. A., Arneson, C. L., Schreiber, J. E., and Gernsbacher, M. A. (2006). A population-based twin study of parentally reported tactile and auditory defensiveness in young children. *J. Abnorm. Child Psychol.* 34, 393–407. doi: 10.1007/s10802-006-9024-0

Greaves-Lord, K., Ferdinand, R. F., Oldehinkel, A. J., Sondeijker, F. E., Ormel, J., and Verhulst, F. C. (2007). Higher cortisol awakening response in young adolescents with persistent anxiety problems. *Acta Psychiatr. Scand.* 116, 137–144. doi: 10.1111/j.1600-0447.2007.01001.x

Green, S. A., and Ben-Sasson, A. (2010). Anxiety disorders and sensory over-responsivity in children with autism spectrum disorders: is there a causal relationship? *J. Autism Dev. Disord.* 40, 1495–1504. doi: 10.1007/s10803-010-1007-x

Green, S. A., Ben-Sasson, A., Soto, T. W., and Carter, A. S. (2012). Anxiety and sensory over-responsivity in toddlers with autism spectrum disorders: bidirectional effects across time. *J. Autism Dev. Disord.* 42, 1112–1119. doi: 10.1007/s10803-011-1361-3

Greenfield, D. B., Iruka, U. I., and Munis, P. (2004). Assessment of social competence in high-risk preschoolers: evaluation of the adaptive social behavior inventory (ASBI) across home and school settings. *J. Psychoeduc. Assess.* 22, 220–232. doi: 10.1177/073428290402200303

Grogan, K., Gormley, C. I., Rooney, B., Whelan, R., Kiiski, H., Naughton, M., et al. (2018). Differential diagnosis and comorbidity of ADHD and anxiety in adults. *Br. J. Clin. Psychol.* 57, 99–115. doi: 10.1111/bjc.12156

Hastings, P. D., Fortier, I., Utendale, W. T., Simard, L. R., and Robaey, P. (2009). Adrenocortical functioning in boys with attention-deficit/hyperactivity disorder: examining subtypes of ADHD and associated comorbid conditions. *J. Abnorm. Child Psychol.* 37, 565–578. doi: 10.1007/s10802-008-9292-y

Herpertz, S. C., Mueller, B., Wenning, B., Qunaibi, M., Lichterfeld, C., and Herpertz-Dahlmann, B. (2003). Autonomic responses in boys with externalizing disorders. *J. Neural Transm.* 110, 1181–1195. doi: 10.1007/s00702-003-0026-6

Hinshaw, S. P. (2007). Moderators and mediators of treatment outcome for youth with ADHD: understanding for whom and how intervention works. *Ambul. Pediatr.* 7, 91–100. doi: 10.1016/j.ambp.2006.04.012

Hirvikoski, T., Lindholm, T., Nordenström, A., Nordström, A. L., and Lajic, S. (2009). High self-perceived stress and many stressors, but normal diurnal cortisol rhythm in adults with ADHD. *Horm. Behav.* 55, 418–424. doi: 10.1016/j.yhbeh.2008.12.004

Hochhauser, M., and Engel-Yeger, B. (2010). Sensory processing abilities and their relation to participation in leisure activities among children with high-functioning autism spectrum disorder (HFASD). *Res. Autism Spectr. Disord.* 4, 746–754. doi: 10.1016/j.rasd.2010.01.015

Hong, H. J., Shin, D. W., Lee, E. H., Oh, Y. H., and Noh, K. S. (2003). Hypothalamic-pituitary-adrenal reactivity in boys with attention deficit hyperactivity disorder. *Yonsei Med. J.* 44, 608–614.

Ismael, N. T., Lawson, L. A., and Cox, J. A. (2015). The relationship between children's sensory processing patterns and their leisure preferences and participation patterns. *Can. J. Occup. Ther.* 82, 316–324. doi: 10.1177/0008417415577421

Jensen, P., Hinshaw, S. P., Kraemer, H. C., Lenora, N., Newcorn, J. H., Abikoff, H. B., et al. (2001). ADHD comorbidity findings from the MTA study: comparing comorbid subgroups. *J. Am. Acad. Child Adolesc. Psychiatry* 40, 147–158. doi: 10.1097/00004583-200102000-00009

Johnson-Ecker, C. L., and Parham, L. D. (2000). The evaluation of sensory processing: a validity study using contrasting groups. *Am. J. Occup. Ther.* 54, 494–503. doi: 10.5014/ajot.54.5.494

Kalpogianni, D. (2002). Sensory characteristics of boys with attention deficit hyperactivity disorder: a comparison of their performance on the Sensory Profile to boys without disabilities. *Br. J. Occup. Ther.* 65:475.

Kamradt, J. M., Momany, A. M., and Nikolas, M. A. (2018). A meta-analytic review of the association between cortisol reactivity in response to a stressor and attention-deficit hyperactivity disorder. *Atten. Defic. Hyperact. Disord.* 10, 99–111. doi: 10.1007/s12402-017-0238-5

Kariyawasam, S. H., Zaw, F., and Handley, S. L. (2002). Reduced salivary cortisol in children with comorbid attention deficit hyperactivity disorder and oppositional defiant disorder. *Neuroendocrinol. Lett.* 23, 45–48.

King, J. A., Barkley, R. A., and Barrett, S. (1998). Attention-deficit hyperactivity disorder and the stress response. *Biol. Psychiatry* 44, 72–74. doi: 10.1016/S0006-3223(97)00507-6

Kinnealey, M., and Oliver, B. (1995). Study of sensory defensiveness in adults. *Am. J. Occup. Ther.* 49, 444–451. doi: 10.5014/ajot.49.5.444

Koziol, L. F., and Budding, D. (2012). ADHD and sensory processing disorders: placing the diagnostic issues in context. *Appl. Neuropsychol. Child* 1, 137–144. doi: 10.1080/21622965.2012.709422

Koziol, L. F., Budding, D. E., and Chidekel, D. (2011). Sensory integration, sensory processing, and sensory modulation disorders: putative functional neuroanatomic underpinnings. *Cerebellum* 10, 770–792. doi: 10.1007/s12311-011-0288-8

Lackschewitz, H., Hüther, G., and Kröner-Herwig, B. (2008). Physiological and psychological stress responses in adults with attention-deficit/hyperactivity disorder (ADHD). *Psychoneuroendocrinology* 33, 612–614.

Lane, S. J. (2019). "Disorders of sensory modulation," in *Sensory Integration Theory and Practice*, 3rd Edn, eds A. C. Bundy and S. J. Lane (Philadelphia, PA: F.A. Davis), 151–180.

Lane, S. J., Reynolds, S., and Dumenci, L. (2012). Sensory over-responsivity and anxiety in typical children and children with autism and attention deficit hyperactivity disorder: cause or co-existence? *Am. J. Occup. Ther.* 66, 595–603. doi: 10.5014/ajot.2012.004523

Lane, S. J., Reynolds, S., and Thacker, L. (2010). Sensory over-responsivity and ADHD: differentiating using electrodermal responses, cortisol, and anxiety. *Front. Integr. Neurosci.* 4:8. doi: 10.3389/fnint.2010.00008

Levy, F. (2004). Synaptic gating and ADHD: a biological theory of comorbidity of ADHD and anxiety. *Neuropsychopharmacology* 29, 1589–1596. doi: 10.1038/sj.npp.1300469

Liston, C., Malter Cohen, M., Teslovich, T., Levenson, D., and Casey, B. J. (2011). Atypical prefrontal connectivity in attention-deficit/hyperactivity disorder: pathway to disease or pathological end point? *Biol. Psychiatry* 69, 1168–1177. doi: 10.1016/j.biopsych.2011.03.022

Little, L. M., Ausderau, K., Sideris, J., and Baranek, G. T. (2015). Activity participation and sensory features among children with autism spectrum disorders. *J. Autism Dev. Disord.* 45, 2981–2990. doi: 10.1007/s10803-015-2460-3

MacKinnon, D. P. (2008). *Introduction to Statistical Mediation Analysis*. New York, NY: Erlbaum.

Maldonado, E. F., Trianes, M. V., Cortés, A., Moreno, E., and Escobar, M. (2009). Salivary cortisol response to a psychosocial stressor on children diagnosed with attention-deficit/hyperactivity disorder: difference between diagnostic subtypes. *Span. J. Psychol.* 12, 707–714. doi: 10.1017/s1138741600002079

Mangeot, S. D., Miller, L. J., McIntosh, D. N., McGrath-Clarke, J., Simon, J., Hagerman, R. J., et al. (2001). Sensory modulation dysfunction in children with attention-deficit-hyperactivity disorder. *Dev. Med. Child Neurol.* 43, 399–406.

March, J. S., Swanson, J. M., Arnold, L. E., Hoza, B., Conners, C. K., Hinshaw, S. P., et al. (2000). Anxiety as a predictor and outcome variable in the multimodal treatment study of children with ADHD (MTA1). *J. Abnorm. Child Psychol.* 28, 527–541.

Marco, E., Owen, J., Desai, S., Hill, S., Harris, J., and Mukherjee, P. (2013). "White matter microstructural abnormalities in children with sensory processing disorders (SPD). Neurology," in *Proceedings of the 65th American Academy of Neurology Annual Meeting*, San Diego, CA.

Mazor-Karsenty, T., Parush, S., Bonneh, Y., and Shalev, L. (2015). Comparing the executive attention of adult females with ADHD to that of females with sensory modulation disorder (SMD) under aversive and non-aversive auditory conditions. *Res. Dev. Disabil.* 37, 17–30. doi: 10.1016/j.ridd.2014.10.041

McCormick, C., Hepburn, S., Young, G. S., and Rogers, S. J. (2015). Sensory symptoms in children with autism spectrum disorder, other developmental disorders and typical development: a longitudinal study. *Autism* 20, 572–579. doi: 10.1177/1362361315599755

McIntosh, D. N., Miller, L. J., Shyu, V., and Hagerman, R. J. (1999). Sensory-modulation disruption, electrodermal responses, and functional behaviors. *Dev. Med. Child Neurol.* 41, 608–615. doi: 10.1017/s0012162299001267

Meredith, P. J., Bailey, K. J., Strong, J., and Rappel, G. (2016). Adult attachment, sensory processing, and distress in healthy adults. *Am. J. Occup. Ther.* 70, 7001250010p1–8. doi: 10.5014/ajot.2016.017376

Miller, L. J., Anzalone, M. E., Lane, J. J., Cermak, S. A., and Osten, E. T. (2007). Concept evolution in sensory integration: a proposed nosology for diagnosis. *Am. J. Occup. Ther.* 21, 135–140. doi: 10.5014/ajot.61.2.135

Morris, E. S., and Cuthbert, B. N. (2012). Research domain criteria: cognitive systems, neural circuits, and dimensions of behavior. *Dialogues Clin. Neurosci.* 14, 29–37. doi: 10.1016/s0924-977x(17)31010-6

Muris, P., Merckelbach, H., Ollendick, T., King, N., and Bogie, N. (2002). Three traditional and three new childhood anxiety questionnaires: their reliability and validity in a normal adolescent sample. *Behav. Res. Ther.* 40, 753–772. doi: 10.1016/s0005-7967(01)00056-0

Nigg, J. T. (2006). Temperament and developmental psychopathology. *J. Child Psychol. Psychiatry* 47, 395–422. doi: 10.1111/j.1469-7610.2006.01612.x

Nigg, J. T., Willcutt, E. G., Doyle, A. E., and Sonuga-Barke, E. J. (2005). Causal heterogeneity in attention-deficit/hyperactivity disorder: do we need neuropsychologically impaired subtypes? *Biol. Psychiatry* 57, 1224–1230. doi: 10.1016/j.biopsych.2004.08.025

Overton, P. G. (2008). Collicular dysfunction in attention deficit hyperactivity disorder. *Med. Hypotheses* 70, 1121–1127. doi: 10.1016/j.mehy.2007.11.016

Owen, J. P., Marco, E. J., Desai, S., Fourie, E., Harris, J., Hill, S. S., et al. (2013). Abnormal white matter microstructure in children with sensory processing disorders. *Neuroimage. Clin.* 2, 844–853. doi: 10.1016/j.nicl.2013.06.009

Owens, E. B., Hinshaw, S. P., Kraemer, H. C., Arnold, L. E., Abikoff, H. B., Cantwell, D. P., et al. (2003). Which treatment for whom for ADHD? Moderators of treatment response in the MTA. *J. Consult. Clin. Psychol.* 71, 540–552. doi: 10.1037/0022-006x.71.3.540

Panagiotidi, M., Overton, P. G., and Stafford, T. (2017). Multisensory integration and ADHD-like traits: evidence for an abnormal temporal integration window in ADHD. *Acta Psychol.* 181, 10–17. doi: 10.1016/j.actpsy.2017.10.001

Panagiotidi, M., Overton, P. G., and Stafford, T. (2018). The relationship between ADHD traits and sensory sensitivity in the general population. *Comprehensive Psychiatry* 80, 179–185. doi: 10.1016/j.comppsych.2017.10.008

Parham, L. D., and Ecker, C. (2007). *Sensory Processing Measure*. Los Angeles, CA: Western Psychological Service.

Parham, L. D., and Johnson-Ecker, C. (2002). "Evaluation of sensory processing: research version 4," in *Sensory Integration: Theory and Practice*, 2nd Edn, eds A. C. Bundy, S. J. Lane, and E. A. Murray (Philadelphia, PA: F.A. Davis), 194–196.

Parush, S., Sohmer, H., Steinberg, A., and Kaitz, M. (2007). Somatosensory function in boys with ADHD and tactile defensiveness. *Physiol. Behav.* 90, 553–558. doi: 10.1016/j.physbeh.2006.11.004

Pfeiffer, B., Brusilovskiy, J., Bauer, J., and Salzer, M. S. (2014). Sensory processing, participation, and recovery in adults with serious mental illnesses. *Psychiatr. Rehabil. J.* 37, 289–296. doi: 10.1037/prj0000099

Pfeiffer, B., Daly, B. P., Nicholls, E. G., and Gullo, D. F. (2015). Assessing sensory processing problems in children with and without attention deficit hyperactivity disorder. *Phys. Occup. Ther. Pediatr.* 35, 1–12.

Piller, A., and Pfeiffer, B. (2016). The sensory environment and participation of preschool children with autism spectrum disorder. *OTJR*36, 103–111. doi: 10.1177/1539449216665116

Piñeiro-Dieguez, B., Balanzá-Martínez, V., García-García, P., Soler-López, B., and the Cat Study Group (2016). Psychiatric co-morbidity at the time of diagnosis in adults with ADHD: the CAT study. *J. Attent. Disord.* 20, 1066–1075. doi: 10.1177/1087054713518240

Provost, B., Crowe, T. K., Acree, K., Osbourn, P. L., and McClain, C. (2009). Sensory behaviors of preschool children with and without autism spectrum disorders. *N. Z. J. Occup. Ther.* 56, 9–17.

Rasmussen, P., and Gillberg, C. (2000). Natural outcome of ADHD with developmental coordination disorder at age 22 years: a controlled, longitudinal, community-based study. *J. Am. Acad. Child Adolesc. Psychiatry* 39, 1424–1431. doi: 10.1097/00004583-200011000-00017

Raz, S., and Leykin, D. (2015). Psychological and cortisol reactivity to experimentally induced stress in adults with ADHD. *Psychoneuroendocrinology* 60, 7–17. doi: 10.1016/j.psyneuen.2015.05.008

Reimherr, F. W., Marchant, B. K., Gift, T. E., and Steans, T. A. (2017). ADHD and anxiety: clinical significance and treatment implications. *Curr. Psychiatry Rep.* 19:109. doi: 10.1007/s11920-017-0859-6

Reynolds, C. R., and Richmond, B. O. (2005). *Revised Children's Manifest Anxiety Scale (RCMAS)*, 9th Edn. Los Angeles, CA: Western Psychological Services.

Reynolds, S., Bendixen, R. M., Lawrence, T., and Lane, S. J. (2011a). A pilot study examining activity participation, sensory responsiveness, and competence in children with high functioning autism spectrum disorder. *J. Autism Dev. Disord.* 41, 1496–1506. doi: 10.1007/s10803-010-1173-x

Reynolds, S., and Lane, S. J. (2008). Diagnostic validity of sensory over-responsivity: a review of the literature and case reports. *J. Autism Dev. Disord.* 38, 516–529. doi: 10.1007/s10803-007-0418-9

Reynolds, S., and Lane, S. J. (2009). Sensory over-responsivity and anxiety in children with ADHD. *Am. J. Occup. Ther.* 63, 433–440.

Reynolds, S., Lane, S. J., and Gennings, C. (2010). The Moderating role of sensory over-responsivity in HPA activity: a pilot study with children diagnosed with ADHD. *J. Attent. Disord.* 13, 468–478. doi: 10.1177/1087054708329906

Reynolds, S., Lane, S. J., and Thacker, L. (2011b). Sensory processing, physiological stress, and sleep behaviors in children with and without autism spectrum disorder. *OTJR* 31, 246–257. doi: 10.3928/15394492-20110513-02

Schoen, S. A., Miller, L. J., and Green, K. E. (2008). Pilot study of the sensory over-responsivity scales: assessment and inventory. *Am. J. Occup. Ther.* 62, 393–406. doi: 10.5014/ajot.62.4.393

Shimizu, V. T., Bueno, O. F., and Miranda, M. C. (2014). Sensory processing abilities of children with ADHD. *Braz. J. Phys Ther.* 18, 343–352. doi: 10.1590/bjpt-rbf.2014.0043

Snicova, E., Marcincakova-Husarova, V., Hrtanek, I., Kulhan, T., Ondrejka, I., and Nosalova, G. (2016). Anxiety reduction during atomoxetine and methylphenidate medication in children with ADHD. *Pediatr. Int.* 58, 476–481. doi: 10.1111/ped.12847

Syu, Y. C., and Lin, L. Y. (2018). Sensory over-responsivity, loneliness, and anxiety in Taiwanese adults with autism spectrum disorder. *Occup. Ther. Int.* 2018:9165978. doi: 10.1155/2018/9165978

Tannock, R. (2009). "ADHD with anxiety disorders," in *ADHD Comorbidities: Handbook for ADHD Complications in Children and Adults*, ed. T. E. Brown (Washington, DC: American Psychiatric Association), 131–155.

Turgeon, L., and Chartrand, E. (2003). Reliability and validity of the revised children's manifest anxiety scale in a French Canadian sample. *Psychol. Assess.* 15, 378–383. doi: 10.1037/1040-3590.15.3.378

Valor, S., and Tannock, R. (2010). Diagnostic instability of DSM-IV ADHD Subtypes: effects of informant source, instrumentation and method for combining symptom reports. *J. Clin. Child Adolesc. Psychol.* 39, 749–760. doi: 10.1080/15374416.2010.517172

Van Ameringen, M., Mancini, C., Simpson, W., and Patterson, B. (2011). Adult attention deficit hyperactivity disorder in an anxiety disorders population.

CNS Neurosci. Therapuet. 17, 221–226. doi: 10.1111/j.1755-5949.2010.00148

Van Hulle, C., Lemery-Chalfant, K., and Goldsmith, H. (2015). Trajectories of sensory over-responsivity from early to middle childhood: birth and temperament risk factors. *PLoS One* 10:e0129968. doi: 10.1371/journal.pone.0129968

Van Hulle, C. A., Schmidt, N. L., and Goldsmith, H. H. (2012). Is sensory over-responsivity distinguishable from childhood behavior problems? A phenotypic and genetic analysis. *J. Child Psychol. Psychiatry*53, 64–72. doi: 10.1111/j.1469-7610.2011.02432.x

Van West, D., Claes, S., and Deboutte, D. (2009). Differences in hypothalamic-pituitary-adrenal axis functioning among children with ADHD predominately inattentive and combined types. *Eur. Child Adolesc. Psychiatry* 18, 543–553. doi: 10.1007/s00787-009-0011-1

White, B. P., and Mulligan, S. (2005). Behavioral and physiologic response measures of occupational task performance: a preliminary comparison between typical children and children with attention disorder. *Am. J. Occup. Ther.* 59, 426–436. doi: 10.5014/ajot.59.4.426

Williams, K. L., Kirby, A. V., Watson, L. R., Sideris, J., Bulluck, J., and Baranek, G. T. (2018). Sensory features as predictors of adaptive behaviors: a comparative longitudinal study of children with autism spectrum disorder and other developmental disabilities. *Res. Dev. Disabil.* 81, 103–112. doi: 10.1016/j.ridd.2018.07.002

Woodard, C. R., Goodwin, M. S., Zelazo, P. R., Aube, D., Scrimgeour, M., Ostholthoff, T., et al. (2012). A comparison of autonomic, behavioral, and parent-report measures of sensory sensitivity in young children with autism. *Res. Autism Spectr. Disord*. 6, 1234–1246. doi: 10.1016/j.rasd.2012.03.012

Wright, S. (1921). Correlation and causation. *J. Agric. Res.* 20, 557–585.

Yochman, A., Alon-Beery, O., Sribman, A., and Parush, S. (2013). Differential diagnosis of sensory modulation disorder (SMD) and attention deficit hyperactivity disorder (ADHD): participation, sensation, and attention. *Front. Hum. Neurosci.* 7:862. doi: 10.3389/fnhum.2013.00862

Yochman, A., Parush, S., and Ornoy, A. (2004). Response of preschool children with and without ADHD to sensory events in daily life. *Am. J. Occup. Ther.* 58, 294–302. doi: 10.5014/ajot.58.3.294

Conflict of Interest Statement: The authors declare that the research was conducted in the absence of any commercial or financial relationships that could be construed as a potential conflict of interest.

Copyright © 2019 Lane and Reynolds. This is an open-access article distributed under the terms of the Creative Commons Attribution License (CC BY). The use, distribution or reproduction in other forums is permitted, provided the original author(s) and the copyright owner(s) are credited and that the original publication in this journal is cited, in accordance with accepted academic practice. No use, distribution or reproduction is permitted which does not comply with these terms.

frontiers in Integrative Neuroscience

ORIGINAL RESEARCH
published: 12 November 2019
doi: 10.3389/fnint.2019.00065

Effectiveness of Noise-Attenuating Headphones on Physiological Responses for Children With Autism Spectrum Disorders

Beth Pfeiffer[1], Leah Stein Duker[2], AnnMarie Murphy[1] and Chengshi Shui[3]*

[1]*Department of Health and Rehabilitation Sciences, Temple University, Philadelphia, PA, United States,* [2]*USC Chan Division of Occupational Science and Occupational Therapy, University of Southern California, Los Angeles, CA, United States,* [3]*School of Nursing, University of California, Los Angeles, Los Angeles, CA, United States*

Objective: The purpose of this study was to evaluate the proof of concept of an intervention to decrease sympathetic activation as measured by skin conductivity (electrodermal activity, EDA) in children with an autism spectrum disorder (ASD) and auditory hypersensitivity (hyperacusis). In addition, researchers examined if the intervention provided protection against the negative effects of decibel level of environmental noises on electrodermal measures between interventions. The feasibility of implementation and outcome measures within natural environments were evaluated.

Method: A single-subject multi-treatment design was used with six children, aged 8–16 years, with a form of Autism (i.e., Autism, PDD-NOS). Participants used in-ear (IE) and over-ear (OE) headphones for two randomly sequenced treatment phases. Each child completed four phases: (1) a week of baseline data collection; (2) a week of an intervention; (3) a week of no intervention; and (4) a week of the other intervention. Empatica E4 wristbands collected EDA data. Data was collected on 16–20 occasions per participant, with five measurements per phase.

Results: Separated tests for paired study phases suggested that regardless of intervention type, noise attenuating headphones led to a significance difference in both skin conductance levels (SCL) and frequency of non-specific conductance responses (NS-SCRs) between the baseline measurement and subsequent phases. Overall, SCL and NS-SCR frequency significantly decreased between baseline and the first intervention phase. A protective effect of the intervention was tested by collapsing intervention results into three phases. Slope correlation suggested constant SCL and NS-SCR frequency after initial use of the headphones regardless of the increase in environmental noises. A subsequent analysis of the quality of EDA data identified that later phases of data collection were associated with better data quality.

Conclusion: Many children with ASD have hypersensitivities to sound resulting in high levels of sympathetic nervous system reactivity, which is associated with problematic behaviors and distress. The findings of this study suggest that the use of

OPEN ACCESS

Edited by:
Jonathan T. Delafield-Butt, University of Strathclyde, United Kingdom

Reviewed by:
Elias Manjarrez, Meritorious Autonomous University of Puebla, Mexico
David R. Simmons, University of Glasgow, United Kingdom

****Correspondence:***
Beth Pfeiffer
bpfeiffe@temple.edu

Received: *07 November 2018*
Accepted: *21 October 2019*
Published: *12 November 2019*

Citation:
Pfeiffer B, Stein Duker L, Murphy A and Shui C (2019) Effectiveness of Noise-Attenuating Headphones on Physiological Responses for Children With Autism Spectrum Disorders. Front. Integr. Neurosci. 13:65. doi: 10.3389/fnint.2019.00065

noise attenuating headphones for individuals with ASD and hyperacusis may reduce sympathetic activation. Additionally, results suggest that the use of wearable sensors to collect physiological data in natural environments is feasible with established protocols and training procedures.

Keywords: hyperacusis, autism spectrum disorder (ASD), noise-attenuating headphones, noise canceling headphone, electrodermal responses (EDR), autonomic nervous system, stress, anxiety

INTRODUCTION

Unusual responses to sensory stimuli are experienced by up to 90% of individuals with autism spectrum disorder (ASD; Ben-Sasson et al., 2009). Although it is unclear as to whether sensory processing difficulties are a trait of ASD or a trait of comorbid disorders (Landon et al., 2016), behavioral responses to sensory stimuli have become so prevalent, that the most recent criteria in the Diagnostic and Statistical Manual of Mental Disorders 5th edition (DSM-V) for ASD added a diagnostic component of hyper- and hypo- reactivity to sensory stimuli (American Psychiatric Association, 2013). When studying the neurobiological differences in those with sensory difficulties, research indicates those with sensory over responsivity (SOR), or hypersensitivities, present with atypical sympathetic and parasympathetic functions of the nervous system (Miller et al., 2009). Of the various sensory responses, one of the most commonly reported challenges for those with ASD is hypersensitivity to sound (Baranek et al., 2006; Kern et al., 2006; Tomchek and Dunn, 2007; Stiegler and Davis, 2010; Bolton et al., 2012). Despite varying findings when analyzing cortical auditory sensory processing, neurophysiological studies have consistently identified atypical neural activity early in the processing stream in individuals with ASD (Marco et al., 2011).

Common in children with ASD, hyperacusis is a term used to describe the negative and/or exaggerated response to environmental stimuli occurring within the auditory pathways (Asha'ari et al., 2010; American Speech-Language-Hearing Association, 2016)[1]. Individuals with hyperacusis have an increased sensitivity to auditory input (Palumbo et al., 2018), and report experiencing auditory information at unbearably loud levels (Kuiper et al., 2019). Although hyperacusis is one of the most commonly identified auditory responses in children with ASD (Rogers et al., 2003), the cause of the disorder is not fully understood. Research suggests that the relationship between the central auditory system and the limbic system contribute to the development of the fear and anxiety frequently experienced with hyperacusis (Brout et al., 2018). In comparison to neurotypical peers, research on multi-sensory integration suggests that children with SOR may not process incoming information in lower level cortical regions. In conjunction with difficulties with sensory gating, challenges with modulation may prevent the central nervous system from appropriately identifying the intensity, frequency, duration, and complexity of environmental stimuli lending to issues filtering meaningful from non-meaningful sounds in the environment (Miller et al., 2009). This inability to filter may lead to an overwhelming amount of incoming stimuli, resulting in hyper-reactions due to sensory overload (Kuiper et al., 2019). The continual stress from perceived noxious stimuli and sensory overload can result in physiological changes (Rance et al., 2017). More specifically, decreased basal respiratory sinus arrhythmia and basal heart rate hyperarousal have been associated with social, language, and cognitive difficulties (Kushki et al., 2014).

Additionally, recent research has examined the role of medial olivocochlear efferent reflexes (MOC) in hyperacusis. Findings suggest that when comparing those with ASD with severe hyperacusis, those with ASD without hyperacusis, and neurotypicals, the MOC reflexes were twice as strong in individuals who have ASD with severe hyperacusis (Wilson et al., 2017). Despite this new understanding of the MOC reflexes and hyperacusis, research is inconsistent in identifying physiological differences in auditory pathways in individuals with hyperacusis (Tharpe et al., 2006; Jones et al., 2009).

Some emerging evidence suggests that SOR, such as hyperacusis, is associated with decreased inhibitory processes. For example, a fMRI study found slower habituation in youth with ASD and SOR in the amygdala and somatosensory cortex from both tactile and auditory input, as compared to youth with ASD without SOR (Green et al., 2015). Chang et al. (2012) found a significant association between electrodermal activity (EDA) and parent reported problem behaviors on the Sensory Processing Measure (SPM) Hearing and Total scale score categories. As discussed previously it is thought that hyperacusis may be linked to a difficulty in sensory modulation for children with ASD. Supporting this, Chang et al. (2012) found that participants with strong sympathetic reactivity were reported to have behaviors indicative of both over- and under-responsiveness. Through use of EDA, Schoen et al. (2008) also found two significant patterns of habituation in response to sensory stimuli (i.e., tone, strobe light, siren, smell, feather, chair movement). Within the population of children with ASD, their results grouped to show: (1) high tonic electrodermal arousal, high reactivity, and slower habituation; and (2) low tonic arousal, lower reactivity, and faster habituation.

When researching hyperacusis in adults with ASD, however, Kuiper et al. (2019) found no significant positive correlation between habituation rate and self-reported auditory hypersensitivity. Despite habituating at similar rates, it is noted that those with ASD had a higher skin conductance level (SCL) at baseline, indicating higher physiological arousal (Kuiper et al., 2019). Another study examined time-course responses of the auditory cortex to repeated auditory stimuli, as measured by magnetoencephalography, between boys with ASD who had

[1]https://www.asha.org/uploadedFiles/AIS-Hyperacusis.pdf

auditory SOR, boys with ASD without auditory SOR, and neurotypical peers. The boys with ASD and auditory SOR exhibited prolonged response duration when compared to the other groups, suggesting decreased inhibition as found in abnormal sensory gating or dysfunction of inhibitory neurons (Matsuzaki et al., 2014). This was further supported in autism model rats that presented with a decrease in morphological size of the medial nucleus of the trapezoid body in the superior olivary complex, which holds an inhibitory role in auditory processing (Ida-Eto et al., 2017).

Regardless of the underlying cause, hyperacusis has been associated with anxiety and stress surrounding perceived noxious auditory stimuli, resulting in strong reactions (Jastreboff and Jastreboff, 2000; Brout et al., 2018). Illustrating this, children with ASD are frequently reported to cover their ears to block out sounds, as well as exhibit anxious or distressing reactions to some sounds (Rimland and Edelson, 1995; Jastreboff and Jastreboff, 2000). Intense and atypical responses to auditory stimuli can result in increased stress; avoidance of certain environments and interactions; decreased participation or engagement in key life activities and events; and distractibility impacting performance in home and school (Pfeiffer et al., 2019). These adverse effects on school performance and social interactions have been reported to influence overall quality of life (Grinker, 2007; Rowe et al., 2011; Smith and Riccomini, 2013). In a qualitative study by Landon et al. (2016), adult participants with ASD and noise sensitivity (NS) described particular sounds as causing physical discomfort and frustration. One participant with ASD and NS described "...the buzzing (of the fluorescent lightbulb) was so annoying that it got to the point where I couldn't turn it on. So I sat there in the dark in my room for half the year because I couldn't turn the light on (p. 48)". Palumbo et al. (2018) note that characteristically, individuals with hyperacusis tend to become hyper-focused on listening for trigger sounds within their natural environments, resulting in a "perpetual state of anxiety" (p. 2) while they wait for the noxious stimuli to occur. This hyper-focused state was reported to cause emotional and physical discomfort by those with hyperacusis (Palumbo et al., 2018). In addition to experiencing emotional and physical discomfort, research indicates that chronic stress associated with hyperacusis may lead to negative mental and physical health conditions (McEwen and Gianaros, 2011).

Researchers have also examined the impact of noise on health in the general population. The World Health Organization (WHO) reports that environmental noise exposure can lead to a variety of negative health outcomes including sleep disturbance, cognitive impairments in children, stress-related mental health risks, as well as tinnitus (World Health Organization, 2018)[2]. Research suggests that autonomic nervous system and endocrine responses to sound correlate with particular night-time noises such as road traffic, aircrafts and railway noises, resulting in increased blood pressure, changes in heart rate, and leading to the release of stress hormones (Münzel et al., 2014). Research also suggests that individuals with non-supported coping strategies, such as children, may experience psychological stress in addition to physiological imbalance due to noise (Basner et al., 2014).

Due to the impact on participation and overall quality of life, a number of interventions that target the reduction of auditory hypersensitivity have been developed and trialed. One intervention, the listening project protocol (LPP), proposes to increase the neural tone to the inner ear muscles. During LPP, participants spend 45 min per day for 5 days listening to computer altered acoustic stimuli *via* headphones. This protocol was developed with insight from the Borg and Counter model, which suggests that auditory hypersensitivity in ASD may be due to atypical regulation of the middle ear as it tries to extract human speech from environmental noise (Porges et al., 2014). Research on this protocol showed a decrease in auditory hypersensitivity as well as an increase of spontaneous sharing behavior in children with ASD (Porges et al., 2014). However, several limitations were noted; for example, improvements were seen in both treatment and control groups, suggesting that the social engagement system utilized may have been a confounder. Although some research on this protocol has been conducted focusing on reducing auditory hypersensitivity in those with ASD, most of the clinical trials focus on its impact on emotional regulation and trauma[3].

Another method currently utilized to reduce sound sensitivity in those with auditory hypersensitivities is auditory integration training (AIT; Sokhadze et al., 2016). Through filtered and modulated frequencies, AIT aims to suppress the peaks of frequency by random dampening of high and low frequencies in order to normalize the sounds and retrain the brain of someone who is hypersensitive (Sinha et al., 2006). Although different types of AIT, including the Listening Program, Berard Method and Tomatis Method are used, there is limited scientific research to support their ability to decrease auditory hypersensitivity (Dawson et al., 2007; Miller and Schoen, 2015; Sokhadze et al., 2016).

Researchers have also tested whether cognitive behavioral therapy (CBT) can alter learned patterns and behaviors, as well as faulty ways of thinking, related to particular noises in the environment. A randomized controlled trial was conducted in which a licensed psychologist trained in CBT provided six therapy sessions using CBT principles, psychoeducation, exposure therapy, applied relaxation and behavioral activation (Jüris et al., 2014). The use of CBT limits escape behavior by role playing potential problem scenarios (i.e., loud sounds or environments with unwanted noises) and learning to be calm (American Psychological Association, 2018). One of the benefits of using CBT for those with hyperacusis is the learning of new behaviors which can be used long after the study and intervention are completed (Jüris et al., 2014). The limitation of using CBT for those with ASD and hyperacusis, however, is that it requires recognition and awareness of the aversive stimuli. Event-related potential and magnetic field research on ASD (Orekhova and Stroganova, 2014) suggest that problems only arose when novel stimuli were outside of the individual's focus of attention, suggesting CBT may be limited with those not aware of the actual trigger.

[2]http://www.who.int/sustainable-development/transport/health-risks/noise/en/

[3]https://integratedlistening.com/bing-safe-sound-protocol/

One common non-invasive intervention to improve the auditory environments for individuals with ASD are noise-attenuating headphones, which block sound transmission to the ears (Pfeiffer et al., 2019). Ikuta et al. (2016) conducted a pilot study on the effectiveness of noise-canceling (NC) headphones in children with ASD of varying intelligence. Participants in this study had difficulty using the NC headphones when they had hypersensitivity to human voices. As noted previously, one theory suggests that auditory hypersensitivity in those with ASD may be due to the inability of the middle ear to filter human voices from environmental noise (Porges et al., 2014). Research did find, however, that behavioral responses improved for children who perceived environmental noises (i.e., noisy classroom sounds) as noxious (Ikuta et al., 2016). Additionally, a single case design study identified an increase in attention to task for a child with ASD and auditory hypersensitivity when wearing the headphones (Rowe et al., 2011). Although this is often a low-cost and easily implemented intervention, there is limited research documenting its effectiveness. Additionally, to our knowledge, there is no current research examining the impact of environmental adaptation, such as use of noise-attenuating headphones, on the core issue of physiological anxiety and stress exhibited by individuals with ASD and hyperacusis.

Therefore, the purpose of this study was to examine the proof of concept for two types of noise attenuating headphones in reducing physiological stress and anxiety in children with ASD when in natural environments with noise perceived as aversive. Further investigation examined how the intervention provided a buffer for children with ASD against the negative effects of environmental noises on their physiological stress and anxiety. Historically, research assessing physiological responses to noise has been conducted in laboratory environments that does not reflect the natural environment. In children with ASD, participation in such studies do not accurately reflect the milieu of auditory stimuli encountered in the real world. For example, recent research has used fMRI to provide insight on neuronal correlations of auditory processing, although there is a loud noise associated with the imaging (Talavage et al., 2014) that is not typically encountered in natural environments. These imaging techniques, along with other psychophysiological measures such as EDA, require the participant to remain still for the duration of the recording (Boucsein et al., 2012; Boucsein, 2012; Wilson et al., 2017). Additionally, participating in these laboratory-based experiments may lead to increased stress as the child must deviate from his or her typical routine while in an unfamiliar environment with unfamiliar people. Because many children with ASD cannot express their distress in context-specific situations and their actions/reactions are often misunderstood, outcome measures of environmentally-based interventions in the natural context of the child are important to truly understand their experiences. Therefore, in this study, wearable sensors were used as the primary source of data collection with the intervention implemented in the natural environment. Due to complexities of collecting data within natural environments, we also evaluated the feasibility of the study measures and the quality of the wearable sensor data.

MATERIALS AND METHODS

Design

The purpose of this study was to evaluate the proof of concept for an intervention to decrease physiological stress and anxiety among children with ASD within their natural environment. Single-subject multi-treatment design was used to compare two different noise attenuating headphone devices. These devices were over-ear (OE) BOSE Quiet Comfort 15 Acoustic Noise Attenuating Headphones and in-ear (IE) BOSE QuietComfort 20i Acoustic Noise Attenuating Headphones. The headphones were used to assess if noise attenuation would impact physiological responses during identified target activities with noxious auditory stimuli in natural environments. An ABAC design was used at random, assigning two different sequences of the intervention to the participants (Group A: ABAC or Group B: ACAB). Regardless of sequence, participants completed all four phases including: (1) a week of baseline data collection; (2) a week of an intervention; (3) a week of no intervention; and (4) a week of the other intervention. Participants did not wear the noise attenuating headphones during baseline or the week of non-intervention. During the 2 weeks of intervention, either the OE or IE attenuating headphones were used. Data collection occurred on 20 occasions per participant, with five measurements per phase. Participants were randomly assigned to one of two groups, with one group having phases sequenced ABAC and the other group having phases sequenced ACAB.

Participants

In total, six children between the ages of 8 and 16 diagnosed with an ASD completed the study. Participant demographics are outlined in **Table 1**. Participants were only included in the study if they were diagnosed with a form of Autism using DSM-IV criteria. Diagnosis was confirmed through parent report and the completion of the Gilliam Autism Rating Scale 3rd edition (GARS-3; Gilliam, 2013)[4]. All participants had a score of 70 or higher, which is indicative of very high probability of ASD. Additionally, participants had to score in the probable or definite difference range on the Auditory Filtering and Auditory Sensitivity Scales of the Short Sensory Profile (SSP; Dunn, 1999) for inclusion as an indicator of hyperacusis.

Initially, 12 participants responded to recruitment efforts. However, six dropped out of the study before completing data collection. Reasons cited for participant drop-out included feeling overwhelmed or having problems with using technology; having no access to child during activities that were noisy and stimulating (i.e., school); confidentiality issues with conducting the experiment within the school setting; disruption of child's routine; lack of time to do the data collection; constant monitoring of child to prevent destruction of headphones; and resistance of the child to wear the wristband collecting data.

[4]https://www.pearsonassessments.com/store/usassessments/en/Store/Professional-Assessments/Behavior/Gilliam-Autism-Rating-Scale-%7C-Third-Edition/p/100000802.html?tab=product-details

TABLE 1 | Participant characteristics.

Participant Number	Age	Diagnosis	Order of Intervention (B = OE; C = IE)	Score Range: Auditory Filtering (SSP)	Score Range: Visual/Auditory Sensitivity (SSP)	Activities and Environments Targeted for the NAH	Ethnicity of Child
3	8 years	PDD-NOS (DSM-IV); ADHD	ABAC	13/30 Definite Difference (range 6–19)	18/25 Probable Difference (range 15–18)	In car; Learning time with music	Caucasian
4	8 years	Autism (DSM-IV)	ACAB	14/30 Definite Difference (range 6–19)	18/25 Probable Difference (range 15–18)	Therapy session with music in background	Caucasian
8	8 years	Autism (DSM-IV)	ABAC	16/30 Definite Difference (range 6–19)	18/25 Probable Difference (range 15–18)	After school time; In the car	Caucasian
10	16 years	PDD-NOS (DSM-IV)	ABAC	15/30 Definite Difference (range 6–19)	14/25 Definite Difference (range 5–15)	Video games; Driving in car with music on; Grocery store; Homework	Caucasian
11	9 years	Autism (DSM-IV), ADD, SPD	ACAB	13/30 Definite Difference (range 6–19)	8/25 Definite Difference (range 5–15)	Playground; Occupational Therapy	Latin American or Hispanic
12	11 years	Asperger's Disorder (DSM-IV), SPD, Anxiety	ABAC	16/30 Definite Difference (range 6–19)	15/25 Definite Difference (range 5–15)	Practicing drums; Playground	Latin American or Hispanic

Procedure

Recruitment was conducted through social media, schools with individuals with ASD, private therapy practices, and community organizations in the Philadelphia area. Information about the study was posted on social media sites, such as Facebook. Flyers were provided to school administration, private therapy practices, and organizations that support individuals with ASD. If participants were interested, they contacted the research coordinator directly.

When an interested participant contacted the researchers, written informed consent was obtained from the parents of the participants who also completed a Demographic Questionnaire, GARS-3, and SSP to determine preliminary inclusion. If scores on the GARS-3 were 70 or higher, and scores on the Auditory Scales of the SSP fell in the range of probable to definite difference, a second meeting was scheduled to obtain child assent. All children provided assent through either verbal (i.e., verbal response of yes or no) or non-verbal indicators (i.e., nodding of head). Additionally, after having the child assent language read to them, the child signed an assent form if they were able. Once child assent was obtained, an occupational therapy evaluation was completed to identify activities/environments that were avoided or caused stress due to auditory stimuli, and to provide training on data collection methods. Target environments varied from child to child, including activities on the playground, playing with drums or video games, going grocery shopping, as well as other activities with and without music present (i.e., driving in a car, doing homework). During the study no was music played into the headphones so that the function was limited to providing noise attenuation rather than noise masking. Parents were provided with step-by-step training for use of equipment and other data collection procedures. See **Table 2** for the Quick Reference Data Collection document provided to parents (the full Pictorial Direction Manual can be requested from authors).

TABLE 2 | iPad with data plan instructions: procedures for BOSE data collection—quick reference.

	Getting Started
Step 1:	Put wristband on participant @ 20 min prior to start of activity, cover with sweatband.
Step 2:	Turn on iPod.
Step 3:	Press wristband power button for 2 s, it will blink green.
Step 4:	Open Empatica RT app.
Step 5:	Touch "start a new session," then select Empatica E4 from device list.
Step 6:	Make a Visual Scan of environment.
Step 7:	Make a Decibel Reading of environment.
	During Session
Step 8:	Make a Visual Scan of Environment at middle and end of activity.
Step 9:	Make a Decibel Reading at middle and end of activity.
	Ending Session
Step 10:	Press the red X on Empatica RT App and confirm "ok?" to end data collection.
Step 11:	Remove wristband from participant and store in carrying case.
	AFTER
Step 14:	Open Notes App on iPod. Complete Momentary Assessment Questions.
Step 15:	Take screen shots of all decibel readings.
Step 16:	Close apps. Turn of iPod. Charge unit for next use.

Children had the opportunity to wear all study-related devices for a week before data collection began in order to help the child feel comfortable with the headphones as well as the wearable sensors within an environment/activity that was not targeted for the study. Participants who demonstrated refusal or discomfort after the one-week trial were excluded from the study. Throughout the study duration, a research team member checked in with participants regularly and provided technical support, as needed, throughout the data collection period. A gift card was given to the parent of a child who participated in the culmination of the study.

Intervention

Two different types of noise-attenuating headphones, designed to block out environmental noises, were used during the intervention phases. The technology used in these headphones compares and reacts to environmental sounds. When reacting to the environmental sound, a signal is provided to counteract the noise in the environment, thus canceling out the noise in the environment (BOSE, 2018)[5]. No music was played into the headphones during the study, so the headphones solely provided a noise attenuating function rather than noise masking. Although BOSE provided the equipment for the study, it is important to note that there are other organizations that produce headphone equipment that has noise attenuating features (e.g., QuietComfort, Velodyne, Etymotic and Westone).

Two types of noise attenuating headphones, IE and OE, were used during this study. The IE BOSE design used in this research has built-in "aware mode" technology. This allows the wearer to switch the processing applied to the microphones on the outside of each earbud creating an auditory approximation to removing the headphones (BOSE, 2018). In essence, the wearer could control how much of the environmental background noise they could hear or block out. The second, an OE device, did not have this mode and continually blocked noise in the environment. During the trial, the children/students wore these headphones during activities that had either large amounts of auditory stimuli or during activities that the child found aversive due to their perception of the auditory stimuli. Five points of data were collected in the 4 phases of: (1) a week of baseline data collection; (2) a week of an intervention; (3) a week of no intervention; and (4) a week of the other intervention.

EDA was collected using an Empatica E4 wireless wearable wristband device to measure arousal state. This wristband allows for researchers to receive data either in real-time or up to 60 h of data through a secure storage system (Empatica, 2018). For purposes of this study, the Empatica RT App was utilized to collect EDA data. Momentary assessment data was collected on types of daily activity, setting, and the number of people in the environment. This data was collected *via* Qualtrics on a provided iPod or iPad mini (Qualtrics, 2019)[6]. In addition, a visual scan of the environment was captured on the device's camera application while in video mode to confirm reported data. For researchers to gain insight on actual environmental sound, smartphone technologies VenueDB app was used to collect decibel readings two times per session (EarMachine, 2018)[7].

Measures

Child Descriptor Measures

All parents of children participating in the study reported diagnosis based on the DSM-IV (i.e., PDD-NOS, Asperger Disorder, Autism), as their children were originally diagnosed using that classification system (American Psychiatric Association, 2000). Participant ASD diagnoses included Autism (n = 3), PDD-NOS (n = 2), and Asperger Disorder (n = 1). Additionally, ASD diagnosis was confirmed through completion of the GARS-3 (Gilliam, 2013). The GARS-3 is a widely used instrument to identify ASD and estimate its severity. A GARS-3 Autism Index score of $\geq$70 was used to confirm diagnosis (Gilliam, 2013).

The SSP (Dunn, 1999) was utilized to characterize auditory-specific sensory processing differences of study participants. This 38-item caregiver questionnaire is standardized for children ages 3–10 years. Using a five-point Likert scale, caregivers report how their child processes sensory information in day-to-day situations. On the *Auditory Filtering* subtests, all participants (n = 6) scored in the "definite difference" category, indicating difficulty filtering auditory stimuli in comparison to peers their age. On the *Visual/Auditory Sensitivity* subtest, three children scored "probable difference" and three children scored "definite difference."

Outcome Variables

EDA reflects the skin conductance of the palmar sweat glands controlled by the sympathetic nervous system (Dawson et al., 2007), a marker of psychophysiological stress and anxiety. EDA was collected using the wireless Empatica E4, which was placed on the child's non-dominant wrist and covered with a lightweight fabric band to ensure continuous contact between the electrode and the child's wrist. The E4 utilized Ag/AgCl dry electrodes and sampled data at 8 Hz. Although the wrist is a non-traditional recording site, it has been found to be correlated with standard measurement locations (van Dooren et al., 2012) and previous research has utilized this equipment (or its predecessor, the Q-sensor) to collect EDA from the wrist in children with ASD (Baker et al., 2015, 2018, 2019; Fenning et al., 2017; Prince et al., 2017). EDA was recorded continuously throughout the study, beginning with a minimum of 20 min in order to allow sufficient buildup of moisture between the electrodes and the skin, followed by a baseline period and subsequent application of the experimental condition phase (baseline, IE, no intervention, OE). In longer-lasting situations, measurement of tonic SCL and frequency of non-specific skin conductance responses (NS-SCRs) are the most useful electrodermal measures (Dawson et al., 2007). It is well-documented that these tonic EDA readings increase in stressful or anxiety-producing situations (Dawson et al., 2007).

[5]https://www.bose.com/en_us/products/headphones/noise_cancelling_headphones.html

[6]https://www.qualtrics.com

[7]https://www.earmachine.com/venuedb/

Covariates

Covariates were used to adjust for the estimation of the treatment effects including: presence of other people (1: 1–2 people; 2: 3–5 people; 3: 5–10 people; 4: 10–20 people, and 5: 20 + people); levels of visual stimuli (1: minimal, 2: moderate, and 3: a lot); levels of noise (1: quiet minimal, 2: moderate, and 3: a lot); setting (1: home, 2: community, and 3: school), and average value of the two decibel readings per session.

Management of Electrodermal Activity (EDA) Data

For EDA data, the number of NS-SCRs were totaled for each participant and converted to a rate of fluctuations per minute and only counted when the amplitude was greater than or equal to 0.05 μs, as suggested by Dawson et al. (2007). Due to the skewed nature of our SCL and NS-SCR frequency data, and as is common practice with EDA data (Dawson et al., 2007), the Yeo-Johnson transformation (Yeo and Johnson, 2000) was applied to both SCL and NS-SCR frequency prior to modeling.

Data were visualized and downloaded in CSV format from the Empatica Connect Webportal for analysis. Data were imported into the BIOPAC program Acq*Knowledge* and a low-pass filter was applied to remove artifacts (Boucsein, 2012). Although ambulatory EDA datasets often preclude traditional quality assessment (e.g., "rigorous and methodical visual inspection and human coding"; Kleckner et al., 2018, pp. 1461; Boucsein, 2012; Boucsein et al., 2012), traditional visual inspection was possible due to the limited duration of each data recording in this study. Data cleaning was completed by hand, offline using Acq*Knowledge* to visualize the data in order to ensure deletion of movement artifacts (SCR data with a rise time <1 s, indicating an increase too quick to be attributable to physiological processes) and/or any abrupt drops which likely reflected the loss of contact between the skin and E4 electrodes. Both SCL and NS-SCRs were computer-scored off-line using the BIOPAC program Acq*Knowledge* and hand-checked to ensure no skin conductance responses were missed or incorrectly marked (Boucsein, 2012; Boucsein et al., 2012). Ten percent of the hand-coded data were double coded to ensure that the identification of NS-SCRs was reliable, with a minimum of 90% agreement (calculated as the number of matching NS-SCRs divided by the total number of NS-SCRs coded by the researchers). Overall, 88% of data were usable and included for analysis. Excluded data were flat line waveforms (SCL < 0.1 μs) with zero or few NS-SCRs. The unusable flat-lined data were due to equipment error/problems and not participants being electrodermal non-responders (Schoen et al., 2008; Keith et al., 2018), as other recordings from those participants yielded usable data. No data from one participant was initially usable; however, the participant collected a second round of data with 100% usability.

Data Analysis

Analysis of Data Quality

To investigate how data quality varied systematically across study designs and under different conditions, we used a random effects ordered logistic model. Random effects models were chosen because the observations came from the same participants, violating the assumption of mutual independence. Ordered logistic models were utilized because the outcome variable (quality of data) had three ordered categories (1: not acceptable, 2: acceptable, and 3: highest quality). We regressed the outcome variable on selected variables, including the study design factors (intervention sequence: ABAC or ABAC; study phases: intervention or non-intervention) and covariates to identify potential associations. Finally, we conducted the Brant test to investigate the extent to which the ordered logistic model followed the assumption of parallel regression with this sample, which requires effects of the exploratory variables to be consistent across thresholds in the outcome variable. A cluster-robust estimator was used for statistical inferences.

Analysis of Preliminary Efficacy

A random-effects model, Moeyaert's model parametrization (Manolov and Moeyaert, 2017), was used to evaluate the intervention's treatment effects. Radom effects models account for auto-correlations among observations due to repeated measurements from the same participants, but can also take into consideration individual variations; for these reasons, random effects models are recommended when the main interest is to estimate the treatment effects of an intervention with repeated measurements (Manolov and Moeyaert, 2017).

This study adapts Moeyaert et al.'s (2014) multilevel models (Model 1A and 1B; p. 193). In these model specifications, the average treatment effects are captured by the mean values of the outcome variables among the observations during the specific study phases, adjusted for other covariates. We fitted two models with transformed NS-SCR frequency and transformed SCL as the outcomes and selected variables as the predictors (e.g., study design factors and covariates). We computed the adjusted average treatment effects using the fitted models and visualized the data to assist in clear interpretation. To determine the preliminary efficacy of the interventions, Wald-test was used to compare the adjusted average treatment effects between and across phases Although there were six completed cases with 108 observations, we limited our analysis to the acceptable data, yielding 95 observations across six participants. With this sample size, the model is limited regarding model complexity and numbers of independent variables. To better account for within-person correlations, we used robust estimator, maximum likelihood, and identity covariance structure in estimations. The unusable data (excluded and missing values) are of lower concern for this data as there were fewer than 12% of unusable values. Finally, we conducted statistical diagnosis and investigated the distributions of the residuals. Shapiro–Wilk normality test (W statistics) and Skewness/Kurtosis test ($\chi^2_{(2)}$) were applied to test for normality.

Additionally, we conducted supplementary testing to investigate potential mechanisms through which the interventions can effect SCL and NS-SCR frequency values. We hypothesized that the interventions could provide protection against the influence of decibel level of environmental noises on SCL and NS-SCR frequency. In other words, we sought to test

the moderating effects of the interventions on the relationships between decibel levels and psychohysiological outcomes. To examine this, we completed the following three steps. First, the study phases were collapsed into three phases: (1) "No Intervention" (baseline + washout phases); (2) "In-Ear"; and (3) "Over-Ear." Second, an additional interaction term between intervention and decibel reading was created and entered into the model to investigate the interaction effect. Third, a continuous time variable was created and entered into the model to adjust for potential time effects to account for the 4 week duration of the study. For these analyses, the random-effects model was used with robust estimator to handle clustering effects as we had to adjust for covariates, including noise levels, presence of other people, presence of visual stimulation, and activity types. All statistics were conducted in Stata 13.

RESULTS

Data Quality Analysis

The ordered logistic model passed the Brant test ($\chi^2_{(11)}$ = 13.55, p = 0.259), suggesting that the model did not significantly violate the parallel regression assumption. As shown in **Table 3**, data quality was significantly associated with Phase 2 (first intervention in sequence), Phase 4 (second intervention sequence), and presence of other people. More specifically, the first intervention phase (Phase 2) was less likely to have higher quality data compared to baseline (Phase 1; 80% lower in odds; a.OR = 0.20, 95% CI: 0.06–0.65, $p < 0.01$). In contrast, the second intervention phase (Phase 4) was more likely to have higher quality data compared to baseline (197% higher in odds (a.OR = 2.97, 95% CI: 1.07–8.26, $p < 0.05$). Additionally, when an additional unit of people were present (e.g., 1: 1–2 people; 2: 3–5 people; 3: 5–10 people; etc.), the odds of obtaining higher data quality increased 82% (a.OR = 1.82, 95% CI: 1.48–2.25, $p < 0.01$). None of the other study design factors and covariates (e.g., activity type) significantly correlated with the data quality.

Preliminary Intervention Efficacy

Results indicate that the residuals from both models followed normal distributions (for transformed NS-SCR frequency: W = 0.97931, p = 0.14687 and $\chi^2_{(2)}$ = 3.49, p = 0.1747; for transformed SCL: W = 0.99098, p = 0.78370 and $\chi^2_{(2)}$ = 0.71, p = 0.6997). Additionally, none of the predictors in the two models were significantly associated with the residuals. These results suggest that the risks of model misspecifications are low. The results of the model fitting are summarized in **Table 4**. For the transformed NS-SCR frequency, the main effect of Phase 2 (β = −0.58, 95% CI: −0.81 to −0.36, $p < 0.01$) and the interaction effect between Phase 2 and Group B (β = −0.74, 95% CI: −1.31 to −0.17, $p < 0.05$) were significantly associated with the outcome. In contrast, for transformed SCL, the interaction effect between Phase 2 and Group B (β = −1.16, 95% CI: −1.91 to −0.42, $p < 0.01$), as well as between Phase 4 and Group B (β = −1.19, 95% CI: −2.07 to −0.31, $p < 0.01$) were significantly associated with the outcome.

To assist in interpretation, we computed the model-adjusted average treatment effects across study groups and study phases, and applied Wald-test ($\chi^2_{(1)}$) to compare their average treatment effects (see **Figures 1A–D**). As illustrated in **Figures 1A,B**, Groups A and B followed similar patterns regarding participants' psychophysiological responses to the interventions. More specifically, in Group A (**Figure 1A**), NS-SCR frequency was significantly lower in Phase 2 (Over Ear) in comparison with Phase 1 (Baseline; $\chi^2_{(1)}$ = 26.35, $p < 0.001$). Similarly, in Group B (**Figure 1B**), NS-SCR frequency was significantly lower in Phase 2 (In Ear) in comparison with Phase 1 (Baseline; $\chi^2_{(1)}$ = 42.75, $p < 0.001$), as well as in Phase 4 (Over Ear) in comparison with Phase 3 (Washout; $\chi^2_{(1)}$ = 12.76, $p < 0.001$). As illustrated in **Figures 1C,D**, we observed similar patterns in the SCL data. Although we did not find evidence of treatment effects in Group A for SCL scores (**Figure 1C**), in Group B (**Figure 1D**), the SCL scores were significantly lower in Phase 2 (In Ear) in comparison with Phase 1 (Baseline; $\chi^2_{(1)}$ = 53.72, $p < 0.001$), as well as in Phase 4 (Over Ear) in comparison with Phase 3 (Washout; $\chi^2_{(1)}$ = 54.72, $p < 0.001$).

Additionally, we investigated potential mechanisms in which the intervention may lower psychophysiological responses. We hypothesized that the intervention may provide protection such that when decibel values increased during the intervention phases both NS-SCR frequencies and SCL remained low. We fitted two random-effect models with an interaction effect between intervention phases and average decibel readings (see **Table 5**). Although we did not find evidence for the interaction effect between intervention and environmental decibel values for the transformed NS-SCR frequency, some significant relationships were found for the transformed SCL. Specifically, the interaction effects between decibel and In Ear (β = −0.02, 95% CI: −0.04 to −0.002, $p < 0.05$), as well as decibel and Over Ear (β = −0.02, 95% CI: −0.04 to −0.004, $p < 0.05$) were significantly associated with the transformed SCL scores.

To assist in interpretation, we computed model-adjusted EDA measures across interventions and over the levels of environmental decibel readings (see **Figures 2A,B** for NS-SCR frequency and SCL, respectively). As illustrated in **Figure 2A**, when environmental decibel levels increased, NS-SCR frequency

TABLE 3 | Results of random-effect ordered logistic regression for data quality analysis.

	a.OR	SE	95% CI
Group B (vs. A)	1.49	0.27	(0.09, 25.99)
Study Phases			
Phase 2 (vs. 1)	0.20**	−2.70	(0.06, 0.65)
Phase 3 (vs. 1)	0.16	−0.80	(0.00, 14.27)
Phase 4 (vs. 1)	2.97*	2.09	(1.07, 8.26)
Noise Levels	1.25	0.24	(0.20, 7.92)
Presence of Other People	1.82**	5.64	(1.48, 2.25)
Presence of Visual Stimulation	0.50	−0.98	(0.13, 1.99)
Activity Types			
Stationary (vs. Active)	1.50	0.71	(0.49, 4.59)
Traveling (vs. Active)	3.24	1.21	(0.49, 21.57)
Average Decibel	1.03	1.50	(0.99, 1.08)
Time	1.09	0.40	(0.71, 1.69)

*a.OR: adjusted Odds Ratio; *p < 0.05; **p < 0.01.*

TABLE 4 | Results of random-effect model for evaluation of intervention effects on electrodermal activity across study phases.

	Transformed NS-SCR Frequency			Transformed SCL		
	Beta	**SE**	**95% CI**	**Beta**	**SE**	**95% CI**
Group B (vs. A)	0.76	0.87	(−0.93, 2.46)	1.55†	0.80	(−0.02, 3.12)
Phase 2 (vs. 1)	−0.58**	0.11	(−0.81, −0.36)	−0.34	0.37	(−1.08, 0.39)
Phase 2 × Group B	−0.74*	0.29	(−1.31, −0.17)	−1.16**	0.38	(−1.91, −0.42)
Phase 3 (vs. 1)	0.35	0.66	(−0.95, 1.64)	0.06	0.22	(−0.37, 0.49)
Phase 3 × Group B	0.70	0.80	(−0.88, 2.27)	0.82	0.52	(−0.20, 1.84)
Phase 4 (vs. 1)	−0.03	0.58	(−1.15, 1.10)	0.32	0.41	(−0.48, 1.12)
Phase 4 × Group B	−0.88	0.68	(−2.22, 0.46)	−1.19**	0.45	(−2.07, −0.31)

†$p < 0.1$; *$p < 0.05$; **$p < 0.01$; *the results were further controlled for noise levels, presence of other people, presence of visual stimulation, activity types, and average decibel.*

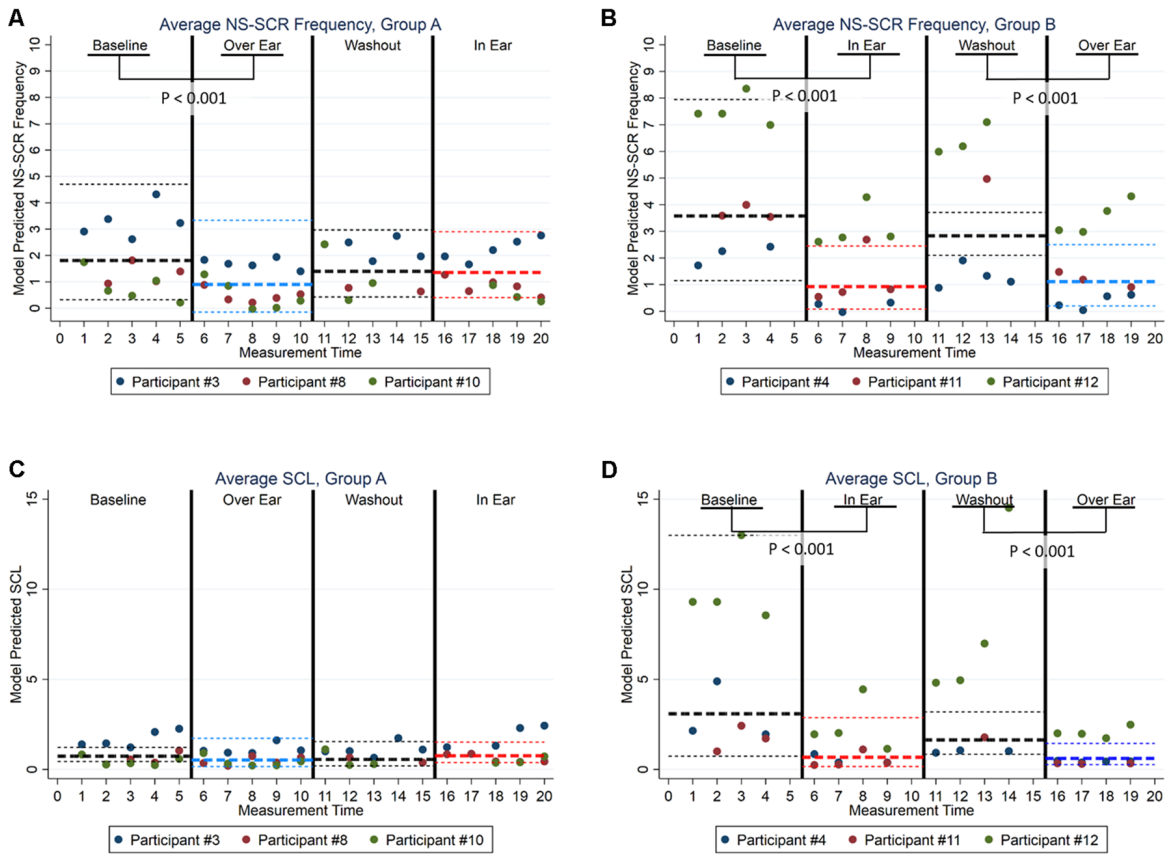

FIGURE 1 | Model Adjusted Back-Transformed Outcomes by Electrodermal Activity (EDA), Study Designs, and Study Phases. **(A)** Group A Average NS-SCR. **(B)** Group B Average NS-SCR. **(C)** Group A Average SCL. **(D)** Group B Average SCL. *Note*. Bold broken lines represent the average values, with thin broken lines representing the 95% CI. Non-transformed values are presented here to increase interpretability; statistical tests were conducted using transformed data.

increased during the stages without intervention, while NS-SCR frequencies remained flat during the stages of interventions, although these differences did not reach statistical significance at 0.05 during formal testing (joint Wald-Test: $\chi^2_{(2)} = 2.09$, $p = 0.3524$). Similarly, in **Figure 2B**, when environmental decibel levels increased, SCL increased during the stages without intervention but remained flat during the stages of intervention. These differences did reach statistical significance at 0.05 during formal testing (joint Wald-Test: $\chi^2_{(2)} = 8.07$, $p = 0.0177$).

DISCUSSION

Research suggests that difficulties with auditory processing are more commonly reported than any other sensory disorder in individuals ASD (Tomchek and Dunn, 2007). Specifically, hyperacusis, a negative and/or exaggerated response to environmental stimuli related to auditory pathways (Asha'ari et al., 2010; American Speech-Language-Hearing Association, 2016), is one of the most identified characteristics of auditory processing differences. Researchers have identified that auditory

TABLE 5 | Results of random-effect models for moderation effects of intervention on the relationship between average decibel and electrodermal activity.

Model parameter	Transformed NS-SCR Frequency			Transformed SCL		
	Beta	SE	95% CI	Beta	SE	95% CI
Intervention						
In Ear (vs. No Intervention)	0.51	1.18	(−1.80, 2.81)	1.39	1.02	(−0.62, 3.40)
Average Decibel	0.02	0.01	(0.00, 0.04)	0.02*	0.01	(0.01, 0.04)
In Ear × Average Decibel	−0.01	0.01	(−0.04, 0.01)	−0.02*	0.01	(−0.04, −0.002)
Over Ear × Average Decibel	−0.01	0.01	(−0.03, 0.01)	−0.02*	0.01	(−0.04, −0.004)

$p < 0.05$; the results were further controlled for noise levels, presence of other people, presence of visual stimulation, and activity types.

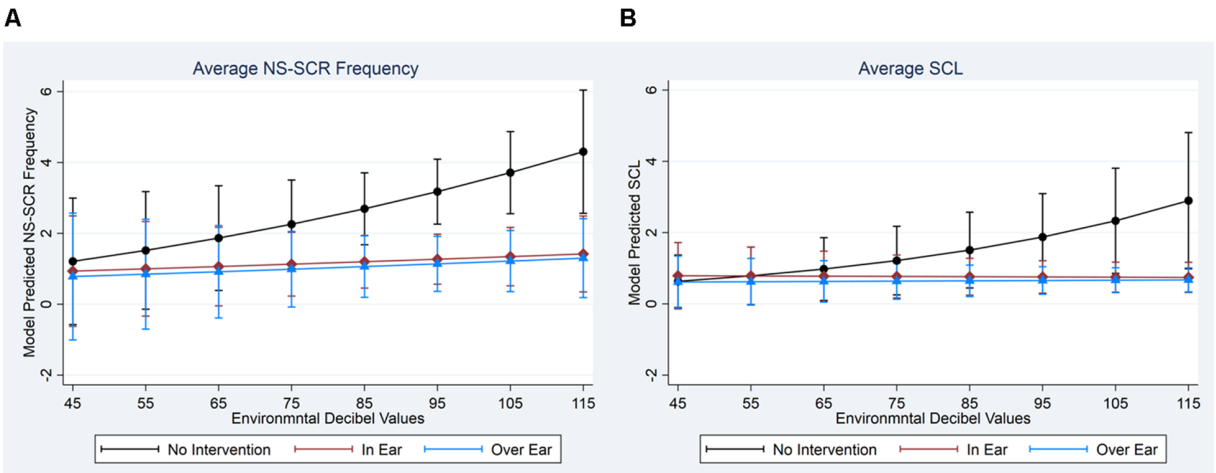

FIGURE 2 | Model Adjusted Back-Transformed Outcomes by EDA and Intervention Types. **(A)** Average NS-SCR Frequency. **(B)** Average SCL. *Note*. Non-transformed values are presented here to increase interpretability; statistical tests were conducted using transformed data.

dysfunction may be due to a slower auditory brain stem response in children with ASD (Lukose et al., 2013; Miron et al., 2018) and that there are anatomical links between the central nervous system and the amygdala (Myne and Kennedy, 2018) contributing to hyperacusis. Although hyperacusis is common in children with ASD, there is minimal scientific evidence to support commonly used interventions such as noise attenuating headphones, which reduces or blocks auditory stimuli in the environment. Results from the current study provide initial support for the use of noise attenuating headphones to reduce psychophysiological stress and anxiety from auditory stimuli, as measured by EDA. Additionally, results identified a clear positive relationship between the level of noise and EDA, which was buffered by the use of noise attenuating headphones.

Despite the neurological links identified between hyperacusis and ASD in research laboratory settings, to our knowledge, there is no research examining the impact of interventions in the natural environment on anxiety and stress levels within this population. As the greatest levels of over-responsiveness are found to be in multi-sensory environments full of potentially unknown experiences (Green et al., 2015), one limitation of laboratory research is that the testing environment does not reflect experiences that occur within natural settings. For example, a child with hyperacusis who has an aversive reaction to sirens on the highway may begin to associate the car with negative physiological experiences related to sounds that are found distressing. Subsequently, this may result in that child presenting with avoidance behaviors (i.e., tantrums, running away, crying) in anticipation of the sound when getting into or traveling in the car, even in the absence of the noise. As discussed previously, this has shown to increase stress for those who cannot communicate their feelings and can lead to the child being misunderstood.

Robertson and Simmons (2015) completed a focus group examining the sensory experiences of six adults with ASD. Results identified that all participants reported strong physical or emotional reactions to sensory stimuli in the environment. Lack of control over the sensory stimuli was identified as a factor that increased the perceived level of stress or anxiety. Prior to this, Smith and Sharp (2013) conducted a qualitative study in which adults with Asperger Syndrome reported sensory stress that contributed to strong emotional responses and coping strategies such as avoidance, fear and social isolation. Specific to the auditory sensory system, Landon et al. (2016) conducted qualitative research on adults with ASD and NS. Participants reported various ways in which hypersensitivity to noise impacted their participation in their day to day lives and the emotions experienced due to perceived noxious auditory stimuli. Despite some participants' employing strategies such as the use of earplugs or verbally discussing their discomfort to sounds with those they knew, escaping from the potential problematic situation was common. Research indicates that a correlation

exists among anxiety, SOR and behavior (Mazurek et al., 2013). Parents and families of children who are over-responsive to sensory stimuli often report avoiding events and activities due to the inability to prepare for potential unknown sensory experiences (Bagby et al., 2012; Demchick et al., 2014; Pfeiffer et al., 2017; Myne and Kennedy, 2018). A common natural context for children is school. Noting that the average noise level in classrooms exceeds WHO noise exposure guidelines, Keith et al. (2018) found that adolescents with ASD, as well as their matched neurotypical peers, performed worse on more difficult tasks when noise was added. Providing individuals with strategies to manage auditory hypersensitivities has the potential to aid them in participating in meaningful occupations rather than experiencing fear and anxiety and engaging in escape and elopement.

The current study employed the use of noise attenuating headphones within the natural environments of participants. On the basis of neural plasticity (Ayres, 1972) and experience-dependent plasticity (Alwis and Rajan, 2014), it is believed that active participation in enriched environments promotes neural change and cognitive behavioral improvements. Research has indicated that biochemical changes occur from engagement in meaningful trial and error learning during sensory and motor tasks (Miller et al., 2009). By decreasing anxiety and stress through the use of noise attenuating headphones, individuals can engage in this trial and error learning within their natural environment. It is further believed that repetition of normal responses to sensory stimuli creates new neural pathways thus providing the platform for successful participation in natural real-world environments (Miller et al., 2009). By providing a strategy that can be used on a day to day basis, individuals can develop the experiences and theoretically build the platform for successful participation. Though limited by small sample size and quasi-experimental design, past research implemented in natural environments identified positive behavioral and academic outcomes when using noise attenuating headphones in children with learning disabilities (Smith and Riccomini, 2013) and ASD (Rowe et al., 2011).

Additionally, the majority of evidence is founded in parent reports *via* questionnaires and interviews, as well as behavioral assessment of retrospective videotape analysis (Tomchek and Dunn, 2007; Myne and Kennedy, 2018). The wearable wireless technology used in the current study allows for the collection of physiological data measuring stress and anxiety within natural environments, creating a real-time picture of events and experiences of participants. As there are unpredictable environmental factors, it is important to consider their potential impact on data collection when using newer measurement systems such as wearable sensors. Analyses were completed for the current study on the quality of data collected from the wearable sensors. Results identified that quality increased over the course of data collection suggesting improvements with additional practice in using the technology. Since the data is collected in natural environments, it is often parents and caregivers who initiated data collection sessions. Although there was a high rate (88%) of useable data, additional practice sessions with the people who collect data may increase the overall quality when implementing research using wearable sensors. Additionally, there was an increase in the quality of data when more people were reported in the environment. It is possible that this resulted in more support for parents and caregivers from other people to ensure that data collection methods were properly implemented (i.e., assistance in maintaining the devices in proper position; ability to maintain focus on data collection methods), although this requires consideration in future research. Most importantly, results identified that neither the activity of the child nor the environmental setting had an impact on the quality of data suggesting that this type of data collection can be used across activity types.

In understanding the physiological responses in conjuction with the perceived experiences of parents/caregivers and individuals with ASD, we can develop and design more targeted interventions for auditory hypersensitivity. Psychologically, triggers may be more easily identified, and treatment/coping strategies can be assessed. If an individual can predict when they will be in an environment leading to this increased sympathetic activation, they may be able to use previously identified environmental interventions, such as noise attenuating headphones or other coping strategies, to continue participation rather than avoid engagement in important life activities and events. When triggered by stress, the emotional motor systems pathway activates one of the branches of the autonomic nervous system, the hypothalamic-pituitary-adrenal axis (HPA-axis; Mayer, 2000). The triggering of the emotional motor systems pathway can lead to emotional feelings and/or vigilance arousal, autonomic responses, sensory modulation and/or neuroendocrine responses. As interoceptive and exteroceptive stress responses occur, the cyclical effects of the triggering of the emotional motor systems pathways begin once again (Mayer, 2000). Thus, the use of noise attenuating headphones may decrease physiological responses in perceived auditory aversive situations, and may also provide opportunity for experiences as triggering of the HPA-axis may be avoided.

Limitations

Similar to limitations of previous research on this topic, the study was limited in the sample size. This is due in part to the substantially varied environments within natural settings and the individualized nature of participants' EDA that requires the use of single-subject design. Another limitation was the high dropout rate (n = 6; 50%). One suggested method to decrease drop-out rate would be to reduce the burden of data collection by using an automated measurement system that is activated at a designated decibel level, although this does not account for aversive responses to types of noises vs. levels of noise. In addition, no data was collected tracking the use of the aware mode during the IE headphone use. This feature could serve as a tool to design individualized interventions and should be explored in future studies.

Future Research

Research has suggested that complete avoidance of sounds can lead to increased anxiety, therefore exacerbating the negative effects of hyperacusis (Jüris et al., 2014). Neurologically it is

suggested that habituation-related plasticity occurs in the central limb of stress-response circuits allowing the hypothalamic pituitary adrenal axis to respond normally and possibly habituate to new environments (Day et al., 2009). Consistent with this neurological understanding, it has been shown that low levels of noise exposure may lead to desensitization of unwanted sounds (Jüris et al., 2014). Therefore, future research should implement methodology to track the use of the "aware-mode" for the IE headphones that allows the wearer to turn off the noise-blocking feature, enabling filtering rather than complete avoidance. This may prove more beneficial long-term in comparison to OE headphones without "aware mode."

Although a link has been found between measures of EDA and parent-report, provider-report, and research-coded behavioral problems, it is highly recommended that future research incorporate behavioral measures of stress in order to examine whether a decrease in sympathetic activity has any relevant impact on child behavior and attention to task. Previous research has examined behavioral outcomes of using NC headphones but did not incorporate measures of sympathetic activity (Ikuta et al., 2016). Methodology could incorporate ecological momentary assessment to collect behavioral data in conjunction with wearable devices to examine the relationship between noise, sympathetic activity, and behavioral responses.

Additionally, there is a hypothesis in the literature that internal neuronal noise is a crucial factor influencing perceptual abilities in ASD. Emerging evidence suggests that high internal neuronal noise and poor external noise filtering impact auditory perception in individuals with ASD (Park et al., 2017). Recent research has implemented new measurement methods using EEG global coherence to examine the relationship between internal neuronal noise and the application of external auditory quasi-Brownian noise vs. absence of external noise (Mendez-Balbuena et al., 2018). Few studies have examined the relationship between EDA and EEG. Of those that have, correlations were found between SCL and specific EEG waveforms in girls with Attention-Deficit/Hyperactivity Disorder (Dupuy et al., 2014), as well as between EDA response amplitude during generalized tonic-clonic seizures and the duration of postictal generalized EEG suppressions in individuals with epilepsy (Poh et al., 2012; Onorati et al., 2017). In order to better understand the influence of auditory interventions, such as noise attenuating headphones, future research should examine the relationship between EDA and EEG global coherence in individuals with ASD during the presence and absence of targeted interventions. This would further expand the understanding of the relationship between internal neuronal noise and external noise filtering that is hypothesized to influence perceptual abilities.

ETHICS STATEMENT

This study was approved by the Temple University IRB.

AUTHOR CONTRIBUTIONS

BP and LS contributed to the conception and design of the study. BP completed all the data collection and LS organized and interpreted all of the physiological data. CS assisted in data organization and analyzed the data. AM assisted in the organization of the data and data base, as well as helping in the writing of the introduction and discussion of the manuscript. BP (introduction, methodology and discussion), LS (parts of the methodology) and CS (data analysis and results) wrote the initial drafts of the manuscript. All authors contributed to manuscript revision, read and approved the submitted version.

FUNDING

This project was partially funded through a contract with Bose Incorporated. The funder provided a grant and small equipment to support the implementation of the study. The funder was not involved in the study design, collection, analysis, interpretation of data, the writing of this article or the decision to submit it for publication. Open access publication fees are provided through a start-up fund of the primary author provided by the College of Public Health at Temple University. LS was supported by the National Institutes of Health under NCMRR K12 HD055929.

REFERENCES

Alwis, D. S., and Rajan, R. (2014). Environmental enrichment and the sensory brain: the role of enrichment in remediating brain injury. *Front. Syst. Neurosci.* 8:156. doi: 10.3389/fnsys.2014.00156

American Psychiatric Association. (2000). *The Diagnostic and Statistical Manual of Mental Disorders: DMS-IV*. 4th Edn. Arlington, VA: American Psychiatric Association.

American Psychiatric Association. (2013). *The Diagnostic and Statistical Manual of Mental Disorders: DSM 5*. 5th Edn. Arlington, VA: American Psychiatric Association.

American Psychological Association. (2018). *What is Cognitive Behavioral Therapy*. Available online at: http://www.apa.org/ptsd-guideline/patients-and-families/cognitive-behavioral.aspx. Accessed October 30, 2019.

American Speech-Language-Hearing Association. (2016). *Hyperacusis*. Available online at: https://www.asha.org/uploadedFiles/AIS-Hyperacusis.pdf. Accessed October 30, 2019.

Asha'ari, Z. A., Mat Zain, N., and Razali, A. (2010). Phonophobia and hyperacusis: practical points from a case report. *Malays. J. Med. Sci.* 17, 49–51.

Ayres, J. (1972). Treatment of sensory integrative dysfunction. *Aust. Occup. Ther. J.* 19:88. doi: 10.1111/j.1440-1630.1972.tb00547.x

Bagby, M. S., Dickie, V. A., and Baranek, G. T. (2012). How sensory experiences of children with and without autism affect family occupations. *Am. J. Occup. Ther.* 66, 78–86. doi: 10.5014/ajot.2012.000604

Baker, J. K., Fenning, R. M., Erath, S. A., Baucom, B. R., Moffitt, J., and Howland, M. A. (2018). Sympathetic under-arousal and externalizing behavior problems in children with autism spectrum disorder. *J. Abnorm. Child Psychol.* 46, 895–906. doi: 10.1007/s10802-017-0332-3

Baker, J. K., Fenning, R. M., Howland, M. A., Baucom, B. R., Moffitt, J., and Erath, S. A. (2015). Brief report: a pilot study of parent-child biobehavioral synchrony in autism spectrum disorder. *J. Autism Dev. Disord.* 45, 4140–4146. doi: 10.1007/s10803-015-2528-0

Baker, J. K., Fenning, R. M., Howland, M. A., and Huynh, D. (2019). Parental criticism and behavior problems in children with autism spectrum disorder. *Autism* 23, 1249–1261. doi: 10.1177/1362361318804190

Baranek, G. T., David, F. J., Poe, M. D., Stone, W. L., and Watson, L. R. (2006). Sensory experiences questionnaire: discriminating sensory features in young children with Autism, developmental delays, and typical development. *J. Child Psychol. Psychiatry* 47, 591–601. doi: 10.1111/j.1469-7610.2005.01546.x

Basner, M., Babisch, W., Davis, A., Brink, M., Clark, C., Janssen, S., et al. (2014). Auditory and non-auditory effects of noise on health. *Lancet* 383, 1325–1332. doi: 10.1016/S0140-6736(13)61613-X

Ben-Sasson, A., Hen, L., Fluss, R., Cermak, S. A., Engel-Yeger, B., and Gal, E. (2009). A meta-analysis of sensory modulation symptoms in individuals with autism spectrum disorders. *J. Autism Dev. Disord.* 39, 1–11. doi: 10.1007/s10803-008-0593-3

Bolton, P. F., Golding, J., Emond, A., and Steer, C. D. (2012). Autism spectrum disorder and autistic traits in the Avon longitudinal study of parents and children: precursors and early signs. *J. Am. Acad. Child Adolesc. Psychiatry* 51, 249.e25–260.e25. doi: 10.1016/j.jaac.2011.12.009

BOSE. (2018). *Noise Cancelling Headphones.* Available online at: https://www.bose.com/en_us/products/headphones/noise_cancelling_headphones.html. Accessed October 30, 2019.

Boucsein, W. (2012). *Electrodermal Activity.* 2nd Edn. New York, NY: Springer.

Boucsein, W., Fowles, D. C., Grimnes, S., Ben-Shakhar, G., Roth, W. T., Dawson, M. E., et al. (2012). Publication recommendations for electrodermal measurements. *Psychophysiology* 49, 1017–1034. doi: 10.1111/j.1469-8986.2012.01384.x

Brout, J. J., Edelstein, M., Erfanian, M., Mannino, M., Miller, L. J., Rouw, R., et al. (2018). Investigating misophonia: a review of the empirical literature, clinical implications, and a research agenda. *Front. Neurosci.* 12:36. doi: 10.3389/fnins.2018.00036

Chang, M. C., Parham, L. D., Blanche, E. I., Schell, A., Chou, C. P., Dawson, M., et al. (2012). Autonomic and behavioral responses of children with autism to auditory stimuli. *Am. J. Occup. Ther.* 66, 567–576. doi: 10.5014/ajot.2012.004242

Dawson, M. E., Schell, A. M., and Fillion, D. L. (2007). "The electrodermal system," in *Handbook of Psychophysiology*, eds T. Cacioppo, L. G. Tassinary and G. G. Bernston (New York, NY: Cambridge University Press), 159–181.

Day, H. E., Masini, C. V., and Campeau, S. (2009). Reversible inactivation of the auditory thalamus disrupts HPA axis habituation to repeated noise stress exposures. *Brain Res.* 1276, 123–130. doi: 10.1016/j.brainres.2009.04.023

Demchick, B. B., Eskow, K. G., and Crabtree, L. A. (2014). Autism and transitioning youth: A pilot study of sensory processing and family quality of life. *J. Occup. Ther. Schools, & Early Intervention* 7, 54–69. doi: 10.1080/19411243.2014.898492

Dunn, W. (1999). *Sensory Profile.* Available online at: https://www.pearsonclinical.com/therapy/products/100000566/sensory-profile.html. Accessed October 30, 2019.

Dupuy, F. E., Clarke, A. R., Barry, R. J., Selikowitz, M., and McCarthy, R. (2014). EEG and electrodermal activity in girls with Attention-Deficit/Hyperactivity disorder. *Clin. Neurophysiol.* 125, 491–499. doi: 10.1016/j.clinph.2013.09.007

EarMachine. (2018). *VenueDB.* Available online at: http://www.earmachine.com/venuedb/. Accessed October 30, 2019.

Empatica. (2018). *E4 Wristband.* Available online at: https://www.empatica.com/research/e4/. Accessed October 30, 2019.

Fenning, R. M., Baker, J. K., Baucom, B. R., Erath, S. A., Howland, M. A., and Moffitt, J. (2017). Electrodermal variability and symptom severity in children with autism spectrum disorder. *J. Autism Dev. Disord.* 47, 1062–1072. doi: 10.1007/s10803-016-3021-0

Gilliam, J. E. (2013). *Gilliam Autism Rating Scale, 3rd Edition (GARS-3).* Available online at: https://www.pearsonassessments.com/store/usassessments/en/Store/Professional-Assessments/Behavior/Gilliam-Autism-Rating-Scale-%7C-Third-Edition/p/100000802.html?tab=product-details. Accessed October 30, 2019.

Green, S. A., Hernandez, L., Tottenham, N., Krasileva, K., Bookheimer, S. Y., and Dapretto, M. (2015). Neurobiology of sensory over-responsivity in youth with autism spectrum disorders. *JAMA Psychiatry* 72, 778–786. doi: 10.1001/jamapsychiatry.2015.0737

Grinker, R. (2007). *Unstrange Minds: Remapping the World of Autism.* New York, NY: Basic Books.

Ida-Eto, M., Hara, N., Ohkawara, T., and Narita, M. (2017). Mechanism of auditory hypersensitivity in human autism using autism model rats. *Pediatr. Int.* 59, 404–407. doi: 10.1111/ped.13186

Ikuta, N., Iwanaga, R., Tokunaga, A., Nakane, H., Tanaka, K., and Tanaka, G. (2016). Effectiveness of earmuffs and noise-cancelling headphones for coping with hyper-reactivity to auditory stimuli in children with Autism Spectrum Disorder: a preliminary study. *Hong Kong J. Occup. Ther.* 28, 24–32.

Jastreboff, P., and Jastreboff, M. (2000). Tinnitus retraining therapy (TRT) as a method for treatment of tinnitus and hyperacusis patients. *J. Am. Acad. Audiol.* 11, 162–177.

Jones, C. R., Happé, F., Baird, G., Simonoff, E., Marsden, A. J., Tregay, J., et al. (2009). Auditory discrimination and auditory sensory behaviours in autism spectrum disorders. *Neuropsychologia* 47, 2850–2858. doi: 10.1016/j.neuropsychologia.2009.06.015

Jüris, L., Andersson, G., Larsen, H. C., and Ekselius, L. (2014). Cognitive behavior therapy for hyperacusis: a randomized controlled trial. *Behav. Res. Ther.* 54, 30–37. doi: 10.1016/j.brat.2014.01.001

Keith, J. M., Jamieson, J. P., and Bennetto, L. (2018). The influence of noise on autonomic arousal and cognitive performance in adolescents with autism spectrum disorder. *J. Autism Dev. Disord.* 49, 113–126. doi: 10.1007/s10803-018-3685-8

Kern, J. K., Trivedi, M. H., Garver, C. R., Grannemann, B. D., Andrews, A. A., Salva, J. S., et al. (2006). The pattern of sensory processing abnormalities in autism. *Autism* 5, 480–494. doi: 10.1177/1362361306066564

Kleckner, I. R., Jones, R. M., Wilder-Smith, O., Wormwood, J. B., Akcakaya, M., Quigley, K. S., et al. (2018). Simple, transparent, and flexible automated quality assessment procedures for ambulatory electrodermal activity data. *IEEE Trans. Biomed. Eng.* 65, 1460–1467. doi: 10.1109/TBME.2017.2758643

Kuiper, M., Verhoeven, E., and Geurts, H. M. (2019). Stop making noise! Auditory sensitivity in adults with autism spectrum disorder diagnosis: physiological habituation and subjective detection thresholds. *J. Autism Dev. Disord.* 49, 2116–2128. doi: 10.1007/s10803-019-03890-9

Kushki, A., Brian, J., Dupuis, A., and Anagnostou, E. (2014). Functional autonomic nervous system profile in children with autism spectrum disorder. *Mol. Autism* 5:39. doi: 10.1186/2040-2392-5-39

Landon, J., Shepherd, D., and Lodhia, V. (2016). A qualitative study of noise sensitivity in adults with autism spectrum disorder. *Res. Autism Spectr. Disord.* 32, 43–52. doi: 10.1016/j.rasd.2016.08.005

Lukose, R., Brown, K., Barber, C. M., and Kulesza, R. J. Jr. (2013). Quantification of the stapedial reflex reveals delayed responses in autism. *Autism Res.* 6, 344–353. doi: 10.1002/aur.1297

Manolov, R., and Moeyaert, M. (2017). Recommendations for choosing single-case data analytical techniques. *Behav. Ther.* 48, 97–114. doi: 10.1016/j.beth.2016.04.008

Marco, E. J., Hinkley, L. B., Hill, S. S., and Nagarajan, S. S. (2011). Sensory processing in autism: a review of neurophysiologic findings. *Pediatr. Res.* 69, 48R–54R. doi: 10.1203/PDR.0b013e3182130c54

Matsuzaki, J., Kagitani-Shimono, K., Sugata, H., Hirata, M. H., Hanaie, R., Nagatani, F., et al. (2014). Progressively increased M50 responses to repeated sounds in autism spectrum disorder with auditory hypersensitivity: a magnetoencephalographic study. *PLoS One* 9:e102599. doi: 10.1371/journal.pone.0102599

Mayer, E. A. (2000). The neurobiology of stress and the gastrointestinal disease. *Gut* 47, 861–869. doi: 10.1136/gut.47.6.861

Mazurek, M. O., Vasa, R. A., Kalb, L. G., Kanne, S. M., Rosenberg, D., Keefer, A., et al. (2013). Anxiety, sensory over-responsivity, and gastrointestinal problems in children with autism spectrum disorders. *J. Abnorm. Child Psychol.* 41, 165–176. doi: 10.1007/s10802-012-9668-x

McEwen, B. S., and Gianaros, P. J. (2011). Stress and allostasis-induced brain plasticity. *Annu. Rev. Med.* 62, 431–445. doi: 10.1146/annurev-med-052209-100430

Mendez-Balbuena, I., Arrieta, P., Huidobro, N., Flores, A., Lemuz-Lopez, R., Trenado, C., et al. (2018). Augmenting EEG-global-coherence with auditory and visual noise. *Medicine* 97:e12008. doi: 10.1097/md.0000000000012008

Miller, L. J., Nielsen, D. M., Schoen, S. A., and Brett-Green, B. A. (2009). Perspectives on sensory processing disorder: a call for translational research. *Front. Integr. Neurosci.* 30:22. doi: 10.3389/neuro.07.022.2009

Miller, L. J., and Schoen, S. (2015). A pilot study of integrated listening system for children with sensory processing problems. *J. Occup. Ther. Sch. Early Interv.* 8, 256–276. doi: 10.1080/19411243.2015.1055418

Miron, O., Beam, A. L., and Kohane, I. S. (2018). Auditory brainstem response in infants and children with autism spectrum disorder: a meta-analysis of wave V. *Autism Res.* 11, 255–363. doi: 10.1002/aur.1886

Moeyaert, M., Ferron, J. M., Beretvas, S. N., and Van den Noortgate, W. (2014). From a single-level analysis to a multilevel analysis of single-case experimental designs. *J. Sch. Psychol.* 52, 191–211. doi: 10.1016/j.jsp.2013.11.003

Münzel, T., Gori, T., Babisch, W., and Basner, M. (2014). Cardiovascular effects of environmental noise exposure. *Eur. Heart J.* 35, 829–836. doi: 10.1093/eurheartj/ehu030

Myne, S., and Kennedy, V. (2018). Hyperacusis in children: a clinical profile.. *Int. J. Pediatr. Otorhinolaryngol.* 107, 80–85. doi: 10.1016/j.ijporl.2018.01.004

Onorati, F., Regalia, G., Caborni, C., Migliorini, M., Bender, D., Poh, M.-Z., et al. (2017). Multicenter clinical assessment of improved wearable multimodal convulsive seizure detectors. *Epilepsia* 58, 1870–1879. doi: 10.1111/epi.13899

Orekhova, E. V., and Stroganova, T. A. (2014). Arousal and attention re-orienting in autism spectrum disorders: evidence from auditory event-related potentials. *Front. Hum. Neurosci.* 8:34. doi: 10.3389/fnhum.2014.00034

Palumbo, D. B., Alsalman, O., Ridder, D. D., Song, J.-J., and Vanneste, S. (2018). Misophonia and potential underlying mechanisms: a perspective. *Front. Psychol.* 9:953. doi: 10.3389/fpsyg.2018.00953

Park, W., Schauder, K. B., Zhang, R., Bennetto, L., and Tadin, D. (2017). High internal noise and poor external noise filtering characterize perception in Autism Spectrum Disorder. *Sci. Rep.* 7:17584. doi: 10.1038/s41598-017-17676-5

Pfeiffer, B., Coster, W., Snethen, G., Derstine, M., Piller, A., and Tucker, C. (2017). Caregivers' perspective on the sensory environment and participation in daily activities of children with autism spectrum disorder. *Am. J. Occup. Ther.* 71, 7104220020p1–7104220028p9. doi: 10.5014/ajot.2017.021360

Pfeiffer, B., Erb, S. R., and Slugg, L. (2019). Impact of noise-attenuating headphones on participation in the home, community, and school for children with autism spectrum disorder. *Phys. Occup. Ther. Pediatr.* 39, 60–76. doi: 10.1080/01942638.2018.1496963

Poh, M.-Z., Loddenkemper, T., Reinsberger, C., Sweenson, N. C., Goyal, S., Madsen, J. R., et al. (2012). Autonomic changes with seizures correlate with postictal EEG suppression. *Neurology* 78, 1868–1876. doi: 10.1212/WNL.0b013e318258f7f1

Porges, S. W., Bazhenova, O. V., Bal, E., Carlson, N., Sorokin, Y., Heilman, K. J., et al. (2014). Reducing auditory hypersensitivities in autistic spectrum disorder: preliminary findings evaluating the listening project protocol. *Front. Pediatr.* 2:80. doi: 10.3389/fped.2014.00080

Prince, E. B., Kim, E. S., Wall, C. A., Gisin, E., Goodwin, M., Schoen Simmons, E., et al. (2017). The relationship between autism symptoms and arousal level in toddlers with autism spectrum disorder, as measured by electrodermal activity. *Autism* 21, 504–508. doi: 10.1177/1362361316648816

Qualtrics, X. M. (2019). *Software to Help Turn Customers Into Fanatics Products Into Obsession Employees Into Ambassadors and Brands Into Religions.* Available online at: https://www.qualtrics.com. Accessed October 30, 2019.

Rance, G., Chisari, D., Saunders, K., and Rault, J.-L. (2017). Reducing listening-related stress in school-aged children with autism spectrum disorders. *J. Autism Dev. Disord.* 47, 2010–2022. doi: 10.1007/s10803-017-3114-4

Rimland, B., and Edelson, S. M. (1995). Brief report: a pilot study of auditory integration training in Autism. *J. Autism Dev. Disord.* 25, 61–70. doi: 10.1007/bf02178168

Robertson, A. E., and Simmons, D. R. (2015). The sensory experiences of adults with autism spectrum disorder: a qualitative analysis. *Perception* 44, 569–586. doi: 10.1068/p7833

Rogers, S. J., Hepburn, S., and Wehner, E. (2003). Parent report of sensory systems in toddlers with autism and those with other developmental disorders. *J. Autism Dev. Disord.* 33, 631–642. doi: 10.1023/b:jadd.0000006000.38991.a7

Rowe, C., Chandler, C., and Neville, M. (2011). Noise reduction headphones and autism: a single case study. *J. Occup. Ther. Sch. Early Interv.* 4, 229–235. doi: 10.1080/19411243.2011.629551

Schoen, S. A., Miller, L. J., Brett-Green, B., and Hepburn, S. L. (2008). Psychophysiology of children with autism spectrum disorder. *Res. Autism Spectr. Disord.* 2, 417–429. doi: 10.1016/j.rasd.2007.09.002

Sinha, Y., Silove, N., Wheeler, D., and Williams, K. (2006). Auditory integration training and other sound therapies for autism spectrum disorders: a systematic review. *Arch. Dis. Child.* 91, 1018–1022. doi: 10.1136/adc.2006.094649

Smith, G. W., and Riccomini, P. J. (2013). The effect of a noise reducing test accommodation on elementary students with learning disabilities. *Learn. Disabil. Res. Pract.* 28, 89–95. doi: 10.1111/ldrp.12010

Smith, R. S., and Sharp, J. (2013). Fascination and isolation: a grounded theory exploration of unusual sensory experiences in adults with Asperger Syndrome. *J. Autism Dev. Disord.* 49, 891–910. doi: 10.1007/s10803-012-1633-6

Sokhadze, E. M., Casanova, M. F., Tasman, A., and Brockett, S. (2016). Electrophysiological and behavioral outcomes of Berard auditory integration training (AIT) in children with autism spectrum disorder. *Appl. Psychophysiol. Biofeedback* 41, 405–420. doi: 10.1007/s10484-016-9343-z

Stiegler, L. N., and Davis, R. (2010). Understanding sound sensitivity in individuals with Autism Spectrum Disorders. *Focus Autism Other Dev. Disabl.* 25, 67–75. doi: 10.1177/1088357610364530

Talavage, T. M., Gonzalez-Castillo, J., and Scott, S. K. (2014). Auditory neuroimaging with fMRI and PET. *Hear. Res.* 307, 4–15. doi: 10.1016/j.heares.2013.09.009

Tharpe, A. M., Bess, F. H., Sladen, D. P., Schissel, H., Couch, S., and Schery, T. (2006). Auditory characteristics of children with autism. *Ear Hear.* 27, 430–441. doi: 10.1097/01.aud.0000224981.60575.d8

Tomchek, S. D., and Dunn, W. (2007). Sensory processing in children with and without autism: a comparative study using the short sensory profile. *Am. J. Occup. Ther.* 61, 190–200. doi: 10.5014/ajot.61.2.190

van Dooren, M., de Vries, J. J. G. G. J., and Janssen, J. H. (2012). Emotional sweating across the body: comparing 16 different skin conductance measurement locations. *Physiol. Behav.* 160, 298–304. doi: 10.1016/j.physbeh.2012.01.020

Wilson, U. S., Sadler, K. M., Hancock, K. E., Guinan, J. J. Jr., and Lichtenhan, J. T. (2017). Efferent inhibition strength in a physiological correlate of hyperacusis in children with autism spectrum disorder. *J. Neurophysiol.* 118, 1164–1172. doi: 10.1152/jn.00142.2017

World Health Organization. (2018). *Noise*. Available online at: http://www.who.int/sustainable-development/transport/health-risks/noise/en/. Accessed October 30, 2019.

Yeo, I.-K., and Johnson, R. A. (2000). A new family of power transformations to improve normality of symmetry. *Biometrika* 87, 954–959. doi: 10.1093/biomet/87.4.954

Conflict of Interest: The authors declare that the research was conducted in the absence of any commercial or financial relationships that could be construed as a potential conflict of interest.

Copyright © 2019 Pfeiffer, Stein Duker, Murphy and Shui. This is an open-access article distributed under the terms of the Creative Commons Attribution License (CC BY). The use, distribution or reproduction in other forums is permitted, provided the original author(s) and the copyright owner(s) are credited and that the original publication in this journal is cited, in accordance with accepted academic practice. No use, distribution or reproduction is permitted which does not comply with these terms.

Advantages of publishing in Frontiers

OPEN ACCESS
Articles are free to read for greatest visibility and readership

FAST PUBLICATION
Around 90 days from submission to decision

HIGH QUALITY PEER-REVIEW
Rigorous, collaborative, and constructive peer-review

TRANSPARENT PEER-REVIEW
Editors and reviewers acknowledged by name on published articles

Frontiers
Avenue du Tribunal-Fédéral 34
1005 Lausanne | Switzerland

Visit us: www.frontiersin.org
Contact us: info@frontiersin.org | +41 21 510 17 00

REPRODUCIBILITY OF RESEARCH
Support open data and methods to enhance research reproducibility

DIGITAL PUBLISHING
Articles designed for optimal readership across devices

FOLLOW US
@frontiersin

IMPACT METRICS
Advanced article metrics track visibility across digital media

EXTENSIVE PROMOTION
Marketing and promotion of impactful research

LOOP RESEARCH NETWORK
Our network increases your article's readership